



TESIS DOCTORAL

**Mecanismos moleculares tempranos de la desregulación
de la homeostasis del calcio inducida por péptidos β -
amiloides y estrategias de neuroprotección**

Joana Margarida de Andrade Poejo

Doctorado en Biomarcadores de Salud y Estados Patológicos (R012)

2022



TESIS DOCTORAL

**Mecanismos moleculares tempranos de la desregulación de la
homeostasis del calcio inducida por péptidos β -amiloides y
estrategias de neuroprotección**

Molecular mechanisms of early cytosolic calcium dysregulation
induced by amyloid β peptides and neuroprotection strategies

Joana Margarida de Andrade Poejo

Doctorado en Biomarcadores de Salud y Estados Patológicos (R012)

La conformidad del director y co-directores consta en el original en papel de esta tesis doctoral

Fdo: Carlos Gutiérrez-Merino (Ph.D.), Director

Fdo: Ana María Mata Durán (Ph.D.), Co-director

Fdo: Alejandro Khalil Samhan Arias (Ph.D.), Co-director

2022

I dedicate this work to:

Afonso, my sun and my everything.

Pedro, my beloved husband.

Mother, the pilar of my life.

Father, my guide-star in the heaven.

ABBREVIATIONS

- [Ca²⁺]_i:** intracellular free calcium concentration
- (-) -BAY-K-8644:** methyl(4S)-2,6-dimethyl-5-nitro-4-[2-(trifluoromethyl)phenyl]-1,4-dihydropyridine-3-carboxylate
- A804598:** N-Cyano-N''-[(1S)-1-phenylethyl]-N'-5-quinolinyl-guanidine
- AC1/AC8:** adenylyl cyclases 1/8
- AChR:** muscarinic acetylcholine receptor
- AD:** Alzheimer's disease
- AMPA:** α-Amino-3-hydroxy-5-methyl-4-isoxazolepropionic acid
- APP:** amyloid precursor protein
- ATP:** adenosine triphosphate
- A.U.:** arbitrary units
- AUC:** area under the curve
- Aβ:** amyloid β
- Aβ(1–42)-HiLyteTM-Fluor555 or Aβ(1-42)*555:** fluorescent labeled amyloid β
- B. w.:** body weight
- BACE1:** β-Site APP-cleaving enzyme 1
- BBG:** brilliant Blue G
- BF:** bright field
- BSA:** bovine serum albumin
- BTP2:** N-{4-[3,5-bis(Trifluoromethyl)-1H-pyrazol-1-yl]phenyl}-4-methyl-1,2,3-thiadiazole-5-carboxamide
- C1q:** complement protein component 1q
- C3:** complement protein component 3
- Ca²⁺:** calcium
- CaCl₂:** calcium chloride
- Calcein-AM:** calcein-acetoxyethyl ester
- CaM:** calmodulin
- CaMBPs:** CaM-binding proteins
- CaMKII:** Ca²⁺/calmodulin-dependent protein kinase isoform II
- CaMKs:** Ca²⁺/calmodulin-dependent protein kinases
- Cav1:** caveoline-1

CGN: cerebellar granule neurons
COX-2: cyclooxygenase-2
CRAC: Ca²⁺ release-activated Ca²⁺
CTB*488: cholera toxin B-Alexa 488
DCF: dichlorofluorescein
Di-E-GSSG: dieosin glutathione disulfide
DMEM: dulbecco's modified eagle medium
DMSO: dimethyl sulfoxide
EDTA: ethylenediaminetetraacetic acid
EGTA: tetra(acetoxyethyl ester)
ER: endoplasmic reticulum
fAD: familial or hereditary Alzheimer's disease
FCCP: trifluoromethoxy carbonylcyanide phenylhydrazone
FeCl₃: ferric chloride
Fluo3 AM: fluo-3 acetoxyethyl ester
FRET: fluorescence resonance energy transfer
Fura2 AM: fura2 acetoxyethyl ester
GF: green fluorescence
GFAP: glial fibrillary acidic protein
GSH: glutathione
H₂DCFDA 2',7': dichlorodihydrofluorescein diacetate
H₂O₂: hydrogen peroxide
HD: Huntington's disease
HEPES: 4-(2-hydroxyethyl)-1-piperazineethanesulfonic acid
HT-22: mouse hippocampal neuronal cell line
I.p. : intraperitoneal
iGluRs: ionotropic glutamate receptors
IL-1 α : interleukin 1 alpha
iNOS: inducible nitric oxide synthase
IP3R: inositol 1,4,5-trisphosphate receptor
KCl: potassium chloride
kD: dissociation constant
KNPA: kaempferol plus NPA group
KOH: potassium hydroxide
LTCC: L-type calcium channel

LTD: long-term depression

LTM: long-term memory

LTP: long-term potentiation

MCB: monochlorobimane

MgCl₂: magnesium chloride

MK801: dizocilpine

MnCl₂: manganese(II) chloride

MTT: 3-(4,5-dimethylthiazol-2-yl)-2,5-diphenyltetra-zolium bromide

MWM: molecular weigh markers

MβCD: methyl-β-cyclodextrin

NaCl: sodium chloride

NaF: sodium fluoride

NaOH: sodium hydroxide

NaVO₃: sodium metavanadate

NCX: sodium-calcium exchanger

NFT: neurofibrillary tangles

NF-κB: nuclear factor kappa B

Ng: neurogranin

Nm: neuromodulin

NMDAR: N-methyl D-aspartate receptors

nNOS: neuronal isoform of nitric oxide synthase

NO: nitric oxide

NPA: 3-Nitropropionic acid

Orai 1,2,3: store-operated channel 1,2 or 3

P2R: type 2 purinergic receptors

P2X: type 2 ligand-gated ionotropic purinergic receptors

P2X7R: type 2 purinergic receptor subtype 7

P2Y: type 2 G-protein-coupled metabotropic purinergic receptors

PAGE: polyacrylamide gel electrophoresis

PBS: phosphate-buffered saline

PBST: PBS supplemented with 0.2% Triton X-100

PD: Parkinson's disease

PDI: protein disulfide isomerase

PKA: protein kinase A

PKC: Protein kinase C

PMCA: plasma membrane calcium pump

PrPc: cellular prion protein

PSEN: presenilin

PVDF: polyvinylidene difluoride

RCS: regulator of CaM signaling

RF: red fluorescence

RNS: reactive nitrogen species

ROC: receptor-operated channels

ROI: region of interest

ROS: reactive oxygen species

RT: room temperature

RyR: ryanodine receptors

sAD: sporadic AD

SDS: sodium dodecyl sulfate

SERCA: sarco(endo)plasmic Ca^{2+} -ATPase

SOCE: store-operated calcium entry

STIM1/2: stromal interactive molecule 1/2

TBS: tris-buffered saline

TBST: TBS supplemented with 0.05% polyoxyethylene sorbitan monolaurate (Tween 20)

Tg: thapsigargin

TMRE: tetramethylrhodamine ethyl ester

TMRM: tetramethylrhodamine

TNF α : tumor necrosis factor alpha

Tris: tris-(hydroxymethyl) aminomethane

Triton X-100: 4-(1,1,3,3-tetramethyl butyl)phenyl-poly-ethylene glycol

TTC: 2,3,5-triphenyltetrazolium chloride

TUNEL: terminal deoxynucleotidyl transferase-mediated deoxyuridine triphosphate nick-end labelling

VGCCs: voltage-gated calcium channels

XeC: xestospongin C

$\Delta\Psi_m$: mitochondrial membrane potential

CONTENTS

Abbreviations	v
Acknowledgments	xi
Abstract	13
Resumen	15
Objectives	17
Introductory overview of the thesis	19
Chapter 1 - The relevance of Aβ-CaM complexation in neurons and brain degeneration in AD	27
Chapter 2 - Binding of Aβ(1–42)-CaM complexes to plasma membrane lipid rafts in CGN alters resting cytosolic Ca$^{2+}$ homeostasis	53
Chapter 3 - Identification of the primary target systems in HT-22 cells that are associated with the early dysregulation of Ca$^{2+}$ homeostasis induced by Aβ	93
Chapter 4 - Kaempferol protects against inflammation and Aβ peptides overproduction induced by the neurotoxin NPA in the brain of Wistar rats	163
Conclusions	199
Conclusiones	201
List of publications	203
Annexes - Publications.....	205

ACKNOWLEDGMENTS

To begin with, I would like to thank to my thesis director, Professor Dr. Carlos Gutiérrez-Merino, for accepting me as Ph.D. student. Thank you for the mentorship and guidance through the fascinating world of neurobiochemistry; for patiently, kindly and wisely taught and helped me during the last years. I am, now, a different and better researcher, thanks to you.

Thanks to my co-directors Dra. Ana M. Mata and Dr. Alejandro K. Samhan-Arias for the support, dedication and mentoring.

I want to express my gratitude to Dr. Virginio Garcia-Martinez and Dra. Mafalda Fernandes for being so kind and introduced me to the benevolent Comendador Rui Nabeiro (Delta Cafés), who helped me when I need it most. Also, I want to thanks to Dr. Alvaro Pacheco for the warm welcome, and for sharing all the knowledge and inspiring stories.

I am grateful to Dra. Carmen Lopez-Sánchez for the guidance through the immunohistochemistry research field and for the good team work spirit that we developed over the last years. I also want to thank to María Berrocal, Laura Ortega Bermejo and Jairo Salazar, my laboratory colleagues at Unex, for teaching me new techniques, for sharing good lab tips, for lending me chemicals or reagents when I needed most and for the relaxed conversations during lab breaks.

I would like to show my recognition and appreciation to my old laboratory co-workers and supervisors from iBET (Portugal): Ana Nunes, Cátia Carmo, Sara Nunes, Vanessa Gonçalves, Dra Catarina Duarte, Dra Ana Matias and Dra Ana Teresa Serra, for the supervision, teaching and friendship. I will never forget the place where I started my path as scientific researcher neither the people that contributed to my professional growth.

To my best friend: Sofia Fortalezas, thank you. I am glad we crossed paths. Thank you for introducing me Dr. Carlos Gutierrez-Merino and for teaching me how to handle primary cell cultures and for the initial guidance through fluorescence microscopy imaging.

To my dear family and friends: Ricardo, Ismael, Nanda, Zé, Gonçalo, Mimi, Muffy and Mouta, thank you for the indirect support shared over these years.

Finally, I would never be able to finish this wonderful lifetime journey without the help and solid support of my husband Pedro and my mother Maria de Lourdes. I am deeply grateful to you two, for the words of encouragement, for being patience and open-minded, and mainly for the immeasurable hours that you spent with my delightful son, Afonso, to allowed me to carry on my Ph.D. thesis.

This work has been supported by grants BFU2014-53641-P and BFU2017-85723-P of the Spanish Plan Nacional de I+D+I, and by Grant GR18118 of the Junta de Extremadura to the Research Group BBB008, all with European Funds for Structural Development (FEDER) co-financing. The author, Joana Poejo, was partially supported by Delta Cafés (Campo Maior, Portugal).



GOBIERNO
DE ESPAÑA



MINISTERIO
DE ECONOMÍA
Y COMPETITIVIDAD



Unión Europea

Fondo Europeo
de Desarrollo Regional
"Una manera de hacer Europa"



JUNTA DE EXTREMADURA

ABSTRACT

Alzheimer's disease (AD) is the most prevalent neurological disorder associated with global population ageing. Amyloid β (A β) peptides are established hallmarks of AD. In the last years, the oligomeric forms of A β have drawn attention in this research field, as there is cumulative evidence showing that these oligomers are the most neurotoxic forms of A β . Dysregulation of intracellular cytosolic calcium (Ca^{2+}) homeostasis has been observed in AD, and it has been suggested that alterations in Ca^{2+} signaling could be an early event of AD pathogenesis. A previous work of our laboratory showed that calmodulin (CaM), which is highly expressed in neurons, has high affinity for neurotoxic A β peptides (dissociation constant (k_D) \approx 1 nM).

Novel molecular mechanisms in A β (1-42) neurotoxicity derived from the complexation of A β (1-42) by CaM are critically evaluated and discussed in this Ph.D. thesis, aiming to identify early biomarkers that trigger the initiation of the progression of A β (1-42) peptide brain neurotoxicity and neurodegeneration; and to develop novel strategies to afford protection against neurodegenerative processes related to overproduction of neurotoxic A β peptides in the brain. To reach this major objective, we have performed the following experimental works: (1) to study the impact of the A β (1-42) peptide internalized after a short time incubation on the dysregulation of Ca^{2+} homeostasis in cultured neurons; (2) to identify the main Ca^{2+} transport systems that are responsible for controlling the resting cytosolic Ca^{2+} concentration ($[\text{Ca}^{2+}]_i$) in these neurons in culture, and study their modulation by the A β (1-42) peptide; and (3) to find a protective agent that efficiently prevents neurotoxic A β peptides overproduction in the brain of an animal model developing a neurodegenerative pathology.

With cerebellar granule neurons (CGN) we have demonstrated the formation of complexes between internalized A β (1:42) and CaM, and extensive co-localization of CaM and A β (1-42) in plasma membrane neuronal lipid rafts submicrodomains. In addition, short time incubation (2 h) with A β (1-42) elicited an early decrease of the resting $[\text{Ca}^{2+}]_i$ of mature CGN, due to the inhibition of L-type calcium channels (LTCC), the main Ca^{2+} transport system responsible for the control of resting $[\text{Ca}^{2+}]_i$ in mature CGN in a partially depolarizing medium.

After identification of the main Ca^{2+} transport systems responsible for the control of resting $[\text{Ca}^{2+}]_i$ in HT-22 cells, we found that short time treatment with A β (1-42) produces an early decrease in the influx of Ca^{2+} through the inhibition of purinergic receptor, subtype 7 (P2X7R). In addition, we observed that internalized A β (1-42) is focalized near the perinuclear region of HT-22 soma up to 5 h incubation, and that induced a decrease in the store-operated Ca^{2+} entry

(SOCE) mechanism, through the modulation of the endoplasmic reticulum (ER) proteins STIM1 (stromal interaction molecule 1) and ligand-gated Ca^{2+} channels ryanodine receptors (RyR) and the inositol 1,4,5-trisphosphate receptor (IP3R).

Finally, intraperitoneal (i.p.) co-administration to Wistar rats of a kaempferol dose that prevented severe neurological impairment induced by acute treatment with 3-nitropropionic acid (NPA), also efficiently inhibited the generation of neurotoxic A β peptides in the *striatum* and *hippocampus*, and completely inhibited the overexpression of brain pro-inflammatory markers (C3 α -fragment of complement protein component C3, cytokines and complement protein component 1q (C1q) that induce the generation of reactive A1 astrocytes and nuclear factor kappa B (NF-kB)).

RESUMEN

La enfermedad de Alzheimer (AD) es la disfunción neurológica más prevalente asociada al envejecimiento de la población humana. Los péptidos amiloides ($A\beta$) son biomarcadores ampliamente aceptados de la AD. Durante los últimos años, los estados oligoméricos de $A\beta$ han focalizado la atención en este campo de investigación, porque se han acumulado numerosas evidencias mostrando que estos oligómeros son las formas más neurotóxicas de $A\beta$. La desregulación de la homeostasis del calcio (Ca^{2+}) citosólico intracelular ha sido reportada en AD, y se ha sugerido que alteraciones de la señalización de Ca^{2+} podría ser un evento temprano en la patogénesis de AD. Un trabajo previo de nuestro laboratorio demostró que la calmodulina (CaM), que se expresa a concentraciones elevadas en neuronas, tiene una elevada afinidad por péptidos $A\beta$ neurotóxicos (constante de disociación ≈ 1 nM).

Nuevos mecanismos moleculares en la neurotoxicidad de $A\beta(1-42)$ derivados de la formación de complejos de $A\beta(1-42)$ con la CaM son críticamente evaluados y discutidos en esta tesis doctoral, con el objetivo de identificar los biomarcadores tempranos que disparan el inicio de la progresión de la neurotoxicidad y neurodegeneración cerebral, y también para desarrollar nuevas estrategias que protejan contra los procesos neurodegenerativos relacionados con la sobreproducción de péptidos $A\beta$ neurotóxicos en el cerebro. En aras a alcanzar este objetivo global, se han desarrollado los siguientes trabajos experimentales: (1) estudio del impacto del péptido $A\beta(1-42)$ internalizado después de un tiempo corto de incubación en la desregulación de la homeostasis del Ca^{2+} en cultivos de neuronas; (2) identificación de los principales sistemas de transporte de Ca^{2+} que son responsables del control de la concentración citosólica del Ca^{2+} ($[Ca^{2+}]_i$) en estos cultivos de neuronas; y (3) búsqueda de un agente protector que prevenga contra la sobreproducción de péptidos $A\beta$ neurotóxicos en el cerebro de un modelo animal de una patología neurodegenerativa.

En neuronas granulares del cerebelo (CGN) hemos demostrado la formación de complejos entre $A\beta(1:42)$ internalizado y CaM, así como la extensiva co-localización de CaM y $A\beta(1:42)$ en los submicrodominios de tipo 'raft' lipídicos de la membrana plasmática neuronal. Además, la incubación con $A\beta(1-42)$ de corta duración (2 h) produjo una disminución temprana de la $[Ca^{2+}]_i$, debido a la inhibición de los canales de calcio de tipo L (LTCC), que son el principal sistema de transporte de Ca^{2+} responsable del control de la $[Ca^{2+}]_i$ en ausencia de estímulo de las CGN en un medio parcialmente despolarizante.

Tras la identificación de los principales sistemas de transporte de Ca^{2+} responsables del control de la $[Ca^{2+}]_i$ en las células HT-22, hemos encontrado que el tratamiento de corta duración

con A β (1-42) produce una disminución temprana del influxo de Ca $^{2+}$ a través del subtipo 7 del receptor purinérgico (P2X7R). Además, hemos observado que el A β (1-42) internalizado está focalizado cerca de la región perinuclear del soma de las células HT-22, hasta 5 h de incubación con A β (1-42), y que produce una atenuación del mecanismo de entrada de Ca $^{2+}$ operado por el vaciado de depósitos intracelulares (SOCE), a través de la modulación de las proteínas del retículo endoplasmático STIM1 (*stromal interaction molecule 1*) y de los canales de calcio operados por ligando: receptores de rianodina (RyR) y receptores de inositol 1,4,5-trifosfato (IP3R).

Finalmente, la co-administración intraperitoneal (i.p.) de dosis de kaempferol que previenen las disfunciones neurológicas severas inducidas por el tratamiento agudo con el ácido 3-nitropropiónico (NPA), también inhiben eficientemente la generación de péptidos A β neurotóxicos en el estriado y en hipocampo y completamente inhiben la sobreexpresión en el cerebro de los biomarcadores proinflamatorios (fragmento C3 α de la proteína del complemento C3, citoquinas y proteína del complemento C1q implicadas en la inducción de astrocitos reactivos de tipo A1 y factor nuclear kappa B (NF- κ B)).

OBJECTIVES

The main objective of this Ph.D. thesis is to identify early biomarkers that trigger the initiation of the progression of A β (1-42) peptide brain neurotoxicity and neurodegeneration; and develop novel strategies to afford protection against neurodegenerative processes developing with overproduction of neurotoxic A β peptides in the brain.

To successfully achieve this major objective, the following concrete aims should be accomplished:

- (1) To study the impact of the A β (1-42) peptide internalized after a short time incubation on the dysregulation of Ca²⁺ homeostasis in cultured neurons;
- (2) To identify the main Ca²⁺ transport systems that are responsible for the control of the resting cytosolic Ca²⁺ in these neurons in culture, and study their modulation by the A β (1-42) peptide.
- (3) To find a protection agent that efficiently prevents neurotoxic A β peptides overproduction in the brain of an animal model developing neurodegenerative pathologies.

INTRODUCTORY OVERVIEW OF THE THESIS

This section introduces to the reader the main structure of this Ph.D. thesis as well as it gives an approach of the main context of each Chapter and explain the integrative work presented in this work.

The core of this Ph.D. thesis is composed by four chapters (**Chapter 1-4**). The work is presented as a compendium of published articles, with the exception of **Chapter 3**, for which the manuscript is being prepared for publication at the time of the delivery of the thesis. **Chapter 1** is an extract of a Review article, which includes an abstract that recapitulates the main key points that are discussed in the state of the art of the review and a conclusions section that outline the most relevant information needed for a better contextualization of the experimental work of this Ph.D. thesis. Then, each chapter (**Chapter 2-4**) includes an abstract with a defined hypothesis of the study and a brief summary of the main experimental findings, an introduction section that reviews the state of the art of the main relevant aspects of the study, the material and methods section of the experimental work, a results section, and finally a discussion section where the results are analyzed and integrated in the context of the existing literature, followed by a final conclusion regarding the significance of the study and the potential impact of the research in the field.

The work presented on this thesis focused on two major goals. The first goal is the identification of early molecular mechanisms and primary major targets that are associated with the initiation of neuropathologies, as there is an urgent need for the discover of reliable biomarkers for the early diagnosis of neurodegenerative diseases like AD and Huntington's disease (HD). The second main goal is to identify and develop novel approaches and strategies to afford protection against the neurodegenerative processes addressed in this work. To successfully accomplish these main proposed objectives, we selected different reliable experimental cell models and an animal model, which are used in the work included in the experimental chapters (**Chapters 2-4**).

Chapter 1 is an introductory section that contains fundamental information for understanding the subsequent chapters enclosed in this thesis. The main subjects addressed in the first Chapter allowed to establish a bridge between chapters, where A β peptide is the main integrative factor of the presented work. In this Chapter is discussed the relevance of A β complexation with a major neuronal protein - CaM - and the main features and consequences of the formation of this complex in brain degeneration in AD. It is widely known that AD is a progressive neurodegenerative disease and the most common cause of dementia in the world,

characterized by memory loss, behavioral dysfunction, and rapid cognitive decline. Despite the intensive years of research and the development of different hypothesis, unfortunately the etiology of the pathophysiology of AD is not yet fully understood. The *postmortem* pathological hallmarks of AD are well known and include the progressive accumulation of deposits of different fragments of the A β peptide and deposition of hyperphosphorylated protein tau, forming neurofibrillary tangles (NFT) inside neurons, leading to damage and death of neurons. However, in the last years, A β oligomers are being recognized as the most neurotoxic form of A β and its production can derive within the neuron or from adjacent neurons or reactive glial cells, as inflammation processes are now recognized to foster AD brain degeneration. Moreover, due to the cumulative experimental studies in the last decade, it has become more evident that dysregulation of Ca²⁺ homeostasis in neurons can play a major role for the initiation of AD pathogenesis. Nevertheless, the lack of the identification of the primary A β -target proteins linked to the functional impairment initiating cytosolic Ca²⁺ homeostasis is an urgent issue that needs to be addressed.

CaM is an essential protein, highly expressed in the brain, that display important neuronal functions linked to metabolism, excitability, and intercellular and intracellular signaling. As demonstrated in a previous work of the laboratory, in neurons, CaM has high affinity for neurotoxic A β peptides ($kD \approx 1$ nM). This finding highlights a novel function of CaM, i.e., the buffering of free A β concentrations in the low nanomolar range; and consequently, the protection afforded against the rise of free concentrations of neurotoxic A β peptides. Noteworthy, it has been found that CaM expression levels is significantly decreased in AD brains. In addition, A β -CaM complexation may play a major role in neuronal Ca²⁺ signaling mediated by calmodulin-binding proteins (CaMBP) by A β , either in sensitivity or activity modulation, and so far, this point has been overlooked. Therefore, in Chapter 1, the following issues are addressed and discussed: i) the main features of A β -CaM complexation in the formation of neurotoxic A β oligomers; ii) the alterations of intracellular cytosolic Ca²⁺ concentration induced by A β and iii) the dysfunction of Ca²⁺-dependent neuronal excitability and activity caused by A β . We concluded that it is of most importance to identify the primary target proteins of non-endogenous intraneuronal A β , that are responsible for the initiation of the dysregulation of cytosolic Ca²⁺ homeostasis, through the following approaches: (1) to assess the total intracellular A β concentration in experiments with cell cultures reporting Ca²⁺ dysregulation; (2) to determine the dissociation constant of the direct interaction between A β and A β -CaM complexes with major target proteins; (3) to measure the oxidative modifications of Ca²⁺ channels and pumps in cell cultures; because it is widely accepted that A β stimulates intracellular reactive oxygen

species (ROS) production and the Ca^{2+} transport systems that are more important for the control of cytosolic Ca^{2+} homeostasis are extremely sensitive to cellular oxidative stress.

In the **Chapter 2** we used primary cultures of mature CGN as a neuronal model, derived from 7-days old Wistar rats, to study the binding of $\text{A}\beta(1-42)$ -CaM complexes to plasma membrane lipid rafts and to evaluate the changes in resting cytosolic Ca^{2+} homeostasis induced by $\text{A}\beta$. In this work we used the $\text{A}\beta(1-42)$, which is the prevalent form of the $\text{A}\beta$ peptide found in AD brains. In addition, the analysis of the $\text{A}\beta(1-42)$ stock solutions used in this work, revealed that $\text{A}\beta$ peptide is in the neurotoxic oligomeric state.

Neuronal lipid rafts are crucial microdomains of the plasma membrane that play a key role in $\text{A}\beta$ oligomerization and cellular uptake, leading to neuronal damage and neurotoxicity. In addition, CGN lipid rafts are composed by high Ca^{2+} sub microcompartments that are composed by the main transport Ca^{2+} systems, that binds to CaM, namely LTCCs and plasma membrane calcium pumps (PMCA). Therefore, CGN lipid rafts play an important role in the modulation of the excitability of CGN. In particular, LTCCs Ca^{2+} activity is fundamental for long-term potentiation/depression (LTP/LTD) in neurons, by playing a major role in neuronal function, memory and cognition. However, the hypothesis that $\text{A}\beta(1-42)$ can disrupt LTCC activity remained to be experimentally evaluated and overlooked until now. Therefore, the **Chapter 2** is focused on the following main goals: i) to demonstrate the complexation between $\text{A}\beta$ -CaM in CGN by using submicromolar concentrations of $\text{A}\beta(1-42)$ through co-immunoprecipitation techniques and Fluorescence Resonance Energy Transfer (FRET) imaging; ii) to evaluate the co-localization of $\text{A}\beta(1-42)$ and $\text{A}\beta(1-42)$ -CaM complexes in CGN neuronal lipid rafts using well-established protein markers of these microdomains, through fluorescence microscopy imaging; and iii) to evaluate the alteration in LTCC activity regarding the resting Ca^{2+} concentration induced by $\text{A}\beta(1-42)$ after a short period of incubation, using a specific Ca^{2+} -fluorometric probe. The results of this work showed the formation of $\text{A}\beta$ -CaM complexation in mature CGN and the high co-localization of $\text{A}\beta$ with neuronal lipid rafts. In addition, our results highlight that after a very short time of incubation (up to 2 h), $\text{A}\beta(1-42)$ is already internalized in mature CGN and disturbing the LTCC activity by decreasing the influx of Ca^{2+} . This finding suggests that the cytosolic Ca^{2+} dysregulation observed in CGN is an early event that precedes the neurotoxic cascade of events associated with cell dysfunction induced by $\text{A}\beta(1-42)$. Of note, the extracellular addition of purified CaM to fixed and permeabilized CGN cells stained with a fluorescent compound of $\text{A}\beta(1-42)$, demonstrates that CaM largely reverses the $\text{A}\beta(1-42)$ fluorescence intensity of CGN. This outcome corroborates with it was described in the **Chapter 1**: CaM display an important role in neurons through the formation of complexes with $\text{A}\beta$ peptides and eventually protects against the rise of free concentrations of neurotoxic $\text{A}\beta$.

peptides until the saturation point, avoiding neuronal impairment in an early stage of AD initiation. Ultimately, it is important to mention that the elevated concentration of CaM found in neurons and the numerous functions that this major protein display in neuronal excitability and metabolism for brain development, are major features that make extremely difficult the use of silencing-RNA of CaM in cultured neurons, as well as the use of CaM knock-out animal models, restricting in-depth studies of the alteration of the molecular mechanism induced by A β . Consequently, it could be applied other strategies to afford neuroprotection against A β (1-42)-induced neurodegeneration through the development of novel specific peptides or other compounds that could be able to antagonize A β -CaM complexation.

The work described in **Chapter 3** was developed in the immortalized mouse hippocampal cell line, HT-22, which is a cell culture model widely used to study excitotoxicity induced by glutamate, as it is already demonstrated that this cell line lacks ionotropic glutamate receptors (iGluRs) like NMDAR (N-methyl-D-aspartate receptor). In addition, there is no consensus about the activity of muscarinic acetylcholine receptor (AChR) in HT-22 cells, suggesting that this cell line has poor AChR activity or is practically nonexistent. Besides the importance and contribution of LTCC as Ca²⁺ influx system in neurons, it is highly recognized that purinergic receptors (P2R) display an important role in Ca²⁺ regulation in excitable cells. P2R are activated by ATP and have key functions in controlling metabolic activities, proliferation, and differentiation in neurons. In addition, the elevation of cytosolic Ca²⁺ concentration in neurons can also derive from the release of Ca²⁺ from the intracellular stores, such as the endoplasmic reticulum (ER), which is mediated by SOCE mechanism.

The main goals of the Chapter 3 are: i) to measure the amount of internalized A β (1-42) after a short period of incubation (up to 5 h) with submicromolar concentration of A β oligomers added to the extracellular medium; ii) to identify the main subcellular distribution of A β (1-42) inside HT-22 cells by fluorescence microscopy imaging; iii) to identify the main Ca²⁺ cell systems that are responsible for cytosolic Ca²⁺ regulation homeostasis in HT-22 cells and evaluate the effect of A β (1-42) in those systems through the measurement of the alteration of resting cytosolic Ca²⁺ concentration, and iv) to measure the levels of oxidative stress induced by A β (1-42) in the immortalized cell model HT-22 after a short period of incubation using different methodologies .

The results obtained in the **Chapter 3** highlight that LTCCs are present but inactive in the HT-22 cell model as we demonstrated by the lack of activity induced by KCl depolarization and by the poor activity measured after the addition of a LTCC agonist. Also, we found that, the addition of ATP to the extracellular medium of HT-22 cells elicits a significant increase in Ca²⁺ influx mediated by P2R. Taking into consideration that HT-22 lacks NMDAR, and both LTCC and

AChR activity are practically nonexistent, we concluded that P2R are the main Ca^{2+} transport systems responsible for the influx of Ca^{2+} in HT-22. We also found that, after only 2 h incubation with submicromolar concentration of A β (1-42), the Ca^{2+} influx is significantly decreased by P2R activity inhibition, mainly through the inhibition of the P2X7R subtype (a member of the P2R family). To the best of our knowledge this is the first study to show that P2R is the main plasma membrane system responsible for the influx of extracellular Ca^{2+} , in HT-22 cells and that A β (1-42) significantly alters the activity of this receptors in HT-22 cell line. In addition, it is important to mention, that the lack of or the poor activity of these Ca^{2+} channels and receptors (NMDAR, AChR and LTCC) in the plasma membrane of HT-22 cells, opens the possibility of using HT-22 as a good model system to study molecular mechanisms associated with modulation of P2R activity.

Through fluorescence microscopy imaging we measured the internalized A β (1-42) and observed that A β (1-42) presented a subcellular distribution mainly near the perinuclear region, up to 5 h incubation, showing moderate co-localization with the ER and the mitochondria, without affecting significantly the mitochondrial membrane potential. Moreover, internalized A β (1-42) induced a decrease in the biphasic SOCE mechanism after 2 h incubation, through the modulation of STIM1, and by stimulation of the activity of both ligand-gated calcium channels RyR and the IP3R, without significantly affecting the steady-state cytosolic Ca^{2+} concentration up to 5 h incubation with A β (1-42) added to the extracellular medium. Finally, there is only a small increase in ROS generation after 2 h and 5 h incubation, making unlikely that the alterations observed with A β (1-42) are caused by oxidative stress. Altogether, the results presented in **Chapter 3**, revealed that both P2R and the molecular components of SOCE: STIM1, IP3R and RyR are main targets of internalized A β (1-42) in the HT-22 cell model, after only 2 h incubation, suggesting that these systems could be considered as main primary targets of A β (1-42) for Ca^{2+} dysregulation in an early stage of the AD progression. These findings create new possibilities for the development of novel strategies to investigate potential therapeutic agents to target P2R and SOCE mechanism in an early stage of Ca^{2+} disruption homeostasis induced by A β .

Because of A β (1-42) binds with high affinity to CaM and other intracellular proteins which are of utmost importance for neuronal survival and activity, neuroprotection strategies preventing the rise of A β (1-42) in the brain are likely the best way to avoid A β (1-42)-induced neurotoxicity and to slowdown brain neurodegeneration in AD and other related neurodegenerative diseases. In the **Chapter 4**, we used an animal model that mimics the motor neurological dysfunctions of the HD aiming to identify biomarkers linked to an early stage of the progression of HD and test for neuroprotection. 3-Nitropropionic acid (NPA) is a neurotoxin that

when administrated to rodents, mimics HD motor neurological dysfunctions. Studies have demonstrated that NPA treatment induces brain degeneration and mediates inflammatory events. In addition, mitochondrial dysfunction and generation of ROS lead to activation of innumerable cell death pathways, which are directly implicated in NPA neurotoxicity and also in HD. Most recently, it was demonstrated that activated microglia induces the production of a specific type of reactive neurotoxic astrocytes, called A1, via the secretion of specific pro-inflammatory cytokines like interleukin-1 alpha (IL-1 α) and tumor necrosis factor alpha (TNF- α) and also through the secretion of C1q. Likewise, it was also found an increase in A1 astrocytes in *post-mortem* tissues of HD patients. Furthermore, it has been published that C3 is a highly upregulated gene in A1 astrocytes, proposing that the increased expression of C3 could be used as marker of the induction of reactive neurotoxic A1 astrocytes in neurodegenerative disorders. Interestingly, it was proven that reactive astrocytes can generate neurotoxic A β peptides and this possibility deserved to be studied in NPA-induced brain neurodegeneration because it has been recently shown that this neurodegenerative process is also a tauopathy. Remarkably, it has been seen an increase in tau phosphorylation in a mouse model of HD and the excess of α -synuclein expression, which is a hall mark of Parkinson disease's (PD), is associated with increased mutant huntingtin aggregation, a protein that is overexpressed in HD. These findings suggest that HD share similar molecular pathways with PD and Tau pathology.

In a previous works of our laboratory, it is shown that intraperitoneal (i.p.) co-administration of kaempferol efficiently protects against NPA-induced brain damage in adult Wistar rats. Moreover, kaempferol, which has antioxidant and anti-inflammatory properties, have been shown to be effective to treat numerous diseases in animal models. In addition, the low toxicity of this natural compound in humans suggests that kaempferol could be seen as potential candidate against brain damage induce by insults and/or neurodegenerative diseases.

Based on all arguments previously presented, we defined two major objectives for this final **Chapter:** 1) to setup an experimental protocol using adult male Wistar rats with progressive brain degeneration through administration of NPA by i.p injections, and to identify early biomarkers of the disease; 2) to test the hypothesis that i.p administration of kaempferol protects against NPA-acute treatment in the brain regions that become dysfunctional. The results demonstrated that NPA treatment induced the production of reactive A1 astrocytes through the increase of C3 fragment expression in *striatum*, *hippocampus* and *cerebellum*, without observation of neurodegeneration in rat brain, suggesting that C3 complement could be used as early biomarker of NPA-induced treatment. Besides, we also demonstrated by Western blots an increase in the levels of pro-inflammatory cytokines TNF α and IL-1 α .

After acute administration of NPA to induce severe neurodegenerative damage and dysfunction in Wistar rats, we evaluated the protective effect of kaempferol in the most affected rat brain areas reported: *striatum* and *hippocampus*. We saw a significant decrease of C3 complement expression by Western blot in the rat group treated with kaempferol and NPA, showing very similar results with the control-group. Moreover, kaempferol prevented the NPA-induced increase of cytokines expression levels and NF- κ B expression in the *striatum* and *hippocampus*. Notably, acute NPA-induced brain degeneration increased the expression of A β and kaempferol clearly reverted A β overproduction in our experimental model, as demonstrated by Western blot. As far as we know this is a novel finding in NPA-induced brain neurodegeneration and it has a special relevance, because exposure to NPA has been recently shown to induce taupathology in tangle-mouse model and also in wild type-mice. Therefore, this neurodegenerative process shares these molecular biomarkers with AD, in which reactive A1 astrocytes have been reported to be generated as well. Thus, this work highlights novel biological roles of this antioxidant flavonoid. The inhibition by kaempferol of C3 proteolytic activation in the brain suggests a potential novel therapeutic use of this flavonoid, because induction of neurotoxic reactive A1 astrocytes has been found in *post-mortem* samples of several neurodegenerative diseases.

CHAPTER 1

The relevance of A β -CaM complexation in
neurons and brain degeneration in AD

Index

1. Abstract.....	31
2. Intracellular A β oligomers in neuronal cytotoxicity and CaM as a major high affinity A β -binding protein in neurons.	31
3. The roles of CaM in neurons as cytosolic Ca $^{2+}$ buffering and Ca $^{2+}$ signaling molecule: subcellular distribution of CaM-Binding Proteins (CaMBPs) in neurons ...	32
4. Modulation by A β of CaMBPs, which play major roles in A β production in neuronal Ca $^{2+}$ homeostasis and LTP.	35
4.1 The relevance of A β -CaM complexation for the regulation of neurotoxic A β peptides production.	35
4.2 The relevance of A β -CaM complexation for the alteration of intracellular Ca $^{2+}$ homeostasis induced by A β	36
4.3 The relevance of A β -CaM complexation for dysregulation of Ca $^{2+}$ -dependent neuronal activity and excitability induced by A β	38
5. Conclusions.....	40
6. References	41

1. Abstract

Intraneuronal A β oligomer accumulation precedes the appearance of A β plaques or NFT and is neurotoxic. In AD-affected brains, intraneuronal A β oligomers can derive from A β peptide production within the neuron and, also, from vicinal neurons or reactive glial cells. Ca $^{2+}$ homeostasis dysregulation and neuronal excitability alterations are widely accepted to play a key role in A β neurotoxicity in AD. However, the identification of primary A β -target proteins, in which functional impairment initiating cytosolic Ca $^{2+}$ homeostasis dysregulation and the critical point of no return are still pending issues. The micromolar concentration of CaM in neurons and its high affinity for neurotoxic A β peptides ($kD \approx 1$ nM) highlight a novel function of CaM, i.e., the buffering of free A β concentrations in the low nanomolar range. In turn, the concentration of A β -CaM complexes within neurons will increase as a function of time after the induction of A β production, and free A β will rise sharply when accumulated A β exceeds all available CaM. Thus, A β -CaM complexation could also play a major role in neuronal Ca $^{2+}$ signaling mediated by CaM-binding proteins by A β ; a point that has been overlooked until now. In this chapter, we address the implications of A β -CaM complexation in the formation of neurotoxic A β oligomers, in the alteration of intracellular Ca $^{2+}$ homeostasis induced by A β , and of dysregulation of the Ca $^{2+}$ -dependent neuronal activity and excitability induced by A β .

2. Intracellular A β oligomers in neuronal cytotoxicity and CaM as a major high affinity A β -binding protein in neurons

Intraneuronal A β accumulation has been shown to mediate neuronal cytotoxicity, and it has been suggested to be an early pathological biomarker for the onset of AD¹. This is also supported by the finding that intraneuronal A β accumulation precedes the appearance of A β plaques or tangles in transgenic mice^{2–5}, and that it also correlates with alteration of long-term potentiation (LTP), synaptic dysfunction and memory impairment in a triple transgenic model of AD^{3,6}. The prevalent A β peptide found in the A β plaques of AD patients is A β (1–42)⁷. It has been shown that microinjection of A β (1–42) or cDNA encoding A β (1–42) is neurotoxic to human neurons in culture⁸. Furthermore, oligomeric species of A β (1–42) are tightly linked to AD pathogenesis and are likely to be the cause of neuronal damage^{9–11}. In addition, neuronal uptake and accumulation of A β (1–42) aggregates correlated with metabolic inhibition¹², while extracellular A β , applied to hippocampal slices, seems to preferentially target synapses, leading

to a decrease in the synaptic marker synaptophysin¹³, as well as endocytosis of N-methyl-D-aspartate receptors (NMDAR)¹⁴ and low-density lipoprotein receptor-related protein-1^{15,16}. In addition, the binding of extracellular A β to other proteins, such as the α 7 nicotinic cholinergic receptor, ApoE and ApoE receptors, integrins and the receptor for advanced glycation end products, has been shown to be implicated in A β uptake by neurons and was reviewed in¹⁷.

CaM is a Ca²⁺ buffering protein which is expressed in neurons at much higher concentrations than in non-excitable cells, reaching micromolar concentrations in neurons¹⁸. The levels of CaM expressed in the brain are within 4 and 15 μ g/mg wet tissue, with highest content in cortical regions, *striatum*, *hippocampus*, amygdala and *substantia nigra*¹⁹. We showed that Ca²⁺-saturated CaM binds with high affinity to A β (1–42) and A β (25–35) peptides, as demonstrated by a dissociation constant of the A β :(Ca²⁺)₄-CaM complex close to 1 nM²⁰. As a result, CaM could have a high capacity to buffer intracellular free A β concentrations. Other proteins known to bind A β peptides with dissociation constants close to 1 nM, i.e., with an affinity similar to that of CaM, are cellular prion protein²¹ and glycogen synthase kinase 3 α ²². However, the expression level of these proteins in neurons is several orders of magnitude lower than that of CaM. Therefore, in neurons, CaM seems to be a major sink for neurotoxic intracellular A β peptides, and this, in turn, suggests that CaM could play a key role in protecting against an increase of free intracellular A β concentrations above 1–2 nM. Based on this, it can be expected that down-regulation of the expression of CaM should make neurons more prone to A β -induced neurotoxicity, because they will suffer a stronger rise in the free intracellular concentration of A β peptides upon β -secretase activation or extracellular A β uptake. Of note, it has been reported a decrease in the CaM expression levels in brains affected by AD²³.

However, CaM is not only a major protein in cytosolic Ca²⁺ buffering in neurons; it also has a major role in neuronal metabolism, excitability, and intercellular and intracellular signaling. Thus, A β (1–42)-CaM complexes can also function as intracellular transducers for focalized actions of A β peptides, and will be analyzed in the following sections of this chapter.

3. The roles of CaM in neurons as cytosolic Ca²⁺ buffering and Ca²⁺ signaling molecule: subcellular distribution of CaM-Binding Proteins (CaMBPs) in neurons

Khachaturian²⁴ proposed the “calcium hypothesis of brain aging and AD”, which defended the idea that sustained changes in Ca²⁺ homeostasis could be a common pathway for aging and the neuropathological changes associated with AD. Later, Ca²⁺ dyshomeostasis in AD received further experimental support. For example, Kuchibhotla and colleagues²⁵ reported that the resting Ca²⁺ concentrations in the spines and dendrites of pyramidal neurons in the

neocortex are higher than normal in neurons located close to A β deposits. Similarly, the resting level of Ca $^{2+}$ in cortical neurons of 3xTg-AD animals was 247 nmol/L, which was twice that found in non-Tg controls (110 nmol/L)²⁶. These measurements were consistent with many other studies that indicate that Ca $^{2+}$ signaling is up-regulated in AD²⁷.

Steady resting cytosolic Ca $^{2+}$ ranges between 70 and 150 nM in different types of neurons in culture, and peaks below 1 μ M upon transient plasma membrane depolarization by action potentials or upon stimulation by excitatory neurotransmitters^{28–32}. In addition, there are large time-dependent and space-dependent fluctuations in Ca $^{2+}$ concentrations within different cytosolic regions, soma and axo-dendritic extensions upon neuronal stimulation. Since the dissociation constant of Ca $^{2+}$ from CaM is relatively high, i.e., between 0.2 and 0.5 μ M^{20,24}, the potency of CaM as a Ca $^{2+}$ buffer in different cytosolic compartments in neurons is, not only dependent on the local concentration of CaM, but also on the local concentration of free Ca $^{2+}$. In addition, fluctuations of cytosolic Ca $^{2+}$ in neurons strongly shift the equilibrium between the Ca $^{2+}$ -saturated open conformation of Ca $^{2+}$ -CaM (Ca $^{2+}$)₄-CaM, and the close conformation of apo-CaM (minus Ca $^{2+}$)³³. Although the interaction of A β (1–42) with CaM did not significantly alter Ca $^{2+}$ binding to CaM, the affinity of A β (1–42) for apoCaM was found to be approximately 20-fold lower²⁰.

The CaM conformation changes from a closed to open configuration upon Ca $^{2+}$ -binding and allows Ca $^{2+}$ /CaM to bind target proteins with high affinity ($kD = 10^{-7}$ to 10^{-11} M)^{34,35}. The majority of CaMBPs bind Ca $^{2+}$ -CaM, while a small number of proteins, such as neuromodulin and neurogranin, only bind to apo-CaM³⁶. CaMBPs play a major role in neuronal function and excitability, and many of them present significant compartmentation within subcellular neuronal structures. In this chapter, we will focus on CaMBPs expressed in specific brain areas (*hippocampus* and cerebral entorhinal, and temporal and frontal cortex), which are prone to degeneration in AD and of which functional impairment has been suggested to underlie the loss of neuronal functions and/or intracellular Ca $^{2+}$ dysregulation in this disease.

Tau and A β peptides are components of neuropathological hallmarks of AD, and tau, A β precursor protein (APP), and β -site APP-cleaving enzyme 1 (BACE1) are CaMBPs^{37,38}. In addition, CaM binds and modulates the activity of several protein kinases involved in tau hyperphosphorylation, such as CaMKII, cyclin-dependent kinase 5 and glycogen synthase kinase 3 α ^{22,37}. Tau belongs to the family of microtubule-associated proteins that function in microtubule assembly and stability; tubulin itself and microtubule-associated protein 2 are also CaMBPs^{39,40}.

Calcineurin is a Ca $^{2+}$ and calmodulin-dependent protein phosphatase⁴¹, which is activated by nanomolar concentrations of Ca $^{2+}$ ⁴². Calcineurin regulates proteins that play key

roles in synaptic transmission and neuronal excitability⁴³. Depending on the strength, duration and site of Ca²⁺ stimulus, calcineurin may either increase or decrease synaptic efficacy and cell excitability through the modulation of ion channels, neurotransmitter receptors, cytoskeletal proteins, kinases, other phosphatases, and transcription factors⁴⁴.

Neuronal nitric oxide synthase (nNOS) and adenylyl cyclases 1 and 8 (AC1 and AC8) are other types of Ca²⁺/CaM-stimulated enzymes that generate second intracellular messengers of high relevance for learning and memory^{45–47}. Besides, ion channels, such as the small-conductance potassium (SK) channels, KCNQ potassium channels, cyclic nucleotide-gated channels, NMDAR, transient receptor potential channels, RyR, voltage-gated Ca²⁺ channels (VGCCs), and voltage-gated Na channels, are also modulated by CaM⁴⁸.

Ca²⁺ influx through VGCCs is crucial for vesicular release of neurotransmitters, intracellular signaling pathways, gene expression, and synaptic plasticity⁴⁹. Among them, LTCC plays an important role in neuronal plasticity, learning and memory, and an alteration in the function and/or regulation of these channels has been associated with neuropsychiatric diseases, migraine headaches, cerebellar ataxia, autism, schizophrenia, bipolar disorder, and depression^{50,51}. The isoforms of LTCC, Cav1.2 and Cav1.3, are more highly expressed in the brain, and they have received increased attention regarding their role in neurological and psychiatric diseases⁵⁰. Both Cav1.2 and Cav1.3 can be found in neuronal cell bodies and proximal dendrites in the *hippocampus* and have been involved in the regulation of many Ca²⁺-dependent functions, e.g., protein phosphorylation, enzyme activity, gene expression and neurotransmission⁵². Furthermore, Ca²⁺ influx through LTCC is limited by constitutively bound CaM, which leads to Ca²⁺-dependent inactivation⁵³ and prevents neuronal damage due to excessive Ca²⁺ entry⁵⁴. Briefly, the CaM conformational change upon Ca²⁺ binding promotes inactivation of LTCC by interaction with additional effector sites of the C-terminal domain in Cav1.2, and, in case of Cav1.3, also of the N-terminal domain⁵⁴. The strength of Ca²⁺-dependent inactivation can be adjusted by regulating the strength of CaM binding by displacement of CaM from its C-terminal interaction sites^{54,55}.

Other neuronal CaMBPs expressed in the *hippocampus*, such as myosin light chain kinase^{56,57}, spectrin⁵⁸, and fodrin⁵⁹, play major roles in the cytoskeleton structure and dynamics, and they also play key roles in neuronal activity and interneuronal connectivity. In addition, Ras-guanine nucleotide-releasing factor 1 (Ras-GRF1), which is also expressed in CA1 neurons of the *hippocampus*, has been shown to be involved in the induction of LTP and LTD associated with spatial learning and long-term memory^{60,61}. Finally, glycogen phosphorylase kinase, in addition to its role in the regulation of glycogenolysis in the brain⁶², can also phosphorylate the apo-CaM-

binding regulatory regions of neuromodulin (Nm) and neurogranin (Ng)⁶³, which are neuronal specific proteins that are known to play major roles in neuronal plasticity and LTP (see below).

However, at normal resting cytosolic Ca²⁺ concentrations close to 100 nM or lower in neurons, CaM is mainly in the apo-CaM conformation. Apo-CaM is largely associated with three proteins in neurons: Nm, Ng, and regulator of CaM signaling (RCS)¹⁸. Nm is an abundant presynaptic protein and accumulates in axonal growth cones and helps their navigation to appropriate target sites during the development of the nervous systems⁶⁴. Furthermore, it is involved in neurite extension and neuronal plasticity, neuroregeneration, regulation of neurotransmitter release at the presynaptic terminal, and in LTP⁶⁵. It has been demonstrated that Nm binds to apo-CaM at the presynaptic membrane and releases it locally under two different mechanisms: (1) when there is an increase in intracellular Ca²⁺ or (2) upon phosphorylation at Ser41 by protein kinase C (PKC), which blocks apo-CaM-binding to Nm^{65,66}.

RCS is a protein kinase A (PKA)-regulated phosphoprotein expressed in brain regions receiving dopaminergic innervation⁶⁷. RCS is enriched in *caudate-putamen*, *substantia nigra*, *nucleus accumbens* and olfactory tubercle, but also displays intermediate levels of expression in the cerebral cortex and *hippocampus*⁶⁴. The G protein-coupled receptor (GPCR)-dependent activation of PKA leads to phosphorylation of RCS at Ser55, and increases its binding to CaM⁶⁸, preventing CaM from binding to CaM-regulated phosphatase calcineurin¹⁸.

4. Modulation by A β of CaMBPs, which play major roles in A β production in neuronal Ca²⁺ homeostasis and LTP.

4.1 The relevance of A β -CaM complexation for the regulation of neurotoxic A β oligomers production

Clinically, AD is divided into sporadic AD (sAD) and familial AD (fAD). The fundamental role of A β in AD is derived from studies of fAD, which accounts for 1–5% of patients with AD⁶⁹, who have autosomal dominant mutations or duplications in the APP or mutations in the presenilin-1 (PSEN1) and presenilin-2 (PSEN2) genes^{70,71}. These mutations result from changes in APP proteolysis by the γ -secretase complex, leading to an increase in the formation of toxic A β (42/40) oligomers, which induce synapse loss and neuronal toxicity^{72,73}. As fAD is pathologically similar to sAD, with the difference being that fAD generally has an early onset and the symptoms progress more rapidly, it is believed that A β (1–42) over-production is also a main factor in sAD⁷³. PSEN mutations contributes to over 90% of fAD cases, and several studies have shown that intracellular Ca²⁺ dysregulation due to these mutations takes place before the

formation of A β plaques and NFT in AD brains, highlighting that modifications in cytoplasmic Ca $^{2+}$ may be an early event at the onset of AD^{74,75}. The increase of cytosolic Ca $^{2+}$, in turn, leads to a CaM-mediated stimulation of the amyloidogenic protease, BACE1³⁸. Moreover, Giliberto and colleagues⁷⁶ showed that the treatment of neuronal and neuroblastoma cells with 1 μ M soluble A β (1–42) increased BACE1 transcription and that this was reverted by an anti-A β (1–42) antibody. It has been suggested that this could be due to A β -induced oxidative stress, because this increase in BACE1 transcription was shown to be mediated by the activity of NF- κ B⁷⁷. Furthermore, an up-regulation of BACE1 expression in several vascular risk factors for AD development, including hypoxia, hyperglycemia and hypercholesterolemia, has been shown and was reviewed in⁷⁸. Therefore, free A β generates a positive feedback loop of A β production, and this is likely to play a major role in brain degeneration, both in fAD and sAD. On these grounds, lowering of free A β by complexation with CaM can be seen as a cellular defense response to slow down the formation of neurotoxic A β in neurons. In addition, the increase of A β (1–42)-CaM complexes elicited by the rise in A β production reduces the availability of free CaM for stimulation of BACE1 activity, providing feedback inhibition of amyloidogenic A β production. To the best of our knowledge, the possibility that A β (1–42)-CaM complexes may also inhibit BACE1 activity has not yet been experimentally assessed.

4.2 The relevance of A β -CaM complexation for the alteration of intracellular Ca $^{2+}$ homeostasis induced by A β

PSENs modulate intracellular Ca $^{2+}$ homeostasis through direct interaction with three components of the ER, namely, IP3R, RyR, and sarco(endo)plasmic reticulum Ca $^{2+}$ -ATPase (SERCA)⁷⁹. Mutations of the PSEN2 gene enhanced Ca $^{2+}$ release through IP3R⁸⁰ and mutations in PSENs can also modulate capacitative Ca $^{2+}$ entry, a refilling mechanism for depleted Ca $^{2+}$ stores^{74,81,82}. SOCE disruption is consistently observed in AD and is manifested as attenuated Ca $^{2+}$ entry in the primary neurons of AD mice with human mutant PSEN1 knocked in, or in skin fibroblasts from familial AD patients⁸³. In addition, it has been reported that STIM2 expression levels are down-regulated by fAD-linked PS1 mutations and, thus, insufficient signal is transferred to the plasma membrane to activate SOCE when ER Ca $^{2+}$ is depleted⁸⁴. In addition, PSEN also acts as an ER Ca $^{2+}$ leak channel and fAD mutations in PSEN1 disrupt this function^{85,86}, leading to overloaded ER Ca $^{2+}$ stores and increased ER Ca $^{2+}$ release in PSEN double knockout fibroblasts and in fibroblasts transfected with mutant PSEN1 and PSEN2 constructs⁷³. Additionally, in fAD, PSEN mutations increase RyR-mediated Ca $^{2+}$ release, either due to enhanced expression of channel proteins or sensitization of the channel activity through PSEN–

RyR protein interactions^{85,87}. In addition, apoE4, a genetic risk factor for AD, may also amplify ER Ca²⁺ release through RyR, thereby stimulating the formation of Aβ plaques and neurofibrillary tangles^{88,89}. *In vitro* experiments have shown that application of soluble AβO causes a large increase in RyR activity due to an approximately 10-fold increase in the channel open probability⁹⁰ and stimulates RyR-mediated Ca²⁺ release in hippocampal neurons in culture⁹¹. It must be noted that the increase of the open channel activity of RyR was measured with the application of micromolar concentrations of Aβ(1–42) to skeletal muscle fibers. Thus, it seems that Aβ oligomers may only further potentiate excessive ER Ca²⁺ release by direct interaction with RyR at concentrations that are not reached within the neurons at the early stage of AD brain degeneration. However, indirect modulation by Aβ-induced oxidative stress may underlie the Aβ-induced activation of RyR observed in hippocampal neurons in culture after 2–3 h of incubation with concentrations of Aβ(1–42) oligomers ≥ 500 nM⁹¹. Therefore, sequestration of Aβ oligomers by CaM could be expected to protect against the increase of ER Ca²⁺ release through RyR. In addition, it has been reported that mutation or deletion of PSEN alters the ER Ca²⁺ refilling process through the SERCA pump and may contribute to the pathogenesis of AD⁹². Indeed, it has been recently shown that increasing SERCA activity helps to maintain ER Ca²⁺ and improves memory and cognition in APP/PSEN1 mice, as SERCA activation can sequester more cytosolic Ca²⁺ and prevent the apoptosis induced by mitochondrial signaling⁹³.

While ER Ca²⁺ release stimulates Aβ peptide production (see above), the produced Aβ can inhibit the activity of plasma membrane Ca²⁺ extrusion systems: plasma membrane Ca²⁺ ATPase (PMCA) and sodium-calcium exchanger (NCX). According to Mata and colleagues, PMCA is the only Ca²⁺ pump in which Ca²⁺ dependence activity is altered in membranes of AD brains compared to control brains and, also, is the only pump in the brain which is directly inhibited by Aβ^{94,95}. In addition, the inhibitory effect of Aβ could be blocked by pretreating the purified protein with Ca²⁺/CaM, the main endogenous activator of PMCA⁹⁵. Additionally, Aβ can inhibit NCX activity, either by direct interaction with the hydrophobic surface of NCX and/or with the lipid bilayer of the plasma membrane⁹⁶. It has been shown that 1 μM Aβ(1–40) stimulates NCX activity three-fold in the reverse mode in human astrocyte-derived glioblastoma cells with a time delay of 400–500 seconds after application of this peptide⁹⁷. The short time for NCX activity modulation by Aβ(1–40) suggests that this may be due to the direct interaction between this peptide and NCX; however, a titration with submicromolar concentrations of Aβ(1–40) was not reported by these authors and data are not available to obtain a dissociation constant of this peptide from NCX.

Since Aβ can inhibit the major Ca²⁺ extrusion systems of the neuronal plasma membrane, it can be foreseen that an increased ER Ca²⁺ release, induced by mutations in PSEN proteins,

should eventually lead to mitochondrial Ca^{2+} overload and apoptotic pathways. Indeed, this is an effect of exogenous A β peptides that has been experimentally demonstrated^{98,99}. Cumulative lines of evidence have demonstrated that mitochondrial Ca^{2+} signaling is altered in AD due to mutations in the PSEN proteins^{100,101}. The excess in cytosolic Ca^{2+} caused by enhanced ER Ca^{2+} release caused by mutant PSENs is, at least in part, counterbalanced by the Ca^{2+} uptake through the voltage-dependent anion-selective channel protein and the Ca^{2+} uniporter of the mitochondria. A sustained increase in mitochondrial Ca^{2+} concentration impairs ATP production, increases ROS production, and the opening of the mitochondrial permeability transition pore¹⁰². Several studies have proposed that enhanced neuronal apoptosis and increased ROS production are major factors in the neurodegeneration observed in AD, and the accumulation of mitochondrial Ca^{2+} has been shown to be significantly implicated in these neurotoxic pathways^{101,102}.

4.3 The relevance of A β -CaM complexation for dysregulation of Ca^{2+} -dependent neuronal activity and excitability induced by A β

The direct modulation of CaMKII by A β has a strong impact on neuronal activity and excitability. It has been shown that treating hippocampal neurons with A β oligomers impairs α CaMKII activation^{103,104} and that A β prevents the activation of CaMKII during hippocampal LTP¹⁰⁵. The inhibition of CaMKII by A β may be primarily a neuronal defense mechanism because APP can be phosphorylated *in vitro* by several kinases, including CaMKII¹⁰⁶, and CaMKII is also a tau kinase, which has been suggested to act in priming tau phosphorylation by cyclin-dependent kinase 5 and glycogen synthase kinase (GSK) β ^{107,108}. It should be observed here that A β (1–42) has been reported to bind to GSK3 α and GSK3 β with high affinity²². Indeed, the reported dissociation constants of A β (1–42) from the GSK3 α isoenzyme²² and from CaM²⁰ are almost identical, \approx 1 nM. Furthermore, Dunning et al. demonstrated that binding of A β (1–42) to GSK3 α stimulates hyperphosphorylation of tau²². In addition, GSK3 α has been proposed to enhance A β production through γ -secretase stimulation¹⁰⁹. Therefore, the inhibition of CaMKII by A β may counteract, at least in part, the stimulation of GSK3-dependent tau phosphorylation by nanomolar A β concentrations. Moreover, it has been proposed that, outside of synapses, α CaMKII is hyperactive and could contribute to NFT formation since it co-localizes with NFT in the AD brain¹⁰⁴. To the best of our knowledge, the possibility that CaMKII could also bind A β -CaM complexes has not been experimentally assessed, nor has the putative role of these complexes in A β -induced CaMKII inhibition.

In vivo, the activation of CaMKII is under the negative control of calcineurin-dependent phosphatase activity^{110,111} and is essential for LTP generation^{112,113}. Calcineurin-dependent subcellular relocation of autophosphorylated αCaMKII also occurs in Aβ oligomer-treated primary neuronal cultures^{114,115}. A shift of p(T286)-αCaMKII from apical dendrites/spines to the soma of CA3 pyramidal neurons, which is blocked by inhibition of the phosphatase calcineurin, is also found in a mouse model of sAD, in which Aβ oligomers are injected into the ventricles¹¹⁵. *Post-mortem* analyses and studies with AD models indicate that T286-autophosphorylation of αCaMKII is decreased at the synapses in the disease¹⁰⁴. This autophosphorylation is essential for NMDAR-dependent LTP at CA1 synapses and for spatial memory formation^{116,117}. Indeed, knockdown of CaMKII mimics the reduced surface expression of AMPA receptor subunit GluA1 and decreased AMPA receptor-mediated synaptic transmission, which is reversed by CaMKII overexpression¹¹⁴. An analogous observation is seen when treating rat hippocampal slices with Aβ(1–42). In this experimental model, Aβ inhibits CaMKII activation and blocks the stimulation-dependent phosphorylation of a CaMKII-specific site on GluA1¹⁰⁵. Moreover, treatment that enhances CaMKII activity also improves long-term memory in a mouse model of AD¹¹⁸.

Acute application of synthetic Aβ elicits inhibition of LTP in the CA1 area, or dentate gyrus, of rat *hippocampus*^{119–122}, as well as in conditioned culture medium containing Aβ species secreted by cells transfected with human APP¹²³. In the dentate gyrus Aβ inhibition of LTP was blocked by specific inhibitors for calcineurin, indicating that increased calcineurin activity contributes to Aβ-induced LTP inhibition¹²⁰. Thus, Aβ can also alter LTP by disrupting the dynamic balance between protein phosphorylation and dephosphorylation of CaMKII. It has been proposed that the increase in cytosolic Ca²⁺ induced by Aβ triggers calcineurin hyperactivity¹¹⁵; however, the possibility that Aβ and/or Aβ-CaM complexes might bind to calcineurin does not seem to have been explored until now. At least, this is *a priori* relevant for the dynamics of tau:calcineurin complexes and ultimately for the modulation of the extent of tau phosphorylation, since binding of Ca²⁺-CaM to calcineurin disrupts its interaction with tau and lowers its ability to dephosphorylate tau¹²⁴. In addition, despite the fact that extracellular Aβ applied to hippocampal slices preferentially targets synapses¹³, experimental data are lacking to exclude that Aβ could alter the association/dissociation kinetics of apo-CaM with CaM reservoir proteins, such as Nm, Ng, or RCS, in synaptic terminals.

LTCC have long been implicated in aging and AD¹²⁵. A decrease in LTCC activity has been reported in the *hippocampus* of APP/PS1 double-transgenic mice¹²⁶. Owing to the high contribution of Ca²⁺ influx through LTCC to increasing the resting cytosolic Ca²⁺ in neurons^{32,127–129}, the inhibition of LTCC by Aβ seems another compensatory neuroprotection mechanism to prevent pathogenic cytosolic Ca²⁺ dysregulation. Adaptive control of the activity of LTCC upon

exposure to A β is also suggested by experiments with astrocytes cultures, since acute exposure of astrocytes to murine A β (1–42) increased the expression of the Cav1.2 α 1-subunit, whereas chronic treatment decreased it, showing that A β can differentially regulate LTCC expression, depending on the incubation time¹³⁰. Noteworthy, nimodipine, a dihydropyridine derivative and LTCC antagonist, has beneficial effects in AD patients and slows the progression of the disease¹³¹. Although two large-population, long-term cohort studies have proved the protective role of Ca $^{2+}$ channel blockers over other types of antihypertensive drugs on the risk of dementia among elderly hypertensive populations^{132,133}, the clinical effects of each specific LTCC blocker remain controversial¹³⁴.

5. Conclusions

The high affinity of small A β oligomers for CaM and the high concentration of CaM in neurons reveal a major role of CaM for A β buffering in neurons, which protects against the rise of free concentrations of neurotoxic A β peptides. In turn, the concentration of A β -CaM complexes within neurons increases as a function of time after induction of A β production, and free A β will rise sharply when accumulated A β exceeds all available CaM, i.e., when it reaches total micromolar A β . Intraneuronal A β oligomers found in the AD brain can arise from endogenous A β peptide production as well as from vicinal reactive glial cells¹³⁵, as inflammation is now recognized to foster AD brain degeneration. The slow kinetics of A β uptake and its internalization by neurons^{12,136} is likely one of the factors that slows down the time course of the neurotoxicity of exogenous A β , and is relevant for the comparison and integration of the results and conclusions of studies performed in cell cultures after exposure to exogenous A β . On these grounds, it is to be expected that the A β -triggering of molecular mechanisms for the onset of neuronal cytosolic Ca $^{2+}$ dysregulation will be different for endogenously generated A β in the early stages of fAD and for the A β produced by vicinal reactive glial cells, probably a major source of A β during AD brain degeneration. In addition, A β -CaM complexation is likely to play a major role in the functional regulation of CaMBPs by A β , either in sensitivity or activity modulation. This has been largely overlooked until now, and it may have relevant implications for neuronal A β production, since APP and BACE1 are CaMBPs, for tau phosphorylation and for neuronal Ca $^{2+}$ dysregulation in AD, which mediates loss-of-function and neurodegeneration in AD brains. The identification of the primary target proteins for non-endogenous intraneuronal A β , of which functional impairment initiates cytosolic Ca $^{2+}$ homeostasis dysregulation as well as the critical point of no return, are still pending issues due to the following major reasons: (1) a lack of assessment of total intracellular A β concentrations in experiments with cell cultures reporting

cytosolic Ca^{2+} dysregulation; (2) a lack of the dissociation constant of the direct interaction between A β and A β -CaM complexes with target proteins; and (3) a lack of measurements of the putative oxidative modifications of Ca^{2+} channels and pumps in cell cultures after different times of exposure to exogenous A β . It should be recalled that A β stimulates intracellular ROS production¹³⁷ and that the Ca^{2+} transport systems that are more relevant for the control of intracellular Ca^{2+} homeostasis are highly sensitive to a sustained cellular oxidative stress^{32,138,139}. However, the experimental data accumulated so far allow us to envisage cellular adaptive responses, i.e., up-regulation and down-regulation of gene and protein expression levels, to compensate for the alteration of intracellular Ca^{2+} homeostasis upon acute and chronic exposure of neurons both *in vitro* (cell culture) and *in vivo* (animal models) to A β stress.

6. References

1. D'Andrea, M.R., Nagel, R.G., Wang, H.Y., Peterson, P.A., Lee, D. H. Evidence that neurons accumulating amyloid can undergo lysis to form amyloid plaques in Alzheimer's disease. *Histopathology* **38**, 120–34 (2001).
2. Wirths, O., Multhaup, G., Czech, C., Blanchard, V., Moussaoui, S., Tremp, G., Pradier, L., Beyreuther, K., Bayer, T. A. In-traneuronal A β accumulation precedes plaque formation in β amyloid precursor protein and presenilin-1 double-transgenic mice. *Neurosci. Lett.* **306**, 116–120 (2001).
3. Oddo, S., Caccamo, A., Shepherd, J.D., Murphy, M.P., Golde, T.E., Kayed, R., Metherate, R., Mattson, M.P., Akbari, Y., LaFerla, F. M. Triple-transgenic model of Alzheimer's Disease with plaques and tangles: Intracellular A β and synaptic dysfunction. *Neuron* **39**, 409–421 (2003).
4. Oakley, H., Cole, S.L., Logan, S., Maus, E., Shao, P., Craft, J., Guillozet-Bongaarts, A., Ohno, M., Disterhoft, J., Van Eldik, L. & Al, E. Intraneuronal β -amyloid aggregates, neurodegeneration, and neuron loss in transgenic mice with five familial Alzheimer's disease mutations: Potential factors in amyloid plaque formation. *J. Neurosci.* **26**, 10129–10140 (2006).
5. Knobloch, M., Konietzko, U., Krebs, D.C., Nitsch, R. M. Intracellular Abeta and cognitive deficits precede beta-amyloid deposition in transgenic arcAbeta mice. *Neurobiol. Aging* **28**, 1297–1306. (2007).
6. Billings, L. M., Oddo, S., Green, K. N., McGaugh, J. L. & LaFerla, F. M. Intraneuronal A β causes the onset of early Alzheimer's disease-related cognitive deficits in transgenic mice. *Neuron* **45**, 675–688 (2005).

7. Younkin, S. G. The role of A β -42 in Alzheimer's disease. *J Physiol.* **92**, 289–292 (1998).
8. Zhang, Y., McLaughlin, R., Goodyer, C.G., Leblanc, A. C. Selective cytotoxicity of intracellular amyloid β peptide 1–42 through p53 and Bax in cultured primary human neurons. *J. Cell Biol.* **156**, 519–529 (2002).
9. Walsh, D.M., Klyubin, I., Fadeeva, J.V., Cullen, W.K., Anwyl, R., Wolfe, M.S., Rowan, M.J., Selkoe, D. J. Naturally secreted oligomers of amyloid beta protein potently inhibit hippocampal long-term potentiation in vivo. *Nature* **416**, 535–539 (2002).
10. Hu, X., Crick, S.L., Bu, G., Frieden, C., Pappu, R.V., Lee, J. M. Amyloid seeds formed by cellular uptake, concentration, and aggregation of the amyloid-beta peptide. *Proc. Natl. Acad. Sci. U. S. A.* **106**, 20324–20329 (2009).
11. Friedrich, R.P., Tepper, K., Rönicke, R., Soom, M., Westermann, M., Reymann, K.I., Kaether, C., Fändrich, M. Mechanism of amyloid plaque formation suggests an intracellular basis of A β pathogenicity. *Proc. Natl. Acad. Sci. U. S. A.* **107**, 1942–1947 (2010).
12. Jin, S., Kedia, N., Illes-Toth, E., Haralampiev, I., Prisner, S., Herrmann, A., Wanker, E.E., Bieschke, J. Amyloid- β (1- 42) Aggregation Initiates Its Cellular Uptake and Cytotoxicity. *J. Biol. Chem.* **291**, 19590–19606 (2016).
13. Bahr, B.A., Hoffman, K.B., Yang, A.J., Hess, U.S., Glabe, C.G., Lynch, G. Amyloid β protein is internalized selectively by hippocampal field CA1 and causes neurons to accumulate amyloidogenic carboxyterminal fragments of the amyloid precursor protein. *J. Comp. Neurol.* **397**, 139–147 (1998).
14. Tang, B. L. Neuronal protein trafficking associated with Alzheimer's Disease: From APP and BACE1 to glutamate receptors. *Cell Adhes. Migr.* **3**, 118–128 (2009).
15. Zerbinatti, C.V., Wahrle, S.E., Kim, H., Cam, J.A., Bales, K., Paul, S.M., Holtzman, D.M., Bu, G. Apolipoprotein E and Low Density Lipoprotein Receptor-related Protein Facilitate Intraneuronal A β 42 Accumulation in Amyloid Model Mice. *J. Biol. Chem.* **281**, (2006).
16. Fuentealba, R.A., Liu, Q., Zhang, J., Kanekiyo, T., Hu, X., Lee, J.-M., Ladu, M.J., Bu, G. Low-Density Lipoprotein Receptor-Related Protein 1 (LRP1) Mediates Neuronal A β 42 Uptake and Lysosomal Trafficking. *PLoS One* **5**, (2010).
17. Lai, A.Y., McLaurin, J. Mechanisms of amyloid-beta peptide uptake by neurons: The role of lipid rafts and lipid raft-associated proteins. *Int. J. Alzheimers. Dis.* **2011**, 11 (2011).
18. Xia, Z. & Storm, D. R. The role of calmodulin as a signal integrator for synaptic plasticity. *Nat. Rev. Neurosci.* **6**, 267–276 (2005).
19. Biber, A., Schmid, G. & Hempel, K. Calmodulin content in specific brain areas. *Exp Brain Res* 323–326 (1984).

20. Corbacho, I., Berrocal, M., Török, K., Mata, A.M., Gutierrez-Merino, C. High affinity binding of amyloid β -peptide to calmodulin: Structural and functional implications. *Biochem Biophys Res Commun.* **486**, 992–997 (2017).
21. Laurén, J., Gimbel, D.A., Nygaard, H.B., Gilbert, J.W., Strittmatter, S. M. Cellular Prion Protein Mediates Impairment of Synaptic Plasticity by Amyloid- β Oligomers. *Nature* **457**, :1128-32 (2009).
22. Dunning, C.J., McGauran, G., Willén, K., Gouras, G.K., O'Connell, D.J., Linse, S. Direct High Affinity Interaction between A β 42 and GSK3 α Stimulates Hyperphosphorylation of Tau. A New Molecular Link in Alzheimer's Disease? *ACS Chem. Neurosci.* **7**, 161–170 (2016).
23. McLachlan, D.R., Wong, L., Bergeron, C., Baimbridge, K. G. Calmodulin and calbindin D28K in Alzheimer disease. *Alzheimer Dis Assoc Disord.* **1**, 171–9 (1987).
24. Khachaturian, Z. S. Calcium Hypothesis of Alzheimer's Disease and Brain Aging a. 1–11 (1993).
25. Kuchibhotla, K. V., Goldman, S. T., Lattarulo, C. R., Wu, H. Y., Hyman, B. T., & Bacskai, B. J. A β plaques lead to aberrant regulation of calcium homeostasis in vivo resulting in structural and functional disruption of neuronal networks. *Neuron* **59**, 214–225 (2008).
26. Lopez, J.R., Lyckman, A., Oddo, S., Laferla, F.M., Querfurth, H.W., Shtifman, A. Increased intraneuronal resting [Ca $^{2+}$] in adult Alzheimer's disease mice. *J Neurochem.* **105**, 262–71 (2008).
27. Berridge, M. J. Calcium Signalling and Alzheimer's Disease. *Neurochem. Res.* **36**, 1149–1156 (2011).
28. Berridge, M. J. Neuronal Calcium Signaling. *Neuron* **21**, 13–26 (1998).
29. Garcia, M.L., Strehler, E. E. Plasma membrane calcium ATPases as critical regulators of calcium homeostasis during neuronal cell function. *Front. Biosci.* D869–D882 (1999).
30. La Ferla, F. Calcium dyshomeostasis and intracellular signalling in Alzheimer's disease. *Nat. Rev. Neurosci.* **3**, 862–872 (2002).
31. Brini, M., Carafoli, E. Calcium Pumps in Health and Disease. *Physiol. Rev.* 1341–1378 (2009).
32. Gutierrez-Merino, C., Marques-da-Silva, D., Fortalezas, S., Samhan-Arias, A. K. Chapter: *Cytosolic Calcium Homeostasis in Neurons — Control Systems, Modulation by Reactive Oxygen and Nitrogen Species, and Space and Time Fluctuations*. In book: *Neurochemistry*. (InTech, 2014).
33. Chin, D. & Means, A. R. Calmodulin: A prototypical calcium sensor. *Trends Cell Biol.* **10**, 322–328 (2000).
34. Crivici A. & Ikura, M. Molecular and structural basis of target recognition by calmodulin.

- Annu Rev Biophys Biomol Struct* **24**, 85–116 (1995).
- 35. Zhang, M., Tanaka, T. & Ikura, M. Calcium-induced conformational transition revealed by the solution structure of apo calmodulin. *Nature* **2**, 758–767 (1995).
 - 36. Kaleka, K.S., Petersen, A.N., Florence, M.A., Gerges, N. Z. Pull-down of calmodulin-binding proteins. *J Vis Exp* **59**, 1–5 (2012).
 - 37. Padilla, R., Maccioni, R., Avila, J. Calmodulin binds to a tubulin binding site of the microtubule-associated protein tau. *Mol. Cell. Biochem* **97**, 35–41 (1990).
 - 38. O'Day, D. H., Eshak, K. & Myre, M. A. Calmodulin binding proteins and Alzheimer's disease. *J. Alzheimer's Dis.* **46**, 553–569 (2015).
 - 39. Hammond, J. W., Cai, D. & Verhey, K. J. Tubulin modifications and their cellular functions. *Curr. Opin. Cell Biol.* **20**, 71–76 (2008).
 - 40. Sánchez, C., Díaz-Nido, J. & Avila, J. Phosphorylation of microtubule-associated protein 2 (MAP2) and its relevance for the regulation of the neuronal cytoskeleton function. *Prog. Neurobiol.* **61**, 133–168 (2000).
 - 41. Sharma, R. K. & Parameswaran, S. Calmodulin-binding proteins: A journey of 40 years. *Cell Calcium* **75**, 89–100 (2018).
 - 42. Klee, C. B., Ren, H. & Wang, X. Regulation of the calmodulin-stimulated protein phosphatase, calcineurin. *J. Biol. Chem.* **273**, 13367–13370 (1998).
 - 43. Baumgärtel, K. & Mansuy, I. M. Neural functions of calcineurin in synaptic plasticity and memory. *Learn. Mem.* **19**, 375–384 (2012).
 - 44. Groth, R. D., Dunbar, R. L. & Mermelstein, P. G. Calcineurin regulation of neuronal plasticity. *Biochem. Biophys. Res. Commun.* **311**, 1159–1171 (2003).
 - 45. Wang, H. & Storm, D. R. Calmodulin-regulated adenylyl cyclases: Cross-talk and plasticity in the central nervous system. *Mol. Pharmacol.* **63**, 463–468 (2003).
 - 46. Conti, A.C., Maas, J.W.Jr., Muglia, L.M., Dave, B.A., Vogt, S.K., Tran, T.T., Rayhel, E.J., Muglia, L. J. Distinct regional and subcellular localization of adenylyl cyclases type 1 and 8 in mouse brain. *Neuroscience* **146**, 713–729 (2007).
 - 47. Zhou, L. & Zhu, D. Y. Neuronal nitric oxide synthase: Structure, subcellular localization, regulation, and clinical implications. *Nitric Oxide - Biol. Chem.* **20**, 223–230 (2009).
 - 48. Yue, D. Towards a unified theory of calmodulin regulation (calmodulation) of voltage-gated calcium and sodium channels. *Curr Mol Pharmacol* **8**, 188–205 (2016).
 - 49. Turner, R. W., Anderson, D. & Zamponi, G. W. Signaling complexes of voltage-gated calcium channels. *Channels* **5**, (2011).
 - 50. Berger, S. M. & Bartsch, D. The role of L-type voltage-gated calcium channels Cav1.2 and Cav1.3 in normal and pathological brain function. *Cell Tissue Res.* **357**, 463–476 (2014).

51. Nanou, E. & Catterall, W. A. Calcium Channels, Synaptic Plasticity, and Neuropsychiatric Disease. *Neuron* **98**, 466–481 (2018).
52. Hell, J.W., Westenbroek, R.E., Warner, C., Ahlijanian, M.K., Prystay, W., Gilbert, M.M., Snutch, T.P., & Catterall, W. A. Identification and differential subcellular localization of the neuronal class C and class D L-type calcium channel $\alpha 1$ subunits. *J. Cell Biol.* **123**, 949–962 (1993).
53. Liang, H., DeMaria, C.D., Erickson, M.G., Mori, M.X., Alseikhan, B.A., Yue, D. T. Unified mechanisms of Ca^{2+} regulation across the Ca^{2+} channel family. *Neuron* **39**, 951–960 (2003).
54. Striessnig, J., Pinggera, A., Kaur, G., Bock, G. & Tuluc, P. L-type Ca^{2+} channels in heart and brain. *Wiley Interdiscip. Rev. Membr. Transp. Signal.* **3**, 15–38 (2014).
55. Yang, P.S., Alseikhan, B.A., Hiel, H., Grant, L., Mori, M.X., Yang, W., Fuchs, P.A., & Yue, D. T. Switching of Ca^{2+} -dependent inactivation of $\text{CaV}1.3$ channels by calcium binding proteins of auditory hair cells. *J. Neurosci.* **26**, 10677–10689 (2006).
56. Lei, S., Czerwinska, E., Czerwinski, W., Walsh, M. P. & MacDonald, J. F. Regulation of NMDA receptor activity by F-actin and myosin light chain kinase. *J. Neurosci.* **21**, 8464–8472 (2001).
57. Li, L., Wu, X., Yue, H. Y., Zhu, Y. C. & Xu, J. Myosin light chain kinase facilitates endocytosis of synaptic vesicles at hippocampal boutons. *J. Neurochem.* **60**–73 (2016) doi:10.1111/jnc.13635.
58. Liu, C. H. & Rasband, M. N. Axonal spectrins: Nanoscale organization, functional domains and spectrinopathies. *Front. Cell. Neurosci.* **13**, (2019).
59. Nellikka., R.K, Sreeja, J.S., Dharmapal, D., John, R., Monteiro, A., Macedo, J.C., Conde, C., Logarinho, E., Sunkel, C.E., Sengupta, S. α -Fodrin is required for the organization of functional microtubules during mitosis. *Cell Cycle* **18**, 2713–2726 (2019).
60. Li, S., Tian, X., Hartley, D. M. & Feig, L. A. Distinct roles for Ras-guanine nucleotide-releasing factor 1 (Ras-GRF1) and Ras-GRF2 in the induction of long-term potentiation and long-term depression. *J. Neurosci.* **26**, 1721–1729 (2006).
61. Manyes, L., Holst, S., Lozano, M., Santos, E. & Fernandez-Medarde, A. Spatial learning and long-term memory impairments in RasGrf1 KO, Pttg1 KO, and double KO mice. *Brain Behav.* **8**, 1–10 (2018).
62. Nadeau, O. W., Fontes, J. D. & Carlson, G. M. The regulation of glycogenolysis in the brain. *J. Biol. Chem.* **293**, 7099–7107 (2018).
63. Paudel, H. K., Zwiers, H. & Wang, J. H. Phosphorylase kinase phosphorylates the calmodulin-binding regulatory regions of neuronal tissue-specific proteins B-50 (GAP-43)

- and neurogranin. *J. Biol. Chem.* **268**, 6207–6213 (1993).
64. Shen, Y., Mani, S., Donovan, S. L., Schwob, J. E. & Meiri, K. F. Growth-associated protein-43 is required for commissural axon guidance in the developing vertebrate nervous system. *J. Neurosci.* **22**, 239–247 (2002).
65. Denny, J. Molecular Mechanisms, Biological Actions, and Neuropharmacology of the Growth-Associated Protein GAP-43. *Curr. Neuropharmacol.* **4**, 293–304 (2006).
66. Apel, E. D., Byford, M. F., Au, D., Walsh, K. A. & Storm, D. R. Identification of the Protein Kinase C Phosphorylation Site in Neuromodulin. *Biochemistry* **29**, 2330–2335 (1990).
67. Ouimet, C. C., Hemmings, H. C. & Greengard, P. ARRP-21, a cyclic AMP-regulated phosphoprotein enriched in dopamine-innervated brain regions. II. Immunocytochemical localization in rat brain. *J. Neurosci.* **9**, 865–875 (1989).
68. Rakhilin, S.V., Olson, P.A., Nishi, A., Starkova, N.N., Fienberg, A.A., Nairn, A.C., Surmeier, D.J., Greengard, P. A network of control mediated by of regulator of calcium/calmodulin-dependent signaling. *Science (80-).* **306**, 698–701 (2004).
69. Reitz, C., Mayeux, R. Alzheimer disease: Epidemiology, diagnostic criteria, risk factors and biomarkers. *Biochem. Pharmacol.* **88**, 640–651 (2014).
70. Goate, A., Chartier-Harlin, M.C., Mullan, M., Brown, J., Crawford, F., Fidani, L., Giuffra, L., Haynes, A., Irving, N., James, L., et al. Segregation of a missense mutation in the amyloid precursor protein gene with familial Alzheimer's disease. *Nature* **349**, 704–6 (1991).
71. Schellenberg, G., Bird, T.D., Wijsman, E.M., Orr, H.T., Anderson, L., Nemens, E., White, J.A., Bonnycastle, L., Weber, J.L., Alonso, M. E. Genetic Linkage Evidence for a Familial Alzheimer's Disease Locus on Chromosome 14. *Science (80-).* **258**, 668–671 (1992).
72. Hardy, J., Selkoe, D. J. The amyloid hypothesis of Alzheimer's disease: Progress and problems on the road to therapeutics. *Science (80-).* **297**, 353–356 (2002).
73. Supnet, C. & Bezprozvanny, I. The dysregulation of intracellular calcium in Alzheimer's disease. *Cell Calcium* **47**, 183–189 (2010).
74. Leisring, M.A., Akbari, Y., Fanger, C.M., Cahalan, M.D., Mattson, M. P. & LaFerla, F. M. Capacitative calcium entry deficits and elevated luminal calcium content in mutant presenilin-1 knockin mice. *J. Cell Biol.* **149**, 793–797 (2000).
75. Ryazantseva, M., Skobeleva, K. & Kaznacheyeva, E. Familial Alzheimer's disease-linked presenilin-1 mutation M146V affects store-operated calcium entry: Does gain look like loss? *Biochimie* **95**, 1506–1509 (2013).
76. Giliberto, L., Borghi, R., Piccini, A., Mangerini, R., Sorbi, S., Cirmena, G., Garuti, A., Ghetti, B., Tagliavini, F., Mughal, M. R., Mattson, M. P., Zhu, X., Wang, X., Guglielmo, M., Tamagni, E., & Tabaton, M. Mutant presenilin 1 increases the expression and activity of

- BACE1. *J. Biol. Chem.* **284**, 9027–9038 (2009).
77. Buggia-Prevot, V., Sevalle, J., Rossner, S., Checler, F. NFkappaB dependent control of BACE1 promoter transactivation by Abeta42. *J. Biol. Chem.* **283**, 10037–10047 (2008).
 78. Tamagno, E., Guglielmo, M., Monteleone, D., Tabaton, M. Amyloid- β production: major link between oxidative stress and BACE1. *Neurotox Res.* 208–19 (2012).
 79. Hermes, M., Eichhoff, G. & Garaschuk, O. Intracellular calcium signalling in Alzheimer's disease. **14**, 30–41 (2010).
 80. Leissring, M. A., Parker, I. & LaFerla, F. M. Presenilin-2 mutations modulate amplitude and kinetics of inositol 1,4,5-trisphosphate-mediated calcium signals. *J. Biol. Chem.* **274**, 32535–32538 (1999).
 81. Yoo, A.S., Cheng, I., Chung, S., Grenfell, T.Z., Lee, H., Pack-Chung, E., Handler, M., Shen, J., Xia, W., Tesco, G. et al. Presenilin-mediated modulation of capacitative calcium entry. *Neuron* **27**, 561–572 (2000).
 82. Popugaeva, E., Pchitskaya, E., Bezprozvanny, I. Dysregulation of neuronal calcium homeostasis in Alzheimer's disease - A therapeutic opportunity? *Biochem Biophys Res Commun* **483**, 998–1004 (2017).
 83. Zeiger, W., Vetrivel, K.S., Buggia-prévet, V., Nguyen, P.D., Wagner, S.L., Villereal, M.L., Thinakaran, G. Ca2+ Influx through Store-operated Ca2+ Channels Reduces Alzheimer's Disease β -Amyloid Peptide Secretion. *Mol. bases Dis.* **288**, 26955–26966 (2013).
 84. Sun, S., Zhang, H., Liu, J., Popugaeva, E., Xu, N.-j., Feske, S., White III, C.L., Bezprozvanny, I. Reduced Synaptic STIM2 Expression and Impaired Store-Operated Calcium Entry Cause Destabilization of Mature Spines in Mutant Presenilin Mice. *Neuron* **82**, 79–93 (2014).
 85. Tu, H., Nelson, O., Bezprozvanny, A., Wang, Z., Lee, S.F., Hao, Y.H., Serneels, L., De Strooper, B., Yu, G., Bezprozvanny, I. Presenilins Form ER Ca2+ Leak Channels, a Function Disrupted by Familial Alzheimer's Disease-Linked Mutations. *Cell* **126**, 981–993 (2006).
 86. Nelson, O., Tu, H., Lei, T., Bentahir, M., De Strooper, B., Bezprozvanny, I. Familial Alzheimer's disease-linked mutations specifically disrupt Ca2+ leak function of presenilin 1. *J. Clin. Invest.* **117**, 1230–1239 (2007).
 87. Rybalchenko, V., Hwang, S., Rybalchenko, N. & Koulen, P. The cytosolic N-terminus of presenilin-1 potentiates mouse ryanodine receptor single channel activity. **40**, 84–97 (2008).
 88. Namba, Y., Tomonaga, M., Kawasaki, H., Otomo, E. & Ikeda, K. Apolipoprotein E immunoreactivity in cerebral amyloid deposits and neurofibrillary tangles in Alzheimer's disease and kuru plaque amyloid in Creutzfeldt-Jakob disease. **541**, 163–166 (1991).
 89. Ohkubo, N., Mitsuda, N., Tamatani, M., Yamaguchi, A., Lee, Y.-d., Ogihara, T., Vitek, M.P.,

- Tohyama, M. Apolipoprotein E4 Stimulates cAMP Response Element-binding Protein Transcriptional Activity through the Extracellular Signal-regulated Kinase Pathway. **276**, 3046–3053 (2001).
90. Shtifman, A., Ward, C.W., Laver, D.R., Bannister, M.L., Lopez, J.R., Kitazawa, M., LaFerla, F.M., Ikemoto, N., Querfurth, H. W. Amyloid- β protein impairs Ca $^{2+}$ release and contractility in skeletal muscle. *Neurobiol. Aging* **31**, 2080–2090 (2010).
91. Paula-Lima, A. & Hidalgo, C. Amyloid β -peptide oligomers, ryanodine receptor-mediated Ca $^{2+}$ release and Wnt-5a/Ca $^{2+}$ signaling: Opposing roles in neuronal mitochondrial dynamics? *Front. Cell. Neurosci.* **7**, 2011–2013 (2013).
92. Green, K.N., Demuro, A., Akbari, Y., Hitt, B.D., Smith, I.F., Parker, I., LaFerla, F. M. SERCA pump activity is physiologically regulated by presenilin and regulates amyloid β production. *J. Cell Biol.* **181**, 1107–1116 (2008).
93. Krajnak, K. & Dahl, R. A new target for Alzheimer's disease: A small molecule SERCA activator is neuroprotective in vitro and improves memory and cognition in APP/PS1 mice. *Bioorganic Med. Chem. Lett.* **28**, 1591–1594 (2018).
94. Berrocal, M., Marcos, D., Sepúlveda, M.R., Pérez, M., Ávila, J., Mata, A. M. Altered Ca $^{2+}$ dependence of synaptosomal plasma membrane Ca $^{2+}$ -ATPase in human brain affected by Alzheimer's disease. *FASEB J.* **23**, 1826–1834 (2009).
95. Berrocal, M., Sepulveda, M. R., Vazquez-Hernandez, M. & Mata, A. M. Calmodulin antagonizes amyloid- β peptides-mediated inhibition of brain plasma membrane Ca $^{2+}$ -ATPase. *Biochim. Biophys. Acta* **1822**, 961–969 (2012).
96. Wu, A., Derrico, C. A., Hatem, L. & Colvin, R. A. Alzheimer's amyloid-beta peptide inhibits sodium/calcium exchange measured in rat and human brain plasma membrane vesicles. **80**, 675–684 (1997).
97. Unlap, M.T., Williams, C., Morin, D., Siroky, B., Fintha, A., Fuson, A., Dodgen, L., Kovacs, G., Komlosi, P., Ferguson, W., Bell, P. D. Amyloid beta peptide 1-40 stimulates the Na $^{+}$ /Ca $^{2+}$ exchange activity of SNCX. *Curr Neurovasc Res* **2**, 3–12 (2005).
98. Ferreiro, E., Oliveira, C.R., Pereira, C. M. F. The release of calcium from the endoplasmic reticulum induced by amyloid-beta and prion peptides activates the mitochondrial apoptotic pathway. *Neurobiol Dis.* **30**, 331–342 (2008).
99. Fonseca, A.C., Ferreiro, E., Oliveira, C.R., Cardoso, S.M., Pereira, C. F. Activation of the endoplasmic reticulum stress response by the amyloid-beta 1-40 peptide in brain endothelial cells. *Biochim Biophys Acta* **1832**, 2191–203 (2013).
100. Magi, S., Castaldo, P., Macrì, M.L., Maiolino, M., Matteucci, A., Bastioli, G., Gratteri, S., Amoroso, S., Lariccia, V. Intracellular Calcium Dysregulation: Implications for Alzheimer's

Disease. *Biomed Res Int* **2016**, (2016).

101. Ryan, K.C., Ashkavand, Z., Norman, K. R. The Role of Mitochondrial Calcium Homeostasis in Alzheimer's and Related Diseases. *Int J Mol Sci* **21**, 9153 (2020).
102. Toglia, P., Cheung, K.H., Mak, D.O., Ullah, G. Impaired mitochondrial function due to familial Alzheimer's disease-causing presenilins mutants via Ca²⁺ disruptions. *Cell Calcium* **59**, 240–250 (2016).
103. Min, D., Guo, F., Zhu, S., Xu, X., Mao, X., Cao, Y., Lv, Xi., Gao, Q. & Wang, L., Chen, T., Shaw, C., Hao, Li., Cai, J. The alterations of Ca²⁺/calmodulin/CaMKII/CaV1.2 signaling in experimental models of Alzheimer's disease and vascular dementia. *Neurosci. Lett.* **538**, 60–65 (2013).
104. Ghosh, A. & Giese, K. P. Calcium/calmodulin-dependent kinase II and Alzheimer's disease. *Mol. Brain* **8**, 1–7 (2015).
105. Zhao, D., Watson, J. B. & Xie, C. W. Amyloid β prevents activation of calcium/calmodulin-dependent protein kinase II and AMPA receptor phosphorylation during hippocampal long-term potentiation. *J. Neurophysiol.* **92**, 2853–2858 (2004).
106. Gandy, S., Czernik, A.J., Greengard, P. Phosphorylation of Alzheimer disease amyloid precursor peptide by protein kinase C and Ca²⁺/calmodulin-dependent protein kinase II. *Proc Natl Acad Sci USA* **85**, 6218–21 (1988).
107. Sengupta, A., Kabat, J., Novak, M., Wu, Q., Grundke-Iqbali, I., Iqbal, K. Phosphorylation of tau at both Thr 231 and Ser 262 is required for maximal inhibition of its binding to microtubules. *Arch Biochem Biophys.* **357**, 299–30 (1998).
108. Wang, J.Z., Grundke-Iqbali, I., Iqbal, K. Kinases and phosphatases and tau sites involved in Alzheimer neurofibrillary degeneration. *Eur J Neurosci.* **25**, 59–68 (2007).
109. Phiel, C.J., Wilson, C.A., Lee, V.M., Klein, P. S. GSK-3alpha regulates production of Alzheimer's disease amyloid-beta peptides. *Nature* **423**, 435–9 (2003).
110. Lisman, J. The CaM kinase II hypothesis for the storage of synaptic memory. *Trends Neurosci.* **17**, 406–412 (1994).
111. Lisman, J., Schulman, H., Cline, H. T. The molecular basis of CaMKII function in synaptic and behavioural memory. *Nat. Rev. Neurosci.* **3**, 175–190 (2002).
112. Hudmon, A. & Schulman, H. Neuronal Ca 2+ /Calmodulin-Dependent Protein Kinase II: The Role of Structure and Autoregulation in Cellular Function . *Annu. Rev. Biochem.* **71**, 473–510 (2002).
113. Silva, A., Stevens, C., Tonegawa, S., Wang, Y. Deficient hippocampal long-term potentiation in alpha-calcium-calmodulin kinase II mutant mice. *Science (80-.)* **257**, 201–206 (1992).

114. Gu, Z., Liu, W., Yan, Z. {beta}-Amyloid impairs AMPA receptor trafficking and function by reducing Ca²⁺/calmodulin-dependent protein kinase II synaptic distribution. *J Biol Chem* **284**, 10639–49 (2009).
115. Reese, L.C., Laezza, F., Woltjer, R., Taglialatela, G. Dysregulated phosphorylation of Ca(2+)/calmodulin-dependent protein kinase II- α in the hippocampus of subjects with mild cognitive impairment and Alzheimer's disease. *J Neurochem* **119**, 791–804 (2011).
116. Giese, K.P., Fedorov, N.B., Filipkowski, R.K., Silva, A. J. Autophosphorylation at Thr286 of the alfa Calcium-Calmodulin Kinase II in LTP and Learning. *Science (80-.).* **270**, 870–873 (1998).
117. Cooke, S.F., Bliss, T. V. Plasticity in the human central nervous system. *Brain* **129**, 1659–1673 (2006).
118. Wang, D.M., Yang, Y.J., Zhang, L., Zhang, X., Guan, F.F., Zhang, L. F. Naringin Enhances CaMKII Activity and Improves Long-Term Memory in a Mouse Model of Alzheimer's Disease. *Int J Mol Sci* **14**, 5576–86. (2013).
119. Chen, Q.S., Kagan, B.L., Hirakura, Y., Xie, C. W. Impairment of hippocampal long-term potentiation by Alzheimer amyloid beta-peptides. *J Neurosci Res* **60**, 65–72 (2000).
120. Chen, Q.S., Wei, W.Z., Shimahara, T., Xie, C. W. Alzheimer amyloid beta-peptide inhibits the late phase of long-term potentiation through calcineurin-dependent mechanisms in the hippocampal dentate gyrus. *Neurobiol Learn Mem* **77**, 354–71 (2002).
121. Kim, J.H., Anwyl, R., Suh, Y.H., Djamgoz, M.B., Rowan, M. J. Use-dependent effects of amyloidogenic fragments of (beta)-amyloid precursor protein on synaptic plasticity in rat hippocampus in vivo. *J. Neurosci.* **21**, 1327–1333 (2001).
122. Wang, H.W., Pasternak, J.F., Kuo, H., Ristic, H., Lambert, M.P., Chromy, B., Viola, K.L., Klein, W.L., Stine, W.B., Krafft, G.A., Trommer, B. L. Soluble oligomers of beta amyloid (1–42) inhibit long-term potentiation but not long-term depression in rat dentate gyrus. *Brain Res.* **924**, 133–40 (2002).
123. Walsh, D.M., Klyubin, I., Fadeeva, J.V., Cullen, W.K., Anwyl, R., Wolfe, M.S., Rowan, M.J., Selkoe, D. J. Naturally secreted oligomers of amyloid β protein potently inhibit hippocampal long-term potentiation in vivo. *Nature* **416**, 535–539 (2002).
124. De Felice, F.G., Velasco, P.T., Lambert, M.P., Viola, K., Fernandez, S.J., Ferreira, S.T., Klein, W. L. A β oligomers induce neuronal oxidative stress through an N-methyl-D-aspartate receptor-dependent mechanism that is blocked by the Alzheimer drug memantine. *J. Biol. Chem.* **282**, 11590–11601 (2007).
125. Agostini, M. & Fasolato, C. When, where and how? Focus on neuronal calcium dysfunctions in Alzheimer's Disease. *Cell Calcium* **60**, 289–298 (2016).

126. Thibault, O., Pancani, T., Landfield, P.W., Norris, C. M. Reduction in neuronal L-type calcium channel activity in a double knock-in mouse model of Alzheimer's disease. *Biochim Biophys Acta* **1822**, 546–549 (2012).
127. Gutierrez-Merino, C., Marques-da-Silva, D., Fortalezas, S., Samhan-Arias, A. K. The critical role of lipid rafts nanodomains in the cross-talk between calcium and reactive oxygen and nitrogen species in cerebellar granule neurons apoptosis by extracellular potassium deprivation. *AIMS Mol. Sci.* **3**, 12–29 (2016).
128. Fortalezas, S., Marques-da-Silva, D., Gutierrez-Merino, C. Methyl- β -Cyclodextrin Impairs the Phosphorylation of the β 2 Subunit of L-Type Calcium Channels and Cytosolic Calcium Homeostasis in Mature Cerebellar Granule Neurons. *Int J Mol Sci.* **19**, 3667 (2018).
129. Willis, M., Kaufmann, W.A., Wietzorek, G., Hutter-Paier, B., Moosmang, S., Humpel, C., Hofmann, F., Windisch, M., Knaus, H.G., Marksteiner, J. L-Type calcium channel CaV 1.2 in transgenic mice overexpressing human A β PP751 with the London (V717I) and Swedish (K670M/N671L) Mutations. *J. Alzheimer's Dis.* **20**, 1167–1180 (2010).
130. Daschil, N., Geisler, S., Obermair, G. J. & Humpel, C. Short-and long-term treatment of mouse cortical primary astrocytes with β -amyloid differentially regulates the mRNA Expression of L-type calcium channels. *Pharmacology* **93**, 24–31 (2014).
131. Birks, J., López-Arrieta, J. Nimodipine for primary degenerative, mixed and vascular dementia. *Cochrane Database Syst. Rev.* **3**, (2002).
132. Wu, C. L. & Wen, S. H. A 10-year follow-up study of the association between calcium channel blocker use and the risk of dementia in elderly hypertensive patients. *Med. (United States)* **95**, (2016).
133. Hwang, D., Kim, S., Choi, H., Oh, I.H., Kim, B.S., Choi, H.R., Kim, S.Y., Won, C. W. Calcium-channel blockers and dementia risk in older adults – National health insurance service – Senior cohort (2002–2013). *Circ. J.* **80**, 2336–2342 (2016).
134. Wang, X. & Zheng, W. Ca $^{2+}$ homeostasis dysregulation in Alzheimer's disease : a focus on plasma membrane and cell organelles. *40*, 6697–6712 (2019).
135. Zhao, J., O'Connor, T., Vassar, R. The contribution of activated astrocytes to A β production: Implications for Alzheimer's disease pathogenesis. *J Neuroinflammation* **8**, 150. *J Neuroinflammation* **8**, 150 (2011).
136. Saavedra, L., Mohamed, A., Ma, V., Kar, S. & De Chaves, E. P. Internalization of β -amyloid peptide by primary neurons in the absence of apolipoprotein E. *J. Biol. Chem.* **282**, 35722–35732 (2007).
137. Green, K. N. Calcium in the initiation, progression and as an effector of Alzheimer's disease pathology. *J. Cell. Mol. Med.* **13**, 2787–2799 (2009).

138. Hidalgo, C., Donoso, P. Crosstalk between Calcium and Redox Signaling: From Molecular Mechanisms to Health Implications. *Antioxid. Redox Signal.* **10**, 1275–1312 (2008).
139. Gutierrez-Merino, C. *Redox modulation of neuronal calcium homeostasis and its deregulation by reactive oxygen species.* In *Free Radicals in Biology and Medicine.* (Research Signpost: Kerala, 2008).

CHAPTER 2

Binding of A β (1–42)-CaM complexes to plasma membrane lipid rafts in CGN alters resting cytosolic Ca²⁺ homeostasis

Index

1. Abstract	57
2. Introduction	57
3. Materials and Methods	59
3.1 Chemicals.....	59
3.2 Preparation of rat CGN	59
3.3 A β (1–42) solutions and aggregation state	60
3.4 Cell viability	60
3.5 Co-Immunoprecipitation	61
3.6 Western blotting	61
3.7 Measurements of internalization of A β (1–42)-HiLyte TM -Fluor555 (A β (1-42)*555) in mature CGN	62
3.8 FRET imaging	62
3.9 Measurement of the intracellular free Ca ²⁺ Concentration ([Ca ²⁺] _i)	64
3.10 Statistical analysis	64
4. Results	65
4.1 Co-Immunoprecipitation of CaM with submicromolar concentrations of A β (1–42) in CGN lysates	65
4.2 Extensive co-localization between CaM and A β (1–42)*555 in mature CGN demonstrated by FRET imaging.....	67
4.3 FRET imaging highlights the association of A β (1-42)*555 and CaM with lipid rafts markers in mature CGN	70
4.4 A short time incubation with submicromolar concentrations of A β (1–42) decreases the resting cytosolic Ca ²⁺ concentration through inhibition of LTCCs in mature CGN	73
4.5 Extensive FRET between LTCCs and A β (1-42)*555 in fixed mature CGN is largely reversed by addition of exogenous CaM	77
5. Discussion	80
6. Supplementary Figures	84
7. References	85

1. Abstract

Neuronal lipid rafts play a key role in A β binding and uptake, leading to the formation of neurotoxic intracellular A β aggregates. Furthermore, dysregulation of intracellular Ca $^{2+}$ homeostasis has been observed in AD. We demonstrated, in a previous work, that A β (1–42), the prevalent form of A β peptide found in A β plaques of AD patients, have high affinity to purified CaM, with a kD around 1 nM. In this work, we used primary cultures of mature cerebellar granule neurons (CGN) as a neuronal model, to experimentally assess the binding capacity of submicromolar concentrations of A β (1–42) dimers to intracellular CaM. Our results showed the formation of A β (1–42):CaM complexes in GCN, up to 120 ± 13 picomoles of A β (1–42) / 2.5×10^6 cells. We also showed an extensive co-localization of CaM and A β (1–42) in lipid rafts in CGN stained with up to 100 picomoles of A β (1–42)-HiLyteTM-Fluor555, using fluorescence microscopy imaging. Intracellular A β (1–42) concentration in this range was achieved after 2 h incubation with 2 μ M A β (1–42), and this treatment lowered the resting cytosolic Ca $^{2+}$ of mature CGN in partially depolarizing 25 mM potassium medium. We conclude that the primary cause of the resting cytosolic Ca $^{2+}$ decrease is the inhibition of LTCC of CGN by A β (1–42) dimers, whose activity is inhibited by CaM-A β (1–42) complexes bound to lipid rafts.

2. Introduction

Membrane lipid rafts are heterogeneous and highly dynamic small submicrodomains of sizes between 10–100 nm that are composed by cholesterol and gangliosides¹. Different studies demonstrated that A β peptides interact with cholesterol and gangliosides in ganglioside-clustered raft-like microdomains, which potentiate the formation of A β oligomers (A β O) and fibrils in a cholesterol-dependent manner^{2–8}. Consequently, due to the high levels of gangliosides in neurons, membrane lipid rafts could be seen as primary targets for A β peptides cytotoxicity. In fact, several studies reported that membrane lipid rafts play a major role in extracellular A β uptake and internalization in neurons⁹, which was demonstrated not only in cell culture models studies¹⁰ but also in mouse models of AD¹¹.

It has been shown that the reuptake of extracellular A β (1–42), which is the prevalent A β peptide found in the A β plaques of AD patients¹², can result in the development of intracellular aggregates, leading to neuronal damage and neurotoxicity^{13–15} since A β (1–42) are associated with AD pathogenesis¹⁶. This premise was supported by different studies with the triple transgenic (3xTg) AD mice, where they demonstrated that the levels of intraneuronal A β are associated with dysfunction in synaptic activity and also in memory impairment^{17,18}.

Dysregulation of intracellular Ca^{2+} homeostasis it is a common phenomenon of sporadic (sAD) and familial forms of AD (fAD), which is linked to increased levels of intraneuronal A β and tau hyperphosphorylation^{19,20}. Also, the concentration of CaM, a major Ca^{2+} -sensor protein present in neuronal cytosol, is significantly decreased in brains of AD patients²¹. We demonstrated in a previous work that A β (1–42) and A β (25–35) have high affinity for CaM (dissociation constants around 1 nM)²². CaM also plays a key role as intracellular Ca^{2+} signaling messenger, by modulating neuronal functions which impairment results in significant changes in metabolism, excitability and synaptic activity, leading to neuronal death^{23–25}. Therefore, impairment of intracellular Ca^{2+} buffering caused by A β can trigger pathogenic feed-forward cycle, leading consequently to synaptic morphology changes, neuronal apoptosis and cognitive decline²⁶.

Neuronal lipid rafts have also the capacity to generate short lived and dynamic high Ca^{2+} compartments near the plasma membrane^{27,28}. As showed in a previously work of the lab, these high Ca^{2+} sub microcompartments are composed of LTCCs, NMDAR, and PMCA, in mature CGN in culture²⁷. LTCCs and PMCA are proteins that bind CaM^{29–33} and are the main plasma membrane Ca^{2+} transport systems that controls the resting cytosolic Ca^{2+} concentration in CGN in a 25mM potassium medium^{34–36}, therefore lipid rafts play a key role in the modulation of the excitability of CGN. Furthermore, CaMKII^{36,37} and the neuronal isoform of nitric oxide synthase (nNOS)^{28,38–40} are also CaM bindings proteins associated with lipid rafts in mature CGN and other neurons. It have been demonstrated that some of these CaM-biding proteins are inhibited by A β peptides such as, CaMKII^{41,42}, PMCA^{33,43} and nNOS^{44,45}. However, despite the relevance of LTCC activity for resting cytosolic Ca^{2+} concentration in neurons in long-term LTP/LTD⁴⁶, and in neuronal function, memory and cognition⁴⁷, the possibility of LTCC inhibition by A β (1–42) remains to be experimentally assessed.

This work was performed in mature CGN in culture and the main goals were: 1) to demonstrate the formation of CaM-A β (1–42) complexes with submicromolar concentrations of A β (1–42); 2) to determine the co-localization of A β (1–42) and A β (1–42)-CaM complexes in neuronal lipid rafts; 3) to evaluate the change in the resting cytosolic Ca^{2+} concentration induced by internalized A β (1–42); and 4) to identify the main cause of the observed change in cytosolic Ca^{2+} concentration. The results of this work showed that incubation of CGN with A β (1–42) dimers for 2 h induced inhibition of LTCCs and elicited a decrease in the resting cytosolic Ca^{2+} concentration.

3. Materials and Methods

3.1 Chemicals

Human A β (1–42)-HiLyte™-Fluor555 (referred as A β (1-42)*555) was obtained from AnaSpec (Freemont, CA, USA). Unlabeled A β (1–42) and scrambled A β (1–42) were supplied by StabVida (Caparica, Portugal). Purified bovine brain CaM was purchased from Sigma- Aldrich (Madrid, Spain).

Primary antibodies: goat anti-HRas (sc-32026), rabbit anti-caveolin-1 (anti-Cav1, sc-894), rabbit anti- LTCC α 1C subunit (sc-25686), and rabbit anti-LTCC β subunit (sc-25689) antibodies were purchased by Santa Cruz Biotechnology (Santa Cruz, CA, USA). Rabbit anti-CaM (Epitomics 1716-1) antibody was supplied by Abcam (Cambridge, UK) and mouse anti-cellular prion protein antibody (anti-PrPc, Thermo Fisher, 6H4-7500997) was supplied from Thermo Fisher Scientific (Madrid, Spain). Monoclonal mouse anti-A β antibody (A8354) was acquired from Sigma- Aldrich (Madrid, Spain). Fluorescent-labeled secondary antibodies used to label the primary antibodies were anti-rabbit IgG-Alexa488 (A11008), anti-goat IgG-Alexa488 (A11055), anti-mouse IgG-Alexa488 (A11001) and anti-goat IgG-Cy3 (C2821) from Invitrogen (Molecular Probes, Eugene, OR, USA). Anti-rabbit IgG-horseradish peroxidase (A0545), anti-goat IgG-horseradish peroxidase (A8919), and anti-mouse IgG-horseradish peroxidase (A0944) were supplied by Sigma-Aldrich. Bio-Rad Clarity Western ECL substrate was purchased from Bio-Rad (Alcobendas - Madrid, Spain).

Fura-2 acetoxyethyl ester (Fura2 AM) and Pluronic® F-127 were purchased from Biotium (Hayward, CA, USA) and Invitrogen, respectively. Nifedipine was supplied by Sigma- Aldrich (Madrid, Spain). Protein A/G PLUS-Agarose sc-2003 was obtained from Santa Cruz Biotechnology Inc. (Santa Cruz, CA, USA). All other reagents and chemicals were of analytical grade from Sigma-Aldrich (Madrid, Spain) or Roche–Merck (Darmstadt, Germany).

3.2 Preparation of rat CGN

CGNs were prepared from 7-day-old Wistar rats as previously described ^{27,36,40}. Animal care and experimental procedures were performed in accordance with the Spanish regulations and approved by the Ethical Committee of the University of Extremadura.

Cells were plated at a density of 2.5×10^6 cells/dish in Dulbecco's Modified Eagle medium (DMEM) supplemented with 10% heat-inactivated fetal bovine serum, 5 mM glucose, 19.63 mM KCl, 3.7 ng/mL insulin, 7 μ M 4-aminobenzoic acid, 50 U/mL penicillin, 25 U/mL

streptomycin, 0.91 mM pyruvate, and 2 mM glutamine on 35 mm diameter dishes (Corning, NY, USA) coated with poly-D-lysine. Forty-eight hours after plating (2 days *in vitro* – DIV2) CGN were treated with 10 µM cytosine arabinofuranoside to prevent the replication of non-neuronal cells. At DIV7, the culture medium was replaced with the serum-free DMEM:F12 medium (1:1) supplemented with 12.5 mM glucose, 20.82 mM KCl, 5 µg/mL insulin, 0.1 mg/mL apo-transferrin, 20 nM progesterone, 50 U/mL penicillin, 25 U/mL streptomycin, 0.1 mg/mL pyruvate, and 2 mM L-glutamine. CGN cultures were kept at 37 °C in a humidified atmosphere of 95% air/ 5% CO₂ and mature CGN at DIV8-10 were used in all the experiments.

The MLocke's K25 buffer composition (pH 7.4 at 37 °C) was as follows: 4 mM NaHCO₃, 10 mM Tricine, 5 mM glucose, 2.3 mM CaCl₂, 1 mM MgCl₂, 134 mM NaCl and 25 mM KCl.

3.3 Aβ(1–42) solutions and aggregation state

Unlabeled Aβ(1–42), scrambled Aβ(1–42) and human Aβ(1–42)*555 stock solutions were prepared by dissolving the solid lyophilized peptide in 1% NH₄OH, and then diluted with PBS to the desired concentration²². The aggregation states of Aβ(1–42) stock solutions used in this work were evaluated using the rapid photoinduced cross-linking of unmodified proteins approach as described in other works^{48,49}. Briefly, 177 µM of Aβ(1–42) was diluted in 60 mM NaOH and 10 mM phosphate (pH 7) and sonicated in a water bath (Selecta Ultrasons) at 150 watts for 1 min and then centrifuged at 16,000 g during 10 min. The supernatants were collected and treated with 60 µM Tris(2,2'-bipyridyl)dichloro-ruthenium(II) hexahydrate and 4.4 mM (NH₄)₂S₂O₈ and then placed in the sample compartment of a Perkin-Elmer 650-40 fluorimeter (Perkin-Elmer, Waltham, MA, USA) and irradiated at 452 nm emitted by the fluorimeter 150 watts Xenon lamp during 1 s at room temperature (RT). Afterwards, the reaction was stopped by the addition of β-mercaptoethanol (5% v/v) plus sample buffer [95 mM tris-(hydroxymethyl) aminomethane (Tris)-HCl buffer, pH 6.8/ 3% sodium dodecyl sulfate (SDS)/13% glycerol, and 0.005% bromophenol blue] and heated at 37°C during 15 min. Samples were loaded into the gradient Tricine-SDS-polyacrylamide gel and run as previously described⁵⁰.

3.4 Cell viability

Mature CGN were treated with different concentrations of Aβ(1–42) (0.75-5 µM) in serum-free DMEM:F12 medium at 37 °C and 5% CO₂. After 48 h incubation, CGN plates were washed once with 1 mL MLocke's K25 buffer to remove the excess of culture media and cell viability was measured by addition of MTT [3-(4,5-dimethylthiazol-2-yl)-2,5-diphenyltetrazolium

bromide] as described in previous works of our lab^{27,36,51,52}. Untreated cells were regarded as controls (100% cell survival) and the cell survival ratio was expressed as the percentage of the control.

3.5 Co-Immunoprecipitation

CGN lysates were prepared in lysis buffer [25 mM Tris–HCl, pH 7.4, 150 mM NaCl, 5 mM ethylenediaminetetraacetic acid (EDTA), 50 mM NaF, 5 mM NaVO₃, and 0.25% 4-(1,1,3,3-tetramethyl butyl) phenyl-polyethylene glycol (Triton X-100), supplemented with 1x SIGMAFAST™ protease inhibitor cocktail] plus 50% glycerol (v/v). Thereafter, the protein concentration was determined using the Bradford's protocol and samples were kept at -80°C until use.

Before co-immunoprecipitation experiment, CGN lysates were incubated with 10 mM of methyl-β-cyclodextrin (MβCD) during 30 min at 4 °C with continuous shaking. The procedure used for co-immunoprecipitation is described in the technical data sheet of protein A/G PLUS-Agarose. Briefly, lysates (200 µg) were incubated with 5 µg mouse anti-Aβ antibody at 4°C with continuous mixing for 1 h. Then, samples were incubated overnight with 65 µL of protein A/G PLUS-Agarose, at 4°C with continuous shaking. In the next day, control sample was incubated with phosphate buffered saline (PBS) and treated sample was incubated with 250 nM Aβ(1–42) in PBS for 1 h at 4°C with continuous shaking. After centrifugation at 2500 × g during 5 min at 4°C, the supernatant was removed and the precipitated matrix was washed three times with 50 µL PBS (control sample) or 50 µL PBS plus 250 nM Aβ(1–42) (treated sample) and centrifugated (2500 × g, 5 min at 4 °C) between each washing step. At the end, the supernatant was discarded and the matrix was resuspended in 80 µL of electrophoresis sample buffer and boiled for 3 min. Samples were stored at –20 °C until running on a SDS–polyacrylamide gel electrophoresis (SDS-PAGE) for western blotting analysis.

3.6 Western blotting

Depending on the molecular weights of the target proteins, SDS-PAGE were run at concentrations of 7.5%, 10.4%, 13.5% or 15% acrylamide, with 20 µg CGN lysates or 15–20 µL co-immunoprecipitated sample per lane. After gel transference to PVDF (polyvinylidene difluoride) membranes (0.2 µm pore size), the blocking step was performed with 3% BSA in Tris-buffered saline (TBS) supplemented with 0.05% polyoxyethylene sorbitan monolaurate (TBST) for 1 h at RT. Next, membranes were washed six times with TBST (washing step) and incubated

with the respective primary antibody at the dilution of 1:1000 in TBST for anti-Cav1, anti-HRas, and anti-LTCC antibodies and at a dilution of 1:2000 in TBST for anti-CaM and anti-cellular prion protein (PrPc) antibodies. After incubation overnight at 4°C, membranes were submitted to the washing step and incubated with the appropriate secondary IgG antibody conjugated with horseradish peroxidase at a dilution of 1:5000 in TBST, for 1 h at RT. Finally, PVDF membranes were washed (washing step), incubated with the Bio-Rad Clarity Western ECL substrate and Western blots were revealed with Bio-Rad ChemiDocTM XRS+ (Bio-Rad, Hercules, CA, USA). Data was analyzed with Image Lab 6.0.1 software.

3.7 Measurements of internalization of A β (1–42)-HiLyte™-Fluor555 in mature CGN

The internalization of A β (1–42) was measured by fluorescence microscopy with A β (1–42)-HiLyte™-Fluor555 (A β (1-42)*555) as described in other works^{15,53}. The amount of internalized A β (1–42) was determined from the increase in red fluorescence (RF) intensity in CGN somas at different times of incubation (up to 2 h) at 37 °C and 5% CO₂ with a total concentration of 2 μ M of A β (1–42) (1.8 μ M of unlabeled A β (1–42) monomers plus 0.2 μ M of A β (1-42)*555 monomers) added to the serum-free DMEM:F12 medium. After incubation, the medium was replaced by MLocke's K25 and the CGN plates were placed in the holder of the thermostated fluorescence microscope (37°C). Image acquisition was performed with a Hamamatsu Orca-R2 CCD camera (Hamamatsu, Hamamatsu-city, Japan; binning mode 2 \times 2) attached to a Nikon Diaphot 300 epifluorescence microscope (Tokyo, Japan) with a NCF Plan ELWD 40 \times objective, using an excitation filter of 556 nm and a dichroic mirror of 580 nm with an emission filter of 590 nm, and 0.03 s exposure time. The quantitative analysis was done with HClImage software using the region of interest (ROI) tool of the selected neuronal soma.

In parallel experiments, increasing concentrations of A β (1-42)*555 in Mlocke's K25 in the Petri plate was recorded for calibration of the A β (1-42)*555 fluorescence under the same experimental conditions as earlier described. The average intensity readings per pixel in CGN neuronal somas were taken from several fields for a total number of 102 cells, and after subtraction of CGN autofluorescence.

3.8 Fluorescence Resonance Energy Transfer (FRET) imaging

FRET imaging was performed as in previous works of our lab^{27,52,54}. First, CGN were washed with MLocke's K25 and then cells were fixed in the petri plates [2.5% paraformaldehyde, 3 mM MgCl₂, 2 mM EDTA, and 0.32 M sucrose in PBS (5 mM sodium phosphate,

137 mM NaCl and 27 mM KCl, pH 7)]. After, CGN were blocked with 1% BSA in PBS supplemented with 0.2% Triton X-100 (PBST) for 1 h at 37 °C, washed three times with PBS (washing step) and then incubated during 1 h at 37 °C with the target primary antibody in PBS. The primary antibodies used in FRET experiments were: rabbit anti-CaM (1:200), goat anti-HRas (1:100), rabbit anti-Cav1 (1:100), mouse anti-PrPc (1:100), and rabbit anti-LTCC α 1C subunit (1:50). Then, cells were washed (washing step) and incubated with the appropriate Alexa488-labeled secondary antibody in PBST (1:200) for 1 h. Afterwards, cells were washed (washing step) and placed at the holder of the fluorescence microscope for image acquisition of cells only with the donor dye. Images of CGN were acquired with an excitation filter of 470 nm, and 510 nm dichroic mirror/520 nm emission filter (green fluorescence, GF), using the exposure times indicated for each case in the legends for the figures. Of note, the specificity of primary antibodies for the selected target proteins was first assessed by the presence of the major/most intense band at the expected protein molecular weight in the western blotting run with CGN lysates. In most cases, this band accounts for more than 90% of the total band staining (see Supplementary Figure S.1).

After finishing the acquisition of FRET donor images, CGN were incubated with 50 or 100 nM A β (1-42)*555 in PBS for 60 min at 37 °C with gentle mixing. Then, plates were placed at the holder of fluorescence microscopy for cell imaging. Contribution of CGN autofluorescence and secondary Alexa488-antibody in the absence of the primary antibody were also assessed and we found to be lower than 10% of the average fluorescence intensity per pixel obtained with specific primary antibodies. The background signal was subtracted to determine RF/GF ratio obtained with CGN plates. Due to the close absorbance spectrum of Cy3 fluorescent antibody and A β (1-42)*555, significant FRET efficiency using this experimental approach implies that the selected protein was separated by less than 50 nm from A β (1-42)*555, as discussed in detail in previous works^{27,40}.

Regarding FRET imaging using a fluorescent acceptor antibody bound to another protein target (e.g., CaM stained with a Alexa488 fluorescent secondary antibody as donor and HRas stained with a Cy3 fluorescent secondary antibody as acceptor) we used the protocol described in other publications of our laboratory^{27,40}. Briefly, after finishing the acquisition of FRET donor images, CGN were incubated for 1 h at 37 °C with the acceptor target primary antibody as indicated above, washed three times with PBS (washing step), then incubated for 1 h with the appropriate Cy3-labeled secondary antibody in PBST (1:200), and washed again for further image acquisition. Controls were also run in the absence of the second primary antibody to correct for partial loss of the donor fluorescence produced by the treatment to label the second protein, on average between 20 and 25% loss of the donor fluorescence, and also to subtract

background signals. Quantitative analysis of the average fluorescence intensity per pixel of selected neuronal soma was done with the HClImage software using the ROI tool, as in previous works. The mean \pm s.e. intensity reading of fluorescence per pixel within CGN somas were obtained in experiments performed in triplicate ($n > 100$ CGN somas in each case). As discussed in previous works^{27,55} significant FRET efficiency using this experimental approach implies that the selected proteins were separated by ≤ 80 nm.

3.9 Measurement of the intracellular free Ca²⁺ Concentration ([Ca²⁺]_i)

[Ca²⁺]_i was measured as in previous works^{27,34,36,51}. Briefly, mature CGN were treated with 2 μ M A β (1–42) for 2 h or 5 h at 37 °C and 5% CO₂ with continuous and gentle mixing. Before the end of the incubation with A β (1–42), CGN were loaded with 5 μ M Fura2 AM plus 0.025% Pluronic® F-127 at 37 °C for 1 h. Afterwards, cells were washed twice with 1 mL MLocke's K25 buffer and petri dishes placed at the thermostatic holder (37°C) of the Nikon Diaphot 300 inverted epifluorescence microscope. Image acquisition was recorded with 340 and 380 nm excitation filters and a 510 nm dichroic mirror/520 nm emission filter with a Hamamatsu Orca-R2 CCD camera (binning mode 2 \times 2) and Lambda 10–2 filter wheel controller and subsequently analyzed with HClImage software. [Ca²⁺]_i was calculated, using the following equation: [Ca²⁺]_i = kD \times [(R - R_{min})/(R_{max} - R)], where R is the measured fluorescence ratio (340/380), and R_{max} and R_{min} are the ratio values (340/380) for Ca²⁺-bound and Ca²⁺-free Fura2-loaded CGN. R_{max} and R_{min} were experimentally determined from steady-state fluorescence ratio (340/380) measurements after sequential addition to the culture medium of Fura2-loaded CGN of (1) nonfluorescent Ca²⁺ ionophore 4-Bromo-A23187 (5 μ g/ml) or ionomycin (5 μ g/ml), and (2) 10 mM EGTA, respectively. To obtain the values of [Ca²⁺]_i we used the reported dissociation constant (kD) Fura2/Ca²⁺ of 224 nM⁵⁶.

To block LTCC activity we added 10 μ M of nifedipine to the extracellular medium of Fura2-loaded CGN. The 340/380 ratio data given in this work were population averages \pm s.e. intensity reading of fluorescence per pixel within CGN somas obtained using the ROI tool of the HClImage software ($n > 100$ CGN somas in each case).

3.10 Statistical Analysis

Statistical analysis was carried out by the Student's t-test and results were expressed as the mean standard error (s.e.). A significant difference was accepted at the $p < 0.05$ level. All

results were confirmed with duplicate measurements of at least three different CGN preparations.

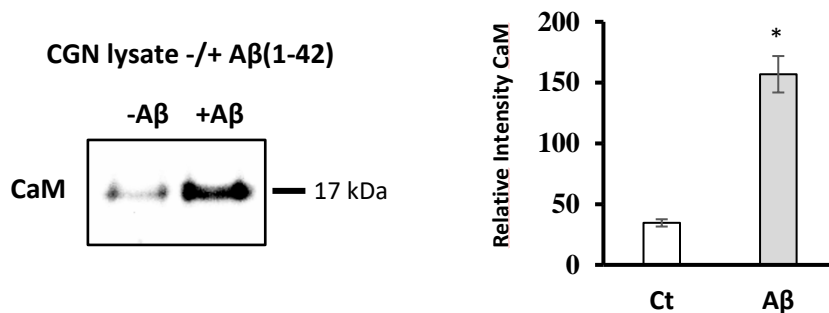
4. Results

4.1 Co-Immunoprecipitation of CaM with submicromolar concentrations of A β (1–42) in CGN lysates

As demonstrated in a previous work of our lab, the kD value of the complex A β (1–42) with purified CaM is around 1 nM²², highlighting that CaM could be a major target for nanomolar concentrations of A β (1–42) in neurons. In this study, we demonstrated the formation of CaM-A β (1–42) complexes in mature CGN (**Figure 1A**) using the co-immunoprecipitation method described in the experimental section of Materials and Methods. After CGN treatment with 10 mM M β CD for 30 min to solubilize and dissociate the proteins in lipid rafts, the formation of CaM-A β (1–42) complexes were demonstrated by the co-immunoprecipitation of CaM with the anti-A β (1–42) antibody in CGN lysates in the presence of 250 nM A β (1–42). Besides the complexation of CaM-A β (1–42), the western blotting in **Figure 1A** shows also a small fraction of CaM molecules in the absence of A β (1–42), which can be explained by its association with poorly solubilized membrane fragments, because as mentioned before CaM binds with high affinity to several proteins that are associated with lipid rafts, such as PMCA^{27,57}, LTCCs^{40,55} and CaMKII^{36,37}.

We quantified the total amount of CaM in CGN lysates by Western blotting using known concentrations of purified CaM and CGN lysates and the results yielded 5.5 ± 0.5 ng of CaM/ μ G of CGN protein (**Figure 1B**). As the 35 mm Petri dishes are seeding with 2.5×10^6 CGN cells, which correspond to 170 ± 20 μ g of CGN protein per plate approximately, we calculated an average of 935 ± 110 ng of CaM per plate (i.e., 56 ± 6 picomoles of CaM per plate). The state of aggregation of A β (1–42) solutions used in this work was determined as described in Materials and Methods section. Results (**Figure 2**) show a major band of a molecular weight close to 9 kDa and a faint band of molecular weight between 12 and 15 kDa. As the monomer molecular weight of A β (1–42) is approximately 4.5 kDa, these results indicate that dimers were the predominant aggregation state of A β (1–42) in the stock solutions used in this work, with a minor (<10%) contribution of trimers, implying that each petri dish contains up to 120 ± 13 picomoles of A β (1–42) that can be bound by CaM. It is also noted that A β (1–42) monomers were not detected in our stock solutions.

A) Co-immunoprecipitation of CaM with A β (1-42)



B) Quantification of CaM in CGN lysates

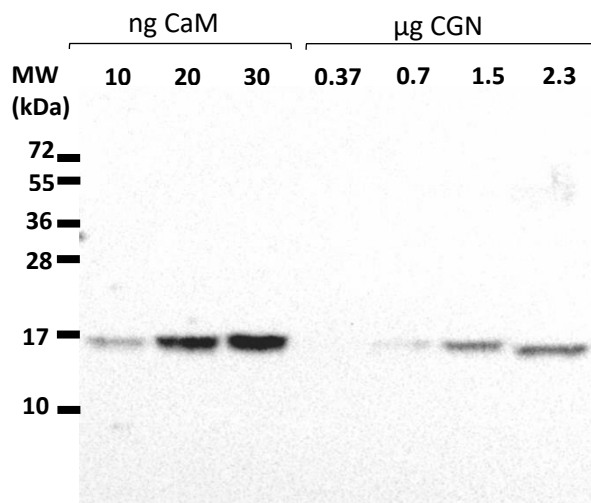


Figure 1. Co-immunoprecipitation between calmodulin (CaM) and A β (1–42) in CGN. **A)** Western blotting of CaM (anti-CaM) after co-immunoprecipitation assay with mouse anti-A β antibody in the absence and presence of 250 nM A β (1-42). **B)** Quantification of CaM content in CGN lysates using known concentrations of purified CaM by Western blotting of CaM.

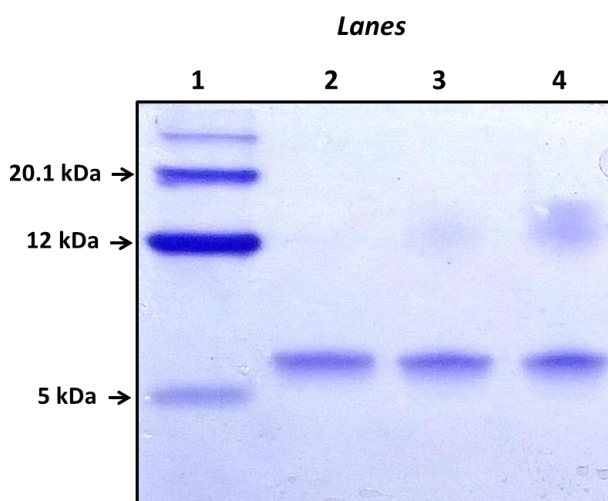


Figure 2. Gradient Tricine-SDS PAGE of A β (1-42) solutions used in this work. Lanes: (1) Low molecular weight markers; (2) 177 μM A β (1-42) in PBS supplemented with 60 mM NaOH after preincubation during 2 h at 37°C; (3) 177 μM A β (1-42) in PBS after preincubation during 2 h at 37°C; (4) 177 μM A β (1-42) in PBS without preincubation at 37°C. Molecular weight of the A β (1-42) monomer = 4.514 kDa.

4.2 Extensive co-localization between CaM and A β (1–42) HiLyteTM-Fluor555 (A β (1–42)*555) in mature CGN demonstrated by Fluorescence Resonance Energy Transfer (FRET) imaging

We used FRET imaging technique to assess the spatial proximity between A β (1–42)*555 and CaM in fixed CGN. First, we had to experimentally define the optimal concentration of A β (1–42)*555 in order to highlight only the subcellular location of the high affinity binding sites for A β (1–42), and for that purpose we used i) the lowest A β (1–42)*555 concentration as possible and ii) an excitation filter of 470 nm as an alternative of 556 nm to minimize the background fluorescence obtained from the binding of A β (1–42)*555 to the Petri plate.

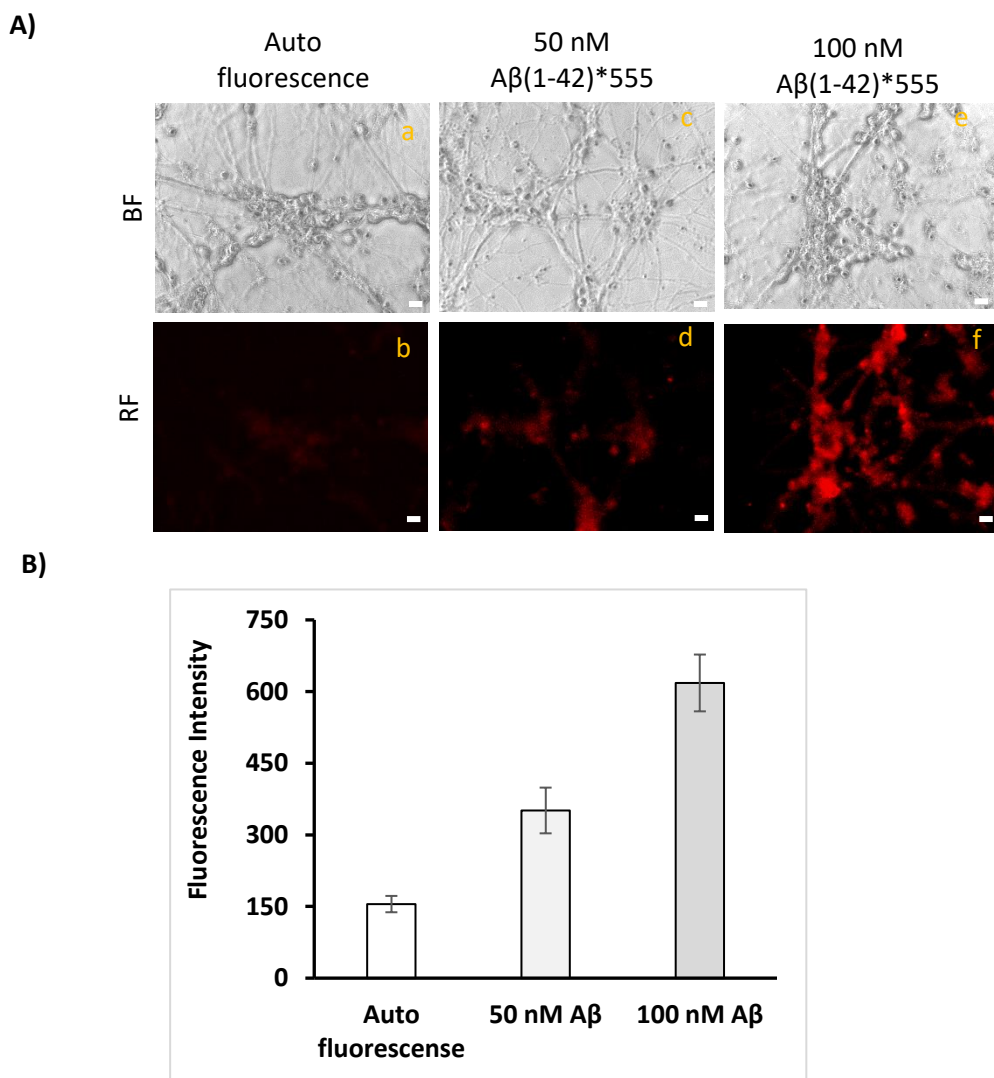


Figure 3. Fluorescence microscopy analysis of fixed CGN stained with A β (1–42)*555. (A) Representative Fluorescence microscopy images of mature CGN without staining-autofluorescence (b) and CGN stained with 50 nM (d) or 100 nM (f) of A β (1–42)*555 incubated for 1 h at 37 °C and 5% CO₂. Bright field (BF) and RF images are shown for representative selected fields. The exposure time for RF images was 0.4 s. Scale bar inserted in fluorescence microscopy images = 10 μ m. (B) Quantitative fluorometric analysis of A β (1–42)*555 bound to CGN. The results yielded a 2.3-fold and 4-fold increase (mean of triplicate experiment

\pm s.e.) of the fluorescence of CGN stained with 50 nM and 100 nM A β (1–42)*555 with respect to the CGN autofluorescence, respectively.

Representative fluorescence microscopy images of CGN stained with 50 and 100 nM of A β (1–42)*555 as well as CGN autofluorescence (without A β (1–42)*555 treatment) are presented in **Figure 3A**, and the quantitative fluorometric analysis (mean of triplicate experiment) are presented in the **Figure 3B**. The results showed that 50 and 100 nM of A β (1–42)*555 gave a fluorescence intensity significantly higher than the CGN autofluorescence, yielding a 2.3 and 4-fold increase in the fluorescence signal, respectively. Aiming to minimize as much as possible the endogenous contribution of red autofluorescence of CGN, we selected a concentration of 100 nM of A β (1–42)*555 for FRET experiments.

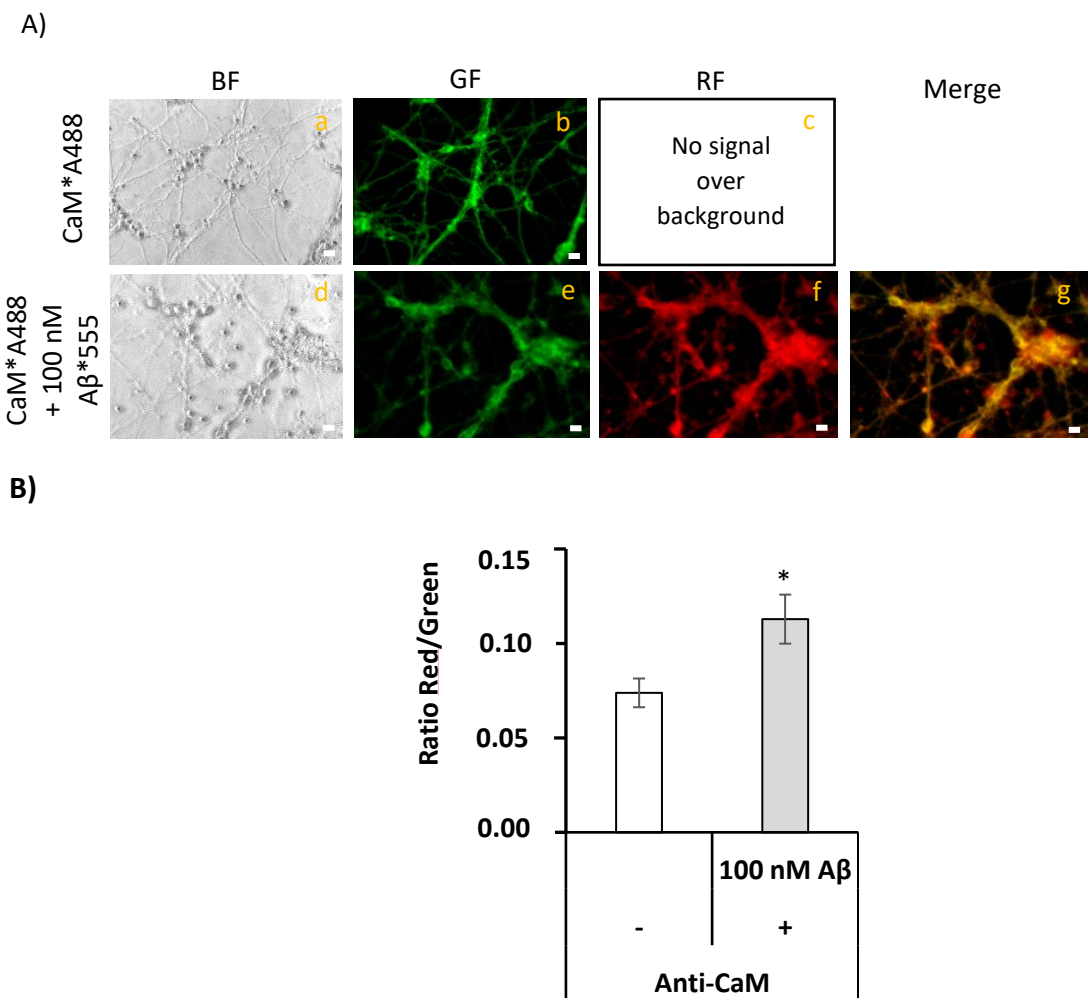


Figure 4. Extensive FRET between anti-CaM antibody stained with a secondary Alexa488 fluorescent antibody and A β (1–42)*555 in fixed and permeabilized mature CGN. (A) Representative fluorescence microscopy images of CGN stained with anti-CaM antibody/ IgG-Alexa488 (CaM* $A488$, a–c) or with anti-CaM/IgG-Alexa488 plus A β (1–42)*555 (CaM* $A488$ / $A\beta^*555$), d–g). BF, GF, and RF images are shown for each one of the selected fields, and the orange-yellow areas (Merge image, g) point out the higher intensity FRET regions. The exposure time for GF and RF images was 0.03 s. Scale bar inserted in fluorescence microscopy images = 10 μ m. (B) Ratio of red/green fluorescence intensity per pixel (RF/GF)

obtained from the analysis of the fluorescence intensity data of CGN somas stained with anti-CaM*IgG-Alexa488 only (CaM*A488) and double stained with anti-CaM*IgG-Alexa488/A β (1-42)*555 (CaM*A488/A β *555). The results shown in (B) are the mean \pm s.e. (*) $p < 0.05$ (i.e., statistically significant with respect to the control (CGN labeled with the Alexa488 FRET donor only)).

Furthermore, part of A β (1-42)*555 were adsorbed non-specifically to the plastic of the Petri dish, which decreases the concentration of A β (1-42)*555 available to bind to the CGN cells. To quantify this unspecific adsorption, 100 nM of A β (1-42)*555 was added to a Petri plate with 1 mL of MLocke's K25 buffer and incubated under mild stirring for 30 min.

The amount of A β (1-42)*555 free in the Petri dish was measured in quartz fluorescence cuvettes in a fluorimeter with excitation and emission wavelengths of 550 and 573 nm and compared with the fluorescence intensity of standard solutions of A β (1-42)*555 prepared directly in the quartz cuvette. We calculate that the free and available concentration of A β (1-42)*555 for binding to CGN cells was half (50 nM of A β (1-42)*555) the total A β (1-42)*555 added to the Petri dish.

FRET imaging was assessed with anti-CaM conjugated with IgG-Alexa 488 (anti-CaM*A488) to experimentally confirm the formation of CaM-A β (1-42) complexes. The **Figure 4A** shows representative fluorescence microscopy images of mature CGN fixed and stained with anti-CaM*A488 in the absence and presence of 100 nM of A β (1-42)*555. The merged image (**Figure 4Ag**) highlights an extensive co-localization (0.2 μ m of pixel size) between anti-CaM*A488 and A β (1-42)*555, both in the neuronal somas and extensions. As demonstrated in **Figure 4B**, the increase in the red/green fluorescence intensity ratio after subtraction of the red intensity by direct excitation of A β (1-42)*555 shows that most of the anti-CaM*A488 molecules lay within an efficient FRET distance range with A β (1-42)*555 (i.e., < 50 nm) for this donor-acceptor pair. Furthermore, after addition of 5 mM CoCl₂ to the Petri plate, we observed about 80% quenching of the RF intensity derived from A β (1-42)*555, yielding RF microscopy images like the CGN autofluorescence image shown in **Figure 3Ab**. Of note, the inner filter effect due to the absorbance of 5 mM Co²⁺ in the wavelength range 470–550 nm, calculated as indicated in the Materials and Methods section, can only account for less than 5% quenching of this fluorescence. At millimolar concentration, Co²⁺ is a well Ca²⁺ channel blocker and also binds to Ca²⁺ sites in proteins^{58,59}. Co²⁺ has a R₀ value of 1.2 nm as the FRET acceptor of the green fluorescence of fluorescein⁶⁰. Therefore, due to the small CaM size, our results were fully consistent with the extensive complexation of A β (1-42)*555 with CaM shown by FRET imaging in CGN.

4.3. FRET imaging highlights the association of A β (1-42)*555 and CaM with lipid rafts markers in mature CGN

Aiming to experimentally assess if A β (1-42)*555 co-localize with lipid rafts of mature CGN, we used antibodies against the protein markers of CGN lipid rafts matured *in vitro*: Cav1 and HRas²⁷. We also used the antibody against PrPc, which is also a neuronal marker of lipid rafts that has been shown to form complexes with A β ^{61,62}. Representative fluorescence microscopy images of CGN stained with anti-Cav1 conjugated with IgG-Alexa 488 (anti-Cav1*A488), anti-HRas conjugated with IgG-Alexa 488 (anti-HRas*A488), and anti-PrPc conjugated with IgG-Alexa488 (anti-PrPc*A488) in the absence and presence of 100 nM of A β (1-42)*555 are shown in the **Figure 5A–C**. In all cases, the addition of A β (1-42)*555 caused a large attenuation of the GF and a significant increase in RF intensity that was higher than the fluorescence intensity obtained derived from direct excitation of the A β (1-42)*555. The **Figure 5D** shows the mean of the red/green fluorescence intensity ratio after correction for the RF due to direct excitation of A β (1-42)*555 and results show extensive FRET between anti-Cav1, anti-HRas, and anti-PrPc and the Fluor555 dye bound to A β (1-42).

It is important to highlight that the donor/acceptor FRET pair with a higher increase in the ratio intensity was anti-PrPc*A488/A β (1-42)*555. This result is in good agreement with the formation of complexes reported elsewhere between PrPc and A β and also with the fact that in this work we did not observed co-immunoprecipitation between Cav1 and HRas with A β (1-42) in GCN lysates (see **Supplementary Figure S.2**). In addition, the merge images also point out for a higher intensity of lipid rafts in neuronal somas, since the extensions are less stained with the protein markers anti-Cav1*A488, anti-HRas*A488 and anti-PrPc*A488, which confirm the results obtained in previous works with anti-Cav1 and anti-HRas^{27,40}. All together, these findings confirmed an extensive association of A β with lipid rafts of mature CGN.

The **Figure 6A** shows representative fluorescence microscopy images of CGN stained with anti-CaM conjugated with IgG-Alexa 488 (anti-CaM*A488), anti-HRas conjugated with IgG*Cy3 (anti-HRas*Cy3), and with both anti-CaM*A488 and anti-HRas*Cy3. There is an extensive co-localization between CaM and HRas showed by the merge image (**Figure 6Ag**), because pixels that maintain the original green and red colors are hardly seen. The large increase in the red/green ratio of fluorescence intensities in CGN double stained with anti-CaM*A488 and anti-HRas*Cy3 with respect to CGN stained only with anti-HRas*Cy3 (**Figure 6B**) pointed out a high efficiency of FRET between Alexa 488 and Cy3. Therefore, these results showed that most of the anti-CaM*A488 and anti-HRas*Cy3 bound to fixed CGN were within the FRET distance using this experimental approach (i.e., < 80 nm^{27,55}).

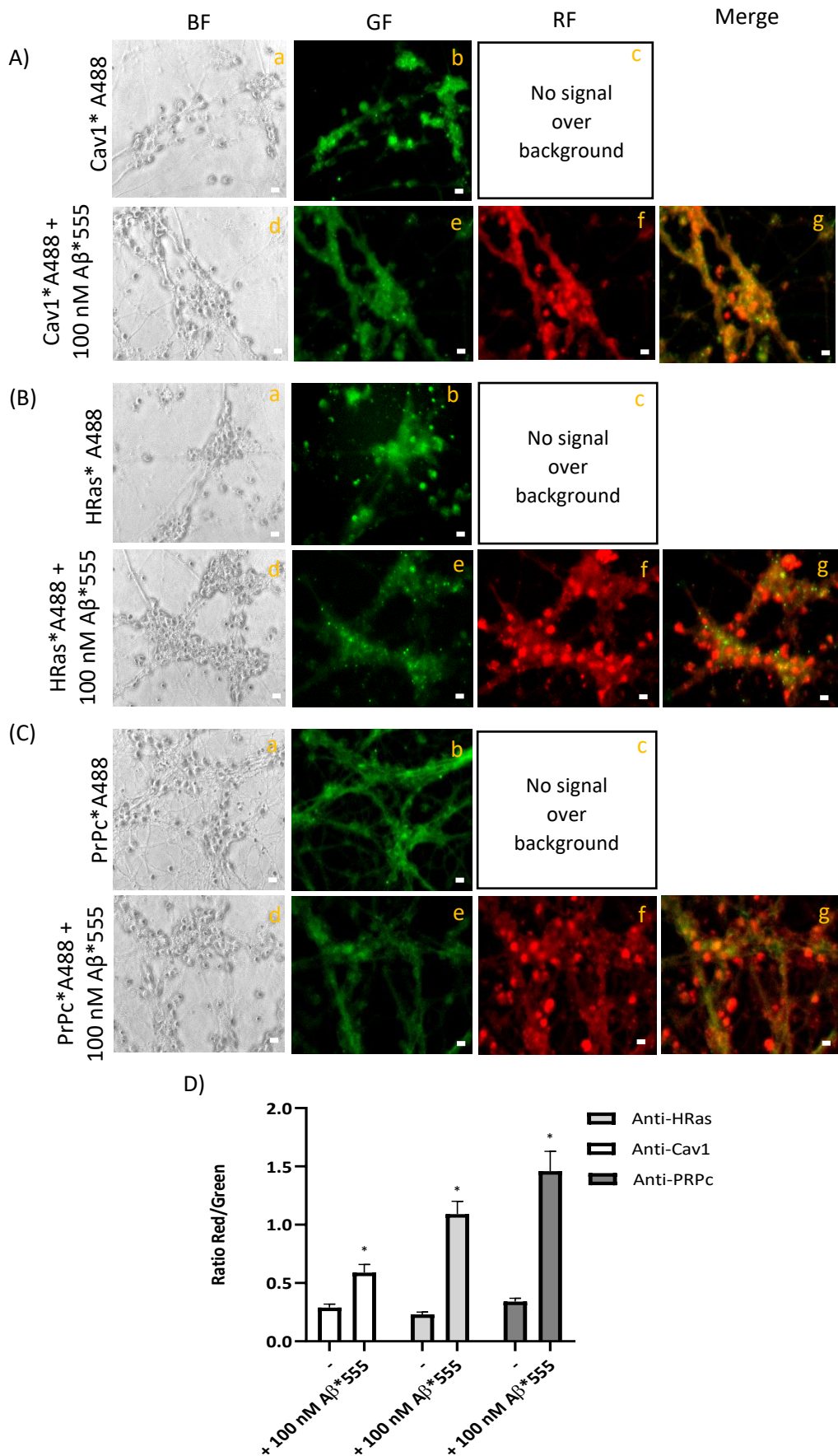


Figure 5. Extensive FRET between the lipid rafts markers Cav1, HRas, PrPc, and A β (1–42)*555.
A) Representative quantitative fluorescence microscopy images of CGN stained with anti-Cav1

antibody/IgG-Alexa488 (Cav1*A488, a–c) or with anti-Cav1/IgG-Alexa488 and A β (1-42)*555 (Cav1*A488/A β *555, d–g). **B)** Representative quantitative fluorescence microscopy images of CGN stained with anti-HRas antibody/IgG-Alexa488 (HRas*A488, a–c) or with anti-HRas/IgG-Alexa488 and A β (1-42)*555 (HRas*A488/A β *555, d–g). **C)** Representative quantitative fluorescence microscopy images of CGN stained with anti-PrPc antibody/IgG-Alexa488 (PrPc*A488, a–c) or with anti-PrPc/IgG-Alexa488 and A β (1-42)*555 (PrPc*A488/A β *555, d–g). Bright-field (BF), green fluorescence (GF), and RF images are shown for each of the selected fields, and the orange-yellow areas (merge image) point out the higher intensity FRET regions (g, (A–C)). The exposure time for GF and RF images was 0.4 s. Scale bar inserted in fluorescence microscopy images = 10 μ m. **D)** Ratio of red/green fluorescence intensity per pixel (RF/GF) obtained from the analysis of fluorescence intensity data of CGN somas stained with (i) anti-Cav1/IgG-Alexa488 only (Cav1*A488) and double stained with anti-Cav1*IgG-Alexa488/A β (1-42)*555 (Cav1*A488/A β *555); (ii) anti-HRas/IgG-Alexa488 only (HRas*A488) and double stained with anti-HRas*IgG-Alexa488/A β (1-42)*555 (HRas*A488/A β *555); and (iii) anti-PrPc/IgG-Alexa488 only (PrPc*A488) and double stained with anti-PrPc*IgG-Alexa488/A β (1-42)*555 (PrPc*A488/A β *555). The results shown in panel D are the mean \pm s.e.(*) $p < 0.05$, (i.e., statistically significant with respect to the control, CGN labeled with the Alexa488 FRET donor only).

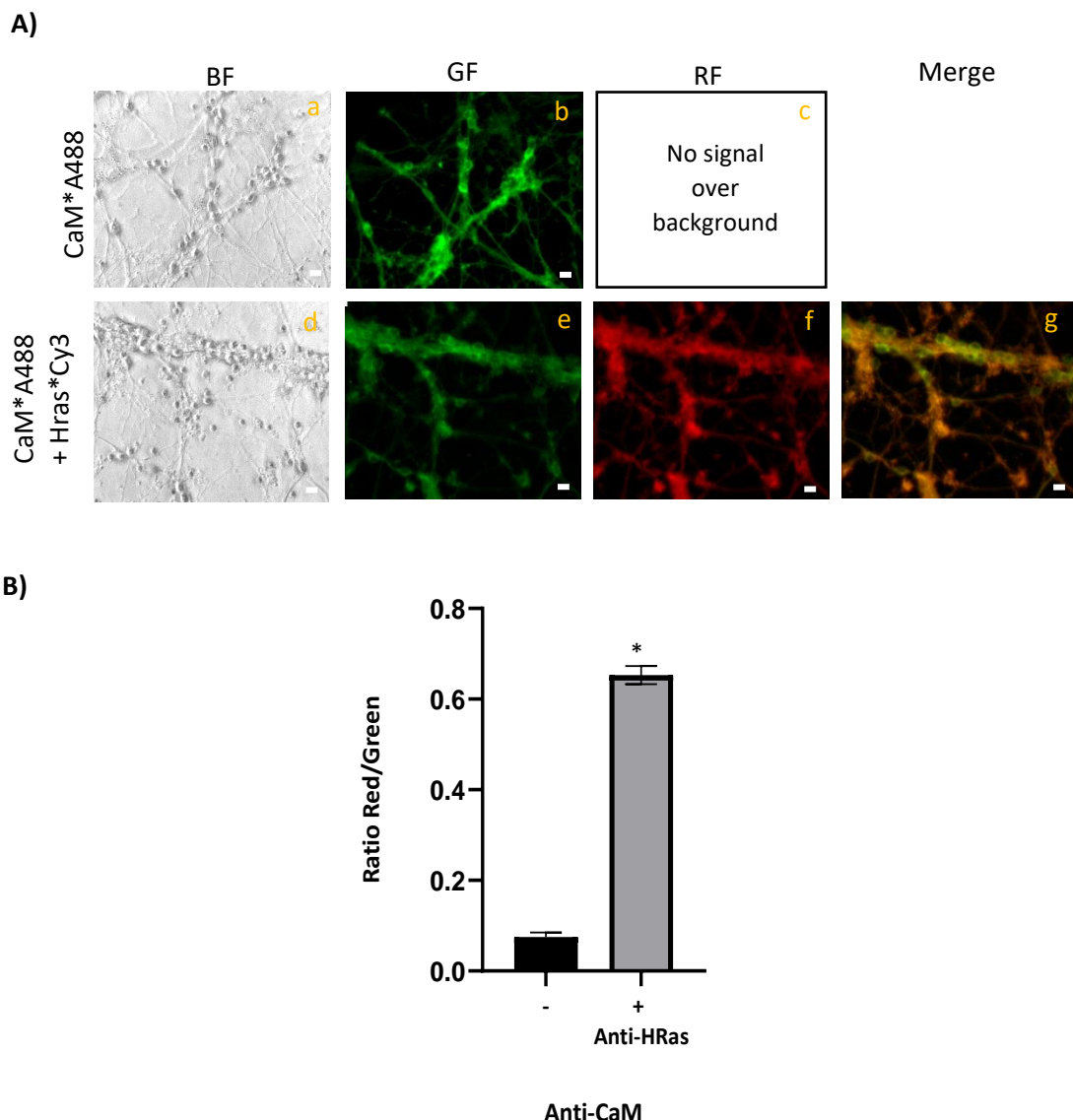


Figure 6. Extensive FRET between CaM and HRas. **A)** Representative quantitative fluorescence microscopy images of CGN stained with the anti-CaM antibody/IgG-Alexa488 (CaM*A488, a–c) or with anti-CaM/IgG-Alexa488 and Anti-HRas antibody/IgG-Cy3 (CaM*A488/HRas*Cy3, d–g). BF, GF, and RF

images are shown for each of the selected fields, and the orange-yellow areas (Merge image, g) point out the higher intensity FRET regions. The exposure time for GF and RF images was 0.05 s. Scale bar inserted in fluorescence microscopy images = 10 μ m. **B)** Ratio of red/green fluorescence intensity per pixel (RF/GF) obtained from the analysis of fluorescence intensity data of CGN somas stained with anti-CaM/IgG-Alexa488 only (CaM*A488) and double stained with anti-CaM*IgG-Alexa488/anti-HRas*IgG-Cy3 (CaM*A488/ HRas*Cy3). The results are the mean \pm s.e. (*) $p < 0.05$ (i.e., statistically significant with respect to the control, CGN labeled with the Alexa488 FRET donor only).

4.4. A short time incubation with submicromolar concentrations of A β (1–42) decreases the resting cytosolic Ca $^{2+}$ concentration through inhibition of LTCCs in mature CGN

The cell viability assay of mature CGN incubated for 48 h with different concentrations of A β (1-42) showed at most 10-20% loss of cell viability up to 5 μ M with A β (1-42) (**Figure 7**).

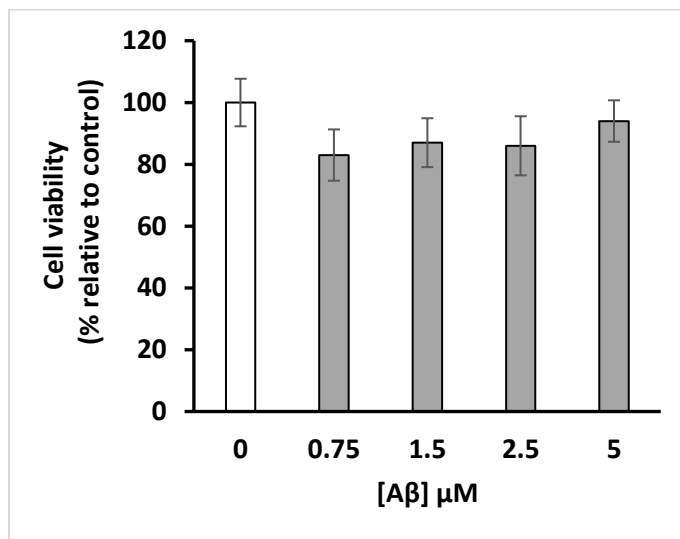


Figure 7. The cell viability of mature CGN was not significantly affected by A β (1–42) at the concentrations tested (0.75–5 μ M) after 48 h of incubation. Cell viability was measured using the MTT assay as indicated in the Materials and Methods section. The results were the average \pm s.e. of experiments done in triplicate, with two different preparations of CGN.

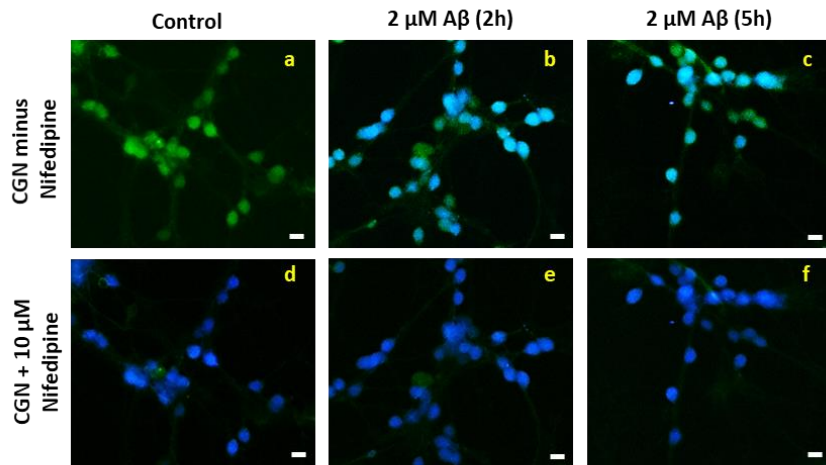
These results allowed us to study the effect of cytosolic Ca $^{2+}$ dysregulation induced by A β (1-42) after incubation in mature CGN for several hours and with micromolar concentrations of this peptide. Nevertheless, we selected a shorter time of incubation (up to 5h) and an extracellular micromolar concentration of 2 μ M A β (1-42) to be able to study the effect of submicromolar concentrations of this peptide on resting Ca $^{2+}$ concentration, because it has been shown that small oligomeric states of this peptide are internalized in neurons with a half-time of 12–14h¹⁵.

After 2 h and 5 h incubation of GCN with 2 μ M A β (1-42) we observed a statistically significant decrease of Fura2 ratio (340/380) from 1.1 \pm 0.1 (control) to 0.71 \pm 0.07 (treated cells

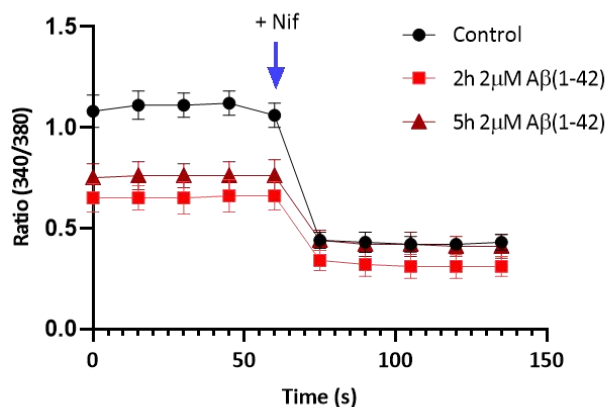
with A β (1-42)) ($p < 0.05$), in other words, A β (1-42) induced a decrease of intracellular Ca²⁺ concentration ([Ca²⁺]_i) from 160 ± 30 nM to 71 ± 7 nM (**Figure 8**). In addition, the LTCC blocker nifedipine did not significantly change the ratio (340/380) of control and CGN cells treated with A β (1-42), demonstrating that A β (1-42) reduces the specific contribution of LTCCs to the resting cytosolic Ca²⁺ concentration in mature CGN in MLocke's K25 medium. In fact, the difference between the ratio (340/380) in the absence and presence of nifedipine decreased from 0.64 in CGN nontreated with A β (1-42) to 0.30 and 0.32 in CGN incubated with 2 μ M A β (1-42) for 2 and 5 h, respectively. Also, controls ran up to 2 h incubation with 2 μ M of scrambled A β (1-42) did not induce alterations of the resting cytosolic Ca²⁺ concentration (data not shown). Therefore, the results obtained in this work pointed out that 2 h of incubation with 2 μ M A β (1-42) in mature CGN, were enough to produce approximately 50% inhibition of LTCC activity.

We measured the concentration of internalized A β after 2 h incubation with 2 μ M A β (1-42) added to the extracellular medium of mature CGN, using A β (1-42)*555. RF images of CGN were acquired with an excitation filter of 556 nm and a dichroic mirror of 580 nm with an emission filter of 590 nm as described in Materials and Methods section. The increase of RF intensity after subtraction of cell's red autofluorescence (**Figure 9A**) was compared with the RF intensity of the medium supplemented with different concentrations of A β (1-42)*555 (**Figure 9B**). From these results obtained, we calculated that after incubation with 2 μ M of A β (1-42) (1.8 μ M of unlabeled A β (1-42) monomers plus 0.2 μ M of A β (1-42)*555 monomers) for 2 h, the intracellular concentration of A β was 193 ± 21 nM of A β (1-42), assuming that there was not a significant difference between the rate of internalization of A β (1-42)*555 and unlabeled A β (1-42) (i.e., a concentration high enough to saturate all CaM present in CGNs).

A) Ratio Images (340/380): before and after Nifedipine



B) Ratio (340/380): kinetic plots before and after Nifedipine



C) Steady ratio (340/380) before and after Nifedipine

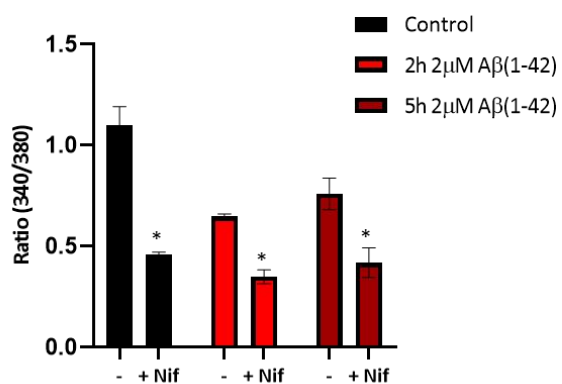
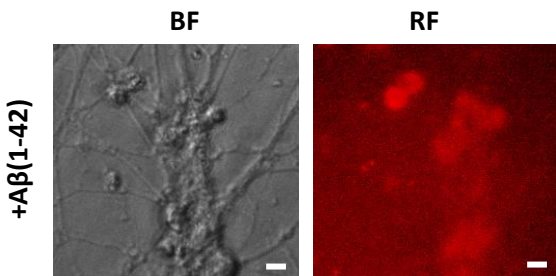


Figure 8. Intracellular cytosolic Ca^{2+} concentration decreases in the neuronal soma after $\text{A}\beta(1-42)$ treatment. Mature CGN were pre-incubated with $2\mu\text{M A}\beta(1-42)$ for 2 h or 5 h at 37°C and 5% CO_2 and loaded with $5\ \mu\text{M Fura2 AM}$ for 1 h, as previously described in Materials and Methods section. Nifedipine ($10\ \mu\text{M}$), a Ca^{2+} channel blocker, was used as positive control to confirm the effect of the total blockade of LTCCs. **A)** Representative ratio (340/380) images of Fura2-loaded CGN of untreated (a) and treated cells with $2\ \mu\text{M A}\beta(1-42)$ for 2 h (b) or 5 h (c) and after the addition of nifedipine in the control group (d) and in cells treated with $2\ \mu\text{M A}\beta(1-42)$ for 2 h (e) or 5 h (f). Scale bar inserted in fluorescence microscopy images = $10\ \mu\text{m}$. **B)** Kinetic plots of the average \pm s.e. fluorescence ratio (340/380) before and after the

addition 10 μ M nifedipine (+Nif) at the time indicated by the blue arrow. **C**) The analysis of fluorescence intensity data for GCN loaded with Fura2 showed a statistically significant decrease (\approx 50%) in the steady ratio (340/380) after A β (1–42) treatment (2 h and 5h) with respect to the control (untreated cells), $p < 0.05$. The addition of nifedipine totally blocks the entry of Ca $^{2+}$ in the soma in untreated and treated cells as demonstrated by the decrease in the ratio showing that A β partially attenuates LTCC function. The ratio (340/380) values shown are the average \pm s.e. of experiments done in triplicate with at least two different preparations of CGN ($n > 400$ neuronal somas of fields taken from at least six plates for each condition).

A)



B)

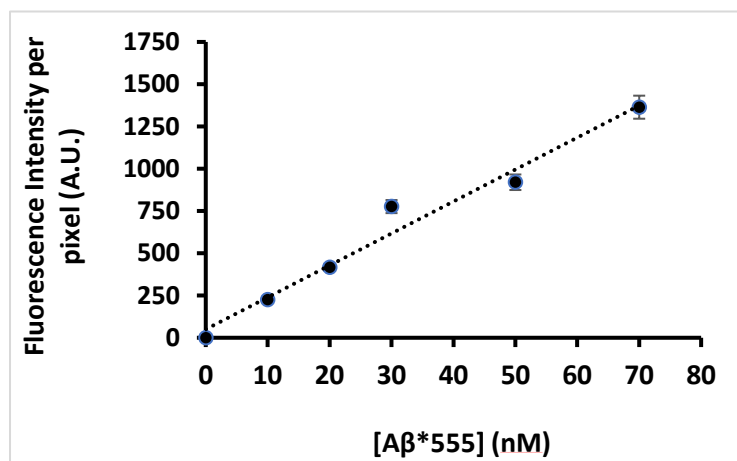
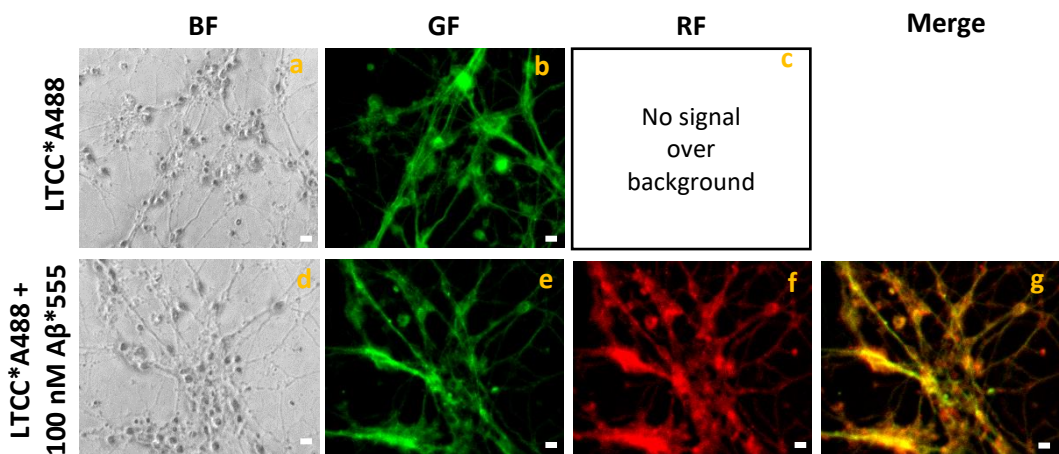


Figure 9. Internalization of A β (1-42)*555 in mature CGN. A) Representative BF and RF images of mature CGN after 2 h incubation with 2 μ M of A β (1–42) (1.8 μ M of A β (1–42) monomers plus 0.2 μ M of A β (1–42)*555 monomers) in DMEM:F12 medium with 25 mM KCl acquired with an excitation filter of 556 nm and a dichroic mirror of 580 nm with emission filter of 590 nm, and 0.03 s exposure time. No significant autofluorescence of CGN in the absence of A β (1-42)*555 was detected over background with these experimental conditions and this short exposition time. After the 2 h incubation of CGN with A β (1-42)*555 the medium was replaced by MLocke's K25 buffer assay and the Petri plate was placed in the holder of the fluorescence microscope (37°C) for images acquisition. Scale bar inserted in fluorescence microscopy images = 10 μ m. **B)** Calibration of the average intensity per pixel obtained with increasing concentrations of A β (1-42)*555 in MLocke's K25 in the Petri plate. A.U. means arbitrary fluorescence units. Dotted line is the result of linear regression, $R^2=0.9729$. The average intensity readings per pixel in CGN neuronal somas were taken from several fields for a total number of 102 cells and after subtraction of CGN autofluorescence yielded an internalized concentration of 193 ± 2.1 nM of A β (1-42) by interpolation in the calibration line shown in the panel (B).

4.5. Extensive FRET between LTCCs and A β (1-42)*555 in fixed mature CGN is largely reversed by addition of exogenous CaM

As mentioned before, we showed, in works of the laboratory, that LTCCs are extensively associated with lipid rafts in primary cultures of mature CGNs^{27,40,55}, therefore this prompted us to experimentally evaluate the possibility that both LTCCs and A β (1–42) are associated within the same lipid rafts in CGN at a concentration of 100 nM A β (1-42). The **Figure 10A** shows representative fluorescence microscopy images of mature CGN stained with anti-LTCC subunit α 1C conjugated with IgG-Alexa 488 (anti-LTCCs*A488) (a-c) and 100 nM A β (1-42)*555 (d-g). The direct observation of images indicated that the GF is attenuated after the addition of A β (1-42)*555 (**Figure 10Ae**). The results of the analysis of the red/green fluorescence ratio showed a 2-fold increase after 100 nM A β (1-42)*555 addition (**Figure 10B**), pointing out the occurrence of FRET between Alexa 488 conjugates of anti-LTCC and the Fluor555 dye bound to A β . In addition, a detailed examination of the merge image (g) revealed significant variations of the extent of FRET between LTCCs and A β *555, as we can see by the color palette of different cellular submicrodomains within the neuronal soma and extensions. More intense yellow/orange-colored pixels highlighted submicrodomains with higher FRET efficiency. It is noteworthy that this leads to a punctate staining appearance of neuronal extensions that is reminiscent of dendritic spines. Therefore, these results demonstrated an extensive co-localization of LTCCs and A β (1-42)*555 within the FRET distance in fixed mature CGN, which using this FRET approach was \leq 50 nm, as indicated in the Materials and Methods section. However, we cannot account for a direct interaction and inhibition of LTCC activity by A β (1-42) due to the absence of co-immunoprecipitation of LTCCs by A β (1-42) as demonstrated in the **Supplementary Figure S.2**.

A)



B)

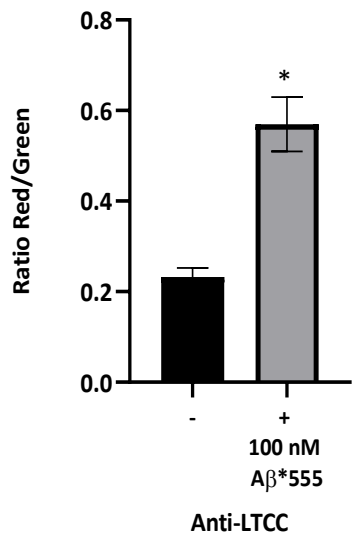


Figure 10. Extensive FRET between LTCC and A β (1-42)*555. **A)** Representative quantitative fluorescence microscopy images of CGN stained with the anti-LTCC subunit α 1C/IgG-Alexa488 antibodies (LTCC*A488, a–c) or with anti-LTCC/IgG-Alexa488 and A β (1-42)*555 (LTCC*A488/A β *555), d–g). BF, GF and RF images are shown for each of the selected fields, and the orange-yellow areas (Merge image) pointed out the higher intensity FRET regions (g). The exposure time for GF and RF images was 0.4 s. Scale bar inserted in fluorescence microscopy images = 10 μ m. **B)** Ratio of red/green fluorescence intensity per pixel (RF/GF) of CGN somas stained with anti-LTCC/IgG-Alexa488 only (LTCC*A488) and double stained with anti-LTCC*IgG-Alexa488/A β (1-42)*555 (LTCC*A488/A β *555). The results shown in (B) are the mean \pm s.e. (*) $p < 0.05$ (i.e., statistically significant with respect to the control, CGN labeled with the Alexa488 FRET donor only).

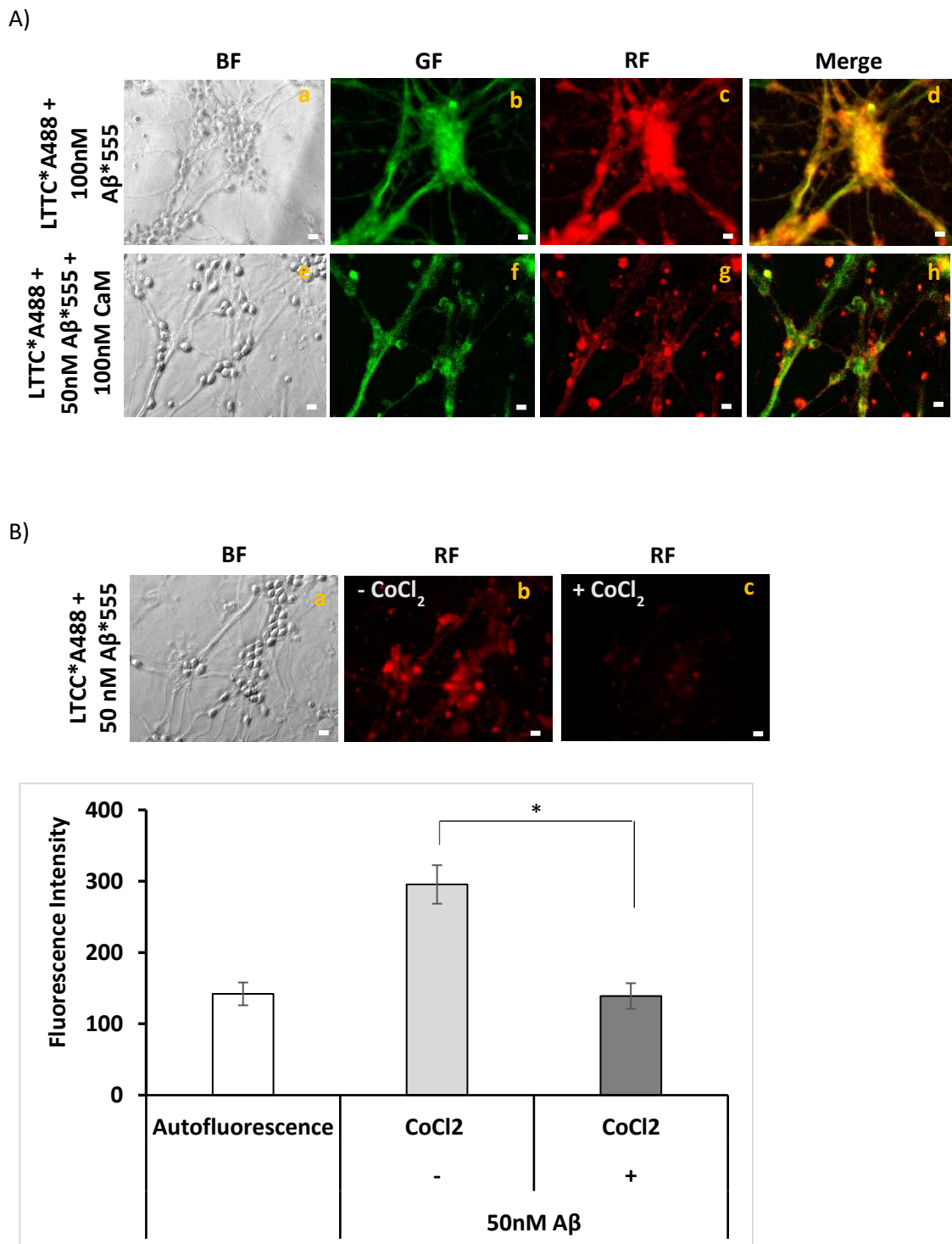


Figure 11. Reversion by CaM of FRET between anti-LTCC/IgG-Alexa488 and $\text{A}\beta(1-42)^*\text{555}$ (A) and quenching by Co^{2+} of the fluorescence of $\text{A}\beta(1-42)^*\text{555}$ (B). **A)** Representative quantitative fluorescence microscopy images of CGN stained with anti-LTCC subunit $\alpha 1\text{C}/\text{IgG-Alexa488}$ and 50 nM of $\text{A}\beta(1-42)^*\text{555}$ (LTCC**A488*/*Aβ**555), after GF and RF image acquisition, 100 nM of purified CaM was added to the medium, and the plate was gently stirred for 15 min before acquisition of the images of selected fields in the presence of CaM. BF, GF, and RF images are shown for the selected fields, and the orange/yellow areas (merge image) point out the higher intensity FRET regions. The exposure time for GF and RF images was 0.5 s. Scale bar inserted in fluorescence microscopy images = 10 μm . **B)** Representative quantitative RF microscopy images of CGN stained with LTCC**A488*/*Aβ*(1-42)*555 in the absence and in the presence

of 5 mM Co²⁺. After acquisition of RF images in the absence of Co²⁺, 5 mM of CoCl₂ was added to the medium and images of the same field were acquired 5 min after incubation. The average intensity per pixel in the neuronal somas of five different fields were measured using HClImage software ($n > 50$ somas for each experimental condition), and are plotted below the fluorescence microscopy images of this panel (B). The results showed that 5 mM Co²⁺ completely quenched the fluorescence of A β *555, because the difference between the average intensity of the autofluorescence and of the fluorescence in the presence of 5 mM Co²⁺ was not statistically significant ($p > 0.05$).

As early mentioned, CaM modulates LTCCs activity directly^{29,30} or indirectly through CaMK activation^{36,63,64}, therefore we experimentally assessed the possibility that CaM provides the major anchor point for A β near LTCCs in lipid rafts of mature CGN. After acquisition of fluorescence microscopy images of CGN sained with anti-LTCCs conjugated with IgG-Alexa 488 (anti-LTCCs*A488) and 50 nM of A β (1-42)*555 we added 100 nM of purified CaM to the extracellular medium. We lowered the concentration of A β (1-42)*555 from 100 to 50 nM for two main reasons: i) to focus on the higher affinity binding sites for A β *555, and ii) to get a CaM/A β (1-42)*555 molar ratio much higher than 1. The **Figure 11A** shows representative images of CGN stained with anti-LTCCs*A488 plus 50 nM of A β (1-42)*555 in the absence (a-d) and presence of 100 nM CaM (e-h). The results clearly show that CaM largely reverses the A β (1-42)*555 fluorescence intensity of CGN in the somas and more extensively in the thicker neuronal extensions connecting aligned neuronal bodies (**Figure 11Ag**). The merge image (**Figure 11Ah**) also indicates the lack of FRET pointed out by the absence of yellow/orange-stained regions, that are widely visible in **Figure 11Ad**. Moreover, the addition of 5 mM Co²⁺ to CGN stained with LTCCs*A488 plus 50 nM of A β (1-42)*555 caused more than 80% quenching of the total RF (**Figure 11B**), resulting in a RF image that was not significantly different to the image of the red autofluorescence of CGN shown in **Figure 3**.

5. Discussion

The results obtained showed that at concentrations lower than 250 nM A β (1-42), structurally, this peptide in solution are present predominantly as dimers species (90%), with approximately 10% of trimers (**Figure 2**), with absence of monomers. Therefore, in this work we used the neurotoxic oligomeric form of A β (1-42).

We observed a large complexation between A β (1-42) (250 nM) and CaM in cell lysates of mature CGN by using the co-immunoprecipitation method (**Figure 1**). This result was further confirmed by extensive FRET between anti-CaM stained with the Alexa 488 fluorescent secondary antibody and 100 nM of A β (1-42)*555 in fixed and permeabilized CGN (**Figure 4**). Moreover, taking into account the high content of CaM showed in other studies^{65,66} and in this

work (**Figure 1**) and the very low kD of the CaM-A β (1–42) complex (~1nM)²², our results pointed out that CaM is a major binding target for A β (1–42) in mature CGN. Since CGN seeded per Petri plate in this work contain 56 ± 6 picomoles of CaM, this implies that in these plates, CaM can bind up to 120 ± 13 picomoles of A β (1–42) monomers. Despite the fact that A β peptides binds also with high affinity with PrPc⁶⁷ and to GSK3 α ⁶⁸ (kD close to 1 nM), it is important to denote that these other target proteins of A β are expressed at much lower levels than CaM in neurons. Therefore, CaM can be seen as the major intracellular target protein for A β peptides in neurons, by playing a major role in keeping free intracellular concentration of A β peptides in the low nanomolar range. Consequently, it should be expected a stronger increase in free intracellular A β peptides and subsequent neuronal degeneration in brains affected with AD, because they contain lower CaM levels compared with normal brains²¹. In addition, it is expected that the formation of CaM-A β (1–42) complexes could act as intracellular transducers for focalized actions of A β peptides, because CaM plays a key role in neuronal metabolism, excitability and signaling through direct interaction with proteins that play a major role in neuronal functions in neurons.

A β peptides have been found associated with neuronal lipid rafts, promoting specific signaling alterations^{69,70}. As reviewed in the Introduction section of this chapter, A β peptides bind to highly expressed cholesterol and gangliosides in lipid rafts, and also to phosphatidylserine, a lipid enriched in the neuronal plasma membrane. Moreover, PrPc, which is also expressed in neuronal lipid rafts, has been shown to bind A β peptides^{61,62,71} providing further direct interaction points for the anchorage of A β to lipid rafts. Using the fluorescent A β (1-42) peptide (A β (1-42)*555), we experimentally assessed by FRET imaging and using specific antibodies, that A β binding sites were within the FRET distance from the protein markers of lipid rafts: Cav1, HRas and PrPc in fixed and permeabilized CGN (**Figure 5**). Between all these three protein markers, the pair with higher increase in the RF/GF ratio was anti-PrPc stained with the Alexa 488 fluorescent secondary antibody/A β *555, indicating a higher co-localization of PrPc and A β (1–42) within FRET distance, which is consistent with the formation of PrPc-A β complexes reported elsewhere (see above). These results were obtained with the addition of only 100 nM of A β (1-42)*555 to a Petri plate containing 2.5×10^6 cells in 1 mL PBS, in order to minimize the contribution of low affinity intracellular binding sites for A β . Moreover, using this experimental approach, the FRET distance limit is less than 60 nm, indicating that the A β binding sites are within the same lipid rafts or in close proximity to them. In addition, despite the extensive co-localization between A β (1-42)*555 and the neuronal lipid rafts protein markers Cav-1 and HRas demonstrated by FRET technique, there is no co-immunoprecipitation by the anti-A β (1–42) antibody in the presence of 250 nM A β (1–42), pointing out that neither Cav1 nor

HRas provide direct anchoring points of A β (1–42) in neuronal lipid rafts (see **Supplementary figure S.2**). On the other hand, the results obtained with FRET imaging with anti-CaM*Alexa488 antibody (as FRET donor) and anti-HRas*Cy3 antibody (as FRET acceptor) pointed out that a significant fraction of CaM were separated by less than 80 nm (i.e., at a distance lower than the maximum 100 nm size reported for lipid rafts). This is in good agreement with the known association of several CaM-binding proteins with lipid rafts in mature CGN, such as, nNOS, LTCCs, PMCA, and CaMKII^{27,36,40}.

It has been demonstrated that LTCCs associated with lipid rafts play a fundamental role in the control of resting cytosolic Ca²⁺ homeostasis in mature CGN *in vitro*, in partially depolarizing medium containing 25 mM KCl^{35,36}. Also, LTCC activity is stimulated by phosphorylation mediated by CaMKII^{36,63,64}, but CaM binding to the LTCC α 1C subunit produces inactivation of these channel^{29,30}. In this work, we demonstrated that A β (1–42) internalizes inside mature CGN, yielding approximately 193 ± 21 nM of A β after 2 h of incubation (**Figure 9**). Moreover, the internalized A β (1–42) produced approximately 50 % inhibition of the activity of LTCCs, and that incubation up to 5h did not significantly increase this inhibition (**Figure 8**). Since, in this work, the predominantly aggregation state of the solutions of A β (1–42) is as a dimer, this means that less than 100 nM A β (1–42) dimers inhibited by 50% the LTCC's activity. Also, we did not observe a significant change in the resting cytosolic Ca²⁺ concentration of CGN measured once LTCCs were blocked with nifedipine after these treatments with A β (1–42). These results indicate that LTCC is the main Ca²⁺ transport system involved in the control of resting cytosolic Ca²⁺ in mature CGN, and is highly sensitive to A β (1–42) under our experimental conditions. Moreover, it is expected that the decrease in resting cytosolic Ca²⁺ elicited by A β (1–42) should attenuate CGN excitability because of the strong requirement of synaptic activity upon cytosolic Ca²⁺ concentration.

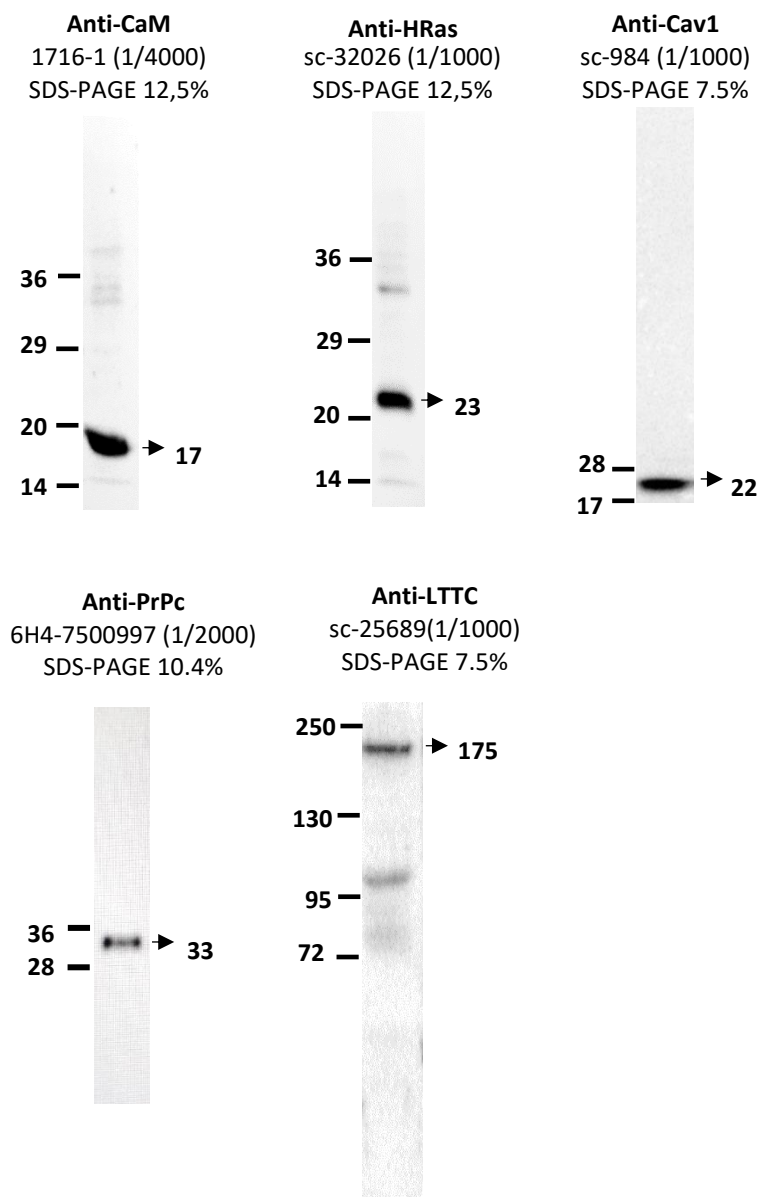
Noteworthy, it is remarkable that upon blockade of LTCCs with nifedipine, the resting cytosolic Ca²⁺ of CGN was not significantly altered by A β (1–42), indicating that the formation of Ca²⁺ pores in plasma membrane by intracellular A β is very unlikely at the short time of exposure and in the nanomolar range of internalized A β attained in this work. This result also suggests that the activity of other Ca²⁺ transport systems in CGN are not significantly impaired by the treatment with A β (1–42) that is enough to elicit inhibition of LTCCs. PMCA is the main transport system responsible for the extrusion of Ca²⁺ in neurons³². It has been reported that A β (1–42) partially inhibit PMCA^{33,43}, however it is to be noted that only a very slight inhibition of PMCA by 2.5 μ M A β (1–42) should be expected in a Ca²⁺ concentration range below 0.2 μ M⁴³, the resting cytosolic concentration range measured in mature CGN in this work and in previous works^{27,35,36}.

Besides, other works have shown that CaM and cholesterol antagonize the inhibition of PMCA caused by A β (1–42)^{43,72}. Additionally, it is important to highlight that the sustained dropping of cytosolic Ca²⁺ in CGN is a cellular stress response observed at short times of incubation and with low nanomolar free intracellular concentrations of A β . In that sense, probably at higher concentrations of A β and/or at longer times of exposure to A β , this may trigger Ca²⁺ release from intracellular stores, mainly from endoplasmic reticulum (ER), as a compensatory or adaptive cellular response. In fact, it was reported enhanced Ca²⁺ release form ER in AD^{73,74}. Furthermore, it has been shown that familial AD mutations of presenilins induce ER Ca²⁺ leak thus causing early-onset inherited AD^{75,76}.

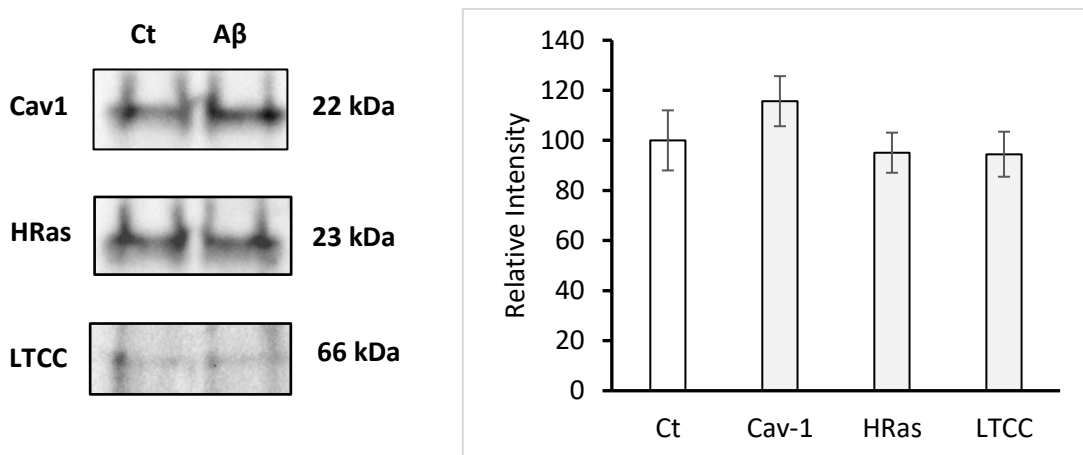
Despite the inhibition of LTCC activity by A β , then, we observed that LTCCs are not co-immunoprecipitated by anti-A β (1–42) antibody (**Supplementary figure S.2**), which excludes the hypothesis of the blockade of these Ca²⁺ channels by direct binding of A β (1–42) to LTCCs. Noteworthy, fluorescence microscopy imaging showed efficient FRET between anti-LTCC*A488 antibody and A β (1–42)*555 (**Figure 10**). Therefore, probably A β (1–42) is binding to a modulatory site in the CGN lipid rafts located very close to the LTCC structure (i.e., less than few nanometers distance from LTCC subunits since the overall size of the complex between the anti-LTCC primary antibody and the Alexa 488 fluorescent secondary antibody is approximately 40 nm)^{27,55}. Since most of the internalized A β (1–42) should be bound to CaM, we can rationalized that the inhibition of LTCC activity by A β (1–42) must be due the known inhibition of CaMKII by A β peptides^{41,42}, and also in terms of potentiation by A β (1–42) of the inactivation of LTCC by direct interaction with CaM. The premise that CaM-A β (1–42) complexes modulate LTCC activity, was experimentally supported by a large reversion of the co-localization between anti-LTCC*A488 and A β (1–42)*555, after addition of CaM to the extracellular medium of permeabilized CGN (**Figure 11A**). In addition, the nearly 80% quenching of A β (1–42)*555 fluorescence intensity caused by addition of 5 mM Co²⁺ (**Figure 11B**) suggests that the binding sites of A β (1–42)*555 in fixed and permeabilized CGN were separated by less than 2 nm from high affinity Ca²⁺ sites, as expected for A β (1–42)*555-CaM complexes²². It has been shown that A β prevents CaMKII activation in rat hippocampal slices⁴¹, and impairment of the phosphorylation of the β -subunit of LTCC by CaMK inhibitors cause inhibition of LTCC in partial depolarizing MLocke's K25 mM medium³⁶. Moreover, it has been proposed that the dysregulation of CaMKII may be a modulator event of toxicity in AD⁴². Nevertheless, we cannot reject the hypothesis that the formation of A β (1–42)-CaM complexes may also potentiate the inactivation of LTCC activity by direct binding of CaM, a possibility which to the best of our knowledge has been overlooked until now. In that way, further extensive experimental studies are required for critical evaluation of this point.

In conclusion, we showed a large complexation between CaM and submicromolar concentrations of A β (1–42) dimers, and also an extensive co-localization of CaM and A β (1–42) within the same lipid rafts in mature CGN with up to 100 nM A β (1–42)*555 monomers. Moreover, we showed that the extracellular addition of 2 μ M A β (1–42) after 2 h incubation reduced to half the resting cytosolic Ca $^{2+}$ concentration in mature CGN, in partially depolarizing 25 mM potassium medium; conditions that produced an internalization of less than 100 nM of A β (1–42) dimers in neuronal somas. Finally, we identified that the primary cause of the decrease of resting cytosolic Ca $^{2+}$ was the inhibition of LTCCs induced by A β (1–42) dimers.

6. Supplementary Figures



Supplementary Figure S.1. Western blotting of CGN lysates with the primary antibodies used in fluorescence microscopy images. The reference number is included for each primary antibody, as well as the dilution used for the Western blotting and the percentage of acrylamide used to run SDS-PAGE in each case.



Supplementary Figure S.2. Western blotting of Cav1 (anti-Cav1, sc 894), HRas (anti-HRas, sc 32026) and LTCC (anti-LTCC β subunit, sc 25689) after co-immunoprecipitation assay with mouse anti-Aβ antibody as described in the Materials and Methods. The results show that there is not a significant co-immunoprecipitation of these proteins by the anti-Aβ antibody.

7. References

- Pike, L. J. Rafts defined: A report on the Keystone symposium on lipid rafts and cell function. *J. Lipid Res.* **47**, 1597–1598 (2006).
- Choo-Smith, L.P.I. & Surewicz, W. K. The interaction between Alzheimer amyloid β(1-40) peptide and ganglioside G(M1)-containing membranes. *FEBS Lett.* **402**, 95–98 (1997).
- Choo-Smith, L., Garzon-Rodriguez, W., Glabe, C. G. & Surewicz, W. K. Acceleration of amyloid fibril formation by specific binding of Aβ-(1-40) peptide to ganglioside-containing membrane vesicles. *J. Biol. Chem.* **272**, 22987–22990 (1997).
- Ariga, T., Kobayashi, K., Hasegawa, A., Kiso, M., Ishida, H., Miyatake, T. Characterization of high-affinity binding between gangliosides and amyloid β-protein. *Arch. Biochem. Biophys.* **388**, 225–230 (2001).
- Matsuzaki, K., Kato, K., Yanagisawa, K. Aβ polymerization through interaction with membrane gangliosides. *Biochim. Biophys. Acta - Mol. Cell Biol. Lipids* **1801**, 868–877 (2010).
- Kakio, A., Nishimoto, S.I., Yanagisawa, K., Kozutsumi, Y., Matsuzaki, K. Cholesterol-dependent Formation of GM1 Ganglioside-bound Amyloid β-Protein, an Endogenous

- Seed for Alzheimer Amyloid. *J. Biol. Chem.* **276**, 24985–24990 (2001).
- 7. Kakio, A., Nishimoto, S.I., Yanagisawa, K. & Kozutsumi, Y., Matsuzaki, K. Interactions of amyloid β -protein with various gangliosides in raft-like membranes: Importance of GM1 ganglioside-bound form as an endogenous seed for Alzheimer amyloid. *Biochemistry* **41**, 7385–7390 (2002).
 - 8. Wood, W. G., Schroeder, F., Igbavboa, U., Avdulov, N. A. & Chochina, S. V. Brain membrane cholesterol domains, aging and amyloid beta-peptides. *Neurobiol. Aging* **23**, 685–694 (2002).
 - 9. Lai, A.Y., McLaurin, J. Mechanisms of amyloid-beta peptide uptake by neurons: The role of lipid rafts and lipid raft-associated proteins. *Int. J. Alzheimers. Dis.* **2011**, 11 (2011).
 - 10. Williamson, R., Usardi, A., Hanger, D. P. & Anderton, B. H. Membrane-bound β -amyloid oligomers are recruited into lipid rafts by a fyn-dependent mechanism. *FASEB J.* **22**, 1552–1559 (2008).
 - 11. Kawarabayashi, T., Shoji, M., Younkin, L.H., Wen-Lang, L., Dickson, D.W., Murakami, T., Matsubara, E., Abe, K., Ashe, K.H., Younkin, S. G. Dimeric Amyloid β Protein Rapidly Accumulates in Lipid Rafts followed by Apolipoprotein E and Phosphorylated Tau Accumulation in the Tg2576 Mouse Model of Alzheimer’s Disease. *J. Neurosci.* **24**, 3801–3809 (2004).
 - 12. Younkin, S. G. The role of AB-42 in Alzheimer’s disease. *J Physiol.* **92**, 289–292 (1998).
 - 13. Hu, X., Crick, S.L., Bu, G., Frieden, C., Pappu, R.V., Lee, J. M. Amyloid seeds formed by cellular uptake, concentration, and aggregation of the amyloid-beta peptide. *Proc. Natl. Acad. Sci. U. S. A.* **106**, 20324–20329 (2009).
 - 14. Friedrich, R.P., Tepper, K., Rönicke, R., Soom, M., Westermann, M., Reymann, K.I., Kaether, C., Fändrich, M. Mechanism of amyloid plaque formation suggests an intracellular basis of A β pathogenicity. *Proc. Natl. Acad. Sci. U. S. A.* **107**, 1942–1947 (2010).
 - 15. Jin, S., Kedia, N., Illes-Toth, E., Haralampiev, I., Prisner, S., Herrmann, A., Wanker, E.E., Bieschke, J. Amyloid- β (1- 42) Aggregation Initiates Its Cellular Uptake and Cytotoxicity. *J. Biol. Chem.* **291**, 19590–19606 (2016).
 - 16. Walsh, D.M., Klyubin, I., Fadeeva, J.V., Cullen, W. K. & Anwyl, R., Wolfe, M.S., Rowan, M.J., Selkoe, D. J. Naturally secreted oligomers of amyloid β protein potently inhibit hippocampal long-term potentiation in vivo. *Nature* **416**, 535–539 (2002).
 - 17. Oddo, S., Caccamo, A., Shepherd, J.D., Murphy, M.P., Golde, T.E., Kayed, R., Metherate, R., Mattson, M.P., Akbari, Y., LaFerla, F. M. Triple-transgenic model of Alzheimer’s Disease with plaques and tangles: Intracellular A β and synaptic dysfunction. *Neuron* **39**,

- 409–421 (2003).
18. Billings, L. M., Oddo, S., Green, K. N., McGaugh, J. L. & LaFerla, F. M. Intraneuronal A β causes the onset of early Alzheimer's disease-related cognitive deficits in transgenic mice. *Neuron* **45**, 675–688 (2005).
 19. La Ferla, F. Calcium dyshomeostasis and intracellular signalling in alzheimer's disease. *Nat. Rev. Neurosci.* **3**, 862–872 (2002).
 20. Bezprozvanny, I. & Mattson, M. P. Neuronal calcium mishandling and the pathogenesis of Alzheimer's disease. *Trends Neurosci.* **31**, 454–463 (2008).
 21. McLachlan, D.R., Wong, L., Bergeron, C., Bainbridge, K, G. Calmodulin and calbindin D28K in Alzheimer disease. *Alzheimer Dis Assoc Disord.* **1**, 171–9 (1987).
 22. Corbacho, I., Berrocal, M., Török, K., Mata, A.M., Gutierrez-Merino, C. High affinity binding of amyloid β -peptide to calmodulin: Structural and functional implications. *Biochem Biophys Res Commun.* **486**, 992–997 (2017).
 23. Chin, D. & Means, A. R. Calmodulin: A prototypical calcium sensor. *Trends Cell Biol.* **10**, 322–328 (2000).
 24. Berridge, M. J. Calcium regulation of neural rhythms, memory and Alzheimer's Disease. *J. Physiol.* **592**, 281–293 (2014).
 25. O'Day, D. H., Eshak, K. & Myre, M. A. Calmodulin binding proteins and Alzheimer's disease. *J. Alzheimer's Dis.* **46**, 553–569 (2015).
 26. Demuro, A., Parker, I. & Stutzmann, G. E. Calcium signaling and amyloid toxicity in Alzheimer disease. *J. Biol. Chem.* **285**, 12463–12468 (2010).
 27. Marques-da-Silva, D. & Gutierrez-Merino, C. Caveolin-rich lipid rafts of the plasma membrane of mature cerebellar granule neurons are microcompartments for calcium/reactive oxygen and nitrogen species cross-talk signaling. *Cell Calcium* **56**, 108–123 (2014).
 28. Gutierrez-Merino, C., Marques-da-Silva, D., Fortalezas, S., Samhan-Arias, A. K. Chapter: *Cytosolic Calcium Homeostasis in Neurons — Control Systems, Modulation by Reactive Oxygen and Nitrogen Species, and Space and Time Fluctuations*. In book: *Neurochemistry*. (InTech, 2014).
 29. Peterson, B. Z., DeMaria, C. D. & Yue, D. T. Calmodulin is the Ca $^{2+}$ sensor for Ca $^{2+}$ -dependent inactivation of L-type calcium channels. *Neuron* **22**, 549–558 (1999).
 30. Zühlke, R. D., Pittt, G. S., Deisseroth, K., Tsien, R. W. & Reuter, H. Calmodulin supports both inactivation and facilitation of L-type calcium channels. *Nature* **399**, 159–162 (1999).
 31. Di Leva, F., Domi, T., Fedrizzi, L., Lim, D. & Carafoli, E. The plasma membrane Ca $^{2+}$ ATPase

- of animal cells: Structure, function and regulation. *Arch. Biochem. Biophys.* **476**, 65–74 (2008).
- 32. Brini, M., Carafoli, E. & Calì, T. The plasma membrane calcium pumps: focus on the role in (neuro)pathology. *Biochem. Biophys. Res. Commun.* **483**, 1116–1124 (2017).
 - 33. Mata, A. M. Functional interplay between plasma membrane Ca²⁺-ATPase, amyloid β-peptide and tau. *Neurosci. Lett.* **663**, 55–59 (2018).
 - 34. Gutiérrez-Martín Y, Martín-Romero FJ, Henao F, G.-M. C. Alteration of cytosolic free calcium homeostasis by SIN-1: high sensitivity of L-type Ca²⁺ channels to extracellular oxidative/nitrosative stress in cerebellar granule cells. *J Neurochem.* **92**, 973–89 (2005).
 - 35. Gutierrez-Merino, C., Marques-da-Silva, D., Fortalezas, S., Samhan-Arias, A. K. The critical role of lipid rafts nanodomains in the cross-talk between calcium and reactive oxygen and nitrogen species in cerebellar granule neurons apoptosis by extracellular potassium deprivation. *AIMS Mol. Sci.* **3**, 12–29 (2016).
 - 36. Fortalezas, S., Marques-da-Silva, D., Gutierrez-Merino, C. Methyl-β-Cyclodextrin Impairs the Phosphorylation of the β2 Subunit of L-Type Calcium Channels and Cytosolic Calcium Homeostasis in Mature Cerebellar Granule Neurons. *Int J Mol Sci.* **19**, 3667 (2018).
 - 37. Suzuki, T., Du, F., Tian, Q. B., Zhang, J. & Endo, S. Ca²⁺/calmodulin-dependent protein kinase IIα clusters are associated with stable lipid rafts and their formation traps PSD-95. *J. Neurochem.* **104**, 596–610 (2008).
 - 38. Sato, Y., Sagami, I. & Shimizu, T. Identification of caveolin-1-interacting sites in neuronal nitric-oxide synthase: Molecular mechanism for inhibition of no formation. *J. Biol. Chem.* **279**, 8827–8836 (2004).
 - 39. Zhou, L. & Zhu, D. Y. Neuronal nitric oxide synthase: Structure, subcellular localization, regulation, and clinical implications. *Nitric Oxide - Biol. Chem.* **20**, 223–230 (2009).
 - 40. Marques-da-Silva, D. & Gutierrez-Merino, C. L-type voltage-operated calcium channels, N-methyl-d-aspartate receptors and neuronal nitric-oxide synthase form a calcium/redox nano-transducer within lipid rafts. *Biochem. Biophys. Res. Commun.* **420**, 257–262 (2012).
 - 41. Zhao, D., Watson, J. B. & Xie, C. W. Amyloid β prevents activation of calcium/calmodulin-dependent protein kinase II and AMPA receptor phosphorylation during hippocampal long-term potentiation. *J. Neurophysiol.* **92**, 2853–2858 (2004).
 - 42. Ghosh, A. & Giese, K. P. Calcium/calmodulin-dependent kinase II and Alzheimer's disease. *Mol. Brain* **8**, 1–7 (2015).
 - 43. Berrocal, M., Marcos, D., Sepúlveda, M.R., Pérez, M., Ávila, J., Mata, A. M. Altered Ca²⁺ dependence of synaptosomal plasma membrane Ca²⁺ -ATPase in human brain affected

- by Alzheimer's disease. *FASEB J.* **23**, 1826–1834 (2009).
- 44. Padayachee, E. R. & Whiteley, C. G. Spectrofluorimetric analysis of the interaction of amyloid peptides with neuronal nitric oxide synthase: Implications in Alzheimer's disease. *Biochim Biophys Acta*. **1810**, 1136–1140 (2011).
 - 45. Padayachee, E., Ngqwala, N. & Whiteley, C. G. Association of β -amyloid peptide fragments with neuronal nitric oxide synthase: Implications in the etiology of Alzheimers disease. *J. Enzyme Inhib. Med. Chem.* **27**, 356–364 (2012).
 - 46. Wankerl, K., Weise, D., Gentner, R., Rumpf, J. J. & Classen, J. L-type voltage-gated Ca²⁺ channels: A single molecular switch for long-term potentiation/long-term depression-like plasticity and activity-dependent metaplasticity in humans. *J. Neurosci.* **30**, 6197–6204 (2010).
 - 47. Berger, S. M. & Bartsch, D. The role of L-type voltage-gated calcium channels Cav1.2 and Cav1.3 in normal and pathological brain function. *Cell Tissue Res.* **357**, 463–476 (2014).
 - 48. Fancy, D. A. & Kodadek, T. Chemistry for the analysis of protein-protein interactions: Rapid and efficient cross-linking triggered by long wavelength light. *Proc. Natl. Acad. Sci. U. S. A.* **96**, 6020–6024 (1999).
 - 49. Bitan, G. & Teplow, D. B. Rapid photochemical cross-linking - A new tool for studies of metastable, amyloidogenic protein assemblies. *Acc. Chem. Res.* **37**, 357–364 (2004).
 - 50. Schägger, H. & von Jagow, G. Tricine-sodium dodecyl sulfate-polyacrylamide gel electrophoresis for the separation of proteins in the range from 1 to 100 kDa. *Anal. Biochem.* **166**, 368–379 (1987).
 - 51. Fortalezas, S., Marques-da-Silva, D. & Gutierrez-Merino, C. Creatine Protects Against Cytosolic Calcium Dysregulation, Mitochondrial Depolarization and Increase of Reactive Oxygen Species Production in Rotenone-Induced Cell Death of Cerebellar Granule Neurons. *Neurotox. Res.* **34**, 717–732 (2018).
 - 52. Samhan-Arias, A.K., Garcia-Bereguaia, M.A., Martin-Romero, F.X., Gutierrez-Merino, C. Clustering of plasma membrane-bound cytochrome b5 reductase within 'lipid raft' microdomains of the neuronal plasma membrane. *Mol. Cell. Neurosci.* **40**, 14–26 (2009).
 - 53. Saavedra, L., Mohamed, A., Ma, V., Kar, S. & De Chaves, E. P. Internalization of β -amyloid peptide by primary neurons in the absence of apolipoprotein E. *J. Biol. Chem.* **282**, 35722–35732 (2007).
 - 54. Samhan-Arias, A. K., Marques-da-Silva, D., Yanamala, N. & Gutierrez-Merino, C. Stimulation and clustering of cytochrome b5 reductase in caveolin-rich lipid microdomains is an early event in oxidative stress-mediated apoptosis of cerebellar granule neurons. *J. Proteomics* **75**, 2934–2949 (2012).

55. Marques-da-Silva, D., Samhan-Arias, A. K., Tiago, T. & Gutierrez-Merino, C. L-type calcium channels and cytochrome b5 reductase are components of protein complexes tightly associated with lipid rafts microdomains of the neuronal plasma membrane. *J. Proteomics* **73**, 1502–1510 (2010).
56. McCormack, J.G., Cobbold, P. H. *Cellular Calcium: A Practical Approach - The Practical Approach Series.* (1991).
57. Sepúlveda, M. R., Berrocal-Carrillo, M., Gasset, M. & Mata, A. M. The plasma membrane Ca²⁺-ATPase isoform 4 is localized in lipid rafts of cerebellum synaptic plasma membranes. *J. Biol. Chem.* **281**, 447–453 (2006).
58. Cuenda, A., Henao, F., Gutierrez-Merino, C. Distances between functional sites of the Ca^{2+ + Mg(2+)}-ATPase from sarcoplasmic reticulum using Co²⁺ as a spectroscopic ruler. *Eur. J. Biochem.* **194**, 663–670 (1990).
59. Nguyen, D. M., Chen, L. S., Jeng, G., Yu, W. P. & Chen, T. Y. Cobalt ion interaction with TMEM16A calcium-activated chloride channel: Inhibition and potentiation. *PLoS One* **15**, 1–23 (2020).
60. Highsmith, S. & Murphy, A. J. Nd³⁺ and Co²⁺ binding to sarcoplasmic reticulum CaATPase. An estimation of the distance from the ATP binding site to the high-affinity calcium binding sites. *J. Biol. Chem.* **259**, 14651–14656 (1984).
61. Chen, S., Yadav, S. P. & Surewicz, W. K. Interaction between human prion protein and amyloid-β (Aβ) oligomers: Role of N-terminal residues. *J. Biol. Chem.* **285**, 26377–26383 (2010).
62. Zhang, Y., Zhao, Y., Zhang, L., Yu, W., Wang, Y., Chang, W. Cellular Prion Protein as a Receptor of Toxic Amyloid-β42 Oligomers Is Important for Alzheimer's Disease. *Front. Cell. Neurosci.* **13**, 1–9 (2019).
63. Hudmon, A., Schulman, H., Kim, J., Maltez, J.M., Tsien, R.W. Pitt, G. S. CaMKII tethers to L-type Ca²⁺ channels, establishing a local and dedicated integrator of Ca²⁺ signals for facilitation. *J. Cell Biol.* **171**, 537–547 (2005).
64. Lee, T.S., Karl, R., Moosmang, S., Lenhardt, P., Klugbauer, N., Hofmann, F., Kleppisch, T., Welling, A. Calmodulin kinase II is involved in voltage-dependent facilitation of the L-type Cav1.2 calcium channel: Identification of the phosphorylation sites. *J. Biol. Chem.* **281**, 25560–25567 (2006).
65. Cheung, W. Calmodulin. *Sci. Am.* **246**, 62–70 (1982).
66. Biber, A., Schmid, G. & Hempel, K. Calmodulin content in specific brain areas. *Exp Brain Res* 323–326 (1984).
67. Laurén, J., Gimbel, D.A., Nygaard, H.B., Gilbert, J.W., Strittmatter, S. M. Cellular Prion

- Protein Mediates Impairment of Synaptic Plasticity by Amyloid- β Oligomers. *Nature* **457**, :1128-32 (2009).
- 68. Dunning, C.J., McGauran, G., Willén, K., Gouras, G.K., O'Connell, D.J., Linse, S. Direct High Affinity Interaction between A β 42 and GSK3 α Stimulates Hyperphosphorylation of Tau. A New Molecular Link in Alzheimer's Disease? *ACS Chem. Neurosci.* **7**, 161–170 (2016).
 - 69. Cecchi, C., Nichino, D., Zampagni, M., Bernacchioni, C., Evangelisti, E., Pensalfini, A., Liguri, G., Gliozi, A., Stefani, M., Relini, A. A protective role for lipid raft cholesterol against amyloid-induced membrane damage in human neuroblastoma cells. *Biochim. Biophys. Acta - Biomembr.* **1788**, 2204–2216 (2009).
 - 70. Vetrivel, K.S. & Thinakaran, G. Membrane rafts in Alzheimer's Disease beta-amyloid production. *Biochim Biophys Acta* **1801**, 860–7 (2010).
 - 71. Samhan-Arias, A. K., Martín-Romero, F. J. & Gutiérrez-Merino, C. Kaempferol blocks oxidative stress in cerebellar granule cells and reveals a key role for reactive oxygen species production at the plasma membrane in the commitment to apoptosis. *Free Radic. Biol. Med.* **37**, 48–61 (2004).
 - 72. Berrocal, M., Sepulveda, M. R., Vazquez-Hernandez, M. & Mata, A. M. Calmodulin antagonizes amyloid- β peptides-mediated inhibition of brain plasma membrane Ca $^{2+}$ -ATPase. *Biochim. Biophys. Acta* **1822**, 961–969 (2012).
 - 73. Ito, E., Oka, K., Etcheberrigaray, R., Nelson, T.J., McPhie, D.L., Tofel-Grehl, B., Gibson, G.E., Alkon, D. L. Internal Ca $^{2+}$ mobilization is altered in fibroblasts from patients with Alzheimer's Disease. *Proc Natl Acad Sci USA* **91**, 534–538 (1994).
 - 74. Emilsson, L., Saetre, P. & Jazin, E. Alzheimer's disease: mRNA expression profiles of multiple patients show alterations of genes involved with calcium signaling. *Neurobiol. Dis.* **21**, 618–625 (2006).
 - 75. Tu, H., Nelson, O., Bezprozvanny, A., Wang, Z., Lee, S.F., Hao, Y.H., Serneels, L., De Strooper, B., Yu, G., Bezprozvanny, I. Presenilins Form ER Ca $^{2+}$ Leak Channels, a Function Disrupted by Familial Alzheimer's Disease-Linked Mutations. *Cell* **126**, 981–993 (2006).
 - 76. Zhang, H., Sun, S., Herreman, A., De Strooper, B. & Bezprozvanny, I. Role of presenilins in neuronal calcium homeostasis. *J. Neurosci.* **30**, 8566–8580 (2010).

CHAPTER 3

Identification of the primary target systems in HT-
22 cells that are associated with the early
dysregulation of Ca^{2+} homeostasis induced by $\text{A}\beta$

Index

1. Abstract	97
2. Introduction	97
3. Materials and Methods	101
3.1 Chemicals	101
3.2 A β (1–42) solutions and aggregation state	101
3.3 HT-22 cell culture	102
3.4 HT-22 cell differentiation	102
3.5 Intracellular cytosolic Ca $^{2+}$ measurements	102
3.6 HT-22 cell staining with LTCC, NMDAR and Sypnasin-1 antibodies	104
3.7 Cell viability using the MTT assay.....	104
3.8 Measurement of internalized A β (1–42)*555 and evaluation of subcellular colocalization with mitochondria and ER.....	105
3.9 Mitochondrial membrane potential ($\Delta\Psi_m$)	106
3.10 FRET imaging	106
3.11 Co-immunoprecipitation.....	107
3.12 Fluorescence measurements and calculation of the FRET parameters J and R ₀ .	108
3.13 Western blotting	108
3.14 PDI-dependent disulfide reduction assay	108
3.15 Generation of ROS.....	109
3.16 Measurement of glutathione levels	109
3.17 Measurement of lipid peroxidation	109
3.18 Iron influx assay using Calcein-AM.....	110
3.19 Images of HT-22 cells plus cholera toxin B-Alexa*555.....	110
3.20 Statistical Analysis	110
4. Results	110
4.1 Ca $^{2+}$ entry systems from the extracellular medium in HT-22 cells in culture.	110
4.1.1 LTCC are expressed in low levels in HT-22 cells in culture: LTCC activation through the LTCC-selective agonist (-)-BAY-K-8644.	110
4.1.2 NMDAR and LTCCs are expressed in morphologically differentiated HT-22, but they are inactive	112
4.1.3. P2R activation can elicit large peaks of cytosolic Ca $^{2+}$ concentration in HT-22 cells.	116

4.1.4 SOCE mechanism in HT22 cell cultures	118
4.2 Modulation of Ca ²⁺ homeostasis by Aβ(1-42) after a short-period of incubation in HT-22 cell culture.	119
4.2.1. Extracellularly added Aβ(1-42) is partially internalized inside HT-22 cells in a short period of time and largely localizes at the perinuclear region.	119
4.2.2. Internalized Aβ(1-42) colocalizes with mitochondria and ER in living HT-22 cells.....	121
4.2.2.1 Incubation during 2 h and 5 h with 2 μM Aβ(1-42) do not alter significantly the ΔΨm in the HT-22 cell culture.....	123
4.2.2.2. FRET imaging shows colocalization between PDI and Aβ(1- 42)*555 in HT-22 cell line, but Aβ(1-42) does not directly modulate PDI activity.	125
4.2.3. FRET imaging highlights the association of Aβ(1-42)*555 with CaM in HT- 22 cells.	128
4.2.4. Aβ(1-42) inhibits SOCE activity after a short period of incubation in HT-22 cells.	130
4.2.4.1 Binding of STIM1 with Aβ(1-42) in lysates of HT-22 cells.	133
4.2.4.2 Aβ(1-42) stimulates Ca ²⁺ release from ER through IP3R and to a lesser extent, through RyR in HT-22 cells.	134
4.2.5 Incubation of HT-22 cells during 2 h with 2 μM Aβ(1-42) decreases the influx of Ca ²⁺ from the extracellular medium through P2R.	137
4.2.5.1. The subtype P2X7R contributes to 48% of the total P2R activity and is inhibited by Aβ(1-42).	140
4.3. Aβ(1-42) induces a moderate increase in the production ROS after 2 h and 5 h incubation in HT-22 cells.	142
5. Discussion	147
6. References	152

1. Abstract

During many years, AD was attributed to the abnormal accumulation of insoluble fibrils of A β peptides, but in the last years accumulative evidence have been show that the oligomeric form of A β is the main cytotoxic form of this peptide. It is widely accepted that Ca²⁺ dysregulation homeostasis plays a major role in AD neurodegeneration and several studies have supported the premise that Ca²⁺ unbalance may be the proximal origin of the AD pathology. However, the main cellular and molecular events that induce alterations in Ca²⁺ triggered by A β peptides in an early stage of AD remain to be fully elucidated. In this work we used the immortalized mouse hippocampal cell line HT-22 to measure the amount of internalized A β (1-42) after a short period of incubation (up to 5 h) with submicromolar concentration of A β oligomers added to the extracellular medium (2 μ M A β (1-42)) and evaluated the alteration of resting cytosolic Ca²⁺ concentration. We showed that A β (1-42) internalize inside HT-22 in submicromolar concentration after only 2 h incubation and colocalize in the perinuclear region with ER and mitochondria up to 5 h , without significantly affecting the mitochondrial membrane potential. The modulation of ER induced by A β (1-42) after 2 h incubation impaired the SOCE mechanism through the modulation of STIM1 and the ER ligand-gated Ca²⁺-channels: RyR and IP3R, without a significant alteration in the cytosolic Ca²⁺ concentration up to 5 h incubation. Moreover internalized A β (1-42) induced the decrease of Ca²⁺ influx from the extracellular medium through P2R after 2 h incubation. These results suggest that ER proteins which modulate SOCE (STIM1, RyR and IP3R) and P2R are good candidates to become primary targets for therapeutic interventions in an early stage of the progression of AD.

2. Introduction

Structurally A β displays a large molecular polymorphism from monomers that assemble to form a variety of oligomeric species, and aggregate to form short, flexible, irregular protofibrils and then finally mature to form insoluble fibrils^{1,2}. The relative neurotoxicity of fibrillar versus oligomeric A β has been an area of debate. During many years, the neurodegeneration of AD was attributed to the abnormal accumulation of insoluble fibrils (amyloid cascade hypothesis of AD) due to the observation of A β plaques in various regions of the brain³. However, accumulative studies in cell models^{4,5}, mouse AD models^{6,7} and in AD brain tissues^{8,9}, have proposed that the small and soluble oligomeric form of A β (e.g., dimers, trimers, tetramers, dodecamers, higher oligomers) is the main cytotoxic form of AD, and A β plaques could serve as reservoirs for the assembly of the neurotoxic A β oligomers¹⁰. As an example, it

has been demonstrated in a study performed in rat brains *in vivo* that the rats infused with soluble A β (1-42) oligomers exhibited more neurodegeneration, a greater inflammatory response and a much greater decline in spatial learning and memory, than the rats that received insoluble A β (1-42) fibrils¹¹. In another study, it has been demonstrated that A β oligomers injected in the lateral ventricle of rats and macaques diffused into the brain and accumulated in several regions associated with memory and cognitive functions, with consequent induction of tau phosphorylation, microglial activation, and synaptic loss in macaques where A β oligomers accumulated and without detection of fibrillar A β aggregates¹². The conclusions of this work revealed to be of extreme importance to understand the main mechanism implicated in AD pathogenesis, since humans and macaques brains share significant similarities¹².

It has been reported that A β oligomers also triggers other neurodegenerative mechanism such as Ca²⁺ dysregulation, ER stress, mitochondrial dysfunction and the activation of pro-apoptotic pathways leading to cell death^{13,14}. There is a growing body of evidence demonstrating that dysregulation in signaling pathways that handle Ca²⁺ play a major role in the initiation of AD pathogenesis. Ca²⁺ is a second messenger and has a key role as regulator of neuronal synaptic plasticity, growth and differentiation, action potential properties and learning and memory¹⁵. Accordingly with the “calcium hypothesis of brain aging and AD”, proposed first by Khachaturian¹⁶, sustained changes in Ca²⁺ homeostasis could be a common pathway for aging and the neuropathological changes associated with AD. In the last decades several studies have confirmed that Ca²⁺ signaling is upregulated in AD¹⁷. For example, Kuchibhotla and colleagues reported higher basal Ca²⁺ concentrations in neurons close to A β in APP mice, comparing with the wild-type mice¹⁸. Likewise, the resting levels of Ca²⁺ in cortical neurons of 3xTg-AD animals was twice that found in non-Tg animals¹⁹. In addition, presenilin (PS1 and PS2) mutations, which contributes to 90% of early-onset familial AD (fAD, counting for less 5% all cases) have been shown to be related with the dysregulation of cytoplasmic Ca²⁺ homeostasis in AD neurons¹⁵. Accumulative evidence has shown that Ca²⁺ imbalance due to PS mutations takes place before the formation of A β plaques or NFT in AD, suggesting once more that dysregulation of Ca²⁺ may be the proximal origin of the pathology¹⁵.

Immortalized cell lines have been extensively used as valuable and reliable tools to understand the molecular mechanism associated with diseases. HT-22 is an immortalized mouse hippocampal sub-line derived from parent HT4 cells that were originally immortalized from primary mouse hippocampal neuronal culture²⁰⁻²². HT-22 culture is extensively used to study the non-receptor mediated oxidative glutamate toxicity because HT-22 cells lack ionotropic glutamate receptors (iGluRs) like NMDAR and AMPAR (α -amino-3-hydroxy-5-methyl-4-isoxazolepropionic acid receptor) but are still sensitive to high concentrations of extracellular

glutamate²³. Besides glutamate excitotoxicity, HT-22 has also been used a reliable model to study different neurophysiologic and neurodegenerative processes associated with the disruption of molecular mechanisms^{24,25}, mitochondrial impairment²⁶, ER stress and alteration in SOCE mechanism^{27,28} and changes in redox homeostasis^{29,30} among others. Also, HT-22 cells have been used in the study of cell death induced by stressors compounds like H₂O₂^{31,32} and Aβ²⁶, and to assess the protective effect of natural compounds^{33,34} in cell dysfunction and neuronal death.

There is no consensus regarding the expression of AChR in HT-22 cells. It has been reported by Liu and colleagues that HT-22 cells differentiated in Neurobasal medium display expression of cholinergic markers, compared with HT-22 cultured in Dulbecco's modified Eagle's medium (DMEM) (undifferentiated cells), but with low levels of AChR markers, although both undifferentiated and differentiated HT-22 possessed weak cholinergic activity³⁵. However, a more recent study demonstrated the lack of acetylcholinesterase activity in the HT-22 cell line³⁶. The lack of more scientific publications and the discrepancy of results regarding the activity of AChR in the HT-22 culture could possibly indicate that AChR are expressed in low levels and/or possess low activity or/and are inactive in normal conditions of culture, suggesting that AChR are not the main plasma membrane system responsible for the influx and modulation of cytosolic Ca²⁺ in HT-22 culture.

Despite the absence of ionotropic glutamate receptors in HT-22 and the apparently poor activity of AChR, there are not scientific publications regarding the main plasma membrane transport system that can allow for the influx of Ca²⁺ from the extracellular medium in HT-22 cells. It is already reported that in excitable cells, Ca²⁺ influx could also be mediated by type 2 P2R or through LTCC³⁷. P2R are activated by ATP, and have drawn a lot of attention due to their wide expression in almost every cell types, including stem cells³⁸. P2R play a major role in controlling metabolic activities and many physiological functions including signal transmission, proliferation and differentiation in neurons³⁸. LTCC are high-voltage-activated channels that present slow activation kinetics and play major roles in regulating gene expression, cell survival, and synaptic plasticity³⁹. Due to the relevance of P2R and LTCC in Ca²⁺ modulation in neurons their activity in HT-22 cells deserves to be studied.

Besides the Ca²⁺ influx mediated through voltage operated channels (VOC) or receptor-operated channels (ROC) in the plasma membrane, the elevation of cytosolic Ca²⁺ concentration in neurons can also derive from the release of Ca²⁺ from the intracellular stores, such as the ER, which is mediated by SOCE mechanism. The principal function of SOCE is to refill the intracellular Ca²⁺-stores to preserve the primary source of intracellular Ca²⁺ and therefore to maintain a favorable environment for protein folding in the ER lumen⁴⁰. The basic components of SOCE include a mechanism for Ca²⁺ stores depletion through ligand-gated Ca²⁺ channels RyR and the

IP3R; a sensor in the ER that also serves as an activator of the plasma membrane channel named STIM1 and STIM2, and the store-operated channel (Orai1, 2 or 3)⁴¹. Many studies have concluded that SOCE modulation via STIM1 or/and Orai1 may serve as a key target for neurological disorders in which oxidative stress play a key role, either in the etiology or in the progression of the disease. In HT-22 cells, SOCE function has been evaluated after glutamate-induced oxidative injury^{27,28} or hydrogen peroxide-induced apoptosis³². In addition, it was demonstrated that HT-22 express all three IP3R subtypes⁴² and the RyR subtype 2⁴³ and subtype 3⁴⁴.

The main goal of this work was to study the alteration of resting cytosolic Ca²⁺ concentration and of cytosolic Ca²⁺ dynamics induced by extracellular addition of 2 μM Aβ(1-42) after a short time incubation (up to 5 h) in HT-22 culture. Using fluorescence microscopy imaging, we calculated the concentration and the subcellular distribution of internalized Aβ(1-42) in HT-22 cells incubated up to 5 h with 2 μM Aβ(1-42) added to the extracellular medium. We evaluated the changes induced by this exposure to extracellular Aβ(1-42) in the cytoplasmic Ca²⁺ concentration and dynamics in Fluo3-loaded HT-22 cells. The main results obtained in this work indicated that Aβ(1-42) internalize inside HT-22 cells in submicromolar concentration after only 2 h of incubation and colocalize mainly in the perinuclear region after 5 h incubation. Also, internalized Aβ(1-42) showed moderate colocalization with mitochondria without affecting significantly the mitochondrial membrane potential and showed colocalization with ER. After 2 h incubation, internalized Aβ(1-42) caused a decrease in SOCE mechanism function through the modulation of STIM1, and by stimulation of the activity of both ligand-gated calcium channels: RyR and IP3R. However, there is not a significative alteration in the steady-state cytosolic Ca²⁺ concentration up to 5 h incubation with 2 μM Aβ(1-42) added to the extracellular medium. In addition internalized Aβ(1-42) induced the decrease of Ca²⁺ influx from the extracellular medium through P2R after 2 h incubation. Furthermore, Aβ(1-42) incubated for 2 h and 5 h in HT-22 cells only induced a small increase in oxidative stress monitored with dihydrolchlorofluorescein. These results indicate that P2R and the molecular components of SOCE STIM1, IP3R and RyR are main targets for internalized Aβ(1-42) after a short time incubation with 2 μM Aβ(1-42) added to the extracellular medium, suggesting that these systems could be considered as candidates for therapeutic intervention in early stages of AD.

3. Materials and Methods

3.1 Chemicals

Human A β (1–42)-HiLyte™-Fluor555 was obtained from AnaSpec (Freemont, CA, USA). Unlabeled A β (1–42) and scrambled A β (1–42) were synthesized and supplied by StabVida (Caparica, Portugal). Fura-2 acetoxyethyl ester (Fura2 AM), Fluo-3-pentaacetoxyethyl ester (Fluo3 AM), 4-Bromo-A23187 and Pluronic®F-127 were obtained from Biotium (Hayward, CA, USA). Thapsigargin (Tg), A804598 and Calcein-AM were obtained from Sigma-Aldrich (Madrid, Spain) and BTP2 was from Merck Roche–Merck (Darmstadt, Germany). Ryanodine, LTCC and (-)-BAY-K-8644 were purchased from Tocris (Bristol, UK). MitoTracker™ Green FM (M7514), ER dye ER-Tracker™ Green FM (glibenclamide BODIPY® FL), tetramethylrhodamine ethyl ester (TMRE), C11-BODIPY^{581/591} and of 2',7' dichlorodihydrofluorescein diacetate (H₂DCFDA) were supplied by Invitrogen (Molecular Probes, Eugene, Oregon, USA). Monochlorobimane (MCB) was purchased from Calbiochem (San Diego, CA, USA). Xestospongin C (XeC) and Protein A/G PLUS-Agarose sc-2003 were purchased from Santa Cruz Biotechnology Inc. (Santa Cruz, CA, USA).

Primary antibodies: anti-LTCC subunit α 1C (sc-25686), anti synapsin-1 (sc-8295), anti-NMDA ϵ 1 subunit α 1C (sc-1468) or goat anti-protein disulfide isomerase (PDI) (sc17222) antibodies were supplied by Santa Cruz Biotechnology (Santa Cruz, CA, USA). Rabbit anti-calmodulin (CaM) (Epitomics 1716-1) antibody was supplied by Abcam (Cambridge, UK). Anti-STIM1 ps621 was kindly supplied by Dr. Francisco Javier Martin-Romero. Monoclonal mouse anti-A β antibody (A8354) was purchased from Sigma- Aldrich (Madrid, Spain). Fluorescent-labeled secondary antibodies used to label the primary antibodies listed above were: anti-rabbit IgG-Alexa488 (A11008) and anti-goat IgG-Alexa488 (A11055) from Invitrogen (Molecular Probes, Eugene, OR, USA). Anti-goat IgG-horseradish peroxidase was supplied by Sigma-Aldrich. Bio-Rad Clarity Western ECL substrate was purchased from Bio-Rad (Alcobendas, Madrid, Spain).

All other reagents and chemicals were of analytical grade from Sigma-Aldrich (Madrid, Spain) or Roche–Merck (Darmstadt, Germany).

3.2 A β (1–42) solutions and aggregation State

A 4 mg/mL A β (1–42) stock solution was prepared by solubilization of the peptide in 1% NH₄OH and further dilution with 100 mM HEPES/KOH (pH 7.4), as previously described⁴⁵. The aggregation state of A β (1–42) stock solutions used in this work was evaluated using the rapid

photoinduced cross-linking of unmodified proteins approach described in chapter 2 of this work⁴⁶.

3.3 HT-22 cell culture

The immortalized mouse hippocampal neuronal HT-22 cells were cultured in Dulbecco's modified Eagle's medium (DMEM)-high glucose, supplemented with 10% inactivated fetal bovine serum (FBS), 4 mM glutamine, 1 mM pyruvic acid, 100 U/mL penicillin and 100 µg/mL streptomycin, and kept at 37 °C in a humidified atmosphere of 95% air/5% CO₂ until reaching 70-80% confluence in the T-flask. For all experiments, HT-22 cells were seeded in 35 mm dishes at a density of 8x10³ cells/cm² in the culture media described above and allowed to grow for 48h at 37°C and 5% CO₂ before performing each experiment.

3.4 HT-22 cell differentiation

HT-22 cell differentiation was performed as previously described in other studies^{34,47-49}. Briefly, HT-22 cells were seeded in 35 mm dishes at a density of 4x10³ cells/cm² in the culture media described above for 24h at 37 °C and 5% CO₂. After 24h incubation the culture media was replaced for the differentiation culture media: DMEM-high glucose medium supplemented with 1x N2 supplement, 50 ng/ml nerve growth factor-β, 100 µM phorbol 12,13-dibutyrate and 100 µM dibutyryl cAMP, for 48h.

HT-22 cells cultured in differentiation medium were used in this work only to evaluate the activity of LTCC and NMDAR, through intracellular Ca²⁺ measurements with Fluo3 AM assay and for HT-22 cell staining with LTCC, NMDAR and Synapsin-1 antibodies.

3.5 Intracellular cytosolic Ca²⁺ measurements

Cytosolic Ca²⁺ imaging was assessed in the HT-22 cell culture with the fluorescent probes Fluo3 AM and Fura2 AM. Briefly, after cell seeding in 35 mm dishes, HT-22 cells were incubated with 2µM Aβ(1–42) for 2 h and 5 h in culture medium at 37 °C and 5% CO₂ with continuous and gentle mixing. Untreated cells were regarded as controls. One hour before the end of the incubation with Aβ(1–42), HT-22 cells were loaded with 5µM of Fura2 AM or Fluo3 AM plus 0.025% Pluronic® F-127 with continuous and gentle mixing. Then, cells were washed once with 1 mL of MLocke's K5 buffer and the 35 mm culture dishes were placed in the thermostatic plate at 37 °C (Warner Instrument Co., Hamden, CT, USA) of the Nikon Diaphot 300 inverted

epifluorescence microscope (Tokyo, Japan) with a NCF Plan ELWD 40× objective (pixel size of the images shown in this work 0.2 μm). Images of Fluo3-loaded cells were acquired with the Hamamatsu Orca-R2 CCD camera (binning mode 2 x 2) with an excitation filter of 470 nm and a dichroic mirror of 510 nm with an emission filter of 520 nm, and 0.3 s exposure time. Images of Fura2-loaded cells have been acquired as described in chapter 2 and in previous publications of this laboratory^{46,50,51}.

For the determination of Ca²⁺ cytosolic concentration using the Fluo3 probe⁵², 5mM MnCl₂ (Ca²⁺ quencher) and 5 μg/mL of the nonfluorescent Ca²⁺ ionophore 4-Bromo-A23187 were added to HT-22 cells and the fluorescence microscopy images were recorded in the kinetic mode to obtain the fluorescence intensity of Fluo3 saturated with Mn²⁺ [F(Mn-Fluo3)], which has been reported to be 20% of the value of fluorescence intensity at saturating Ca²⁺ (F_{max})⁵³. The fluorescence value of free Fluo3 (not bound to Ca²⁺), F_{min} , is about 0.01· F_{max} ⁵³. Intracellular Ca²⁺ concentration ([Ca²⁺]_i) was measured using the formula: [Ca²⁺]_i = kD [(F - F_{min})/(F_{max} - F)], where F is the fluorescence intensity obtained with an excitation filter of 470 nm, and 510 nm dichroic mirror/520 nm emission filter with 0.1 s exposure time. The dissociation constant (kD) for Fluo3/Ca²⁺ complex used to obtain the [Ca²⁺]_i was 390nM⁵⁴.

The activation of LTCCs in HT-22 cells loaded with Fluo3 were assessed by addition of different concentrations of potassium chloride (KCl, 5-200 mM) to the medium assay or by addition of 50 μM of the LTCC agonist (-)-BAY-K-8644. The activity of NMDAR was evaluated after addition of 10 μM glycine plus 100 μM glutamate to the extracellular medium or by addition of the antagonist MK801 (10 μM). These experiments were performed in HT-22 cells cultured in DMEM (designated as undifferentiated) and in HT-22 cells cultured in differentiated medium (designated as differentiated), as described above.

The response of P2R was performed in loaded-Fluo3 HT-22 cultured in DMEM medium, in the absence (control) or presence of 2 μM Aβ(1-42) incubated for 0.5 h or 2 h at 37 °C and 5% CO₂ and gentle mixing. The activation of P2R was evaluated after addition of the agonist ATP (100 μM) to the extracellular medium assay of HT-22 cells. The inhibition of P2X7R (a subtype of the P2R family) was evaluated with two different antagonists: i) 5μM Brilliant Blue G (BBG) preincubated in MLocke's K5 buffer for 5 minutes before the addition of ATP, or ii) 200 nM of A804598 preincubated for 0.5 h in HT-22 culture media, followed by a cell wash with MLocke's 5 buffer and addition of ATP.

The response of SOCE was performed in loaded-Fluo3 HT-22 cultured in DMEM medium, in the absence (control) or presence of 2 μM Aβ(1-42), incubated for 2 h at 37 °C and 5% CO₂ and gentle mixing-. The depletion of Ca²⁺ stores was triggered by adding the SERCA pump blocker thapsigargin (Tg, 2 μM) plus EGTA (1 mM), in Ca²⁺- free MLockeK'5 buffer. Then, SOCE

was measured after the addition of 3 mM CaCl₂ to the Tg-containing medium. As a positive control of this experiment, we measured SOCE in the presence of the selective inhibitor BTP2 (3 μM) preincubated for 15 min in HT-22 culture media. Activities of the ligand-gated Ca²⁺ channels RyR and the IP3R from ER were evaluated by incubation with 100 μM of the RyR antagonist ryanodine for 1h in HT-22 culture media or by incubation of 3 μM XeC for 15 min in Ca²⁺-free MLocke's K5 buffer. In all experiments with antagonists, we performed the respective DMSO vehicle controls. Also, the response of P2R and SOCE was evaluated in the presence of 2 μM scrambled Aβ(1-42) incubated for 2 h at 37 °C and 5% CO₂.

Data acquisition and analysis were done with HClImage software after the selection of the cells using the ROI (region of interest) tool of this software. The average intensity of fluorescence per pixel within HT-22 cells were performed at least in 8-10 petri plates in 4 or 5 independent assays, n> 60-80 cells in each case.

3.6 HT-22 cell staining with LTCC, NMDAR and Synapsin-1 antibodies

Undifferentiated and differentiated HT-22 cells were cultured in 35 mm dishes as described above and washed with MLocke's K5 buffer to remove the phenol red remaining in the plates. Afterwards, cells were fixed with 2.5% para-formaldehyde, 3 mM MgCl₂, 2 mM EGTA and 0.32 M sucrose in PBS (5 mM sodium phosphate, 137 mM NaCl, and 27 mM KCl, pH 7). Fixed and permeabilized cells were blocked with 1% bovine serum albumin (BSA) in PBS supplemented with 0.2% Triton X-100 (PBST) for 1 h at 37 °C and washed three times with PBS (washing step). Then, cells were incubated during 1 h at 37 °C with the respective target primary antibody in PBST: anti-LTCC subunit α1C, anti synapsin-1 or anti-NMDAε1 subunit α1C. Thereafter, HT-22 cells were washed and incubated for 1 h with the appropriate Alexa488-labeled secondary antibody in PBST (1:200) and washed again. Images of undifferentiated and differentiated HT-22 cells were acquired with an excitation filter of 470 nm, and 510 nm dichroic mirror/520 nm emission filter (GF) using the exposure times indicated for each case in the legends of the figures. Quantitative analysis of the average fluorescence intensity per pixel of selected neuronal soma was done with the HClImage software using the ROI tool, as in previous works.

3.7 Cell viability using the MTT assay

HT-22 cells were incubated with 2 μM Aβ(1-42) for 5 h at 37 °C and 5% CO₂ and gentle mixing. Then, cells were washed with 1 mL MLocke's K5 buffer and cell viability was experimentally assessed measuring the amount of colored formazan by the reduction of 3-(4,5-

dimethylthiazol-2-yl)-2,5-diphenyltetrazolium bromide (MTT) as in previous works^{46,50,55,56}. Untreated cells were regarded as controls (100% cell survival) and the cell survival ratio was expressed as the percentage of the control.

3.8 Measurement of internalized Aβ(1–42)-HiLyte™-Fluor555 and evaluation of subcellular colocalization with mitochondria and endoplasmic reticulum

The internalization of Aβ(1–42)-HiLyte™-Fluor555 (referred as Aβ(1–42)*555) in the HT-22 cell culture was measured using a similar experimental approach described earlier with some modifications⁴⁶. The amount of Aβ(1–42) internalized was estimated from the increase in RF in HT-22 cells at different times of incubation (2 h and 5 h) at 37 °C and 5%CO₂ with a total concentration of 2 μM of Aβ(1–42) (1.6 μM of Aβ(1–42) + 0.4 μM of Aβ(1–42)*555) added to the culture medium. Then, cells were washed once with 1mL of MLocke's K5 and the 35mm dishes were placed in the holder of the microscope at 37 °C for RF imaging. Fluorescence microscopy images of HT-22 were acquired with a Hamamatsu Orca-R2 CCD camera (binning mode 2 × 2) camera (Hamamatsu, Hamamatsu-city, Japan) attached to a Nikon Diaphot 300 epifluorescence microscope (Tokyo, Japan) with a NCF Plan ELWD 40× objective, using an excitation filter of 556 nm and a dichroic mirror of 580 nm with an emission filter of 590 nm, and 0.06 s exposure time. The ROI tool of the HCImage software was used for the quantitative analysis. The average fluorescence intensity readings per pixel in HT-22 cells were taken from several fields for a total number of 80 cells, and after subtraction of autofluorescence. In a parallel experiment, the average intensities per pixel obtained with increasing concentrations of Aβ(1–42)*555 in fixed HT-22 cells were recorded for calibration of the Aβ(1–42)*555 fluorescence under the same experimental conditions.

After cell incubation with Aβ(1–42)*555 for 5 h and RF imaging , HT-22 were incubated with 20 nM of the mitochondria fluorescent dye MitoTracker™ Green FM or with 100 nM of the ER dye ER-Tracker™ Green FM for 5 min at 37 °C and 5% CO₂ and gentle mixing. Then, cells were washed with MLocke's K5 buffer and placed again in the holder of the microscope at 37 °C. GF imaging was acquired with an excitation filter of 470 nm, and 510 nm dichroic mirror/520 nm emission filter with an exposure time between 0.4 - 0.6 s and RF imaging was acquired with direct excitation filter (556nm) with a dichroic mirror of 580 nm/590 nm emission filter, with an exposure time of 0.06 s respectively. The software ImageJ was used for color processing and to merge the pseudocolor green images (MitoTracker™ Green FM or ER-Tracker™ Green FM) and red images (Aβ(1–42)*555).

3.9 Mitochondrial membrane potential ($\Delta\Psi_m$)

Mitochondrial depolarization was monitored with the fluorescent dye tetramethylrhodamine ethyl ester (TMRE) as previously described with some modifications^{56,57}. Briefly, HT-22 cells were incubated with 2 μ M of A β (1-42) for 2 h or 5 h at 37 °C and 5% CO₂. Next, untreated cells (control) and cells treated with A β (1-42) were washed once with MLock's K5 buffer and loaded with 100 nM of TMRE for 10 min at 37 °C and 5% CO₂ and with continuous and gentle mixing, as previously described. Then, HT-22 culture dishes were placed in the thermostatic plate at 37 °C of the inverted epifluorescence microscope and the fluorescence kinetic was recorded at 556 nm excitation filter and a dichroic mirror of 580 nm with an emission filter of 590 nm and a time of exposure 0.01 s. To assess the level of the mitochondrial membrane depolarization, it was added 5 μ M of a potent mitochondrial oxidative phosphorylation uncoupler -FCCP - (Trifluoromethoxy carbonylcyanide phenylhydrazone) to the medium. The ROI tool of the HClImage software was used for the quantitative analysis. The average fluorescence intensity readings per pixel in HT-22 cells were taken from several fields for a total number of 80 cells.

3.10 FRET imaging

FRET imaging was performed as described in the previous chapter of this thesis and in previous works of the laboratory^{46,50,58}. First, HT-22 cells were stained with different concentrations of A β (1-42)*555 (25-100nM) in order to perform the measurements with the lowest A β (1-42)*555 concentrations to highlight only the subcellular location of the high affinity binding sites for A β (1-42). Fixed and permeabilized HT-22 cells were blocked with 1% BSA in PBST for 1 h at room temperature (RT) and washed three times with PBS (washing step). Then, cells were incubated only with PBST for 2 h at 37 °C (to simulate the incubation with primary and secondary antibodies) and after the washing step, 25 nM of A β (1-42)*555 was added to the plate and incubated for 15 at RT and gentle mixing. HT-22 cells were placed at the inverted epifluorescence microscope and imaging acquisition was performed using an excitation filter of 556 nm and 470 nm and a dichroic mirror of 580 nm with an emission filter of 590 nm (RF), and 0.03 s exposure time. Afterwards, the same procedure was repeated for 50, 75 and 100 nM A β (1-42)*555.

The following selected protein targets for FRET imaging were used: protein disulfide isomerase (goat anti-PDI, 1:50) and calmodulin (rabbit anti-CaM, 1:200). After blocking with 1% BSA in PBST for 1 h, HT-22 cells were incubated for 1h with the respective primary antibodies

(anti-PDI or anti-CaM) diluted in PBST. Next, HT-22 were incubated for 1 h with the appropriate Alexa488-labeled secondary antibody in PBST (1:200) and washed again before acquisition of fluorescence microscopy images stained only with the donor dye. Image acquisition was performed with an excitation filter of 470 nm, and 510 nm dichroic mirror/520 nm emission filter (GF), using the exposure times indicated for each case in the legends of the figures. After finishing the acquisition of FRET donor images, HT-22 cells were incubated for 15 min at RT with 25, 50 or 100 nM A β (1–42)*555 in PBS with continuous and gentle mixing. GF and RF imaging acquisitions were performed as early described. Contribution of HT-22 autofluorescence and secondary Alexa488-antibody in the absence of the primary antibody were assessed before running FRET experiments and were found to be lower than 5% of the average fluorescence intensity per pixel obtained with specific primary antibodies. This background signal was subtracted for calculations of the RF/GF ratio obtained with HT-22 plates

3.11 Co-immunoprecipitation

The formation of STIM1:A β (1-42) complexes was evaluated using the co-immunoprecipitation protocol described previously, with some modifications⁴⁶. HT-22 cells were lysed in buffer: 25 mM Tris-HCl, pH 7.4, 150 mM NaCl, 5 mM EDTA, 50 mM NaF, 5 mM NaVO₃, 0.25% 4-(1,1,3,3-tetramethyl butyl) phenyl-polyethylene glycol (Triton X-100), 5 mM of methyl- β -cyclodextrin, supplemented with 1x SIGMAFAST™ protease inhibitor cocktail. After cell centrifugation at 2000 g for 2 min at 4°C, the supernatant was collected and supplemented with 50% glycerol. The Bradford's method was used to measure the protein concentration in HT22 lysates using bovine serum albumin as the standard. Co-immunoprecipitation was carried out using the protein A/G PLUS-Agarose, following the instructions described in the technical data sheet. Briefly, in an eppendorf tube, 500 μ g of HT-22 lysate was incubated for 1h with 10 μ g mouse anti- β -amyloid antibody at 4 °C with continuous shaking. Afterwards, 50 μ L protein A/G PLUS-Agarose was added and incubated overnight at 4 °C with continuous shaking. The next day, the PBS control sample or 0.25 μ M A β (1–42) in PBS (treated sample) was added and incubated for 1 h at 4 °C with continuous shaking. The matrix was precipitated by centrifugation at 2500 g during 5 min at 4 °C in a refrigerated Eppendorf microcentrifuge. Then, the precipitated matrix was subjected to three washes with 50 μ L PBS (control sample) or 50 μ L PBS plus 0.25 μ M A β (1–42) (treated sample). A centrifugation step (2500 g, 5 min at 4 °C) was performed in a refrigerated Eppendorf in each washing step. The supernatant was carefully removed, and the matrix precipitate was resuspended in 25 μ L of electrophoresis sample buffer, boiled during 4 min, and stored at –20 °C until running on an SDS-PAGE gel for western blotting analysis.

3.12 Fluorescence measurements and calculation of the FRET parameters J and R₀

Fluorescence measurements were performed using a Fluoromax+ fluorescence Spectrophotometer (Jovin Yvon technologies) at RT (24-25°C), in quartz cells of 1 cm light-pathlength, with excitation and emission slits set to 2 nm. The FRET parameters J and R₀ for the donor/acceptor pair GFP-STIM1/Aβ(1-42)*555 have been measured and calculated as in previous works of our laboratory^{59,60}. A value of 0.6 has been used for the quantum yield of GFP⁶¹, and we have calculated a value of R₀ = 6.3 nm.

3.13 Western blotting

SDS-PAGE was run at a concentration of 7.5% acrylamide, using 20 µL co-immunoprecipitated sample per lane, as described in chapter 2 with some modifications⁴⁶. Gels were transferred to polyvinylidene difluoride (PVDF) membranes of 0.2 µm pore size and blocked with 3% BSA in Tris-buffered saline (TBS) supplemented with 0.05% polyoxyethylene sorbitan monolaurate (Tween 20) (TBST) for 1 h at RT. Membranes were washed three times with TBST (washing step) and incubated with the primary antibody anti-STIM1 ps621 (1µg/mL) diluted in TBST for 1h at RT. After the washing step, membranes were incubated with the secondary IgG antibody conjugated with horseradish peroxidase (anti-Goat HRP) at a dilution of 1:2000 in TBST for 1h at RT. Then, membranes were washed three times with TBST followed by incubation for 3 min with the Bio-Rad Clarity Western ECL substrate. Western blots were revealed with Bio-Rad ChemiDoc™ XRS+ (Bio-Rad, Hercules, CA, USA) and data analyzed with Image Lab 6.0.1 software.

3.14 PDI-dependent disulfide reduction assay

PDI reduction activity was measured as previously described with some modifications⁶². Briefly, 34 µg of protein of HT-22 lysate was incubated with 150mM of the pseudo subtract of PDI, dieosin glutathione disulfide (Di-E-GSSG) in PDI buffer assay (100 mM phosphate plus 2 mM EDTA, pH 7.0) in the absence (control) or presence of 200 nM Aβ(1-42). Fluorescence intensity was measured at room temperature (24 ± 1 °C), with excitation and emission wavelengths of 522 and 550 nm, respectively.

3.15 Generation of ROS

For the detection of intracellular ROS levels it was measured the oxidation of H₂DCFDA to the fluorescent compound dichlorofluorescein (DCF) as previously described⁵⁵ with minor modifications. Briefly, untreated HT-22 (control) and treated cells incubated with 2 µM of Aβ(1-42) for 2 h or 5 h at 37 °C and 5% CO₂ were washed once with MLocke's K5 buffer and placed in the thermostatic controlled plate at 37 °C of the Nikon Diaphot 300 inverted epifluorescence microscope. Then, 10 µM of H₂DCFDA was added to the medium and the fluorescence intensity was recorded each 15 s for 10 min with an excitation filter of 470 nm, and 510 nm dichroic mirror/520 nm emission filter (GF), using an exposure time of 0.2 s.

3.16 Measurement of glutathione levels

Glutathione (GSH) levels were determined using MCB as previously described, with minor modifications⁶³. Briefly, untreated HT-22 cells (control) and cells treated with 2 µM Aβ(1-42) for 2 h and 5 h at 37° C and 5% CO₂ were washed once with MLocke's K5 buffer and placed in the thermostatic controlled plate at 37 °C of the epifluorescence microscope. Afterwards, 10 µM MCB was added to the extracellular medium and the fluorescence intensity was recorded every 10 s for 5 min with an excitation filter of 380 nm and a dichroic mirror DM510 plus an emission filter of 510 nm, using an exposure time of 0.7 s.

3.17 Measurement of lipid peroxidation

Lipid peroxidation was measured as previously described⁶⁴. HT-22 cells were incubated with 1 µM of the fluorescent ratio probe C11-BODIPY^(581/591) for 30 min in untreated cells (control) and for 2 h and 5 h at 37 °C and 5 % CO₂ in cells treated with 2 µM Aβ(1-42). Afterwards, cells were washed with MLocke's K5 buffer and placed at the holder of the microscope (37 °C). Cell imaging was acquired with an excitation filter of 470 nm and a dichroic mirror of 580 nm/emission filter of 590 nm (RF, reduced form C11-BODIPY^(581/591)) with an exposure time of 0.2 s and with a 510 nm dichroic mirror/520 nm emission filter (GF, oxidized form of C11-BODIPY^(581/591)) with an exposure time of 1 s.

3.18 Iron influx assay using Calcein-AM

Ferrous iron influx into HT-22 cells was measured by the quenching of Calcein fluorescence as previously described, with minor modifications⁶⁵. Briefly, untreated (control) and HT-22 cells treated with 2 µM Aβ(1-42) for 2 h, were loaded with 0.1 µM Calcein-AM plus 0.025% Pluronic® F 127 for 30 min. Afterwards, cells were washed once with Ca²⁺ and EGTA free-MLocke's K5 buffer (medium assay) and placed at the holder of the fluorescence microscope (37 °C) for imaging acquisition with an excitation filter of 470 nm, and 510 nm dichroic mirror/520 nm emission filter. Fluorescence intensity was measured every 30 s during 20 min with an exposure time of 0.2 s, before and after the addition of 200 µM FeCl₃ plus 400 µM L-ascorbate.

3.19 Images of HT-22 cells plus cholera toxin B-Alexa*555

HT-22 cells seeding in 35 mm dishes were incubated with 1 µg/mL of cholera toxin B-Alexa*555 (CTB*555) for 30 min at 37 °C and 5% CO₂. Next, HT-22 plates were placed at the holder of the microscope and imaging acquisition was performed at 556 nm and a dichroic mirror of 580 nm with an emission filter of 590 nm with an exposure time up to 1 s.

3.20 Statistical Analysis

Statistical analysis was carried out by the Student's t-test and results were expressed as the mean standard deviation (s.d.). A significant difference was accepted at the *p* < 0.05 level. All results were done at least in 8 - 10 petri plates in 4 - 5 independent assays (*n* > 60 - 80 cells) for each condition.

4. Results

4.1 Ca²⁺ entry systems from the extracellular medium in HT-22 cells in culture.

4.1.1 LTCC are expressed in low levels in HT-22 cells in culture: LTCC activation through the LTCC-selective agonist (-)-BAY-K-8644

The addition of KCl to the culture medium is a method extensively used to depolarize the plasma membrane of cultured neurons, leading to the sustained increase of cytosolic Ca²⁺

influx through mainly the LTCCs⁶⁶. Besides, the dihydropyridine (-)-BAY-K-8644 allows LTCCs to open at significantly lower levels of depolarization, increasing Ca^{2+} influx⁶⁷. In this work we used 25 mM KCl or 50 μM of the agonist (-)-BAY-K-8644 to study the alteration of the resting cytosolic Ca^{2+} concentration in HT-22 cells loaded with the Ca^{2+} indicator Fluo3. The results are shown in the **Figure 1**, and demonstrated that the addition of 25 mM KCl to the extracellular medium (MLocke's K5 buffer) did not altered the resting cytosolic Ca^{2+} concentration, whereas the addition of 50 μM (-)-BAY-K-8644 elicited the cytosolic Ca^{2+} influx in the HT-22 cells, leading to a peak increase of Fluo3 fluorescence of $31 \pm 3\%$, comparing with the basal levels of Fluo3 fluorescence before addition of (-)-BAY-K-8644. However, these results show that the effect of (-)-BAY-K-8644 on cytosolic Ca^{2+} concentration is transient, lasting less than 2 min and with a half-peak width of around 60 s.

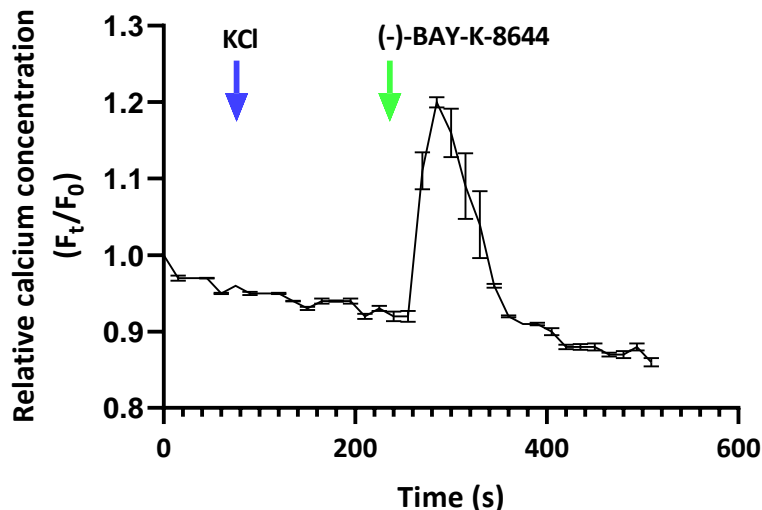


Figure 1. Intracellular cytosolic Ca^{2+} concentration changes after HT-22 cells treatment with i) 25mM KCl and ii) 50 μM (-)-BAY-K-8644. HT-22 cells were incubated with 5 μM Fluo3 AM plus 0.025% Pluronic® F-127 for 1h at 37 °C and washed once with MLocke's K5 buffer. HT-22 cells loaded with Fluo3 were placed at the holder of the fluorescence microscope (37 °C) for Ca^{2+} imaging as described in Materials and Methods section. The kinetic trace shows the average of fluorescence intensity per pixel (F_t/F_0 ; F_t is fluorescence value at any time; F_0 fluorescence value at time 0) in the HT-22 cells before and after the addition of 25 mM KCl (indicated by the blue arrow) and after the addition of 50 μM of the agonist (-)-BAY-K-8644 (indicated by the green arrow). Other experimental parameters: exposure time of 0.3 s and time intervals of 15 s. The results show no alteration in Ca^{2+} concentration after KCl addition to the extracellular medium and a peak increase of Fluo3 fluorescence of $31 \pm 3\%$ due the entry of Ca^{2+} after addition of 50 μM (-)-BAY-K-8644. Results presented are the mean \pm s.d. of experiments done at least in 10 petri plates in 5 independent assays ($n > 80$ cells).

The lack of effect in membrane depolarization after addition of 25 mM KCl in HT-22 cells and the large variability in KCl concentration treatments published in scientific papers⁶⁶ lead us

to test different concentrations of KCl, ranging between 5 and 200 mM. Our results indicated no significant increase in Ca^{2+} influx after application of different KCl concentrations (data not shown). This result can account for the lack of scientific studies about LTCCs in this cell model. Nevertheless, considering the positive response with the agonist (-)-BAY-K-8644, we tested for the presence of LTCCs in HT-22 cells by fluorescence microscopy imaging, by staining fixed and permeabilized HT-22 cells with anti-LTCC subunit $\alpha 1\text{C}$ antibody conjugated with IgG-Alexa 488 (anti-LTCC*A488) (**Figure 2**). A direct observation of the representative image of HT-22 cells stained with anti-LTCC*A488 (**Figure 2b**) allow us to confirm the presence of LTCCs with a higher expression in central somatic regions. However, it is of note that we needed to increase the time of exposure up to 1 s to be able to detect LTCCs, highlighting that these channels are expressed in low levels in the HT-22 cell model.

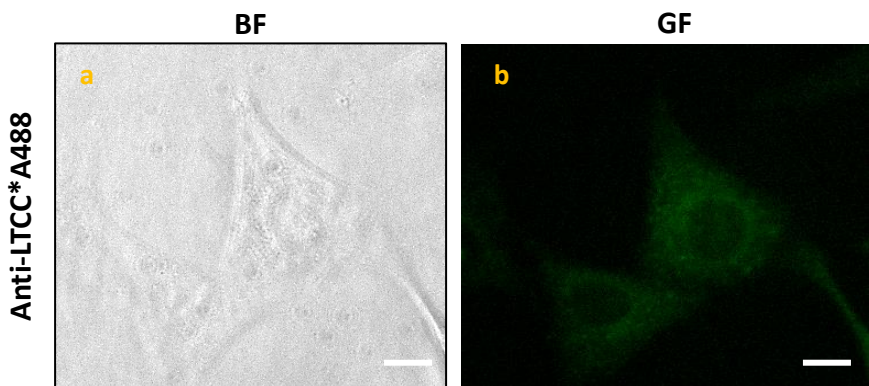


Figure 2. HT-22 cells express LTCCs. Representative microscopy images of fixed HT-22 BF (Figure 2a) and HT-22 cells stained with anti-LTCC subunit $\alpha 1\text{C}$ conjugated with the respective secondary antibody IgG-Alexa488 (GF, Figure 2b). The exposure time for GF was 1s. Scale bar inserted in fluorescence microscopy images = 20 μm .

With these findings we demonstrated that HT-22 cells do not respond to KCl depolarization because LTCCs are inactive under normal culture conditions, and the low levels of LTCC expressed in this cell model are transiently activated only through the addition of 50 μM of the agonist (-)-BAY-K-8644. Therefore, we can conclude that LTCCs do not play a significant role for the control of Ca^{2+} homeostasis in HT-22 cell model.

4.1.2 NMDAR and LTCCs are expressed in morphologically differentiated HT-22, but they are inactive

During the last years some efforts have been made to differentiate HT-22 to express NMDAR^{34,48,68} using several cell differentiation methods. In this work we used a differentiation

protocol as previously described (see Materials and Methods section) aiming to differentiate the immortalized HT-22 cell line in more mature-like neurons, and we have experimentally evaluated its ability to functionally express NMDAR.

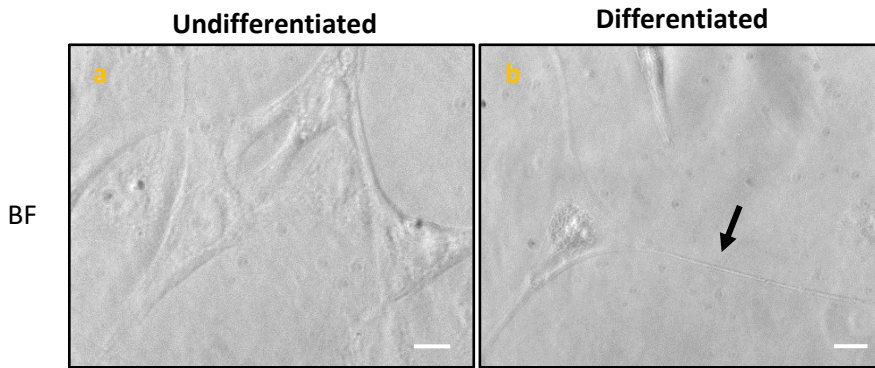


Figure 3. Representative BF images of undifferentiated (a) and differentiated (b) HT-22 cells. HT-22 cells were cultured in DMEM (undifferentiated) or in the differentiation medium (differentiated) as indicated in the Materials and Methods section. The black arrow in Figure 3b indicates neurites. Scale bar = 20 μ m.

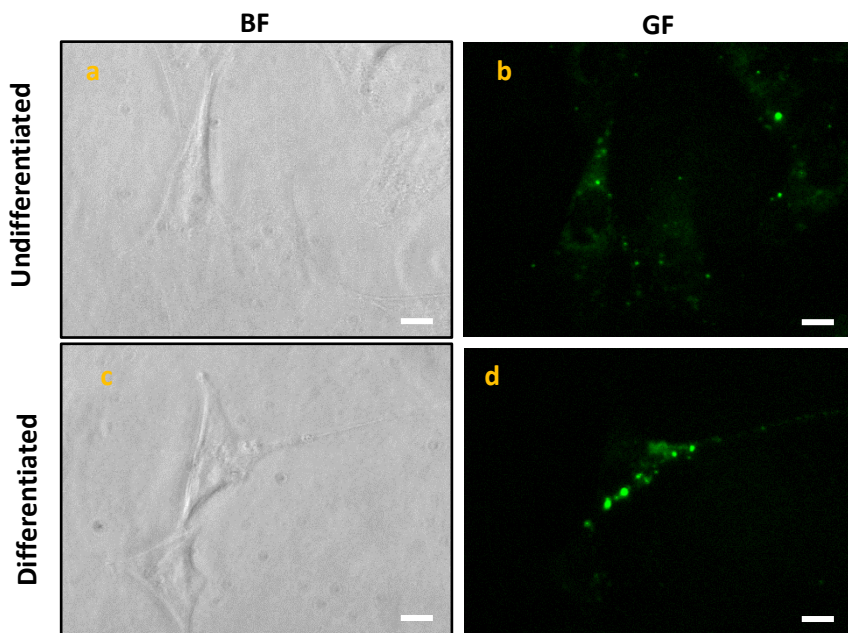


Figure 4. Differences of synapsin-1 expression pattern in undifferentiated (b) and differentiated cells (d). Undifferentiated and differentiated HT-22 were stained with anti-synapsin-1 conjugated with IgG-Alexa488 secondary antibody. The representative microscopy images indicate BF (Figure 4a and b) and the GF (Figure 4b and d) of undifferentiated and differentiated HT-22 cells. The exposure time to acquire GF images was 1s. Scale bar = 20 μ m.

After 48h in differentiation medium, some of the HT-22 cells differentiated to a mature neuronal state through the development of extended neurites (**Figure 3b**), comparing with undifferentiated cells (**Figure 3a**). Besides the evident morphological changes between undifferentiated and differentiated HT-22, we stained fixed and permeabilized cells with the

pre-synaptic marker anti-synapsin-1 conjugated with IgG-Alexa 488 (anti-synapsin-1*A488) to evaluate the neuronal differentiation. The results show (**Figure 4**) a higher and focalized expression of synapsin-1 in differentiated HT-22, comparing with undifferentiated cells, demonstrating once more that HT-22 were able to be differentiated in mature neurons.

Next, we assessed the expression and activity of LTCCs and NMDARs through fluorescence microscopy imaging of fixed HT-22 and by evaluating the Ca^{2+} response of HT-22 cells loaded with Fluo3, respectively. The direct observation of the representative images of cells stained with anti-LTCC*A488 (**Figure 5**) shows clear differences in the LTCC expression pattern in undifferentiated (**Figure 5b**) and differentiated HT-22 cells (**Figure 5d**). While undifferentiated cells have a more diffuse pattern through all the soma, differentiated HT-22 cells present a stronger cluster-like pattern with focalized expression of LTCC.

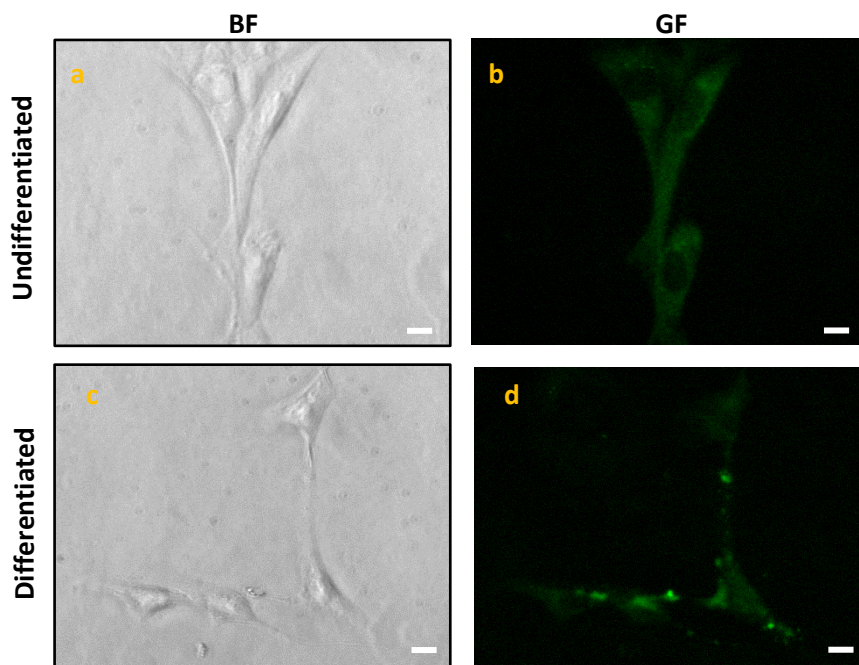


Figure 5. Differences of LTCC expression pattern in undifferentiated and differentiated cells. HT-22 cells were cultured for 2 days in DMEM (undifferentiated) or in the differentiation medium (differentiated) as indicated in the Materials and Methods section and stained with anti-LTCC subunit $\alpha 1\text{C}$ /IgG-Alexa488 antibody. The representative microscopy images indicate the BF (Figure 5a and b) and the GF (Figure 5b and d) of undifferentiated and differentiated HT-22 cells. The exposure time to acquire GF images was 0.8–1 s. Scale bar inserted in microscopy images = 20 μm .

However, the results obtained with the Fluo3-loaded HT-22 cells show that plasma membrane depolarization produced by increasing KCl up to 200 mM in the extracellular medium does not significantly increase the resting cytosolic Ca^{2+} concentration (data not shown) in undifferentiated cells.

The expression of NMDAR in both differentiated and undifferentiated HT-22 was

assessed by staining cells with anti-NMDA ϵ 1 antibody conjugated with IgG-Alexa 488 (anti-NMDA ϵ 1*A488) and the NMDAR activity evaluated by studying the Ca $^{2+}$ response through extracellular addition of the agonist glutamate plus glycine or by addition of the antagonist MK801. In this case, the representative images in **Figure 6** show no significant differences in NMDAR expression pattern between undifferentiated (**Figure 6b**) and differentiated cells (**Figure 6d**). Also, the addition of 10 μ M glycine plus 100 μ M glutamate to the extracellular medium of HT-22 loaded with the Ca $^{2+}$ indicator Fluo3, showed no difference in Ca $^{2+}$ influx in both undifferentiated and differentiated HT-22, as well as no response to the antagonist MK801 (10 μ M) (data not shown).

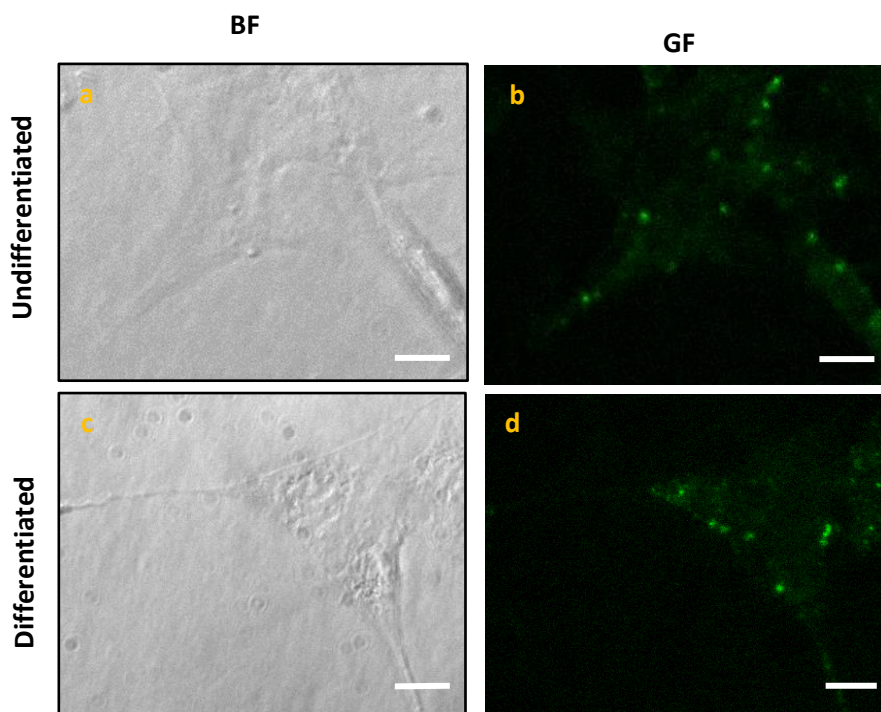


Figure 6. NMDAR expression pattern in undifferentiated and differentiated cells. HT-22 cells were culture for 2 days in DMEM (undifferentiated) or in the differentiation medium (differentiated) as indicated in the Materials and Methods section, and stained with anti-NMDA ϵ 1 subunit α 1C /IgG-Alexa488 antibody. The representative microscopy images indicate the BF (Figure 6a and b) and the GF (Figure 6b and d) of undifferentiated and differentiated HT-22 cells. The exposure time to acquire GF images was 0.6-0.8 s. Scale bar inserted in microscopy images = 20 μ m.

With the results obtained herein we can conclude that the differentiation protocol used in this study was able to change morphologically HT-22 cells for a more neuron-like pattern with the development of neurites, and with high expression of synapsin-1 and LTCCs. However, despite the increase in LTCC expression and change in LTCC pattern, HT-22 cells differentiated in the differentiation medium described in the Materials and Methods remained inactive after KCl induced depolarization, as well as undifferentiated cells in DMEM. Therefore, we decided to

continue with the experimental studies with HT-22 cultured in normal DMEM media displaying the morphological appearance of differentiated neurons with large axons.

4.1.3. P2R activation can elicit large peaks of cytosolic Ca²⁺ concentration in HT-22 cells

As the LTCC and NMDAR are inactive as previously demonstrated and the AChRs are expressed in very low levels or inactive as mentioned in introduction section, next we wanted to identify the neuronal ionotropic receptors expressed in HT-22 cells that could be responsible for large Ca²⁺ influx from the extracellular medium. Taking into account that P2R whose activation can elicit large peaks of cytosolic Ca²⁺ concentration in neurons, and that they are expressed in the *hippocampus*^{69,70}, we have evaluated the possibility that activation of P2R can provide a major pathway for Ca²⁺ entry from the extracellular medium in the HT-22 cell cultures used in this work. P2R can be classified into two subfamilies: G-protein-coupled metabotropic (P2Y) and ligand-gated ionotropic (P2X) receptors⁷¹. All the seven P2X receptors subtypes (P2X1r-P2X7R) and two subtypes of P2Y receptors (P2Y2 and P2Y11) exhibit high Ca²⁺ permeability upon activation by extracellular ATP treatment⁷¹. Therefore, aiming to evaluate the effect of ATP on the resting Ca²⁺ cytosolic concentration, we added 100 µM ATP to the extracellular medium of HT-22 cells loaded with Fluo3 (**Figure 7**).

As observed in the **Figure 7**, there is a rapid increase of the fluorescence intensity of Fluo3-loaded HT-22 after the addition of the P2R agonist ATP (100 µM), reaching a peak of 2.0-fold increase of fluorescence. These results confirmed the presence of functional Ca²⁺ ionotropic P2R in HT-22 cell culture. In fact, it is important to note and highlight the differences in P2R and LTCC Ca²⁺ responses (**Figure 8**) after treatment with their respective stimuli (ATP or (-)-BAY-K-8644). The **Figure 8A** clearly shows that P2R open faster in response to extracellular addition of 100 µM ATP than LTCC responds to 50 µM of (-)-BAY-K-8644 and also that the Ca²⁺ influx after treatment with 100 µM ATP is about 1.5-fold higher comparing to the response with the agonist (-)-BAY-K-8644. Furthermore, the time duration of Ca²⁺ entry through P2R is larger than the LTCC response, as demonstrated not only by the kinetic plot (**Figure 8A**) but also by the Area Under Cure (A.U.C., **Figure 8B**) which is 4.5-fold higher for P2R, comparing with LTCC activation by (-)-BAY-K-8644.

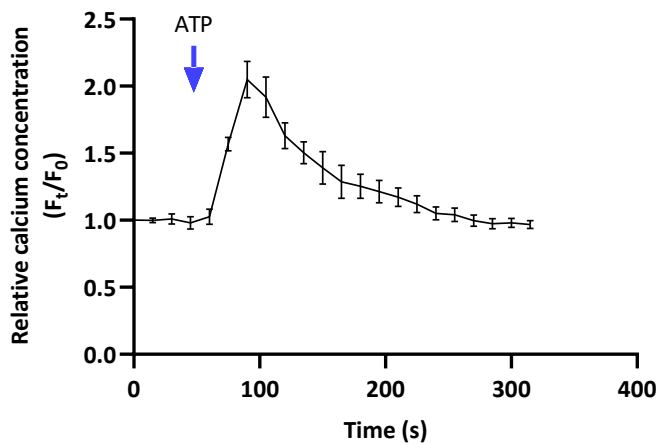


Figure 7. Representative kinetic trace of intracellular Ca^{2+} concentration after addition of ATP. HT-22 cells were incubated with 5 μM Fluo3 AM plus 0.025% Pluronic® F-127 for 1h at 37 °C and then changed to MLocke's K5 buffer (37 °C). The kinetic trace shows the average fluorescence intensity per pixel (F_t/F_0) in the HT-22 cells before and after the addition of 100 μM ATP (indicated by the blue arrow). Other experimental parameters: exposure time of 0.3 s and time intervals of 15 s. Results are the mean \pm s.d. of experiments done at least in 10 petri plates in 5 independent assays ($n > 80$ cells).

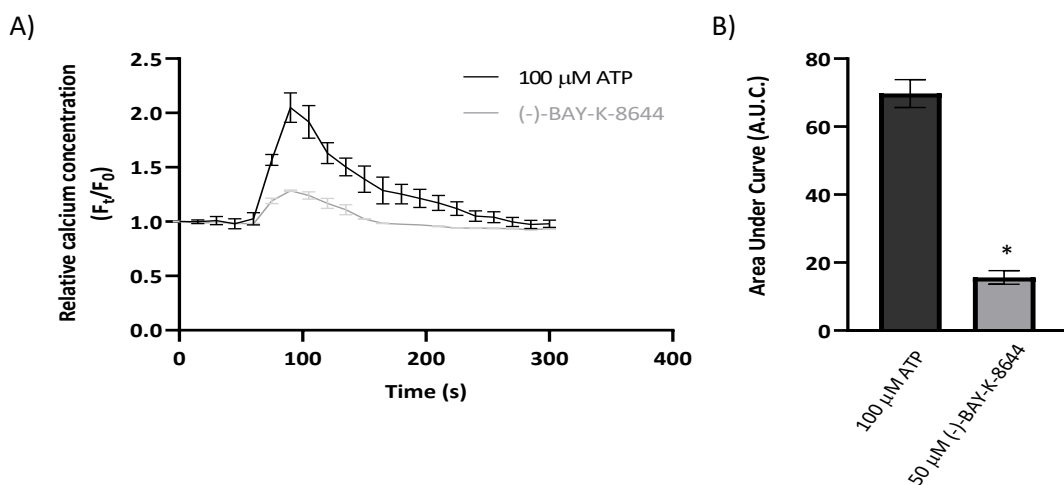


Figure 8. Increase in cytosolic Ca^{2+} influx after HT-22 cells treatment with ATP or (-)-BAY-K-8644. HT-22 cells were loaded with Fluo3 in culture media for 1h at 37 °C and 5% CO_2 and then washed with MLocke's K5 buffer. HT-22 plates were placed at the holder of the fluorescence microscopy for Ca^{2+} imaging as described in Materials and Methods section. **A)** Changes in Ca^{2+} signals were evaluated as time-series curves of the average of fluorescence intensity per pixel (F_t/F_0) after addition of 100 μM ATP or 50 μM (-)-BAY-K-8644. Results show that P2R opens faster and that the influx of Ca^{2+} is 1.5-fold higher in response to extracellular addition of 100 μM ATP than LTCC respond to 50 μM of (-)-BAY-K-8644. **B)** The Area Under Curve (AUC), calculated for both treatments demonstrated that Ca^{2+} entry through P2R with ATP is 4.5-fold higher than the LTCC response to (-)-BAY-K-8644 (* $p < 0.05$). Results presented are the mean \pm s.d. of experiments done at least in 10 petri plates in 5 independent assays ($n > 80$ cells).

Since LTCCs and NMDAR are inactive as we demonstrated before, the results indicate that P2R could be the main plasma membrane transport systems that are responsible for Ca^{2+} influx from the extracellular medium in the HT-22.

4.1.4 SOCE mechanism in HT22 cell cultures

In this study, we have monitored SOCE by measurement of ER Ca^{2+} depletion after the addition of 2 μM Tg, a SERCA inhibitor, plus 1mM EGTA in the Ca^{2+} -free MLocke's K5 buffer, and then we recorded the increase in cytosolic Ca^{2+} concentration by adding 3 mM of CaCl_2 to the Tg-containing medium. The results in **Figure 9** show an increase in cytosolic Ca^{2+} concentration in HT-22 cells due to Ca^{2+} release from the ER induced by the SERCA blocker Tg, and then, an increase in the cytosolic Ca^{2+} concentration after the addition of Ca^{2+} to the extracellular medium. The increase of the fluorescence of Fluo3-loaded HT-22 cells after ER depletion was about 2-fold comparing the peak height with the basal conditions, whereas the fluorescence of Fluo3-loaded HT-22 cells after CaCl_2 addition to the extracellular medium increased about 2.4-fold. These results are in good agreement with the results reported in a published study²⁷ where they used similar Tg and Ca^{2+} concentrations to elicit SOCE in HT-22 cells.

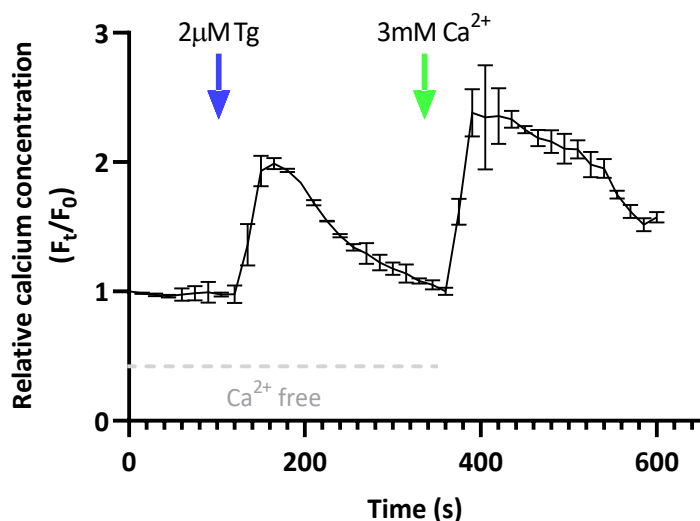


Figure 9. Representative kinetic trace of SOCE in HT-22 cells. HT-22 were incubated with 5 μM Fluo3 AM plus 0.025% Pluronic® F-127 for 1 h at 37 °C and then changed to Ca^{2+} -free MLocke's K5 buffer supplemented with 50 μM EGTA. The kinetics was recorded with 0.3 s time of exposure and shows the average fluorescence intensity per pixel (F_t/F_0) in the HT-22 cells after triggering the emptying of intracellular stores with 2 μM Tg plus 1mM EGTA (indicated by the blue arrow) and after the addition of 3 mM of Ca^{2+} to the medium (indicated by the green arrow) after store emptying. Results presented are the mean \pm s.d. of experiments done at least in 10 petri plates in 5 independent assays ($n>80$ cells).

4.2 Modulation of Ca²⁺ homeostasis by Amyloid-β peptide (1-42) after a short-period of incubation in HT-22 cell culture

4.2.1 Extracellularly added Aβ(1-42) is partially internalized inside HT-22 cells in a short period of time and largely localizes at the perinuclear region

As mentioned in Chapter 2, the aggregation state of Aβ(1–42) in the stock solutions used in this work were predominantly dimers (90 %), with a minor (<10 %) contribution of trimers, highlighting that we added to the extracellular medium of HT-22 cells, the oligomeric neurotoxic form of Aβ in this work (Aβ). However, it is important to note, that we don't know the state of aggregation of internalized Aβ inside HT-22 cells after 2 h and 5 h of incubation, therefore independently of the state of Aβ peptide aggregation, in this work we will referred as Aβ(1-42).

The putative cytotoxicity of 2 μM Aβ(1-42) was evaluated up to 5 h incubation in HT-22 cells through the MTT assay, which measures the cellular mitochondrial activity as indicator of cell viability. The results in **Figure 10** show only a 10 % loss of cell viability after 5 h incubation with 2 μM Aβ(1-42), compared with control, which is statistically nonsignificant ($p>0.05$).

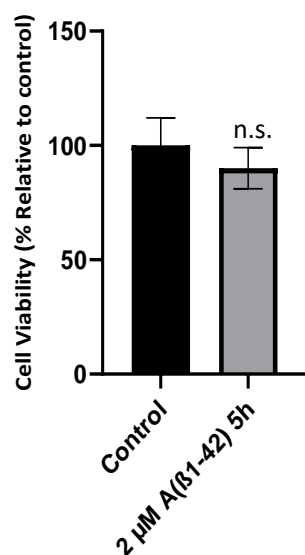


Figure 10. The 10% loss of cell viability of HT-22 cells after incubation with 2 μM Aβ(1-42) for 5 h is statistically non-significant ($p>0.05$). Untreated cells (control) and HT-22 cells incubated with 2 μM Aβ(1-42) for 5 h at 37 °C and 5% CO₂ were incubated with MTT. The absorbance of the formazan MTT product was measured at 590 nm. Cell viability is expressed as percentage relative to the control. Results presented are the mean ± s.d. of experiments done at least in 8 petri plates in 4 independent assays ($n > 60$ cells); n.s. – non significant.

The concentration of internalized Aβ(1-42) after 2 h and 5 h of incubation in HT-22 with a total concentration of 2 μM Aβ(1–42) (1.8 μM of Aβ(1–42) plus 0.2 μM of Aβ(1–42)-HiLyteTM-

Fluor555), added to the extracellular medium, was measured as previously described⁴⁶. RF images of HT-22 were acquired with an excitation filter of 556 nm and a dichroic mirror of 580 nm with an emission filter of 590 nm and a time of exposure of 0.06 s. The RF intensity obtained after 2 h and 5 h of incubation was subtracted from the red autofluorescence intensity of the cells ($n > 80$ cells) and the concentration was calculated with a calibration curve obtained with different A β (1–42)-HiLyte™-Fluor555 (A β (1-42)*555) concentrations added to the extracellular medium of fixed and permeabilized HT-22 cells (**Figure 11**). From these data, we calculated a concentration of 62 ± 11 nM and 135 ± 15 nM of A β (1-42), after 2 h and 5 h of incubation in HT-22 cells, respectively, assuming that there was not a significant difference between the rate of internalization of A β (1–42)*555 and unlabeled A β (1–42). Besides de amount of internalized A β (1-42), we have assessed the subcellular distribution of A β in HT-22. The **Figure 12** show representative BF, RF and merge images (BF plus RF image) of A β (1–42)*555 after incubation in HT-22 cells for 2 h and 5 h, respectively.

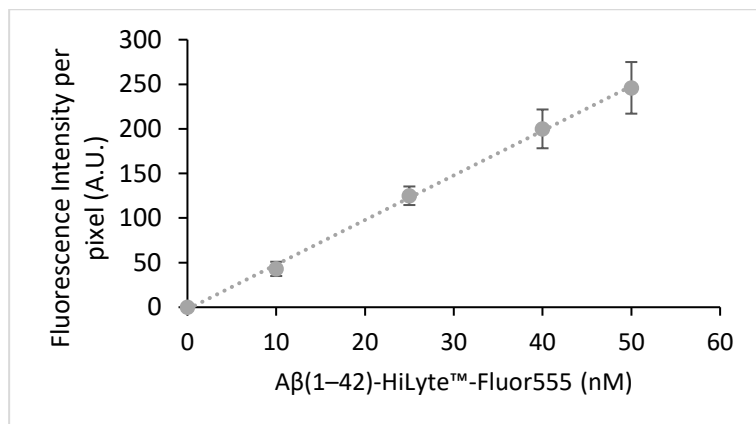


Figure 11. Calibration curve of internalized A β (1–42)*555 in fixed and permeabilized HT-22 cells to calculate the internalized concentration of A β (1–42) in living HT-22 cells.

The direct observation of the representative merge images demonstrate a clear internalization of A β (1–42)*555 inside living HT-22 cells (**Figure 12c** and **f**). After 2 h of incubation it seems that A β (1–42) is distributed through all the cytoplasm, with focalized points near the nuclear region. However, after 5 h of incubation (**Figure 12f-g**) the subcellular distribution of A β (1–42)*555 is mainly near the perinuclear region. These results demonstrated that: i) extracellular A β (1–42) added to the HT-22 medium is being internalized inside cells only after a short period of time of incubation, and ii) A β (1–42) is largely interacting with cytoplasmatic organelles, possibly mainly with the ER, mitochondria and/or lysosomes. Noteworthy, these subcellular organelles have been reported to be targets for interaction and

modulation by intracellular A β peptides in studies performed with other cells^{72–75} and also in HT-22 cells²⁶.

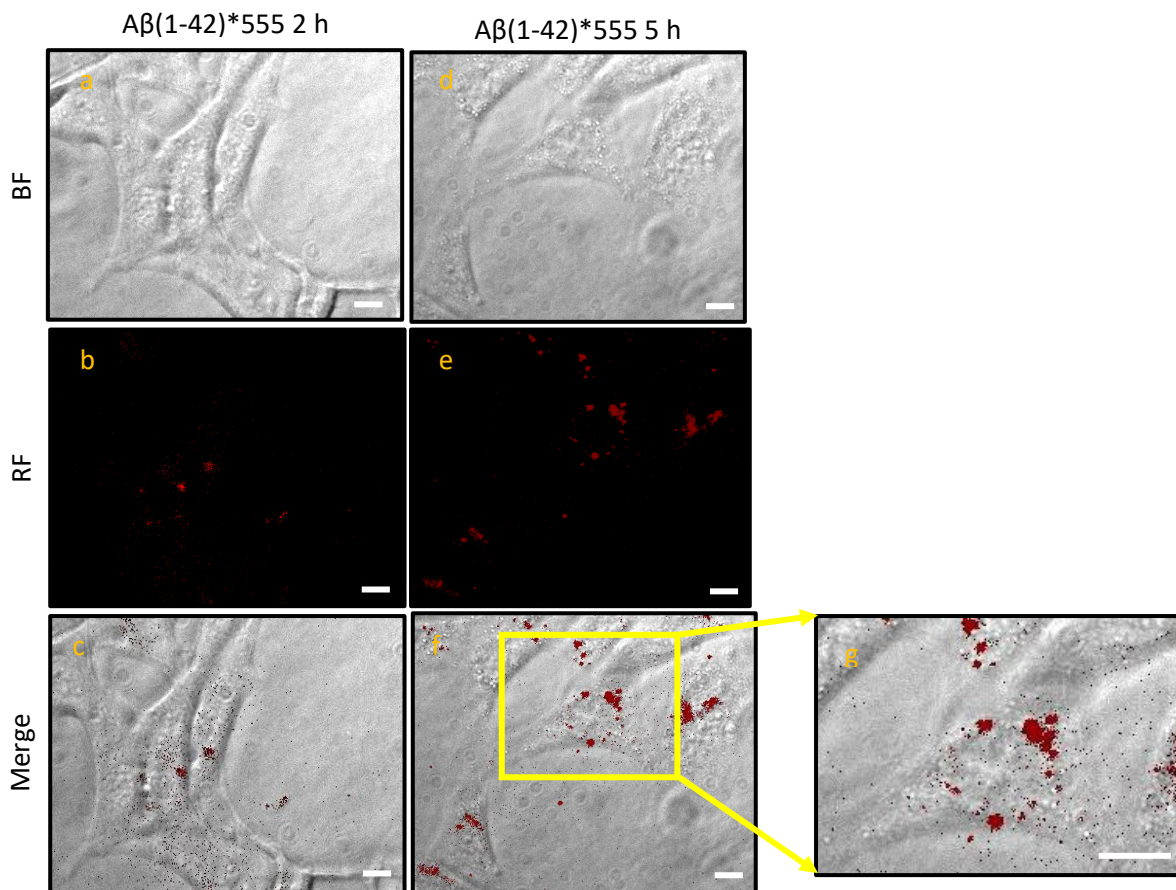


Figure 12. Subcellular distribution of A β (1–42)*555 after 2 h and 5 h incubation in HT-22 cells. HT-22 were incubated with of 2 μ M A β (1–42) (1.8 μ M of A β (1–42) plus 0.2 μ M of A β (1–42)*555) for 2 h and 5 h at 37 °C and 5% CO₂. Then cells were washed once with MLocke's K5 buffer and placed in the holder of the fluorescence microscope thermostated at 37 °C for image acquisition, as described in Material and Methods section. Figure 12a-c shows representative images of BF, RF, and Merge (BF plus RF) of HT-22 incubated for 2 h with A β (1–42). Figure 12d-f shows representative images of BF, RF and Merge of HT-22 cells incubated for 5 h with A β (1–42). Figure 12g shows a focalized zoom of the Figure 12f to highlight the subcellular distribution of A β (1–42)*555 near the perinuclear region of HT-22 soma. Scale bar inserted in fluorescence microscopy images = 20 μ m.

4.2.2 Internalized A β (1-42) colocalizes with mitochondria and ER in living HT-22 cells.

We added to the extracellular medium of HT-22 loaded with A β (1–42)*555, the fluorescent dyes MitoTracker™ Green FM or ER-Tracker™ Green, to evaluate if A β (1–42) colocalize with mitochondria and/or ER, respectively. We decided to assess the co-localization between A β (1–42) and ER and mitochondria only after 5 h of incubation with A β (1–42)*555 because at 2 h of incubation the fluorescence intensity signal is low, compared with the background, making difficult to accurately evaluate the subcellular distribution of A β due to the

poor signal. The **Figure 13** shows representative images of HT-22 loaded with A β (1–42)*555 (RF) plus 20 nM MitoTracker™ Green FM (GF).

The MitoTracker™ Green FM is a green-fluorescent dye that stain cellular mitochondria regardless of mitochondrial membrane potential. As opposed to A β (1–42)*555 that show a preferential distribution near the nucleus (**Figure 13b**), mitochondria are distributed throughout all the HT-22 cells, including the extensions as can be seen in the representative image of HT-22 cells stained with MitoTracker™ Green FM (**Figure 13c**). The merge image (**Figure 13d**) show a moderate co-localization between A β (1–42)*555 and MitoTracker™ Green FM, which can be more easily observed by the yellow-orange stained regions of HT-22 cells, marked by the white arrows in the **Figure 13e**.

The ER-Tracker™ Green is a live cell-permeant highly selective for the ER. In the representative image of HT-22 cells stained with ER-Tracker™ Green (**Figure 14c**) it can be seen the ER distribution in HT-22. In this case, the ER has a more diffuse distribution pattern in the HT-22 soma (compared with mitochondria) and a very poor presence in the extensions. Of note, it is important to highlight the higher density of ER near the perinuclear region like we saw before for A β (1–42)*555. The merge image (**Figure 14d**) show a moderate co-localization between A β (1–42)*555 and ER-Tracker™ Green FM, which is pointed out by the yellow-orange stained regions in HT-22 cells near the perinuclear region (**Figure 14e**).

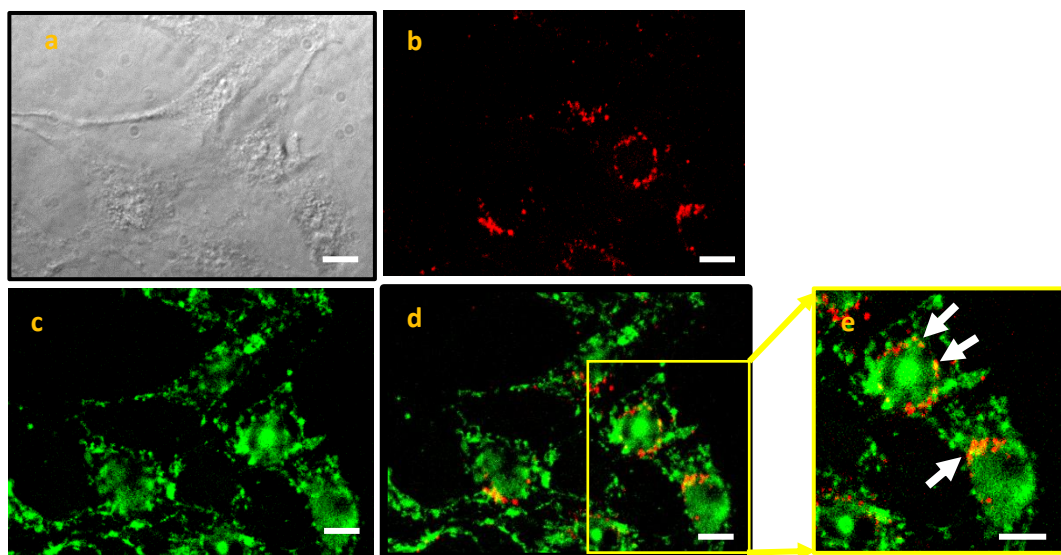


Figure 13. Moderate co-localization between internalized A β (1–42)*555 and mitochondria, after 5 h of A β (1–42) incubation in HT-22 cell line. HT-22 were incubated with 2 μ M A β (1–42) (1.8 μ M of A β (1–42) plus 0.2 μ M of A β (1–42)*555) for 5 h at 37 °C and 5% CO₂. Then cells were washed once with MLocke's K5 buffer and placed in the holder of the fluorescence microscope thermostated at 37 °C for fluorescence imaging of A β (1–42)*555 (Figure 13b). Next, cells were incubated with 20 nM MitoTracker™ Green FM for 5 min at 37 °C and 5% CO₂ and placed again in the holder of the fluorescence microscope for fluorescence imaging acquisition (Figure 13c). Figure 13d shows a merge image between A β (1–42)*555 and MitoTracker™ Green FM. Figure 13e shows a focalized zoom of Figure 13d and the white arrows point

out regions of higher co-localization between A β (1–42)*555 and MitoTracker™ Green FM. Scale bar inserted in fluorescence microscopy images = 20 μ m.

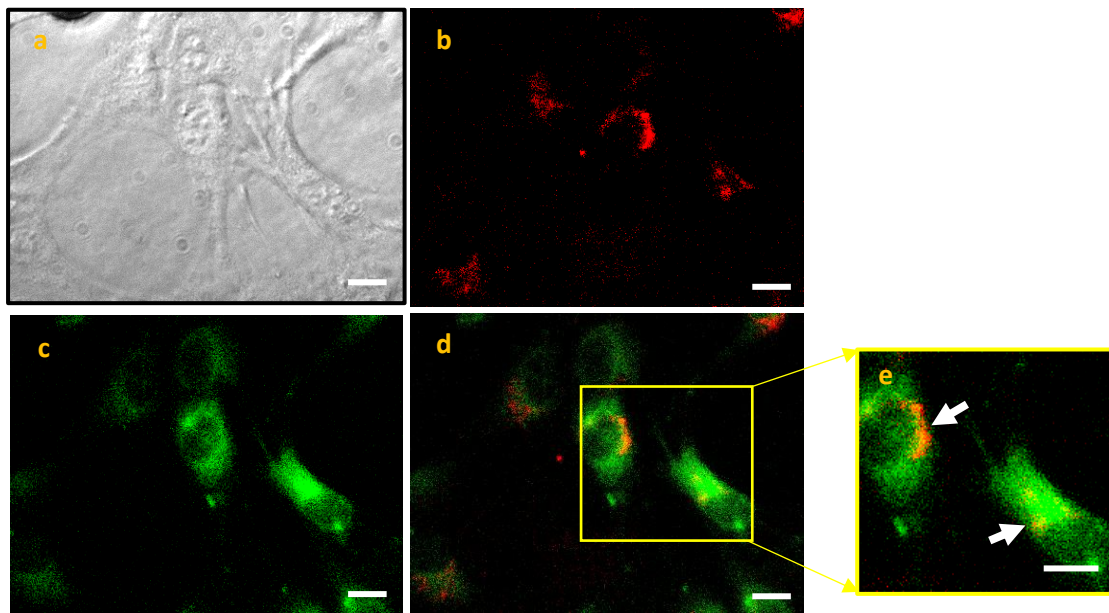


Figure 14. Moderate co-localization between internalized A β (1–42)*555 and ER, after 5 h of A β (1–42) incubation in HT-22 cell line. HT-22 were incubated with 2 μ M A β (1–42) (1.8 μ M of A β (1–42) plus 0.2 μ M of A β (1–42)*555) for 5 h at 37 °C and 5% CO₂. Then cells were washed once with MLocke's K5 buffer and placed in the holder of the fluorescence microscope thermostated at 37 °C for fluorescence imaging of A β (1–42)*555 (Figure 14b). Next, cells were incubated with 100 nM ER-Tracker™ Green FM for 5 min at 37 °C and 5% CO₂ and placed again in the holder of the fluorescence microscope for GF imaging acquisition of ER-Tracker™ Green FM (Figure 13c) and RF of A β (1–42)*555. Figure 14d shows a merge image between A β (1–42)*555 and ER-Tracker™ Green FM. Figure 14e shows a focalized zoom of Figure 13d and the white arrows point out regions where the co-localization between A β (1–42)*555 and ER-Tracker™ Green FM is higher. Scale bar inserted in fluorescence microscopy images = 20 μ m.

4.2.2.1 Incubation during 2 h and 5 h with 2 μ M A β (1–42) do not alter significantly the mitochondria membrane potential ($\Delta\Psi_m$) in the HT-22 cell culture

The results obtained for the localization of internalized A β (1–42) prompted us to evaluate the effect of A β (1–42) in the $\Delta\Psi_m$ after incubation with 2 μ M A β (1–42) for 2 h and 5 h in HT-22 cells. To this end, we used the fluorescent dye TMRE, which accumulates in non-depolarized mitochondria. As shown in a previous work of our laboratory⁵⁶, the degree of mitochondria depolarization is proportional to the decrease of the average number of high intensity fluorescence pixels in HT-22. As positive control, and for complete mitochondrial depolarization, we added to the extracellular medium, 5 μ M of FCCP a potent mitochondrial oxidative phosphorylation uncoupler. Representative kinetic traces of the average fluorescence intensity per pixel (F_t/F_0) of control cells and HT-22 incubated with 2 μ M A β (1–42) during 2 h and 5 h are shown in the Figure 15A.

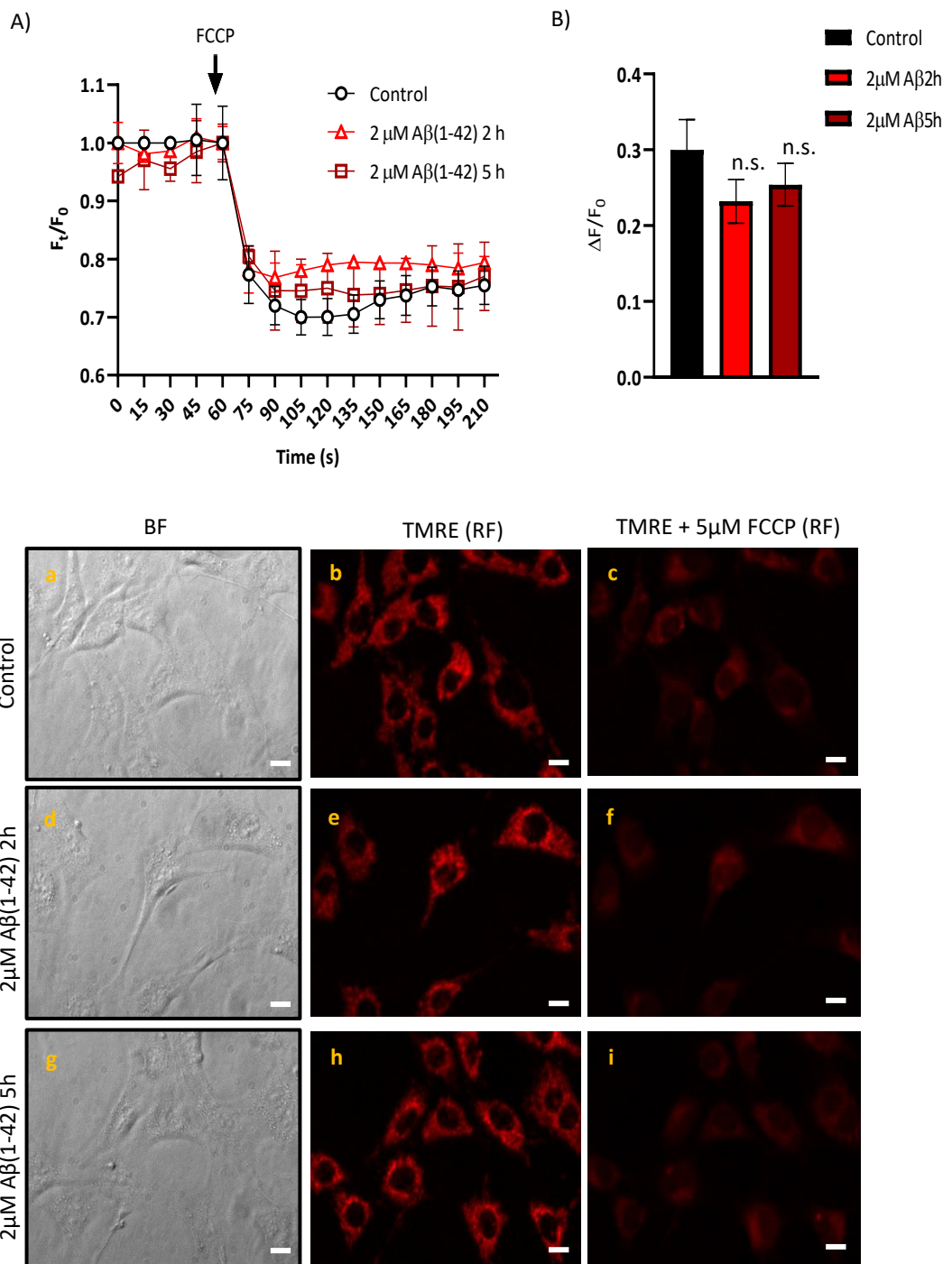


Figure 15. The mitochondria membrane potential is not statistically significant affected by Aβ(1-42) in a short period of time ($p>0.05$). Untreated cells (control) and HT-22 cells incubated with 2 μM Aβ(1-42) for 2 h and 5 h at 37 °C and 5%CO₂ were loaded with 100 nM TMRE for 10 min and placed in the holder (37 °C) of the fluorescence microscope for cell imaging. **A)** Representative kinetic traces of the average fluorescence intensity (F_t/F_0) recorded over time with a 556 nm excitation filter/ 590 nm emission filter and a dichroic mirror of 580 nm with a time of exposure 0.01 s. The black arrow indicates the addition of 5 μM FCCP with a subsequent extinction of the mitochondria membrane potential. **B)** Means of the difference of the average fluorescent intensity before and after the addition of 5 μM FCCP normalized for the baseline fluorescent intensity ($\Delta F/F_0$). **C)** Representative BF images and fluorescence microscopy images of TMRE-loaded HT-22 cells, before and after addition of 5 μM FCCP in untreated HT-22 cells (control, a-c) and in cells treated with 2 μM Aβ(1-42) for 2 h (d-f) and for 5 h (g-i). Results show that the mitochondria membrane potential ($\Delta\psi_m$) is not statistically affected by Aβ(1-42) incubated for 2 h or 5 h

in HT-22 cells, comparing with untreated cells (control). Scale bar inserted in fluorescence microscopy images = 20 μ m. n.s.- non significative.

The results show a fast and large decrease in $\Delta\Psi_m$ after addition of 5 μ M FCCP, as expected, being this decrease higher in the control group compared with HT-22 cells treated with A β (1-42). However, this difference is not statistically significant ($p>0.05$), as demonstrated by the difference of the average fluorescent intensity before and after the addition of FCCP (**Figure 15 B**). The **Figure 15C**, shows representative images of HT-22 BF and TMRE-loaded HT-22 cells, before and after addition of 5 μ M FCCP in the control group (a-c) and in cell-treated with 2 μ M A β (1-42) for 2 h (d-f) and for 5 h (g-i).

4.2.2.2 FRET imaging shows colocalization between PDI and A β (1-42)*555 in HT-22 cell line, but A β (1-42) does not directly modulate PDI activity

The protein disulfide isomerase (PDI) is highly expressed in ER and play a major role as molecular chaperone by catalyzing disulfide bond oxidation, reduction, and isomerization ⁷⁶. More recent studies have revealed unconventional roles for PDI in neurodegenerative diseases (i.e. AD), distinct from its normal function in the ER ⁷⁷. According to Erickson and co-workers the PDI family has an important role to prevent A β oligomerization ⁷⁸. Besides, it was demonstrated that PDI levels are significantly decreased in oligodendrocytes in the brains of AD patients and also in an AD mouse model, before the animals displayed AD pathology ⁷⁹. On these grounds, we further assessed if A β (1-42) and PDI are within FRET distance in fixed and permeabilized HT-22 cells, by using the Fluorescence Resonance Energy Transfer (FRET), and evaluated if the PDI activity is modulated by A β (1-42). First, we stained HT-22 cells with increasing concentrations of A β (1-42)*555 (25-100nM) as described in Materials and Methods section, aiming to perform the measurements with the lowest A β (1-42)*555 concentrations to highlight only the subcellular location of the high affinity binding sites for A β (1-42). The representative images in **Figure 16** show HT-22 cells stained with 25, 50, 75 and 100 nM of A β (1-42)*555. As expected, the RF intensity increases as the A β (1-42)*555 concentration increases. The 3D surface plots highlight once more the subcellular distribution of A β (1-42)*555, which is more focalized near the HT-22 nucleus, as we demonstrated before in HT-22 living cells (**Figure 12**). Then, we selected the concentrations of 25, 50 and 100 nM of A β (1-42)*555 to experimentally assess the occurrence of FRET between anti-PDI conjugated with IgG-Alexa488 (Anti-PDI*A488) and A β (1-42)*555. The **Figure 17A** shows a high co-localization within FRET distance between anti-PDI*A488 and A β (1-42)*555, demonstrated by the increase in the red/green fluorescence

intensity ratio in the presence of 50 and 100 nM of A β (1–42)*555. After subtraction of the red intensity by direct excitation of A β (1–42)*555, we have calculated a 2.2-fold and 5.2-fold increases of the red/green fluorescence intensity ratio, respectively. On the other hand, there is no co-localization within FRET distance between anti-PDI and 25 nM of A β (1–42)*555, as the same ratio values were calculated for anti-PDI in the absence or presence of 25 nM A β (1–42)*555.

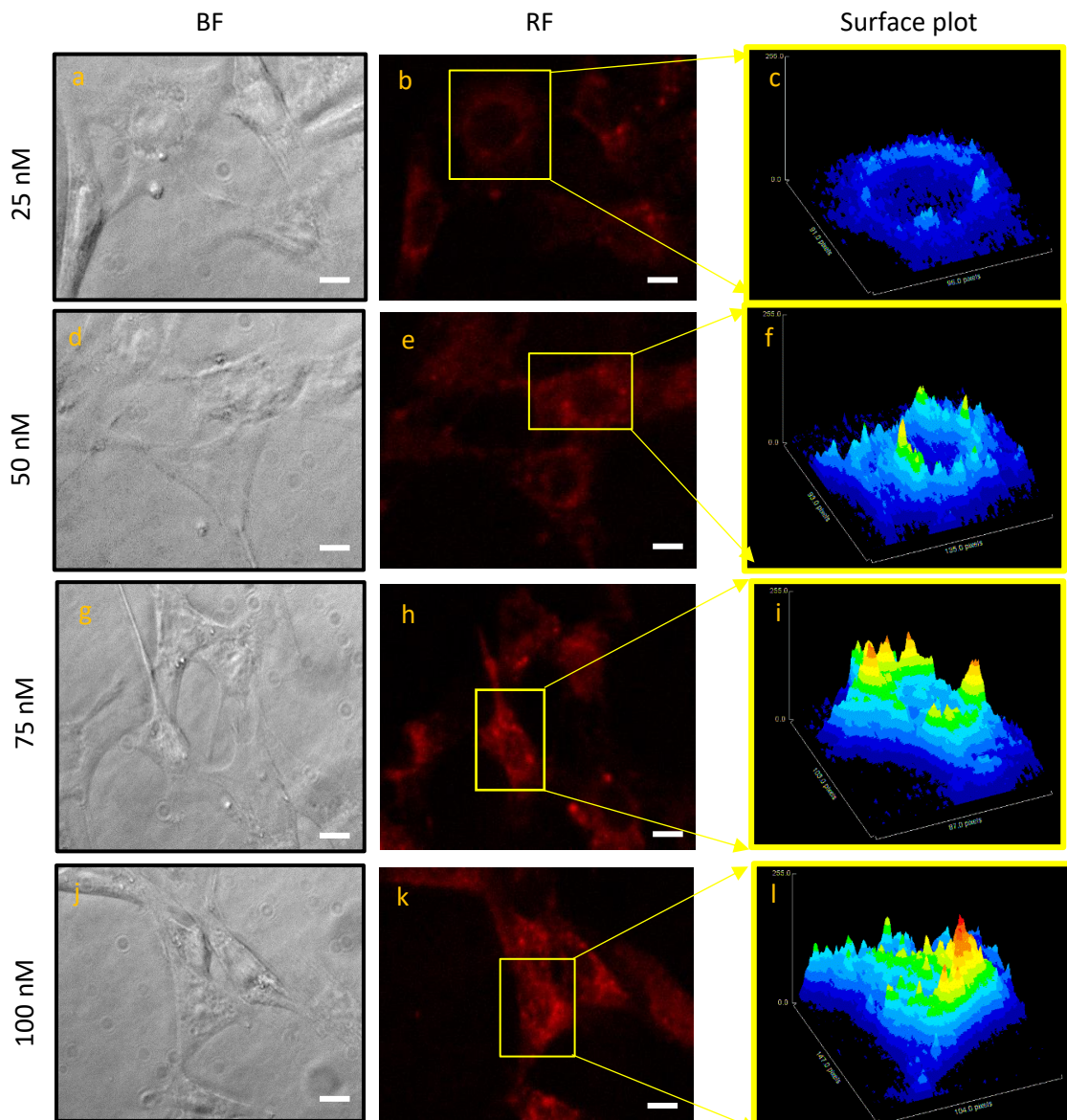


Figure 16. Fluorescence microscopy images of fixed HT-22 stained with increased concentrations of A β (1–42)*555. Representative fluorescence microscopy images of permeabilized HT-22 staining with 25, 50, 75 and 100 nM of A β (1–42)*555. BF and RF images are shown for representative selected fields. Surface plots are shown for each concentration tested, highlighting the focalized subcellular distribution of A β (1–42) mainly in the perinuclear region of HT-22 soma. The exposure time for RF images was 0.03 s. Scale bar inserted in fluorescence microscopy images = 20 μ m.

Representative fluorescence microscopy images of HT-22 stained with anti-PDI*A488 in the absence and presence of 50 nM A β (1–42)*555 are shown in **Figure 17B**. The direct observation of the images allows to visualize a decrease in the GF intensity after addition of 50 nM A β (1–42)*555 (**Figure 17e**), compared with cells stained only with anti-PDI (**Figure 17b**). The merge image highlights the existence of *punctata* colocalization between anti-PDI*A488 and 50 nM A β (1–42)*555 in the neuronal soma, as showed by the yellow-orange pixels.

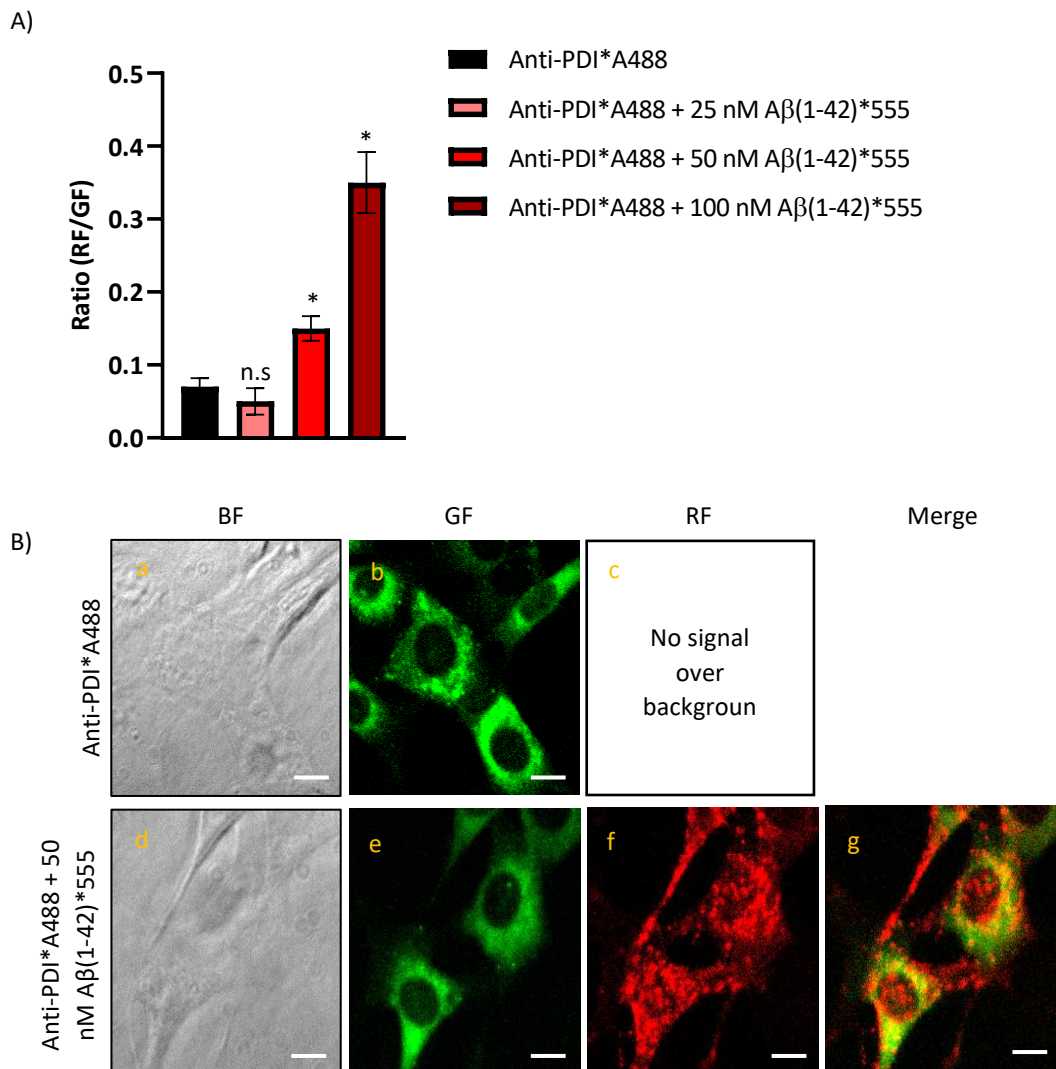


Figure 17. Extensive FRET between anti-PDI and A β (1–42)*555. **A)** Ratio of red/green fluorescence intensity per pixel (RF/GF) obtained from the analysis of fluorescence intensity data of HT-22 stained with anti-PDI/IgG-Alexa488 only (PDI*A488) and double stained with anti-PDI*IgG-Alexa488 plus 25, 50 or 100 nM A β (1–42)*555. The results shown are the mean \pm s.d. (*) $p < 0.05$, (i.e., statistically significant with respect to the control; n.s. – non significant). **B)** Representative fluorescence microscopy images of HT-22 stained with anti-PDI/IgG-Alexa488 (PDI*A488, a–c) or with anti-PDI/IgG-Alexa488 plus 50 nM A β (1–42)*555 (PDI*A488/A β (1–42)*555, d–g). BF, GF and RF images are shown for each of the selected fields, and the orange-yellow areas (merge image, g) point out the higher intensity FRET regions. The exposure time for GF and RF images was 0.4 s. Scale bar inserted in fluorescence microscopy images = 20 μ m.

As we saw colocalization between PDI and A β (1–42)*555 within FRET distance, we have experimentally evaluated the effect of A β (1–42) on PDI activity, by measuring PDI activity through the isomerase assay as described in Materials and Methods section. The **Figure 18** show representative kinetic traces of the disulfide reductase activity of PDI acquired after 10 min of incubation, a time needed to reach the linear steady-state rate of substrate reduction with HT-22 lysates using this assay method (data not shown). The results obtained demonstrated that A β (1–42) do not significantly alter the activity of PDI in HT-22 cell lysates at the concentrations attained within HT-22 cells. These results allow to conclude that A β (1–42) and PDI are within FRET distance, but A β (1–42) concentrations internalized within HT-22 in our experimental protocols do not inhibit the activity of PDI.

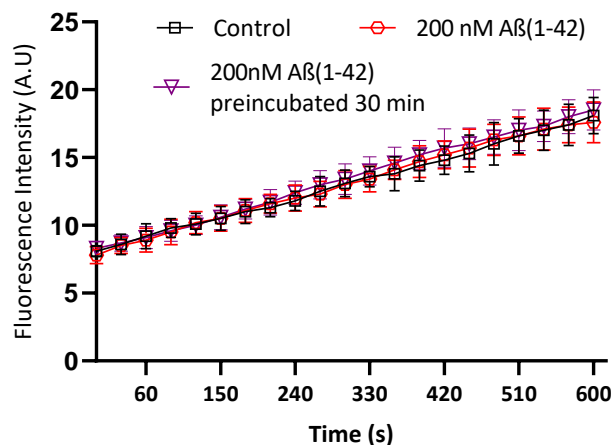


Figure 18. A β (1–42) do not alter the activity of PDI in HT-22 cell lysates. The pseudo substrate of PDI, Di-E-GSSG (150 nM) was incubated with HT-22 cell lysates (34 μ g protein) in the absence (black squares) or presence of 200 nM A β (1–42) (red hexagons) or 200 nM A β (1–42) preincubated with cell lysate (purple triangles) in PDI's buffer assay. Fluorescence intensity was measured at room temperature (24 ± 1 °C) with excitation and emission wavelengths of 522 and 550 nm, respectively. The results show no statistically significant differences in the kinetic activity of PDI in the absence or presence of A β (1–42).

4.2.3. FRET imaging highlights the association of A β (1–42)*555 with CaM in HT-22 cells

In a previous work, described in Chapter 2, we showed through co-immunoprecipitation and FRET techniques that CaM is a major target protein for A β (1–42) in mature CGN ⁴⁶. Therefore, we decided to experimentally assess if CaM and A β (1–42) are also within FRET distance in fixed and permeabilized mouse hippocampal HT-22 cells in culture. To this end, we stained HT-22 cells with anti-CaM conjugated with the secondary antibody IgG Alexa488 (anti-CaM*A488) in the absence and presence of 50 and 100 nM of A β (1–42)*555. As can be seen in

Figure 19A, there is a large increase in the red/green fluorescence intensity ratio in the presence of 50 and 100 nM of A β (1–42)*555, after subtraction of the red intensity by direct excitation of A β (1–42)*555. The results yielded a 3.4-fold and 6.9-fold increase, after addition of 50 and 100 A β (1–42)*555, respectively, demonstrating an extensive colocalization within FRET distance between CaM and A β (1–42) in HT-22 cells. **Figure 19B** shows representative fluorescence microscopy images of HT-22 stained with anti-CaM*A488 in the absence and in the presence of 50 A β (1–42)*555. The orange-yellow pixels presented in the merge image (**Figure 19g**) reveal the regions with high colocalization between CaM and A β (1–42). Therefore, these results confirms once more that CaM is a major binding target protein for A β (1–42).

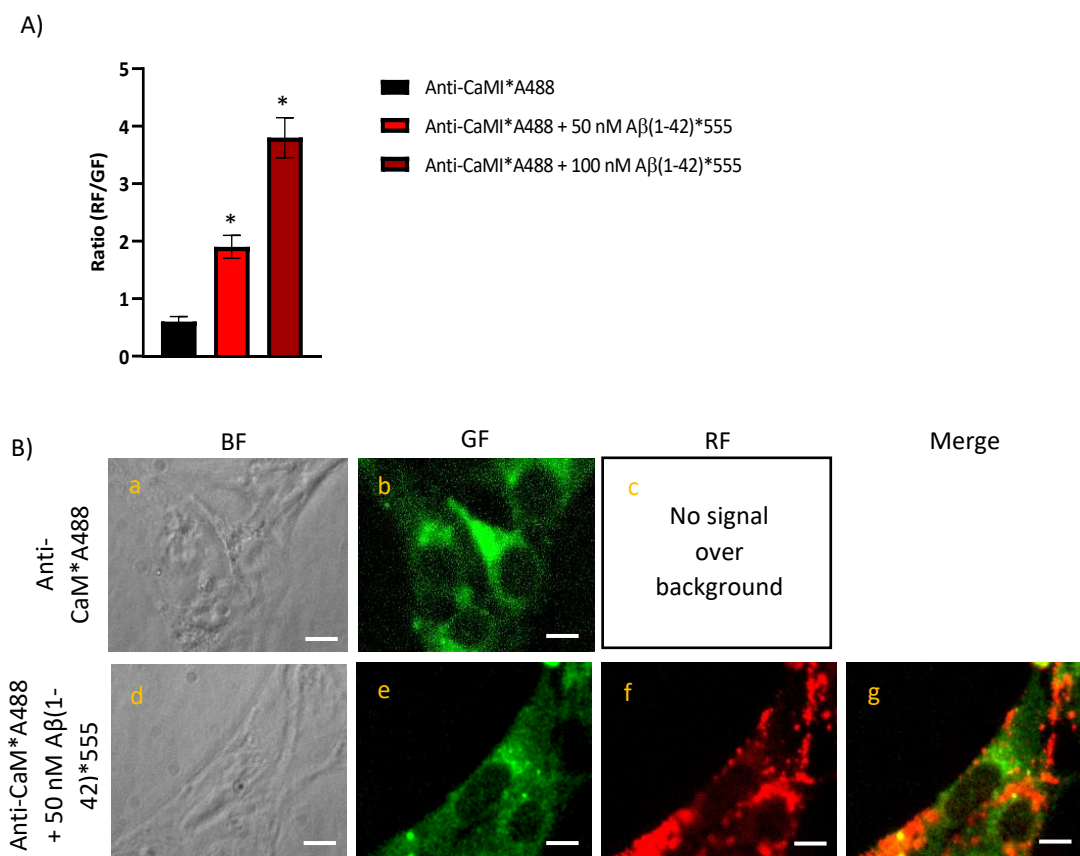


Figure 19. Extensive FRET between calmodulin (CaM) and A β (1–42)*555. **A)** Ratio of red/green fluorescence intensity per pixel (RF/GF) obtained from the analysis of fluorescence intensity data of HT-22 stained with anti-CaM/IgG-Alexa488 only (CaM*A488) and double stained with anti-CaM/IgG-Alexa488 plus 50 or 100 nM of A β (1–42)*555. The results shown are the mean \pm s.d. (*) $p < 0.05$, (i.e., statistically significant with respect to the control). **B)** Representative quantitative fluorescence microscopy images of HT-22 stained with anti-CaM/IgG-Alexa488 (CaM*A488, a–c) or with anti-CaM/IgG-Alexa488 plus 50 nM A β (1–42)*555 (CaM*A488/A β (1–42)*555, d–g). BF, GF and RF images are shown for each of the selected fields, and the orange-yellow areas (merge image, g) point out for higher intensity FRET regions. The exposure time for GF and RF images was 0.4 s. Scale bar inserted in fluorescence microscopy images = 20 μ m.

4.2.4. A β (1-42) inhibits SOCE activity after a short period of incubation in HT-22 cells

As demonstrated earlier (**Figures 14 and 17**), internalized A β (1-42) interacts with ER in HT-22 cells. Due to this, we evaluated the effect of A β (1-42) in SOCE mechanism after 2 h of incubation with 2 μ M A β (1-42) in HT-22 cells loaded with Fluo3. The **Figure 20A**, shows representative kinetic traces of SOCE in untreated HT-22 cells (control, black trace) or cells treated with 2 μ M A β (1-42) for 2 h (red trace) and the results demonstrate a significant decrease of SOCE after HT-22 treatment with A β (1-42). Accordingly with the **Figure 20B**, there is an inhibition of both Ca $^{2+}$ release from stores and Ca $^{2+}$ entry through the plasma membrane, being the Ca $^{2+}$ decrease about 37 \pm 7% and 32 \pm 6%, respectively, compared with control. These results are also shown by the representative fluorescence microscopy images of HT-22 cells **Figure 20C**. It is important to note that controls run with 2 μ M of scrambled A β (1-42) for 2 h did not produce alterations of the Ca $^{2+}$ in SOCE experiments, compared with untreated cells (control) (**Figure 21**).

To confirm that A β (1-42) is modulating the SOCE mechanism, we tested a selective SOCE inhibitor, named BTP2 (also known as YM58483) as positive control. BTP2 is considered selective because it does not affect Ca $^{2+}$ signaling by the ER or mitochondria or other channel activities such as voltage-operated Ca $^{2+}$ channels (that are inactive in HT-22 cells) or K $^{+}$ channels in T-cells^{80,81}. We added 3 μ M of BTP2 to the HT-22 culture medium 15 min before the end of the incubation with Fluo3 AM (control cells) or before the end of the incubation with Fluo3 AM plus 2 μ M A β (1-42) 2 h in treated cells. The results are shown in **Figure 22**. The **panel A** shows that there is no significative difference in Ca $^{2+}$ release from stores between the control cells in the absence (black trace) and presence of 3 μ M BTP2 (blue trace), which are in good agreement with the expected results, because BTP2 do not affect Ca $^{2+}$ signaling through ER. On the other hand, there is a large decrease in the entry of Ca $^{2+}$ through the plasma membrane, i.e. 71 \pm 8% in control cells incubated with BTP2, relative to the control without BTP2 (**Figure 22B**), which confirms the effect of the STIM1-mediated SOCE inhibitor BTP2 by blockade of Ca $^{2+}$ influx. Concerning the results obtained with HT-22 cells incubated with A β (1-42), there is no statistically significant difference in Ca $^{2+}$ release from stores in HT-22 cells treated with only 2 μ M A β (1-42) for 2 h (37 \pm 7% inhibition, **Figure 20B**) and cells treated with both 2 μ M A β (1-42) 2 h and 3 μ M BTP2 (42 \pm 6 % inhibition, **Figure 22B**). Regarding the Ca $^{2+}$ entry, the results show a 2-fold decrease in Ca $^{2+}$ influx after HT-22 incubation with 2 μ M A β (1-42) for 2 h plus 3 μ M BTP2, a decrease that is the same to that observed with HT-22 cells incubated with only A β (1-42). These results indicate that A β (1-42) is partially inhibiting SOCE through the inhibition of STIM1-operated Ca $^{2+}$ entry.

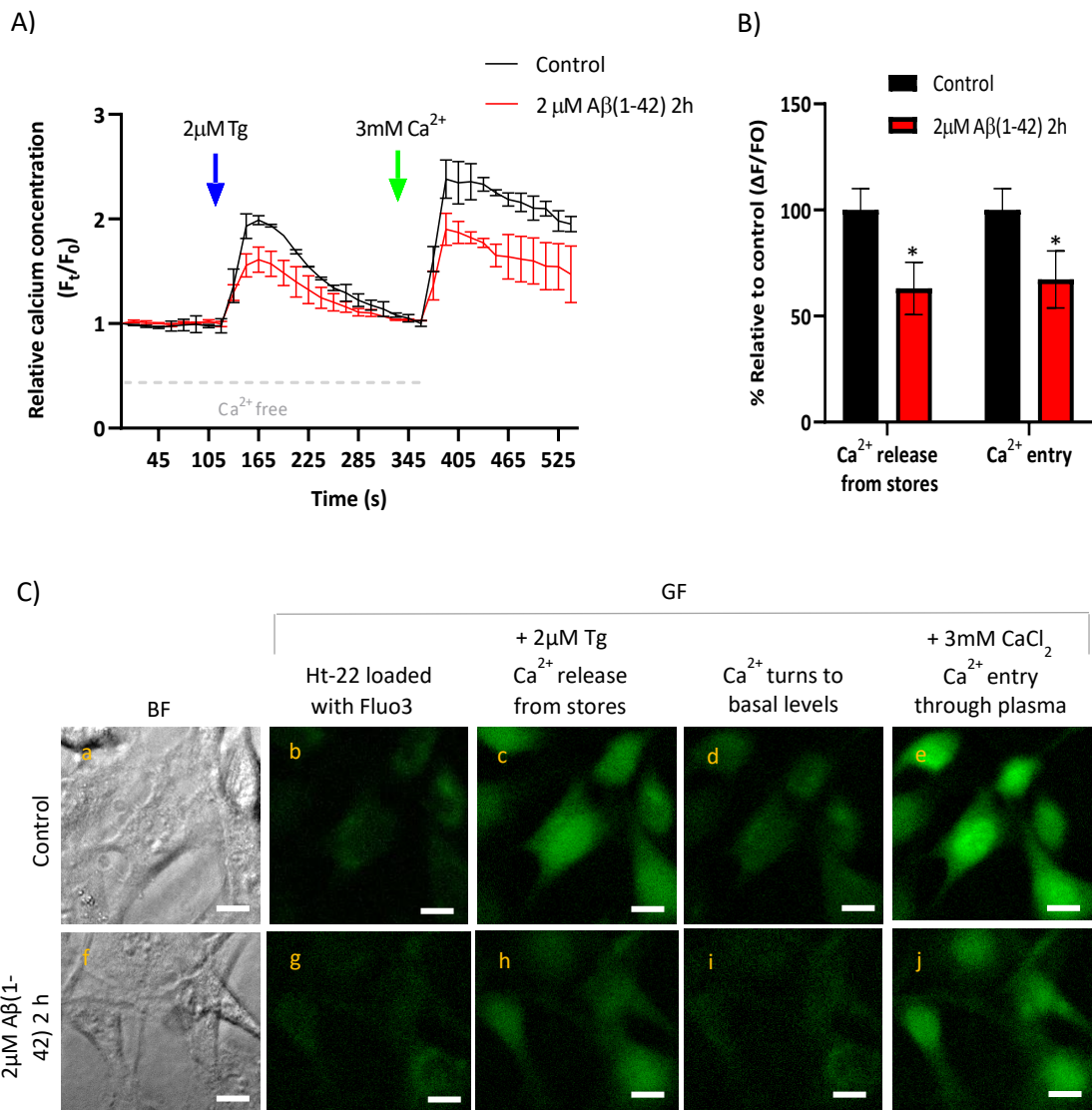


Figure 20. SOCE inhibition by A β (1-42) in HT-22 cells after 2 h of incubation. Untreated (control) a treated HT-22 cells incubated with 2 μ M A β (1-42) for 2 h at 37 °C and 5% CO₂ were loaded with 5 μ M Fluo3 AM and 0.025% Pluronic® F-127 for 1 h. Then cells were washed once with Ca²⁺-free MLocke's K5 buffer (medium assay) and placed at the holder (37 °C) of the fluorescence microscopy for Ca²⁺ imaging of SOCE. **A)** Representative kinetic traces of untreated HT-22 cells (black trace) and HT-22 cells incubated with 2 μ M A β (1-42) for 2 h (red trace) after addition of 2 μ M Tg (indicated by the blue arrow) for Ca²⁺ release from stores and after addition of 3 mM Ca²⁺ to evaluate the extension of Ca²⁺ entry inside HT-22 cells through the plasma membrane (indicated by the green arrow). The experiment was performed at 0.3 s exposure time. **B)** Means of the average fluorescent intensity ($\Delta F/F_0$) relatively to control, after addition of Tg (Ca²⁺ release from stores) or after addition Ca²⁺ (Ca²⁺ entry). Results show that A β (1-42) inhibits about 37 ± 7 % and 32 ± 6 % of Ca²⁺ release from stores and Ca²⁺ entry, respectively, compared with control. Data are presented as the mean ± s.d. of experiments done at least in 10 petri plates in 5 independent assays (n>80 cells, *p<0.05, relatively to each control). **C)** Representative fluorescence images of untreated HT-22 (control) and cells treated with 2 μ M A β (1-42) 2 h, loaded with Fluo3 and after SOCE experiments. Scale bar = 20 μ m.

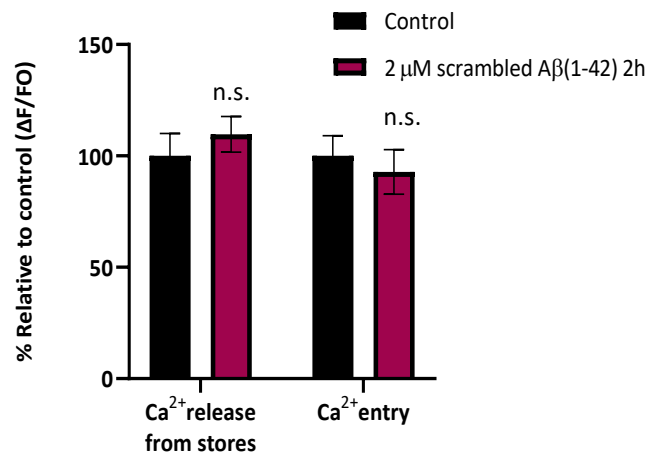


Figure 21. Scrambled Aβ(1-42) did not alter the resting cytosolic Ca²⁺ concentration peaks in SOCE experiment. Untreated cells (control) and HT-22 treated with 2 μM scramble Aβ(1-42) for 2 h at 37 °C and 5% CO₂ were loaded with Fluo3 AM plus Pluronic® F-127 and submitted to SOCE experiments as described in the Materials and Methods section. The results presented do not show statistically difference, neither in Ca²⁺ release from stores after addition of Tg, nor in the Ca²⁺ influx after Ca²⁺ addition to the extracellular medium. Data are presented as the means of the average fluorescent intensity ($\Delta F/F_0$) represented by percentage (%), relatively to control cells, of experiments done at least in 8 petri plates in 4 independent assays (n>60 cells;). n.s. – non significant.

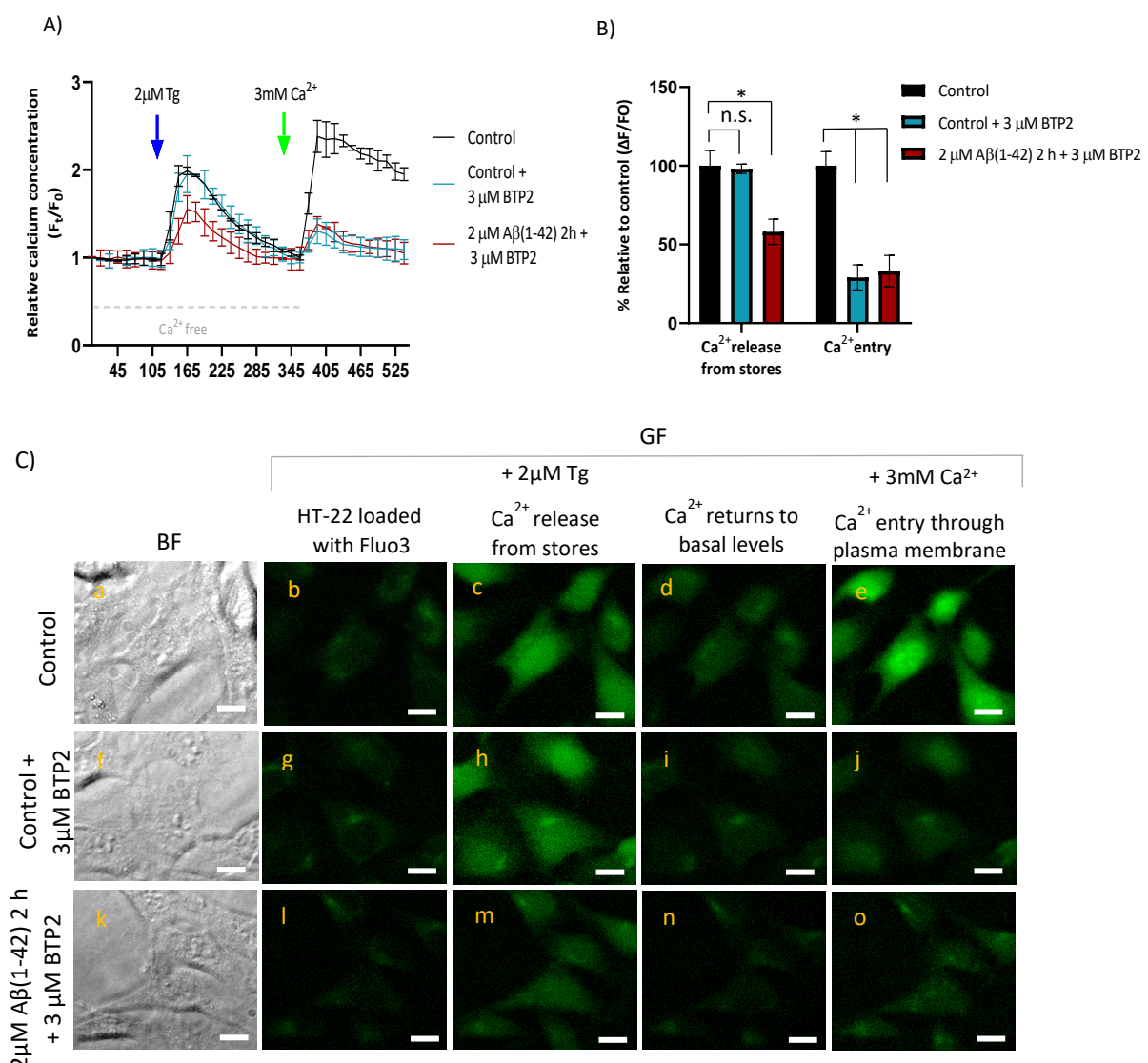


Figure 22. Effect of the SOCE inhibitor BTP2 in untreated (control) and treated HT-22 cells [A β (1-42)]. Untreated HT-22 cells (control) and treated cells with 2 μ M A β (1-42) for 2 h were incubated with 3 μ M of BTP2 for 15 min, as described in Materials and Methods section. Plates were placed at the holder (37 °C) of the fluorescent microscopy for Ca $^{2+}$ imaging of SOCE. **A)** Representative kinetic traces of HT-22 control with (blue trace line) or without BTP2 (black trace line) and HT-22 cells incubated with 2 μ M A β (1-42) for 2 h plus BTP2 (*bordeaux* trace line) after addition of 2 μ M Tg (indicated by blue arrow) for Ca $^{2+}$ release from stores and addition of 3 mM Ca $^{2+}$ to evaluate the extension of Ca $^{2+}$ entry inside HT-22 cells (indicated by the green arrow). The experiment was performed at 0.3 s exposure time. **B)** Means of the average fluorescent intensity ($\Delta F/F_0$) represented by percentage (%), relatively to control cells. BTP2 do not elicit Ca $^{2+}$ depletion but inhibits the Ca $^{2+}$ influx in about 71 ± 8% in control cells and HT-22 cells incubated with 2 μ M A β (1-42) 2 h, comparing with the respective controls. Data are presented as the mean ± s.d. of experiments done at least in 10 petri plates in 5 independent assays (n>80 cells for each condition) (* $p<0.05$, relatively to each control). **C)** Representative fluorescence images of untreated HT-22 (control), cells with 3 μ M BTP2, and cells treated with A β (1-42) plus 3 μ M BTP2. Scale bar = 20 μ m.

4.2.4.1 Binding of STIM1 with A β (1-42) in lysates of HT-22 cells

In order to gain a deeper insight into the possible mechanism underlying the SOCE inhibition induced by a short time incubation with A β (1-42), we assessed the interaction between STIM1 and A β (1-42), since as explained earlier in the Introduction, STIM1 and Orai1 proteins are well established as the building blocks of SOCE⁸² and, therefore, are functionally coupled in store-operated Ca $^{2+}$ currents⁸³. We used the co-immunoprecipitation method to evaluate the formation of STIM1-A β (1-42) complexes in HT-22 cell lysates with the anti-A β (1-42) antibody and in the presence of 250 nM A β (1-42) (Figure 23).

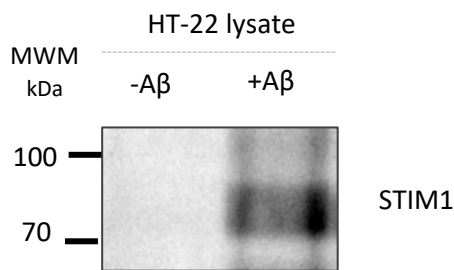


Figure 23. Co-immunoprecipitation between STIM1 and A β (1-42). Western blotting of STIM1 (anti-STIM1 ps621) after co-immunoprecipitation assay with mouse anti-A β antibody, as described in the Materials and Methods section.

The western blotting clearly reveal the formation of STIM1-A β complexes in HT-22 cell lysates, demonstrating that STIM1 is a target molecule of A β (1-42). Of note, other studies have demonstrated that STIM1 protein expression level decreased with the progression of neurodegeneration in AD⁸⁴.

Owing to the relevance of these co-immunoprecipitation results, we have also assessed the binding of A β oligomers with STIM1 using FRET between GFP-STIM1 and A β (1-42)*555.

Samples of the membrane fraction of hypotonic lysates of HEK 293 cells expressing GFP-STIM1, prepared as described in⁸⁵, have been kindly supplied by Dr. Francisco Javier Martín-Romero.

Figure 24 shows the results of the titration of GFP-STIM1-containing membranes with Aβ(1–42)*555. These results show that Aβ(1–42)*555 produces about 18% quenching of GFP-STIM1 fluorescence at saturation by FRET to Aβ(1–42)*555, but not of GFP-empty used as control, excluding the possibility that the observed quenching was due to a direct interaction of Aβ(1–42)*555 with the GFP protein attached to STIM1. Assuming that about 50% of the membranes are inverted with respect to the right-side out orientation, from the maximum quenching of GFP-STIM1 fluorescence by Aβ(1–42)*555 we can calculate that Aβ(1–42)*555 binds to a site that is at \approx 6 - 7 nm distance from GFP in GFP-STIM1, using the R_0 value for the FRET pair GFP (donor)/Aβ(1–42)*555 (acceptor) given in the Materials and Methods section. In addition, the results shown in the **Figure 24** allows to obtain a dissociation constant of \approx 10 nM Aβ(1–42)*555 from its complex with GFP-STIM1.

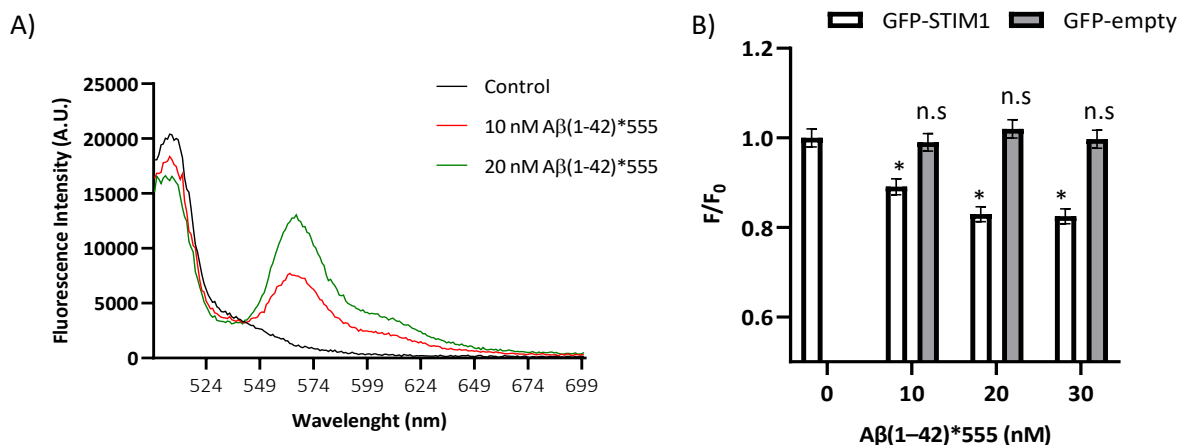


Figure 24. Titration of the fluorescence of GFP-STIM1 with Aβ(1–42)*555. **A)** Emission fluorescence spectra of 10 µg/mL of HEK 293 cell lysate containing GFP-STIM1 in the absence (black trace) and after the addition of 10 nM (red trace) and 20 nM (green trace) of Aβ(1–42)*555. Fluorescence spectra were recorded at RT in buffer: 50 mM Hepes, 100 mM KCl, 2 mM MgCl₂ and 50 µM CaCl₂ (pH 7.05). The spectra were acquired between 20 and 30 min after the addition of the indicated Aβ(1–42)*555 concentration, with excitation wavelength of 488 nm, and excitation and emission slits of 2 nm. **B)** Fluorescence of the emission peak of GFP-STIM1 (white-filled bars) and of GFP-empty (gray-filled bars) in the presence of different Aβ(1–42)*555 concentrations. F and F₀ are the fluorescence in the presence and in the absence of Aβ(1–42)*555, respectively. The results shown are the average of triplicate experiments \pm the standard error. (*) $p < 0.05$; n.s.- no statistically significant.

4.2.4.2 Aβ(1–42) stimulates Ca²⁺ release from ER through IP3R and to a lesser extent, through RyR in HT-22 cells

As the amount of Ca^{2+} release from stores is also decreased by $\text{A}\beta(1\text{-}42)$ (**Figure 20**) and SERCA is not inhibited by concentrations of $\text{A}\beta(1\text{-}42)$ up to $2 \mu\text{M}$ ⁸⁶ we hypothesized that the ligand-gated Ca^{2+} channels RyR and/or the IP3R from ER are being modulated by $\text{A}\beta(1\text{-}42)$. To confirm this hypothesis, we used inhibitors of RyR and IP3R and assessed the effect of $\text{A}\beta(1\text{-}42)$ in Ca^{2+} dynamics using fluorescence microscopy imaging.

Ryanodine, an alkaloid derived from the plant *Ryania speciosa*, binds with high selectivity and affinity to RyR. At high concentrations ($> 100 \mu\text{M}$) ryanodine blocks RyR, while at nanomolar concentrations locks the channel in an open subconductance state⁸⁷. We incubated untreated (control) and treated HT-22 cells ($2 \mu\text{M A}\beta(1\text{-}42)$ 2 h) with $100 \mu\text{M}$ ryanodine for 1 h in culture medium at 37°C and proceeded to SOCE experiments. The results are presented in **Figure 25** and show a significant increase (2.2-fold) in Ca^{2+} release from stores after HT-22 cells were incubated with $100 \mu\text{M}$ ryanodine, compared with the control in absence of ryanodine, which demonstrated the blockade of RyR by ryanodine. Furthermore, there is a decrease in Ca^{2+} release from ER in HT-22 cells treated with $\text{A}\beta(1\text{-}42)$ plus $100 \mu\text{M}$ ryanodine ($\pm 20\%$) compared with cells treated only with ryanodine, indicating that $\text{A}\beta(1\text{-}42)$ is partially stimulating RyR.

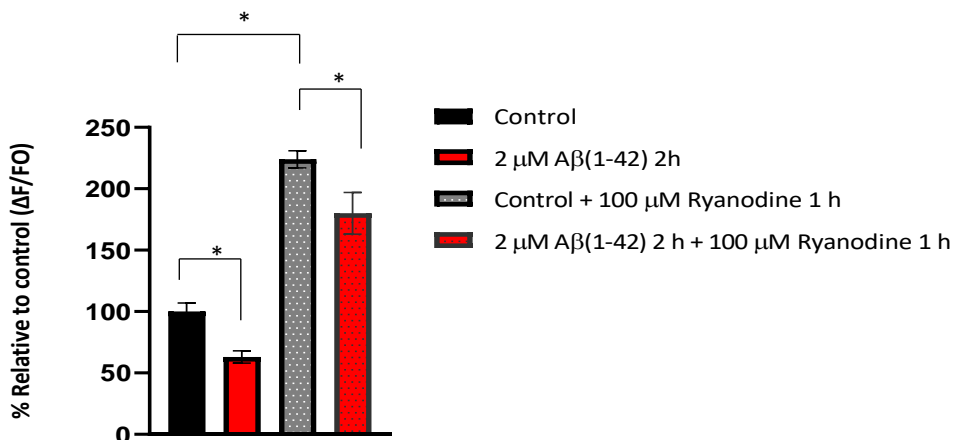


Figure 25. $\text{A}\beta(1\text{-}42)$ partially stimulates RyR activity after 2 h of incubation in HT-22 cells. Untreated (control) and treated HT-22 cells ($2 \mu\text{M A}\beta(1\text{-}42)$) were loaded with Fluo3 AM plus 0.025% Pluronic® F-127 in the absence and presence of the RyR inhibitor ryanodine ($100 \mu\text{M}$) for 1 h. After, cells were washed once with Ca^{2+} -free MLocke's K5 buffer and placed at the holder of the fluorescent microscope for SOCE experiments as described in Materials and Methods section. The graphic represents the means of the average of fluorescence intensity per pixel after addition of $2 \mu\text{M Tg}$ to the extracellular Ca^{2+} -free MLocke's K5 medium in untreated cells (control) and HT-22 treated with $2 \mu\text{M A}\beta(1\text{-}42)$, in absence and presence of $100 \mu\text{M}$ ryanodine. The results indicated that ryanodine blocks the RyR, as demonstrated by the significant increase in Ca^{2+} release from stores (2.2-fold) in control cells incubated with the inhibitor, compared with control cells without ryanodine. Also, there is a decrease in Ca^{2+} release from stores ($\pm 20\%$) in HT-22 cells treated with $\text{A}\beta(1\text{-}42)$ plus $100 \mu\text{M}$ ryanodine, comparing with cells incubated only with ryanodine (control plus ryanodine) indicating that $\text{A}\beta(1\text{-}42)$ partially stimulates the RyR activity.

Xestospongin C (XeC), a marine alkaloid isolated from the Okinawan sponge *Xestospongia* sp, has been used as IP3R blocker^{88,89}. In fact, Wang and co-workers (2019)

demonstrated that XeC could ameliorate the cognitive impairments and pathological damage in APP/PS1 mice, suggesting that XeC might be considered as novel therapeutic for AD⁹⁰. However, other studies have been suggesting that XeC is not selective only for IP3R, and equally blocks SERCA activity^{91,92}. Due to the lack of more specific and selective IP3R blockers, we used XeC as inhibitor to evaluate the effect of Aβ(1-42) in Ca²⁺ release from stores. We incubated 3 μM of XeC for 15 min at 37 °C and 5 %CO₂ in untreated (control) and treated cells (2 μM Aβ(1-42)) and placed Fluo3-loaded HT-22 cells in the thermostated fluorescence microscope for SOCE experiments. The results (**Figure 26**) show that 3 μM of XeC inhibits about 56 ± 4 % the amount of Ca²⁺ released from stores (after tg addition) in untreated HT-22 cells, compared with the respective control (untreated HT-22 cells without XeC). The same result was obtained with HT-22 cells treated with 2 μM Aβ(1-42) plus XeC (57 ± 5 % inhibition). These findings allow us to conclude that the decrease of Ca²⁺ release from ER in HT-22 cells treated with Aβ(1-42) (about 37% inhibition) is largely due the stimulation of IP3R activity.

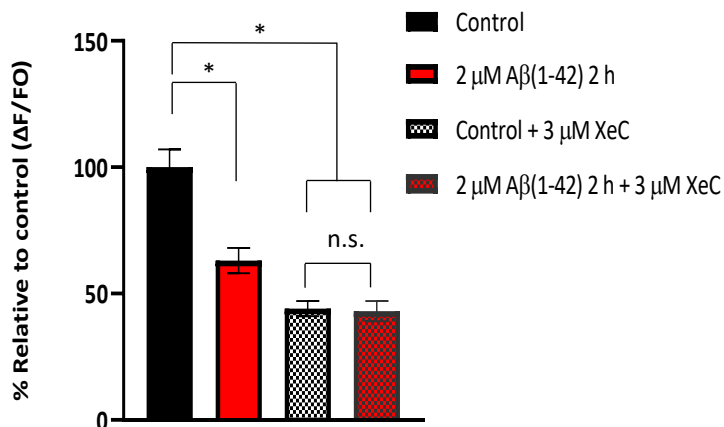


Figure 26. Aβ(1-42) stimulates IP3R activity in HT-22 cells. Untreated (control) and HT-22 cells treated with 2 μM Aβ(1-42) for 2 h were loaded with Fluo3 AM plus 0.025% Pluronic® F-127 for 1h. After, cells were washed once with Ca²⁺-free MLocke's K5 buffer and incubated with 3 μM of XeC for 15 min at 37 °C and placed at the holder of the fluorescent microscope for SOCE experiments. The graphic represents the mean of the average of fluorescence intensity after addition of 2 μM tg to the extracellular Ca²⁺-free medium in untreated cells (control) and HT-22 treated with 2 μM Aβ(1-42), in the absence and presence of 3 μM XeC. The results show that 3 μM of XeC inhibits about 56 ± 4 % the amount of Ca²⁺ released from stores (after tg addition) in control HT-22 cells, and inhibits about 57 ± 5 % in cells treated with Aβ(1-42) compared with the respective controls, suggesting that Aβ(1-42) stimulates IP3R activity (37% ± 7%) ($p<0.05$).

As RyR and IP3R activities are stimulated by Aβ(1-42), we measured the [Ca²⁺]_i. The results in **Figure 27** show that the [Ca²⁺]_i is not significantly altered after 2 h and 5 h with 2 μM Aβ(1-42) in Fura2-loaded nor in Fluo3-loaded HT-22 cells.

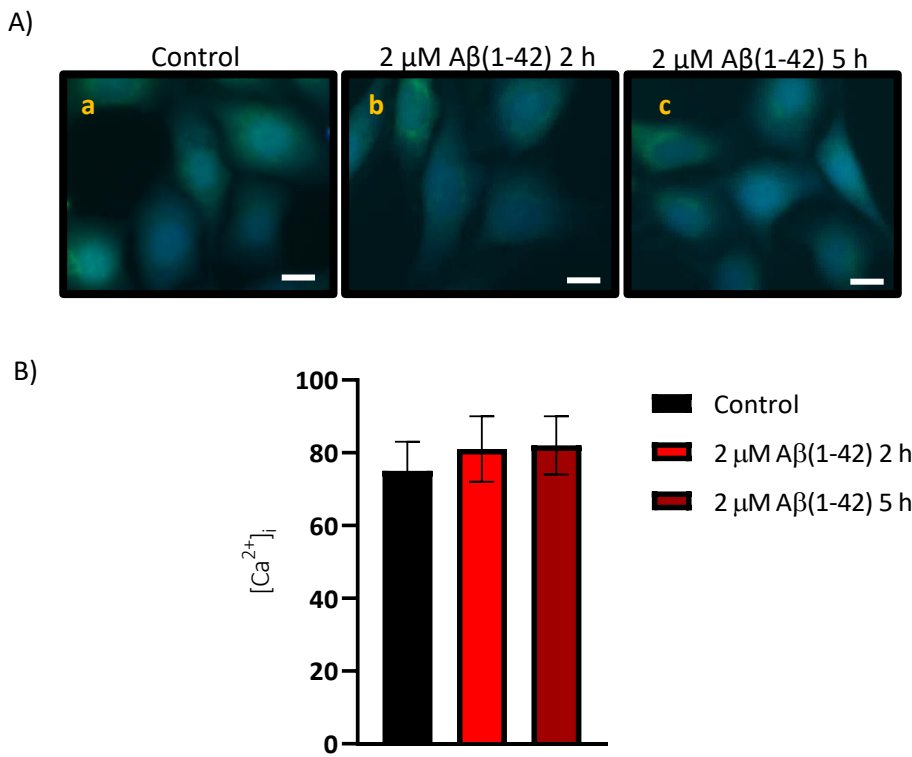


Figure 27. Intracellular Ca²⁺ concentration ([Ca²⁺]_i) is not significantly altered after 2 h and 5 h with 2 μ M A β (1-42) in HT-22 cells. Untreated (control) and treated HT-22 cells with 2 μ M A β (1-42) for 2 h and 5 h were loaded with 5 μ M Fura2 AM or Fluo3 AM plus 0.025 Pluronic® F-127 for [Ca²⁺]_i measurements, as described in Materials and Methods section. **A)** Representative fluorescence images of Fura2-loaded untreated HT-22 cells (control, a) and HT-22 cells treated with 2 μ M A β (1-42) for 2 h (b) and 5 h (c). Scale bar = 20 μ m. **B)** [Ca²⁺] obtained for untreated cells (control, 75 \pm 8 nM) and HT-22 cells incubated with 2 μ M A β (1-42) for 2 h (81 \pm 9 nM) and 5 h (82 \pm 8 nM).

4.2.5 Incubation of HT-22 cells during 2 h with 2 μ M A β (1-42) decreases the influx of Ca²⁺ from the extracellular medium through P2R

As demonstrated earlier in the 3.1 section of this chapter, P2R are the main plasmatic membrane receptors responsible for the influx of Ca²⁺ in HT-22 cell model. For that reason it became relevant to study the effect of A β (1-42) in the activity of P2R. The results obtained by measurements of the cytosolic Ca²⁺ of HT-22 cells (untreated and treated with 2 μ M A β (1-42) 2 h) before and after addition of 100 μ M ATP (the P2R agonist) are shown in the **Figure 28A**. These results show that treatment with A β (1-42) elicits an attenuation of 40 \pm 4% of the ATP-induced Ca²⁺ cytosolic influx in HT-22 cells, see also **Figure 28B**, and the representative fluorescence microscopy images of HT-22 loaded with Fluo3 (**Figure 28C**). We also tested the effect of 2 μ M of scrambled A β (1-42) for 2 h in the activity of P2R and we saw no significant difference in Ca²⁺ signaling after addition of 100 μ M ATP, compared with untreated cells (control) (**Figure 29**).

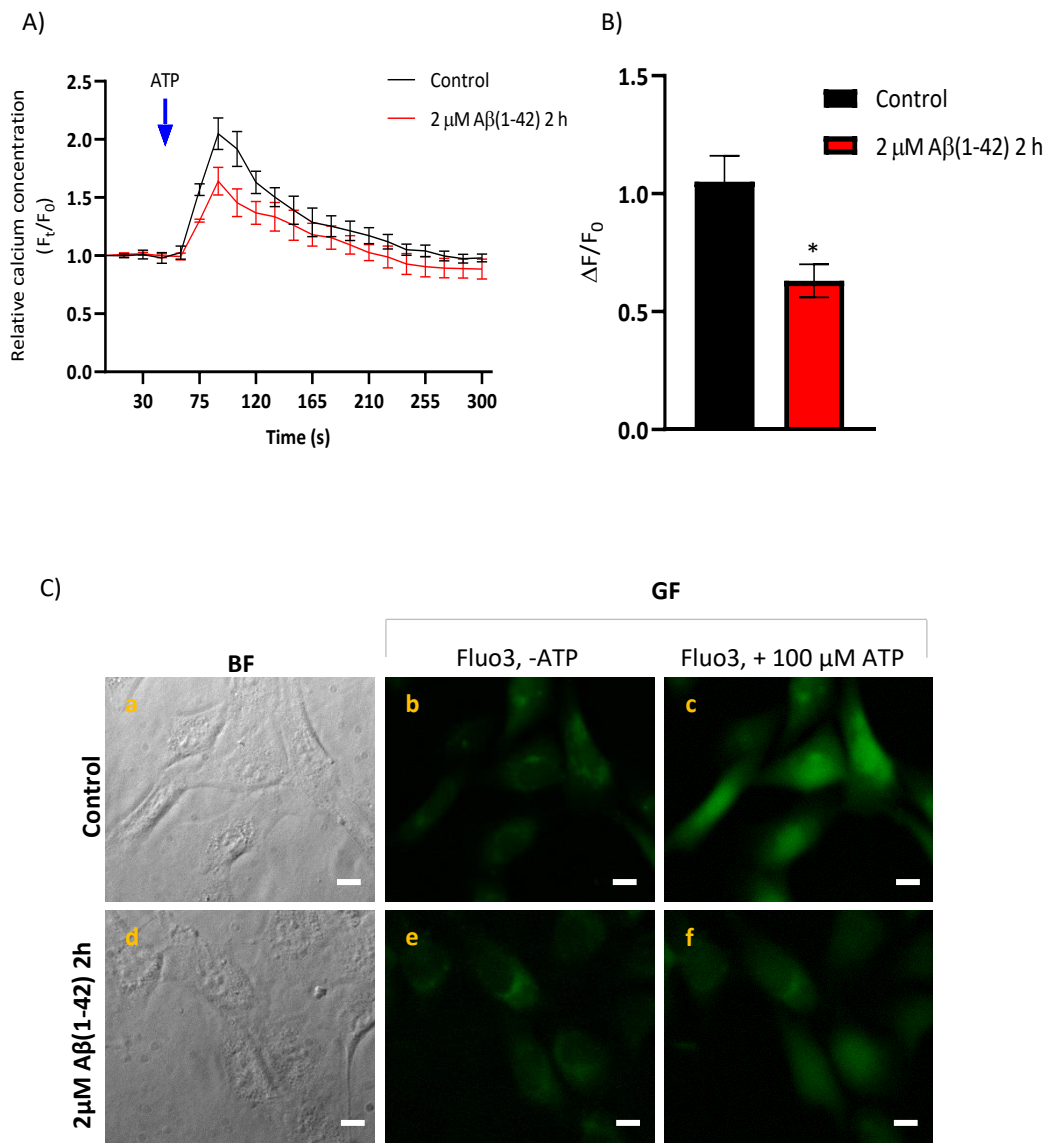


Figure 28. A short time incubation with A β (1-42) decreases the influx of Ca $^{2+}$ from the extracellular medium through P2R in HT-22 cells. HT-22 cells were incubated with 2 μ M A β (1-42) for 2 h at 37 °C and 5% CO₂. One hour before the end of the incubation with A β (1-42), HT-22 were loaded with 5 μ M Fluo3 AM and 0.025% Pluronic® F-127 for 1 h. Then cells were washed once with MLocke's K5 buffer and placed at the holder (37 °C) of the fluorescence microscopy for Ca $^{2+}$ imaging before and after addition of 100 μ M ATP (P2R agonist). **A)** Representative kinetic traces of untreated HT-22 cells (control, black trace) and HT-22 cells incubated with 2 μ M A β (1-42) for 2 h (red trace) after addition of 100 μ M ATP (indicated by the blue arrow). The experiment was performed at 0.3 s exposure time. **B)** Means of the average fluorescent intensity per pixel ($\Delta F/F_0$) of HT-22 cells after addition of 100 μ M ATP. A β (1-42) inhibits about 40 ± 4 % of the Ca $^{2+}$ entry through P2R. Data are presented as the mean ± s.d. at least in 10 petri plates in 5 independent assays (n>80 cells, *p<0.05). **C)** Representative fluorescence images of untreated HT-22 (control) and cells treated with 2 μ M A β (1-42) 2 h, loaded with Fluo3, before and after addition of 100 μ M ATP. Scale bar = 20 μ m.

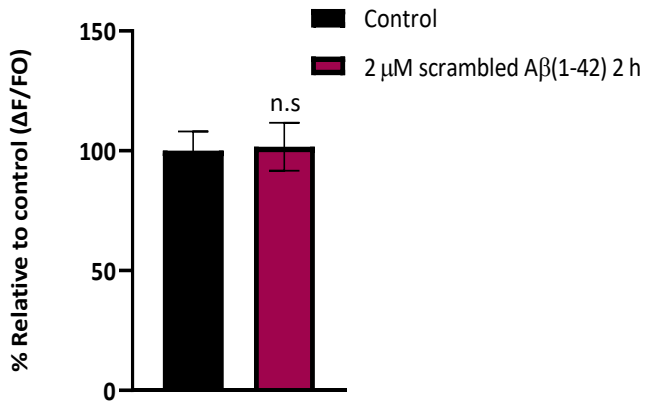


Figure 29. Scrambled A β (1-42) did not alter the resting cytosolic Ca $^{2+}$ concentration through P2R inhibition. HT-22 were incubated with Fluo3 AM (1h) and 2 μ M scrambled A β (1-42) for 2 h at 37 °C and 5% CO₂ and placed at the holder of the fluorescent microscope for Ca $^{2+}$ imaging, as described in the Materials and Methods section. The results presented show not statistically difference in Ca $^{2+}$ signaling after addition of 100 μ M ATP (P2R agonist), compared with the control (untreated cells). Data are presented as the means of the average fluorescent intensity ($\Delta F/F_0$) represented by percentage (%), relatively to control cells, of at least 8 petri plates in 4 independent assays (n > 60 cells). N.s. – non significant.

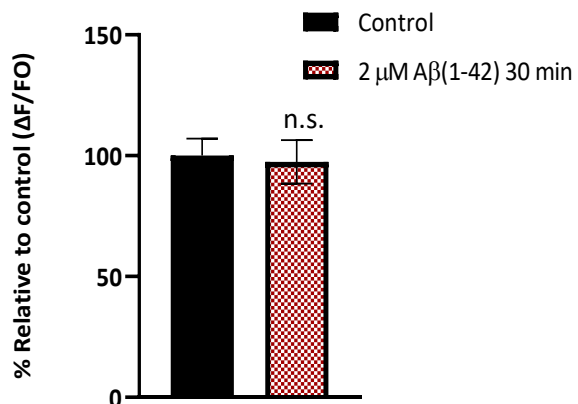


Figure 30. A β (1-42) incubation for 30 min did not change the influx of Ca $^{2+}$ from the extracellular medium through P2R in HT-22 cells. Untreated (control) and treated HT-22 cells with 2 μ M A β (1-42) 0.5 h were incubated with Fluo3 AM (1h) and placed at the holder of the fluorescent microscope for Ca $^{2+}$ imaging, as described in Materials and Methods section. The results presented show no statistically difference in Ca $^{2+}$ influx in HT-22 treated with 2 μ M A β (1-42) for 30 min, compared with untreated cells (control), suggesting that A β (1-42) needs an extended time of incubation to modulate Ca $^{2+}$ influx through these receptors. Data are presented as the means of the average fluorescent intensity ($\Delta F/F_0$) represented by percentage (%), relatively to control cells, of at least 8 petri plates in 4 independent assays (n > 60 cells); n.s. – non significant.

Aiming to evaluate if A β (1-42) binds to putative P2R modulatory site in the extracellular side of the plasma membrane or needs to be internalized inside HT-22 cells to exert its inhibitory effect, we further tested the Ca $^{2+}$ influx in P2R system after incubation with only 30 min of A β (1-42) (2 μ M). The results obtained (Figure 30) indicate that there is not a statistically significant difference in Ca $^{2+}$ influx after addition of 100 μ M ATP to the HT-22 extracellular medium between HT-22 cells treated during 30 min with 2 μ M A β (1-42) and untreated cells (control).

These findings point out that A β (1-42) attenuation of the activity of P2R is not due to direct binding to an extracellularly oriented P2R site, because an extended time of incubation with A β (1-42) is needed to modulate Ca $^{2+}$ influx through these receptors.

4.2.5.1. The subtype P2X7R contributes to 48% of the total P2R activity and is inhibited by A β (1-42)

In the last years, several studies have demonstrated altered expression levels and function of P2X7R (one of the 7 subtypes of the P2R family) in mouse models and AD patients, suggesting that P2X7R is upregulated in AD pathology⁹³. Since the P2X7R has been directly linked to AD, we have evaluated the contribution of this P2R subtype in Ca $^{2+}$ signaling in untreated (control) and treated cells (with A β (1-42)) using two different antagonists of the P2X7R, namely BBG⁹⁴ and compound A804598.

The BBG dye is well known for its use in staining proteins in gel electrophoresis and as a color additive in foods, drugs and cosmetics, yet in the last years BBG has been recognized as a potential pharmacological agent⁹⁵. In fact, *in vivo* administration of BBG in a mouse model of AD, demonstrated that BBG protected against amyloid-induced neuronal loss⁹⁶. Despite the intensive use of BBG as P2X7R antagonist, there are several studies reporting that BBG also blocks P2X1R, P2X4R, and sodium channels, highlighting the lack of specificity of BBG⁹⁷. For this reason, we have also used a novel and more selective P2X7R antagonist, the compound A804598⁹⁸. The results in **Figure 31** show that both treatments: i) 5 μ M of BBG incubated for 5 min in the MLocke's 5 buffer assay or ii) 200 nM of A804598 incubated previously in HT-22 cultured medium for 30 min, had similar inhibitory effects in P2R activity, by decreasing the extracellular ATP-induced influx of Ca $^{2+}$ about 57 \pm 6% and 48 \pm 4%, respectively, comparing with untreated cells (control). The decrease of cytosolic Ca $^{2+}$ concentration is higher with the antagonist BBG, suggesting that BBG could be interact with other receptor(s) (P2X1R and/or P2X4R), since it is not as selective as A804598. However, the difference between both antagonists is not statistically significant. Therefore, these results allow to conclude that P2X7R contributes with 48 \pm 4%, of the Ca $^{2+}$ influx across all P2R activity in HT-22 cells.

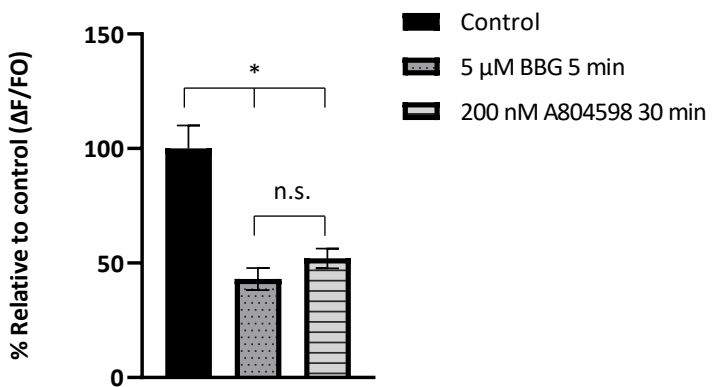


Figure 31. The subtype P2X7R contributes for 48% of all P2R activity in the HT-22 cell culture.

HT-22 cells were loaded with 5 μ M Fluo3 AM and 0.025% Pluronic® F-127 for 1 h and submitted to two different P2X7R antagonist treatments as described in the Materials and Methods section: i) 5 μ M BBG for 5 min in MLocke's K5 buffer or ii) 200 nM A804598 for 30 min in culture media. The results show that both BBG and A804598 antagonists decrease Ca^{2+} influx after addition of ATP (100 μ M) to the extracellular medium. As A809045 is more selective than BBG for P2X7R, these results pointed out that the subtype P2X7R represents 48% of all P2R activity in HT-22 cells. Data are presented as the means of the average fluorescent intensity ($\Delta F/F_0$) represented by percentage (%), relatively to control cells, of at least 8 petri plates in 4 independent assays ($n > 60$ cells; * $p < 0.05$; n.s. – non significant).

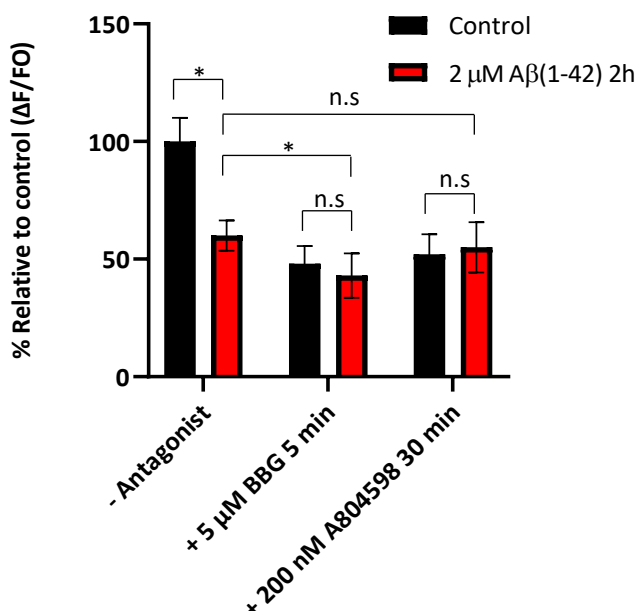


Figure 32. A β (1-42) decreases the influx of cytosolic Ca^{2+} through inhibition of P2X7R subtype of the P2R family. Untreated (control) and treated HT-22 cells (2 μ M A β (1-42) 2 h) were loaded with 5 μ M Fluo3 AM and 0.025% Pluronic® F-127 for 1 h and submitted to two different P2X7R antagonist treatments (BBG and A804598) as described in the Materials and Methods section. The results show similar values of Ca^{2+} inhibition (non-significant) between HT-22 treated with A β (1-42) and cells treated with the most selective antagonist, A804598, and cells treated both with A β (1-42) and A804598. Therefore, these results highlight that A β (1-42) inhibits the flux of Ca^{2+} through inhibition of the subtype P2X7R activity of P2R. Data are presented as the means of the average fluorescent intensity ($\Delta F/F_0$) represented by percentage (%), relatively to control cells, of 3 independent assays ($n > 50$ cells for each condition, $p < 0.05$).

The effect of the incubation with A β (1-42) plus antagonists in HT-22 cells is represented in **Figure 32**. It can be observed that the decrease of the extracellular ATP-induced Ca $^{2+}$ influx in cells treated with A β (1-42) plus the antagonists BBG ($57 \pm 5\%$) is higher than in HT-22 cells incubated only with A β (1-42) ($40 \pm 4\%$). Moreover, the inhibition of P2R activity is similar (no significant differences) between HT-22 treated with A β (1-42) and cells treated with only the P2X7R A804598 antagonist and cells treated both with A β (1-42) and A804598. These results allow us to conclude that A β (1-42) is inhibiting the activity of P2R by blockade of the subtype P2X7R. However, future studies are needed to further experimentally assess the putative contribution of other types of P2R present in this cell line.

4.3. A β (1-42) induces a moderate increase in the production of ROS after 2 h and 5 h incubation in HT-22 cells

It is widely accepted that oxidative stress plays an important role in AD pathology, but there is a large controversy concerning if free radicals are cause or consequence in AD. We evaluated the generation of the intracellular ROS production by monitoring H₂DCF-DA oxidation to the highly fluorescent DCF in HT-22 cells after a short period of incubation with A β (1-42). The results of fluorescence intensity in untreated HT-22 (control) and treated cells with 2 μ M A β (1-42) for 2 h or 5 h, after 15 min incubation with 10 μ M H₂DCF-DA are presented in **Figure 32**. The results show a moderate increase in ROS generation in HT-22 cells treated with A β (1-42). More specifically, there is a 1.3-fold and 1.7-fold increase in ROS production in HT-22 cells treated with 2 μ M A β (1-42) for 2 h and 5 h, respectively, compared to untreated cells (control), as can be seen in **Figure 33 panel A and B**.

As ROS levels are higher in HT-22 cells treated with A β (1-42), we then evaluated the levels of another markers of cellular oxidative stress, namely, reduced glutathione (GSH) content, lipid peroxidation and iron influx in the HT-22 cell after incubation with A β (1-42).

GSH is a major antioxidant in neurons and it is already known that GSH is significantly depleted in AD patients compared to healthy old subjects⁹⁹. We measured GSH levels in untreated and treated HT-22 cells with A β (1-42) using the compound MCB, since it is quickly converted to a fluorescent GSH conjugate (GS-MCB) in culture cells. The results are presented in **Figure 34** and show the means of fluorescent intensity per pixel (**Figure 34A**) and representative HT-22 images (**Figure 34B**) acquired 2 minutes after addition of MCB (10 μ M). The results reveal that GSH levels were not altered by 2 μ M A β (1-42) after 2 h and 5 h incubation in HT-22 cells.

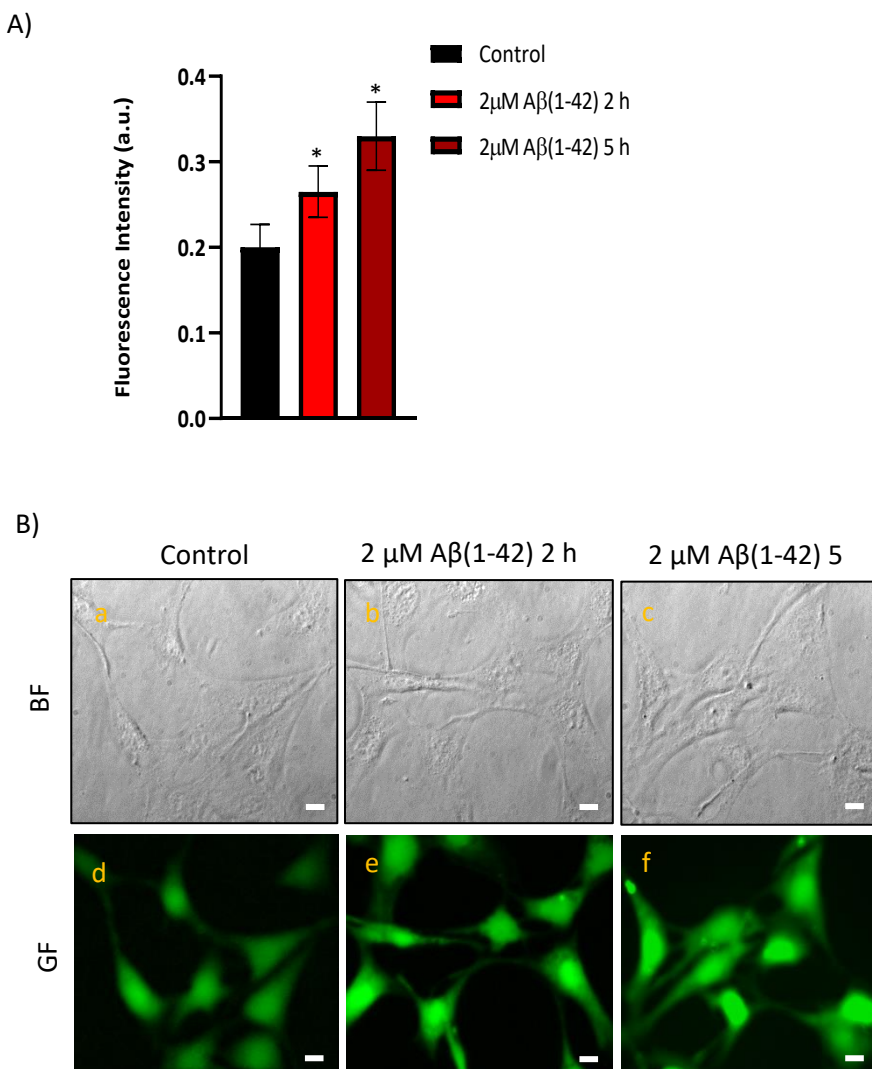


Figure 33. A β (1-42) induces a moderate increase in ROS production after 2 h and 5 h incubation in HT-22 cells. Untreated HT-22 cells (control) and treated cells (incubated with 2 μ M A β (1-42) for 2 h and 5 h) were incubated with 10 μ M of H₂DCF-DA and the extent of H₂DCF-DA oxidation to DCF was monitored by the increase in fluorescent intensity in HT-22 cells 15 min after addition of 10 μ M H₂DCF-DA. **A)** Means of the average fluorescence per pixel in HT-22 cells. The results show a 1.3-fold and 1.7-fold increase in ROS generation in HT-22 cells treated with 2 μ M A β (1-42) for 2 h and 5 h, respectively, compared with untreated cells (control) (* p <0.05). **B)** Representative fluorescence microscopy images of untreated HT-22 cells and treated cells incubated with 2 μ M A β (1-42) for 2 h and 5 h after addition of 10 μ M H₂DCF-DA for 15 min. Scale bar = 20 μ m.

Lipid peroxidation in AD brain's has received special attention, because this form of oxidative stress has been involved in early AD development and therefore strong efforts have been made to discover reliable biomarkers related with lipid peroxidation for early AD diagnosis¹⁰⁰. We assessed the levels of lipid peroxidation in HT-22 cells treated with 2 μ M A β (1-42) for 2 h or 5 h incubation by adding 1 μ M of the fluorescent ratio probe C11-BODIPY^(581/591) in culture media for 30 min (**Figure 35**).

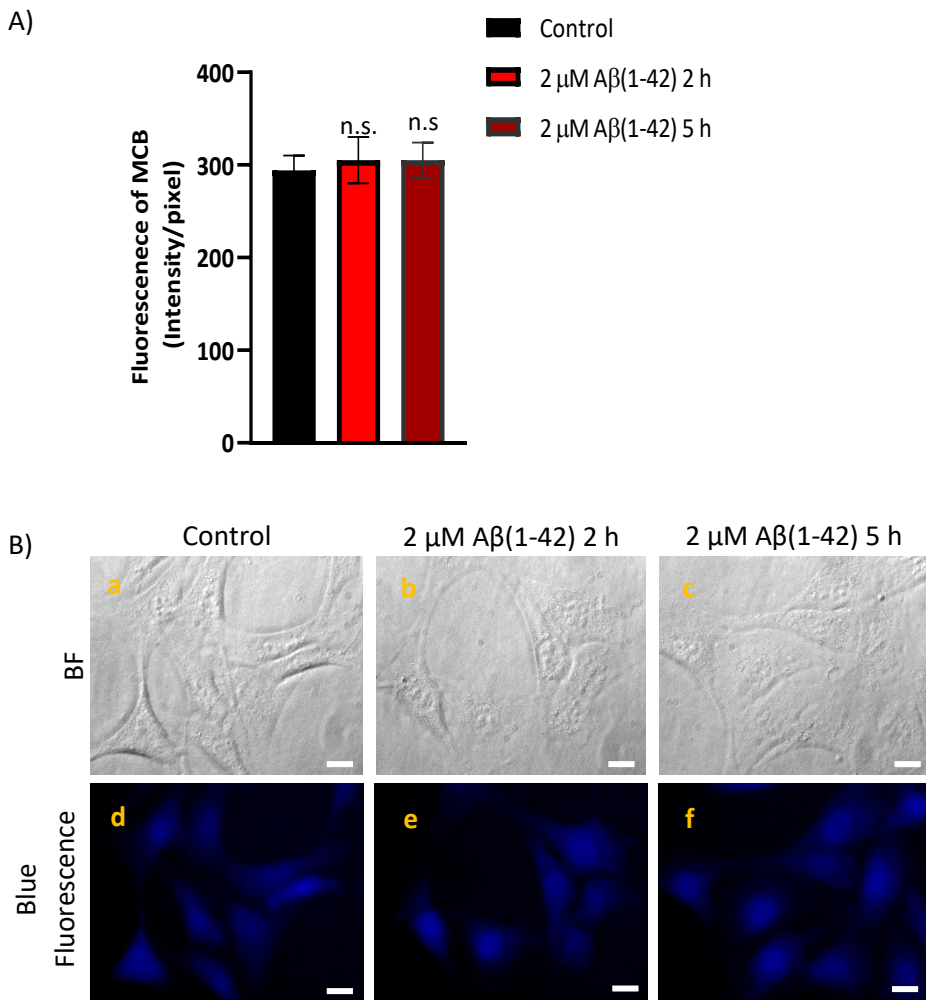


Figure 34. GSH levels are not altered after 2 h and 5 h incubation with 2 μM Aβ(1-42) in HT-22 cells. Untreated HT-22 cells and cells treated with 2 μM Aβ(1-42) for 2 h or 5 h were washed once with MLocke's K5 buffer and placed at holder of the fluorescence microscope (37 °C) for cell imaging before and after the addition of 10 μM MCB as described in the Material and Methods section. **A)** Means of fluorescence intensity per pixel of HT-22 cells after 2 min of incubation with MCB (10 μM). **B)** Representative BF and blue fluorescence images (GS-MCB) acquired 2 min after MCB addition of untreated cells HT-22 (control) and treated cells with 2 μM Aβ(1-42). The time of exposure was 0.7 s and scale bar inserted = 20 μm. Results show no statistically difference in GSH levels between untreated cells (control) and cells treated with 2 μM Aβ(1-42) for 2 h and 5 h (n.s.- non significant).

Figure 35 shows the reduced form of C11-BODIPY^(581/591) indicated by representative RF images of untreated (control) and HT-22 cells treated with Aβ(1-42) and the lack of lipid oxidation in HT-22 cells by the absence of GF (the oxidized form), demonstrating that Aβ(1-42) do not induce a detectable lipid peroxidation in this experimental conditions used.

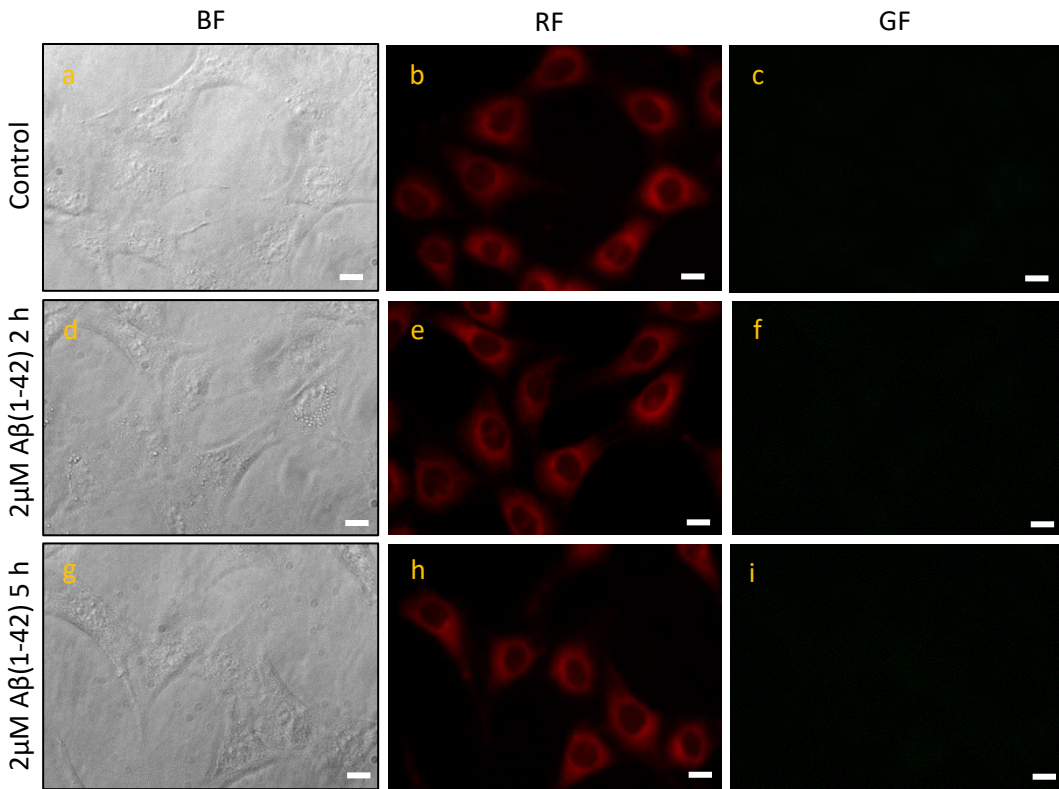


Figure 35. A β (1-42) do not induce alteration in lipid peroxidation in HT-22 cells after a short period of incubation. Representative images of untreated (control) and treated cells with 2 μ M A β (1-42) for 2 h and 5 h, after incubation with the fluorescent ratio probe C11-BODIPY $^{(581/591)}$ (1 μ M for 30 min), acquired with an excitation filter of 470 nm, and a dichroic mirror of 580 nm/emission filter of 590 nm (RF) with an exposure time of 0.2 s and with a 510 nm dichroic mirror/520 nm emission filter (GF) with an exposure time of 1 s. Results show HT-22 images loaded with the reduced form of C11-BODIPY $^{(581/591)}$ (RF) and the lack of GF (oxidized form of C11-BODIPY $^{(581/591)}$), indicating that A β (1-42) do not induce lipid peroxidation after 2 h and 5 h of incubation. Scale bar = 20 μ m.

In the last years several studies have demonstrated that dysregulation of iron homeostasis is associated with AD, showing that high concentrations of iron are present in the insoluble amyloid plaques and neurofibrillary tangles¹⁰¹. Therefore, we used the iron influx assay by loading HT-22 cells with calcein-AM to evaluate if A β (1-42) induces changes in intracellular iron concentration after a short period of incubation in HT-22 cells. Figure 36 presents the means of fluorescence intensity per pixel (F_t/F_0) of untreated HT-22 cells (control, black trace) and cells treated with 2 μ M A β (1-42) for 2 h (red trace) before and after addition of 200 μ M FeCl₃ plus 400 μ M L-ascorbate to loaded calcein HT-22 cells (Figure 36A) and representative fluorescence images of untreated and treated HT-22 loaded with calcein (Figure 36B). The results clearly show no differences in the kinetics of calcein quenching between control (untreated cells) and cells treated with A β (1-42) for 2 h after addition of Fe³⁺ and L-ascorbate. Therefore, exposure of HT-22 cells during 2 h to 2 μ M A β (1-42) do not stimulate iron uptake by these cells.

The results obtained herein indicated that A β (1-42) is inducing a moderate production of ROS, without affecting the GSH and iron levels and with no induction in lipid peroxidation, after a short incubation of time in HT-22 cells.

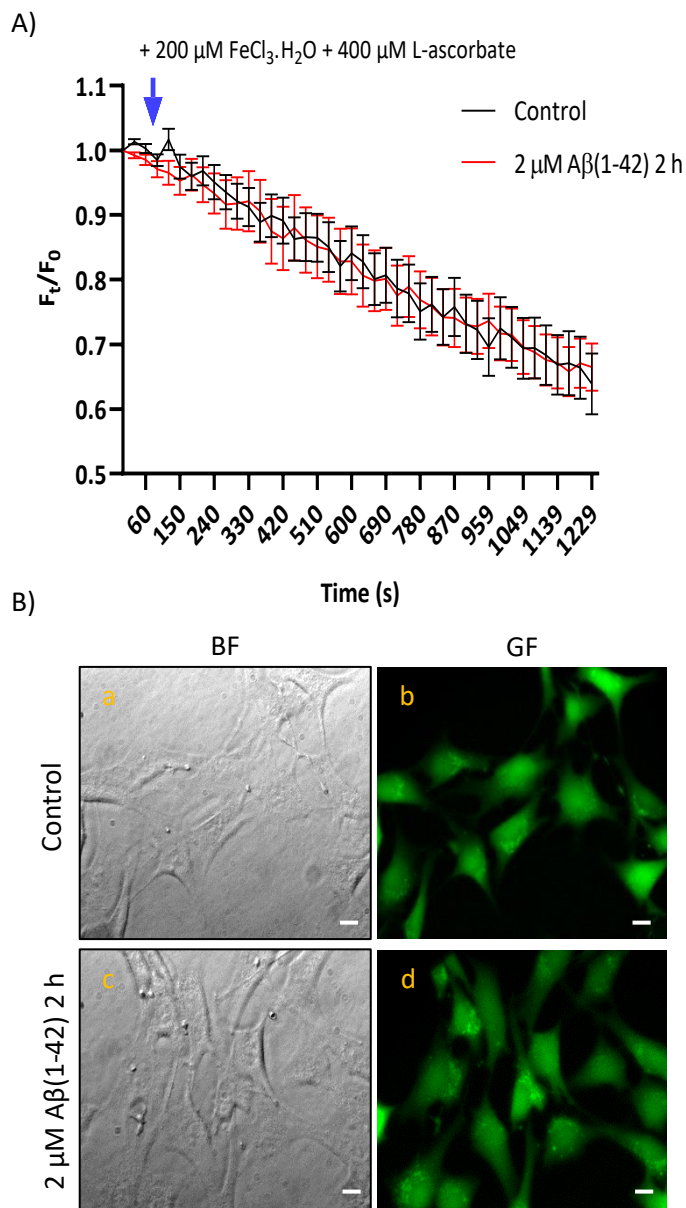


Figure 36. A β (1-42) does not induce alteration in iron concentration in HT-22 cells after 2 h of incubation. Untreated (control) and treated HT-22 cells (2 μ M A β (1-42) incubated for 2 h) were loaded with 0.1 μ M calcein-AM plus 0.025% Pluronic® F-127 for 30 min and washed once with Ca²⁺ and EGTA free-MLocke's K5 buffer (medium assay) and placed at the holder of the fluorescence microscope (37 °C) for imaging acquisition as described in Materials and Methods section. **A)** Means of fluorescence intensity per pixel of untreated HT-22 (control, black trace) and HT-22 cells treated with A β (1-42) (Red trace) before and after addition of FeCl₃ and L-ascorbate as pointed by the blue arrow. Results show no significant differences in calcein quenching between control and treated cells with A β (1-42). **B)** Representative images of HT-22 BF and loaded with calcein (GF images) of untreated (control) and treated with A β (1-42). Scale bar = 20 μ m.

5. Discussion

The internalization of A β peptides in neurons and the subsequent initiation of the neurotoxic cascade of molecular events associated with Ca $^{2+}$ dysregulation represents early pathological features in the progression of AD. In the last years, the study of the mechanism associated with the early stages of AD has drawn attention in the medical field as there is an urgent need for the discover of reliable biomarkers for the early diagnosis of AD.

In this work we added micromolar concentrations of A β (1-42) oligomers (A β (1-42)) to the extracellular medium of HT-22 cells, to study the effect of internalized submicromolar A β peptides in the dysregulation of Ca $^{2+}$ homeostasis after a short time of incubation, without significant loss of cell viability up to 5 h (**Figure 10**). The results obtained show that extracellular addition of 2 μ M A β (1-42) to HT-22 cells, yielded approximately 62 \pm 11 nM and 135 \pm 15 nM of internalized A β (1-42), after 2 h and 5 h of incubation, respectively. In the previous chapter of this work we showed that mature CGN (cerebellar granule neurons) internalized about 193 \pm 21 nM of A β (1-42) only after 2 h of incubation⁴⁶, i.e. three times more than HT-22 cells. It is well accepted that membrane lipid composition plays a key role in conformational changes of A β peptides, including stiffness/elasticity and polarity, affecting the neuronal uptake of A β peptides^{102,103}. Furthermore, increasing evidence suggest that A β peptides are internalized in neuronal cells through different pathways and also it depends of cell type^{74,104,105}. It has been reported both in cell cultures^{106,107} and in the Tg2576 mouse model of AD¹⁰⁸, that A β internalization is mediated mainly by clathrin endocytosis. Besides, lipid rafts microdomains play an important role in A β formation and oligomerization and in A β uptake by neurons, as briefly summarized in the Introduction section of chapter 2. In previous works of our laboratory, it has been shown that mature CGN express high levels of protein lipid rafts markers like caveolin-1, flotillin and HRas⁵⁰. In addition, CGN staining with the fluorescent lipid rafts marker cholera toxin B-Alexa 488 (CTB*488) demonstrated that lipid rafts are widely present in the plasma membrane of CGN in culture⁵¹. However, HT-22 cells were not stained with CTB*488, demonstrating the lack of lipid rafts in the mouse hippocampal cell line HT-22 (data not shown). Furthermore, the lipid rafts-mediated endocytosis does not require the organization of a complex clathrin coat and, therefore, takes place faster than the clathrin-mediated endocytosis¹⁰⁹. Thus, the differences in the amount of internalized A β (1-42) in HT-22 and mature CGN after 2 h of incubation could be explained by the differences in the endocytosis mechanism of A β peptides uptake. However, future studies are needed to experimentally assess the main mechanisms responsible for the uptake of A β (1-42) in both CGN and HT-22 in culture.

We showed by fluorescence microscopy imaging that after 2 h of incubation, internalized A β (1-42) is distributed through all the cytoplasm of HT-22 cells, with some focalized points near the nuclear region (**Figure 12c**) and up to 5 h incubation, A β (1-42) presented a subcellular distribution mainly near the perinuclear region (**Figure 12f and g**). These results are in agreement with other studies that demonstrated that A β 40 and/or A β 42 peptides are predominately distributed in the perinuclear region in differentiated PC12 cells and rat primary hippocampal neurons (RPH)¹⁰⁴ and in the neuroblastoma cell line SH-SY5Y¹⁰⁵⁻⁷⁴. The intracellular distribution of internalized A β (1-42) in HT-22 cells suggest that A β (1-42) could be interacting with mitochondria, ER and/or lysosomes, as these cytoplasm organelles are main targets for A β interaction and modulation as earlier described in other studies in cell cultures and mouse models^{26,72-75}. We have focused our investigation in the intracellular binding of internalized A β (1-42) with mitochondria and ER in HT-22 cells. Our results showed a moderate colocalization between A β (1-42) and mitochondria and ER by using the fluorescent dies MitoTracker™ Green FM (**Figure 13**) and ER-Tracker™ Green, respectively (**Figure 14**) after 5 h incubation in HT-22 cells. These results suggested that A β (1-42) is interacting and possibly modulating mitochondria and/or ER. The effect of A β (1-42) in the $\Delta\Psi_m$ was evaluated with TMRE and the results showed no significative differences between untreated (control) and HT-22 cell treated with 2 μ M A β (1-42). It is to be recalled that another study performed in HT-22 cells concluded that exogenous treatment of A β (1-42) induced mitochondrial impairment, but it is important to note that HT-22 cells were incubated with 5 μ M of A β (1-42), i.e. 2.5-fold the concentration used in this work, and the mitochondrial dysfunction (assessed by TMRM, ROS and ATP generation) was evaluated 6 h after A β (1-42) incubation in HT-22 cells. Therefore, we can conclude that up to 5 h incubation with 2 μ M A β (1-42) added to the extracellular medium, internalized A β (1-42) is interacting with mitochondria as demonstrated by the colocalization with MitoTracker™ Green FM, but is not affecting significantly the $\Delta\Psi_m$ in HT-22.

The moderate colocalization showed between internalized A β (1-42)*555 and the cell permeant ER-Tracker™ Green in living HT-22 cells and the extensive FRET between 50 and 100 nM of A β (1-42)*555 and the ER, which was evaluated using the highly expressed chaperone PDI antibody conjugated with the Alexa 488 fluorescent secondary antibody in fixed HT-22 cells, confirmed the high colocalization between A β peptide and ER (**Figure 17**). It has been reported that nitric oxide (NO) generated in AD, induce S-nitrosylation of PDI and inhibits its enzymatic activity leading to unfolded protein response, which induce ER stress and may cause apoptosis of neuronal cells through S-nitrosylation and down-regulation of PDI in AD¹¹⁰. Therefore, PDI has been seen as potential target for AD therapy¹¹¹. In this work we tested the direct modulation of A β (1-42) in the activity of PDI through the isomerase assay and results show that up to 200 nM,

$\text{A}\beta(1\text{-}42)$ do not significantly alter the activity of PDI in HT-22 cell lysates, suggesting that $\text{A}\beta(1\text{-}42)$ cannot directly modulate the activity of PDI.

SOCE is a ubiquitous Ca^{2+} signaling mechanism triggered by Ca^{2+} depletion of the ER lumen. The activation of SOCE channels induces the entry of extracellular Ca^{2+} into the cytosol, thereby promoting the refilling of the depleted ER Ca^{2+} stores as well as the generation of long-lasting Ca^{2+} signals¹¹². The indication that internalized $\text{A}\beta(1\text{-}42)$ is interacting with ER suggest the possibility that SOCE mechanisms could be affected by $\text{A}\beta(1\text{-}42)$. Our results show that incubation of HT-22 cells with 2 μM $\text{A}\beta(1\text{-}42)$ for 2 h is affecting the biphasic Ca^{2+} signaling mechanism of SOCE, involving both the depletion of Ca^{2+} stores by the SERCA blocker Tg and the Ca^{2+} influx through plasma membrane after addition of Ca^{2+} to the extracellular medium (**Figure 20**). The decrease in the ER Ca^{2+} content is pointed out by 37 \pm 7% decrease of the Tg-induced peak of the fluorescence intensity of Fluo3-loaded HT-22 pre-incubated during 2 h with $\text{A}\beta(1\text{-}42)$. In addition, the incubation of HT-22 cells with 2 μM $\text{A}\beta(1\text{-}42)$ for 2 h also produced a 32 \pm 6% inhibition of the Ca^{2+} influx through plasma membrane Ca^{2+} channels activated by depletion of intracellular Ca^{2+} stores. As positive control of SOCE inhibition we used the cell-permeable pyrazole BTP2 that act as potent blocker of STIM1 and Orai1-coupled CRAC (Ca^{2+} release-activated Ca^{2+}) channel-mediated SOCE. The incubation of HT-22 cells with 3 μM BTP2 for 15 min showed a significative decrease in the Ca^{2+} influx (71 \pm 8 %) after addition of Ca^{2+} to the extracellular medium (**Figure 22**), without affecting the amount of Ca^{2+} released from ER. These results demonstrated that $\text{A}\beta(1\text{-}42)$ is partially inhibiting the Ca^{2+} influx (32 \pm 6%) only after 2 h incubation in HT-22 cells. This suggested the possibility that STIM1 is a major target of internalized $\text{A}\beta(1\text{-}42)$ in HT-22 cells. The possibility of the formation of STIM1: $\text{A}\beta(1\text{-}42)$ complexes in HT-22 was experimentally assessed by co-immunoprecipitation assays with the anti- $\text{A}\beta(1\text{-}42)$ antibody and in the presence of 250 nM $\text{A}\beta(1\text{-}42)$. The western blotting of anti-STIM1 (**Figure 23**) clearly show the presence of STIM1- $\text{A}\beta$ complexes in HT-22 cell lysates, demonstrating that STIM1 is a target molecule of $\text{A}\beta(1\text{-}42)$ at concentrations of this $\text{A}\beta$ peptide close to those reached in HT-22 cells after incubation for 2 h with 2 μM $\text{A}\beta(1\text{-}42)$ added to the extracellular medium. The formation of $\text{A}\beta(1\text{-}42)$ -STIM1 complexes was also confirmed by the measurements of the titration of the fluorescence of GFP-STIM1 with $\text{A}\beta(1\text{-}42)^*\text{555}$, which give a kD close to 10 nM of $\text{A}\beta(1\text{-}42)^*\text{555}$ from these complexes (**Figure 24**). Moreover, the efficiency of FRET obtained in these experiments allows to conclude that $\text{A}\beta(1\text{-}42)^*\text{555}$ binds to a site located \approx 6 – 7 nm from the donor dye of the GFP protein attached to the C-terminal amino acid of STIM1, which is in the cytosolic side of the ER membrane. This result points out to a site close to the CaM binding site in STIM1. Noteworthy, binding of CaM to STIM1 promotes STIM1/Orai1 disassembly^{113,114} and there is extensive FRET between internalized $\text{A}\beta(1\text{-}42)$ and CaM in HT-22

cells (**Figure 19**). Since the dissociation constant of the A β (1-42)-CaM complexes is ≈ 1 nM¹¹⁵, a value much lower than the concentration of internalized A β (1-42) in HT-22 cells after 2 h incubation with 2 μ M A β (1-42) in the extracellular medium, a simple hypothesis is that A β (1-42)-CaM complexes potentiate CaM inhibition upon binding to STIM1.

Accumulating evidence have shown that SOCE function is diminished in AD, resulting in instability of dendric spines and enhanced amyloid genesis¹¹⁶. A large number of studies performed in fAD have provided mechanistic insights regarding altered SOCE function in AD¹¹⁶. Other studies have shown attenuated Ca $^{2+}$ entry in skin fibroblasts from fAD patients^{117,118}. Furthermore, it has been demonstrated that STIM1 is cleaved by the PS1-secretase, leading to the dysregulation of Ca $^{2+}$ homeostasis in SH-SY5Y and in fibroblasts from familial AD patients¹¹⁹. In addition, it was reported that the levels of STIM1 expression in brain tissues of medium frontal gyrus is decreased with the progression of neurodegeneration⁸⁴.

Besides the inhibition of SOCE-dependent Ca $^{2+}$ influx through the plasma membrane, incubation of HT-22 for 2 h with 2 μ M A β (1-42) also induced a partial depletion of Ca $^{2+}$, namely, a 37% decrease of the amount of Ca $^{2+}$ in the ER. This result prompted us to further study the modulation of A β (1-42) in the activity of ligand-gated Ca $^{2+}$ channels RyR and the IP3R from ER, as SERCA is not inhibited by concentrations of A β (1-42) up to 2 μ M⁸⁶. Our results show that ryanodine (100 μ M), the selective blocker of RyR, increased the ER Ca $^{2+}$ content about 2.2-fold, comparing with control in the absence of ryanodine. This result supports the presence of significant activity of RyR in morphologically differentiated HT-22 cells (**Figure 25**). In addition, in HT-22 cells treated with A β (1-42) plus ryanodine there is a decrease in the ER Ca $^{2+}$ content (about 20%) after addition of Tg to the extracellular medium. Indeed, *in vitro* experiments showed that application of A β caused a large increase in RyR activity due to an approximately 10-fold increase in the channel open probability¹²⁰ and stimulates RyR-mediated Ca $^{2+}$ release in hippocampal neurons in culture¹²¹. Therefore, our results lend support to the hypothesis that intracellular A β (1-42) is also partially stimulating the RyR activity in HT-22 cells after incubation for 2 h with 2 μ M A β (1-42).

The results obtained with XeC, the inhibitor of IP3R activity, showed a similar depletion in ER Ca $^{2+}$ content in both untreated (control) and HT-22 cells treated with A β (1-42) in the presence of XeC (**Figure 26**). Since in the absence of XeC incubation of HT-22 cells for 2 h with 2 μ M A β (1-42) led to a $37 \pm 7\%$ depletion of the ER Ca $^{2+}$ content relative to control cells, our results point out that internalized A β (1-42) is also partially stimulating the activity of IP3R. Our results are in good agreement with the results reported by Ferreiro and co-workers with cortical neurons, which demonstrated that A β (1-40) induced an early increase of intracellular Ca $^{2+}$ levels due to the release of Ca $^{2+}$ from ER through RyR and IP3R, leading to the consequent perturbation

of Ca^{2+} homeostasis¹²². However, we have not observed a significant increase in cytosolic Ca^{2+} concentration neither in Fura2-loaded nor in Fluo3-loaded HT-22 cells up to 5 h incubation with 2 μM $\text{A}\beta(1-42)$ added to the extracellular medium (**Figure 27**). Indeed, our results also demonstrate that the kinetics of the decay of cytosolic Ca^{2+} concentration after Tg-induced ER Ca^{2+} release is not significantly altered with respect to control cells after incubation of HT-22 cells for 2 h with 2 μM $\text{A}\beta(1-42)$. Therefore, our results strongly support that the activity of the main cytosolic Ca^{2+} extrusion systems can counterbalance the ER Ca^{2+} release induced by the intracellular $\text{A}\beta(1-42)$ concentration reached in HT-22 cells. In addition, both the decrease in Ca^{2+} influx through P2R inhibition (the main Ca^2 entry system in HT-22 cells) (**Figure 28**) and through plasma membrane Ca^{2+} channels activated by STIM1 upon depletion of intracellular Ca^{2+} stores, help to maintain the intracellular Ca^{2+} homeostasis in HT-22 exposed to $\text{A}\beta(1-42)$ for a short period of time. Of note, HT-22 cells do not express functional AChR³⁶ neither NMDAR²³ which in many neuronal cells are responsible of neurotransmitter-dependent large influx of Ca^{2+} from the extracellular medium.

It has been demonstrated that the subtype P2X7R of the P2R is upregulated in AD pathology, suggesting that this receptor can be a potential target for the AD therapy⁹³. Our results (**Figure 31**) demonstrated, through the selective antagonist A804598, that P2X7R contributes for approximately 48% of the P2R activity in HT-22 cells. To the best of our knowledge this is the first study that show that P2R are the main plasma membrane systems responsible for the influx of extracellular Ca^{2+} , in HT-22 cells, where LTCC are present but inactive, and that $\text{A}\beta(1-42)$ is inhibiting the influx of Ca^{2+} thought the P2X7R subtype after a short incubation of 2 h in HT-22 cells.

It is well accepted that the oxidative stress is linked to AD in early and late stages of AD pathology and several efforts have been made with the aim to define if oxidative stress is a cause for the progression of the disease or if it is a consequence of the indirect neurotoxic events. We evaluated the levels of oxidative stress generated in HT-22 cells induced by $\text{A}\beta(1-42)$ using different experimental assays, aiming to reveal if the changes in Ca^{2+} in SOCE mechanism and in the influx of HT-22 through P2R could be due to indirect modulation mediated by ROS. The results obtained in HT-22 culture, suggests only a moderate increase of ROS production after 2 h and 5 h incubation with 2 μM $\text{A}\beta(1-42)$ (**Figure 33**), without affecting the GSH levels (**Figure 34**) and the degree of lipid peroxidation of HT-22 cells (**Figure 35**). Besides, we did not observed alterations in iron uptake between untreated cells (control) and cells treated for 2 h with $\text{A}\beta(1-42)$ (**Figure 36**). Therefore, we hypothesize that $\text{A}\beta(1-42)$ is inducing the generation of H_2O_2 likely through a mechanism that involves the iron and/or copper-bound to this amyloid peptide via Fenton-type reactions, a known property of this amyloid peptide^{123,124}. Also, the moderate

generation of ROS suggest that A β (1-42) is not affecting SOCE mechanism neither P2R influx through indirect modulation by ROS-signaling pathways associated with a widespread intracellular oxidative stress.

In summary, we showed that A β (1-42) internalizes inside HT-22 cells in submicromolar concentration after a short period of incubation and colocalizes mainly in the perinuclear region up to 5 h incubation in HT-22 cells, before inducing a significant loss of cell viability. A β (1-42) showed moderate colocalization with mitochondria without affecting significantly the mitochondrial membrane potential and also showed colocalization with the ER. The modulation of ER induced by A β (1-42) after 2 h incubation caused a decrease in SOCE mechanism through the modulation of STIM1, and the ER ligand-gated calcium-release channels: RyR and IP3R. Other novel targets for A β (1-42) unveiled in this work are P2X7R. These results suggest that these molecular components of SOCE and P2X7R are good candidates to become targets for therapeutic interventions in an early stage of the progression of AD.

6. References

1. Penke, B., Szucs, M. & Bogár, F. Oligomerization and conformational change turn monomeric β -amyloid and tau proteins toxic: Their role in Alzheimer's pathogenesis. *Molecules* **25**, 1–29 (2020).
2. Reiss, A. B., Arain, H. A., Stecker, M. M., Siegart, N. M. & Kasselman, L. J. Amyloid toxicity in Alzheimer's disease. *Rev. Neurosci.* **29**, 613–627 (2018).
3. Hardy, J.A. & Higgins, G. A. Alzheimer's disease: The amyloid cascade hypothesis. *Science (80-.).* **256**, 184–185 (1992).
4. Podlisny, M. B., Ostaszewski, B. L., Squazzo, S. L., Koo, E. H., Rydell, R. E., Teplow, D. B., Selkoe, D. J. Aggregation of secreted amyloid β -protein into sodium dodecyl sulfate-stable oligomers in cell culture. *J. Biol. Chem.* **270**, 9564–9570 (1995).
5. Walsh, D.M., Klyubin, I., Fadeeva, J.V., Cullen, W.K., Anwyl, R., Wolfe, M.S., Rowan, M.J., Selkoe, D. J. Naturally secreted oligomers of amyloid β protein potently inhibit hippocampal long-term potentiation in vivo. *Nature* **416**, 535–539 (2002).
6. Lesné, S., Ming, T.K., Kotilinek, L., Kayed, R., Glabe, C.G., Yang, A., Gallagher, M., Ashe, K. H. A specific amyloid- β protein assembly in the brain impairs memory. *Nature* **440**, 352–357 (2006).
7. Shankar, G.M., Leissing, M.A., Adame, A., Sun, X., Spooner, E., Masliah, E., Selkoe, D.J., Lemere, C.A., Walsh, D. M. Biochemical and immunohistochemical analysis of an

- Alzheimer's disease mouse model reveals the presence of multiple cerebral A β assembly forms throughout life. *Neurobiol Dis.* **36**, 293–302 (2009).
- 8. Gong, Y., Chang, L., Viola, K.L., Lacor, P.N., Lambert, M.P., Finch, C.E., Krafft, G.A., Klein, W. L. Alzheimer's disease-affected brain: Presence of oligomeric A β ligands (ADDLs) suggests a molecular basis for reversible memory loss. *Proc. Natl. Acad. Sci. U. S. A.* **100**, 10417–10422 (2003).
 - 9. Shankar, G.M., Li, S., Mehta, T.H., Garcia-Munoz, A., Shepardson, N.E., Smith, I., Brett, F.M., Farrell, M.A., Rowan, M.J., Lemere, C.A., Regan, C.M., Walsh, D.M., Sabatini, B.L., Selkoe, D. J. Amyloid β -Protein Dimers Isolated Directly from Alzheimer Brains Impair Synaptic Plasticity and Memory. *Nat Med* **14**, 837–42 (2008).
 - 10. Mucke, L. & Selkoe, D. J. Neurotoxicity of amyloid β -protein: Synaptic and network dysfunction. *Cold Spring Harb. Perspect. Med.* **2**, 1–18 (2012).
 - 11. He, Y., Zheng, M.M., Ma, Y., Han, X.J., Ma, X.Q., Qu, C.Q., Du, Y. F. Soluble oligomers and fibrillar species of amyloid β -peptide differentially affect cognitive functions and hippocampal inflammatory response. *Biochem. Biophys. Res. Commun.* **429**, 125–130 (2012).
 - 12. Forny-Germano, L., Lyra e Silva, N.M., Batista, A.F., Brito-Moreira, J., Gralle, M., Boehnke, S.E., Coe, B.C., Lablans, A., Marques, S.A., Martinez, A. M. et al. Alzheimer's disease-like pathology induced by amyloid- β oligomers in nonhuman primates. *J. Neurosci.* **34**, 13629–13643 (2014).
 - 13. Ferreira, S. T. The A β oligomer hypothesis for synapse failure and memory loss in Alzheimer's disease. *Neurobiol Learn Mem* **96**, 529–543 (2011).
 - 14. Walsh, D. M. & Selkoe, D. J. A β oligomers - A decade of discovery. *J. Neurochem.* **101**, 1172–1184 (2007).
 - 15. Tong, B. C. K., Wu, A. J., Li, M. & Cheung, K. H. Calcium signaling in Alzheimer's disease & therapies. *Biochim. Biophys. Acta - Mol. Cell Res.* **1865**, 1745–1760 (2018).
 - 16. Khachaturian, Z. S. Calcium Hypothesis of Alzheimer's Disease and Brain Aging a. 1–11 (1993).
 - 17. Berridge, M. J. Calcium Signalling and Alzheimer's Disease. *Neurochem. Res.* **36**, 1149–1156 (2011).
 - 18. Kuchibhotla, K.V., Goldman, S.T., Lattarulo, C.R., Wu, H., Hyman, B.T., Bacskai, B. J. Amyloid β Plaques Lead to Aberrant Regulation of Calcium Homeostasis In Vivo Resulting in Structural and Functional Disruption of Neuronal Networks. *Neuron.* 214–225 (2008).
 - 19. Lopez, R., Lyckman, A., Oddo, S., Laferla, F.M., Querfurth, H.W., Shtifman, A. Increased intraneuronal resting [Ca 2+] in adult Alzheimer's disease mice. *J Neurochem* **105**, 262–

- 271 (2008).
- 20. Frederiksen, K., Jat, P. S., Valtz, N., Levy, D. & McKay, R. Immortalization of precursor cells from the mammalian CNS. *Neuron* **1**, 439–448 (1988).
 - 21. Lendahl, U. & McKay, R. D. The use of cell lines in neurobiology. *Trends Neurosci.* **13** (4), 132–137 (1990).
 - 22. Morimoto, B.H. & Koshland Jr, D. E. Induction and expression of long- and shortterm neurosecretory potentiation in a neural cell line. *Neuron* **5**, 875–880 (1990).
 - 23. Kritis, A. A., Stamoula, E. G., Paniskaki, K. A. & Vavilis, T. D. Researching glutamate – induced cytotoxicity in different cell lines: A comparative/collective analysis/study. *Front. Cell. Neurosci.* **9**, 1–18 (2015).
 - 24. Luo, L., Lü, L., Lu, Y., Zhang, L., Li, B., Guo, K., Chen, L., Wang, Y., Shao, Y., Xu, J. Effects of hypoxia on progranulin expression in HT22 mouse hippocampal cells. *Mol. Med. Rep.* **9**, 1675–1680 (2014).
 - 25. Zhong, S., Pei, D., Shi, L., Cui, Y. & Hong, Z. Ephrin-B2 inhibits A β 25-35 -induced apoptosis by alleviating endoplasmic reticulum stress and promoting autophagy in HT22 cells. *Neurosci. Lett.* **704**, 50–56 (2019).
 - 26. Cha, M.Y., Han, S.H., Son, S.M., Hong, H.S., Choi, Y.J., Byun, J., Mook-Jung, I. Mitochondria-specific accumulation of amyloid β induces mitochondrial dysfunction leading to apoptotic cell death. *PLoS One* **7**, (2012).
 - 27. Rao, W., Peng, C., Zhang, L., Su, N., Wang, K., Hui, H., Dai, S.H., Yang, Y.F., Luo, P., Fei, Z. Homer1a attenuates glutamate-induced oxidative injury in HT-22 cells through regulation of store-operated calcium entry. *Sci. Rep.* **6**, 1–12 (2016).
 - 28. Henke, N., Albrecht, P., Bouchachia, I., Ryazantseva, M., Knoll, K., Lewerenz, J., Kaznache耶eva, E., Maher, P., Methner, A. The plasma membrane channel ORAI1 mediates detrimental calcium influx caused by endogenous oxidative stress. *Cell Death Dis.* **4**, e470-9 (2013).
 - 29. Behl, C. Effects of glucocorticoids on oxidative stress-induced hippocampal cell death: implications for the pathogenesis of Alzheimer's disease. *Exp Gerontol* **33**, 689–96 (1998).
 - 30. Song, J.H., Shin, M.S., Hwang, G.S., Oh, S.T., Hwang, J.J., Kang, K. S. Chebulinic acid attenuates glutamate-induced HT22 cell death by inhibiting oxidative stress, calcium influx and MAPKs phosphorylation. *Bioorganic Med. Chem. Lett.* **28**, 249–253 (2018).
 - 31. Zhao, Z.Y., Luan, P., Huang, S.X., Xiao, S.H., Zhao, J., Zhang, B., Gu, B.B., Pi, R.B., Liu, J. Edaravone protects HT22 neurons from H₂O₂-induced apoptosis by inhibiting the MAPK signaling pathway. *CNS Neurosci. Ther.* **19**, 163–169 (2013).
 - 32. Rao, W., Zhang, L., Su, N., Wang, K., Hui, H., Wang, L., Chen, T., Luo, P., Yang, Y.F., Liu,

- Z.B., Fei, Z. Blockade of SOCE protects HT22 cells from hydrogen peroxide-induced apoptosis. *Biochem. Biophys. Res. Commun.* **441**, 351–356 (2013).
33. Zhu, B., Zhang, Y. & Herrup, K. Testing the neuroprotective properties of PCSO-524® using a neuronal cell cycle suppression assay. *Mar. Drugs* **17**, (2019).
34. Bonaterra, G.A., Schwendler, A., Hüther, J., Schwarzbach, H., Schwarz, A., Kolb, C., Abdel-Aziz, H., Kinscherf, R. Neurotrophic, cytoprotective, and anti-inflammatory effects of St. John's wort extract on differentiated mouse hippocampal HT-22 neurons. *Front. Pharmacol.* **8**, 1–13 (2018).
35. Liu, J., Li, L. & Suo, W. Z. HT22 hippocampal neuronal cell line possesses functional cholinergic properties. *Life Sci.* **84**, 267–271 (2009).
36. Naime, A.A., Lopes, M.W., Colle, D., Dafré, A.L., Suñol, C., da Rocha, J.B.T., Aschner, M., Leal, R.B., Farina, M. Glutathione in Chlorpyrifos-and Chlorpyrifos-Oxon-Induced Toxicity: a Comparative Study Focused on Non-cholinergic Toxicity in HT22 Cells. *Neurotox. Res.* **38**, 603–610 (2020).
37. Koshimizu, T.A., Van Goor, F., Tomić, M., Wong, A.O., Tanoue, A., Tsujimoto, G., Stojilkovic, S. S. Characterization of calcium signaling by purinergic receptor-channels expressed in excitable cells. *Mol. Pharmacol.* **58**, 936–945 (2000).
38. Glaser, T., Resende, R. R. & Ulrich, H. Implications of purinergic receptor-mediated intracellular calcium transients in neural differentiation. *Cell Commun. Signal.* **11**, 1–9 (2013).
39. Lipscombe, D., Helton, T. D. & Xu, W. L-type calcium channels: The low down. *J. Neurophysiol.* **92**, 2633–2641 (2004).
40. Bagur, R. & Hajnóczky, G. Intracellular Ca²⁺ sensing: role in calcium homeostasis and signaling. *Mol Cell* **66**, 780–788 (2017).
41. Putney, J.W., Steinckwich-Besançon, N., Numaga-Tomita, T., Davis, F.M., Desai, P.N., D'Agostin, D.M., Wu, S., Bird, G. S. The functions of store-operated calcium channels. *Biochim. Biophys. Acta - Mol. Cell Res.* **1864**, 900–906 (2017).
42. Duncan, R. S., Hwang, S. Y. & Koulen, P. Differential inositol 1,4,5-trisphosphate receptor signaling in a neuronal cell line. *Int. J. Biochem. Cell Biol.* **39**, 1852–1862 (2007).
43. Rybalchenko, V., Grillo, M.A., Gastinger, M.J., Rybalchenko, N., Payne, A.J., Koulen, P. The unliganded long isoform of estrogen receptor beta stimulates brain ryanodine receptor single channel activity alongside with cytosolic Ca²⁺. *J Recept Signal Transduct Res* **29**, 326–41 (2009).
44. Li, X., Yao, L., Liang, Q., Qu, H., Cai, H. Propofol Protects Hippocampal Neurons from Hypoxia-Reoxygenation Injury by Decreasing Calcineurin-Induced Calcium Overload and

- Activating YAP Signaling. *Oxid Med Cell Longev* **2018**, 1–12 (2018).
45. Berrocal, M., Saez, L. & Mata, A. M. Sorcin activates the brain pmca and blocks the inhibitory effects of molecular markers of alzheimer's disease on the pump activity. *Int. J. Mol. Sci.* **22**, (2021).
 46. Poejo, J., Salazar, J., Mata, A. M. & Gutierrez-merino, C. Binding of amyloid β (1–42)-calmodulin complexes to plasma membrane lipid rafts in cerebellar granule neurons alters resting cytosolic calcium homeostasis. *Int. J. Mol. Sci.* **22**, 1–23 (2021).
 47. Zhang, M., Zheng, H., Zhang, X., Tian, X., Xu, S., Liu, Y., Jiang, S., Liu, X., Shi, R., Gong, K., Yan, S., Wang, H., Shao, G., Yang, Z. Involvement of nerve growth factor in mouse hippocampal neuronal cell line (HT22) differentiation and underlying role of DNA methyltransferases. *J. Toxicol. Environ. Heal. - Part A Curr. Issues* **81**, 1116–1122 (2018).
 48. Zhao, Z., Lu, R., Zhang, B., Shen, J., Yang, L., Xiao, S., Liu, J., Suo, W. Z. Differentiation of HT22 neurons induces expression of NMDA receptor that mediates homocysteine cytotoxicity. *Neurol. Res.* **34**, 38–43 (2012).
 49. Suo, Z., Wu, M., Citron, B. A., Palazzo, R. E. & Festoff, B. W. Rapid tau aggregation and delayed hippocampal neuronal death induced by persistent thrombin signaling. *J. Biol. Chem.* **278**, 37681–37689 (2003).
 50. Marques-da-Silva, D. & Gutierrez-Merino, C. Caveolin-rich lipid rafts of the plasma membrane of mature cerebellar granule neurons are microcompartments for calcium/reactive oxygen and nitrogen species cross-talk signaling. *Cell Calcium* **56**, 108–123 (2014).
 51. Fortalezas, S., Poejo, J., Samhan-arias, A. K. & Gutierrez-merino, C. Cholesterol-Rich Plasma Membrane Submicrodomains Can Be a Major Extramitochondrial Source of Reactive Oxygen Species in Partially Depolarized Mature Cerebellar Granule Neurons in Culture. *Jnnd* **5**, (2019).
 52. McCormack, J.G., Cobbold, P. H. *Cellular Calcium: A Practical Approach - The Practical Approach Series.* (1991).
 53. Kao, J.P.Y., Li, G., Auston, D. A. *Methods in Cell Biology. Chapter 5 - Practical Aspects of Measuring Intracellular Calcium Signals with Fluorescent Indicators.* (2010).
 54. Fluo Calcium Indicators. Invitrogen Handbook. *Mol. Probes* 1–5 (2011).
 55. Fortalezas, S., Marques-da-Silva, D., Gutierrez-Merino, C. Methyl- β -Cyclodextrin Impairs the Phosphorylation of the β 2 Subunit of L-Type Calcium Channels and Cytosolic Calcium Homeostasis in Mature Cerebellar Granule Neurons. *Int J Mol Sci.* **19**, 3667 (2018).
 56. Fortalezas, S., Marques-da-Silva, D. & Gutierrez-Merino, C. Creatine Protects Against Cytosolic Calcium Dysregulation, Mitochondrial Depolarization and Increase of Reactive

- Oxygen Species Production in Rotenone-Induced Cell Death of Cerebellar Granule Neurons. *Neurotox. Res.* **34**, 717–732 (2018).
- 57. Chazotte, B. Labeling Mitochondria with TMRM or TMRE. *Cold Spring Harb Protoc* **7**, 895–7 (2011).
 - 58. Samhan-Arias, A.K., Marques-da-Silva, D., Yanamala, N., Gutierrez-Merino, C. Stimulation and clustering of cytochrome b5 reductase in caveolin-rich lipid microdomains is an early event in oxidative stress-mediated apoptosis of cerebellar granule neurons. *J Proteomics* **75**, 2934–49 (2012).
 - 59. Gutiérrez-Merino, C., Molina A., Escudero, B., Diez, A., Laynez, J. Interaction of the local anesthetics dibucaine and tetracaine with sarcoplasmic reticulum membranes. Differential scanning calorimetry and fluorescence studies. *Biochemistry* **28**, 3398–406 (1989).
 - 60. Centeno, F. and Gutiérrez, Merino, C. Location of functional centers in the microsomal cytochrome P450 system. *Biochemistry* **31**, 8473–8481 (1992).
 - 61. Wall, K.P., Dillon, R., Knowles, M. K. Fluorescence quantum yield measurements of fluorescent proteins: A laboratory experiment for a biochemistry or molecular biophysics laboratory course. *Biochem. Mol. Biol. Educ.* **43**, 52–59 (2015).
 - 62. Raturi, A. & Mutus, B. Characterization of redox state and reductase activity of protein disulfide isomerase under different redox environments using a sensitive fluorescent assay. *Free Radic. Biol. Med.* **43**, 62–70 (2007).
 - 63. Keelan, J., Allen, N. J., Antcliffe, D., Pal, S. & Duchen, M. R. Quantitative imaging of glutathione in hippocampal neurons and glia in culture using monochlorobimane. *J. Neurosci. Res.* **66**, 873–884 (2001).
 - 64. Pap, E.H.W., Drummen, G.P.C., Winter, V. J., Kooij, T.W.A., Rijken, P., Wirtz, K.W.A., Op Den Kamp, J. A.F., Hage, W. J., Post, J. A. Ratio-fluorescence microscopy of lipid oxidation in living cells using C11-BODIPY(581/591). *FEBS Lett.* **453**, 278–282 (1999).
 - 65. Xu, Y. Y., Wan, W. P., Zhao, S. & Ma, Z. G. L-type Calcium Channels are Involved in Iron-induced Neurotoxicity in Primary Cultured Ventral Mesencephalon Neurons of Rats. *Neurosci. Bull.* **36**, 165–173 (2020).
 - 66. Rienecker, K. D. A., Poston, R. G. & Saha, R. N. Merits and Limitations of Studying Neuronal Depolarization-Dependent Processes Using Elevated External Potassium. *ASN Neuro* **12**, (2020).
 - 67. Collins, F. & Lile, J. D. The role of dihydropyridine-sensitive voltage-gated calcium channels in potassium-mediated neuronal survival. *Brain Res.* **502**, 99–108 (1989).
 - 68. He, M., Liu, J., Cheng, S., Xing, Y. & Suo, W. Z. Differentiation renders susceptibility to

- excitotoxicity in HT22 neurons. *Neural Regen. Res.* **8**, 1297–1306 (2013).
- 69. Song, Z., Vijayaraghavan, S. & Sladek, C. D. ATP increases intracellular calcium in supraoptic neurons by activation of both P2X and P2Y purinergic receptors. *Am. J. Physiol. - Regul. Integr. Comp. Physiol.* **292**, 423–431 (2007).
 - 70. Pankratov, Y., Lalo, U., Krishtal, O. A. & Verkhratsky, A. P2X receptors and synaptic plasticity. *Neuroscience* **158**, 137–148 (2009).
 - 71. Zarrinmayeh, H. & Territo, P. R. Purinergic Receptors of the Central Nervous System: Biology, PET Ligands, and Their Applications. *Mol. Imaging* **19**, 1–26 (2020).
 - 72. Umeda, T., Tomiyama, T., Sakama, N., Tanaka, S., Lambert, M.P., Klein, W.L., Mori, H. Intraneuronal Amyloid b Oligomers Cause Cell Death Via Endoplasmic Reticulum Stress, Endosomal/Lysosomal Leakage, and Mitochondrial Dysfunction In Vivo. *J Neuropathol Exp Neurol* **1042**, 1031–1042 (2011).
 - 73. Jiao, Y., Zhang, Y., Wei, Y., Liu, Z., An, W., Guo, M. Direct Observation of Internalization and ROS Generation of Amyloid β -Peptide in Neuronal Cells at Subcellular Resolution. *ChemBioChem* **13**, 2335–2338 (2012).
 - 74. Lana, E., Khanbolouki, M., Degavre, C., Samuelsson, E.B., Åkesson, E., Winblad, B., Alici, E., Lithner, C.U., Behbahani, H. Perforin Promotes Amyloid Beta Internalisation in Neurons. *Mol. Neurobiol.* **54**, 874–887 (2017).
 - 75. He, Z., Wang, M., Zhao, Q., Li, X., Liu, P., Ren, B., Wu, C., Du, X., Li, N., Liu, Q. Bis(ethylmaltolato)oxidovanadium (IV) mitigates neuronal apoptosis resulted from amyloid-beta induced endoplasmic reticulum stress through activating peroxisome proliferator-activated receptor γ . *J. Inorg. Biochem.* **208**, 111073 (2020).
 - 76. Ferrari, D. M. & Soling, H.-D. The protein disulphide-isomerase family: unravelling a string of folds. *Biochem. J.* **339**, 1–10 (1999).
 - 77. Perri, E. R., Thomas, C. J., Parakh, S., Spencer, D. M. & Atkin, J. D. The unfolded protein response and the role of protein disulfide isomerase in neurodegeneration. *Front. Cell Dev. Biol.* **3**, 1–17 (2016).
 - 78. Erickson, R.R., Dunning, L. M., Olson, D.A., Cohen, S. J., Davis, A.T., Wood, W. G. & Kratzke, R.A., Holtzman, J. L. In cerebrospinal fluid ER chaperones ERp57 and calreticulin bind β -amyloid. *Biochem. Biophys. Res. Commun.* **332**, 50–57 (2005).
 - 79. Honjo, Y., Ayaki, T., Tomiyama, T., Horibe, T., Ito, H., Mori, H., Takahashi, R., Kawakami, K. Decreased levels of PDI and P5 in oligodendrocytes in Alzheimer's disease. *Neuropathology* **37**, 495–501 (2017).
 - 80. Ishikawa, J., Ohga, K., Yoshino, T., Takezawa, R., Ichikawa, A., Kubota, H., Yamada, T. A Pyrazole Derivative, YM-58483, Potently Inhibits Store-Operated Sustained Ca²⁺ Influx

- and IL-2 Production in T-Lymphocytes. *J. Immunol.* **170**, 4441–4449 (2003).
81. Zitt, C., Strauss, B., Schwarz, E.C., Spaeth, N., Rast, G., Hatzelmann, A., Hoth, M. Potent Inhibition of Ca²⁺ Release-activated Ca²⁺ Channels and T-lymphocyte Activation by the Pyrazole Derivative BTP2. *J. Biol. Chem.* **279**, 12427–12437 (2004).
 82. Moccia, F., Zuccolo, E., Soda, T. & Tanzi, F., Guerra, G., Mapelli, L., Lodola, F., D’angelo, E. STIM and Orai proteins in neuronal Ca²⁺ signaling and excitability. *Front. Cell. Neurosci.* **9**, 1–14 (2015).
 83. Derler, I., Jardin, I. & Romanin, C. Molecular mechanisms of STIM/Orai communication. *Am. J. Physiol. - Cell Physiol.* **310**, C643–C662 (2016).
 84. Pascual-Caro, C., Berrocal, M., Lopez-Guerrero, A.M., Alvarez-Barrientos, A., Pozo-Guisado, E., Gutierrez-Merino, C., Mata, A.M., Martin-Romero, F. J. STIM1 deficiency is linked to Alzheimer’s disease and triggers cell death in SH-SY5Y cells by upregulation of L-type voltage-operated Ca²⁺ entry. *J. Mol. Med.* **96**, 1061–1079 (2018).
 85. Pascual-Caro, C., Orantos-Aguilera, Y., Sanchez-Lopez, I., de Juan-Sanz, J., Parys, J. B., Area-Gomez, E., Pozo-Guisado, E., & Martin-Romero, F. J. STIM1 Deficiency Leads to Specific Down-Regulation of ITPR3 in SH-SY5Y Cells. *Int J Mol Sci* **21**, 6598 (2020).
 86. Berrocal, M., Marcos, D., Sepúlveda, M.R., Pérez, M., Ávila, J., Mata, A. M. Altered Ca²⁺ dependence of synaptosomal plasma membrane Ca²⁺ -ATPase in human brain affected by Alzheimer’s disease. *FASEB J.* **23**, 1826–1834 (2009).
 87. Lanner, J.T, Georgiou, D.K., Joshi, A.D., Hamilton, S. L. Ryanodine Receptors: Structure, Expression, Molecular Details, and Function in Calcium Release. *Cold Spring Harb Perspect Biol* 2:a003996 (2010).
 88. Miyamoto, S., Izumi, M., Hori, M., Kobayashi, M., Ozaki, H., Karaki, H. Xestospongin C, a selective and membrane-permeable inhibitor of IP₃ receptor, attenuates the positive inotropic effect of α-adrenergic stimulation in guinea-pig papillary muscle. *Br. J. Pharmacol.* **130**, 650–654 (2000).
 89. Oka, T., Sato, K., Hori, M., Ozaki, H. & Karaki, H. Xestospongin C, a novel blocker of IP₃ receptor, attenuates the increase in cytosolic calcium level and degranulation that is induced by antigen in RBL-2H3 mast cells. *Br. J. Pharmacol.* **135**, 1959–1966 (2002).
 90. Wang, Z.J., Zhao, F., Wang, C.F., Zhang, X.M., Xiao, Y., Zhou, F., Wu, M.N., Zhang, J., Qi, J.S., Yang, W. Xestospongin C, a Reversible IP₃ Receptor Antagonist, Alleviates the Cognitive and Pathological Impairments in APP/PS1 Mice of Alzheimer’s Disease. *J. Alzheimer’s Dis.* **72**, 1217–1231 (2019).
 91. De Smet, P., Parys, J. B., Callewaert, G., Weidema, A. F. & Hill, E., De Smedt, H., Erneux, C., Sorrentino, V., Missiaen, L. Xestospongin C is an equally potent inhibitor of the inositol

- 1,4,5-trisphosphate receptor and the endoplasmic-reticulum Ca²⁺ pumps. *Cell Calcium* **26**, 9–13 (1999).
92. Castonguay, A. & Robitaille, R. Xestospongin C is a potent inhibitor of SERCA at a vertebrate synapse. *Cell Calcium* **32**, 39–47 (2002).
93. Francistiová, L., Bianchi, C., Di Lauro, C., Sebastián-Serrano, Á., de Diego-García, L., Kobolák, J., Dinnyés, A., Díaz-Hernández, M. The Role of P2X7 Receptor in Alzheimer's Disease. *Front. Mol. Neurosci.* **13**, 1–14 (2020).
94. Soares-Bezerra, R.J., Ferreira, N.C., Alberto, A.V., Bonavita, A.G., Fidalgo-Neto, A.A., Calheiros, A.S., Frutuoso, Vda. S, Alves, L. A. An improved method for P2X7R antagonist screening. *PLoS One* **10**, 1–15 (2015).
95. Jo, S. & Bean, B. P. Inhibition of neuronal voltage-gated sodium channels by Brilliant blue G. *Mol. Pharmacol.* **80**, 247–257 (2011).
96. Ryu, J. K. & McLarnon, J. G. Block of purinergic P2X7 receptor is neuroprotective in an animal model of Alzheimer's disease. *Neuroreport* **19**, 1715–1719 (2008).
97. Savio, L. E. B., Mello, P. de A., da Silva, C. G. & Coutinho-Silva, R. The P2X7 receptor in inflammatory diseases: Angel or demon? *Front. Pharmacol.* **9**, (2018).
98. Freire, D., Reyes, R.E., Baghram, A., Davies, D.L., Asatryan, L. P2X7 Receptor Antagonist A804598 Inhibits Inflammation in Brain and Liver in C57BL/6J Mice Exposed to Chronic Ethanol and High Fat Diet. *J Neuroimmune Pharmacol* **14**, 263–277 (2019).
99. Mandal, P. K., Shukla, D., Tripathi, M. & Ersland, L. Cognitive Improvement with Glutathione Supplement in Alzheimer's Disease: A Way Forward. *J. Alzheimer's Dis.* **68**, 531–535 (2019).
100. Peña-Bautista, C., Baquero, M., Vento, M. & Cháfer-Pericás, C. Free radicals in Alzheimer's disease: Lipid peroxidation biomarkers. *Clin. Chim. Acta* **491**, 85–90 (2019).
101. Ward, R. J., Zucca, F. A., Duyn, J. H., Crichton, R. R., & Zecca, L. The role of iron in brain ageing and neurodegenerative disorders. *Lancet Neurol.* **13**, 1045–1060 (2014).
102. Waschuk, S. A., Elton, E. A., Darabie, A. A., Fraser, P. E. & McLaurin, J. A. Cellular Membrane Composition Defines Aβ-Lipid Interactions. *J. Biol. Chem.* **276**, 33561–33568 (2001).
103. Bharadwaj, P., Solomon, T., Malajczuk, C.J., Mancera, R. L., Howard, M., Arrigan, D.W.M., Newsholme, P., Martins, R. N. Role of the cell membrane interface in modulating production and uptake of Alzheimer's beta amyloid protein. *Biochim. Biophys. Acta - Biomembr.* **1860**, 1639–1651 (2018).
104. Kandimalla, K. K., Scott, O. G., Fulzele, S., Davidson, M. W. & Poduslo, J. F. Mechanism of Neuronal versus endothelial cell uptake of Alzheimer's disease amyloid β protein. *PLoS*

One **4**, (2009).

105. Wesén, E., Jeffries, G. D. M., Dzebo, M. M. & Esbjörner, E. K. Endocytic uptake of monomeric amyloid- β peptides is clathrin-and dynamin-independent and results in selective accumulation of A β (1-42) compared to A β (1-40). *Sci. Rep.* **7**, 1–14 (2017).
106. Shi, J.M., Zhu, L., Lan, X., Zhao, D.W., He, Y.J., Sun, Z.Q., Wu, D., Li, H. Y. Endocytosis Is a Key Mode of Interaction between Extracellular β -Amyloid and the Cell Membrane. *Biophys. J.* **119**, 1078–1090 (2020).
107. Kuboyama, T., Lee, Y. A., Nishiko, H. & Tohda, C. Inhibition of clathrin-mediated endocytosis prevents amyloid β -induced axonal damage. *Neurobiol. Aging* **36**, 1808–1819 (2015).
108. Thomas, R. S., Lelos, M. J., Good, M. A. & Kidd, E. J. Clathrin-mediated endocytic proteins are upregulated in the cortex of the Tg2576 mouse model of Alzheimer's disease-like amyloid pathology. *Biochem. Biophys. Res. Commun.* **415**, 656–661 (2011).
109. El-Sayed, A. & Harashima, H. Endocytosis of gene delivery vectors: From clathrin-dependent to lipid raft-mediated endocytosis. *Mol. Ther.* **21**, 1118–1130 (2013).
110. Honjo, Y., Horibe, T., Torisawa, A., Ito, H., Nakanishi, A., Mori, Hi., Komiya, T., Takahashi, R., Kawakami, K. Protein disulfide isomerase P5-immunopositive inclusions in patients with Alzheimer's disease. *J. Alzheimer's Dis.* **38**, 601–609 (2014).
111. Nomura, J., Hosoi, T., Kaneko, M., Ozawa, K., Nishi, A., Nomura, Y. Neuroprotection by Endoplasmic Reticulum Stress-Induced HRD1 and Chaperones: Possible Therapeutic Targets for Alzheimer's and Parkinson's Disease. *Med. Sci.* **4**, 14 (2016).
112. Shen, W.-W., Frieden, M., Demaurex, N. Remodelling of the endoplasmic reticulum during store-operated calcium entry. *Biol. Cell* **103**, 365–380 (2011).
113. Li, X., Wu, G., Yang, Y., Fu, S., Liu, X., Kang, H., Yang, X., Su, X.C., Shen, Y. Calmodulin dissociates the STIM1-Orai1 complex and STIM1 oligomers. *Nat Commun.* **8**, 1042 (2017).
114. Bhardwaj, R., Augustynek, B.S., Ercan-Herbst, E., Kandasamy, P., Seedorf, M., Peinelt, C., Hediger, M. A. Ca $^{2+}$ /calmodulin binding to STIM1 hydrophobic residues facilitates slow Ca $^{2+}$ -dependent inactivation of the ORAI1 channel. *Cell. Physiol. Biochem.* **54**, 252–270 (2020).
115. Corbacho, I., Berrocal, M., Török, K., Mata, A.M., Gutierrez-Merino, C. High affinity binding of amyloid β -peptide to calmodulin: Structural and functional implications. *Biochem Biophys Res Commun.* **486**, 992–997 (2017).
116. Huang, A.S., Tong, B.C.K., Wu, A.J., Chen, X., Sreenivasaraghavan, S.G., Zhu, Z., Liu, J. Su, C., Li, M., Cheung, K.-H. Rectifying Attenuated Store-Operated Calcium Entry as a Therapeutic Approach for Alzheimer's Disease. *Curr. Alzheimer Res.* **17**, 1072–1087

(2021).

117. Peterson, C., Gibson, G.E., Blass, J. P. Altered calcium uptake in cultured skin fibroblasts from patients with Alzheimer's disease. *N Engl J Med* **312**, 1063–1065 (1985).
118. Ito, E., Oka, K., Etcheberrigaray, R., Nelson, T.J., McPhie, D.L., Tofel-Grehl, B., Gibson, G.E., Alkon, D. L. Internal Ca²⁺ + mobilization is altered in fibroblasts from patients with Alzheimer's Disease. *Proc Natl Acad Sci USA* **91**, 534–538 (1994).
119. Tong, B.C., Lee, C.S., Cheng, W.H., Lai, K.O., Foskett, J.K., Cheung, K. H. Familial Alzheimer's disease-associated presenilin 1 mutants promote γ-secretase cleavage of STIM1 to impair store-operated Ca²⁺ entry. *Sci. Signal.* **9**, 1–12 (2016).
120. Shtifman, A., Ward, C.W., Laver, D.R., Bannister, M.L., Lopez, J.R., Kitazawa, M., LaFerla, F.M., Ikemoto, N., Querfurth, H. W. Amyloid-β protein impairs Ca²⁺ release and contractility in skeletal muscle. *Neurobiol. Aging* **31**, 2080–2090 (2010).
121. Paula-Lima, A. & Hidalgo, C. Amyloid β-peptide oligomers, ryanodine receptor-mediated Ca²⁺ release and Wnt-5a/Ca²⁺ signaling: Opposing roles in neuronal mitochondrial dynamics? *Front. Cell. Neurosci.* **7**, 2011–2013 (2013).
122. Ferreiro, E., Resende, R., Costa, R., Oliveira, C. R. & Pereira, C. M. F. An endoplasmic reticulum-specific apoptotic pathway is involved in prion and amyloid-beta peptides neurotoxicity. *Neurobiol. Dis.* **23**, 669–678 (2006).
123. Rival, T., Page, R.M., Chandraratna, D.S., Sendall, T.J., Ryder, E., Liu, B., Lewis, H., Rosahl, T., Hider, R. Camargo, L. M., Shearman, M.S., Crowther, D.C., Lomas, D. A. Fenton chemistry and oxidative stress mediate the toxicity of the -amyloid peptide in a Drosophila model of Alzheimer's disease. *Eur. J. Neurosci.* **29**, 1335–1347 (2009).
124. Syme, C. D., Nadal, R. C., Rigby, S. E. J. & Viles, J. H. Copper binding to the amyloid-β (aβ) peptide associated with Alzheimer's disease: Folding, coordination geometry, pH dependence, stoichiometry, and affinity of Aβ-(1-28): Insights from a range of complementary spectroscopic techniques. *J. Biol. Chem.* **279**, 18169–18177 (2004).

CHAPTER 4

Kaempferol protects against inflammation and
A β peptides overproduction induced by the
neurotoxin NPA in the brain of Wistar rats

Index

1. Abstract	167
2. Introduction	168
3. Materials and Methods	170
3.1 Chemicals	170
3.2 Animals and treatments	171
3.2.1 Subacute NPA treatment	171
3.2.2 Acute NPA treatment and protection	172
3.3 Preparation of rat brain slices and TTC Staining	172
3.4 Immunostaining with anti-neurogranin	172
3.5 Terminal deoxynucleotidyl transferase-mediated deoxyuridine triphosphate nick-end labelling (TUNEL).	173
3.6 Brain samples homogenization and Western blotting	173
3.7 Statistical analysis	174
4. Results	174
4.1 The increase of activated complement C3 protein, a reactive A1 Astrocyte marker, precedes significant NPA-induced brain degeneration	174
4.2 The increase of pro-inflammatory cytokines IL-1 α and TNF α also precedes significant NPA-induced brain degeneration	178
4.3. Kaempferol prevents the increase of complement C3 protein expression and activation, a reactive A1 astrocyte marker in NPA-induced brain damage	180
4.4. Kaempferol prevents the increase of pro-inflammatory cytokines (IL-1 α and TNF α) and complement C1q in the <i>striatum</i> and <i>hippocampus</i> of NPA-treated rats	182
4.5. Kaempferol prevents the NPA-induced increase of NF- κ B expression in the <i>striatum</i> and <i>hippocampus</i>	184
4.6. Kaempferol protects against the increase of A β peptides production in the <i>hippocampus</i> and <i>striatum</i> of NPA-treated rats.....	186
5. Discussion.....	187
6. Supplementary Figure	192
7. References	193

1. Abstract

NPA is a potent neurotoxin that when administrated to rodents, mimics HD motor neurological dysfunctions. Several studies have demonstrated that NPA treatment induce brain degeneration mediated by inflammatory events. Activated microglia induce a specific type of reactive neurotoxic astrocytes, named A1, which have been detected in *post-mortem* brain samples of HD, AD, and PD. Kaempferol is a natural antioxidant found in vegetables and fruits and has been showed to have neuroprotective properties against several diseases. In the first part of this work we used an experimental model based on NPA i.p. injection in adult Wistar rats at doses that can elicit progressive brain degeneration (daily dose of 25 mg/Kg b. w.), to identify early biomarkers of NPA-induced neurodegeneration. Brain samples were collected before and after extensive brain damage and monitored using 2,3,5-triphenyltetrazolium chloride (TTC) staining, immunostaining with anti-neurogranin and the presence of apoptotic cells was evaluated by TUNEL assay. Results indicated that after 24 days of subacute NPA treatment (G24 group) there is an extensive neurodegeneration degree, compared with the lack of significant neurodegeneration in the rat group treated only for 17 days (G17). Western blots of the G17 group showed that i.p. NPA injections elicit significant increased expression levels of C3 α fragment, a marker of generation of neurotoxic A1 astrocytes. In addition, the pro-inflammatory cytokines IL-1 α and TNF α are also significantly highly expressed within the *striatum*, *hippocampus* and *cerebellum*, before the appearance of the HD-related neurological dysfunctions and neuronal death induced by NPA. By applying an acute NPA treatment to Wistar rats (2 doses/day of 25 mg/Kg b. w.) we evaluated the protective effect of kaempferol (21 mg/Kg b. w.) against severe neurodegeneration in our animal model. Our results showed that kaempferol administration prevents against proteolytic activation of complement C3 protein and generation of reactive A1 astrocytes NPA-induced in the *striatum* and *hippocampus*. Also, it blocked the NPA-induced increase of NF- κ B expression and enhanced secretion of C1q and cytokines (IL-1 α and TNF α), which have been linked to the generation of reactive A1 astrocytes. In addition, kaempferol administration prevented enhanced production of A β peptides in *striatum* and *hippocampus*, a novel finding in NPA-induced brain degeneration found in this work. We concluded that the activation of complement C3 protein in the brain of Wistar rats is an early event in NPA-induced brain neurodegeneration and that kaempferol provides a strong neurological protection against acute NPA treatment.

2. Introduction

NPA is a highly toxic compound that derived from natural sources like leguminous plants and fungi^{1–4}. It has been reported that the systemic administration of NPA to rodents and non-human primates induce neurological impairment that mimic the motor neurological dysfunctions of HD. More exactly, systemic NPA administration induce degeneration in the dorso-lateral region of the striatum^{5–10}, showing similar severe damage observed in the caudate and dorso-lateral putamen of human brains affected by HD¹¹. Furthermore, it has been reported preferential degeneration of the medium-sized GABAergic spiny striatal neurons after NPA systemic administration, an these alterations are also observed in HD *striatum*^{5,7}. The main early symptoms of HD include executive dysfunction, perceptual deficits, memory loss, visuospatial deficits and also difficulty in learning new skills^{12,13}. Systemic NPA administration to rodents is also associated with memory impairment^{14,15} and significant metabolic alterations in the *striatum*, vicinal cortical areas as well in *hippocampus*¹⁵. Additionally, NPA administration to rats also elicits significant changes in the *cerebellum*, which are associated with metabolism and neurotransmitters alterations^{16,17}. In fact, recently, it has been reported damage in cerebellar cortex with extensive Purkinje cells loss in *post-mortem* samples of HD patients¹⁸.

Generation of ROS and mitochondrial dysfunction that activate cell death pathways, play a major role in NPA neurotoxicity^{19–21} as well as in HD²². NPA is a suicide inhibitor of succinate dehydrogenase causing rapid loss of ATP in neurons *in vitro*^{19,23} and consequently leads to a sustained rise in cytosolic Ca²⁺ due to the large consumption of ATP to restore plasma membrane potential after repetitive synaptic activity in brain neurons. This fact potentiates secretion of excitatory neurotransmitters and, eventually, neuronal death through calpains activation. Besides, NPA promotes excitotoxic neuronal death, mediated by the excitatory neurotransmitters L-glutamate and dopamine^{17,24,25}, and by calpains activation^{19,26,27} in both cellular and animal models. Additionally, it has been shown that NPA produces indirect excitotoxic damage to the *striatum*²⁸, making it unlikely that NPA-induced selective damage of neurons in specific regions of the brain can be solely related with the metabolic rate and density of receptors for L-glutamate and dopamine.

In the brain, activated microglia is the main source of ROS and nitric oxide (NO), which consequently can lead to mitochondrial respiratory chain function impairment²⁹. In a previous publication, we showed a large increase of protein nitrotyrosines in parallel with a large decrease of reduced glutathione in the *striatum* of adult Wistar rats' brain after NPA systemic administration¹⁰. These results are in good agreement with activation of neuroinflammatory microglia by NPA administration reported by others studies^{30–32} and strongly suggests that

inflammation mediates NPA-induced brain degeneration. Remarkably, non-invasive imaging of the brain of HD patients, revealed significant microglial activation in the *striatum* and cortical areas³³. In fact, it has been suggested that pro-inflammatory cytokines stimulate the development of neurodegenerative diseases like HD, AD, and PD, where it is reported a progressive and slow damage of different cerebral cortical areas such as *striatum*, *substantia nigra* and *hippocampus*³⁴. Pro-inflammatory cytokines may exacerbate oxidative stress-induced cell death through the increase of ROS and NO generation and stimulation of L-glutamate release to the extracellular space³⁵. Moreover, during brain degeneration, the release of endogenous cell molecules (Damage Associated Molecular Patterns or DAMPs) can potentiate further microglial activation, creating a positive feedback loop in brain areas undergoing a more extensive degeneration, like the *striatum* and vicinal somatomotor cortex³⁶.

However, it remains unclear what are the molecular mechanisms through which brain inflammation can selectively produce cell death in specific neuronal structures. It has been observed the loss of astrocytes and also astrogliosis, in the brain *striatum* in rats treated with NPA^{28,31,32,37}. More recently, it was demonstrated that the activation of neuroinflammatory microglia induce the production of a specific type of reactive neurotoxic astrocytes, namely A1, via the secretion of complement component 1q (C1q) and secretion of specific pro-inflammatory cytokines like interleukin-1 alpha (IL-1 α) and tumor necrosis factor alpha (TNF α). Also, it has been found an increase in reactive A1 astrocytes generation in *post-mortem* tissue of HD patients³⁸. Furthermore, it has been reported that complement component 3 (C3) gene is highly upregulated in A1 astrocytes, but not in ischemic reactive astrocytes (A2)³⁸, suggesting that the increased expression of C3 could be used as a reactive A1 astrocyte marker in neurodegenerative disorders.

Recently, it has been shown that rat astrocytes are more sensitive than microglia to 2-chloroethanol, an intermediate metabolite in subacute poisoning with 1,2-dichloroethane, and that reactive astrocytes induced by 2-chloroethanol poisoning can stimulate microglia polarization³⁹. Therefore, reactive astrocytes induced by some chemical insults can also lead to microglia activation. In addition, reactive astrocytes can produce neurotoxic A β peptides⁴⁰⁻⁴², and this possibility deserved to be studied in NPA-induced brain neurodegeneration because, it has been recently shown that this neurodegenerative process is also linked to tangle-pathologies linked to dementia⁴³.

Many natural compounds, like flavonoids are well-known inhibitors of pro-inflammatory cytokines, iNOS, as well as COX-2 gene expression in the brain through inhibition of NF- κ B activation⁴⁴. Therefore, it could be expected that flavonoids provide protection against brain neurodegeneration induced by systemic NPA-administration. Kaempferol is a natural compound

with antioxidant properties that belongs to the flavonols group of flavonoids and is found in vegetables and fruits. In a previous work of the lab, we reported that kaempferol protected against brain neurodegeneration of the *striatum* and motor neurological dysfunctions induced by NPA by means of preventing the decrease of reduced glutathione, the increase of protein nitrotyrosines and the inhibition of creatine kinase activity¹⁰. In addition, we also showed that intravenous administration of kaempferol attenuates brain damage induced by ischemia-reperfusion in a rat model of transient focal ischemia caused by occlusion of the middle cerebral artery⁴⁵. Our findings alongside with other publications regarding the protective effect of kaempferol in several diseases⁴⁶ and the low toxicity of kaempferol in humans, suggest that this natural compound can be potentially used as protective therapeutic agent against brain damage induced by insults and/or neurodegenerative diseases. In agreement, *Ginkgo biloba* extract EGb761, whose major component is kaempferol, showed neuroprotective properties in brain ischemia models⁴⁷. Also, the administration of the flavonol quercetin, has demonstrated to have beneficial effects to improve behavioral deficiencies and restore astrocytes and microglia in the NPA-induced rat model of HD³¹.

On these grounds, the main goals of this work were: 1) to setup an experimental protocol of daily i.p. injections of the neurotoxin NPA in adult Wistar rats that elicits a slow progressive brain neurodegeneration which allows to identify early biomarkers; 2) to test the hypothesis that kaempferol protects against NPA degeneration in brain regions with severe dysfunction induced by an acute NPA treatment. Our results demonstrate that NPA treatment induces the generation of reactive A1 astrocytes and increases the expression of activated C3 fragment alongside with an increase in pro-inflammatory cytokines generation and C1q, which is efficiently prevented by administration of kaempferol in rats with acute NPA treatment. In addition, kaempferol also protected against the A β peptides overproduction found in NPA-induced brain degeneration. All together these findings suggest that kaempferol could be used as therapeutic agent against the progression of neurodegenerative diseases linked to the generation of neurotoxic reactive A1 astrocytes, neuroinflammation and A β production in the brain.

3. Methods and Methods

3.1 Chemicals

NPA (>97% by HPLC) and kaempferol (>96% by HPLC) were purchased by Sigma (St. Louis, MO, USA). Glycerol and paraformaldehyde were purchased from Panreac (Barcelona,

Spain). Ketamine was from Pfizer, Madrid, Spain, while diazepam and atropine were obtained from B. Braun (Rubí-Barcelona Spain).

Primary antibodies: rabbit monoclonal anti-C3 (ab200999, dilution 1:2000) and rabbit polyclonal anti-TNF α (ab6671, dilution 1:1000) were purchased from Abcam (Cambridge, UK). Mouse monoclonal anti-IL-1 α (sc-9983, dilution 1:500) was from Santa Cruz Biotechnology (Santa Cruz, CA, USA). Anti-NF- κ B-p65 polyclonal antibody (10745-1-AP produced in rabbit, dilution 1:1000) was from Proteintech (Manchester, UK). Anti-A β antibody (A8354, mouse monoclonal, at 2 μ g/mL), secondary anti-rabbit IgG-Horseradish peroxidase (A0545), anti-mouse IgG-Horseradish peroxidase (A0944) mouse anti- β -actin (A1978, dilution 1:5000) or rabbit polyclonal anti- β -actin (A5060, dilution 1:750) were purchased from Sigma-Aldrich (Madrid, Spain).

All other products were purchased from Sigma-Aldrich or Merck (Darmstadt, Germany), unless specified otherwise.

3.2 Animals and treatments

As animal model we used male Wistar rats with 9–10 weeks old and weighing 290–340 g. They were kept in a 12 h light/dark cycle and allowed free access to food and water. The experimental procedures followed the animal care guidelines of the European Union Council Directive 86/609/EEC and the protocols were approved by the Ethics Committee for Animal Research of the local government.

3.2.1 Subacute NPA treatment

NPA was administered by i.p. injection of a 25 mg/mL solution in normal saline (0.9% w/v NaCl) and the pH was adjusted to 7.4 with NaOH (5 M), and filtered through a 0.2 μ m filter. Rats' treatments were as follow: 25 mg of NPA/kg b. w. was administered every 24 h for 6, 17, and 24 days, and are referred in the text as rats from G6 ($n = 7$), G17 ($n = 7$), and G24 ($n = 7$) groups. Of note, the total number of rats used for the G24 group was 10, because three rats died after developing severe pathological symptoms, an interindividual variability that we observed when adult Wistar rats were treated with doses of 25 mg NPA/kg b. w. every 12 h¹⁰. Rats from control groups ($n = 6$) received 0.4 mL saline solution (NPA vehicle), with the same treatment schedule given in the experimental groups. The animals were evaluated for motor impairment during all the time course of the experiment. They were observed daily, just before the injection,

and rated with a quantitative scale according to their motor deficiencies^{10,48}. This rating scale measures gait abnormalities, hind limbs dystonia, grasping ability, balance, and recumbency.

3.2.2 Acute NPA treatment and protection by kaempferol

Wistar rats were divided into three experimental groups: KNPA (kaempferol plus NPA), NPA and Control. The KNPA group ($n = 6$) received a first injection of kaempferol solution, at a dose of 21 mg/kg b. w., 48 h before initiation of NPA-treatment. From day 0 to 5 of treatment, a dose of 25 mg of NPA/kg b. w. was administered every 12 h. Daily, 30 min before the morning NPA injection, another dose of kaempferol was injected to the rats. Rats from NPA-group ($n = 6$) were treated with 25 mg NPA/kg b. w. every 12 h during 5 days and, instead of kaempferol, received 1-mL injections with 2.4 % v/v DMSO in saline 48 h before NPA-treatment and every day 30 min prior to the morning NPA injection. Control-group ($n = 6$) received 1 mL 2.4% v/v DMSO in saline (kaempferol vehicle) and 0.4 mL saline solution (NPA vehicle), with the same time schedule of treatment groups. Rats in the NPA-group with severe pathological symptoms (motor deficit ≥ 6 or weight loss $\geq 15\%$) were sacrificed at the end of day 4. The rats from the KNPA-group, as well as control-group, were treated until day 5 and sacrificed at this time. At the end of treatments, the animals were anesthetized with ketamine (50 µg/g), diazepam (2.5 µg/g) and atropine (0.05 µg/g). The brains were immediately removed from the skull and washed in cold phosphate-buffered saline (PBS) pH 7.4, and then cut with a tissue slicer. All the immunohistochemistry and Western blots shown in this work have been performed with brain slices vicinal to those used for TTC staining and without signs of micro vessel's hemorrhage.

3.3 Preparation of rat brain slices and TTC Staining

We followed the protocol described early in previous works of our lab^{10,49}. Briefly, sections (1.5 mm thick coronal slice) corresponding to the three regions analyzed (*striatum*, *hippocampus* and *cerebellum*) were immersed in a 2% solution of TTC in PBS for 15 min at 37°C, and observed under a Leica MZ APO stereomicroscope.

3.4 Immunostaining with anti-neurogranin

For this propose we used brain sections of *striatum* of G17 and G24 group. Briefly brain sections were immersed in 4% paraformaldehyde in PBS, dehydrated in a graded series of ethyl alcohol, cleared in xylene, and embedded in paraffin wax, using standard techniques.

Afterwards, tissue blocks were cut in coronal sections (7 µm thick) with a microtome Leica RM2125RT. Slices were hydrated and subjected to immunohistochemistry as followed. Briefly, brain tissue sections were blocked with 1% bovine serum albumin (BSA) in PBS for 0.5 h and then incubated with 5% normal goat serum in 1% BSA and 0.1% 4-(1,1,3,3-tetramethyl butyl)phenyl-poly-ethylene glycol (Triton X-100) for 2 h. Thereafter, slides were blocked with endogenous avidin/biotin blocking kit (Abcam ab 64212) and incubated overnight at 4°C in humidified box, with the primary antibody rabbit anti-neurogranin (Chemicon AB5620) at a dilution of 1:500. After extensive washing in PBS, endogenous peroxidase activity was quenched with 0.5% H₂O₂, again blocked, and incubated with the secondary antibody, a biotinylated goat anti-rabbit immunoglobulin G supplied by Vectastain ABC Kit, Vector Laboratories (PK-6101), for 3 h at room temperature. After rinsing in PBS, the sections were incubated with avidin-biotinylated horseradish peroxidase complex (Vectastain ABC Kit) for 30 min at room temperature. Chromogen development was performed with peroxidase substrate solution (Vector VIP substrate, SK-4600). Slides were washed in distilled water, dehydrated, and mounted in Eukit.

3.5 Terminal deoxynucleotidyl transferase-mediated deoxyuridine triphosphate nick-end labelling (TUNEL)

Tissue sections were treated as previously described⁵⁰ with an in-situ cell death detection kit, POD (Roche). Apoptotic cells were observed under microscopy using a Vector VIP substrate kit (peroxidase detection; Vector Laboratories).

3.6 Brain samples homogenization and Western blotting

Selected dissected brain sections of *striatum*, *hippocampus* and *cerebellum* were weighed, frozen in liquid nitrogen and kept at -80 °C until use. Brain sections were homogenized within an ice-cold recipient with a glass homogenizer followed by sonication (30–40 pulses of 1 s) in lysis buffer 25 mM tris-(hydroxymethyl) aminomethane hydrochloride (Tris-HCl) at pH 7.4 [150 mM NaCl, 5 mM ethylenediaminetetraacetic acid (EDTA), 50 mM NaF, 5 mM NaVO₃, and 0.25% Triton X-100, supplemented with the protease inhibitor cocktail SIGMAFAST™]. Homogenates were centrifuged at 500 g for 10 min at 4 °C to pellet tissue debris and the supernatant was carefully removed and supplemented with 40% glycerol. Protein concentration was determined using Bradford's method using BSA as standard and samples were conserved at -80 °C until use.

Western blotting was carried out as described in the Chapter 2 of this thesis and in another recent works of the lab^{49,51}. The primary antibodies used were rabbit monoclonal anti-C3, mouse monoclonal anti-IL-1 α , rabbit polyclonal anti-TNF α , anti-NF- κ B-p65 polyclonal antibody and anti-A β antibody. The secondary anti-rabbit or anti-mouse IgG-Horseradish peroxidase and anti- β -actin used in this work are described in the Chemicals section.

3.7 Statistical analysis

Results of Western blots are expressed as mean \pm standard error (s.e.). Statistical analysis was carried out by Mann–Whitney non-parametric test. Significant difference was accepted at the $p < 0.05$ level and all the results were confirmed with triplicate experiments.

4. Results

4.1 The increase of activated complement C3 protein, a reactive A1 Astrocyte marker, precedes significant NPA-induced brain degeneration

In the first part of the work, we planned an experimental NPA-treatment aiming to induce progressive brain degeneration, before facing strong neurological defects and neuronal death, to identify early biomarkers. On these grounds, we administered to adult Wistar rats, by i.p. injection, 25 mg of NPA/kg b. w. every 24 h for 6, 17, and 24 days, referred in the text as rats from G6, G17 and G24 groups as mentioned in Materials and Methods section and then evaluated the progression of the neurodegeneration.

Rats in the G24 group showed neurological defects based on increased dystonic movements of hind limbs and an abnormal gait, characterized by a wobbly gait and padding, which are characteristics of a HD experimental model, as we previously described in a previous work¹⁰. Additionally, staining of rat brain slices with TTC clearly showed damage of the *striatum*, as can be seen in **Figure 1**. Moreover, it can be observed neuronal loss, through neurogranin immunostaining and the apoptotic cells observed with TUNEL assay reveals neuronal damage associated with the pathological events early described (**Figure 1**).

It is important to highlight that Wistar rats treated with a daily dose of NPA for 17 days (G17) did not show significant sensorial or motor neurological dysfunctions; nevertheless, after 17 doses some rats developed a hypoactive behavior but kept a normal posture and gait. In fact, G17 rat brain sections staining with TTC showed no differences comparing with untreated control rats (**Figure 2**). The absence of TTC stained areas in the *striatum*, *hippocampus*

and cerebellum of rats treated i.p. with one daily dose of 25 mg NPA/kg b. w., for 17 days, suggest that this treatment did not produce observable degeneration of these brain areas, which is supported by the neuronal soma labeling with neurogranin and the absence of apoptotic cells evaluated by the TUNEL assay in the *striatum* as can be seen in **Figure 1**. Based on these results, we selected the G17 group for experimental evaluation of brain biomarkers at early stages of the neurotoxic process induced by NPA treatment.

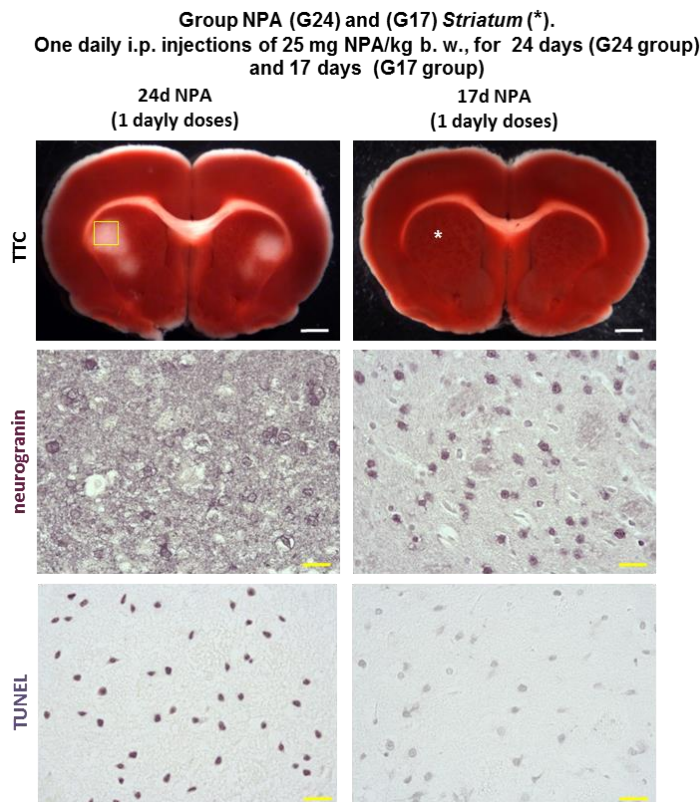


Figure 1. Rats of the G24 group show degeneration of the brain *striatum* (*) with respect to rats of the G17 group. Representative coronal sections stained with TTC, neurogranin and TUNEL assay. Treatment with one daily i.p. injection of 25 mg NPA/kg b. w. for 24 days (G24 group) shows an initial unstained area of the *striatum* after TTC staining with respect to rats of the G17 group. Yellow square mark indicates the selected TTC unstained area for neurogranin and TUNEL staining. Neurogranin immunolabeling reveals a loss of neuronal somas in the *striatum* of rats of the G24 group with respect to rats of the G17 group. TUNEL staining shows neuronal cell death in the *striatum* (*) of rats of the G24 group. White scale bars: 2 mm, yellow scale bars: 25 µm.

Coronal slices illustrating (*) the striatum, hippocampus and cerebellum stained with TTC.

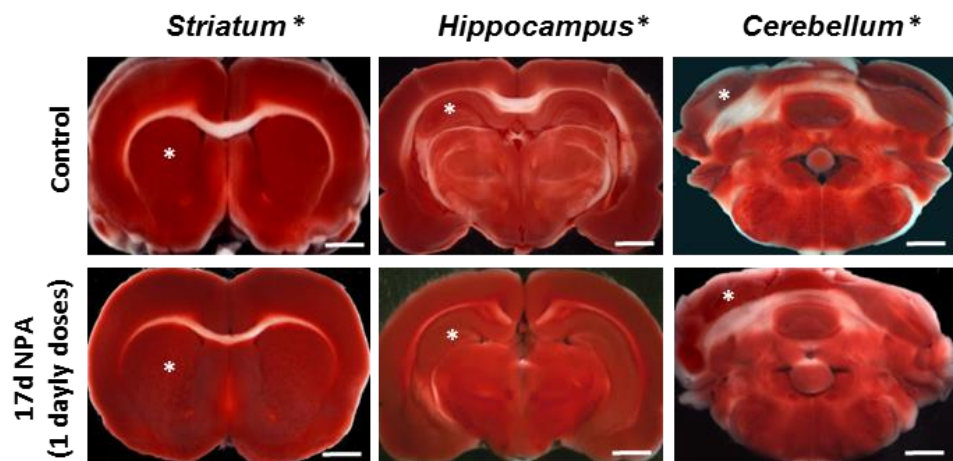
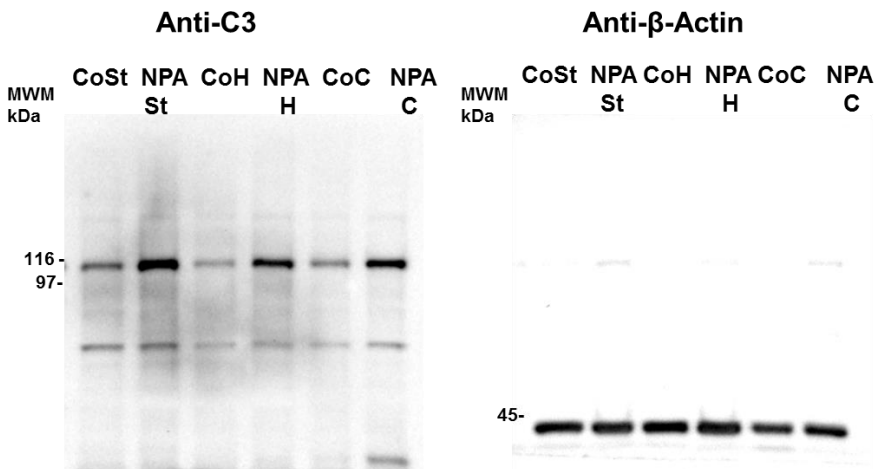


Figure 2. Representative fresh brain 1.5 mm thick coronal slices illustrating the striatum, hippocampus and cerebellum (respectively marked with white asterisk) stained with TTC. Treatment with one daily i.p. injection of 25 mg NPA/kg b. w., for 17 days (G17 group) show no differences with TTC staining comparing with untreated control rats. Scale bars: 2 mm.

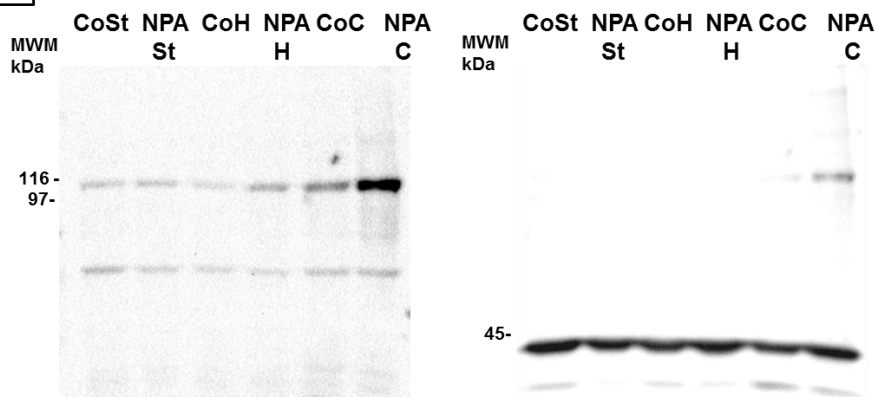
The representative Western blot in **Figure 3A** shows that the levels of the proteolytic fragment C3 α are increased in *striatum*, *hippocampus* and *cerebellum* in the NPA-treatment G17 group more than 2-fold regarding to control untreated rats, namely 2.33 ± 0.17 , 3.7 ± 0.25 and 2.2 ± 0.15 -fold, respectively (**Figure 3C**). Particularly, it has been shown that reactive A1 astrocytes are also produced upon neuronal axotomy³⁸, which can account for the low levels of C3 α observed in these brain regions in control untreated rats. This result indicates that the generation of A1 astrocytes induced by NPA treatment for 17 days (G17) can be observed before significant brain damage (detected through TTC, neurogranin and TUNEL staining) and precedes NPA-induced neurological dysfunctions. In addition, **Figure 3B** and **C** highlight that Wistar rats treated with a daily dose of 25 mg NPA/kg b. w. for only 6 days (G6) show statistically significant increase in C3 α levels in *hippocampus* and *cerebellum* (but not *striatum*), compared with the untreated control group, with an increase of 2.5 ± 0.2 and 2.4 ± 0.2 -fold, respectively. This result pointed out an early generation of reactive A1 astrocytes in *hippocampus* and *cerebellum* regions.

In addition, immunohistochemistry performed in rat brain sections, demonstrated an increase in reactive A1 astrocytes, expressing C3 α and increased expression of the astrocytic marker glial fibrillary acidic protein (GFAP) in specific regions of *striatum*, *hippocampus* and *cerebellum*, in NPA treated rats in the experimental G17 group (data not shown here, but included in the attached published article⁴⁹).

A Western blot anti-C3 of rats control and G17 group



B Western blot anti-C3 of rats control and G6 group



C

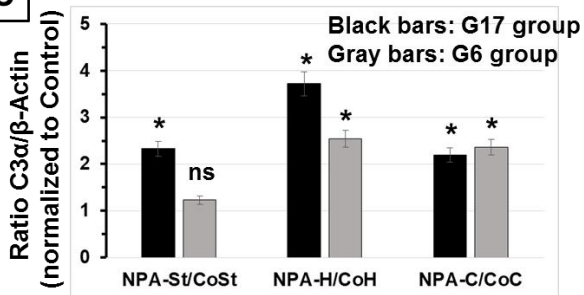


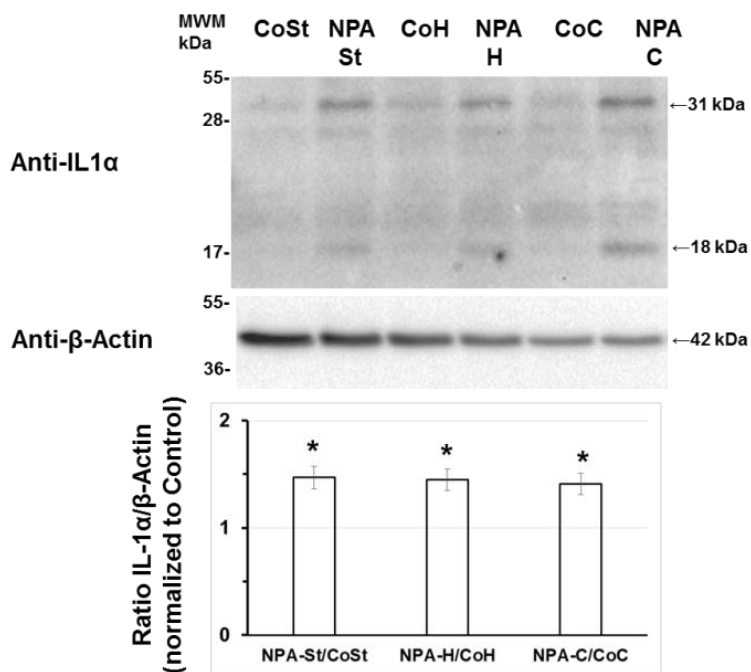
Figure 3. Western blots of C3 α fragment in G17 and G6 rat groups. Wistar Rats treated i.p. with one daily dose of 25 mg NPA/kg b. w., for 17 days (G17 group) show a large increase of the C3 α proteolytic fragment in the *striatum*, *hippocampus* and *cerebellum* with respect to rats of the untreated control group, while the C3 α proteolytic fragment only significantly increases in the *hippocampus* and *cerebellum* in the rats of the G6 group (daily i.p. dose of 25 mg NPA/kg b. w. for 6 days). Representative Western blots of C3 and β-actin of *striatum* (St), *hippocampus* (H), and *cerebellum* (C) homogenates of rats of control (Co) and G17 group (NPA rats) (**A**) and of control (Co) and G6 group (NPA rats) (**B**). After acquisition of images of the Western blot with anti-C3, the PVDF membrane was stripped and processed for the Western blot of anti-β-actin, as indicated in Materials and Methods section. The molecular weights of the protein markers (MWM) closer to the target proteins (C3 α proteolytic fragment and β-actin) are indicated on the left-hand side. (**C**) Plot of the ratio of (C3 α /β-actin) in *striatum*, *hippocampus* and *cerebellum* homogenates of rats of G17 (black bars) and G6 (gray bars) groups relative to control rats. The results shown are the average ± s.e. of triplicate experiments. (*) $p < 0.05$ with respect to control rats; ns, statistically non-significant difference with respect to control rats.

4.2 The increase of pro-inflammatory cytokines IL-1 α and TNF α also precedes significant NPA-induced brain degeneration

Recently, it has been reported that cytokines IL-1 α and TNF α are specifically expressed in activated microglia induced by different brain injuries inducing reactive A1 astrocyte^{38,52,53}. Therefore, we measured the expression levels of these pro-inflammatory cytokines in the *striatum*, *hippocampus* and *cerebellum* of rats treated i.p. with one daily dose of 25 mg NPA/kg b.w. for 17 days (G17), using Western blotting technique. As can be seen in **Figure 4A** and **B**, both IL-1 α and TNF α expression levels are increased in all brain areas, compared with untreated control group (Co). The quantitative analysis showed a similar increase of \approx 50% of IL-1 α levels in all brain areas whereas the increase of TNF α was higher in the *striatum* (160%) than in the *hippocampus* (80%) and *cerebellum* (70%).

In addition to Western blots, the immunohistochemical analysis in rat brains of the regions of interest (*striatum*, *hippocampus* and *cerebellum*) showed an increase in IL-1 α and TNF α expression in NPA treatment group (G17), comparing with untreated control group as can be seen in our published work (data not shown, but included in the attached published article⁴⁹). Moreover, other studies reported that activated microglia in HD, is associated with an increase in C1q biosynthesis, which correlates with the increase in the activation of C3^{38,54,55}. We demonstrated a similar increase in C1q distribution in the three regions under analysis (data not shown, but included in the attached published article⁴⁹). In general, the pattern of increased expression of cytokines (IL-1 α , TNF α) and C1q in *striatum*, *hippocampus* and *cerebellum* correlated with the regionalization of C3 positive reactive A1 astrocytes⁴⁹.

A Western blot anti-IL1 α of rats control and G17 group



B Western blot anti-TNF α of rats control and G17 group

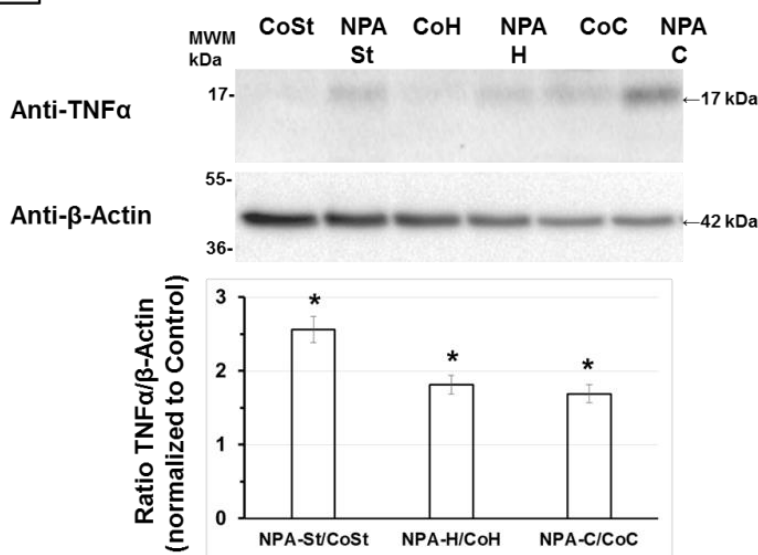


Figure 4. Rats of the G17 group show a significant increase of IL-1 α and TNF α in the striatum, hippocampus and cerebellum with respect to rats of the control group. Representative Western blots of IL-1 α and β -actin (A) and of TNF α and β -actin (B) of striatum (St), hippocampus (H), and cerebellum (C) homogenates of rats of control (Co) and G17 group (NPA treated rats). After acquisition of images of the Western blot with anti-IL-1 α and anti-TNF α , PVDF membranes were stripped and processed for the Western blot of anti- β -actin, as indicated in Materials and Methods section of this chapter. The estimated molecular weights of the target proteins IL-1 α , TNF α , and β -actin are indicated on the right-hand side, and on the left-hand side the molecular weights of the protein markers (MWM) closer to the target protein are included. Plots of the ratios of (IL-1 α / β -actin) and (TNF α / β -actin) in striatum, hippocampus, and cerebellum homogenates of rats of G17 group relative to untreated control rats are also inserted, respectively. The results shown are the average \pm s.e. of triplicate experiments. (*) $p < 0.05$ with respect to control rats.

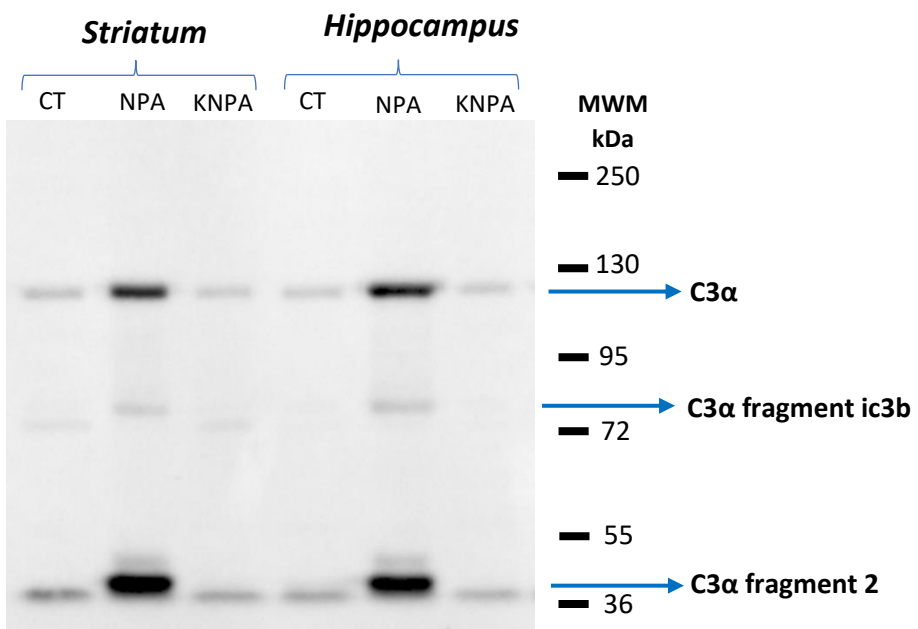
4.3 Kaempferol prevents the increase of complement C3 protein expression and activation, a reactive A1 astrocyte marker in NPA-induced brain damage

In order to evaluate the protective effect of the natural compound kaempferol against an advanced stage of brain neurodegeneration induced by NPA treatment, we followed the protocol early described¹⁰ to promote acute brain neurodegeneration in Wistar rats. Of note, systemic administration of NPA at a dose of 25 mg/kg b. w. every 12 h caused marked behavioral alterations in the rats, as reported in a previous work¹⁰. After the first and second NPA injections, the animals showed reduced reactive activity during handlings with respect to control animals, although maintained a normal posture and gait. Through days 2 and 3, the animals showed dystonic movements of hind limbs and wobbling gait and paddling. On the 4th day, the animals lost grasping ability and balance capacity. By day 4-5, the rats became recumbent, with a progressive limbs paralysis and moribund appearance.

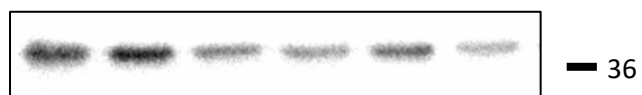
The protection afforded by kaempferol was investigated in two main regions of the brain: *striatum* and *hippocampus*. Brain samples were taken from brain slices adjacent to those that display brain damage in TTC-stained slices as can be seen in **Supplementary Figure S.1**, and homogenized as indicated in the Materials and Methods section.

The representative Western blot showed in **Figure 5** clearly demonstrated increased levels of C3 α in *striatum* and *hippocampus* in rats of the NPA group with respect to control group (CT), namely 4.4 ± 0.4 and 5.9 ± 0.5 -fold, respectively. This result is in good agreement with the results obtained early in this chapter where rats submitted with only one daily dose of NPA treatment for 17 days also showed increased expression in C3 α (**Figure 3**). Additionally, the Western blot also revealed an enhanced proteolytic processing of C3 α in the NPA-group with lower molecular weight fragments, i.e. C3 protein activation. The increase is much higher if is calculated from the sum of the C3 α and all C3 α fragments detected by the anti-C3 antibody used in this work. **Figure 5** also shows that the increase of C3 α was statistically non-significant ($p > 0.05$) in the *striatum* and *hippocampus* of rats treated with kaempferol and NPA (KNPA-group). Therefore, all these results pointed out an increased generation of reactive A1 astrocytes in the brain areas that have been shown in many studies to be more prone to NPA-induced degeneration (*striatum* and *hippocampus*) and highlight the protection of kaempferol against the generation of C3 α in acute NPA-induced treatment. Noteworthy, no significant increase of C3 α and all C3 α fragments were observed in brain stem of rats of the NPA-group comparing with rats of the control-group (data not shown).

(A) Anti-C3 α



(B) Anti- β -actin



(C) Plot ratio: C3 α / β -actin

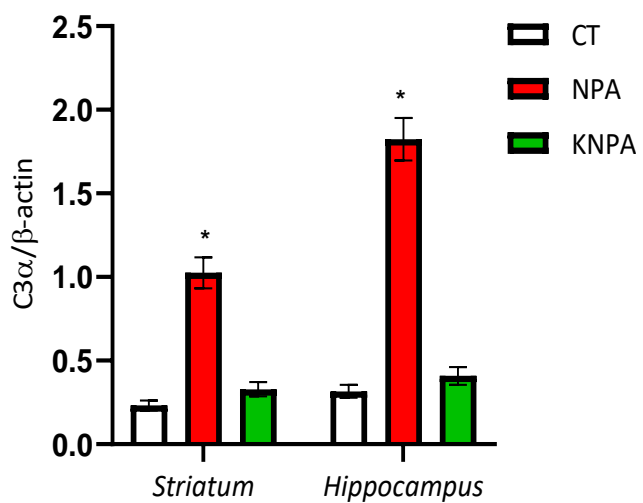


Figure 5 Kaempferol i.p. administration protects against the increase of C3 α and C3 α proteolytic fragments induced by i.p. administration of NPA in the *striatum* and *hippocampus* with respect to rats of the control-group. (A) Representative Western blot of C3 protein and β -actin of *striatum* and *hippocampus* homogenates of rats of control-group (CT), NPA-group (NPA) and kaempferol plus NPA, KNPA-group (KNPA). (B) After acquisition of images of the Western blot with anti-C3 antibody, the PVDF membrane was stripped as described in Materials and Methods section and processed for the Western blot of anti- β -actin. The molecular weights of the protein markers (MWM) are indicated on the right-hand

side. (**C**) Plot of the ratio of (C3 α /β-actin) in *striatum* and *hippocampus* homogenates of rats of CT-, NPA- and KNPA-groups. The results shown are the average ± s.e. of Western blots of n = 6 homogenate samples of each group of rats. (*) p<0.05 with respect to Control rats.

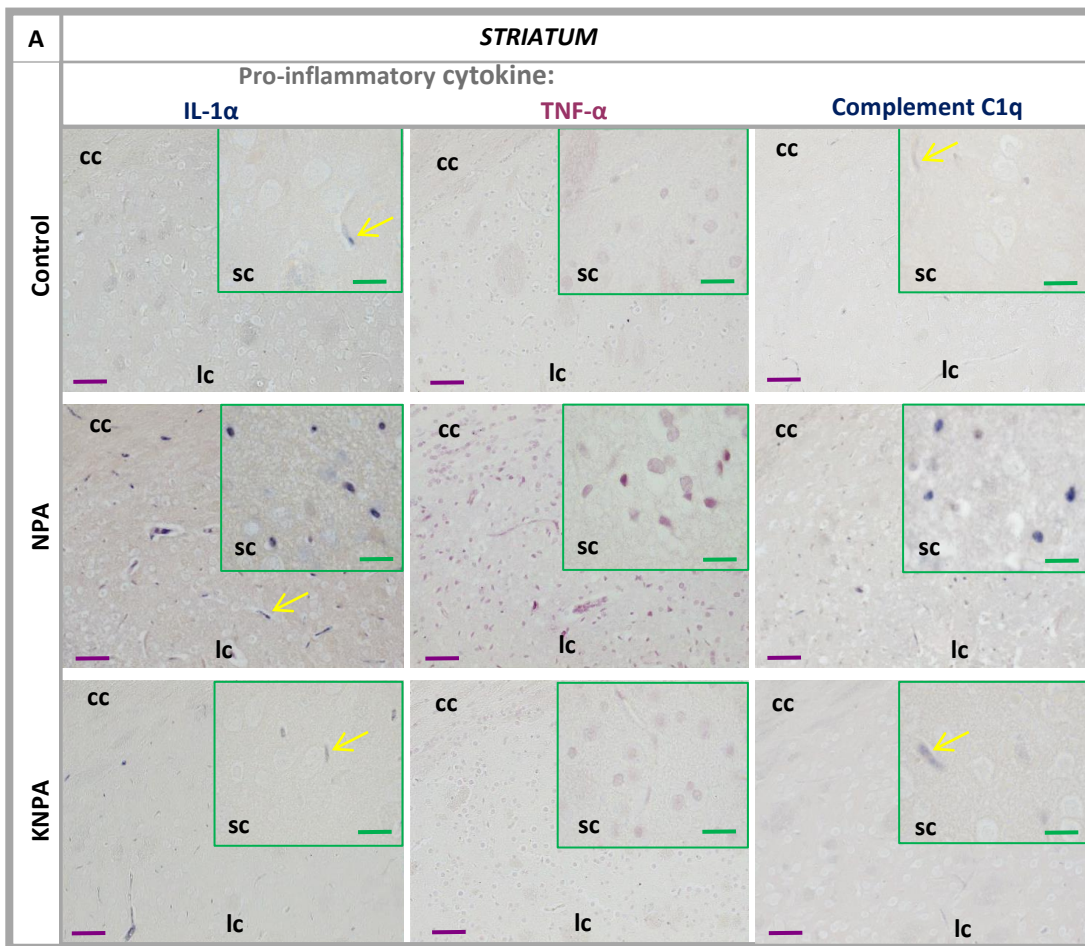
Using immunohistochemical analysis, we confirmed the increased expression of the complement C3 protein in regionalized brain areas of *striatum* and *hippocampus* as well as the presence of reactive A1 astrocytes in rats of NPA-group (data not shown, but included in the attached manuscript submitted for publication). In addition, immunohistochemistry of the brain slices showed that kaempferol treatment fully prevented the increase of C3 induced by the treatment with NPA, because immunostaining pattern was almost identical to that of the control-group (data not shown, but included in the attached manuscript submitted for publication).

4.4. Kaempferol prevents the increase of pro-inflammatory cytokines (IL-1 α and TNF α) and complement C1q in the *striatum* and *hippocampus* of NPA-treated rats

As showed earlier in this chapter, daily i.p. administration of NPA to Wistar rats in a single dose (25 mg/kg b. w.) for 17 days induced an increase in the levels of pro-inflammatory cytokines IL-1 α and TNF α (**Figure 4**) and an increment in C1q levels demonstrated by immunostaining of brain slices (data not shown, but included in the published article⁴⁹). These cytokines and C1q have been shown to trigger the generation of A1 astrocytes³⁸.

After acute NPA treatment (two doses of 25 mg/kg b. w. /day) for five days we analyzed the brain slices of the regions of interest (*striatum* and *hippocampus*) by immunohistochemistry with specific antibodies. The **Figure 6A** show an increase in IL-1 α , TNF α and C1q in *striatum* brain slices of rats of the NPA-group with respect to control-group, highlighted by the frames with higher magnification in this figure. The small apparent particle size of the cells heavily stained with TNF α is consistent with the known nuclear translocation of this cytokine. In addition, the *striatum* brain slices from KNPA-group present a similar pattern of immunostaining with the cytokines and complement C1q comparing with control-group (**Figure 6A**). Results obtained with *hippocampus* brain-slices show also an increase in the expression of these cytokines and complement C1q in NPA-group, regarding the Control-group as can be seen in **Figure 6B**, which was fully prevented by co-administration of kaempferol (KNPA-group) at the dose that prevent C3 α activation. Moreover, the representative images showed in **Figure 6B** pointed out that NPA treatment induced a large increase of these cytokines in the Ammon's horn CA1 and CA3 regions, by strongly staining the soma of pyramidal neurons. This is not observed in the

hippocampus slices of KNPA-group, whose immunostaining pattern is not significantly different from those of rats of the control-group.



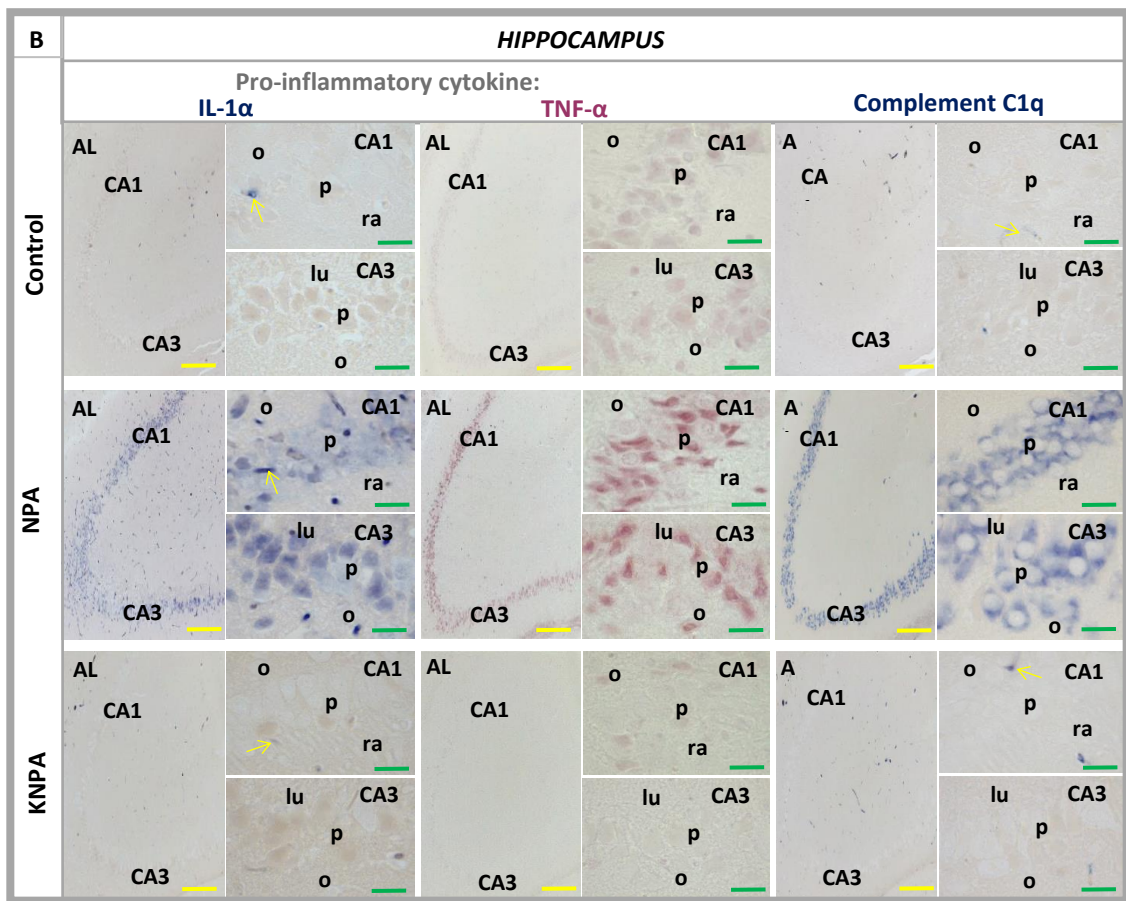


Figure 6. Kaempferol prevents an increase in pro-inflammatory cytokines (IL-1 α and TNF α) and complement C1q in the striatum (A) and in the hippocampus (B) of NPA-treated rats. Representative coronal sections of striatum (A) and hippocampus (B) after immunohistochemistry with anti-IL-1 α , anti-TNF α and anti-C1q antibodies corresponding to control-, NPA- and KNPA-groups. In NPA-group note the cellular somas stained in the area surrounding the core (sc) in the striatum (A), and in CA1 and in CA3 (Ammon's horn) fields in the hippocampus (B). Brain sections of rats treated with kaempferol (KNPA-group) show a low immunoreactivity, similar to the control-group. No staining in the cellular soma is observed in Control- and KNPA-groups. As a significant characteristic of anti-IL-1 α and anti-C1q antibodies, small blood vessels are marked in the three groups (yellow arrows). Abbreviations used in this Figure: AL, alveus; cc, corpus callosum; lc, lesion core area; lu, stratum lucidum; o, stratum oriens; p, pyramidal layer; ra, stratum radiatum. Yellow scale bars: 100 μ m. Purple scale bars: 50 μ m. Green scale bars: 10 μ m.

4.5 Kaempferol prevents the NPA-induced increase of NF- κ B expression in the striatum and hippocampus

It has been shown that the NF- κ B pathway is activated in NPA-induced brain neurodegeneration^{30–32} which is a molecular mechanism underlying the increased expression of many cytokines⁴⁴. Therefore, next we evaluated if the co-administration of kaempferol with NPA, could prevent the NPA-induced increase of NF- κ B expression. The representative Western blot (**Figure 7**) showed increased levels of NF- κ B in rats of NPA-group with respect to control-

group in *striatum* and *hippocampus*. This increase is fully prevented by co-administration of kaempferol at the same dose that prevented the C3 α activation and gliosis. These results were confirmed using double immunohistochemistry of anti-NF-kB and anti-GFAP of coronal slices of the regions of interest (data not shown, but included in the manuscript submitted for publication attached in this thesis). Of note, it has been found high basal constitutive NF-kB activity in glutamatergic neurons of the CNS, such as the *hippocampus* granule cells and CA1 and CA2 pyramidal neurons^{56,57}, which can explain the high levels of NF-kB expression in the control-group of the *hippocampus* that can be seen in the Western blot of **Figure 7**.

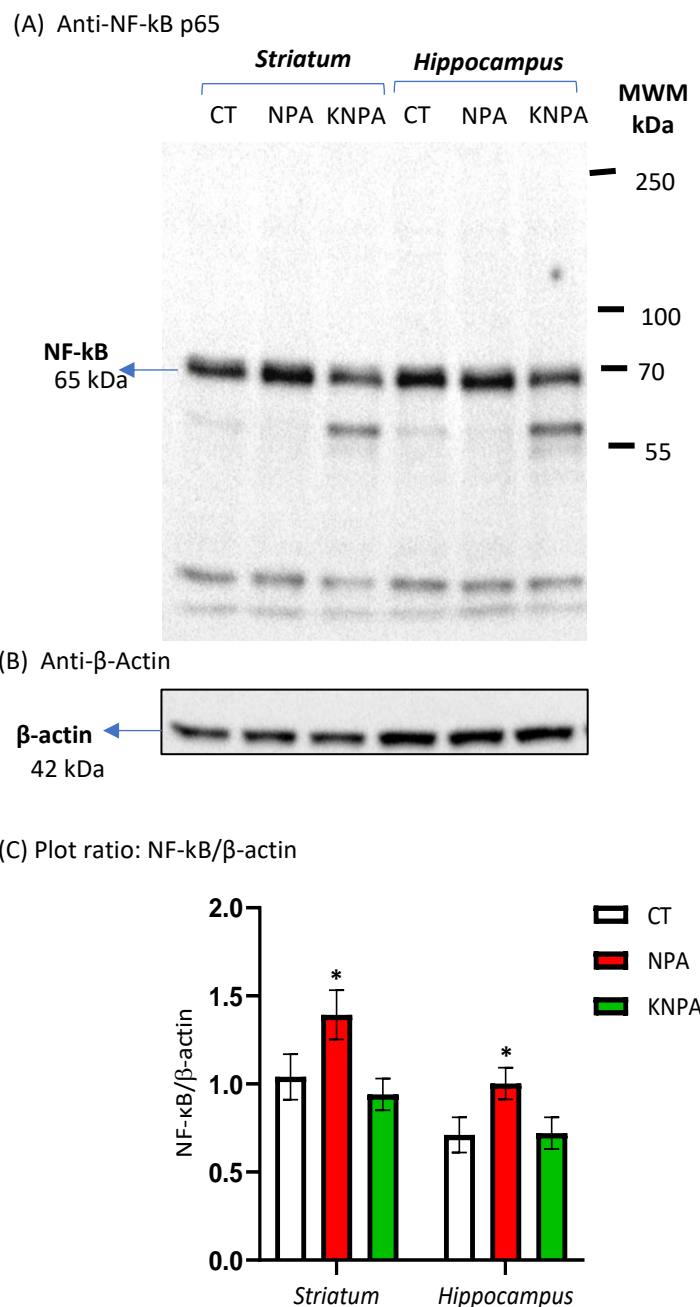


Figure 7. Co-administration of kaempferol and NPA, prevents the increase of NF-kB activity induced by NPA treatment. (A) Representative Western blot of NF-kB and β -actin of *striatum* and *hippocampus*

homogenates of rats of control-group (CT), NPA-group (NPA) and KNPA-group (KNPA). **(B)** After acquisition of images of the Western blot with anti-NF- κ B-p65 antibody, the PVDF membrane was stripped and processed for the Western blot of anti- β -actin, as indicated in the Materials and Methods section. The MWM are indicated on the right-hand side. **(C)** Plot of the ratio of (NF- κ B / β -actin) in *striatum* and *hippocampus* homogenates of rats of CT-, NPA- and KNPA-groups. The results shown are the average \pm s.e. of Western blots of n = 6 homogenate samples of each group of rats. (*) p<0.05 with respect to Control rats.

4.6 Kaempferol protects against the increase of A β peptides production in the *hippocampus* and *striatum* of NPA-treated rats

Recently, it has been reported that NPA induces tau pathology in tangle-mouse model and in wild type mice⁴³. The generation of neurofibrillary tangles of tau and A β peptides are major hallmarks of AD and also it has been reported the production of reactive A1 astrocytes in this neurodegenerative disease³⁸. Therefore, it became important to investigate if the activation of astroglia leads to an increased generation of A β peptides in the brain regions of interest during NPA-induced neurodegeneration. The representative Western blot in **Figure 8** show an enhanced A β expression in rats treated with NPA, which was clearly reverted by the co-administration of kaempferol (KNPA-group) at the dose that prevent C3 α . Of note, **Figure 8** also shows the analysis of the ratio C99-cleavage fragment of APP/ β -actin (a band at \approx 50-55 kDa that is expected to appear with the anti-A β antibody used in this work, as reported in its technical data sheet) but a similar trend is observed in the protein bands corresponding to smaller size A β peptides (between 35 and 50 kDa) and peptides of less than 15 kDa migrating near the front of the gel.

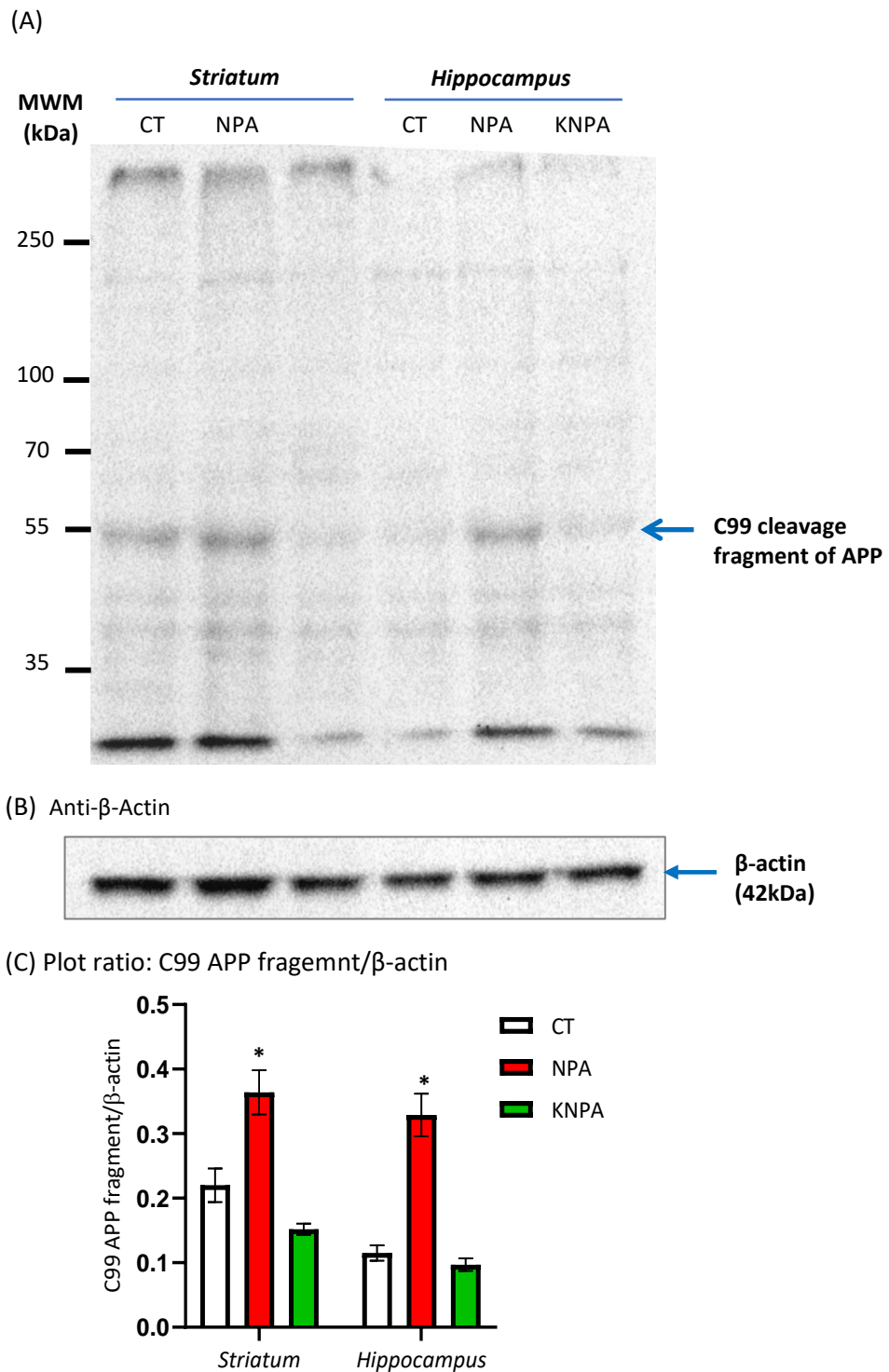


Figure 8. Kaempferol co-administration prevents the increase of A β peptides induced by NPA-treatment. (A) Representative Western blot of A β peptides and β -actin of *striatum* and *hippocampus* homogenates of rats of control-group (CT), NPA-group (NPA) and KNPA-group (KNPA). (B) After acquisition of images of the Western blot with anti-A β antibody, the PVDF membrane was stripped and processed for the Western blot of anti- β -actin, as indicated in the Materials and Methods. The MWM are indicated on the left-hand side. (C) Plot of the ratio of (C99 cleavage fragment of APP of \approx 50–55 kDa / β -actin) in *striatum* and *hippocampus* homogenates of rats of CT, NPA- and KNPA-groups. The results shown are the average \pm s.e. of Western blots of $n = 6$ homogenate samples of each group of rats. (*) $p < 0.05$ with respect to Control rats.

5. Discussion

Administration of NPA to rodent's mimic HD motor neurological dysfunctions. This work had two main objectives: (i) to identify early biomarkers of brain neurodegeneration before to achieve strong neuronal damage, in an animal model of Wistar rats subjected a subacute NPA treatment (i.p. injection of 25 mg NPA/kg b. w.) for 6 (G6), 17 (G17) and 24 (G24) days; and ii) administration of acute NPA treatment by i.p. injections (25 mg NPA/kg b. w. every 12h) for 5 days to induce severe neurotological damage and dysfunction, and to evaluate the protective effect of the natural compound kaempferol (21 mg NPA/kg b. w.) against neurological impairment.

In the first part of this work, the TTC staining of the rat brain slices, the neuronal loss through neurogranin immunostaining and the apoptotic cells observed with the TUNEL assay (**Figure 1**) showed a stronger degree of neurodegeneration in *striatum* of G24 group, compared with the G17 group. In addition, the absence of TTC staining in the three regions analyzed in the first part of this work (*striatum, hippocampus* and *cerebellum*) (**Figure 2**) confirmed the lack of tissue neurodegeneration in G17-group brain sections analyzed. Moreover, the G17-group of rats did not show significant sensorial or motor neurological dysfunctions, compared with the G24-group, pointing out that after 17 days of daily NPA treatment we did not observe strong neuronal damage. The comparison between the Western blots of C3 α fragment expression, a reactive A1 astrocyte marker, in G6 and G17 groups (**Figure 3**) suggested that 6 days with a daily dose of NPA is not enough time to ensure that all rat brain regions of interest are affected by this neurotoxin, because after 6 days of treatment we did not observe a significant increase in C3 α expression in *striatum*. Therefore, all these results suggested that 17 days of NPA treatment (daily i.p. injection of 25mg NPA/kg b. w.) are needed to guarantee that the three regions considered in this study are affected by NPA treatment but in an early stage of the progression of the disease. Other publications reported the expression of complement C3 in astrocytes in the *striatum* obtained from HD *post-mortem* brain samples^{38,54}. However, unlike our observations in early stages of NPA neurotoxicity, these authors described C3 expression in the white matter and neurons in the *striatum* from the same patients⁵⁴, which is possibly well justified due to an advanced lesion stage, when neuronal loss is already evident. Hence, as a novel finding in NPA-induced neurotoxicity, our results demonstrate an earlier activation of complement C3 protein in the brain from Wistar rats that are treated with this neurotoxin.

It is well known that neurodegenerative diseases are associated with a neuroinflammatory processes mediated by microglial activation in the brain, including HD^{34,36}. The secretion of pro-inflammatory cytokines promotes neuronal death through induction of ROS

and reactive nitrogen species (RNS) production^{29,58,59}, excitotoxicity caused by the release of L-glutamate³⁵ and damage associated to molecular products^{59,60}, as well as activation and proliferation of astrocytes⁵⁹. It has been reported that the secretion of IL-1 α , TNF α , and C1q upon reactive microglial activation can induce the generation of reactive A1 astrocytes³⁸. We showed in a previous work¹⁰ that there is a large increase of protein nitrotyrosines in parallel with a depletion of reduced glutathione in NPA-induced degeneration of adult Wistar rat brains, pointing out a large induction of ROS and also RNS in this animal model of HD. In this work we showed an increased expression of the cytokines IL-1 α and TNF α in the *striatum*, *hippocampus* and *cerebellum* of adult Wistar rats treated with daily i.p. injections of 25 mg NPA/kg b.w. for 17 days, demonstrated by the western blots presented in **Figure 4** and confirmed later by immunostaining of rat brain slices of the three regions with the respective antibodies (data not shown in this thesis, but included in the published article, attached in the dissertation⁴⁹). In addition, we found an increase in C1q expression through immunohistochemical analysis of rat brain slices (data not shown in this thesis, but included in the published article⁴⁹).

In our experimental model, we showed that a daily dose of NPA induced a gradual increase of C3 α fragment, a reactive A1 astrocyte marker, as well as an increased generation of cytokines IL-1 α and TNF- α starting long before the observation of any significant neurological motor impairment in treated rats, indicating an early induction of reactive microglia in the three regions under study (*striatum*, *hippocampus* and *cerebellum*). These findings supported the hypothesis that these cytokines play a major early role in the neuroinflammatory process. Moreover, the increase of IL-1 α , TNF α , and C1q expression co-localizes with the appearance of C3 positive astrocytes in the three regions (data not shown in this thesis, but included in the published article⁴⁹). Therefore, considering all these data, we conclude that, in our HD experimental animal model, extensive reactive microglial activation takes place in the brain, along with a reactive astrogliosis with generation of neurotoxic A1 astrocytes near or at neuronal structures which play a major role in brain motor coordination. These processes are early events that precede brain neurodegenerative processes that elicit motor disorders observed at an advanced stage of this neurological disease. Therefore, our results further validate the use of NPA i.p. administration to shed light on molecular mechanisms in the initial stages of neurotoxicity in HD.

In the second part of this work, we administered an acute NPA treatment to Wistar rats (i.p. injection of 25 mg NPA/kg b. w. every 12 h for 5 days) to induce severe neurological damage to evaluate the protective effect of the natural compound kaempferol against neurological impairment. The kaempferol dose used was 21 mg/kg b. w., according to a previous study of our

laboratory with this experimental model of i.p. injections of NPA¹⁰. Lower doses of kaempferol afforded only a partial protection against *striatum* degeneration¹⁰.

The results obtained in this work show that i.p. administration of kaempferol resulted in an almost complete blockade of the NPA-induced increase of C3α and other proteolytic fragments of C3 (iC3b, C3α fragment 2 and lower molecular weight fragments) in the *striatum* and *hippocampus*. Of note, brain slices stained with TTC (**Supplementary Figure S.1**) showed that kaempferol bears a large therapeutical potential to protect against NPA induced brain degeneration in both regions affected by NPA. In addition, the immunostaining patterns of IL-1α, C1q and TNFα antibodies obtained with *striatum* and *hippocampus* slices of the rats of the KNPA-group are not significantly or only weakly different to those obtained from the rats of the control-group (**Figure 6A and B**). Therefore, we can conclude that i.p. administration of kaempferol at the dose used in this work efficiently prevented against the activation of complement C3 protein and generation of reactive A1 astrocytes induced by acute treatment with NPA in the *striatum* and *hippocampus*.

As previously mentioned, we showed in other lab work that i.p. co-administration of 21 mg of kaempferol/kg b.w. largely prevents the increase of cellular oxidative stress markers in NPA-induced brain degeneration¹⁰. In this work, we demonstrated that i.p. co-administration of this dose of kaempferol clearly prevents against the enhancement of NF-κB expression in both *striatum* and *hippocampus* of NPA-treated rats. In addition, it has been shown that the secretion of pro-inflammatory cytokines that mediate NPA-induced brain degeneration is elicited by NF-κB activation^{30–32}. Therefore, our results support the hypothesis that the activation of NF-κB signaling pathway by cellular oxidative stress is the major molecular mechanism underlying the increased production of C1q and pro-inflammatory cytokines IL-1α and TNFα and in NPA-induced degeneration of the *striatum* and of the *hippocampus*. Nevertheless, the putative implication of other cellular stress signaling pathways in the production of these cytokines cannot be excluded. Therefore, the molecular mechanisms associated with the blockade of reactive A1 astrocyte generation by kaempferol in the rat brain induced by i.p. administration of NPA needs to be further investigated. Yet, the results reported herein reveal a potential novel therapeutic use of this flavonoid, because induction of neurotoxic reactive A1 astrocytes has been found in *post-mortem* samples of many human neurodegenerative diseases, like AD, PD and HD, and in amyotrophic lateral sclerosis and multiple sclerosis³⁸. In fact, Stanek and colleagues⁶¹ using the YAC128 mouse model of HD have suggested that astrocyte dysfunction may display a critical role on HD pathogenesis, although this is still a controversial point because it has been questioned by other authors using another mouse models⁶².

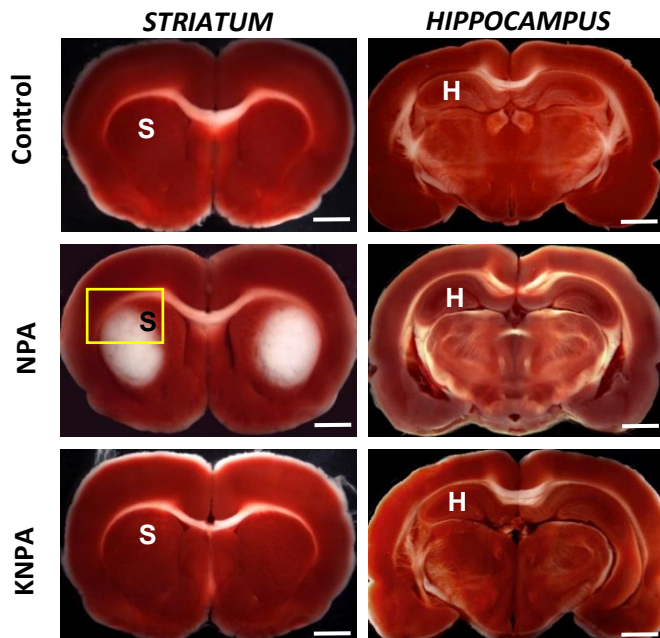
The effective doses of kaempferol to afford protection against activation of complement C3 protein in the brain are strongly dependent upon the administration route of this flavonoid. In a previous work we showed that intravenous injections of only 100-200 µM of kaempferol in the blood produced an extensive protection against the striatal neurodegeneration caused by transient focal cerebral ischemia induced by middle cerebral artery occlusion in adult rats⁴⁵. For comparison, the amount of kaempferol used for intravenous injections were 0.16-0.25 mg of kaempferol/kg b. w.⁴⁵, while i.p. injections used in this work have been 21 mg of kaempferol/kg b. w. In another study, Babaei and colleagues (2021)⁶³ administered kaempferol using the same method described here (i.p injection) and used 10 mg/Kg b. w. (for 21 days) to evaluate the protective effect of kaempferol in the mouse model of sporadic AD. In a study performed in an mice model of PD, they administered 50 mg/Kg b. w of kaempferol by i.p. injection, to experimentally assess the protective effect of this natural compound⁶⁴. Another work developed in an animal model of chronic social defeat stress (CDSD) evaluated the anti-depressive effect of kaempferol by using 10 and 20 mg/kg b. w., also administrated through the route that we used in our work⁶⁵. Therefore, the amount of kaempferol used in this work (21 mg/kg b. w.) is consistent with the doses used in all these studies performed in animal models that mimic neurodegenerative or depressive disorders. Also, our study as well as the other animals' studies reported, strongly suggest that the administration of kaempferol via i.p. injection required higher doses than intravenous injection to afford effective neuroprotection.

Finally, in this work we observed an increase in Aβ peptides production in the *striatum* and a higher increase in the *hippocampus* of NPA-treated rats (**Figure 8**). To the best of our knowledge this is a novel finding in NPA-induced brain neurodegeneration and it has a special relevance, because exposure to NPA has been recently shown to induce tau pathology in tangle-mouse model and also in wildtype-mice⁴³. Therefore, this neurodegenerative process shares these molecular biomarkers with AD, in which reactive A1 astrocytes have been reported to be generated as well³⁸. In addition, the results obtained herein showed that kaempferol prevented the generation of Aβ peptides induced by NPA treatment (**Figure 8**), which could be due the protection afforded by kaempferol against the generation of reactive astrocytes, once it has been shown that astrocytes can produce neurotoxic Aβ peptides⁴⁰⁻⁴². Yet, the putative beneficial effects of kaempferol in AD is a pending issue, although clinical trials have reported improvements in cognitive function and memory impairment from treatment with the flavonoid-rich *Ginkgo biloba* extract^{66,67}, an extract that contains kaempferol.

In summary, the major result of this work is the protection against proteolytic activation of complement C3 protein and generation of reactive A1 astrocytes, by i.p. administration of kaempferol at a dose that also protects efficiently against the rise of markers of

neurodegeneration and against the neurological dysfunctions induced by acute i.p. injections of the neurotoxin NPA in male adult Wistar rats, as shown by the good neurological scores of the rats of the KNPA-group, which are in good agreement with those reported in an earlier work¹⁰. To the best of our knowledge this is a novel finding not previously reported elsewhere. Kaempferol blocked the activation of the NF-κB signaling pathway, suggesting that this is the major molecular mechanism inducing the enhanced secretion of C1q and cytokines IL- 1 α and TNF α that elicits the generation of reactive A1 astrocytes in the rat model used in this study. In addition, an enhanced production of A β peptides has been found in NPA induced brain degeneration, which is also prevented by kaempferol i.p. administration. Therefore, this work highlights novel biological roles of this antioxidant flavonoid. The inhibition by kaempferol of C3 proteolytic activation in the brain suggest a potential novel therapeutic use of this flavonoid, because induction of neurotoxic reactive A1 astrocytes has been found in *post-mortem* samples of many human neurodegenerative diseases.

6. Supplementary Figure



Supplementary Figure S.1. Kaempferol reduces NPA-induced brain degeneration as demonstrated by TTC brain slides staining. The images show representative fresh brain 1.5 mm thick coronal sections of the *striatum* (S) and *hippocampus* (H), stained with TTC in the three groups. The white areas observed in the *striatum* reveal large lesions in NPA-group. In KNPA-group no damaged tissue is observed, showing similar TTC staining to control-group. The yellow square mark indicates those *striatum* areas illustrated in the immunohistochemistry images. In the hippocampus is observed a weaker TTC staining in NPA-group with respect to Control- and KNPA-groups. Scale bars: 2mm.

7. References

1. Alston, T.A., Mela, L., Bright, H. J. 3-Nitropropionate, the toxic substance of Indigofera, is a suicide inactivator of succinate dehydrogenase. *Proc Natl Acad Sci USA* **74**, 3767–3771 (1977).
2. Liu, X., Luo, X., Hu, W. Studies on the epidemiology and etiology of moldy sugarcane poisoning in China. *Biomed Env. Sci.* **5**, 161–77 (1992).
3. Ming, L. Moldy sugarcane poisoning--a case report with a brief review. *J Toxicol Clin Toxicol.* **33**, 363–7 (1995).
4. Blumenthal, C. Z. Production of toxic metabolites in *Aspergillus niger*, *Aspergillus oryzae*, and *Trichoderma reesei*: Justification of mycotoxin testing in food grade enzyme preparations derived from the three fungi. *Regul. Toxicol. Pharmacol* **39**, 214–228 (2004).
5. Beal, M., Brouillet, E., Jenkins, B., Ferrante, R., Kowall, N., Miller, J., Storey, E., Srivastava, R., Rosen, B., Hyman, B. Neurochemical and histologic characterization of striatal excitotoxic lesions produced by the mitochondrial toxin 3-nitropropionic acid. *J. Neurosci.* **13**, 4181–4192 (1993).
6. Beal, M. F. Neurochemistry and toxin models in Huntington's disease. *Curr. Opin. Neurol.* **7**, 542–547 (1994).
7. Brouillet, E., Jenkins, B.G., Hyman, B.T., Ferrante, R.J., Kowall, N.W., Srivastava, R., Roy, D.S., Rosen, B. R. & Beal, M. F. Age-Dependent Vulnerability of the Striatum to the Mitochondrial Toxin 3-Nitropropionic Acid. *J. Neurochem.* **60**, 356–359. (1993).
8. Brouillet, E., Condé, F., Beal, M.F., Hantraye, P. Replicating Huntington's disease phenotype in experimental animals. *Prog. Neurobiol.* **59**, 427–468 (1999).
9. Blum, D., Gall, D., Cuvelier, L., Schiffmann, S.N., Blum, D., Gall, D., Cuvelier, L., Schiffmann, S. N. Topological analysis of striatal lesions induced by 3-nitropropionic acid in the Lewis rat. *Neuroreport* **12**, 1769–1772 (2001).
10. Lagoa, R., Lopez-Sanchez, C., Samhan-Arias, A.K., Gañan, C.M., Garcia-Martinez, V., Gutierrez-Merino, C. Kaempferol protects against rat striatal degeneration induced by 3-nitropropionic acid. *J. Neurochem.* **111**, 473–487 (2009).
11. Vonsattel, J.P., Myers, R.H., Stevens, T.J., Ferrante, R.J., Bird, E.D., Richardson, E. P. J. Neuropathological classification of Huntington's disease. *J. Neuropathol. Exp. Neurol.* **44**, 559–577 (1985).
12. Ho, A.K., Sahakian, B.J., Brown, R.G., Barker, R.A., Hodges, J.R., Ané, M.-N., Snowden, J., Thompson, J., Esmonde, T., Gentry, R., Moore, J.W., Bodner, T. Profile of cognitive progression in early Huntington's disease. *Neurology* **61**, 1702–1706 (2003).

13. Phillips, W., Shannon, K.M., Barker, R. A. The current clinical management of Huntington's disease. *Mov Disord.* **23**, 491–504 (2008).
14. Browne, S.E., Ferrante, R.J., Beal, M. F. Oxidative Stress in Huntington's Disease. *Brain Pathol.* **9**, 147–163 (1999).
15. Menze, E.T., Esmat, A., Tadros, M.G., Abdel-Naim, A.B., Khalifa, A. E. Genistein Improves 3-NPA-Induced Memory Impairment in Ovariectomized Rats: Impact of Its Antioxidant, Anti-Inflammatory and Acetylcholinesterase Modulatory Properties. *PLoS One* **10**, e0117223 (2015).
16. Tsang, T.M., Haselden, J.N. & Holmes, E. Metabonomic Characterization of the 3-Nitropropionic Acid Rat Model of Huntington's Disease. *Neurochem Res* **34**, 1261–1271 (2009).
17. Peraza, A.V., Guzmán, D.C., Brizuela, N.O., Herrera, M.O., Olguin, H.J., Silva, M.L., Tapia, B.J., Mejía, G. B. Riboflavin and pyridoxine restore dopamine levels and reduce oxidative stress in brain of rats. *BMC Neurosci* **19**, (2018).
18. Singh-Bains, M.K., Mehrabi, N.F., Sehji, T., Austria, M.D.R., Tan, A.Y.S., Tippett, L.J., Dragunow, M., Waldvogel, H.J., Faull, R. L. M. Cerebellar degeneration correlates with motor symptoms in Huntington disease. *Ann Neurol* **85**, 396–405 (2019).
19. Nasr, P., Gursahani, H.I., Pang, Z., Bondada, V., Lee, J., Hadley, R.W., Geddes, J. Influence of cytosolic and mitochondrial Ca²⁺, ATP, mitochondrial membrane potential, and calpain activity on the mechanism of neuron death induced by 3-nitropropionic acid. *Neurochem. Int.* **43**, 89–99 (2003).
20. Rosenstock, T.R., Carvalho, A.C.P., Jurkiewicz, A., Frussa-Filho, R., Smaili, S. Mitochondrial calcium, oxidative stress and apoptosis in a neurodegenerative disease model induced by 3-nitropropionic acid. *J. Neurochem.* **88**, 1220–1228 (2004).
21. Brouillet, E., Jacquard, C., Bizat, N., Blum, D. 3-Nitropropionic acid: A mitochondrial toxin to uncover physiopathological mechanisms underlying striatal degeneration in Huntington's disease. *J Neurochem* **95**, 1521–40 (2005).
22. Gil, J.M., Rego, A. C. Mechanisms of neurodegeneration in Huntington's disease. *Eur. J. Neurosci.* **27**, 2803–2820. (2008).
23. Zeevalk, G.D., Derr-Yellin, E., Nicklas, W. J. NMDA receptor involvement in toxicity to dopamine neurons in vitro caused by the succinate dehydrogenase inhibitor 3-nitropropionic acid. *J. Neurochem* **64**, 455–458 (1995).
24. Greene, J.G., Sheu, S.-S., Gross, R.A., Greenamyre, J. T. 3-Nitropropionic acid exacerbates N-methyl-d-aspartate toxicity in striatal culture by multiple mechanisms. *Neuroscience* **84**, 503–510 (1998).

25. Calabresi, P., Gubellini, P., Picconi, B., Centonze, D., Pisani, A., Bonsi, P., Greengard, P., Hipskind, R.A., Borrelli, E., Bernardi, G. Inhibition of Mitochondrial Complex II Induces a Long-Term Potentiation of NMDA-Mediated Synaptic Excitation in the Striatum Requiring Endogenous Dopamine. *J. Neurosci.* **21**, 5110–5120. (2001).
26. Bizat, N., Hermel, J.-M., Boyer, F., Jacquard, C., Creminon, C., Ouary, S., Escartin, C., Hantraye, P., Krajewski, S., Brouillet, E. Calpain Is a Major Cell Death Effector in Selective Striatal Degeneration Induced In Vivo by 3-Nitropropionate: Implications for Huntington’s Disease. *J. Neurosci.* **23**, 5020–5030 (2003).
27. Crespo-Biel, N., Camins, A., Pelegrí, C., Vilaplana, J., Pallàs, M., Canudas, A. 3-Nitropropionic acid activates calpain/cdk5 pathway in rat striatum. *Neurosci. Lett.* **421**, 77–81 (2007).
28. Fu, Y. 3-Nitropropionic acid produces indirect excitotoxic damage to rat striatum. *Neurotoxicol. Teratol.* **17**, 333–339 (1995).
29. Stewart, V.C., Sharpe, M.A., Clark, J.B., Heales, S. J. R. Astrocyte-Derived Nitric Oxide Causes Both Reversible and Irreversible Damage to the Neuronal Mitochondrial Respiratory Chain. *J. Neurochem.* **75**, 694–700 (2002).
30. Ryu, J.K., Nagai, A., Kim, J., Lee, M.C., McLarnon, J.G., Kim, S. U. Microglial activation and cell death induced by the mitochondrial toxin 3-nitropropionic acid: In vitro and in vivo studies. *Neurobiol. Dis.* **12**, 121–132 (2003).
31. Chakraborty, J., Singh, R., Dutta, D., Naskar, A., Rajamma, U., Mohanakumar, K. P. Quercetin Improves Behavioral Deficiencies, Restores Astrocytes and Microglia, and Reduces Serotonin Metabolism in 3-Nitropropionic Acid-Induced Rat Model of Huntington’s Disease. *CNS Neurosci. Ther.* **20**, 10–19 (2013).
32. Jin, X., Riew, T.-R., Kim, H.L., Choi, J.-H., Lee, M.-Y. Morphological characterization of NG2 glia and their association with neuroglial cells in the 3-nitropropionic acid-lesioned striatum of rat. *Sci. Rep.* **8**, 5942 (2018).
33. Niccolini, F., Politis, M. Neuroimaging in Huntington’s disease. *World J. Radiol.* **6**, 301–312 (2014).
34. Hong, H., Kim, B., Im, H.-I. Pathophysiological Role of Neuroinflammation in Neurodegenerative Diseases and Psychiatric Disorders. *Int. Neurourol. J.* **20**, (Suppl. 1), S2–S7 (2016).
35. Takeuchi, H., Jin, S., Wang, J., Zhang, G., Kawanokuchi, J., Kuno, R., Sonobe, Y., Mizuno, T., Suzumura, A. Tumor Necrosis Factor- Induces Neurotoxicity via Glutamate Release from Hemichannels of Activated Microglia in an Autocrine Manner. *J. Biol. Chem.* **281**, 21362–21368 (2006).

36. Crotti, A., Glass, C. K. The choreography of neuroinflammation in Huntington's disease. *Trends Immunol.* **36**, 364–373 (2015).
37. Nishino, H., Kumazaki, M., Fukuda, A., Fujimoto, I., Shimano, Y., Hida, H., Sakurai, T., Deshpande, S.B., Shimizu, H., Morikawa, S., et al. Acute 3-nitropropionic acid intoxication induces striatal astrocytic cell death and dysfunction of the blood-brain barrier: Involvement of dopamine toxicity. *Neurosci. Res.* **27**, 343–355 (1997).
38. Liddelow, S.A., Guttenplan, K.A., Clarke, L.E., Bennett, F.C., Bohlen, C.J., Schirmer, L., Bennett, M.L., Münch, A.E., Chung, W.-S., Peterson, T.C., et al. Neurotoxic reactive astrocytes are induced by activated microglia. *Nature* 481–487 (2017).
39. Wang, T., Sun, Q., Yang, J., Wang, G., Zhao, F., Chen, Y., Jin, Y. Reactive astrocytes induced by 2-chloroethanol modulate microglia polarization through IL-1 β , TNF- α , and iNOS upregulation. *Food Chem. Toxicol.* **157**, 112550 (2021).
40. Nadler, Y., Alexandrovich, A., Grigoriadis, N., Hartmann, T., Rao, K.S.J., Shohami, E., Stein, R. Increased expression of the gamma-secretase components presenilin-1 and nicastrin in activated astrocytes and microglia following traumatic brain injury. *Glia* **56**, 552–567 (2008).
41. Zhao, J., O'Connor, T., Vassar, R. The contribution of activated astrocytes to A β production: Implications for Alzheimer's disease pathogenesis. *J Neuroinflammation* **8**, 150. *J Neuroinflammation* **8**, 150 (2011).
42. Frost, G.R., Li, Y. M. The role of astrocytes in amyloid production and Alzheimer's disease. *Open Biol.* **7**, 170228 (2017).
43. Lahiani-Cohen, I., Touloumi, O., Lagoudaki, R., Grigoriadis, N., Rosenmann, H. Exposure to 3-Nitropropionic Acid Mitochondrial Toxin Induces Tau Pathology in Tangle-Mouse Model and in Wild Type-Mice. *Front. Cell Dev. Biol.* **7**, 321 (2020).
44. Gutierrez-Merino, C., Lopez-Sanchez, C., Lagoa, R., Samhan-Arias, A.K., Bueno, C., G.- & Martinez, V. Neuroprotective actions of flavonoids. *Curr. Med. Chem.* **18**, 1195-1212. (2011).
45. Lopez-Sanchez, C., Martin-Romero, F.J., Sun, F., Luis, L., Samhan-Arias, A.K., G.-M. & V., Gutierrez-Merino, C. Blood micromolar concentrations of kaempferol afford protection against ischemia/reperfusion induced damage in rat brain. *Brain Res.* **1182**, 123–137 (2007).
46. Ren, J., Lu, Y., Qian, Y., Chen, B., Wu, T., Ji, G. Recent progress regarding kaempferol for the treatment of various diseases. *Exp. Ther. Med.* **18**, 2759–277 (2019).
47. Saleem, S., Zhuang, H., Biswal, S., Christen, Y., Doré, S. Ginkgo biloba extract neuroprotective action is dependent on heme oxygenase 1 in ischemic reperfusion brain

- injury. *Stroke* **39**, 3389–3396 (2008).
- 48. Ouary, S., Bizat, N., Altairac, S., Ménétrat, H., Mittoux, V., Condé, F., Hantraye, P., Brouillet, E. Major strain differences in response to chronic systemic administration of the mitochondrial toxin 3-nitropropionic acid in rats: Implications for neuroprotection studies. *Neuroscience* **97**, 521–530 (2000).
 - 49. Lopez-Sanchez, C., Garcia-Martinez, V., Poejo, J., Garcia-Lopez, V., Salazar, J., Gutierrez-Merino, C. Early reactive a1 astrocytes induction by the neurotoxin 3-nitropropionic acid in rat brain. *Int. J. Mol. Sci.* **21**, (2020).
 - 50. Sun, F., López-Sánchez, C., Martin-Romero, F.J., Luis, L., Gutierrez-Merino, C., Garcia-Martinez, V. Transfemoral selective “intraluminal wiring” technique for transient middle cerebral artery occlusion in rats. *J. Neurosci. Methods* **149**, 82–89 (2005).
 - 51. Poejo, J., Salazar, J., Mata, A. M. & Gutierrez-merino, C. Binding of amyloid β (1–42)-calmodulin complexes to plasma membrane lipid rafts in cerebellar granule neurons alters resting cytosolic calcium homeostasis. *Int. J. Mol. Sci.* **22**, 1–23 (2021).
 - 52. Zhang, Y., Chen, K., Sloan, S., Bennett, M.L., Scholze, A.R., O’Keeffe, S., Phatnani, H.P., Guarnieri, P., Caneda, C., Ruderisch, N., et al. An RNA-sequencing transcriptome and splicing database of glia, neurons, and vascular cells of the cerebral cortex. *J. Neurosci.* **34**, 11929–11947 (2014).
 - 53. Bennett, M.L., Bennett, F.C., Liddelow, S.A., Ajami, B., Zamanian, J., Fernho, N.B., Mulinyawe, S.B., Bohlen, C.J., Adil, A., Tucker, A., et al. New tools for studying microglia in the mouse and human CNS. *Proc. Natl. Acad. Sci. USA* **113**, E1738–E1746 (2016).
 - 54. Singhrao, S., Neal, J., Morgan, B.P., Gasque, P. Increased Complement Biosynthesis By Microglia and Complement Activation on Neurons in Huntington’s Disease. *Exp. Neurol.* **159**, 362–376 (1999).
 - 55. Färber, K., Cheung, G., Mitchell, D., Wallis, R., Weihe, E., Schwaebel, W., Kettenmann, H. C1q, the recognition subcomponent of the classical pathway of complement, drives microglial activation. *J. Neurosci. Res.* **87**, 644–652 (2009).
 - 56. Kaltschmidt, C., Kaltschmidt, B., Neumann, H., Wekerle, H., Baeuerle, P. A. Constitutive NF-kappa B activity in neurons. *Mol Cell Biol.* **14**, 3981–3992 (1994).
 - 57. Kaltschmidt, C., Kaltschmidt, B., Henkel, T., Stockinger, H., Baeuerle, P.A. Selective recognition of the activated form of transcription factor NF-kappa B by a monoclonal antibody. *Biol Chem Hoppe Seyler* **376**, 9–16 (1995).
 - 58. Boje, K.M., Arora, P. K. Microglial-produced nitric oxide and reactive nitrogen oxides mediate neuronal cell death. *Brain Res.* **587**, 250–256 (1992).
 - 59. Murray, K.N., Parry-Jones, A.R., Allan, S. M. Interleukin-1 and acute brain injury. *Front.*

Cell. Neurosci. **2015**, *9*, 1662–5102. **9**, 1662 (2015).

60. Marinelli, C., Di Liddo, R., Facci, L., Bertalot, T., Conconi, M., Zusso, M., Skaper, S., Giusti, P. Ligand engagement of Toll-like receptors regulates their expression in cortical microglia and astrocytes. *J. Neuroinflamm.* **12**, 244 (2015).
61. Stanek, L.M., Bu, J., Shihabuddin, L. S. Astrocyte transduction is required for rescue of behavioral phenotypes in the YAC128 mouse model with AAV-RNAi mediated HTT lowering therapeutics. *Neurobiol. Dis.* **129**, 29–37 (2019).
62. Diaz-Castro, B., Gangwani, M.R., Yu, X., Coppola, G., Khakh, B. S. Astrocyte molecular signatures in Huntington’s disease. *Sci. Transl. Med.* **11**, eaaw8546 (2019).
63. Babaei, P., Eyvani, K., Kouhestani, S. Sex-Independent Cognition Improvement in Response to Kaempferol in the Model of Sporadic Alzheimer’s Disease. *Neurochem. Res.* **46**, 1480–1486 (2021).
64. Han, X., Zhao, S., Song, H., Xu, T., Fang, Q., Hu, G., Sun, L. Kaempferol alleviates LD-mitochondrial damage by promoting autophagy: Implications in Parkinson’s disease. *Redox Biol.* **41**, 101911 (2021).
65. Gao, W., Wang, W., Peng, Y. & Deng, Z. Antidepressive effects of kaempferol mediated by reduction of oxidative stress, proinflammatory cytokines and up-regulation of AKT/β-catenin cascade. *Metab. Brain Dis.* **34**, 485–494 (2019).
66. Praticò, D., Delanty, N. Oxidative injury in diseases of the central nervous system: Focus on Alzheimer’s disease. *Am. J. Med.* **109**, 577–585 (2000).
67. Ward, C.P., Redd, K., Williams, B.M., Caler, J.R., Luo, Y., McCoy, J. G. Ginkgo biloba extract: cognitive enhancer or antistress buffer. *Pharmacol. Biochem. Behav.* **72**, 913–922 (2002).

CONCLUSIONS

In summary, the main conclusions of this work are:

- (1) A novel function of CaM in neurons demonstrated in this Ph.D. thesis is its high binding capacity to the neurotoxic A β (1-42) peptide in the nanomolar range, the prevalent A β peptide found in the amyloid plaques of AD patients.
- (2) A β (1-42) and CaM form complexes in primary rat cultures of mature CGN, and co-localize with lipid rafts, as showed by extensive FRET assays, using lipid raft markers.
- (3) A β (1-42) can be significantly internalized into mature CGN cells by short time incubation (2 h), leading to a decrease of resting cytosolic Ca²⁺ concentration through the inhibition of LTCC activity.
- (4) A β (1-42) is also internalized into HT-22 mouse hippocampal cells by short time incubation, leading to a significant decrease of Ca²⁺ entry through P2X7R, a subtype of PR2, which are the main Ca²⁺ influx transport system in these cells. Besides, internalized A β (1-42) causes a decrease in SOCE mechanism by modulating of STIM1 function, and by stimulating the activity of both, RyR and IP3R, ligand-gated calcium channels.
- (5) Subcellular distribution of internalized A β (1-42) into living HT-22 cells by short time incubation shows, a predominant localization near the perinuclear region of the soma, and moderate co-localization with ER and mitochondria, although it does not significantly alter the mitochondrial membrane potential. In addition, this internalized A β (1-42) up to 5 h incubation does not alter the resting cytosolic Ca²⁺ concentration.
- (6) A daily dose of the neurotoxin NPA administrated by i.p. injection to Wistar rats for 17 days, results in inflammatory events, as shown by the increase of C3 α generation (an early marker of generation of neurotoxic A1 astrocytes) in *striatum*, *hippocampus* and *cerebellum*, as well an increase of pro-inflammatory cytokines (TNF- α and IL-1 α) and secretion of C1q.
- (7) The antioxidant kaempferol exerts a strong neurological protection against acute NPA treatment of Wistar rats (two doses per day, for 5 days). Co-administration of NPA and kaempferol completely prevents the rise of the levels of C3 α , pro-inflammatory cytokines, complement C1q and NF- κ B, in *striatum* and *hippocampus*.

(8) A novel finding in NPA-induced brain degeneration reported in this work is that kaempferol i.p. administration also prevents the overproduction of A β peptides in *striatum* and *hippocampus*.

CONCLUSIONES

En resumen, las principales conclusiones alcanzadas en este trabajo son las siguientes:

- (1) Una nueva función de la CaM en neuronas demostrada en esta tesis doctoral es su elevada capacidad para unir concentraciones nanomolares del péptido neurotóxico A β (1-42), el péptido de A β más enriquecido en las placas amiloides de los enfermos de AD.
- (2) A β (1-42) y CaM forman complejos en los cultivos primarios de CGN de ratas maduradas *in vitro* que co-localizan con *lipid rafts*, como lo demuestran los estudios de FRET realizados utilizando varios marcadores de *lipid rafts*.
- (3) A β (1-42) se internaliza significativamente en CGN maduras tras un corto tiempo de incubación (2 h), produciendo la disminución de la concentración citosólica de Ca $^{2+}$ en ausencia de estímulo por inhibición de la actividad de los LTCC.
- (4) A β (1-42) se internaliza también en células de hipocampo de ratón inmortalizadas HT-22 tras un corto tiempo de incubación, produciendo una disminución significativa de la entrada de Ca $^{2+}$ a través de P2X7R, un subtipo de receptores P2, que es el sistema con mayor capacidad de catalizar el influjo de Ca $^{2+}$ extracelular en estas células. Además, el A β (1-42) internalizado induce una atenuación del mecanismo SOCE a través de la modulación de la función de STIM1 y de la estimulación de la actividad de RyR y de IP3R, canales de calcio activados por ligando.
- (5) La distribución subcellular del A β (1-42) internalizado en células HT-22 vivas tras un corto tiempo de incubación muestra una localización predominante cerca de la región perinuclear del soma, con una moderada co-localización con el ER y mitocondrias, aunque no altera significativamente el potencial de membrana mitocondrial. Además, el A β (1-42) internalizado hasta las 5 h de incubación no altera la concentración citosólica de Ca $^{2+}$ en ausencia de estímulo.
- (6) Una dosis diaria de la neurotoxina NPA administrada por inyecciones i.p. a ratas Wistar durante 17 días, produce eventos inflamatorios que incrementan la producción de C3 α (un marcador temprano de la generación de astrocitos A1 neurotóxicos) en el estriado, el hipocampo y el cerebelo, así como un incremento de las citoquinas proinflamatorias (TNF- α e IL-1 α) y de la secreción de C1q.

- (7) El antioxidante kaempferol ejerce una fuerte protección neurológica contra el tratamiento agudo de ratas Wistar con NPA (dos dosis cada día, durante 5 días). La co-administración de NPA y kaempferol previene completamente la subida de los niveles de C3 α , de citoquinas proinflamatorias, de la proteína de complemento C1q y de NF- κ B en el estriado y en hipocampo.
- (8) Un hallazgo novedoso reportado en este trabajo es que la administración i.p. de kaempferol también previene la sobreproducción de péptidos A β en el estriado y en hipocampo en el proceso neurodegenerativo inducido por NPA.

LIST OF PUBLICATIONS

Publications directly related with this Ph.D. thesis:

- (1) **Joana Poejo**, Jairo Salazar, Ana M. Mata, Carlos Gutierrez-Merino. The Relevance of Amyloid β -Calmodulin Complexation in Neurons and Brain Degeneration in Alzheimer's Disease. *Int. J. Mol. Sci.* 2021, 22, 4976. Doi: 10.3390/ijms22094976. (**ANNEX I**).
- (2) **Joana Poejo**, Jairo Salazar, Ana M. Mata, Carlos Gutierrez-Merino. Binding of Amyloid β (1–42)-Calmodulin Complexes to Plasma Membrane Lipid Rafts in Cerebellar Granule Neurons Alters Resting Cytosolic Calcium Homeostasis. *Int. J. Mol. Sci.* 2021, 22, 1984. Doi: 10.3390/ijms22041984. (**ANNEX II**).
- (3) Carmen Lopez-Sanchez, Virginio Garcia-Martinez, **Joana Poejo**, Virginio Garcia-Lopez, Jairo Salazar, Carlos Gutierrez-Merino. Early Reactive A1 Astrocytes Induction by the Neurotoxin 3-Nitropropionic Acid in Rat Brain. *Int J Mol Sci.* 2020, 21, 3609. Doi: 10.3390/ijms21103609. (**ANNEX III**).
- (4) Carmen Lopez-Sanchez[†], **Joana Poejo**[†], Virginio Garcia-Lopez, Jairo Salazar, Virginio Garcia-Martinez, Carlos Gutierrez-Merino. Kaempferol Prevents the Activation of Complement C3 Protein and the Generation of Reactive A1 Astrocytes that Mediate Rat Brain Degeneration Induced by 3-Nitropropionic Acid. *Food Chem. Toxicol.* 2022. Submitted for publication on 21/12/21. (**ANNEX IV**).
- (5) Manuscript in preparation to be submitted before the defense of the Ph.D. thesis: "Downregulation of Store-Operated Calcium Entry Function by the Amyloid β (1-42) Peptide in HT-22 cell".

Other publications in this period:

- (1) Sofia Fortalezas, **Joana Poejo**, Alejandro K. Samhan-Arias and Carlos Gutierrez-Merino. Cholesterol-Rich Plasma Membrane Submicrodomains Can Be a Major Extramitochondrial Source of Reactive Oxygen Species in Partially Depolarized Mature

Cerebellar Granule Neurons in Culture. J. Neurophysiol. Neurol. Disord 2019, 5, 1-22. Doi: :10.17303/jnnd.2019.5.204.

- (2) Salazar, **Joana Poejo**, Ana M. Mata, Alejandro K. Samhan-Arias and Carlos Gutierrez-Merino. Design and experimental evaluation of a peptide antagonist against amyloid β (1-42) interactions with calmodulin and calbindin-D28k. Int. J. Mol. Sci. 2022. Submitted for publication on 20/01/22.

† Both should be considered first authors

PUBLICATIONS - ANNEXES



Review

The Relevance of Amyloid β -Calmodulin Complexation in Neurons and Brain Degeneration in Alzheimer's Disease

Joana Poejo ¹ ID, Jairo Salazar ^{1,2}, Ana M. Mata ^{1,3} ID and Carlos Gutierrez-Merino ^{1,3,*} ID

¹ Instituto de Biomarcadores de Patologías Moleculares, Universidad de Extremadura, 06006 Badajoz, Spain; joanapoejo86@gmail.com (J.P.); jairochemsalazar@gmail.com (J.S.); anam@unex.es (A.M.M.)

² Departamento de Química, Universidad Nacional Autónoma de Nicaragua-León, León 21000, Nicaragua

³ Departamento de Bioquímica y Biología Molecular y Genética, Facultad de Ciencias, Universidad de Extremadura, 06006 Badajoz, Spain

* Correspondence: carlosgm@unex.es

Abstract: Intraneuronal amyloid β ($A\beta$) oligomer accumulation precedes the appearance of amyloid plaques or neurofibrillary tangles and is neurotoxic. In Alzheimer's disease (AD)-affected brains, intraneuronal $A\beta$ oligomers can derive from $A\beta$ peptide production within the neuron and, also, from vicinal neurons or reactive glial cells. Calcium homeostasis dysregulation and neuronal excitability alterations are widely accepted to play a key role in $A\beta$ neurotoxicity in AD. However, the identification of primary $A\beta$ -target proteins, in which functional impairment initiating cytosolic calcium homeostasis dysregulation and the critical point of no return are still pending issues. The micromolar concentration of calmodulin (CaM) in neurons and its high affinity for neurotoxic $A\beta$ peptides (dissociation constant ≈ 1 nM) highlight a novel function of CaM, i.e., the buffering of free $A\beta$ concentrations in the low nanomolar range. In turn, the concentration of $A\beta$ -CaM complexes within neurons will increase as a function of time after the induction of $A\beta$ production, and free $A\beta$ will rise sharply when accumulated $A\beta$ exceeds all available CaM. Thus, $A\beta$ -CaM complexation could also play a major role in neuronal calcium signaling mediated by calmodulin-binding proteins by $A\beta$; a point that has been overlooked until now. In this review, we address the implications of $A\beta$ -CaM complexation in the formation of neurotoxic $A\beta$ oligomers, in the alteration of intracellular calcium homeostasis induced by $A\beta$, and of dysregulation of the calcium-dependent neuronal activity and excitability induced by $A\beta$.



Citation: Poejo, J.; Salazar, J.; Mata, A.M.; Gutierrez-Merino, C. The Relevance of Amyloid β -Calmodulin Complexation in Neurons and Brain Degeneration in Alzheimer's Disease. *Int. J. Mol. Sci.* **2021**, *22*, 4976. <https://doi.org/10.3390/ijms22094976>

Academic Editor: Maurizio Battino

Received: 1 April 2021

Accepted: 5 May 2021

Published: 7 May 2021

Publisher's Note: MDPI stays neutral with regard to jurisdictional claims in published maps and institutional affiliations.



Copyright: © 2021 by the authors. Licensee MDPI, Basel, Switzerland. This article is an open access article distributed under the terms and conditions of the Creative Commons Attribution (CC BY) license (<https://creativecommons.org/licenses/by/4.0/>).

1. Intracellular Amyloid β ($A\beta$) Oligomers in Neuronal Cytotoxicity and Calmodulin (CaM) as a Major High Affinity $A\beta$ -Binding Protein in Neurons

Intraneuronal $A\beta$ accumulation has been shown to mediate neuronal cytotoxicity, and it has been suggested to be an early pathological biomarker for the onset of Alzheimer's disease (AD) [1]. This is also supported by the finding that intraneuronal $A\beta$ accumulation precedes the appearance of amyloid plaques or tangles in transgenic mice [2–5], and that it also correlates with alteration of long-term potentiation, synaptic dysfunction, and memory impairment in a triple transgenic model of AD [3,6]. The prevalent $A\beta$ peptide found in the amyloid plaques of AD patients is $A\beta(1–42)$ [7]. It has been shown that microinjection of $A\beta(1–42)$ or cDNA encoding $A\beta(1–42)$ is neurotoxic to human neurons in culture [8]. Furthermore, oligomeric species of $A\beta(1–42)$ are tightly linked to AD pathogenesis and are likely to be the cause of neuronal damage [9–11]. In addition, neuronal uptake and accumulation of $A\beta(1–42)$ aggregates correlated with metabolic inhibition [12], while extracellular $A\beta$, applied to hippocampal slices, seems to preferentially target synapses, leading to a decrease in the synaptic marker synaptophysin [13], as well as endocytosis of N-methyl-D-aspartate receptors (NMDAR) [14] and low-density lipoprotein receptor-related

protein-1 (LRP1) [15,16]. Of note, the plasma membrane distribution and internalization of NMDARs are modulated by LRP1 [17], and it has been proposed that physical interactions with LRP1 may also mediate the functional modulation of NMDAR by LRP1 [18,19]. In addition, the binding of extracellular A β to other proteins, such as the α 7 nicotinic cholinergic receptor, ApoE and ApoE receptors, integrins and the receptor for advanced glycation end products, has been shown to be implicated in A β uptake by neurons and was reviewed in [20].

Calmodulin (CaM) is a calcium buffering protein which is expressed in neurons at much higher concentrations than in non-excitable cells, reaching micromolar concentrations in neurons [21]. The levels of CaM expressed in the brain are within 4 and 15 μ g/mg wet tissue, with highest content in cortical regions, striatum, hippocampus, amygdala, and substantia grisea [22]. We showed that calcium-saturated CaM binds with high affinity to A β (1–42) and A β (25–35) peptides, as demonstrated by a dissociation constant of the A β :Ca $^{2+}$ -CaM complex close to 1 nM [23]. As a result, CaM could have a high capacity to buffer intracellular free A β concentrations. We have recently shown [24] that primary cultures of mature cerebellar granule neurons express 5.5 ± 0.5 ng of CaM per μ g of total protein, i.e., approximately 1 μ g of CaM or 56 ± 6 picomoles of CaM in a plate seeded with 2.5×10^6 neurons. Additionally, we found that CaM extensively binds A β (1–42) dimers in cerebellar granule neurons after only 2 hours of incubation at 37 °C with micromolar concentrations of A β (1–42) dimers added to the extracellular medium, which allowed to calculate that the CaM present in these neurons can bind up to around 120 picomoles of A β /2.5 $\times 10^6$ neurons [24]. This latter result leads to the complexation of the micromolar intracellular CaM concentration, considering the size and the internal volume of mature cerebellar granule neurons. Other proteins known to bind A β peptides with dissociation constants close to 1 nM, i.e., with an affinity similar to that of CaM, are cellular prion protein [25] and glycogen synthase kinase 3 α [26]. However, the expression level of these proteins in neurons is several orders of magnitude lower than that of CaM. Therefore, in neurons, CaM seems to be a major sink for neurotoxic intracellular A β peptides, and this, in turn, suggests that CaM could play a key role in protecting against an increase of free intracellular A β concentrations above 1–2 nM. Based on this, it can be expected that down-regulation of the expression of CaM should make neurons more prone to A β -induced neurotoxicity, because they will suffer a stronger rise in the free intracellular concentration of A β peptides upon β -secretase activation or extracellular A β uptake. Of note, a decrease in the CaM expression level in brains affected by AD has been reported [27].

However, CaM is not only a major protein in cytosolic calcium buffering in neurons; it also has a major role in neuronal metabolism, excitability, and intercellular and intracellular signaling. Thus, A β (1–42):CaM complexes can also function as intracellular transducers for focalized actions of A β peptides, and will be analyzed in the following sections of this review.

2. The Roles of CaM in Neurons as Cytosolic Calcium Buffering and Calcium Signaling Molecule—Subcellular Distribution of CaM-Binding Proteins (CaMBPs) in Neurons

Khachaturian [28] proposed the “calcium hypothesis of brain aging and AD”, which defended the idea that sustained changes in calcium homeostasis could be a common pathway for aging and the neuropathological changes associated with AD. Later, calcium dyshomeostasis in AD received further experimental support. For example, Kuchibhotla et al. [29] reported that the resting Ca $^{2+}$ concentrations in the spines and dendrites of pyramidal neurons in the neocortex are higher than normal in neurons located close to amyloid deposits. Similarly, the resting level of Ca $^{2+}$ in cortical neurons of 3xTg-AD animals was 247 nmol/L, which was twice that found in non-Tg controls (110 nmol/L) [30]. These measurements were consistent with many other studies that indicate that Ca $^{2+}$ signaling is up-regulated in AD [31].

Steady resting cytosolic calcium ranges between 70 and 150 nM in different types of neurons in culture, and peaks below 1 μ M upon transient plasma membrane depolar-

ization by action potentials or upon stimulation by excitatory neurotransmitters [32–36]. In addition, there are large time-dependent and space-dependent fluctuations in calcium concentrations within different cytosolic regions, soma, and axo-dendritic extensions upon neuronal stimulation. Furthermore, the association with plasma membrane lipid raft nanodomains of voltage-operated calcium channels, NMDA and AMPA-glutamate receptors, and plasma membrane calcium pumps, leads to the generation of high calcium concentration transients near the plasma membrane, both in the soma and synapses [36,37]. Since the dissociation constant of calcium from CaM is relatively high, i.e., between 0.2 and 0.5 μM [23,38], the potency of CaM as a calcium buffer in different cytosolic compartments in neurons is, not only dependent on the local concentration of CaM, but also on the local concentration of free calcium. In addition, fluctuations of cytosolic calcium in neurons strongly shift the equilibrium between the calcium-saturated open conformation of $\text{Ca}^{2+}\text{-CaM}$ ($\text{Ca}^{2+}_4\text{-CaM}$) and the close conformation of apo-CaM (minus Ca^{2+}) [38]. Although the interaction of $\text{A}\beta(1\text{-}42)$ with CaM did not significantly alter calcium binding to CaM, the affinity of $\text{A}\beta(1\text{-}42)$ for apoCaM was found to be approximately 20-fold lower [23].

The CaM conformation changes from a closed to open configuration upon calcium-binding and allows $\text{Ca}^{2+}\text{/CaM}$ to bind target proteins with high affinity ($K_d = 10^{-7}$ to 10^{-11} M) [39,40]. The majority of CaMBPs bind $\text{Ca}^{2+}\text{-CaM}$, while a small number of proteins, such as neuromodulin and neurogranin, only bind to apo-CaM [41].

CaM binds and modulates the activity of the plasma membrane calcium pump (PMCA), a protein that has a recognized major role in the control of the homeostasis of cytosolic calcium in neurons [35,42,43]. In addition, CaMBPs play a major role in neuronal function and excitability, and many of them present significant compartmentation within subcellular neuronal structures. In this review, we will focus on CaMBPs expressed in specific brain areas (hippocampus and cerebral entorhinal, and temporal and frontal cortex), which are prone to degeneration in AD and of which functional impairment has been suggested to underlie the loss of neuronal functions and/or intracellular calcium dysregulation in this disease.

Tau and $\text{A}\beta$ peptides are components of neuropathological hallmarks of AD, and tau, amyloid β precursor protein, and β -site APP-cleaving enzyme 1 (BACE1) are CaMBPs [44,45]. In addition, CaM binds and modulates the activity of several protein kinases involved in tau hyperphosphorylation, such as CaMKII, cyclin-dependent kinase 5, and glycogen synthase kinase 3 α [26,46]. Tau belongs to the family of microtubule-associated proteins that function in microtubule assembly and stability; tubulin itself and microtubule-associated protein 2 are also CaMBPs [47,48].

CaMKs (CaMKI-IV) are a family of serine/threonine (Ser/Thr) protein kinases [49], which are abundantly expressed in the brain; in some regions, such as the hippocampus, CaMKII levels can reach to 2% of total proteins [50]. Upon activation by $\text{Ca}^{2+}\text{/CaM}$ binding, CaMKs phosphorylate Ser/Thr residues of their target proteins and trigger the activity of different substrates [51]. The multiplicity of substrates is a key feature of multifunctional CaMKs, since this modulates the activity of many neuronal Ca^{2+} effectors that mediate a wide range of neuronal processes that are critical for cognition and many other brain functions. CaMKII is the most studied member of the CaMK family owing to its central role in neuronal plasticity and cognitive functions, such as learning [52]. CaMKII has different properties according to its subunit composition and isoform type (α , β , γ , and δ), because each isoform has different features, such as calcium trapping kinetics, subcellular distribution, and affinity for other proteins [53,54]. The $\text{Ca}^{2+}\text{/CaM}$ complex binds to the regulatory region of CaMKII and produces a conformational change that activates the phosphorylation of its substrates [55] as well as autophosphorylation at Thr286 in the α isoform and Thr287 in the β , γ , and δ isoforms [54]. Autophosphorylation prevents the enzyme from reverting to its inactive form and maintains CaMKII activity, even after the intracellular Ca^{2+} levels decrease, which allows for CaMKII-autonomous and Ca^{2+} -independent activities [56]. Many studies have shown that α -CaMKII activity is essential

for the induction of long-term potentiation (LTP) in hippocampal slices, spatial learning, and memory [57–63].

Calcineurin (or protein phosphatase 2B) is a Ca^{2+} and calmodulin-dependent Ser/Thr protein phosphatase [64], which is activated by nanomolar concentrations of Ca^{2+} [65]. Calcineurin regulates proteins that play key roles in synaptic transmission and neuronal excitability [66]. Calcineurin is mostly expressed in the cerebral cortex, hippocampus, and striatum, as well as in the cerebellum [67]. In neurons, calcineurin is found in the perikarya and nucleus [67] and in synaptic terminals [68]. Depending on the strength, duration, and site of Ca^{2+} stimulus, calcineurin may either increase or decrease synaptic efficacy and cell excitability through the modulation of ion channels, neurotransmitter receptors, cytoskeletal proteins, kinases, other phosphatases, and transcription factors [69].

Neuronal nitric oxide synthase (nNOS) and adenylyl cyclases 1 and 8 (AC1 and AC8) are other types of $\text{Ca}^{2+}/\text{CaM}$ -stimulated enzymes that generate second intracellular messengers of high relevance for learning and memory [70–72]. nNOS is highly expressed in the hippocampus with a widespread intracellular distribution (nucleus, cytoplasm, plasma membrane, and synaptic spines) and mediates synaptic plasticity, including LTP and neuronal survival and signaling [72,73]. AC1 is the only adenylyl cyclase specific to neurons and is expressed in the hippocampus and cerebellum [71,74], while AC8 is expressed mainly in the hippocampus and slightly in the cortex [70,71]. AC1 is directly stimulated by CaM and calcium at a concentration just above that of resting free Ca^{2+} in neurons (150–200 nM) [70,75]. AC8 is also stimulated by CaM, but its Ca^{2+} sensitivity is approximately five-fold lower than that of AC1 [76]. Both ACs are required for some types of synaptic plasticity, including LTP and long-term memory formation (LTM) [70,77]. In addition, overexpression of AC1 in mouse forebrain showed an increase in memory for novel objects and enhanced L-LTP [21,78]; however, as noted above, a sustained dysregulation of calcium homeostasis has been reported in AD [31,41] and it should be noted that $\text{Ca}^{2+}/\text{CaM}$ -dependent phosphodiesterase isoforms modulate intracellular cAMP dynamics in response to elevation of cytosolic Ca^{2+} [79].

Ion channels, such as the small-conductance potassium (SK) channels, KCNQ potassium channels, cyclic nucleotide-gated channels, NMDAR, transient receptor potential channels, ryanodine receptors (RyR), voltage-gated Ca^{2+} channels (VGCCs), and voltage-gated Na channels, are also modulated by CaM [80]. In this work, we will only highlight the modulation of Ca^{2+} channels that are recognized to play a major role in learning and memory, two brain functions that are largely impaired in AD, by CaM.

Calcium influx through VGCCs is crucial for vesicular release of neurotransmitters, intracellular signaling pathways, gene expression, and synaptic plasticity [81]. Among them, L-type VGCC (LTCC) plays an important role in neuronal plasticity, learning and memory, and an alteration in the function and/or regulation of these channels has been associated with neuropsychiatric diseases, migraine headaches, cerebellar ataxia, autism, schizophrenia, bipolar disorder, and depression [82,83]. The isoforms of LTCC, Cav1.2 and Cav1.3, are more highly expressed in the brain, and they have received increased attention regarding their role in neurological and psychiatric diseases [82]. Both Cav1.2 and Cav1.3 can be found in neuronal cell bodies and proximal dendrites in the hippocampus and have been involved in the regulation of many Ca^{2+} -dependent functions, e.g., protein phosphorylation, enzyme activity, gene expression, and neurotransmission [84]. Furthermore, calcium influx through LTCC is limited by constitutively bound CaM, which leads to Ca^{2+} -dependent inactivation [85] and prevents neuronal damage due to excessive Ca^{2+} entry [86]. Briefly, the CaM conformational change upon Ca^{2+} binding promotes inactivation of LTCC by interaction with additional effector sites of the C-terminal domain in Cav1.2, and, in case of Cav1.3, also of the N-terminal domain [86]. The strength of Ca^{2+} -dependent inactivation can be adjusted by regulating the strength of CaM binding by displacement of CaM from its C-terminal interaction sites [86,87].

NMDAR are critical for the expression of LTP in hippocampal and cortical regions [88,89], and overexpression of the NR2B subunit in the hippocampus has been found to increase

the amplitude of LTP in the CA1 region and to enhance learning in mice [90]. NMDAR can be directly or indirectly modulated by CaM or CaMKII, respectively [91]. In direct CaM-NMDAR modulation, after calcium entry, CaM induces inactivation of NMDAR through a reduction of its open rate and mean open time by binding to two regions of the C terminal domain of the NR1 subunit, i.e., a high affinity site at the alternatively spliced C1 exon ($K_d \approx 4$ nM) and a lower affinity site at the neighboring C0 region ($K_d \approx 87$ nM) [92]. This Ca^{2+} -dependent inactivation provides an important feedback inhibition of Ca^{2+} influx, preventing excessive Ca^{2+} entry through NMDAR that can lead to neurodegeneration and excitotoxicity [93]. In addition, the indirect modulation of NMDAR by CaMKII is crucial for LTP and long-term depression (LTD) in the brain [94], as disruption of the interaction of NMDAR/CaMKII produces deficits in hippocampal LTP and spatial learning [95]. In the postsynaptic compartment, Ca^{2+} influx through NMDAR activates CaMKII and its translocation from cytosol to postsynaptic density membranes, where it binds to NMDAR subunit 2B (NR2B) [96]. CaMKII/NR2B binding requires an initial Ca^{2+} /CaM stimulus, but this interaction persists, even after dissociation of CaM from the complex due to the autophosphorylation of CaMKII at Thr286 [94].

Other neuronal CaMBPs expressed in the hippocampus, such as myosin light chain kinase [97,98], spectrin [99], and fodrin [100], play major roles in the cytoskeleton structure and dynamics, and they also play key roles in neuronal activity and interneuronal connectivity. In addition, Ras-guanine nucleotide-releasing factor 1 (Ras-GRF1), which is also expressed in CA1 neurons of the hippocampus, has been shown to be involved in the induction of LTP and LTD associated with spatial learning and long-term memory [101,102]. Finally, glycogen phosphorylase kinase, in addition to its role in the regulation of glycogenolysis in the brain [103], can also phosphorylate the apo-CaM-binding regulatory regions of neuromodulin (Nm) and neurogranin (Ng) [104], which are neuronal specific proteins that are known to play major roles in neuronal plasticity and LTP (see below).

However, at normal resting cytosolic calcium concentrations close to 100 nM or lower in neurons, CaM is mainly in the apo-CaM conformation. Apo-CaM is largely associated with three proteins in neurons: Nm, Ng, and regulator of CaM signaling (RCS) [21]. Nm, also known as GAP43 or B-50 or P-57, is an abundant presynaptic protein and was the first CaMBP discovered to have a higher affinity for CaM in the absence of Ca^{2+} [21]. Nm accumulates in axonal growth cones and helps their navigation to appropriate target sites during the development of the nervous systems [105]. Furthermore, it is involved in neurite extension and neuronal plasticity, neuroregeneration, regulation of neurotransmitter release at the presynaptic terminal, and in LTP [106]. It has been demonstrated that Nm binds to apo-CaM at the presynaptic membrane and releases it locally under two different mechanisms: (1) when there is an increase in intracellular Ca^{2+} or (2) upon phosphorylation at Ser41 by protein kinase C (PKC), which blocks apo-CaM-binding to Nm [106,107].

Ng (also known as RC3, BICKS and P17) is a postsynaptic neuronal-specific CaMBP that is expressed in the cerebral cortex and hippocampus [108]. In neurons, it is expressed in the cytoplasm and in dendritic spines, where it participates in synaptic signaling via regulation of CaM availability [109]. Ng binds to CaM only in calcium-free medium, suggesting that Ng could serve as a reservoir for apo-CaM and as a Ca^{2+} sensor [110]. An IQ motif of Ng mediates its interaction with apo-CaM and with phosphatidic acid, and phosphorylation by PKC at Ser36 blocks the binding of Ng with apo-CaM or phosphatidic acid [111]. Ng-knockout mice display an apparently normal phenotype, but show severe deficits in spatial and emotional learning and a decrease in LTP induction [111] as well as a slightly enhanced LTD [112]. Indeed, Ng mutants lacking the ability to bind to apo-CaM are unable to potentiate synaptic transmissions [110]. In conclusion, similar to Nm, Ng has an important role in the neuroplasticity mechanism of learning and memory [113].

RCS, also known as ARPP-21 or cAMP-regulated phosphoprotein 21kDa, is a PKA-regulated phosphoprotein expressed in brain regions receiving dopaminergic innervation [114]. RCS is enriched in *caudate-putamen*, *substantia nigra*, *nucleus accumbens* and

olfactory tubercle, but also displays intermediate levels of expression in the cerebral cortex and hippocampus [115]. The G protein-coupled receptor (GPCR)-dependent activation of protein kinase A (PKA) leads to phosphorylation of RCS at Ser55, and increases its binding to CaM [116], preventing CaM from binding to CaM-regulated phosphatase calcineurin [21].

3. Modulation by A β of CaMBPs, Which Play Major Roles in A β Production in Neuronal Calcium Homeostasis and LTP

3.1. The Relevance of A β :CaM Complexation for the Regulation of Neurotoxic A β Oligomer Formation

Clinically, AD is divided into sporadic AD (sAD) and familial AD (fAD). The fundamental role of A β in AD is derived from studies of fAD, which accounts for 1–5% of patients with AD [117], who have autosomal dominant mutations or duplications in the amyloid precursor protein (APP) or mutations in the presenilin-1 (PSEN1) and presenilin-2 (PSEN2) genes [118,119]. These mutations result from changes in APP proteolysis by the γ -secretase complex, leading to an increase in the formation of toxic A β (42/40) oligomers, which induce synapse loss and neuronal toxicity [120,121]. As fAD is pathologically similar to sAD, with the difference being that fAD generally has an early onset and the symptoms progress more rapidly, it is believed that A β (1–42) over-production is also a main factor in sAD [121]. PSEN mutations contributes to over 90% of fAD cases, and several studies have shown that intracellular calcium dysregulation due to these mutations takes place before the formation of A β plaques and neurofibrillary tangles (NFT) in AD brains, highlighting that modifications in cytoplasmic calcium may be an early event at the onset of AD [122,123]. The increase of cytosolic calcium, in turn, leads to a CaM-mediated stimulation of the amyloidogenic protease, BACE1. In vitro experiments have shown that this calcium–CaM dependent stimulation of BACE1 is about 2.5-fold [45]. Moreover, Giliberto et al. [124] showed that the treatment of neuronal and neuroblastoma cells with 1 μ M soluble A β (1–42) increased BACE1 transcription and that this was reverted by an anti-A β (1–42) antibody. It has been suggested that this could be due to A β -induced oxidative stress, because this increase in BACE1 transcription was shown to be mediated by the activity of NF κ B [125]. Furthermore, an up-regulation of BACE1 expression in several vascular risk factors for AD development, including hypoxia, hyperglycemia and hypercholesterolemia, has been shown and was reviewed in [126]. Therefore, free A β generates a positive feedback loop of A β production, and this is likely to play a major role in brain degeneration, both in fAD and sAD. On these grounds, lowering of free A β by complexation with CaM can be seen as a cellular defense response to slow down the formation of neurotoxic A β in neurons. In addition, the increase of A β (1–42):CaM complexes elicited by the rise in A β production reduces the availability of free CaM for stimulation of BACE1 activity, providing feedback inhibition of amyloidogenic A β production. Of note, it has been shown that the CaM antagonist W7 stimulates cleavage of APP through a non-amyloidogenic pathway [127,128]. To the best of our knowledge, the possibility that A β (1–42):CaM complexes may also inhibit BACE1 activity has not yet been experimentally assessed.

3.2. The Relevance of A β :CaM Complexation for the Alteration of Intracellular Calcium Homeostasis Induced by A β

PSENs modulate intracellular Ca²⁺ homeostasis through direct interaction with three components of the endoplasmic reticulum (ER), namely, inositol triphosphate receptors (IP3R), RyR, and sarko(endo)plasmic reticulum Ca²⁺-ATPase (SERCA) [129]. Mutations of the PSEN2 gene enhanced Ca²⁺ release through IP3R [130] and mutations in PSENs can also modulate capacitative calcium entry, a refilling mechanism for depleted Ca²⁺ stores [122,131,132]. Store-operated calcium entry (SOCE) disruption is consistently observed in AD and is manifested as attenuated Ca²⁺ entry in the primary neurons of AD mice with human mutant PSEN1 knocked in, or in skin fibroblasts from familial AD patients [133]. In addition, it has been reported that STIM2 expression levels are down-regulated by fAD-linked PS1 mutations and, thus, insufficient signal is transferred to

the plasma membrane to activate SOCE when ER Ca^{2+} is depleted [134]. In addition, PSEN also acts as an ER Ca^{2+} leak channel and fAD mutations in PSEN1 disrupt this function [135,136], leading to overloaded ER Ca^{2+} stores and increased ER Ca^{2+} release in PSEN double knockout fibroblasts and in fibroblasts transfected with mutant PSEN1 and PSEN2 constructs [121]. Additionally, in fAD, PSEN mutations increase RyR-mediated Ca^{2+} release, either due to enhanced expression of channel proteins or sensitization of the channel activity through PSEN–RyR protein interactions [135,137]. In addition, apoE4, a genetic risk factor for AD, may also amplify ER Ca^{2+} release through RyR, thereby stimulating the formation of A β plaques and neurofibrillary tangles [138,139]. In vitro experiments have shown that application of soluble A β oligomers causes a large increase in RyR activity due to an approximately 10-fold increase in the channel open probability [140] and stimulates RyR-mediated Ca^{2+} release in hippocampal neurons in culture [141]. It must be noted that the increase of the open channel activity of RyR was measured with the application of micromolar concentrations of A β (1–42) to skeletal muscle fibers. Thus, it seems that oligomeric A β may only further potentiate excessive ER Ca^{2+} release by direct interaction with RyR at concentrations that are not reached within the neurons at the early stage of AD brain degeneration. However, indirect modulation by A β -induced oxidative stress may underlie the A β -induced activation of RyR observed in hippocampal neurons in culture after 2–3 h of incubation with concentrations of A β (1–42) oligomers $\geq 500 \text{ nM}$ [141]. Therefore, sequestration of A β oligomers by CaM could be expected to protect against the increase of ER Ca^{2+} release through RyR. In addition, it has been reported that mutation or deletion of PSEN alters the ER calcium refilling process through the SERCA pump and may contribute to the pathogenesis of AD [142]. Indeed, it has been recently shown that increasing SERCA activity helps to maintain ER calcium and improves memory and cognition in APP/PSEN1 mice, as SERCA activation can sequester more cytosolic Ca^{2+} and prevent the apoptosis induced by mitochondrial signaling [143].

While ER calcium release stimulates A β production (see above), the produced A β can inhibit the activity of plasma membrane Ca^{2+} extrusion systems, PMCA, and sodium–calcium exchanger (NCX). According to Mata and colleagues, PMCA is the only Ca^{2+} pump in which Ca^{2+} dependence activity is altered in membranes of AD brains compared to control brains and, also, is the only pump in the brain which is directly inhibited by A β [144,145]. Mechanistic studies indicated that A β aggregates are more potent inhibitors of PMCA activity than monomers [145] and the A β inhibitory effect is due to the interaction of A β with the C-terminal tail of PMCA [43]. In addition, the inhibitory effect of A β could be blocked by pretreating the purified protein with $\text{Ca}^{2+}/\text{CaM}$, the main endogenous activator of PMCA [145]. Additionally, A β can inhibit NCX activity, either by direct interaction with the hydrophobic surface of NCX and/or with the lipid bilayer of the plasma membrane [146]. It has been shown that $1 \mu\text{M}$ A β (1–40) stimulates NCX activity three-fold in the reverse mode in human astrocyte-derived glioblastoma cells with a time delay of 400–500 seconds after application of this peptide [147]. The short time for NCX activity modulation by A β (1–40) suggests that this may be due to the direct interaction between this peptide and NCX; however, a titration with submicromolar concentrations of A β (1–40) was not reported by these authors and data are not available to obtain a dissociation constant of this peptide from NCX. Of note, impaired hippocampal LTP and memory-related behaviors have been recently reported for NCX2 $+/-$ or NCX3 $+/-$ mice [148]. The synaptosomal expression of NCX1, NCX2, and NCX3, the three variants of NCX, were investigated in AD parietal cortex by Sokolow et al. [149]. These authors found that NCX2-positive terminals were increased in the AD cohort, while NCX3-positive terminals were reduced, and they demonstrated that the three isoforms co-localized with A β in synaptic terminals [149]. This co-localization could increase the local concentration of A β near NCX, and this would favor the modulation of NCX activity by its direct interaction with A β peptides at lower cytoplasmic free A β concentrations. If this is the case, complexation of A β with CaM should antagonize NCX modulation by A β peptides, protecting against the rise of cytosolic calcium by calcium entry through NCX. Although

these authors also reported that all three variants are up-regulated in nerve terminals containing A β [149], a recent study carried out in APP23 and APP-KI transgenic mice demonstrated that both protein and mRNA levels of NCX2 and NCX3 isoforms were down-regulated in hippocampal CA1 neurons [148]. These findings suggest that further studies are required to unveil the functional modifications and expression patterns of all NCX isoforms and their roles in AD pathology.

Since A β can inhibit the major Ca $^{2+}$ extrusion systems of the neuronal plasma membrane, it can be foreseen that an increased ER Ca $^{2+}$ release, induced by mutations in PSEN proteins, should eventually lead to mitochondrial Ca $^{2+}$ overload and apoptotic pathways. Indeed, this is an effect of exogenous A β peptides that has been experimentally demonstrated [150,151]. Cumulative lines of evidence have demonstrated that mitochondrial Ca $^{2+}$ signaling is altered in AD due to mutations in the PSEN proteins [152,153]. The excess in cytosolic Ca $^{2+}$ caused by enhanced ER Ca $^{2+}$ release caused by mutant PSENs is, at least in part, counterbalanced by the Ca $^{2+}$ uptake through the voltage-dependent anion-selective channel protein and the calcium uniporter of the mitochondria. A sustained increase in mitochondrial Ca $^{2+}$ concentration impairs ATP production, increases reactive oxygen species (ROS) production, and the opening of the mitochondrial permeability transition pore [154]. Several studies have proposed that enhanced neuronal apoptosis and increased ROS production are major factors in the neurodegeneration observed in AD, and the accumulation of mitochondrial Ca $^{2+}$ has been shown to be significantly implicated in these neurotoxic pathways [153,154]. Upregulation of genes related to mitochondrial energy metabolism and apoptosis has been already reported in an AD transgenic mouse model overexpressing a mutant form of APP at different stages of AD progression [155]. This upregulation is likely an adaptive response to restore the mitochondrial functions impaired by the sustained increase in cytosolic Ca $^{2+}$ induced by A β . However, it seems that this is not enough to protect against the loss of mitochondrial function produced by the oxidative damage associated with the overproduction of ROS induced by mutant APP and soluble A β [152]. Indeed, Wang et al. [156,157] demonstrated that essential proteins for mitochondria fission and fusion, which are needed to maintain synaptic activity in healthy neurons, are altered by enhanced A β production when APP is overexpressed in human neuroblastoma cell line M17, and, also, by treatment with oligomeric A β (1–42). Furthermore, these authors showed that altered levels of mitochondrial fission/fusion proteins in M17 cells, and in differentiated hippocampal neurons mimicking changes observed in AD neurons, led to an increase in mitochondrial fragmentation and abnormal distribution, which contribute to mitochondrial and neuronal dysfunction [156,157]. Later, Silva-Álvarez et al. [158] showed that treatment of hippocampal neurons in culture with a concentration of 500 nM A β (1–42) oligomers for 2–5 hours elicits a large loss of mitochondria per neuron with respect to control neurons. In addition, it was shown by Area-Gomez et al. [159] that the contact sites between mitochondria and ER are rich in PSEN, and it was later demonstrated that mutations in PSEN and APP can upregulate mitochondria-associated ER membrane (MAM) functions and generate a substantial increase in ER-mitochondrial connectivity [160]. Since these authors observed the same upregulation in MAM function and ER mitochondrial communication in fibroblasts from patients with sAD, without mutations in PSEN1, PSEN2, and APP, they suggested that MAM-upregulated function is a common feature in both fAD and sAD, and proposed that it may represent a pathogenic initiator of AD [160,161]. In addition, other recent studies have shown that an increase in A β production may perturb mitochondria and mitochondria-ER contact site functions, mediating the neurodegeneration observed in AD, see, e.g., [153,162].

3.3. The Relevance of A β :CaM Complexation for Dysregulation of Calcium-Dependent Neuronal Activity and Excitability Induced by A β

The direct modulation of CaMKII by A β has a strong impact on neuronal activity and excitability. It has been shown that treating hippocampal neurons with A β oligomers impairs α CaMKII activation [163,164] and that A β prevents the activation of CaMKII during hippocampal LTP [165]. The inhibition of CaMKII by A β may be primarily a neu-

ronal defense mechanism because APP can be phosphorylated in vitro by several kinases, including CaMKII [166], and CaMKII is also a tau kinase, which has been suggested to act in priming tau phosphorylation by cyclin-dependent kinase 5 and glycogen synthase kinase β [167,168]. It should be observed here that A β (1–42) has been reported to bind to glycogen synthase kinases 3 α and 3 β with high affinity [26]. Indeed, the reported dissociation constants of A β (1–42) from the glycogen synthase kinase 3 α isoform [26] and from CaM [23] are almost identical, \approx 1 nM. Furthermore, Dunning et al. [26] demonstrated that binding of A β (1–42) to glycogen synthase kinase 3 α stimulates hyperphosphorylation of tau. In addition, glycogen synthase kinase 3 α has been proposed to enhance A β production through γ -secretase stimulation [169]. Therefore, the inhibition of CaMKII by A β may counteract, at least in part, the stimulation of glycogen synthase kinase 3-dependent tau phosphorylation by nanomolar A β concentrations. Moreover, it has been proposed that, outside of synapses, α CaMKII is hyperactive and could contribute to NFT formation since it co-localizes with NFT in the AD brain [164]. To the best of our knowledge, the possibility that CaMKII could also bind A β :CaM complexes has not been experimentally assessed, nor has the putative role of these complexes in A β -induced CaMKII inhibition.

Inhibition of CaMKII prevents against the phosphorylation of nNOS at Ser847, which inhibits the activation of nNOS by Ca $^{2+}$ /CaM [170,171]. This is a neuroprotective effect of CaMKII inhibition by A β , because nitric oxide-induced inhibition of NMDAR protects neurons against the toxicity elicited by the excessive increase in cytosolic Ca $^{2+}$ produced by sustained stimulation of these glutamatergic receptors [172]. It has been shown that nNOS can be inhibited by several A β peptides with inhibitor constants ranging from 0.81 to 14 μ M [173]; however, these high concentrations of A β peptides are unlikely to be reached within the neurons until a late stage of AD brain degeneration.

In vivo, the activation of CaMKII is under the negative control of calcineurin-dependent phosphatase activity [174,175] and is essential for LTP generation [57,176]. Calcineurin-dependent subcellular relocation of autophosphorylated α CaMKII also occurs in A β oligomer-treated primary neuronal cultures [177,178]. A shift of p(T286)- α CaMKII from apical dendrites/spines to the soma of CA3 pyramidal neurons, which is blocked by inhibition of the phosphatase calcineurin, is also found in a mouse model of sAD, in which amyloid oligomers are injected into the ventricles [178]. Post-mortem analyses and studies with AD models indicate that T286-autophosphorylation of α CaMKII is decreased at the synapses in the disease [164]. It should be recalled that this autophosphorylation is essential for NMDAR-dependent LTP at CA1 synapses and for spatial memory formation [179,180]. Indeed, knockdown of CaMKII mimics the reduced surface expression of AMPA receptor subunit GluA1 and decreased AMPA receptor-mediated synaptic transmission, which is reversed by CaMKII overexpression [177]. An analogous observation is seen when treating rat hippocampal slices with A β (1–42). In this experimental model, A β inhibits CaMKII activation and blocks the stimulation-dependent phosphorylation of a CaMKII-specific site on GluA1 [165]. Moreover, treatment that enhances CaMKII activity also improves long-term memory in a mouse model of AD [181].

Acute application of synthetic A β elicits inhibition of LTP in area CA1, or *dentate gyrus*, of rat hippocampus [182–185], as well as in conditioned culture medium containing A β species secreted by cells transfected with human APP [9]. In the *dentate gyrus* A β inhibition of LTP was blocked by specific inhibitors for calcineurin, indicating that increased calcineurin activity contributes to A β -induced LTP inhibition [183]. Thus, A β can also alter LTP by disrupting the dynamic balance between protein phosphorylation and dephosphorylation of CaMKII. It has been proposed that the increase in cytosolic calcium induced by A β triggers calcineurin hyperactivity [186]; however, the possibility that A β and/or A β :CaM complexes might bind to calcineurin does not seem to have been explored until now. At least, this is a priori relevant for the dynamics of tau:calcineurin complexes and ultimately for the modulation of the extent of tau phosphorylation, since binding of Ca $^{2+}$ -CaM to calcineurin disrupts its interaction with tau and lowers its ability to dephosphorylate tau [187]. In addition, despite the fact that extracellular A β applied to

hippocampal slices preferentially targets synapses [13], experimental data are lacking to exclude that A β could alter the association/dissociation kinetics of apo-CaM with CaM reservoir proteins, such as Nm, Ng, or RCS, in synaptic terminals.

Accumulated evidence has demonstrated that soluble A β oligomers bind to NMDAR and induce Ca $^{2+}$ influx [187], which leads to further Ca $^{2+}$ release into the cytosol from internal stores within the spine [188], the major component of spine calcium transients. In addition, it has been demonstrated that A β oligomers associate and co-localize with dendritic trees [189], which are postsynaptic membranes enriched in NMDAR [190]. A direct activation of NMDAR by A β (1–42) oligomers has been demonstrated with NR1/NR2A and NR1/NR2B receptors, heterologously expressed in *Xenopus laevis* oocytes [191], but the binding sites of A β oligomers in NMDAR subunits remain to be identified. This elicits a pathological level of Ca $^{2+}$ signaling, producing a gradual loss of synaptic function and, ultimately, neuronal excitotoxic cell death. However, the molecular mechanisms underlying the activation of NMDAR in the AD brain remain controversial, because NMDAR are activated by oxidative stress [192] and A β oligomers also induce an increase in cellular oxidative stress [187,193]. On the other hand, studies with astroglial and neuronal cells show that A β impairs glutamate uptake/recycling mechanisms, contributing to AD-associated excitotoxicity and neurodegeneration [194,195]. Interestingly, hippocampal neurons are more susceptible to this type of injury than cortical neurons, and in organotypic hippocampal slices, CA1 neurons show greater susceptibility than CA3 or *dentate gyrus* neurons [164]. This reflects the hierarchical decline of brain areas during disease progression [196]. This provides rationale for the clinical trial of memantine, the NMDAR antagonist, as a neuroprotective treatment for AD [197].

LTCC have long been implicated in aging and AD [198]. A decrease in LTCC activity has been reported in the hippocampus of APP/PS1 double-transgenic mice [199]. In a recent study, Poejo et al. [24] reported the inhibition of L-type calcium channels of cerebellar granule neurons by submicromolar cytosolic concentrations of A β (1–42) dimers, likely mediated by A β -CaM complexes. Owing to the high contribution of calcium influx through LTCC to increasing the resting cytosolic calcium in neurons [36,200–202], the inhibition of LTCC by A β seems another compensatory neuroprotection mechanism to prevent pathogenic cytosolic Ca $^{2+}$ dysregulation. Adaptive control of the activity of LTCC upon exposure to A β is also suggested by experiments with astrocytes cultures, since acute exposure of astrocytes to murine A β (1–42) increased the expression of the Cav1.2 $\alpha 1$ -subunit, whereas chronic treatment decreased it, showing that A β can differentially regulate LTCC expression, depending on the incubation time [203]. However, the molecular mechanism(s) accounting for the inhibition of LTCC by A β found in primary cultures of cerebellar granule neurons remains to be settled, as LTCC are activated by CaMK-dependent phosphorylation but are inactivated by CaM binding [204,205]. Noteworthy, nimodipine, a dihydropyridine derivative and LTCC antagonist, has beneficial effects in AD patients and slows the progression of the disease [206]. Although two large-population, long-term cohort studies have proved the protective role of Ca $^{2+}$ channel blockers over other types of antihypertensive drugs on the risk of dementia among elderly hypertensive populations [207,208], the clinical effects of each specific LTCC blocker remain controversial [209].

4. Conclusions

The high affinity of small A β oligomers for CaM and the high concentration of CaM in neurons reveal a major role of CaM for A β buffering in neurons, which protects against the rise of free concentrations of neurotoxic A β peptides. In turn, the concentration of A β -CaM complexes within neurons increases as a function of time after induction of A β production, and free A β will rise sharply when accumulated A β exceeds all available CaM, i.e., when it reaches total micromolar A β . Intraneuronal A β oligomers found in the AD brain can arise from endogenous A β peptide production as well as from vicinal reactive glial cells [210], as inflammation is now recognized to foster AD brain degeneration. The slow kinetics of A β uptake and its internalization by neurons [12,211] is likely one of the factors that

slows down the time course of the neurotoxicity of exogenous A β , and is relevant for the comparison and integration of the results and conclusions of studies performed in cell cultures after exposure to exogenous A β . In addition, lipid rafts have an important function in A β uptake and its internalization in neurons [20,212,213], and associated with them are calcium entry and extrusion systems that control resting cytosolic calcium homeostasis and neuronal excitability, such as PMCA, NCX, LTCC and NMDAR [36,37]. Thus, lipid rafts provide a physical link between the known alteration of cholesterol metabolism and dysregulation of cytosolic calcium in AD. On these grounds, it is to be expected that the A β -triggering of molecular mechanisms for the onset of neuronal cytosolic calcium dysregulation will be different for endogenously generated A β in the early stages of fAD and for the A β produced by vicinal reactive glial cells, probably a major source of A β during AD brain degeneration.

In addition, A β -CaM complexation is likely to play a major role in the functional regulation of CaMBPs by A β , either in sensitivity or activity modulation. This has been largely overlooked until now, and it may have relevant implications for neuronal A β production, since APP and BACE1 are CaMBPs, for tau phosphorylation and for neuronal calcium dysregulation in AD, which mediates loss-of-function and neurodegeneration in AD brains. The identification of the primary target proteins for non-endogenous intraneuronal A β , of which functional impairment initiates cytosolic calcium homeostasis dysregulation as well as the critical point of no return, are still pending issues due to the following major reasons: (1) a lack of assessment of total intracellular A β concentrations in experiments with cell cultures reporting cytosolic calcium dysregulation; (2) a lack of the dissociation constant of the direct interaction between A β and A β -CaM complexes with target proteins; and (3) a lack of measurements of the putative oxidative modifications of calcium channels and pumps in cell cultures after different times of exposure to exogenous A β . It should be recalled that that A β stimulates intracellular ROS production [190] and that the calcium transport systems that are more relevant for the control of intracellular calcium homeostasis are highly sensitive to a sustained cellular oxidative stress [36,214,215]. However, the experimental data accumulated so far allow us to envisage cellular adaptive responses, i.e., up-regulation and down-regulation of gene and protein expression levels, to compensate for the alteration of intracellular calcium homeostasis upon acute and chronic exposure of neurons both in vitro (cell culture) and in vivo (animal models) to A β stress.

Author Contributions: Conceptualization, J.P. and C.G.-M.; methodology, J.P. and C.G.-M.; validation, J.P., J.S., A.M.M. and C.G.-M.; investigation, J.P., J.S., A.M.M. and C.G.-M.; writing—original draft preparation, J.P., J.S. and C.G.-M.; writing—review and editing, J.P., A.M.M. and C.G.-M.; supervision, C.G.-M.; project administration, A.M.M.; funding acquisition, A.M.M. and C.G.-M. All authors have read and agreed to the published version of the manuscript.

Funding: This work has been supported by Grant BFU2017-85723-P of the Spanish Ministerio de Ciencia, Innovación y Universidades (Spanish National R&D program) to Ana M. Mata and Carlos Gutierrez-Merino, and was co-financed by the European Funds for Structural Development (FEDER).

Acknowledgments: Jairo Salazar has been supported by a Predoctoral Fellowship of the Spanish Fundación Carolina (Madrid, Spain).

Conflicts of Interest: The authors declare no conflict of interest. The funders had no role in the design of the study; in the collection, analyses, or interpretation of data; in the writing of the manuscript, or in the decision to publish the results.

Abbreviations

A β	Amyloid β peptide
AC	Adenylate cyclase
AD	Alzheimer's disease
AMPA	α -Amino-3-hydroxy-5-methyl-4-isoxazolepropionic acid
APP	Amyloid precursor protein

BACE1	β -Site APP-cleaving enzyme 1
CaM	Calmodulin
CaMBPs	Calmodulin binding proteins
CaMKs	Ca^{2+} /calmodulin-dependent protein kinases
ER	Endoplasmic reticulum
fAD	Familial or hereditary Alzheimer's disease
IP ₃ R	Inositol trisphosphate receptor
Kd	Dissociation constant
LRP1	Low density lipoprotein receptor-related protein-1
LTCC	L-type calcium channels
LTD	Long-term depression
LTM	Long-term memory
LTP	Long-term potentiation
MAMs	Mitochondria associated ER membranes
NCX	Sodium-calcium exchanger
NFT	Neurofibrillary tangles
Ng	Neurogranin
Nm	Neuromodulin
NMDA	N-methyl D-aspartate
NMDAR	N-methyl D-aspartate receptors
nNOS	Neuronal isoform of nitric oxide synthase
PKA	protein kinase A
PKC	Protein kinase C
PMCA	Plasma membrane calcium pumps
PSEN	Presenilin
RCS	Regulator of calcium signaling
RyR	Ryanodine receptors
ROS	Reactive oxygen species
sAD	Sporadic Alzheimer's disease
SERCA	Sarco(endo)plasmic Ca^{2+} -ATPase
SOCE	Store-operated calcium entry
VGCCs	Voltage-gated calcium channels

References

1. D'Andrea, M.R.; Nagele, R.G.; Wang, H.Y.; Peterson, P.A.; Lee, D.H. Evidence that neurons accumulating amyloid can undergo lysis to form amyloid plaques in Alzheimer's disease. *Histopathology* **2001**, *38*, 120–134. [[CrossRef](#)] [[PubMed](#)]
2. Wirths, O.; Multhaup, G.; Czech, C.; Blanchard, V.; Moussaoui, S.; Tremp, G.; Pradier, L.; Beyreuther, K.; Bayer, T.A. Intraneuronal A β accumulation precedes plaque formation in β -amyloid precursor protein and presenilin-1 double-transgenic mice. *Neurosci. Lett.* **2001**, *306*, 116–120. [[CrossRef](#)]
3. Oddo, S.; Caccamo, A.; Shepherd, J.D.; Murphy, M.P.; Golde, T.E.; Kayed, R.; Metherate, R.; Mattson, M.P.; Akbari, Y.; LaFerla, F.M. Triple-transgenic model of Alzheimer's disease with plaques and tangles: Intracellular A β and synaptic dysfunction. *Neuron* **2003**, *39*, 409–421. [[CrossRef](#)]
4. Oakley, H.; Cole, S.L.; Logan, S.; Maus, E.; Shao, P.; Craft, J.; Guillozet-Bongaarts, A.; Ohno, M.; Disterhoft, J.; Van Eldik, L.; et al. Intraneuronal β -amyloid aggregates, neurodegeneration, and neuron loss in transgenic mice with five familial Alzheimer's disease mutations: Potential factors in amyloid plaque formation. *J. Neurosci.* **2006**, *26*, 10129–10140. [[CrossRef](#)] [[PubMed](#)]
5. Knobloch, M.; Konietzko, U.; Krebs, D.C.; Nitsch, R.M. Intracellular A β and cognitive deficits precede β -amyloid deposition in transgenic arcA β mice. *Neurobiol. Aging* **2007**, *28*, 1297–1306. [[CrossRef](#)]
6. Billings, L.M.; Oddo, S.; Green, K.N.; McGaugh, J.L.; LaFerla, F.M. Intraneuronal A β Causes the Onset of Early Alzheimer's Disease-Related Cognitive Deficits in Transgenic Mice. *Neuron* **2005**, *45*, 675–688. [[CrossRef](#)] [[PubMed](#)]
7. Younkin, S.G. The role of A β 42 in Alzheimer's disease. *J. Physiol. Paris* **1998**, *92*, 289–292. [[CrossRef](#)]
8. Zhang, Y.; McLaughlin, R.; Goodyer, C.G.; Leblanc, A.C. Selective cytotoxicity of intracellular amyloid β peptide1–42 through p53 and Bax in cultured primary human neurons. *J. Cell Biol.* **2002**, *156*, 519–529. [[CrossRef](#)] [[PubMed](#)]
9. Walsh, D.M.; Klyubin, I.; Fadeeva, J.V.; Cullen, W.K.; Anwyl, R.; Wolfe, M.S.; Rowan, M.J.; Selkoe, D.J. Naturally secreted oligomers of amyloid beta protein potently inhibit hippocampal long-term potentiation in vivo. *Nature* **2002**, *416*, 535–539. [[CrossRef](#)]

10. Hu, X.; Crick, S.L.; Bu, G.; Frieden, C.; Pappu, R.V.; Lee, J.-M. Amyloid seeds formed by cellular uptake, concentration, and aggregation of the amyloid- β peptide. *Proc. Natl. Acad. Sci. USA* **2009**, *106*, 20324–20329. [[CrossRef](#)] [[PubMed](#)]
11. Friedrich, R.P.; Tepper, K.; Rönicke, R.; Soom, M.; Westermann, M.; Reymann, K.; Kaether, C.; Fändrich, M. Mechanism of amyloid plaque formation suggests an intracellular basis of A β pathogenicity. *Proc. Natl. Acad. Sci. USA* **2010**, *107*, 1942–1947. [[CrossRef](#)]
12. Jin, S.; Kedia, N.; Illes-Toth, E.; Haralampiev, I.; Prisner, S.; Herrmann, A.; Wanker, E.E.; Bieschke, J. Amyloid- β (1–42) Aggregation Initiates Its Cellular Uptake and Cytotoxicity. *J. Biol. Chem.* **2016**, *291*, 19590–19606. [[CrossRef](#)]
13. Bahr, B.A.; Hoffman, K.B.; Yang, A.J.; Hess, U.S.; Glabe, C.G.; Lynch, G. Amyloid β protein is internalized selectively by hippocampal field CA1 and causes neurons to accumulate amyloidogenic carboxyterminal fragments of the amyloid precursor protein. *J. Comp. Neurol.* **1998**, *397*, 139–147. [[CrossRef](#)]
14. Tang, B.L. Neuronal protein trafficking associated with Alzheimer disease: From APP and BACE1 to glutamate receptors. *Cell Adhes. Migr.* **2009**, *3*, 118–128. [[CrossRef](#)]
15. Zerbinatti, C.V.; Wahrle, S.E.; Kim, H.; Cam, J.A.; Bales, K.; Paul, S.M.; Holtzman, D.M.; Bu, G. Apolipoprotein E and Low Density Lipoprotein Receptor-related Protein Facilitate Intraneuronal A β 42 Accumulation in Amyloid Model Mice. *J. Biol. Chem.* **2006**, *281*, 36180–36186. [[CrossRef](#)]
16. Fuentealba, R.A.; Liu, Q.; Zhang, J.; Kanekiyo, T.; Hu, X.; Lee, J.-M.; Ladu, M.J.; Bu, G. Low-Density Lipoprotein Receptor-Related Protein 1 (LRP1) Mediates Neuronal A β 42 Uptake and Lysosomal Trafficking. *PLoS ONE* **2010**, *5*, e11884. [[CrossRef](#)]
17. Maier, W.; Bednorz, M.; Meister, S.; Roebroek, A.; Weggen, S.; Schmitt, U.; Pietrzik, C.U. LRP1 is critical for the surface distribution and internalization of the NR2B NMDA receptor subtype. *Mol. Neurodegener.* **2013**, *8*, 25. [[CrossRef](#)]
18. Martin, A.M.; Kuhlmann, C.; Trossbach, S.; Jaeger, S.; Waldron, E.; Roebroek, A.; Luhmann, H.J.; Laatsch, A.; Weggen, S.; Lessmann, V.; et al. The functional role of the second NPXY motif of the LRP1 beta-chain in tissue-type plasminogen activator-mediated activation of N-methyl-D-aspartate receptors. *J. Biol. Chem.* **2008**, *283*, 12004–12013. [[CrossRef](#)]
19. Mantuano, E.; Lam, M.S.; Shibayama, M.; Campana, W.M.; Gonias, S.L. The NMDA receptor functions independently and as an LRP1 co-receptor to promote Schwann cell survival and migration. *J. Cell Sci.* **2015**, *128*, 3478–3488. [[CrossRef](#)]
20. Lai, A.Y.; McLaurin, J. Mechanisms of Amyloid-Beta Peptide Uptake by Neurons: The Role of Lipid Rafts and Lipid Raft-Associated Proteins. *Int. J. Alzheimer's Dis.* **2011**, *2011*, 1–11. [[CrossRef](#)]
21. Xia, Z.; Storm, D.R. The role of calmodulin as a signal integrator for synaptic plasticity. *Nat. Rev. Neurosci.* **2005**, *6*, 267–276. [[CrossRef](#)] [[PubMed](#)]
22. Biber, A.; Schmid, G.; Hempel, K. Calmodulin content in specific brain areas. *Exp. Brain Res.* **1984**, *56*, 323–326. [[CrossRef](#)] [[PubMed](#)]
23. Corbacho, I.; Berrocal, M.; Török, K.; Mata, A.M.; Gutierrez-Merino, C. High affinity binding of amyloid β -peptide to cal-modulin: Structural and functional implications. *Biochem. Biophys. Res. Commun.* **2017**, *486*, 992–997. [[CrossRef](#)] [[PubMed](#)]
24. Poejo, J.; Salazar, J.; Mata, A.; Gutierrez-Merino, C. Binding of Amyloid β (1–42)-Calmodulin Complexes to Plasma Membrane Lipid Rafts in Cerebellar Granule Neurons Alters Resting Cytosolic Calcium Homeostasis. *Int. J. Mol. Sci.* **2021**, *22*, 1984. [[CrossRef](#)] [[PubMed](#)]
25. Laurén, J.; Gimbel, D.A.; Nygaard, H.B.; Gilbert, J.W.; Strittmatter, S.M. Cellular prion protein mediates impairment of synaptic plasticity by amyloid- β oligomers. *Nat. Cell Biol.* **2009**, *457*, 1128–1132. [[CrossRef](#)] [[PubMed](#)]
26. Dunning, C.J.; McGauran, G.; Willén, K.; Gouras, G.K.; O'Connell, D.J.; Linse, S. Direct High Affinity Interaction between A β 42 and GSK3 α Stimulates Hyperphosphorylation of Tau. A New Molecular Link in Alzheimer's Disease? *ACS Chem. Neurosci.* **2015**, *7*, 161–170. [[CrossRef](#)]
27. McLachlan, D.R.C.; Wong, L.; Bergeron, C.; Baimbridge, K.G. Calmodulin and Calbindin D28K in Alzheimer Disease. *Alzheimer Dis. Assoc. Disord.* **1987**, *1*, 171–179. [[CrossRef](#)]
28. Khachaturian, Z.S. Calcium Hypothesis of Alzheimer's Disease and Brain Aging. *Ann. N. Y. Acad. Sci.* **1994**, *747*, 1–11. [[CrossRef](#)]
29. Kuchibhotla, K.V.; Goldman, S.T.; Lattarulo, C.R.; Wu, H.-Y.; Hyman, B.T.; Bacskai, B.J. A β Plaques Lead to Aberrant Regulation of Calcium Homeostasis In Vivo Resulting in Structural and Functional Disruption of Neuronal Networks. *Neuron* **2008**, *59*, 214–225. [[CrossRef](#)]
30. Lopez, J.R.; Lyckman, A.; Oddo, S.; LaFerla, F.M.; Querfurth, H.W.; Shtifman, A. Increased intraneuronal resting [Ca $^{2+}$] in adult Alzheimer's disease mice. *J. Neurochem.* **2008**, *105*, 262–271. [[CrossRef](#)]
31. Berridge, M.J. Calcium Signalling and Alzheimer's Disease. *Neurochem. Res.* **2011**, *36*, 1149–1156. [[CrossRef](#)]
32. Berridge, M.J. Neuronal Calcium Signaling. *Neuron* **1998**, *21*, 13–26. [[CrossRef](#)]
33. Garcia, M.L.; Strehler, E.E. Plasma membrane calcium ATPases as critical regulators of calcium homeostasis during neuronal cell function. *Front. Biosci.* **1999**, *4*, D869–D882. [[CrossRef](#)]
34. LaFerla, F.M. Calcium dyshomeostasis and intracellular signalling in Alzheimer's disease. *Nat. Rev. Neurosci.* **2002**, *3*, 862–872. [[CrossRef](#)]
35. Brini, M.; Carafoli, E. Calcium Pumps in Health and Disease. *Physiol. Rev.* **2009**, *89*, 1341–1378. [[CrossRef](#)]
36. Gutierrez-Merino, C.; Marques-Da-Silva, D.; Fortalezas, S.; Samhan-Arias, A.K. Cytosolic Calcium Homeostasis in Neurons—Control Systems, Modulation by Reactive Oxygen and Nitrogen Species, and Space and Time Fluctuations. In *Neurochemistry*; Heinbockel, T., Ed.; InTech: Rijeka, Croatia, 2014; Chapter 3; pp. 59–110.

37. Marques-Da-Silva, D.; Gutierrez-Merino, C. Caveolin-rich lipid rafts of the plasma membrane of mature cerebellar granule neurons are microcompartments for calcium/reactive oxygen and nitrogen species cross-talk signaling. *Cell Calcium* **2014**, *56*, 108–123. [[CrossRef](#)]
38. Chin, D.; Means, A.R. Calmodulin: A prototypical calcium sensor. *Trends Cell Biol.* **2000**, *10*, 322–328. [[CrossRef](#)]
39. Crivici, A.; Ikura, M. Molecular and structural basis of target recognition by calmodulin. *Annu. Rev. Biophys. Biomol. Struct.* **1995**, *24*, 85–116. [[CrossRef](#)]
40. Zhang, M.; Tanaka, T.; Ikura, M. Calcium-induced conformational transition revealed by the solution structure of apo calmodulin. *Nature* **1995**, *2*, 758–767. [[CrossRef](#)]
41. Kaleka, K.S.; Petersen, A.N.; Florence, M.A.; Gerges, N.Z. Pull-down of Calmodulin-binding Proteins. *J. Vis. Exp.* **2012**, *59*, e3502. [[CrossRef](#)]
42. Lopreiato, R.; Giacomello, M.; Carafoli, E. The Plasma Membrane Calcium Pump: New Ways to Look at an Old Enzyme. *J. Biol. Chem.* **2014**, *289*, 10261–10268. [[CrossRef](#)] [[PubMed](#)]
43. Mata, A.M. Functional interplay between plasma membrane Ca^{2+} -ATPase, amyloid β -peptide and tau. *Neurosci. Lett.* **2018**, *663*, 55–59. [[CrossRef](#)]
44. Padilla, R.; Maccioni, R.; Avila, J. Calmodulin binds to a tubulin binding site of the microtubule-associated protein tau. *Mol. Cell. Biochem.* **1990**, *97*, 35–41. [[CrossRef](#)]
45. O’Day, D.H.; Eshak, K.; Myre, M.A. Calmodulin Binding Proteins and Alzheimer’s Disease. *J. Alzheimer’s Dis.* **2015**, *46*, 553–569. [[CrossRef](#)] [[PubMed](#)]
46. Yu, D.-Y.; Tong, L.; Song, G.-J.; Lin, W.-L.; Zhang, L.-Q.; Bai, W.; Gong, H.; Yin, Y.-X.; Wei, Q. Tau binds both subunits of calcineurin, and binding is impaired by calmodulin. *Biochim. Biophys. Acta Mol. Cell Res.* **2008**, *1783*, 2255–2261. [[CrossRef](#)] [[PubMed](#)]
47. Hammond, J.W.; Cai, D.; Verhey, K.J. Tubulin modifications and their cellular functions. *Curr. Opin. Cell Biol.* **2008**, *20*, 71–76. [[CrossRef](#)]
48. Sánchez, C.; Diaz-Nido, J.; Avila, J. Phosphorylation of microtubule-associated protein 2 (MAP2) and its relevance for the regulation of the neuronal cytoskeleton function. *Prog. Neurobiol.* **2000**, *61*, 133–168. [[CrossRef](#)]
49. Wayman, G.A.; Lee, Y.-S.; Tokumitsu, H.; Silva, A.; Soderling, T.R. Calmodulin-Kinases: Modulators of Neuronal Development and Plasticity. *Neuron* **2008**, *59*, 914–931. [[CrossRef](#)]
50. Erondu, N.E.; Kennedy, M.B. Regional distribution of type II Ca^{2+} /calmodulin-dependent protein kinase in rat brain. *J. Neurosci.* **1985**, *5*, 3270–3277. [[CrossRef](#)]
51. Takemoto-Kimura, S.; Suzuki, K.; Horigane, S.-I.; Kamijo, S.; Inoue, M.; Sakamoto, M.; Fujii, H.; Bito, H. Calmodulin kinases: Essential regulators in health and disease. *J. Neurochem.* **2017**, *141*, 808–818. [[CrossRef](#)]
52. Bayer, K.U.; Schulman, H. CaM Kinase: Still Inspiring at 40. *Neuron* **2019**, *103*, 380–394. [[CrossRef](#)]
53. Coultrap, S.J.; Bayer, K.U. CaMKII regulation in information processing and storage. *Trends Neurosci.* **2012**, *35*, 607–618. [[CrossRef](#)]
54. Zalcman, G.; Federman, N.; Romano, A. CaMKII Isoforms in Learning and Memory: Localization and Function. *Front. Mol. Neurosci.* **2018**, *11*, 445. [[CrossRef](#)]
55. Matsuo, N.; Yamasaki, N.; Ohira, K.; Keizo, T.; Keiko, T.; Megumi, E.; Shun, Y.; Tsuyoshi, M. Neural activity changes under-lying the working memory deficit in alpha-CaMKII heterozygous knockout mice. *Front. Behav. Neurosci.* **2009**, *3*, 1–10. [[CrossRef](#)]
56. Hudmon, A.; Schulman, H. Neuronal Ca^{2+} /Calmodulin-Dependent Protein Kinase II: The Role of Structure and Autoregulation in Cellular Function. *Annu. Rev. Biochem.* **2002**, *71*, 473–510. [[CrossRef](#)]
57. Malinow, R.; Schulman, H.; Tsien, R.W. Inhibition of postsynaptic PKC or CaMKII blocks induction but not expression of LTP. *Science* **1989**, *245*, 862–866. [[CrossRef](#)]
58. Silva, A.J.; Paylor, R.; Wehner, J.M.; Tonegawa, S. Impaired spatial learning in α -calcium-calmodulin kinase II mutant mice. *Science* **1992**, *257*, 206–211. [[CrossRef](#)]
59. Bach, M.E.; Hawkins, R.D.; Osman, M.; Kandel, E.R.; Mayford, M. Impairment of spatial but not contextual memory in CaMKII mutant mice with a selective loss of hippocampal ltp in the range of the θ frequency. *Cell* **1995**, *81*, 905–915. [[CrossRef](#)]
60. Mayford, M.; Bach, M.E.; Huang, Y.-Y.; Wang, L.; Hawkins, R.D.; Kandel, E.R. Control of Memory Formation Through Regulated Expression of a CaMKII Transgene. *Science* **1996**, *274*, 1678–1683. [[CrossRef](#)]
61. Frankland, P.W.; O’Brien, C.; Ohno, M.; Kirkwood, A.; Silva, A.J. α -CaMKII-dependent plasticity in the cortex is required for permanent memory. *Nature* **2001**, *411*, 309–313. [[CrossRef](#)]
62. Wang, H.; Shimizu, E.; Tang, Y.-P.; Cho, M.; Kyin, M.; Zuo, W.; Robinson, D.A.; Alaimo, P.J.; Zhang, C.; Morimoto, H.; et al. Inducible protein knockout reveals temporal requirement of CaMKII reactivation for memory consolidation in the brain. *Proc. Natl. Acad. Sci. USA* **2003**, *100*, 4287–4292. [[CrossRef](#)] [[PubMed](#)]
63. Elgersma, Y.; Sweatt, J.D.; Giese, K.P. Mouse Genetic Approaches to Investigating Calcium/Calmodulin-Dependent Protein Kinase II Function in Plasticity and Cognition. *J. Neurosci.* **2004**, *24*, 8410–8415. [[CrossRef](#)] [[PubMed](#)]
64. Sharma, R.K.; Parameswaran, S. Calmodulin-binding proteins: A journey of 40 years. *Cell Calcium* **2018**, *75*, 89–100. [[CrossRef](#)]
65. Klee, C.B.; Ren, H.; Wang, X. Regulation of the Calmodulin-stimulated Protein Phosphatase, Calcineurin. *J. Biol. Chem.* **1998**, *273*, 13367–13370. [[CrossRef](#)]
66. Baumgärtel, K.; Mansuy, I.M. Neural functions of calcineurin in synaptic plasticity and memory. *Learn. Mem.* **2012**, *19*, 375–384. [[CrossRef](#)] [[PubMed](#)]

67. Solà, C.; Tusell, J.M.; Serratosa, J. Comparative study of the distribution of calmodulin kinase II and calcineurin in the mouse brain. *J. Neurosci. Res.* **1999**, *57*, 651–662. [[CrossRef](#)]
68. Kuno, T.; Mukai, H.; Ito, A.; Chang, D.; Kishima, K.; Saito, N.; Tanaka, C. Distinct Cellular Expression of Calcineurin A α and A β in Rat Brain. *J. Neurochem.* **1992**, *58*, 1643–1651. [[CrossRef](#)] [[PubMed](#)]
69. Groth, R.D.; Dunbar, R.L.; Mermelstein, P.G. Calcineurin regulation of neuronal plasticity. *Biochem. Biophys. Res. Commun.* **2003**, *311*, 1159–1171. [[CrossRef](#)]
70. Wang, H.; Storm, D.R. Calmodulin-Regulated Adenylyl Cyclases: Cross-Talk and Plasticity in the Central Nervous System. *Mol. Pharmacol.* **2003**, *63*, 463–468. [[CrossRef](#)]
71. Conti, A.C.; Maas, J.W.; Muglia, L.M.; Dave, B.A.; Vogt, S.K.; Tran, T.T.; Rayhel, E.J.; Muglia, L.J. Distinct regional and sub-cellular localization of adenylyl cyclases type 1 and 8 in mouse brain. *Neuroscience* **2007**, *146*, 713–729. [[CrossRef](#)]
72. Zhou, L.; Zhu, D.-Y. Neuronal nitric oxide synthase: Structure, subcellular localization, regulation, and clinical implications. *Nitric Oxide* **2009**, *20*, 223–230. [[CrossRef](#)]
73. Chen, J.; Tu, Y.; Moon, C.; Matarazzo, V.; Palmer, A.M.; Ronnett, G.V. The localization of neuronal nitric oxide synthase may influence its role in neuronal precursor proliferation and synaptic maintenance. *Dev. Biol.* **2004**, *269*, 165–182. [[CrossRef](#)]
74. Xia, Z.; Refsdal, C.D.; Merchant, K.M.; Dorsa, D.M.; Storm, D.R. Distribution of mRNA for the calmodulin-sensitive adenylyl cyclase in rat brain: Expression in areas associated with learning and memory. *Neuron* **1991**, *6*, 431–443. [[CrossRef](#)]
75. Wu, Z.; Wong, S.T.; Storm, D.R. Modification of the calcium and calmodulin sensitivity of the type I adenylyl cyclase by mu-tagenesis of its calmodulin binding domain. *J. Biol. Chem.* **1993**, *268*, 23766–23768. [[CrossRef](#)]
76. Nielsen, M.D.; Chan, G.C.K.; Poser, S.W.; Storm, D.R. Differential Regulation of Type I and Type VIII Ca²⁺-stimulated Adenylyl Cyclases by Gi-coupled Receptors in Vivo. *J. Biol. Chem.* **1996**, *271*, 33308–33316. [[CrossRef](#)]
77. Wong, S.T.; Athos, J.; Figueroa, X.A.; Pineda, V.V.; Schaefer, M.L.; Chavkin, C.C.; Muglia, L.J.; Storm, D.R. Calcium-Stimulated Adenylyl Cyclase Activity Is Critical for Hippocampus-Dependent Long-Term Memory and Late Phase LTP. *Neuron* **1999**, *23*, 787–798. [[CrossRef](#)]
78. Wang, H.; Ferguson, G.D.; Pineda, V.V.; Cundiff, P.E.; Storm, D.R. Overexpression of type-1 adenylyl cyclase in mouse fore-brain enhances recognition memory and LTP. *Nat. Neurosci.* **2004**, *7*, 635–642. [[CrossRef](#)]
79. Goraya, T.A.; Masada, N.; Ciruela, A.; Willoughby, D.; Clynes, M.A.; Cooper, D.M.F. Kinetic properties of Ca²⁺/calmodulin-dependent phosphodiesterase isoforms dictate intracellular cAMP dynamics in response to elevation of cytosolic Ca²⁺. *Cell Signal.* **2008**, *20*, 359–374. [[CrossRef](#)]
80. Yue, D. Towards a unified theory of calmodulin regulation (calmodulation) of voltage-gated calcium and sodium channels. *Curr. Mol. Pharmacol.* **2016**, *8*, 188–205.
81. Turner, R.W.; Anderson, D.; Zamponi, G.W. Signaling complexes of voltage-gated calcium channels. *Channels* **2011**, *5*, 440–448. [[CrossRef](#)]
82. Berger, S.M.; Bartsch, D. The role of L-type voltage-gated calcium channels Cav1.2 and Cav1.3 in normal and pathological brain function. *Cell Tissue Res.* **2014**, *357*, 463–476. [[CrossRef](#)]
83. Nanou, E.; Catterall, W.A. Calcium Channels, Synaptic Plasticity, and Neuropsychiatric Disease. *Neuron* **2018**, *98*, 466–481. [[CrossRef](#)]
84. Hell, J.W.; Westenbroek, R.E.; Warner, C.; Ahlijanian, M.K.; Prystay, W.; Gilbert, M.M.; Snutch, T.P.; Catterall, W.A. Identification and differential subcellular localization of the neuronal class C and class D L-type calcium channel $\alpha 1$ subunits. *J. Cell Biol.* **1993**, *123*, 949–962. [[CrossRef](#)] [[PubMed](#)]
85. Liang, H.; DeMaria, C.D.; Erickson, M.G.; Mori, M.X.; Alseikhan, B.A.; Yue, D.T. Unified Mechanisms of Ca²⁺ Regulation across the Ca²⁺ Channel Family. *Neuron* **2003**, *39*, 951–960. [[CrossRef](#)]
86. Striessnig, J.; Pinggera, A.; Kaur, G.; Bock, G.; Tuluc, P. L-type Ca²⁺ channels in heart and brain. *Wiley Interdiscip. Rev. Membr. Transp. Signal.* **2014**, *3*, 15–38. [[CrossRef](#)] [[PubMed](#)]
87. Yang, P.S.; Alseikhan, B.A.; Hiel, H.; Grant, L.; Mori, M.X.; Yang, W.; Fuchs, P.A.; Yue, D.T. Switching of Ca²⁺-Dependent Inactivation of CaV1.3 Channels by Calcium Binding Proteins of Auditory Hair Cells. *J. Neurosci.* **2006**, *26*, 10677–10689. [[CrossRef](#)] [[PubMed](#)]
88. Berberich, S.; Punnakkal, P.; Jensen, V.; Pawlak, V.; Seeburg, P.H.; Hvalby, Ø.; Köhr, G. Lack of NMDA Receptor Subtype Selectivity for Hippocampal Long-Term Potentiation. *J. Neurosci.* **2005**, *25*, 6907–6910. [[CrossRef](#)] [[PubMed](#)]
89. Fox, C.J.; Russell, K.I.; Wang, Y.T.; Christie, B.R. Contribution of NR2A and NR2B NMDA subunits to bidirectional synaptic plasticity in the hippocampus in vivo. *Hippocampus* **2006**, *16*, 907–915. [[CrossRef](#)]
90. Tang, Y.-P.; Shimizu, E.; Dube, G.R.; Rampon, C.; Kerchner, G.A.; Zhuo, M.; Liu, G.; Tsien, J.Z. Genetic enhancement of learning and memory in mice. *Nat. Cell Biol.* **1999**, *401*, 63–69. [[CrossRef](#)]
91. Iacobucci, G.J.; Popescu, G.K. Resident Calmodulin Primes NMDA Receptors for Ca²⁺-Dependent Inactivation. *Biophys. J.* **2017**, *113*, 2236–2248. [[CrossRef](#)]
92. Ehlers, M.D.; Zhang, S.; Bernhardt, J.P.; Huganir, R.L. Inactivation of NMDA Receptors by Direct Interaction of Calmodulin with the NR1 Subunit. *Cell* **1996**, *84*, 745–755. [[CrossRef](#)]
93. Wang, C.; Wang, H.-G.; Xie, H.; Pitt, G.S. Ca²⁺/CaM Controls Ca²⁺-Dependent Inactivation of NMDA Receptors by Dimerizing the NR1 C Termini. *J. Neurosci.* **2008**, *28*, 1865–1870. [[CrossRef](#)]

94. Barcomb, K.; Hell, J.W.; Benke, T.A.; Bayer, K.U. The CaMKII/GluN2B Protein Interaction Maintains Synaptic Strength. *J. Biol. Chem.* **2016**, *291*, 16082–16089. [[CrossRef](#)]
95. Zhou, Y.; Takahashi, E.; Li, W.; Halt, A.; Wiltgen, B.; Ehninger, D.; Li, G.-D.; Hell, J.W.; Kennedy, M.B.; Silva, A.J. Interactions between the NR2B Receptor and CaMKII Modulate Synaptic Plasticity and Spatial Learning. *J. Neurosci.* **2007**, *27*, 13843–13853. [[CrossRef](#)]
96. Halt, A.R.; Dallapiazza, R.F.; Zhou, Y.; Stein, I.S.; Qian, H.; Juntti, S.; Wojcik, S.; Brose, N.; Silva, A.J.; Hell, J.W. CaMKII binding to GluN2B is critical during memory consolidation. *EMBO J.* **2012**, *31*, 1203–1216. [[CrossRef](#)]
97. Lei, S.; Czerwinska, E.; Czerwinski, W.; Walsh, M.P.; Macdonald, J.F. Regulation of NMDA Receptor Activity by F-Actin and Myosin Light Chain Kinase. *J. Neurosci.* **2001**, *21*, 8464–8472. [[CrossRef](#)]
98. Li, L.; Wu, X.; Yue, H.; Zhu, Y.; Xu, J. Myosin light chain kinase facilitates endocytosis of synaptic vesicles at hippocampal boutons. *J. Neurochem.* **2016**, *138*, 60–73. [[CrossRef](#)]
99. Liu, C.-H.; Rasband, M.N. Axonal Spectrins: Nanoscale Organization, Functional Domains and Spectrinopathies. *Front. Cell. Neurosci.* **2019**, *13*, 234. [[CrossRef](#)]
100. Nellikka, R.K.; Sreeja, J.S.; Dharmapal, D.; John, R.; Monteiro, A.; Macedo, J.C.; Conde, C.; Logarinho, E.; Sunkel, C.E.; Sengupta, S. α -Fodrin is required for the organization of functional microtubules during mitosis. *Cell Cycle* **2019**, *18*, 2713–2726. [[CrossRef](#)]
101. Li, S.; Tian, X.; Hartley, D.M.; Feig, L.A. Distinct Roles for Ras-Guanine Nucleotide-Releasing Factor 1 (Ras-GRF1) and Ras-GRF2 in the Induction of Long-Term Potentiation and Long-Term Depression. *J. Neurosci.* **2006**, *26*, 1721–1729. [[CrossRef](#)]
102. Manyes, L.; Holst, S.; Lozano, M.; Santos, E.; Fernandez-Medarde, A. Spatial learning and long-term memory impairments in RasGrf1 KO, Ptg1 KO, and double KO mice. *Brain Behav.* **2018**, *8*, e01089. [[CrossRef](#)] [[PubMed](#)]
103. Nadeau, O.W.; Fontes, J.D.; Carlson, G.M. The regulation of glycogenolysis in the brain. *J. Biol. Chem.* **2018**, *293*, 7099–7107. [[CrossRef](#)] [[PubMed](#)]
104. Paudel, H.; Zwiers, H.; Wang, J. Phosphorylase kinase phosphorylates the calmodulin-binding regulatory regions of neuronal tissue-specific proteins B-50 (GAP-43) and neurogranin. *J. Biol. Chem.* **1993**, *268*, 6207–6213. [[CrossRef](#)]
105. Shen, Y.; Mani, S.; Donovan, S.L.; Schwob, J.E.; Meiri, K.F. Growth-Associated Protein-43 Is Required for Commissural Axon Guidance in the Developing Vertebrate Nervous System. *J. Neurosci.* **2002**, *22*, 239–247. [[CrossRef](#)]
106. Denny, J.B. Molecular mechanisms, biological actions, and neuropharmacology of the growth-associated protein GAP-43. *Curr. Neuropharmacol.* **2006**, *4*, 293–304. [[CrossRef](#)]
107. Apel, E.D.; Byford, M.F.; Au, D.; Walsh, K.A.; Storm, D.R. Identification of the protein kinase C phosphorylation site in neuromodulin. *Biochemistry* **1990**, *29*, 2330–2335. [[CrossRef](#)]
108. Neuner-Jehle, M.; Denizot, J.-P.; Mallet, J. Neurogranin is locally concentrated in rat cortical and hippocampal neurons. *Brain Res.* **1996**, *733*, 149–154. [[CrossRef](#)]
109. Huang, K.-P.; Huang, F.L.; Jäger, T.; Li, J.; Reymann, K.G.; Balschun, D. Neurogranin/RC3 Enhances Long-Term Potentiation and Learning by Promoting Calcium-Mediated Signaling. *J. Neurosci.* **2004**, *24*, 10660–10669. [[CrossRef](#)]
110. Zhong, L.; Gerges, N.Z. Neurogranin and synaptic plasticity balance. *Commun. Integr. Biol.* **2010**, *3*, 340–342. [[CrossRef](#)]
111. Díez-Guerra, F.J. Neurogranin, a link between calcium/calmodulin and protein kinase C signaling in synaptic plasticity. *IUBMB Life* **2010**, *62*, 597–606. [[CrossRef](#)]
112. Zhabotinsky, A.M.; Camp, R.N.; Epstein, I.R.; Lisman, J.E. Role of the Neurogranin Concentrated in Spines in the Induction of Long-Term Potentiation. *J. Neurosci.* **2006**, *26*, 7337–7347. [[CrossRef](#)]
113. Kumar, V.; Chichili, V.P.R.; Zhong, L.; Tang, X.; Velazquez-Campoy, A.; Sheu, F.S.; Seetharaman, J.; Gerges, N.Z.; Sivaraman, J. Structural basis for the interaction of unstructured neuron specific substrates neuromodulin and neurogranin with Calmodulin. *Sci. Rep.* **2013**, *3*, 1–9. [[CrossRef](#)]
114. Ouimet, C.C.; Hemmings, H.C.; Greengard, P. ARRP-21, a cyclic AMP-regulated phosphoprotein enriched in dopa-mine-innervated brain regions. II. Immunocytochemical localization in rat brain. *J. Neurosci.* **1989**, *9*, 865–875. [[CrossRef](#)]
115. Girault, J.A.; Walaas, S.I.; Hemmings, H.C.; Greengard, P. ARPP-21, a cAMP-regulated phosphoprotein enriched in dopa-mine-innervated brain regions: Tissue distribution and regulation of phosphorylation in rat brain. *Neuroscience* **1990**, *37*, 317–325. [[CrossRef](#)]
116. Rakshit, S.V.; Olson, P.A.; Nishi, A.; Starkova, N.N.; Fienberg, A.A.; Laird, A.C.; Surmeier, D.J.; Greengard, P. A Network of Control Mediated by Regulator of Calcium/Calmodulin-Dependent Signaling. *Science* **2004**, *306*, 698–701. [[CrossRef](#)]
117. Reitz, C.; Mayeux, R. Alzheimer disease: Epidemiology, diagnostic criteria, risk factors and biomarkers. *Biochem. Pharmacol.* **2014**, *88*, 640–651. [[CrossRef](#)]
118. Goate, A.; Chartier-Harlin, M.C.; Mullan, M.; Brown, J.; Crawford, F.; Fidani, L.; Giuffra, L.; Haynes, A.; Irving, N.; James, L. Segregation of a missense mutation in the amyloid precursor protein gene with familial Alzheimer's disease. *Nature* **1991**, *349*, 704–706. [[CrossRef](#)]
119. Schellenberg, G.; Bird, T.D.; Wijsman, E.M.; Orr, H.T.; Anderson, L.; Nemens, E.; White, J.A.; Bonycastle, L.; Weber, J.L.; Alonso, M.E. Genetic linkage evidence for a familial Alzheimer's disease locus on chromosome 14. *Science* **1992**, *258*, 668–671. [[CrossRef](#)]
120. Hardy, J.; Selkoe, D.J. The amyloid hypothesis of Alzheimer's disease: Progress and problems on the road to therapeutics. *Science* **2002**, *297*, 353–356. [[CrossRef](#)]

121. Supnet, C.; Bezprozvanny, L. The dysregulation of intracellular calcium in Alzheimer disease. *Cell Calcium* **2010**, *47*, 183–189. [[CrossRef](#)]
122. Leissring, M.A.; Akbari, Y.; Fanger, C.M.; Cahalan, M.D.; Mattson, M.P.; LaFerla, F.M. Capacitative Calcium Entry Deficits and Elevated Luminal Calcium Content in Mutant Presenilin-1 Knockin Mice. *J. Cell Biol.* **2000**, *149*, 793–798. [[CrossRef](#)] [[PubMed](#)]
123. Ryazantseva, M.; Skobeleva, K.; Kaznacheyeva, E. Familial Alzheimer's disease-linked presenilin-1 mutation M146V affects store-operated calcium entry: Does gain look like loss? *Biochimie* **2013**, *95*, 1506–1509. [[CrossRef](#)] [[PubMed](#)]
124. Giliberto, L.; Borghi, R.; Piccini, A.; Mangerini, R.; Sorbi, S.; Cirmena, G.; Garuti, A.; Ghetti, B.; Tagliavini, F.; Mughal, M.R.; et al. Mutant Presenilin 1 Increases the Expression and Activity of BACE1. *J. Biol. Chem.* **2009**, *284*, 9027–9038. [[CrossRef](#)] [[PubMed](#)]
125. Buggia-Prevot, V.; Sevalle, J.; Rossner, S.; Checler, F. NFKappaB dependent control of BACE1 promoter transactivation by Abeta42. *J. Biol. Chem.* **2008**, *283*, 10037–10047. [[CrossRef](#)]
126. Tamagno, E.; Guglielmo, M.; Monteleone, D.; Tabaton, M. Amyloid- β Production: Major Link between Oxidative Stress and BACE1. *Neurotox. Res.* **2012**, *22*, 208–219. [[CrossRef](#)]
127. Canobbio, I.; Catricalà, S.; Balduini, C.; Torti, M. Calmodulin regulates the non-amyloidogenic metabolism of amyloid precursor protein in platelets. *Biochim. Biophys. Acta Bioenergy* **2011**, *1813*, 500–506. [[CrossRef](#)]
128. Díaz-Rodríguez, E.; Esparís-Ogando, A.; Monero, J.C.; Yuste, L.; Pandiella, A. Stimulation of cleavage of membrane proteins by calmodulin inhibitors. *Biochem. J.* **2000**, *346*, 359–367. [[CrossRef](#)]
129. Hermes, M.; Eichhoff, G.; Garaschuk, O. Intracellular calcium signalling in Alzheimer's disease. *J. Cell. Mol. Med.* **2009**, *14*, 30–41. [[CrossRef](#)]
130. Leissring, M.A.; Parker, I.; LaFerla, F.M. Presenilin-2 Mutations Modulate Amplitude and Kinetics of Inositol 1,4,5-Trisphosphate-mediated Calcium Signals. *J. Biol. Chem.* **1999**, *274*, 32535–32538. [[CrossRef](#)]
131. Yoo, A.S.; Cheng, I.; Chung, S.; Grenfell, T.Z.; Lee, H.; Pack-Chung, E.; Handler, M.; Shen, J.; Xia, W.; Tesco, G.; et al. Presenilin-Mediated Modulation of Capacitative Calcium Entry. *Neuron* **2000**, *27*, 561–572. [[CrossRef](#)]
132. Popugaeva, E.; Pchitskaya, E.; Bezprozvanny, I. Dysregulation of neuronal calcium homeostasis in Alzheimer's disease—A therapeutic opportunity? *Biochem. Biophys. Res. Commun.* **2017**, *483*, 998–1004. [[CrossRef](#)]
133. Zeiger, W.; Vetrivel, K.S.; Buggia-Prévot, V.; Nguyen, P.D.; Wagner, S.L.; Villereal, M.L.; Thinakaran, G. Ca²⁺ Influx through Store-operated Ca²⁺ Channels Reduces Alzheimer Disease β -Amyloid Peptide Secretion. *J. Biol. Chem.* **2013**, *288*, 26955–26966. [[CrossRef](#)]
134. Sun, S.; Zhang, H.; Liu, J.; Popugaeva, E.; Xu, N.-J.; Feske, S.; White, C.L.; Bezprozvanny, I. Reduced Synaptic STIM2 Expression and Impaired Store-Operated Calcium Entry Cause Destabilization of Mature Spines in Mutant Presenilin Mice. *Neuron* **2014**, *82*, 79–93. [[CrossRef](#)]
135. Tu, H.; Nelson, O.; Bezprozvanny, A.; Wang, Z.; Lee, S.; Hao, Y.; Serneels, L.; Strooper, B.D.; Yu, G.; Bezprozvanny, I. Pre-senilins Form ER Ca²⁺ Leak Channels, a Function Disrupted by Familial Alzheimer's Disease-Linked Mutations. *Cell* **2006**, *126*, 981–993. [[CrossRef](#)]
136. Nelson, O.; Tu, H.; Lei, T.; Bentahir, M.; De Strooper, B.; Bezprozvanny, I. Familial Alzheimer disease-linked mutations specifically disrupt Ca²⁺ leak function of presenilin 1. *J. Clin. Investig.* **2007**, *117*, 1230–1239. [[CrossRef](#)]
137. Rybalchenko, V.; Hwang, S.-Y.; Rybalchenko, N.; Koulen, P. The cytosolic N-terminus of presenilin-1 potentiates mouse ryanodine receptor single channel activity. *Int. J. Biochem. Cell Biol.* **2008**, *40*, 84–97. [[CrossRef](#)]
138. Namba, Y.; Tomonaga, M.; Kawasaki, H.; Otomo, E.; Ikeda, K. Apolipoprotein E immunoreactivity in cerebral amyloid deposits and neurofibrillary tangles in Alzheimer's disease and kuru plaque amyloid in Creutzfeldt-Jakob disease. *Brain Res.* **1991**, *541*, 163–166. [[CrossRef](#)]
139. Ohkubo, N.; Mitsuda, N.; Tamatani, M.; Yamaguchi, A.; Lee, Y.-D.; Ogihara, T.; Vitek, M.P.; Tohyama, M. Apolipoprotein E4 Stimulates cAMP Response Element-binding Protein Transcriptional Activity through the Extracellular Signal-regulated Kinase Pathway. *J. Biol. Chem.* **2001**, *276*, 3046–3053. [[CrossRef](#)]
140. Shtifman, A.; Ward, C.W.; Laver, D.R.; Bannister, M.L.; Lopez, J.R.; Kitazawa, M.; LaFerla, F.M.; Ikemoto, N.; Querfurth, H.W. Amyloid-beta protein impairs Ca²⁺ release and contractility in skeletal muscle. *Neurobiol. Aging* **2010**, *31*, 2080–2090. [[CrossRef](#)]
141. Paula-Lima, A.C.; Hidalgo, C. Amyloid beta-peptide oligomers, ryanodine receptor-mediated Ca⁽²⁺⁾ release, and Wnt-5a/Ca⁽²⁺⁾ signaling: Opposing roles in neuronal mitochondrial dynamics? *Front. Cell Neurosci.* **2013**, *7*, 120–123. [[CrossRef](#)]
142. Green, K.N.; DeMuro, A.; Akbari, Y.; Hitt, B.D.; Smith, I.F.; Parker, I.; LaFerla, F.M. SERCA pump activity is physiologically regulated by presenilin and regulates amyloid β production. *J. Cell Biol.* **2008**, *181*, 1107–1116. [[CrossRef](#)] [[PubMed](#)]
143. Krajnak, K.; Dahl, R. A new target for Alzheimer's disease: A small molecule SERCA activator is neuroprotective in vitro and improves memory and cognition in APP/PS1 mice. *Bioorg. Med. Chem. Lett.* **2018**, *28*, 1591–1594. [[CrossRef](#)] [[PubMed](#)]
144. Berrocal, M.; Marcos, D.; Sepúlveda, M.R.; Pérez, M.; Avila, J.; Mata, A.M. Altered Ca²⁺ dependence of synaptosomal plasma membrane Ca²⁺-ATPase in human brain affected by Alzheimer's disease. *FASEB J.* **2009**, *23*, 1826–1834. [[CrossRef](#)] [[PubMed](#)]
145. Berrocal, M.; Sepulveda, M.R.; Vazquez-Hernandez, M.; Mata, A.M. Calmodulin antagonizes amyloid- β peptides-mediated inhibition of brain plasma membrane Ca²⁺-ATPase. *Biochim. Biophys. Acta Mol. Basis Dis.* **2012**, *1822*, 961–969. [[CrossRef](#)]
146. Wu, A.; Derrico, C.; Hatem, L.; Colvin, R. Alzheimer's amyloid-beta peptide inhibits sodium/calcium exchange measured in rat and human brain plasma membrane vesicles. *Neuroscience* **1997**, *80*, 675–684. [[CrossRef](#)]
147. Unlap, M.T.; Williams, C.; Morin, D.; Siroky, B.; Firtha, A.; Fuson, A.; Dodgen, L.; Kovacs, G.; Komlosi, P.; Ferguson, W.; et al. Amyloid Beta Peptide 1-40 Stimulates the Na⁺/Ca²⁺ Exchange Activity of SNCX. *Curr. Neurovascular Res.* **2005**, *2*, 3–12. [[CrossRef](#)]

148. Moriguchi, S.; Kita, S.; Fukaya, M.; Osanai, M.; Inagaki, R.; Sasaki, Y.; Izumi, H.; Horie, K.; Takeda, J.; Saito, T.; et al. Reduced expression of $\text{Na}^+/\text{Ca}^{2+}$ exchangers is associated with cognitive deficits seen in Alzheimer's disease model mice. *Neuropharmacology* **2018**, *131*, 291–303. [[CrossRef](#)]
149. Sokolow, S.; Luu, S.H.; Headley, A.J.; Hanson, A.Y.; Kim, T.; Miller, C.A.; Vinters, H.V.; Gylys, K.H. High levels of synapto-somal $\text{Na}^+/\text{Ca}^{2+}$ exchangers (NCX1, NCX2, NCX3) co-localized with amyloid-beta in human cerebral cortex affected by Alzheimer's disease. *Cell Calcium* **2011**, *49*, 208–216. [[CrossRef](#)]
150. Ferreira, E.; Oliveira, C.R.; Pereira, C.M. The release of calcium from the endoplasmic reticulum induced by amyloid-beta and prion peptides activates the mitochondrial apoptotic pathway. *Neurobiol. Dis.* **2008**, *30*, 331–342. [[CrossRef](#)]
151. Fonseca, A.C.R.; Ferreira, E.; Oliveira, C.R.; Cardoso, S.M.; Pereira, C.F. Activation of the endoplasmic reticulum stress response by the amyloid-beta 1–40 peptide in brain endothelial cells. *Biochim. Biophys. Acta Mol. Basis Dis.* **2013**, *1832*, 2191–2203. [[CrossRef](#)]
152. Magi, S.; Castaldo, P.; Macrì, M.L.; Maiolino, M.; Matteucci, A.; Bastioli, G.; Gratteri, S.; Amoroso, S.; Lariccia, V. Intracellular Calcium Dysregulation: Implications for Alzheimer's Disease. *BioMed Res. Int.* **2016**, *2016*, 1–14. [[CrossRef](#)]
153. Ryan, K.C.; Ashkavand, Z.; Norman, K.R. The Role of Mitochondrial Calcium Homeostasis in Alzheimer's and Related Diseases. *Int. J. Mol. Sci.* **2020**, *21*, 9153. [[CrossRef](#)]
154. Toglia, P.; Cheung, K.-H.; Mak, D.-O.D.; Ullah, G. Impaired mitochondrial function due to familial Alzheimer's disease-causing presenilins mutants via Ca^{2+} disruptions. *Cell Calcium* **2016**, *59*, 240–250. [[CrossRef](#)]
155. Reddy, P.H.; McWeeney, S.; Park, B.S.; Manczak, M.; Gutala, R.V.; Partovi, D.; Jung, Y.; Yau, V.; Searles, R.; Mori, M.; et al. Gene expression profiles of transcripts in amyloid precursor protein transgenic mice: Up-regulation of mitochondrial metabolism and apoptotic genes is an early cellular change in Alzheimer's disease. *Hum. Mol. Genet.* **2004**, *13*, 1225–1240. [[CrossRef](#)]
156. Wang, X.; Su, B.; Siedlak, S.L.; Moreira, P.I.; Fujioka, H.; Wang, Y.; Casadesus, G.; Zhu, X. Amyloid- β overproduction causes abnormal mitochondrial dynamics via differential modulation of mitochondrial fission/fusion proteins. *Proc. Natl. Acad. Sci. USA* **2008**, *105*, 19318–19323. [[CrossRef](#)]
157. Wang, X.; Su, B.; Lee, H.-G.; Li, X.; Perry, G.; Smith, M.A.; Zhu, X. Impaired Balance of Mitochondrial Fission and Fusion in Alzheimer's Disease. *J. Neurosci.* **2009**, *29*, 9090–9103. [[CrossRef](#)]
158. Silva-Alvarez, C.; Arrázola, M.S.; Godoy, J.A.; Ordenes, D.; Inestrosa, N.C. Canonical Wnt signaling protects hippocampal neurons from $\text{A}\beta$ oligomers: Role of non-canonical Wnt-5a/ Ca^{2+} in mitochondrial dynamics. *Front. Cell. Neurosci.* **2013**, *7*, 97. [[CrossRef](#)]
159. Area-Gomez, E.; de Groof, A.J.; Boldogh, I.; Bird, T.D.; Gibson, G.E.; Koehler, C.M.; Yu, W.H.; Duff, K.E.; Yaffe, M.P.; Pon, L.A.; et al. Presenilins Are Enriched in Endoplasmic Reticulum Membranes Associated with Mitochondria. *Am. J. Pathol.* **2009**, *175*, 1810–1816. [[CrossRef](#)]
160. Area-Gomez, E.; Castillo, M.D.C.L.; Tambini, M.D.; Guardia-Laguarta, C.; De Groof, A.J.C.; Madra, M.; Ikenouchi, J.; Umeda, M.; Bird, T.D.; Sturley, S.L.; et al. Upregulated function of mitochondria-associated ER membranes in Alzheimer disease. *EMBO J.* **2012**, *31*, 4106–4123. [[CrossRef](#)]
161. Schon, E.A.; Area-Gomez, E. Mitochondria-associated ER membranes in Alzheimer disease. *Mol. Cell. Neurosci.* **2013**, *55*, 26–36. [[CrossRef](#)]
162. Schreiner, B.; Hedskog, L.; Wiehager, B.; Ankarcrona, M. Amyloid- β peptides are generated in mitochondria-associated endoplasmic reticulum membranes. *J. Alzheimer's Dis.* **2015**, *43*, 369–374. [[CrossRef](#)]
163. Min, D.; Guo, F.; Zhu, S.; Xu, X.; Mao, X.; Cao, Y.; Lv, X.; Gao, Q.; Wang, L.; Chen, T.; et al. The alterations of $\text{Ca}^{2+}/\text{calmodulin/CaMKII/CaV1.2}$ signaling in experimental models of Alzheimer's disease and vascular dementia. *Neurosci. Lett.* **2013**, *538*, 60–65. [[CrossRef](#)]
164. Ghosh, A.; Giese, K.P. Calcium/calmodulin-dependent kinase II and Alzheimer's disease. *Mol. Brain* **2015**, *8*, 1–7. [[CrossRef](#)]
165. Zhao, D.; Watson, J.B.; Xie, C.-W. Amyloid β Prevents Activation of Calcium/Calmodulin-Dependent Protein Kinase II and AMPA Receptor Phosphorylation During Hippocampal Long-Term Potentiation. *J. Neurophysiol.* **2004**, *92*, 2853–2858. [[CrossRef](#)]
166. Gandy, S.; Czernik, A.J.; Greengard, P. Phosphorylation of Alzheimer disease amyloid precursor peptide by protein kinase C and $\text{Ca}^{2+}/\text{calmodulin}$ -dependent protein kinase II. *Proc. Natl. Acad. Sci. USA* **1988**, *85*, 6218–6221. [[CrossRef](#)]
167. Sengupta, A.; Kabat, J.; Novak, M.; Wu, Q.; Grundke-Iqbali, I.; Iqbal, K. Phosphorylation of tau at both Thr 231 and Ser 262 is required for maximal inhibition of its binding to microtubules. *Arch. Biochem. Biophys.* **1998**, *357*, 299–309. [[CrossRef](#)]
168. Wang, J.Z.; Grundke-Iqbali, I.; Iqbal, K. Kinases and phosphatases and tau sites involved in Alzheimer neurofibrillary degeneration. *Eur. J. Neurosci.* **2007**, *25*, 59–68. [[CrossRef](#)]
169. Phil, C.J.; Wilson, C.A.; Lee, V.M.; Klein, P.S. GSK-3alpha regulates production of Alzheimer's disease amyloid-beta peptides. *Nature* **2003**, *423*, 435–439. [[CrossRef](#)]
170. Hayashi, Y.; Nishio, M.; Naito, Y.; Yokokura, H.; Nimura, Y.; Hidaka, H.; Watanabe, Y. Regulation of Neuronal Nitric-oxide Synthase by Calmodulin Kinases. *J. Biol. Chem.* **1999**, *274*, 20597–20602. [[CrossRef](#)]
171. El-Mliki, N.; Rodrigo, R.; NaghiZadeh, B.; Cauli, O.; Felipo, V. Chronic hyperammonemia reduces the activity of neuronal nitric oxide synthase in cerebellum by altering its localization and increasing its phosphorylation by calcium-calmodulin kinase II. *J. Neurochem.* **2008**, *106*, 1440–1449. [[CrossRef](#)]
172. Lei, S.Z.; Pan, Z.-H.; Aggarwal, S.K.; Chen, H.-S.V.; Hartman, J.; Sucher, N.J.; Lipton, S.A. Effect of nitric oxide production on the redox modulatory site of the NMDA receptor-channel complex. *Neuron* **1992**, *8*, 1087–1099. [[CrossRef](#)]

173. Padayachee, E.; Ngqwala, N.; Whiteley, C.G. Association of β -amyloid peptide fragments with neuronal nitric oxide synthase: Implications in the etiology of Alzheimers disease. *J. Enzym. Inhib. Med. Chem.* **2011**, *27*, 356–364. [CrossRef] [PubMed]
174. Lisman, J. The CaM kinase II hypothesis for the storage of synaptic memory. *Trends Neurosci.* **1994**, *17*, 406–412. [CrossRef]
175. Lisman, J.; Schulman, H.; Cline, H.T. The molecular basis of CaMKII function in synaptic and behavioural memory. *Nat. Rev. Neurosci.* **2002**, *3*, 175–190. [CrossRef]
176. Silva, A.; Stevens, C.; Tonegawa, S.; Wang, Y. Deficient hippocampal long-term potentiation in alpha-calcium-calmodulin kinase II mutant mice. *Science* **1992**, *257*, 201–206. [CrossRef]
177. Gu, Z.; Liu, W.; Yan, Z. {beta}-Amyloid impairs AMPA receptor trafficking and function by reducing Ca^{2+} /calmodulin-dependent protein kinase II synaptic distribution. *J. Biol. Chem.* **2009**, *284*, 10639–10649. [CrossRef]
178. Reese, L.C.; Laezza, F.; Woltjer, R.; Taglialatela, G. Dysregulated phosphorylation of Ca^{2+} /calmodulin-dependent protein kinase II- α in the hippocampus of subjects with mild cognitive impairment and Alzheimer’s disease. *J. Neurochem.* **2011**, *119*, 791–804. [CrossRef]
179. Giese, K.P.; Fedorov, N.B.; Filipkowski, R.K.; Silva, A.J. Autophosphorylation of Thr286 of the alpha Calcium-Calmodulin Kinase II in LTP and Learning. *Science* **1998**, *279*, 870–873. [CrossRef]
180. Cooke, S.F.; Bliss, T.V. Plasticity in the human central nervous system. *Brain* **2006**, *129*, 1659–1673. [CrossRef]
181. Wang, D.M.; Yang, Y.J.; Zhang, L.; Zhang, X.; Guan, F.F.; Zhang, L.F. Naringin Enhances CaMKII Activity and Improves Long-Term Memory in a Mouse Model of Alzheimer’s Disease. *Int. J. Mol. Sci.* **2013**, *14*, 5576–5586. [CrossRef]
182. Chen, Q.S.; Kagan, B.L.; Hirakura, Y.; Xie, C.W. Impairment of hippocampal long-term potentiation by Alzheimer amyloid beta-peptides. *J. Neurosci. Res.* **2000**, *60*, 65–72. [CrossRef]
183. Chen, Q.S.; Wei, W.Z.; Shimahara, T.; Xie, C.W. Alzheimer amyloid beta-peptide inhibits the late phase of long-term potentiation through calcineurin-dependent mechanisms in the hippocampal dentate gyrus. *Neurobiol. Learn. Mem.* **2002**, *77*, 354–371. [CrossRef]
184. Kim, J.H.; Anwyl, R.; Suh, Y.H.; Djamgoz, M.B.; Rowan, M.J. Use-dependent effects of amyloidogenic fragments of (beta)-amyloid precursor protein on synaptic plasticity in rat hippocampus in vivo. *J. Neurosci.* **2021**, *21*, 1327–1333. [CrossRef]
185. Wang, H.W.; Pasternak, J.F.; Kuo, H.; Ristic, H.; Lambert, M.P.; Chromy, B.; Viola, K.L.; Klein, W.L.; Stine, W.B.; Krafft, G.A.; et al. Soluble oligomers of beta amyloid (1–42) inhibit long-term potentiation but not long-term depression in rat dentate gyrus. *Brain Res.* **2002**, *924*, 133–140. [CrossRef]
186. Reese, L.C.; Taglialatela, G. A Role for Calcineurin in Alzheimers Disease. *Curr. Neuropharmacol.* **2011**, *9*, 685–692. [CrossRef]
187. De Felice, F.G.; Velasco, P.T.; Lambert, M.P.; Viola, K.; Fernandez, S.J.; Ferreira, S.T.; Klein, W.L. A β Oligomers Induce Neuronal Oxidative Stress through an N-Methyl-D-aspartate Receptor-dependent Mechanism That Is Blocked by the Alzheimer Drug Memantine. *J. Biol. Chem.* **2007**, *282*, 11590–11601. [CrossRef]
188. Emptage, N.; Bliss, T.V.; Fine, A. Single Synaptic Events Evoke NMDA Receptor–Mediated Release of Calcium from Internal Stores in Hippocampal Dendritic Spines. *Neuron* **1999**, *22*, 115–124. [CrossRef]
189. Lacor, P.N.; Buniel, M.C.; Chang, L.; Fernandez, S.J.; Gong, Y.; Viola, K.L.; Lambert, M.P.; Velasco, P.T.; Bigio, E.H.; Finch, C.E.; et al. Synaptic targeting by Alzheimer’s-related amyloid β oligomers. *J. Neurosci.* **2004**, *24*, 10191–10200. [CrossRef]
190. Green, K.N. Calcium in the initiation, progression and as an effector of Alzheimer’s disease pathology. *J. Cell. Mol. Med.* **2009**, *13*, 2787–2799. [CrossRef]
191. Texidó, L.; Martín-Satué, M.; Alberdi, E.; Solsona, C.; Matute, C. Amyloid β peptide oligomers directly activate NMDA receptors. *Cell Calcium* **2011**, *49*, 184–190. [CrossRef]
192. Aizenman, E.; Lipton, S.A.; Loring, R.H. Selective modulation of NMDA responses by reduction and oxidation. *Neuron* **1989**, *2*, 1257–1263. [CrossRef]
193. Cheignon, C.; Tomas, M.; Bonnefont-Rousselot, D.; Faller, P.; Hureau, C.; Collin, F. Oxidative stress and the amyloid beta peptide in Alzheimer’s disease. *Redox Biol.* **2018**, *14*, 450–464. [CrossRef]
194. Parpura-Gill, A.; Beitz, D.; Uemura, E. The inhibitory effects of β -amyloid on glutamate and glucose uptakes by cultured astrocytes. *Brain Res.* **1997**, *754*, 65–71. [CrossRef]
195. Fernández-Tomé, P.; Brera, B.; Arévalo, M.-A.; De Ceballos, M.L. β -Amyloid25–35 inhibits glutamate uptake in cultured neurons and astrocytes: Modulation of uptake as a survival mechanism. *Neurobiol. Dis.* **2004**, *15*, 580–589. [CrossRef]
196. West, M.; Coleman, P.; Flood, D.; Troncoso, J. Differences in the pattern of hippocampal neuronal loss in normal ageing and Alzheimer’s disease. *Lancet* **1994**, *344*, 769–772. [CrossRef]
197. Wang, R.; Reddy, P.H. Role of Glutamate and NMDA Receptors in Alzheimer’s Disease. *J. Alzheimer’s Dis.* **2017**, *57*, 1041–1048. [CrossRef]
198. Agostini, M.; Fasolato, C. When, where and how? Focus on neuronal calcium dysfunctions in Alzheimer’s Disease. *Cell Calcium* **2016**, *60*, 289–298. [CrossRef]
199. Thibault, O.; Pancani, T.; Landfield, P.W.; Norris, C.M. Reduction in neuronal L-type calcium channel activity in a double knock-in mouse model of Alzheimer’s disease. *Biochim. Biophys. Acta Mol. Basis Dis.* **2012**, *1822*, 546–549. [CrossRef] [PubMed]
200. Gutierrez-Merino, C.; Marques-da-Silva, D.; Fortalezas, S.; Samhan-Arias, A.K. The critical role of lipid rafts nanodomains in the cross-talk between calcium and reactive oxygen and nitrogen species in cerebellar granule neurons apoptosis by extra-cellular potassium deprivation. *AIMS Mol. Sci.* **2016**, *3*, 12–29. [CrossRef]

201. Fortalezas, S.; Marques-Da-Silva, D.; Gutierrez-Merino, C. Methyl- β -Cyclodextrin Impairs the Phosphorylation of the β 2 Subunit of L-Type Calcium Channels and Cytosolic Calcium Homeostasis in Mature Cerebellar Granule Neurons. *Int. J. Mol. Sci.* **2018**, *19*, 3667. [[CrossRef](#)] [[PubMed](#)]
202. Willis, M.; Kaufmann, W.A.; Wietzorrek, G.; Hutter-Paier, B.; Moosmang, S.; Humpel, C.; Hofmann, F.; Windisch, M.; Knaus, H.-G.; Marksteiner, J. L-Type Calcium Channel CaV 1.2 in Transgenic Mice Overexpressing Human A β PP751 with the London (V717I) and Swedish (K670M/N671L) Mutations. *J. Alzheimer's Dis.* **2010**, *20*, 1167–1180. [[CrossRef](#)]
203. Daschil, N.; Geisler, S.; Obermair, G.J.; Humpel, C. Short-and long-term treatment of mouse cortical primary astrocytes with β -amyloid differentially regulates the mRNA Expression of L-type calcium channels. *Pharmacology* **2014**, *93*, 24–31. [[CrossRef](#)]
204. Zühlke, R.D.; Pitt, G.S.; Deisseroth, K.; Tsien, R.W.; Reuter, H. Calmodulin supports both inactivation and facilitation of L-type calcium channels. *Nat. Cell Biol.* **1999**, *399*, 159–162. [[CrossRef](#)]
205. Peterson, B.Z.; DeMaria, C.D.; Yue, D.T. Calmodulin Is the Ca²⁺ Sensor for Ca²⁺-Dependent Inactivation of L-Type Calcium Channels. *Neuron* **1999**, *22*, 549–558. [[CrossRef](#)]
206. Birks, J.; López-Arrieta, J.; López-Arrieta, J.M. Nimodipine for primary degenerative, mixed and vascular dementia. *Cochrane Database Syst. Rev.* **2002**, *2002*, CD000147. [[CrossRef](#)]
207. Wu, C.-L.; Wen, S.-H. A 10-year follow-up study of the association between calcium channel blocker use and the risk of dementia in elderly hypertensive patients. *Medicine* **2016**, *95*, e4593. [[CrossRef](#)]
208. Hwang, D.; Kim, S.; Choi, H.; Oh, I.H.; Kim, B.S.; Choi, H.R.; Kim, S.Y.; Won, C.W. Calcium-channel blockers and dementia risk in older adults—National health insurance service—Senior cohort (2002–2013). *Circ. J.* **2016**, *80*, 2336–2342. [[CrossRef](#)]
209. Wang, X.; Zheng, W. Ca²⁺ homeostasis dysregulation in Alzheimer's disease: A focus on plasma membrane and cell organelles. *FASEB J.* **2019**, *33*, 6697–6712. [[CrossRef](#)]
210. Zhao, J.; Connor, T.O.; Vassar, R. The contribution of activated astrocytes to A β production: Implications for Alzheimer's disease pathogenesis. *J. Neuroinflamm.* **2011**, *8*, 150. [[CrossRef](#)]
211. Saavedra, L.; Mohamed, A.; Ma, V.; Kar, S.; de Chaves, E.P. Internalization of β -Amyloid Peptide by Primary Neurons in the Absence of Apolipoprotein E. *J. Biol. Chem.* **2007**, *282*, 35722–35732. [[CrossRef](#)]
212. Kakio, A.; Nishimoto, S.; Yanagisawa, K.; Kozutsumi, Y.; Matsuzaki, K. Interactions of amyloid β -protein with various gangliosides in raft-like membranes: Importance of GM1 ganglioside-bound form as an endogenous seed for Alzheimer amyloid. *Biochemistry* **2002**, *41*, 7385–7390. [[CrossRef](#)]
213. Williamson, R.; Usardi, A.; Hanger, D.P.; Anderton, B.H. Membrane-bound β -amyloid oligomers are recruited into lipid rafts by a fyn-dependent mechanism. *FASEB J.* **2008**, *1552–1559*. [[CrossRef](#)]
214. Hidalgo, C.; Donoso, P. Crosstalk between Calcium and Redox Signaling: From Molecular Mechanisms to Health Implications. *Antioxid. Redox Signal.* **2008**, *10*, 1275–1312. [[CrossRef](#)]
215. Gutierrez-Merino, C. Redox modulation of neuronal calcium homeostasis and its deregulation by reactive oxygen species. In *Free Radicals in Biology and Medicine*; Gutierrez-Merino, C., Leeuwenburgh, C., Eds.; Research Signpost: Kerala, India, 2008; pp. 67–101.



Article

Binding of Amyloid β (1–42)-Calmodulin Complexes to Plasma Membrane Lipid Rafts in Cerebellar Granule Neurons Alters Resting Cytosolic Calcium Homeostasis

Joana Poejo ¹, Jairo Salazar ^{1,2}, Ana M. Mata ^{1,3} and Carlos Gutierrez-Merino ^{1,3*}

¹ Instituto de Biomarcadores de Patologías Moleculares, Universidad de Extremadura, 06006 Badajoz, Spain; joanapoejo86@gmail.com (J.P.); jairochemsalazar@gmail.com (J.S.); anam@unex.es (A.M.M.)

² Departamento de Química, Universidad Nacional Autónoma de Nicaragua-León, León 21000, Nicaragua

³ Departamento de Bioquímica y Biología Molecular y Genética, Facultad de Ciencias, Universidad de Extremadura, 06006 Badajoz, Spain

* Correspondence: carlosgm@unex.es

Abstract: Lipid rafts are a primary target in studies of amyloid β ($A\beta$) cytotoxicity in neurons. Exogenous $A\beta$ peptides bind to lipid rafts, which in turn play a key role in $A\beta$ uptake, leading to the formation of neurotoxic intracellular $A\beta$ aggregates. On the other hand, dysregulation of intracellular calcium homeostasis in neurons has been observed in Alzheimer’s disease (AD). In a previous work, we showed that $A\beta$ (1–42), the prevalent $A\beta$ peptide found in the amyloid plaques of AD patients, binds with high affinity to purified calmodulin (CaM), with a dissociation constant ≈ 1 nM. In this work, to experimentally assess the $A\beta$ (1–42) binding capacity to intracellular CaM, we used primary cultures of mature cerebellar granule neurons (CGN) as a neuronal model. Our results showed a large complexation of submicromolar concentrations of $A\beta$ (1–42) dimers by CaM in CGN, up to 120 ± 13 picomoles of $A\beta$ (1–42) / 2.5×10^6 cells. Using fluorescence microscopy imaging, we showed an extensive co-localization of CaM and $A\beta$ (1–42) in lipid rafts in CGN stained with up to 100 picomoles of $A\beta$ (1–42)-HiLyteTM-Fluor555 monomers. Intracellular $A\beta$ (1–42) concentration in this range was achieved by 2 h incubation of CGN with 2 μ M $A\beta$ (1–42), and this treatment lowered the resting cytosolic calcium of mature CGN in partially depolarizing 25 mM potassium medium. We conclude that the primary cause of the resting cytosolic calcium decrease is the inhibition of L-type calcium channels of CGN by $A\beta$ (1–42) dimers, whose activity is inhibited by CaM: $A\beta$ (1–42) complexes bound to lipid rafts.

Citation: Poejo, J.; Salazar, J.; Mata, A.M.; Gutierrez-Merino, C. Binding of Amyloid β (1–42)-Calmodulin Complexes to Plasma Membrane Lipid Rafts in Cerebellar Granule Neurons Alters Resting Cytosolic Calcium Homeostasis. *Int. J. Mol. Sci.* **2021**, *22*, 1984. <https://doi.org/10.3390/ijms22041984>

Academic Editor: Jean-Pierre Jaffrézou

Received: 24 January 2021

Accepted: 9 February 2021

Published: 17 February 2021

Publisher’s Note: MDPI stays neutral with regard to jurisdictional claims in published maps and institutional affiliations.



Copyright: © 2021 by the author. Licensee MDPI, Basel, Switzerland. This article is an open access article distributed under the terms and conditions of the Creative Commons Attribution (CC BY) license (<http://creativecommons.org/licenses/by/4.0/>).

1. Introduction

Lipid rafts are plasma membrane submicrodomains of sizes between 10 and 100 nm enriched in cholesterol and gangliosides [1]. Amyloid β ($A\beta$) peptides interact with both cholesterol and gangliosides in ganglioside-clustered raft-like membrane microdomains, which potentiate the formation of $A\beta$ oligomers and fibrils in a cholesterol-dependent manner [2–8]. Therefore, due to the high content of gangliosides in the brain and in particular in neurons, lipid rafts can be seen as primary targets for $A\beta$ peptide cytotoxicity. Indeed, it has been reported that exogenous oligomeric $A\beta$ applied to neurons in culture concentrates in lipid rafts [9]. Noteworthy, dimeric nonfibrillar $A\beta$ has been shown to rapidly accumulate in lipid rafts in the Tg2576 mouse model of Alzheimer’s disease (AD) [10], and several studies have reported that lipid rafts play an active role in extracellular $A\beta$ uptake and internalization in neurons, reviewed in [11]. $A\beta$ (1–42) is the prevalent $A\beta$ peptide found in the amyloid plaques of AD patients [12], and it has been shown that

reuptake of extracellular A β (1–42) into neurons can lead to the formation of intracellular aggregates, resulting in neuronal damage and neurotoxicity [13–15]. It is to be remarked that oligomeric species of A β (1–42) are tightly linked to AD pathogenesis and are presumed to be the cause of neuronal damage [16]. This hypothesis is further supported by the results obtained with the triple transgenic (3xTg) AD mice, where the level of intraneuronal A β correlates with synaptic dysfunction and memory impairment [17,18].

Dysregulation of intracellular calcium homeostasis in neurons is a common metabolic feature in both sporadic and familial forms of AD, which by itself can account for enhanced intraneuronal A β production and tau hyperphosphorylation potentiation [19,20]. Noteworthy, calmodulin (CaM), the major calcium buffering protein present in the neuronal cytosol, is significantly decreased in the brain of AD individuals [21]. In a previous work, we showed that A β (1–42) and A β (25–35) had very high affinity for purified CaM, with dissociation constants around 1 nM [22]. However, CaM is not only a cytosolic calcium buffering protein, it is also an intracellular calcium signaling messenger that modulates many neuronal functions whose impairment can lead to significant alterations in neuronal metabolism, excitability, and synaptic activity, and eventually leads to neuronal death (see for example [23–25]). On these grounds, it has been proposed that impairment of intracellular calcium buffering by A β can trigger a pathogenic feed-forward cycle that leads to altered synaptic morphology, neuronal apoptosis, and cognitive impairment [26].

Neuronal lipid rafts are also platforms that have the ability to generate short lived and dynamic high calcium compartments near the plasma membrane of a thickness lower than 1 micrometer [27,28]. In mature cerebellar granule neurons (CGN) in culture, these high calcium sub-microcompartments are built up by the association with lipid rafts of L-type calcium channels (LTCCs), N-methyl D-aspartate receptors, and plasma membrane calcium pumps (PMCA) [27]. As LTCCs and PMCA are the plasma membrane calcium transport systems that play the major role in the control of resting cytosolic calcium concentration in CGN in culture in a 25 mM potassium medium [29–31], lipid rafts also play a major role in the modulation of the excitability of CGN. Interestingly, both LTCCs and PMCA are proteins that bind CaM [32–36]. In addition, other CaM binding proteins are also associated with lipid rafts in mature CGN and other neurons such as calmodulin-dependent protein kinase II (CaMKII) [31,37] and the neuronal isoform of nitric oxide synthase (nNOS) [28,38–40]. Most of these CaM-binding proteins have been reported to be inhibited by A β peptides, namely, CaMKII [41,42], PMCA [36,43], and nNOS [44,45]. However, the possibility of LTCC inhibition by A β (1–42) remains to be experimentally assessed, despite the relevance of LTCC activity for resting cytosolic calcium concentration in neurons, in long-term potentiation/depression (LTP/LTD) [46], and in neuronal function, memory, and cognition [47].

Furthermore, it has been noted that several proteins linked to the production of A β have putative calmodulin binding domains (CaMBDs), and it has been shown that CaM binds to amyloid β precursor protein and β -secretase (BACE1; beta-site amyloid β precursor protein cleaving enzyme 1) [25,48].

This work was performed with mature CGN in culture with the following major aims: (1) to demonstrate CaM complexation with submicromolar A β (1–42) concentrations in neurons; (2) to experimentally assess the co-localization of A β (1–42) and A β (1–42):CaM complexes in neuronal lipid rafts; (3) to experimentally evaluate the alteration of the resting cytosolic calcium concentration by submicromolar concentrations of internalized A β (1–42); and (4) to identify the primary cause of the observed alteration of the resting cytosolic calcium. Upon reaching all these aims, the results of this work revealed that the inhibition of LTCCs by incubation of CGN with A β (1–42) dimers for 2 h elicited a large decrease of resting cytosolic calcium in a partially depolarizing 25 mM potassium medium.

2. Results

2.1. Co-Immunoprecipitation of Calmodulin (CaM) with Submicromolar Concentrations of A β (1–42) in Cerebellar Granule Neurons (CGN) Lysates

In a previous work [22], we showed that the dissociation constant of the complex of A β (1–42) with purified CaM is around 1 nM. Since CaM is a protein that is highly expressed in neurons, it seems likely that this should be a major protein target for nanomolar concentrations of A β (1–42). Since A β (1–42) has been shown to bind to lipid rafts (see above), before running the co-immunoprecipitation assays, the CGN lysates were treated with 10 mM methyl- β -cyclodextrin during 30 min to solubilize lipid rafts and allow for dissociation of the proteins associated with these subcellular structures. The formation of CaM:A β (1–42) complexes in mature CGN has been demonstrated by the co-immunoprecipitation of CaM with the anti-A β (1–42) antibody in CGN lysates in the presence of 0.25 micromoles of A β (1–42)/L, performed as described in detail in the Materials and Methods section (Figure 1A). Of note, the precipitation of a small fraction of CaM molecules observed in the absence of A β (1–42) is likely due to its association with poorly solubilized membrane fragments, because it has been demonstrated that CaM also binds with high affinity to several proteins that are associated with lipid rafts in mature CGN, like PMCA [27,49], LTCCs [27,40,50], and CaMKII [31,37].

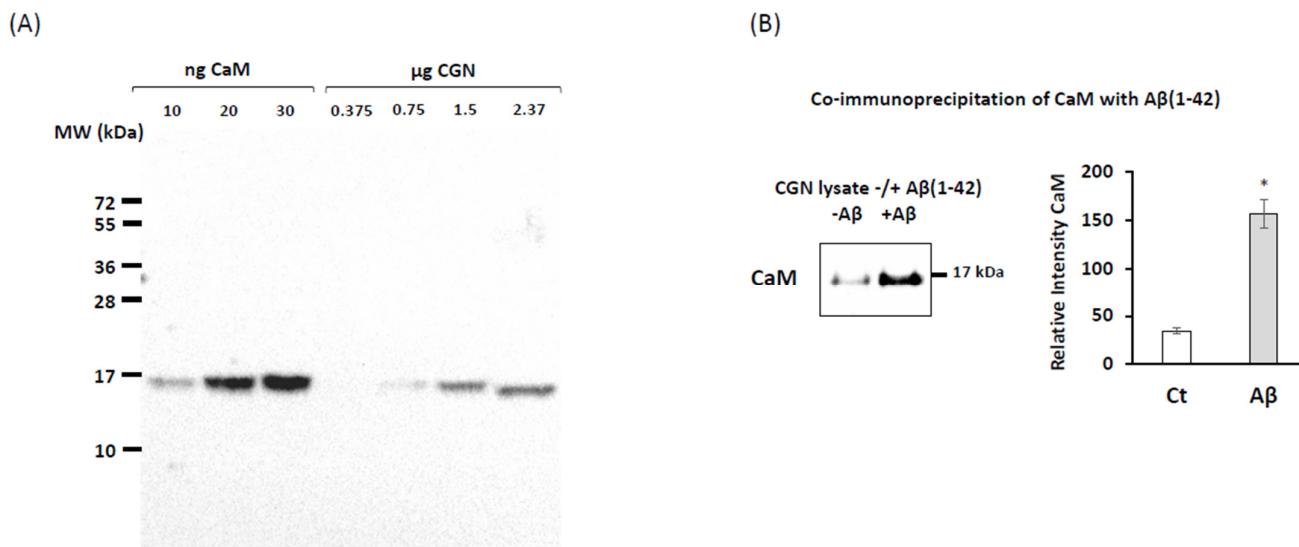


Figure 1. Co-immunoprecipitation between calmodulin (CaM) and A β (1–42). **(A)** Quantification of calmodulin content in cerebellar granule neurons (CGN) lysates. **(B)** Western blotting of CaM (anti-CaM 1716-1, Epitomics) after co-immunoprecipitation assay with mouse anti- β -amyloid antibody (Sigma, A8354), as described in the Materials and Methods section.

The amount of total CaM per microgram of CGN lysate protein was quantified using western blots with different lanes loaded with known amounts of purified CaM and of CGN lysates (Figure 1B). The analysis of the results yielded on average 5.5 ± 0.5 ng of CaM/ μ g of CGN protein. Taking into account that the Petri plates of 35 mm diameter seeded with 2.5×10^6 CGN cells used in this work contained about 170 ± 20 μ g of CGN protein, we calculated that on average, there was 935 ± 110 ng of CaM per plate (i.e., 56 ± 6 picomoles of CaM per plate). Since the A β (1–42) solutions prepared in this work were largely dimers with around 10% of trimers (see Supplementary Figure S1 in the Materials and Methods section), this implies that in these Petri plates containing $2.5 \cdot 10^6$ CGN cells, up to 120 ± 13 picomoles of A β (1–42) can be bound by CaM.

2.2. Fluorescence Resonance Energy Transfer (FRET) Imaging Shows an Extensive Co-Localization between CaM and A β (1–42) HiLyteTM-Fluor555 in Mature CGN

We used fluorescence resonance energy transfer (FRET) imaging to experimentally assess the spatial proximity between A β (1–42) and CaM in mature CGN. To this end, we used the fluorescent derivative A β (1–42) HiLyteTM Fluor555. In addition, we aimed to perform these measurements with the lowest A β (1–42)-HiLyteTM-Fluor555 concentrations as possible to highlight only the subcellular location of the high affinity binding sites for A β (1–42), and using an excitation filter of 470 nm instead of 556 nm to minimize the background fluorescence arising from the binding of A β (1–42)-HiLyteTM-Fluor555 to the Petri plate (see above). Furthermore, these experimental conditions will specifically highlight intracellular A β (1–42) binding sites close to flavoproteins like nNOS and the isoform 3 of cytochrome b₅ reductase, which in mature CGN are associated with lipid rafts [27,40,51,52]. Fluorescence microscopy images of fixed CGN stained with different concentrations of A β (1–42)-HiLyteTM-Fluor555 using an exposure time of 0.4 s (Figure 2) showed that concentrations of A β (1–42)-HiLyteTM-Fluor555 as low as 50–100 nanomoles/L gave a fluorescence intensity significantly higher than the CGN autofluorescence. To minimize the contribution of the endogenous red autofluorescence of CGN, we selected a concentration of 100 nanomoles/L of A β (1–42)-HiLyteTM-Fluor555 for the FRET experiments. In addition, these images and others not shown pointed out that part of A β (1–42)-HiLyteTM-Fluor555 adsorbed non-specifically to the Petri dish plastic. To quantify this unspecific adsorption, 100 picomoles of A β (1–42)-HiLyteTM-Fluor555 monomers was added to a Petri plate with 1 mL of MLocke's K25, incubated under mild stirring during 30 min, and then pipetted from the Petri dish to quartz fluorescence cuvettes. Afterward, the fluorescence was measured in a fluorimeter with excitation and emission wavelengths of 550 and 573 nm and compared with the fluorescence intensity of standard solutions of A β (1–42)-HiLyteTM-Fluor555 prepared directly in the quartz cuvette. The results allowed us to calculate that the free concentration of A β (1–42)-HiLyteTM-Fluor555 readily available for binding to CGN cells was only half of the total A β (1–42)-HiLyteTM-Fluor555 added to the Petri plate (i.e., at most 50 picomoles of A β (1–42)-HiLyteTM-Fluor555 monomers in the total 1 mL volume of each plate).

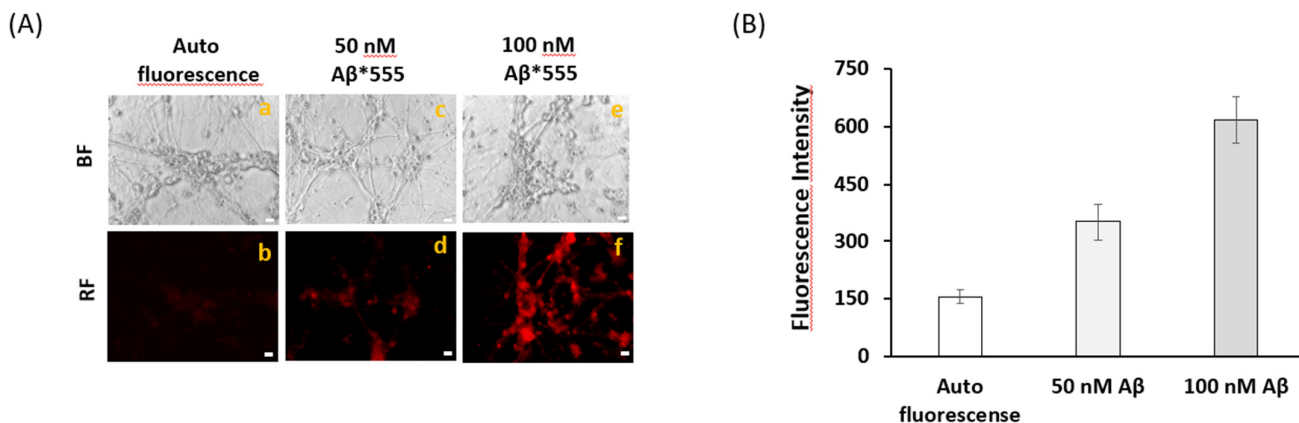


Figure 2. Fluorescence microscopy images of CGN stained with A β (1–42) HiLyteTM-Fluor 555. (A) Representative fluorescence microscopy images of mature CGN without staining-autofluorescence (b) and CGN stained with 50 nM (d) or 100 nM (f) of A β (1–42) HiLyteTM-Fluor 555 incubated for 1 h at 37 °C and 5% CO₂. Bright field (BF) and red fluorescence (RF) images are shown for representative selected fields. The exposure time for RF images was 0.4 s. Scale bar inserted in fluorescence microscopy images = 10 μ m. (B) Quantitative fluorimetric analysis of A β (1–42) HiLyteTM-Fluor 555 bound to CGN. The results yielded a 2.3-fold and 4-fold increase (mean of triplicate experiment \pm s.e.) of the fluorescence of CGN stained with 50 nM and 100 nM A β (1–42) HiLyteTM- Fluor 555 with respect to the CGN autofluorescence, respectively.

FRET imaging between anti-CaM conjugated with IgG-Alexa 488 (anti-CaM*488) was used to experimentally confirm the formation of CaM:A β (1–42) complexes and co-

localization of A β (1–42) with the CaM expressed in mature CGN. Representative fluorescence microscopy images of mature CGN fixed and stained with anti-CaM*A488 in the absence and presence of 100 picomoles of A β (1–42)-HiLyteTM-Fluor555/mL are shown in Figure 3A. The merged image highlighted an extensive co-localization (pixel size 0.2 μ m) between anti-CaM*A488 and A β (1–42)-HiLyteTM-Fluor555, both in the neuronal somas and extensions. The increase in the red/green fluorescence intensity ratio after subtraction of the red intensity by direct excitation of A β (1–42)-HiLyteTM-Fluor555 (Figure 3B) demonstrated that most of the anti-CaM*A488 molecules lay within an efficient FRET distance range with A β (1–42)-HiLyteTM-Fluor555 (i.e., <50 nm) for this donor–acceptor pair. Moreover, the red fluorescence intensity of A β (1–42)-HiLyteTM-Fluor555 was more than 80% quenched by the addition of 5 mM CoCl₂ to the Petri plate, yielding red fluorescence microscopy images like the CGN autofluorescence image shown in Figure 2. Of note, the inner filter effect due to the absorbance of 5 mM Co²⁺ in the wavelength range 470–550 nm, calculated as indicated in the Materials and Methods section, can only account for less than 5% quenching of this fluorescence. Co²⁺ is a well calcium channel blocker at millimolar concentration, and has also been shown to bind to Ca²⁺ sites in proteins (see for example [53,54]). Co²⁺ has a R₀ value of 1.2 nm as the FRET acceptor of the green fluorescence of fluorescein [55]. Therefore, due to the small CaM size, our results were fully consistent with the extensive complexation of A β (1–42)-HiLyteTM-Fluor555 with CaM shown by FRET imaging in CGN.

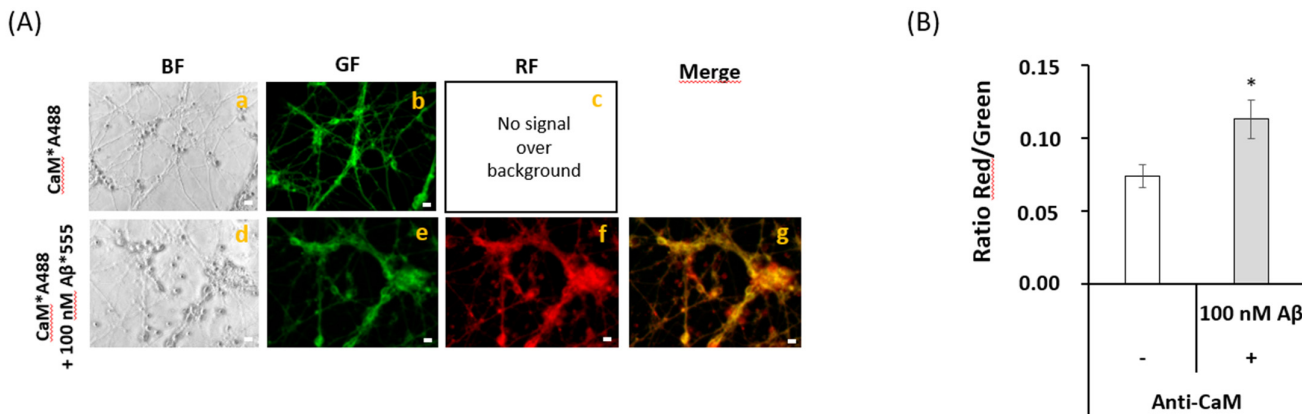


Figure 3. Extensive FRET between anti-CaM antibody stained with a secondary Alexa488 fluorescent antibody and A β (1–42)-HiLyteTM-Fluor 555 in fixed and permeabilized mature CGN. (A) Representative quantitative fluorescence microscopy images of CGN stained with anti-CaM antibody (1716-1)/ IgG-Alexa488 (CaM*A488, a–c) or with anti-CaM/IgG-Alexa488 and A β (1–42) HiLyteTM-Fluor 555 (CaM*A488/A β (1–42), d–g). Bright-field (BF), green fluorescence (GF), and red fluorescence (RF) images are shown for each one of the selected fields, and the orange-yellow areas (Merge image) point out the higher intensity FRET regions (g). The exposure time for GF and RF images was 0.03 s. Scale bar inserted in fluorescence microscopy images = 10 μ m. (B) Ratio of red/green fluorescence intensity per pixel (RF/GF) obtained from the analysis of the fluorescence intensity data of CGN somas stained with anti-CaM*IgG-Alexa488 only (CaM*A488) and double stained with anti-CaM*IgG-Alexa488/A β (1–42) HiLyteTM-Fluor 555 (CaM*A488/A β (1–42)). The results shown in (B) are the mean \pm s.e. (*) p < 0.05 (i.e., statistically significant with respect to the control (CGN labeled with the Alexa488 FRET donor only)).

2.3. FRET Imaging Highlights the Association of A β (1–42)-HiLyteTM-Fluor555 and CaM with Lipid Rafts Markers in Mature CGN

In order to experimentally show that A β (1–42)-HiLyteTM-Fluor555 extensively co-localizes with protein markers of the lipid rafts of mature CGN, we used antibodies against caveolin-1 (Cav-1) and HRas, protein markers of CGN lipid rafts matured in vitro [27], and also cellular prion protein (PrPc), a neuronal marker of lipid rafts that has been shown to form complexes with A β [56,57]. Representative fluorescence microscopy images of mature CGN stained with anti-Cav-1 conjugated with IgG-Alexa 488 (anti-Cav1*A488), anti-HRas conjugated with IgG-Alexa 488 (anti-HRas*A488), and anti-PrPc conjugated

with IgG-Alexa488 (anti-PrPc*A488) in the absence and presence of 100 picomoles of A β (1–42)-HiLyte™-Fluor555/mL are shown in the Figure 4A–C. In all these cases, the addition of A β (1–42)-HiLyte™-Fluor555 elicited a large attenuation of the green fluorescence and an increase in red fluorescence intensity that was higher than the red fluorescence increase expected for the direct excitation of the added A β (1–42)-HiLyte™-Fluor555. The analysis of the red/green fluorescence intensity ratio after correction for the red fluorescence due to direct excitation of A β (1–42)-HiLyte™-Fluor555 pointed out extensive FRET between Alexa 488 conjugates of anti-Cav1, anti-HRas, and anti-PrPc and the Fluor555 dye bound to A β (Figure 4D). Noteworthy, the donor/acceptor FRET pair that showed a higher increase in the ratio of the red/green fluorescence intensity was anti-PrPc*A488/ A β (1–42)-HiLyte™-Fluor555, which is in good agreement with the reported formation of complexes between PrPc and A β , and also with the fact that in this work, we did not find co-immunoprecipitation of Cav-1 and of HRas with A β (see Supplementary Figure S2). This confirmed an extensive association of A β with lipid raft submicrodomains of mature CGN. The merge images also highlight a much larger density of lipid rafts in neuronal somas, since neuronal extensions were less intensely stained with anti-Cav-1*A488, anti-HRas*A488, and anti-PrPc*A488. This latter result is confirmatory of other FRET results reported in previous works with CGN matured in vitro [27,40].

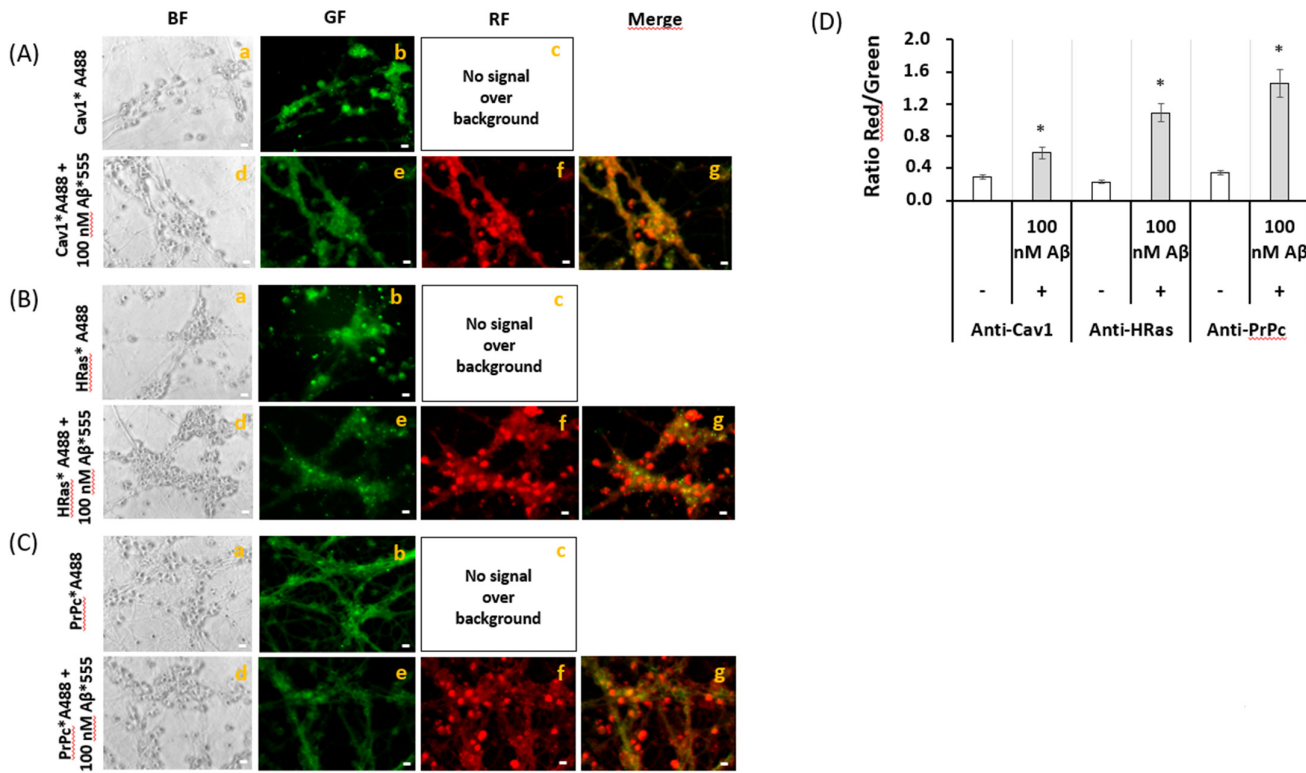


Figure 4. Extensive FRET between the lipid rafts markers Cav1, HRas, PrPc, and A β (1–42). (A) Representative quantitative fluorescence microscopy images of CGN stained with anti-Cav1 antibody (sc-894)/IgG-Alexa488 (Cav1*A488, a–c) or with anti-Cav1/IgG-Alexa488 and A β (1–42) HiLyte™-Fluor 555 (Cav1*A488/A β (1–42), d–g). (B) Representative quantitative fluorescence microscopy images of CGN stained with anti-HRas antibody (sc-32026)/IgG-Alexa488 (HRas*A488, a–c) or with anti-HRas/IgG-Alexa488 and A β (1–42) HiLyte™-Fluor 555 (HRas*A488/A β (1–42), d–g). (C) Representative quantitative fluorescence microscopy images of CGN stained with anti-PrPc antibody (7500997)/IgG-Alexa488 (PrPc*A488, a–c) or with anti-PrPc/IgG-Alexa488 and A β (1–42) HiLyte™-Fluor 555 (PrPc*A488/A β (1–42), d–g). Bright-field (BF), green fluorescence (GF), and red fluorescence (RF) images are shown for each of the selected fields, and the orange-yellow areas (merge image) point out the higher intensity FRET regions (g, (A–C)). The exposure time for GF and RF images was 0.4 s. Scale bar inserted in fluorescence microscopy images = 10 μ m. (D) Ratio of red/green fluorescence intensity per pixel (RF/GF) obtained from the analysis of fluorescence intensity data of CGN somas stained with (i) anti-Cav1/IgG-Alexa488 only (Cav1*A488) and double stained with anti-Cav1*IgG-Alexa488/A β (1–42) HiLyte™-Fluor 555 (Cav1*A488/A β (1–42));

(ii) anti-HRas/IgG-Alexa488 only (HRas*A488) and double stained with anti-HRas*IgG-Alexa488/A β (1–42) HiLyte™-Fluor 555 (HRas*A488/A β (1–42)); and (iii) anti-PrPc/IgG-Alexa488 only (PrPc*A488) and double stained with anti-PrPc*IgG-Alexa488/A β (1–42) HiLyte™-Fluor 555 (PrPc*A488/A β (1–42)). The results shown in panel D are the mean \pm s.e. (*) $p < 0.05$, (i.e., statistically significant with respect to the control, CGN labeled with the Alexa488 FRET donor only).

Representative fluorescence microscopy images of mature CGN stained with anti-CaM conjugated with IgG-Alexa 488 (anti-CaM*A488), anti-HRas conjugated with IgG-Cy3 (anti-HRas*Cy3), and with both anti-CaM*A488 and anti-HRas*Cy3 are shown in Figure 5A. The extensive co-localization of CaM and HRas is shown by the merge image, because pixels that maintain the original green and red colors are hardly seen. The large increase in the red/green ratio of fluorescence intensities in CGN double stained with anti-CaM*A488 and anti-HRas*Cy3 with respect to CGN stained only with anti-HRas*Cy3 (Figure 5B) pointed out a high efficiency of FRET between Alexa 488 and Cy3. Thus, these results showed that most of the anti-CaM*A488 and anti-HRas*Cy3 bound to fixed CGN were within the FRET distance using this experimental approach (i.e., <80 nm [27,50]).

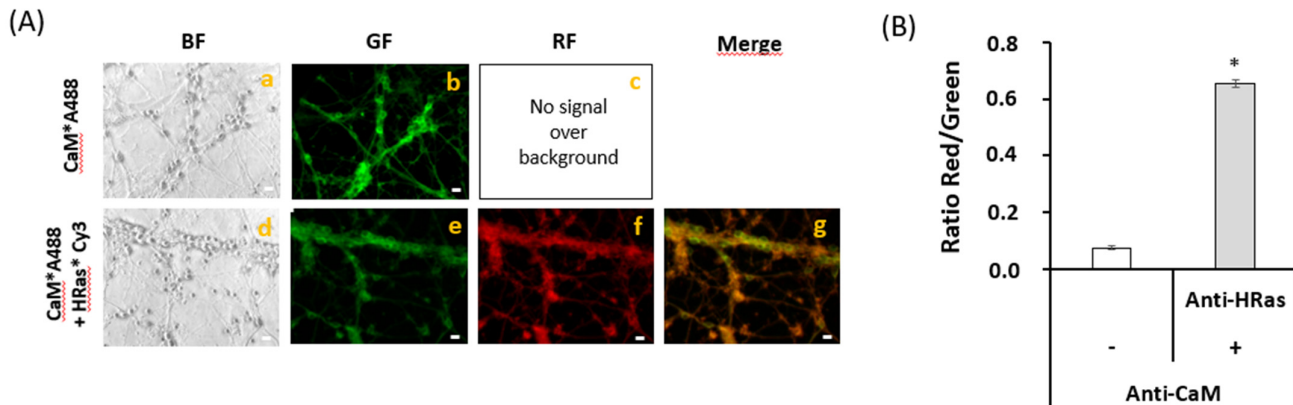


Figure 5. Extensive FRET between CaM and HRas. (A) Representative quantitative fluorescence microscopy images of CGN stained with the anti-CaM antibody (1716-1)/IgG-Alexa488 (CaM*A488, a–c) or with anti-CaM/IgG-Alexa488 and Anti-HRas antibody (sc32026)/IgG-Cy3 (CaM*A488/HRas*Cy3, d–g). Bright-field (BF), green fluorescence (GF), and red fluorescence (RF) images are shown for each of the selected fields, and the orange-yellow areas (Merge image) point out the higher intensity FRET regions (g). The exposure time for GF and RF images was 0.05 s. Scale bar inserted in fluorescence microscopy images = 10 μ m. (B) Ratio of red/green fluorescence intensity per pixel (RF/GF) obtained from the analysis of fluorescence intensity data of CGN somas stained with anti-CaM/IgG-Alexa488 only (CaM*A488) and double stained with anti-CaM*IgG-Alexa488/anti-HRas*IgG-Cy3 (CaM*A488/HRas*Cy3). The results shown in (B) are the mean \pm s.e. (*) $p < 0.05$ (i.e., statistically significant with respect to the control, CGN labeled with the Alexa488 FRET donor only).

2.4. A Short Time Incubation with Submicromolar Concentrations of A β (1–42) Decreases the Resting Cytosolic Calcium Concentration through Inhibition of L-Type Calcium Channels (LTCCs) in Mature CGN

Figure 6 shows that 48 h incubation of mature CGN with up to 5 μ M A β (1–42) produced, at most, 10–20% loss of cell viability assayed with the 3-(4,5-dimethylthiazol-2-yl)-2,5-diphenyltetrazolium bromide (MTT) method. Therefore, this allowed us to study the effects on cytosolic calcium dysregulation produced by the incubation of CGN for several hours with micromolar concentrations of this peptide. However, a shorter time of incubation with extracellular micromolar concentrations of A β (1–42) is needed to study the effect of submicromolar intracellular concentrations of this peptide on resting calcium concentration, because it has been shown that small oligomeric states of this peptide are internalized in neurons with a half-time of 12–14 h [15].

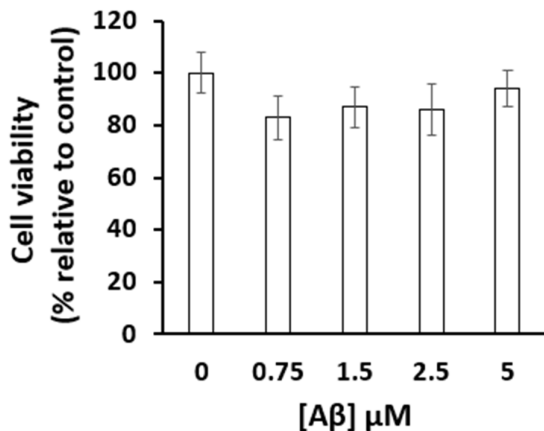


Figure 6. The cell viability of mature CGN was not significantly affected by A β (1–42) at the concentrations tested (0.75–5 μM) after 48 h of incubation at 37 °C and 5%CO₂. Cell viability was measured using the 3-(4,5-dimethylthiazol-2-yl)-2,5-diphenyltetrazolium bromide (MTT) assay as indicated in the Materials and Methods section. The results were the average \pm s.e. of experiments done in triplicate, with two different preparations of CGN.

Figure 7 shows that 2–5 h incubation of CGN in MLocke's K25 medium with 2 μM A β (1–42) produced a statistically significant decrease of the Fura-2 ratio 340/380 from 1.1 \pm 0.1 to 0.71 \pm 0.07 ($p < 0.05$), in other words, from $[\text{Ca}^{2+}]_i$ 160 \pm 30 nM to 71 \pm 7 nM. However, this treatment did not significantly change the ratio 340/380 measured after the addition of the LTCC blocker 2 μM nifedipine ($p > 0.05$), as shown also in Figure 7. Therefore, A β (1–42) reduces the specific contribution of LTCCs to the resting cytosolic calcium concentration in mature CGN in MLocke's K25 medium. Indeed, the difference between the ratio 340/380 in the absence and presence of nifedipine decreased from 0.64 in CGN non-treated with amyloid β (1–42) to 0.30 and 0.32 in CGN incubated with 2 μM A β (1–42) during 2 and 5 h, respectively. Controls run with up to 2 h incubation with 2 μM of scrambled A β (1–42) peptide did not produce alterations of the resting cytosolic calcium (data not shown). Thus, these results pointed out that 2 hours of the incubation of mature CGN with A β (1–42) were enough to produce about 50% inhibition of LTCC activity.

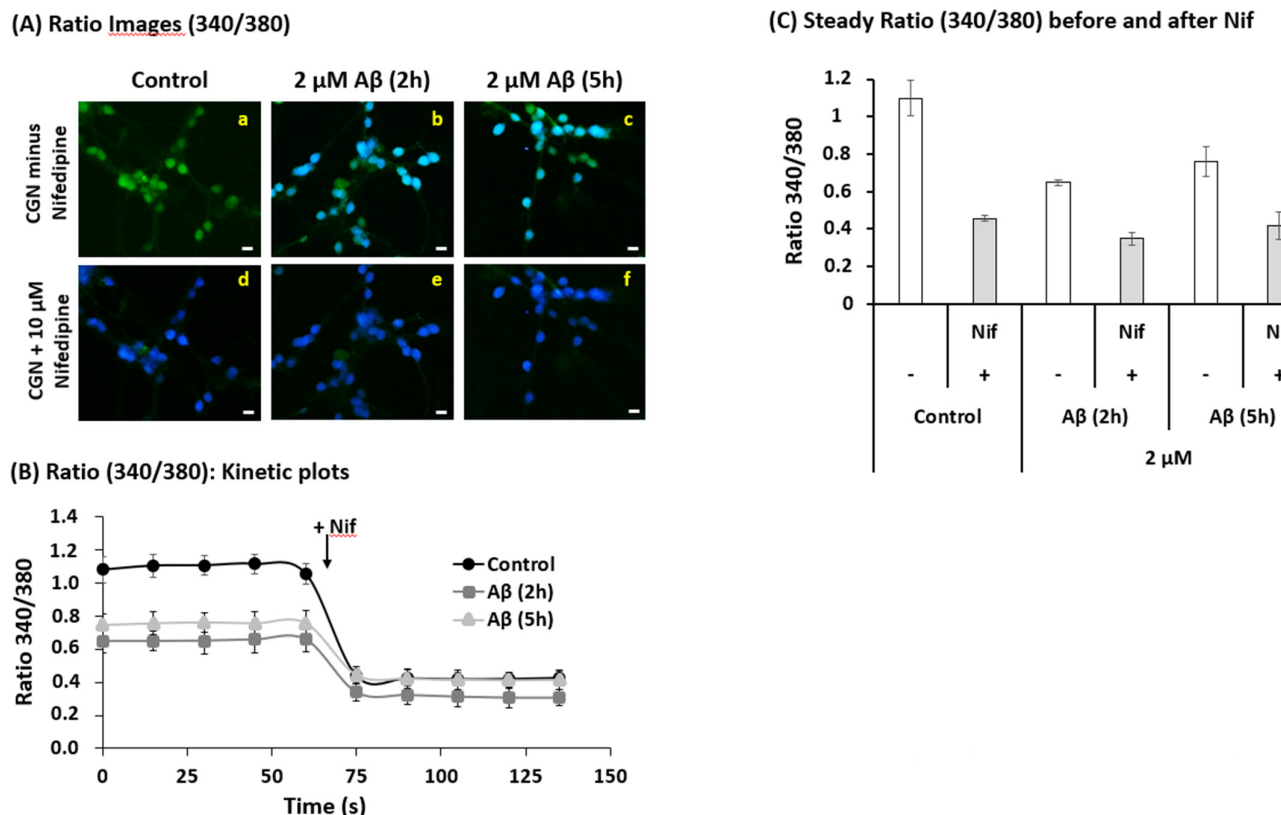


Figure 7. Intracellular cytosolic calcium concentration decreases in the neuronal soma after A β (1–42) treatment. Mature CGN were pre-incubated with 2 μ M A β (1–42) for 2 h or 5 h at 37 °C and 5% CO₂ and loaded with 5 μ M Fura-2 for 60 min, as previously described in Section 2. Nifedipine (10 μ M), a calcium channel blocker, was used as positive control to confirm the effect of the total blockade of LTCCs. (A) Representative ratio (340/380) images of Fura-2-loaded CGN of untreated (a) and treated cells with 2 μ M A β (1–42) for 2 h (b) or 5 h (c) and after the addition of nifedipine in the control group (d) and in cells treated with 2 μ M A β (1–42) for 2 h (e) or 5 h (f). Scale bar inserted in fluorescence microscopy images = 10 μ m. (B) Kinetic plots of the average \pm s.e. fluorescence ratio (340/380) before and after the addition 10 μ M nifedipine (+Nif) at the time indicated by the arrow. (C) The analysis of fluorescence intensity data for GCN loaded with Fura-2 showed a statistically significant decrease (\approx 50%) in the steady ratio (340/380) after A β (1–42) treatment (2 h and 5 h) with respect to the control (untreated cells), p < 0.05. The addition of nifedipine totally blocks the entry of Ca²⁺ in the soma in untreated and treated cells as demonstrated by the decrease in the ratio showing that A β partially attenuates LTCC function. The ratio (340/380) values shown are the average \pm s.e. of experiments done in triplicate with at least two different preparations of CGN (n > 400 neuronal soma of fields taken from at least six plates for each condition).

The concentration of internalized A β after 2 h of incubation of mature CGN with 2 μ M A β added to the extracellular medium was measured using A β (1–42)-HiLyteTM-Fluor555, as indicated in the Materials and Methods section. Red fluorescence images of CGN acquired with an excitation filter of 556 nm and a dichroic mirror of 580 nm with an emission filter of 590 nm were analyzed with HCImage software. The increase of red fluorescence intensity in neuronal somas after subtraction of the red autofluorescence of the cells (see Supplementary Figure S3 in the Materials and Methods section) was compared with the red fluorescence intensity of the medium supplemented with different concentrations of A β (1–42)-HiLyteTM-Fluor555. From these results, we calculated that after 2 h of incubation with 2 μ M A β in the extracellular medium, the intracellular concentration of A β was 193 ± 21 nM of A β monomers (i.e., high enough to saturate all CaM present in CGNs).

2.5. Extensive FRET between LTCCs Labeled with Alexa488 Fluorescent Antibody and A β (1–42)-HiLyte™-Fluor555 in Fixed Mature CGN Is Largely Reversed by Addition of Exogenous CaM

In previous works, we have shown an extensive association of LTCCs with lipid rafts in primary cultures of mature CGNs [27,40,50], and this prompted us to experimentally assess the possibility that both LTCCs and A β (1–42) are associated with the same lipid rafts in mature CGN at a concentration of 100 picomoles of A β (1–42)/mL (e.g., the concentration of A β used in other FRET imaging experiments shown in this work). Representative fluorescence microscopy images of mature CGN stained with anti-LTCC subunit α 1C conjugated with IgG-Alexa 488 (anti-LTCCs*A488) and 100 picomoles of A β (1–42)-HiLyte™-Fluor555/mL are shown in Figure 8A. Images of several fields of the plate were acquired as indicated in the Materials and Methods before and after the addition of A β (1–42)-HiLyte™-Fluor555. A direct inspection of images revealed that the green fluorescence was attenuated after the addition of A β (1–42)-HiLyte™-Fluor555. The analysis of the red/green fluorescence intensity ratio after correction for the red fluorescence due to direct excitation of A β (1–42)-HiLyte™-Fluor555 showed a two-fold increase in this ratio (Figure 8B), pointing out the occurrence of FRET between Alexa 488 conjugates of anti-LTCC and the Fluor555 dye bound to A β . Moreover, a detailed inspection of the merge images revealed significant variations of the extent of FRET between LTCCs and A β (1–42)-HiLyte™-Fluor555, as indicated by the color palette of different cellular submicrodomains within the neuronal soma and extensions. The more intense yellow/orange-colored pixels highlighted submicrodomains with higher FRET efficiency. It is noteworthy that this leads to a punctate staining appearance of neuronal extensions that is reminiscent of dendritic spines. Therefore, these results indicate an extensive co-localization of LTCCs and A β (1–42)-HiLyte™-Fluor555 within the FRET distance in fixed mature CGN, which using this FRET approach was \leq 50 nm, as indicated in the Materials and Methods section.

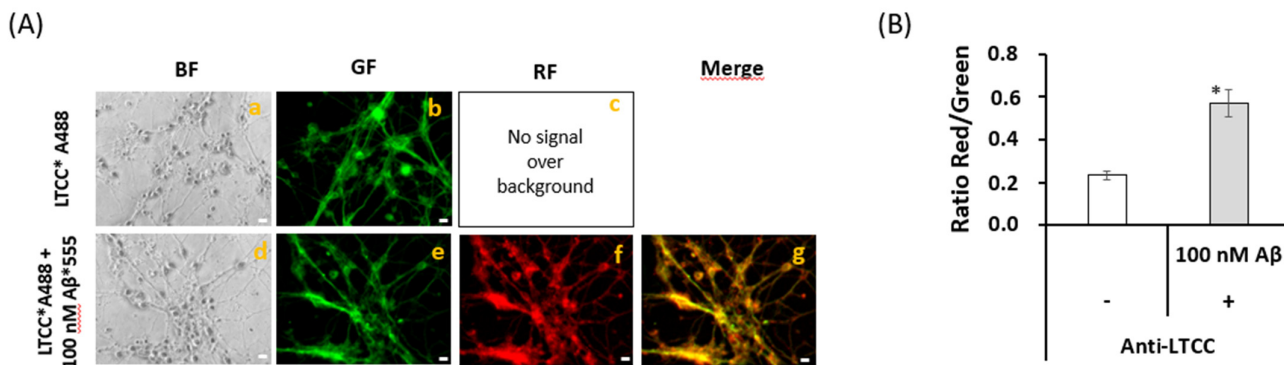


Figure 8. Extensive FRET between LTCC and A β (1–42). (A) Representative quantitative fluorescence microscopy images of CGN stained with the anti-LTCC subunit α 1C (sc-25686)/IgG-Alexa488 antibodies (LTCC*A488, a–c) or with anti-LTCC/IgG-Alexa488 and A β (1–42) HiLyte™ Fluor 555 (LTCC*A488/A β (1–42), d–g). Bright-field (BF), green fluorescence (GF), and red fluorescence (RF) images are shown for each of the selected fields, and the orange-yellow areas (Merge image) pointed out the higher intensity FRET regions (g). The exposure time for GF and RF images was 0.4 s. Scale bar inserted in fluorescence microscopy images = 10 μ m. (B) Ratio of red/green fluorescence intensity per pixel (RF/GF) obtained from the analysis of fluorescence intensity data of CGN somas stained with anti-LTCC/IgG-Alexa488 only (LTCC*A488) and double stained with anti-LTCC*IgG-Alexa488/A β (1–42) HiLyte™ Fluor 555 (LTCC*A488/A β (1–42)). The results shown in (B) are the mean \pm s.e. (*) $p < 0.05$ (i.e., statistically significant with respect to the control, CGN labeled with the Alexa488 FRET donor only).

However, our results excluded significant co-immunoprecipitation of LTCCs by A β (see Supplementary Figure S2). Thus, a direct interaction between LTCCs and A β cannot account for the observed inhibition of LTCCs by A β . Since CaM modulates LTCCs directly [32,33] or indirectly through CaMK activation [31,58,59], we experimentally assessed the

possibility that CaM provides the major anchor point for A β near LTCCs in lipid rafts of mature CGN. To this end, we acquired fluorescence microscopy images before and after the addition of 100 picomoles of purified CaM to the Petri plate with CGN stained with anti-LTCCs conjugated with IgG-Alexa 488 (anti-LTCCs*A488) and A β (1–42)-HiLyteTM-Fluor555 in 1 mL PBS (Figure 9). The concentration of A β (1–42)-HiLyteTM-Fluor555 was lowered to 50 picomoles for two major reasons: (1) to focus on the higher affinity binding sites for A β (1–42)-HiLyteTM-Fluor555 in CGN, and (2) to get a CaM/A β (1–42)-HiLyteTM-Fluor555 monomer molar ratio much higher than 1. The representative images shown in Figure 9A point out that CaM largely reverses the intensity of A β (1–42)-HiLyteTM-Fluor555 red fluorescence staining of CGN in the somas and more extensively in the thicker neuronal extensions connecting aligned neuronal bodies. Moreover, the addition of 5 mM Co²⁺ elicited more than 80% quenching of the total red fluorescence (Figure 9B), yielding a red fluorescence image that was not significantly different to the image of the red autofluorescence of CGN shown in Figure 2.

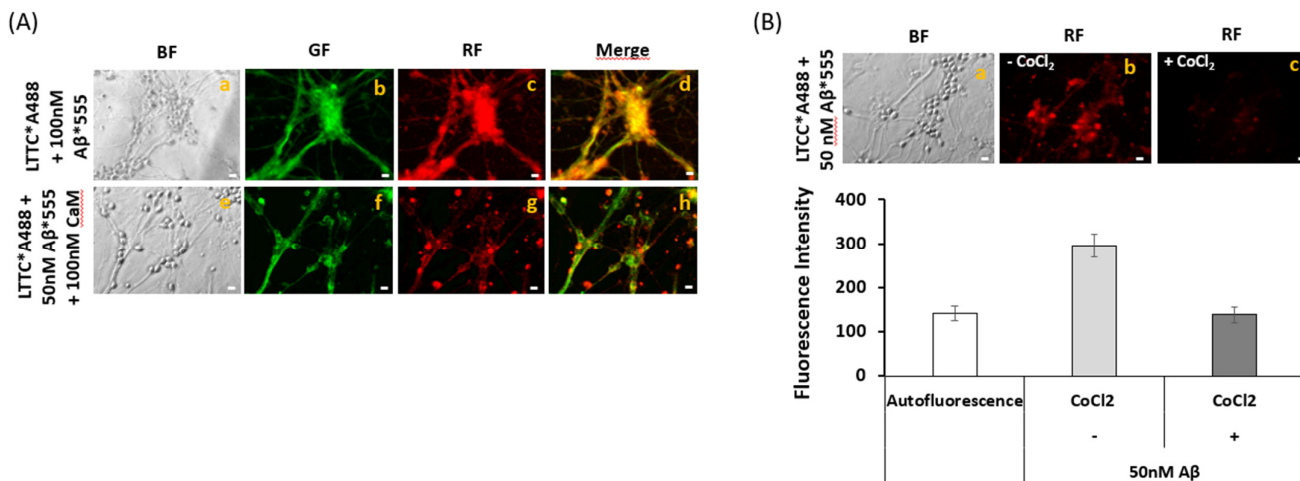


Figure 9. Reversion by CaM of FRET between anti-LTCC/IgG-Alexa488 and A β (1–42)-HiLyteTM-Fluor555 (A) and quenching by Co²⁺ of the fluorescence of A β (1–42)-HiLyteTM-Fluor 555 (B). (A) Representative quantitative fluorescence microscopy images of CGN stained with anti-LTCC subunit α 1C/IgG-Alexa488 and 50 nM of A β (1–42)-HiLyteTM-Fluor 555 (LTCC*A488/A β *555), after GF and RF image acquisition, 100 nM of purified CaM was added to the medium, and the plate was gently stirred for 15 min before acquisition of the images of selected fields in the presence of calmodulin. Bright-field (BF), green fluorescence (GF), and red fluorescence (RF) images are shown for the selected fields, and the orange-yellow areas (merge image) point out the higher intensity FRET regions. The exposure time for GF and RF images was 0.5 s. Scale bar inserted in fluorescence microscopy images = 10 μ m. (B) Representative quantitative red fluorescence microscopy images of CGN stained with LTCC*A488/A β *555 in the absence and in the presence of 5 mM Co²⁺. After acquisition of RF images in the absence of Co²⁺, 5 mM of CoCl₂ was added to the medium and images of the same field were acquired 5 min after the addition of 5 mM Co²⁺. The average intensity per pixel in the neuronal somas of five different fields were measured using HCImage software ($n > 50$ somas for each experimental condition), and are plotted below the fluorescence microscopy images of this panel (B). The results showed that 5 mM Co²⁺ completely quenched the fluorescence of A β (1–42)-HiLyteTM-Fluor 555, because the difference between the average intensity of the autofluorescence and of the fluorescence in the presence of 5 mM Co²⁺ was not statistically significant ($p > 0.05$).

3. Discussion

The results of this work show that at concentrations lower than 0.25 micromoles of A β (1–42)/L, the predominant oligomeric species of this peptide were dimers, with approximately 10% contribution of trimers, and that there was a large complexation of A β (1–42) with CaM in mature CGN. This was supported by extensive FRET between anti-CaM stained with the Alexa 488 fluorescent secondary antibody and 0.1 micromoles of A β (1–42)-HiLyteTM-Fluor555/L in fixed and permeabilized CGN, and also by co-immunoprecipitation of CaM with anti-A β (1–42) in the presence of 0.25 micromoles of A β (1–42)/L. Moreover, taking into account the high content of CaM in neurons ([60,61] and this work) and

the very low dissociation constant of the CaM:A β (1–42) complex, approximately 1 nM [22], our results point that CaM is a major binding target for A β (1–42) in neurons, not only in mature CGN. As our results also showed that 2.5×10^6 mature CGN (the number of cells seeded per Petri plate in this work) contained 56 ± 6 picomoles of CaM, this implies that in these plates, CaM can bind up to 120 ± 13 picomoles of A β (1–42) monomers, decreasing the concentration of free A β (1–42) to approximately 1 nM. Although A β peptides have also been shown to bind with dissociation constants close to 1 nM to PrPc [62] and to glycogen synthase kinase 3 α (GSK3 α) [63], it is to be noted that all these alternate target proteins were expressed at much lower levels than CaM in neurons. Thus, CaM can be seen in neurons as the major intracellular target protein for A β peptides, helping to keep the free intracellular concentration of A β peptides in the low nanomolar range. Therefore, brains affected with Alzheimer’s disease, which contain lower CaM levels than normal brains [21], should be expected to suffer a stronger rise in the free intracellular concentration of A β peptides upon β -secretase activation, being more prone to undergoing neuronal degeneration. In addition, CaM:A β (1–42) complexes can be by themselves intracellular transducers for focalized actions of A β peptides, because CaM has a major role in neuronal metabolism, excitability, and signaling through direct interaction with proteins that play a major regulatory role of neuronal functions in different subcellular locations.

A β peptides have been found in neuronal lipid rafts, where they promote specific signaling alterations [11,64,65]. A β peptides bind to cholesterol and gangliosides, highly enriched in the lipid rafts of the plasma membrane, and also to phosphatidylserine, a lipid enriched in the neuronal plasma membrane. In addition, PrPc, which is constitutively present in lipid rafts, has been shown to bind A β peptides [56,57,62], providing further direct interaction points for the physical anchorage of A β to lipid rafts. Using A β (1–42)-HiLyte™-Fluor555, we experimentally assessed with FRET imaging that in fixed and permeabilized CGN, A β (1–42) binding sites were within the FRET distance from protein markers of plasma membrane lipid rafts stained with specific antibodies. The donor/acceptor FRET pair with higher increase in the red fluorescence/green fluorescence ratio was anti-PrPc stained with the Alexa 488 fluorescent secondary antibody/A β (1–42)-HiLyte™-Fluor555, indicating a more extensive co-localization of PrPc and A β (1–42) within FRET distance. This is in good agreement with the formation of PrPc:A β complexes reported elsewhere (see above). To minimize the contribution of low affinity intracellular binding sites for A β , these results were obtained with the addition of only 100 picomoles of A β (1–42)-HiLyte™-Fluor555 monomers to a Petri plate containing 2.5×10^6 cells in 1 mL PBS. As the FRET distance limit using this experimental approach was less than 60 nm, these results highlight A β binding sites within the same lipid rafts or in close proximity to them. Moreover, fluorescence microscopy images highlighted that there was a large co-localization in the neuronal soma and also in neuronal extensions of A β (1–42)-HiLyte™-Fluor555 and protein markers of lipid rafts stained with specific antibodies labelled with fluorescent Alexa 488 secondary antibodies. However, the raft markers Cav-1 and HRas were not co-immunoprecipitated by the anti-A β (1–42) antibody in the presence of 0.25 μ M A β (1–42), pointing out that neither Cav-1 nor HRas provide direct anchoring points of A β (1–42) in lipid rafts. On the other hand, FRET imaging with anti-CaM stained with the Alexa 488 fluorescent secondary antibody (as FRET donor) and anti-HRas stained with the Cy3 fluorescent secondary antibody (as FRET acceptor) pointed out that a significant fraction of CaM were separated by less than 80 nm (i.e., at a distance lower than the maximum 100 nm size reported for lipid rafts) [1]. This is consistent with the known association of several CaM-binding proteins with lipid rafts in mature CGN, namely, nNOS, LTCCs, PMCA, and CaMKII [27,31,40].

Previous works have shown that LTCCs associated with lipid rafts play a major role in the control of resting cytosolic calcium homeostasis in mature CGN in vitro in the optimum survival medium (i.e., a partially depolarizing medium containing 25 mM KCl) [30,31]. It has also been reported that LTCC activity is stimulated by phosphorylation mediated by CaMKII [31,58,59], but CaM binding to the LTCC α 1C subunit produces

inactivation of these channels [32,33]. In this work, we showed that incubation of CGN with 2 μ M (monomers) A β (1–42) during 2 h, which allowed us to reach 193 \pm 21 nM (monomers) of internalized A β (1–42) in CGN, produced approximately 50% inhibition of the activity of LTCCs, and that incubation up to 5 h did not significantly increase this inhibition. Since the dimer is the predominant aggregation state of the solutions of A β (1–42) used in this work, this means that less than 100 nM A β (1–42) dimers inhibited by 50% the LTCC's activity. Note that there was not a significant change in the resting cytosolic calcium concentration of CGN measured once LTCCs were blocked with nifedipine after these treatments with A β (1–42). This result indicates that LTCC is the calcium transport system involved in the control of resting cytosolic calcium in mature CGN in vitro that is most sensitive to A β (1–42) under our experimental conditions. Additionally, this decrease in resting cytosolic calcium elicited by A β (1–42) should attenuate CGN excitability because of the strong dependence of synaptic activity upon cytosolic calcium concentration.

A remarkable observation is that upon blockade of LTCCs with nifedipine, the resting cytosolic calcium of CGN was not significantly altered by A β (1–42). Thus, the formation of calcium pores by intracellular A β is unlikely at the short times of exposure to the low nanomolar free intracellular concentrations of A β attained in this work. This also implies that the activity of other calcium transport systems involved in the control of cytosolic calcium homeostasis in CGN are not significantly impaired by the treatment with A β (1–42) that is enough to elicit inhibition of LTCCs. The major transport system for calcium homeostasis in neurons, which extrudes cytosolic calcium toward the extracellular medium is the PMCA [35]. Despite that A β (1–42) can bind and partially inhibit PMCA [36,43], it is to be noted that only a weak inhibition of lipid rafts associated with PMCA by intracellular nanomolar concentrations of A β (1–42) should be expected in a calcium concentration range below 0.2 μ M [43], the resting cytosolic concentration range measured in mature CGN in this work and in previous works [27,30,31]. Moreover, previous works have shown that the inhibition of PMCA by A β (1–42) can be antagonized by CaM and cholesterol [43,66]. Furthermore, it is to be noted that the sustained lowering of cytosolic calcium of CGN in a partially depolarizing medium is a cellular stress observed at short times of exposure to low nanomolar free intracellular concentrations of A β . It is likely that at higher concentrations of A β or at longer times of exposure to A β , this may trigger calcium release from intracellular stores, mainly from endoplasmic reticulum, as a compensatory or adaptive cellular response. Indeed, enhanced endoplasmic reticulum calcium release has been shown in AD [67,68]. Moreover, it has been shown that familial AD mutations of presenilins potentiate endoplasmic reticulum calcium leak and cause early-onset inherited AD [69,70].

However, LTCCs are not co-immunoprecipitated by anti-A β (1–42), and this excludes that the inhibition of LTCC activity can be due to the blockade of these calcium channels by direct binding of A β (1–42). However, fluorescence microscopy revealed efficient FRET between anti-LTCC stained with Alexa 488 fluorescent secondary antibody and A β (1–42)-HiLyteTM-Fluor555. Therefore, A β (1–42) must bind to a modulatory site in the lipid rafts located very close to the LTCC structure (i.e., less than few nanometers distance from LTCC subunits since the overall size of the complex between the anti-LTCC primary antibody and the Alexa 488 fluorescent secondary antibody is approximately 40 nm) [27,50]. Since most of this internalized A β (1–42) should be bound to CaM, the inhibition of LTCC by A β (1–42) can be rationalized in terms of the known inhibition of CaMKII by A β peptides [41,42], and also in terms of potentiation by A β (1–42) of the inactivation of LTCC by direct interaction with CaM. The hypothesis that CaM:A β (1–42) complexes are involved in the modulation of LTCC was experimentally supported by a large reversion by exogenously added CaM of the co-localization between anti-LTCC stained with the Alexa 488 fluorescent secondary antibody and A β (1–42)-HiLyte™-Fluor555. Additionally, the large quenching of A β (1–42)-HiLyte™-Fluor555 fluorescence by 5 mM Co²⁺ indicated that the binding sites of A β (1–42)-HiLyte™-Fluor555 in fixed and permeabilized CGN were separated by less than 2 nm from high affinity calcium sites, as expected for A β (1–42)-

HiLyte™-Fluor555:CaM complexes [22]. Noteworthy, A β has been shown to prevent CaMKII activation in rat hippocampal slices [41], and impairment of the phosphorylation of the β -subunit of LTCC by CaMK inhibitors leads to the strong inhibition of LTCC in partial depolarizing MLocke's K25 mM medium [31]. In addition, it has been suggested that CaMKII dysregulation may be a modulator of toxicity in Alzheimer's disease [42]. However, we cannot exclude that A β (1–42) association with CaM may also potentiate the inactivation of LTCC activity by direct binding of CaM, a possibility which to the best of our knowledge has been overlooked until now. However, a critical evaluation of this point requires further extensive experimental studies that are out of the scope of this work.

In summary, by using mature CGN in culture, we showed a large complexation of CaM by submicromolar concentrations of A β (1–42) dimers, and also extensive co-localization of CaM and A β (1–42) within the same lipid rafts in plates seeded with 2.5×10^6 cells and stained with up to 100 picomoles of A β (1–42)-HiLyte™-Fluor555 monomers. In addition, we found that the resting cytosolic calcium of mature CGN in partially depolarizing 25 mM potassium medium was largely lowered by exposure to A β (1–42) dimers during 2 h, conditions that produced an internalization of less than 100 picomoles of A β (1–42) dimers in neuronal somas. As a final conclusion, we identified that the primary cause of this decrease of the resting cytosolic calcium was the inhibition of LTCCs of CGN by A β (1–42) dimers.

4. Materials and Methods

4.1. Preparation of Rat Cerebellar Granule Neurons (CGN)

CGNs were obtained from dissociated cerebella of 7-day-old Wistar rats as described previously [27,29,31,40,51,52,71,72]. Animal handlings were performed in accordance with Spanish regulations and were approved by the Ethical Committee of the University of Extremadura. Briefly, cells were plated in Dulbecco's Modified Eagle medium (DMEM) supplemented with 10% heat-inactivated fetal bovine serum, 5 mM glucose, 19.63 mM KCl, 3.7 ng/mL insulin, 7 μ M 4-aminobenzoic acid, 50 U/mL penicillin, 25 U/mL streptomycin, 0.91 mM pyruvate, and 2 mM glutamine on 35 mm diameter dishes (Corning, NY, USA) coated with poly-D-lysine at a density of 2.5×10^6 cells/dish. CGN cultures were kept at 37 °C in a humidified atmosphere of 95% air/5% CO₂. Cytosine arabinofuranoside (10 μ M) was added to fresh culture medium 48 h after plating to prevent the replication of non-neuronal cells. Seven days after plating, the culture medium was replaced with the serum-free DMEM:F12 medium (1:1) supplemented with 12.5 mM glucose, 20.82 mM KCl, 5 μ g/mL insulin, 0.1 mg/mL apo-transferrin, 20 nM progesterone, 50 U/mL penicillin, 25 U/mL streptomycin, 0.1 mg/mL pyruvate, and 2 mM L-glutamine. Mature CGNs at 8–10 days in vitro (DIV) were used in all of the experiments.

The composition of MLocke's K25 buffer (pH 7.4 at 37 °C) used in this work was as follows: 4 mM NaHCO₃, 10 mM Tricine, 5 mM glucose, 2.3 mM CaCl₂, 1 mM MgCl₂, and 134 mM NaCl/25 mM KCl.

4.2. A β (1–42) Solutions and Aggregation State

A β (1–42) solutions were prepared dissolving the solid lyophilized peptide in 1% NH₄OH, and thereafter diluted with PBS to the desired concentration, as in [22]. The aggregation state of A β (1–42) stock solutions used in this work were evaluated using the rapid photoinduced cross-linking of unmodified proteins approach described in [73,74]. Briefly, A β (1–42) diluted to 177 μ M in 60 mM NaOH and 10 mM phosphate at pH 7 was sonicated in a water bath, Selecta Ultrasons, set at the maximum intensity of 150 watts during 1 min and, thereafter, it was centrifuged at 16,000 g during 10 min. The supernatants were treated with 60 μ M Tris(2,2'-bipyridyl)dichloro-ruthenium(II) hexahydrate and 4.4 mM ammonium persulfate, placed in the sample compartment of a Perkin-Elmer 650-40 fluorimeter (Perkin-Elmer, Waltham, MA, USA) and irradiated with the light of 452 nm emitted by the fluorimeter 150 watts Xenon lamp during 1 s at room temperature.

Immediately after irradiation, the reaction was stopped by the addition of 5% *v/v* β -mercaptoethanol plus sample buffer [95 mM tris-(hydroxymethyl) aminomethane (Tris)-HCl buffer, pH 6.8/ 3% sodium dodecyl sulfate (SDS)/13% glycerol, and 0.005% bromophenol blue], and heated at 37 °C for 15 min, before loading into the gel for Tricine-SDS-polyacrylamide electrophoresis (PAGE) prepared and run as indicated by [75]. The results obtained (Supplementary Figure S1) showed a major band of a molecular weight close to 9 kDa and a faint band of molecular weight between 12 and 15 kDa. As the monomer molecular weight of A β (1–42) is approximately 4.5 kDa, these results indicate that dimers were the predominant aggregation state of A β (1–42) in the stock solutions used in this work, with a minor (<10%) contribution of trimers. A β (1–42) monomers were not detected in our stock solutions.

4.3. Cell Viability

Cells were incubated with different concentrations of A β (1–42) (0.75, 1.5, 2.5 and 5 μ M) in serum-free DMEM:F12 medium at 37 °C and 5% CO₂. After 48 h incubation, CGN plates were washed with 1 mL MLocke's K25 buffer and cell viability was experimentally assessed measuring the amount of colored formazan by the reduction of 3-(4,5-dimethylthiazol-2-yl)-2,5-diphenyltetrazolium bromide (MTT) as in previous works [27,29,31,52,71,72]. Untreated cells were regarded as controls (100% cell survival) and the cell survival ratio was expressed as the percentage of the control.

4.4. Co-Immunoprecipitation

CGN was lysed in buffer 25 mM Tris-HCl, pH 7.4, 150 mM NaCl, 5 mM ethylenediaminetetraacetic acid, 50 mM NaF, 5 mM NaVO₃, and 0.25% 4-(1,1,3,3-tetramethyl butyl)phenyl-polyethylene glycol (Triton X-100), supplemented with 1x SIGMAFAST™ protease inhibitor cocktail (Sigma-Aldrich, St. Louis, MO, USA). Lysates were collected and supplemented with 50% glycerol. The protein concentration of cell lysates was measured by the Bradford's method using bovine serum albumin (BSA) as the standard.

Co-immunoprecipitation was carried out using the protein A/G PLUS-Agarose sc-2003 of Santa Cruz Biotechnology Inc. (Santa Cruz, CA, USA) following the instructions given in their technical data sheets. Prior to the co-immunoprecipitation experiment, cell lysates were treated with 10 mM of methyl- β -cyclodextrin for 30 min at 4 °C in a tube-rotor with continuous shaking. Afterward, in an Eppendorf tube, 200 μ g of CGN lysate was incubated with 5 μ g mouse anti- β -amyloid antibody (Sigma, A8354) at 4 °C with continuous shaking. After 1 h, 65 μ L protein A/G PLUS-Agarose was added and incubated overnight at 4 °C with continuous shaking. The next day, the phosphate buffered saline (PBS) control sample or 0.25 μ M A β (1–42) in PBS (treated sample) was added and incubated for 1 h at 4 °C with continuous shaking. The matrix was precipitated by centrifugation at 2500 \times g during 5 min at 4 °C in a refrigerated Eppendorf microcentrifuge 5415R. The supernatant was removed, and the precipitated matrix was subjected to three washes with 50 μ L PBS (control sample) or 50 μ L PBS plus 0.25 μ M A β (1–42) (treated sample). A centrifugation step (2500 \times g, 5 min at 4 °C) was performed in a refrigerated Eppendorf in each washing step. The supernatant was carefully removed and the matrix precipitate was resuspended in 80 μ L of electrophoresis sample buffer, boiled during 3 min, and stored at -20 °C until running on an SDS-PAGE gel for western blotting analysis.

4.5. Western Blotting

SDS-PAGE was run at concentrations of 7.5%, 10.4%, 13.5%, or 15% acrylamide depending upon the molecular weights of the target proteins using 20 μ g CGN lysates or 15–20 μ L co-immunoprecipitated sample per lane. Gels were transferred to polyvinylidene difluoride (PVDF) membranes of 0.2 μ m average pore size, and PVDF membranes were blocked with 3% BSA in Tris-buffered saline (TBS) supplemented with 0.05% polyoxyethylene sorbitan monolaurate (TBST) for 1 h at room temperature. Before incubation

with the primary antibody, membranes were washed six times with TBST. Immunodetection of proteins was performed with their specific antibodies at a dilution of 1:1000 in TBST for anti-caveolin-1, anti-HRas, and anti-LTCC antibodies, and at a dilution of 1:2000 in TBST for anti-CaM and anti-cellular prion protein (PrP^c) antibodies. After incubation with the first antibody overnight at 4 °C, membranes were washed six times with TBST and incubated for 1 h at room temperature with the appropriate secondary IgG antibody conjugated with horseradish peroxidase at a dilution of 1:5000 in TBST. Then, membranes were washed six times with TBST followed by incubation for 3 min with the Bio-Rad Clarity Western ECL substrate. Western blots were revealed with Bio-Rad ChemiDocTM XRS+ (Bio-Rad, Hercules, CA, USA) and data analyzed with Image Lab 6.0.1 software.

4.6. Measurements of Internalization of A β (1–42)-HiLyteTM-Fluor555 in Mature CGN

The internalization of A β (1–42) was monitored by fluorescence microscopy with A β (1–42)-HiLyteTM-Fluor555 following an experimental approach similar to that used with other fluorescent derivatives of A β (1–42) in cell cultures [15,76]. The extent of internalization of A β (1–42) was measured from the increase in red fluorescence in CGN soma at different times of incubation (up to 2 h) at 37 °C and 5% CO₂ with a total concentration of 2 μ M of A β (1–42) monomers (1.8 μ M of A β (1–42) monomers plus 0.2 μ M of A β (1–42)-HiLyteTM-Fluor555 monomers) added to the serum-free DMEM:F12 medium supplemented as indicated above. After the selected time of incubation, the medium was replaced by MLocke's K25 and the Petri plate was placed in the holder of the fluorescence microscope thermostated at 37 °C for image acquisition. Fluorescence images were acquired with a Hamamatsu Orca-R² CCD camera (binning mode 2 × 2) camera (Hamamatsu, Hamamatsu-city, Japan) attached to a Nikon Diaphot 300 epifluorescence microscope (Tokyo, Japan) with a NCF Plan ELWD 40× objective, using an excitation filter of 556 nm and a dichroic mirror of 580 nm with an emission filter of 590 nm, and 0.03 s exposure time. Quantitative analysis of the average fluorescence intensity per pixel of selected neuronal soma was done with HClImage software using the region of interest (ROI) tool. The results obtained after 2 h incubation are shown in panel A of Supplementary Figure S3. In separate experiments, the average intensity per pixel obtained with increasing concentrations of A β (1–42)-HiLyteTM-Fluor555 in Mlocke's K25 in the Petri plate was recorded for calibration of the A β (1–42)-HiLyteTM-Fluor555 fluorescence under the same experimental conditions, and the results are shown in panel B of Supplementary Figure S3. The average intensity readings per pixel in CGN neuronal somas were taken from several fields for a total number of 102 cells, and after subtraction of CGN autofluorescence, yielded an internalized concentration of 19.3 ± 2.1 nM of A β (1–42)-HiLyteTM-Fluor555 monomers. Assuming that there was not a significant difference between the rate of internalization of A β (1–42)-HiLyteTM-Fluor555 and of A β (1–42), we calculated an internalized concentration of 193 ± 21 nM of total A β monomers by interpolation in the calibration line shown in panel B.

4.7. Fluorescence Resonance Energy Transfer (FRET) Imaging

FRET imaging was performed as in previous works [27,40,50–52]. Fluorescence microscopy images of CGN were acquired with a Hamamatsu Orca-R² CCD camera (Hamamatsu) attached to a Nikon Diaphot 300 epifluorescence microscope (Tokyo, Japan) with a NCF Plan ELWD 40× objective (pixel size of the images shown in this work 0.2 μ m). Quantitative analysis of the average fluorescence intensity per pixel of selected neuronal soma was done with the HClImage software using the ROI tool, as in previous works. Only fields devoid of large aggregates of neurons forming granules or small grain-like structures were selected for image acquisition to minimize the distortion of images by the sum of the fluorescence contributions of juxtaposed layers of neurons. The mean ± s.e. intensity reading of fluorescence per pixel within CGN somas were obtained in experiments performed in triplicate ($n > 100$ CGN somas in each case). Images of CGN were acquired with an excitation filter of 470 nm, and 510 nm dichroic mirror/520 nm emission filter (green

fluorescence), using the exposure times indicated for each case in the legends for the figures. Untreated cells were regarded as controls.

CGN were washed with MLocke's K25 buffer to remove the phenol red remaining in the plates. Then, CGN were fixed with 2.5% para-formaldehyde, 3 mM MgCl₂, 2 mM ethylene glycol-bis(2-aminoethyl ether)-N,N,N,N'-tetraacetic acid, and 0.32 M sucrose in PBS (5 mM sodium phosphate, 137 mM NaCl, and 27 mM KCl, pH 7).

The following selected protein targets for FRET imaging were used: CaM, HRas, caveolin-1 (Cav-1), PrPc, and α 1C subunit of LTCC (Cav1.2). Before their use for fluorescence microscopy image acquisition, the specificity of primary antibodies for the selected target proteins was routinely assessed by the presence of the major and most intense band at the expected protein molecular weight in the western blotting run with CGN lysates. In most cases, this band accounts for more than 90% of the total band staining (Supplementary Figure S4). Primary antibodies used in these experiments were: rabbit anti-CaM (Epitomics, 1716-1, 1:200), goat anti-HRas (Santa Cruz Biotechnology, sc-32026, 1:100), rabbit anti-caveolin-1 (Santa Cruz Biotechnology, sc-894, 1:100), mouse anti-PrPc (Thermo Fisher, 6H4-7500997, 1:100), and rabbit anti-LTCC α 1C subunit (Santa Cruz Biotechnology, sc-25686, 1:50).

After CGN were fixed, cells were blocked with 1% BSA in PBS supplemented with 0.2% Triton X-100 (PBST) for 1 h at 37 °C and then incubated during 1 h at 37 °C with the target primary antibody in PBS and washed three times with PBS (washing step). Thereafter, CGN were incubated for 1 h with the appropriate Alexa488-labeled secondary antibody in PBST (1:200) and washed again three times with PBS before acquisition of fluorescence microscopy images stained only with the donor dye. After finishing the acquisition of FRET donor images, CGN were incubated for 60 min at 37 °C with 50 or 100 nM A β (1–42)-HiLyte™-Fluor 555 in PBS with continuous and gentle mixing. Then, the acquisition of fluorescence microscopy images of selected fields, routinely 5–6 fields of each Petri plate, were performed within the next 20–30 min. Contribution of CGN autofluorescence and secondary Alexa488-antibody in the absence of the primary antibody were assessed before running FRET experiments and were found to be lower than 10% of the average fluorescence intensity per pixel obtained with specific primary antibodies. This background signal was subtracted for calculations of the RF/GF ratio obtained with CGN plates. Due to the close absorbance spectrum of Cy3 and A β (1–42)-HiLyte™-Fluor 555, significant FRET efficiency using this experimental approach implies that the selected protein was separated by less than 50 nm from A β (1–42)-HiLyte™-Fluor 555, as discussed in detail in previous works [27,50].

In the case of FRET imaging using a fluorescent acceptor antibody bound to another protein target (e.g., CaM stained with a Alexa488 fluorescent secondary antibody as donor and HRas stained with a Cy3 fluorescent secondary antibody as acceptor), we followed the protocol described in detail in previous publications of our laboratory [27,50]. Briefly, after finishing the acquisition of FRET donor images, CGN were incubated for 1 h at 37 °C with the acceptor target primary antibody as indicated above, washed three times with PBS, then incubated for 1 h with the appropriate Cy3-labeled secondary antibody in PBST (1:200), and washed again three times with PBS before the acquisition of fluorescence microscopy images. Controls were also run in the absence of the second primary antibody to correct for partial loss of the donor fluorescence produced by the treatment to label the second protein, on average between 20 and 25% loss of the donor fluorescence, and also to subtract background signals.

The average intensity of fluorescence per pixel within CGN somas were taken using the ROI tool of the Hamamatsu HC Image software to select somas as the areas of interest in experiments performed in triplicate, at least, $n > 100$ CGN somas in each case. As discussed in previous works [27,50], significant FRET efficiency using this experimental approach implies that the selected proteins were separated by ≤80 nm.

4.8. Measurement of the Intracellular Free Ca^{2+} Concentration ($[\text{Ca}^{2+}]_{\text{i}}$)

$[\text{Ca}^{2+}]_{\text{i}}$ was measured as indicated in detail in previous works [27,29,31,71]. Briefly, cells were incubated with 2 μM A β (1–42) in DMEM:F12 medium for 2 h or 5 h at 37 °C and 5%CO₂ on a sunflower mini-shaker (BioSan, Labnet, Madrid, Spain) with continuous and gentle mixing. One hour before the end of the incubation with A β (1–42), CGN was loaded with 5 μM Fura-2-acetoxymethyl ester (Fura2-AM) and 0.025% Pluronic-F127 at 37 °C. Next, CGN plates were washed twice with 1 mL MLocke's K25 buffer and the culture dishes were placed in the thermostatic controlled plate (Warner Instrument Co., Hamden, CT, USA) of the Nikon Diaphot 300 inverted epifluorescence microscope. Nifedipine (10 μM) was used to block the L-type calcium channels. Digital images with 340 and 380 nm excitation filters and a 510 nm dichroic mirror/520 nm emission filter were taken with a Hamamatsu Orca-R² CCD camera (binning mode 2 × 2) and Lambda 10–2 filter wheel controller and subsequently analyzed with HCImage software. Data acquisition and analysis were done after the selection of the neuronal soma using the ROI tool of this software. The 340/380 ratio data given in this work were population averages ± s.e. intensity reading of fluorescence per pixel within CGN somas were obtained using the ROI tool of the Hamamatsu HCImage software to select somas as areas of interest in experiments performed in triplicate ($n > 100$ CGN somas in each case).

4.9. Chemicals and Reagents

Human A β (1–42)-HiLyteTM-Fluor555 was obtained from AnaSpec (Freemont, CA, USA). Unlabeled A β (1–42) and scrambled A β (1–42) were synthesized and supplied by StabVida (Caparica, Portugal). Purified bovine brain CaM was purchased from Sigma-Aldrich (Madrid, Spain).

Primary antibodies: goat anti-HRas (sc-32026), rabbit anti-Cav-1 (sc-894), rabbit anti-LTCC $\alpha 1\text{C}$ subunit (sc-25686), and rabbit anti-LTCC β subunit (sc-25689) antibodies were supplied by Santa Cruz Biotechnology (Santa Cruz, CA, USA). Rabbit anti-CaM (Epitomics 1716-1) antibody was supplied by Abcam (Cambridge, UK) and mouse anti-PrPc antibody (Thermo Fisher, 6H4-7500997) was purchased from Thermo Fisher Scientific (Madrid, Spain). Monoclonal mouse anti-A β antibody (A8354) was purchased from Sigma-Aldrich (Madrid, Spain). Fluorescent-labeled secondary antibodies used to label the primary antibodies listed above were anti-rabbit IgG-Alexa488 (cat. no. A11008), anti-goat IgG-Alexa488 (cat. no. A11055), and anti-mouse IgG-Alexa488 (cat. no. A11001) from Invitrogen (Molecular Probes, Eugene, OR, USA). Anti-rabbit IgG-horseradish peroxidase, anti-goat IgG-horseradish peroxidase, and anti-mouse IgG-horseradish peroxidase were supplied by Sigma-Aldrich. Bio-Rad Clarity Western ECL substrate was purchased from Bio-Rad (Alcobendas - Madrid, Spain).

Fura-2 acetoxymethyl ester and pluronic F-127 were obtained from Biotium (Hayward, CA, USA) and Invitrogen, respectively. Nifedipine was supplied by Sigma-Aldrich (Madrid, Spain). Protein A/G PLUS-Agarose sc-2003 was purchased from Santa Cruz Biotechnology Inc. (Santa Cruz, CA, USA).

All other reagents and chemicals were of analytical grade from Sigma-Aldrich (Madrid, Spain) or Roche-Merck (Darmstadt, Germany).

4.10. Statistical Analysis

Results were expressed as the mean standard error (s.e.). Statistical analysis was carried out by the Student's *t*-test. A significant difference was accepted at the $p < 0.05$ level. All results were confirmed with duplicate measurements of at least three different CGN preparations.

Supplementary Materials: The following are available online at www.mdpi.com/1422-0067/22/4/1984/s1, Supplementary Figures file with Supplementary Figures S1–S4. Supplementary Figure S1: Tricine-SDS PAGE of A β (1–42) solutions used in this work. Supplementary Figure S2: Western blotting of caveolin-1 (anti-Cav-1, sc 894), HRas (anti-HRas, sc 32026), and LTCC (anti-LTCC β subunit, sc 25689) after co-immunoprecipitation assay with mouse anti- β -amyloid antibody (Sigma, A8354) as described in the Materials and Methods section. Supplementary Figure S3: Internalization of A β (1–42)-HiLyte™-Fluor555 in mature CGN. Supplementary Figure S4: Western blotting of CGN lysates with the primary antibodies used in fluorescence microscopy images.

Author Contributions: Joana Poejo (J.P.) performed most of the experimental results, analyzed the experimental results, prepared the figures, wrote large parts of the first draft of this manuscript. Jairo Salazar (J.S.) did part of the experimental work and analyzed his results, and prepared the corresponding section of the Materials and Methods and figures. Ana M. Mata (A.M.M.) contributed to defining the experimental conditions for A β handling, revision of the manuscript, and funding of this work. Carlos Gutierrez-Merino (C.G.-M.) designed the overall work plan and aims of this study, supervised the performance of many experiments, revised and analyzed the experimental results, wrote the manuscript and also provided funding for this work. **Specific tasks:** Conceptualization, C.G.-M. and J.P.; Methodology, J.P., J.S., A.M.M., and C.G.-M.; Software, J.P. and C.G.-M.; Validation, J.P. and C.G.-M.; Formal analysis, J.P., J.S., and C.G.-M.; Investigation, J.P., J.S., and C.G.-M.; Resources, C.G.-M. and A.M.M.; Data curation, J.P. and C.G.-M.; Writing—original draft preparation, J.P., J.S., and C.G.-M.; Writing—review and editing, C.G.-M. and A.M.M.; Supervision, C.G.-M.; Project administration, A.M.M. and C.G.-M.; Funding acquisition, A.M.M. and C.G.-M. All authors have read and agreed to the published version of the manuscript.

Funding: This work was supported by Grant BFU2017-85723-P of the Spanish Ministerio de Ciencia, Innovación y Universidades (Spanish National R&D program) to Ana M. Mata and Carlos Gutierrez-Merino, co-financed by the European Funds for Structural Development (FEDER).

Institutional Review Board Statement: Animal handlings were performed in accordance with Spanish regulations and were approved by the Ethical Committee of the University of Extremadura (date of approval October 27, 2014 -Registry code 88/2014 of the University of Extremadura) and also by the Servicio de Sanidad Animal of the Dirección General de Agricultura y Ganadería of the Junta de Extremadura (date of approval October 22, 2015 -REGA code ES 060150001817).

Informed Consent Statement: Not applicable.

Data Availability Statement: Data are available from our laboratory archives.

Acknowledgments: We gratefully acknowledge the Cafés Delta Foundation (Campo Maior, Portugal) for a fellowship/contract to Joana Poejo. Jairo Salazar was supported by a Predoctoral Fellowship of the Spanish Fundación Carolina (Madrid, Spain).

Conflicts of Interest: The authors declare no conflicts of interest.

Abbreviations

A β	amyloid β peptide
AD	Alzheimer's disease
Anti-CaM*A488/Anti-Cav1*A488/Anti-HRas*A488/Anti-LTCC*A488/Anti-PrPc*A488	primary antibody of target protein (CaM, Cav1, HRas, LTCC or PrPc) stained with a secondary Alexa488 fluorescent antibody
Anti-HRas*Cy3	primary antibody of HRas stained with a secondary Cy3 fluorescent antibody
BSA	bovine serum albumin
[Ca $^{2+}$] $_i$	intracellular free calcium concentration
CaM	calmodulin
CaMKII	Ca $^{2+}$ /calmodulin-dependent protein kinase isoform II
CaMBDs	calmodulin binding domains
CGN	cerebellar granule neurons
DMEM	Dulbecco's Modified Eagle medium
FRET	fluorescence resonance energy transfer
Fura2-AM	Fura2 acetoxyethyl ester

LTCC	L-type calcium channels
MTT	3-(4,5-dimethylthiazol-2-yl)-2,5-diphenyltetrazolium bromide
nNOS	neuronal isoform of nitric oxide synthase
PAGE	polyacrylamide gel electrophoresis
PBS	phosphate-buffered saline
PBST	PBS supplemented with 0.2% Triton X-100
PMCA	plasma membrane calcium pump
PrP ^c	cellular prion protein
PVDF	polyvinylidene difluoride
ROI	region of interest
SDS	sodium dodecyl sulfate
TBS	Tris-buffered saline
TBST	TBS supplemented with 0.05% polyoxyethylene sorbitan monolaurate (Tween 20)
Tris	tris-(hydroxymethyl) aminomethane
Triton X-100	4-(1,1,3,3-tetramethyl butyl)phenyl-poly-ethylene glycol

References

1. Pike, L.J. Rafts defined: A report on the Keystone symposium on lipid rafts and cell function. *J. Lipid Res.* **2006**, *47*, 1597–1598, doi:10.1194/jlr.e600002-jlr200.
2. Choo-Smith, L.-P.; Surewicz, W.K. The interaction between Alzheimer amyloid β (1–40) peptide and ganglioside GM1-containing membranes. *FEBS Lett.* **1997**, *402*, 95–98, doi:10.1016/s0014-5793(96)01504-9.
3. Choo-Smith, L.-P.; Garzon-Rodriguez, W.; Glabe, C.G.; Surewicz, W.K. Acceleration of Amyloid Fibril Formation by Specific Binding of $\text{A}\beta$ (1–40) Peptide to Ganglioside-containing Membrane Vesicles. *J. Biol. Chem.* **1997**, *272*, 22987–22990, doi:10.1074/jbc.272.37.22987.
4. Ariga, T.; Kobayashi, K.; Hasegawa, A.; Kiso, M.; Ishida, H.; Miyatake, T. Characterization of high-affinity binding between gangliosides and amyloid β -protein. *Arch. Biochem. Biophys.* **2001**, *388*, 225–230.
5. Matsuzaki, K.; Kato, K.; Yanagisawa, K. $\text{A}\beta$ polymerization through interaction with membrane gangliosides. *Biochim. Biophys. Acta Mol. Cell Biol. Lipids* **2010**, *1801*, 868–877, doi:10.1016/j.bbalip.2010.01.008.
6. Kakio, A.; Nishimoto, S.I.; Yanagisawa, K.; Kozutsumi, Y.; Matsuzaki, K. Cholesterol dependent formation of GM1 ganglioside-bound amyloid β -protein, an endogenous seed for Alzheimer amyloid. *J. Biol. Chem.* **2001**, *276*, 24985–24990.
7. Kakio, A.; Nishimoto, S.I.; Yanagisawa, K.; Kozutsumi, Y.; Matsuzaki, K. Interactions of amyloid β -protein with various gangliosides in raft-like membranes: Importance of GM1 ganglioside-bound form as an endogenous seed for Alzheimer amyloid. *Biochemistry* **2002**, *41*, 7385–7390.
8. Wood, W.; Schroeder, F.; Igbavboa, U.; A. Avdulov, N.; Chochina, S.V.; Avdulov, N. Brain membrane cholesterol domains, aging and amyloid beta-peptides. *Neurobiol. Aging* **2002**, *23*, 685–694, doi:10.1016/s0197-4580(02)00018-0.
9. Williamson, R.; Usardi, A.; Hanger, D.P.; Anderton, B.H. Membrane-bound β -amyloid oligomers are recruited into lipid rafts by a fyn-dependent mechanism. *FASEB J.* **2008**, *22*, 1552–1559.
10. Kawarabayashi, T.; Shoji, M.; Younkin, L.H.; Wen-Lang, L.; Dickson, D.W.; Murakami, T.; Matsubara, E.; Abe, K.; Ashe, K.H.; Younkin, S.G. Dimeric amyloid beta protein rapidly accumulates in lipid rafts followed by apolipoprotein E and phosphorylated tau accumulation in the Tg2576 mouse model of Alzheimer’s disease. *J. Neurosci.* **2004**, *24*, 3801–3809.
11. Lai, A.Y.; McLaurin, J. Mechanisms of Amyloid-Beta Peptide Uptake by Neurons: The Role of Lipid Rafts and Lipid Raft-Associated Proteins. *Int. J. Alzheimer’s Dis.* **2011**, *2011*, 1–11, doi:10.4061/2011/548380.
12. Younkin, S.G. The role of $\text{A}\beta$ 42 in Alzheimer’s disease. *J. Physiol. Paris* **1998**, *92*, 289–292.
13. Hu, X.; Crick, S.L.; Bu, G.; Frieden, C.; Pappu, R.V.; Lee, J.-M. Amyloid seeds formed by cellular uptake, concentration, and aggregation of the amyloid- β peptide. *Proc. Natl. Acad. Sci. USA* **2009**, *106*, 20324–20329.
14. Friedrich, R.P.; Tepper, K.; Rönicke, R.; Soom, M.; Westermann, M.; Reymann, K.; Kaether, C.; Fändrich, M. Mechanism of amyloid plaque formation suggests an intracellular basis of $\text{A}\beta$ pathogenicity. *Proc. Natl. Acad. Sci. USA* **2010**, *107*, 1942–1947, doi:10.1073/pnas.0904532106.
15. Jin, S.; Kedia, N.; Illes-Toth, E.; Haralampiev, I.; Prisner, S.; Herrmann, A.; Wanker, E.E.; Bieschke, J. Amyloid- β (1–42) Aggregation Initiates Its Cellular Uptake and Cytotoxicity. *J. Biol. Chem.* **2016**, *291*, 19590–19606.
16. Walsh, D.M.; Klyubin, I.; Fadeeva, J.V.; Cullen, W.K.; Anwyl, R.; Wolfe, M.S.; Rowan, M.J.; Selkoe, D.J. Naturally secreted oligomers of amyloid β protein potently inhibit hippocampal long-term potentiation in vivo. *Nat. Cell Biol.* **2002**, *416*, 535–539, doi:10.1038/416535a.
17. Oddo, S.; Caccamo, A.; Shepherd, J.D.; Murphy, M.P.; Golde, T.E.; Kayed, R.; Metherate, R.; Mattson, M.P.; Akbari, Y.; LaFerla, F.M. Triple-transgenic model of Alzheimer’s disease with plaques and tangles: Intracellular $\text{A}\beta$ and synaptic dysfunction. *Neuron* **2003**, *39*, 409–421.
18. Billings, L.M.; Oddo, S.; Green, K.N.; McGaugh, J.L.; La Ferla, F.M. Intraneuronal $\text{A}\beta$ Causes the Onset of Early Alzheimer’s Disease-Related Cognitive Deficits in Transgenic Mice. *Neuron* **2005**, *45*, 675–688, doi:10.1016/j.neuron.2005.01.040.

19. La Ferla, F.M. Calcium dyshomeostasis and intracellular signalling in Alzheimer's disease. *Nat. Rev. Neurosci.* **2002**, *3*, 862–872.
20. Bezprozvanny, I.; Mattson, M.P. Neuronal calcium mishandling and the pathogenesis of Alzheimer's disease. *Trends Neurosci.* **2008**, *31*, 454–463.
21. McLachlan, D.R.C.; Wong, L.; Bergeron, C.; Bainbridge, K.G. Calmodulin and calbindin D28K in Alzheimer disease. *Alzheimer Dis. Assoc. Disord.* **1987**, *1*, 171–179, doi:10.1097/00002093-198701030-00009.
22. Corbacho, I.; Berrocal, M.; Török, K.; Mata, A.M.; Gutierrez-Merino, C. High affinity binding of amyloid β -peptide to calmodulin: Structural and functional implications. *Biochem. Biophys. Res. Commun.* **2017**, *486*, 992–997.
23. Chin, D.; Means, A.R. Calmodulin: A prototypical calcium sensor. *Trends Cell Biol.* **2000**, *10*, 322–328, doi:10.1016/s0962-8924(00)01800-6.
24. Berridge, M.J. Calcium regulation of neural rhythms, memory and Alzheimer's disease. *J. Physiol.* **2013**, *592*, 281–293, doi:10.1113/jphysiol.2013.257527.
25. O'Day, D.H.; Eshak, K.; Myre, M.A. Calmodulin Binding Proteins and Alzheimer's Disease. *J. Alzheimer's Dis.* **2015**, *46*, 553–569, doi:10.3233/jad-142772.
26. De Muro, A.; Parker, I.; Stutzmann, G.E. Calcium Signaling and Amyloid Toxicity in Alzheimer Disease. *J. Biol. Chem.* **2010**, *285*, 12463–12468, doi:10.1074/jbc.r109.080895.
27. Marques-da-Silva, D.; Gutierrez-Merino, C. Caveolin-rich lipid rafts of the plasma membrane of mature cerebellar granule neurons are microcompartments for calcium/reactive oxygen and nitrogen species cross-talk signaling. *Cell Calcium* **2014**, *56*, 108–123, doi:10.1016/j.ceca.2014.06.002.
28. Gutierrez-Merino, C.; Marques-da-Silva, D.; Fortalezas, S.; Samhan-Arias, A.K. Cytosolic calcium homeostasis in neurons: Control systems, modulation by reactive oxygen and nitrogen species, and space and time fluctuations. In *Neurochemistry*; Thomas Heinbockel, Ed.; InTech: Rijeka, Croatia, **2014**; Chapter 3, pp. 59–110.
29. Gutiérrez-Martín, Y.; Martín-Romero, F.J.; Henao, F.; Gutiérrez-Merino, C. Alteration of cytosolic free calcium homeostasis by SIN-1: High sensitivity of L-type Ca^{2+} channels to extracellular oxidative/nitrosative stress in cerebellar granule cells. *J. Neurochem.* **2005**, *92*, 973–989, doi:10.1111/j.1471-4159.2004.02964.x.
30. Gutierrez-Merino, C.; Marques-Da-Silva, D.; Fortalezas, S.; Samhan-Arias, A.K. The critical role of lipid rafts nanodomains in the cross-talk between calcium and reactive oxygen and nitrogen species in cerebellar granule neurons apoptosis by extracellular potassium deprivation. *AIMS Mol. Sci.* **2016**, *3*, 12–29.
31. Fortalezas, S.; Marques-da-Silva, D.; Gutierrez-Merino, C. Methyl- β -Cyclodextrin Impairs the Phosphorylation of the $\beta 2$ Subunit of L-Type Calcium Channels and Cytosolic Calcium Homeostasis in Mature Cerebellar Granule Neurons. *Int. J. Mol. Sci.* **2018**, *19*, 3667, doi:10.3390/ijms19113667.
32. Peterson, B.Z.; de Maria, C.D.; Yue, D.T. Calmodulin Is the Ca^{2+} Sensor for Ca^{2+} -Dependent Inactivation of L-Type Calcium Channels. *Neuron* **1999**, *22*, 549–558, doi:10.1016/s0896-6273(00)80709-6.
33. Zühlke, R.D.; Pitt, G.S.; Deisseroth, K.; Tsien, R.W.; Reuter, H. Calmodulin supports both inactivation and facilitation of L-type calcium channels. *Nat. Cell Biol.* **1999**, *399*, 159–162, doi:10.1038/20200.
34. Di Leva, F.; Domi, T.; Fedrizzi, L.; Lim, D.; Carafoli, E. The plasma membrane Ca^{2+} ATPase of animal cells: Structure, function and regulation. *Arch. Biochem. Biophys.* **2008**, *476*, 65–74, doi:10.1016/j.abb.2008.02.026.
35. Brini, M.; Carafoli, E.; Cali, T. The plasma membrane calcium pumps: Focus on the role in (neuro)pathology. *Biochem. Biophys. Res. Commun.* **2017**, *483*, 1116–1124, doi:10.1016/j.bbrc.2016.07.117.
36. Mata, A.M. Functional interplay between plasma membrane Ca^{2+} -ATPase, amyloid β -peptide and tau. *Neurosci. Lett.* **2018**, *663*, 55–59, doi:10.1016/j.neulet.2017.08.004.
37. Suzuki, T.; Du, F.; Tian, Q.-B.; Zhang, J.; Endo, S. Ca^{2+} /calmodulin-dependent protein kinase II α clusters are associated with stable lipid rafts and their formation traps PSD-95. *J. Neurochem.* **2007**, *104*, 596–610, doi:10.1111/j.1471-4159.2007.05035.x.
38. Sato, Y.; Sagami, I.; Shimizu, T. Identification of Caveolin-1-interacting Sites in Neuronal Nitric-oxide Synthase. *J. Biol. Chem.* **2004**, *279*, 8827–8836, doi:10.1074/jbc.m310327200.
39. Zhou, L.; Zhu, D.-Y. Neuronal nitric oxide synthase: Structure, subcellular localization, regulation, and clinical implications. *Nitric Oxide* **2009**, *20*, 223–230, doi:10.1016/j.niox.2009.03.001.
40. Marques-da-Silva, D.; Gutierrez-Merino, C. L-type voltage-operated calcium channels, N-methyl-d-aspartate receptors and neuronal nitric-oxide synthase form a calcium/redox nano-transducer within lipid rafts. *Biochem. Biophys. Res. Commun.* **2012**, *420*, 257–262, doi:10.1016/j.bbrc.2012.02.145.
41. Zhao, D.; Watson, J.B.; Xie, C.-W. Amyloid β Prevents Activation of Calcium/Calmodulin-Dependent Protein Kinase II and AMPA Receptor Phosphorylation During Hippocampal Long-Term Potentiation. *J. Neurophysiol.* **2004**, *92*, 2853–2858, doi:10.1152/jn.00485.2004.
42. Ghosh, A.; Giese, K.P. Calcium/calmodulin-dependent kinase II and Alzheimer's disease. *Mol. Brain* **2015**, *8*, 1–7, doi:10.1186/s13041-015-0166-2.
43. Berrocal, M.; Marcos, D.; Sepúlveda, M.R.; Pérez, M.; Ávila, J.; Mata, A.M. Altered Ca^{2+} dependence of synaptosomal plasma membrane Ca^{2+} -ATPase in human brain affected by Alzheimer's disease. *FASEB J.* **2009**, *23*, 1826–1834, doi:10.1096/fj.08-121459.
44. Padayachee, E.; Whiteley, C.G. Spectrofluorimetric analysis of the interaction of amyloid peptides with neuronal nitric oxide synthase: Implications in Alzheimer's disease. *Biochim. Biophys. Acta* **2011**, *1810*, 1136–1140.

45. Padayachee, E.; Ngqwala, N.; Whiteley, C.G. Association of β -amyloid peptide fragments with neuronal nitric oxide synthase: Implications in the etiology of Alzheimers disease. *J. Enzym. Inhib. Med. Chem.* **2011**, *27*, 356–364, doi:10.3109/14756366.2011.590805.
46. Wankerl, K.; Weise, D.; Gentner, R.; Rumpf, J.-J.; Classen, J. L-Type Voltage-Gated Ca₂₊ Channels: A Single Molecular Switch for Long-Term Potentiation/Long-Term Depression-Like Plasticity and Activity-Dependent Metaplasticity in Humans. *J. Neurosci.* **2010**, *30*, 6197–6204, doi:10.1523/JNEUROSCI.4673-09.2010.
47. Berger, S.M.; Bartsch, D. The role of L-type voltage-gated calcium channels Cav1.2 and Cav1.3 in normal and pathological brain function. *Cell Tissue Res.* **2014**, *357*, 463–476, doi:10.1007/s00441-014-1936-3.
48. O'Day, D.H.; Myre, M.A. Calmodulin-binding domains in Alzheimer's disease proteins: Extending the calcium hypothesis. *Biochem. Biophys. Res. Commun.* **2004**, *320*, 1051–1054, doi:10.1016/j.bbrc.2004.06.070.
49. Sepúlveda, M.R.; Berrocal-Carrillo, M.; Gasset, M.; Mata, A.M. The Plasma Membrane Ca₂₊-ATPase Isoform 4 Is Localized in Lipid Rafts of Cerebellum Synaptic Plasma Membranes. *J. Biol. Chem.* **2006**, *281*, 447–453, doi:10.1074/jbc.m506950200.
50. Marques-Da-Silva, D.; Samhan-Arias, A.K.; Tiago, T.; Gutiérrez-Merino, C. L-type calcium channels and cytochrome b5 reductase are components of protein complexes tightly associated with lipid rafts microdomains of the neuronal plasma membrane. *J. Proteom.* **2010**, *73*, 1502–1510.
51. Samhan-Arias, A.K.; Garcia-Berenguain, M.A.; Martin-Romero, F.J.; Gutierrez-Merino, C. Clustering of plasma membrane-bound cytochrome b5 reductase within 'lipid rafts' microdomains of the neuronal plasma membrane. *Mol. Cell. Neurosci.* **2009**, *40*, 14–26.
52. Samhan-Arias, A.K.; Marques-da-Silva, D.; Yanamala, N.; Gutierrez-Merino, C. Stimulation and clustering of cytochrome b5 reductase in caveolin-rich lipid microdomains is an early event in oxidative stress-mediated apoptosis of cerebellar granule neurons. *J. Proteom.* **2012**, *75*, 2934–2949, doi:10.1016/j.jprot.2011.12.007.
53. Cuenda, A.; Henao, F.; Gutierrez-Merino, C. Distances between functional sites of the Ca₂₊ + Mg₂₊-ATPase from sarcoplasmic reticulum using Co₂₊ as a spectroscopic ruler. *JBIC J. Biol. Inorg. Chem.* **1990**, *194*, 663–670, doi:10.1111/j.1432-1033.1990.tb15666.x.
54. Nguyen, D.M.; Chen, L.S.; Jeng, G.; Yu, W.-P.; Chen, T.-Y. Cobalt ion interaction with TMEM16A calcium-activated chloride channel: Inhibition and potentiation. *PLoS ONE* **2020**, *15*, e0231812, doi:10.1371/journal.pone.0231812.
55. Highsmith, S.; Murphy, A.J. Nd³⁺ and Co²⁺ binding to sarcoplasmic reticulum CaATPase. An estimation of the distance from the ATP binding site to the high-affinity calcium binding sites. *J. Biol. Chem.* **1984**, *259*, 14651–14656, doi:10.1016/s0021-9258(17)42652-4.
56. Chen, S.; Yadav, S.P.; Surewicz, W.K. Interaction between Human Prion Protein and Amyloid-(A β) Oligomers. Role of n-terminal residues. *J. Biol. Chem.* **2010**, *285*, 26377–26383.
57. Zhang, Y.; Zhao, Y.; Zhang, L.; Yu, W.; Wang, Y.; Chang, W. Cellular Prion Protein as a Receptor of Toxic Amyloid- β 42 Oligomers Is Important for Alzheimer's Disease. *Front. Cell. Neurosci.* **2019**, *13*, 339, doi:10.3389/fncel.2019.00339.
58. Hudmon, A.; Schulman, H.; Kim, J.; Maltez, J.M.; Tsien, R.W.; Pitt, G.S. CaMKII tethers to L-type Ca₂₊ channels, establishing a local and dedicated integrator of Ca₂₊ signals for facilitation. *J. Cell Biol.* **2005**, *171*, 537–547, doi:10.1083/jcb.200505155.
59. Lee, T.S.; Karl, R.; Moosmang, S.; Lenhardt, P.; Klugbauer, N.; Hofmann, F.; Kleppisch, T.; Welling, A. Calmodulin kinase II is involved in voltage dependent facilitation of the L-type Cav1.2 calcium channel: Identification of the phosphorylation sites. *J. Biol. Chem.* **2006**, *281*, 25560–25567.
60. Cheung, W.Y. Calmodulin. *Sci. Am.* **1982**, *246*, 62–70, doi:10.1038/scientificamerican0682-62.
61. Biber, A.; Schmid, G.; Hempel, K. Calmodulin content in specific brain areas. *Exp. Brain Res.* **1984**, *56*, 323–326, doi:10.1007/bf00236287.
62. Laurén, J.; Gimbel, D.A.; Nygaard, H.B.; Gilbert, J.W.; Strittmatter, S.M. Cellular prion protein mediates impairment of synaptic plasticity by amyloid- β oligomers. *Nat. Cell Biol.* **2009**, *457*, 1128–1132, doi:10.1038/nature07761.
63. Dunning, C.J.; McGauran, G.; Willén, K.; Gouras, G.K.; O'Connell, D.J.; Linse, S. Direct High Affinity Interaction between A β 42 and GSK3 α Stimulates Hyperphosphorylation of Tau. A New Molecular Link in Alzheimer's Disease? *ACS Chem. Neurosci.* **2015**, *7*, 161–170, doi:10.1021/acscchemneuro.5b00262.
64. Cecchi, C.; Nichino, D.; Zampagni, M.; Bernacchioni, C.; Evangelisti, E.; Pensalfini, A.; Liguri, G.; Glioza, A.; Stefani, M.; Relini, A. A protective role for lipid raft cholesterol against amyloid-induced membrane damage in human neuroblastoma cells. *Biochim. Biophys. Acta Biomembr.* **2009**, *1788*, 2204–2216, doi:10.1016/j.bbamem.2009.07.019.
65. Vetrivel, K.S.; Thinakaran, G. Membrane rafts in Alzheimer's disease beta-amyloid production. *Biochim. Biophys. Acta Mol. Cell Biol. Lipids* **2010**, *1801*, 860–867, doi:10.1016/j.bbalip.2010.03.007.
66. Berrocal, M.; Sepulveda, M.R.; Vazquez-Hernandez, M.; Mata, A.M. Calmodulin antagonizes amyloid- β peptides-mediated inhibition of brain plasma membrane Ca₂₊-ATPase. *Biochim. Biophys. Acta Mol. Basis Dis.* **2012**, *1822*, 961–969, doi:10.1016/j.bbadiis.2012.02.013.
67. Ito, E.; Oka, K.; Etcheberrigaray, R.; Nelson, T.J.; McPhie, D.L.; Tofel-Grehl, B.; Gibson, G.E.; Alkon, D.L. Internal Ca₂₊ mobilization is altered in fibroblasts from patients with Alzheimer disease. *Proc. Natl. Acad. Sci. USA* **1994**, *91*, 534–538.
68. Emilsson, L.; Saetre, P.; Jazin, E. Alzheimer's disease: mRNA expression profiles of multiple patients show alterations of genes involved with calcium signaling. *Neurobiol. Dis.* **2006**, *21*, 618–625, doi:10.1016/j.nbd.2005.09.004.
69. Tu, H.; Nelson, O.; Bezprozvanny, A.; Wang, Z.; Lee, S.-F.; Hao, Y.-H.; Serneels, L.; de Strooper, B.; Yu, G.; Bezprozvanny, I. Presenilins Form ER Ca₂₊ Leak Channels, a Function Disrupted by Familial Alzheimer's Disease-Linked Mutations. *Cell* **2006**, *126*, 981–993, doi:10.1016/j.cell.2006.06.059.

70. Zhang, H.; Sun, S.; Herreman, A.; de Strooper, B.; Bezprozvanny, I. Role of Presenilins in Neuronal Calcium Homeostasis. *J. Neurosci.* **2010**, *30*, 8566–8580, doi:10.1523/jneurosci.1554-10.2010.
71. Fortalezas, S.; Marques-Da-Silva, D.; Gutierrez-Merino, C. Creatine protects against cytosolic calcium dysregulation, mitochondrial depolarization and increase of reactive oxygen species production in rotenone-induced cell death of cerebellar granule neurons. *Neurotox. Res.* **2018**, *34*, 717–732.
72. Samhan-Arias, A.K.; Martin-Romero, F.J.; Gutierrez-Merino, C. Kaempferol blocks oxidative stress in cerebellar granule cells and reveals a key role for the plasma membrane NADH oxidase activity in the commitment of apoptosis. *Free Radic. Biol. Med.* **2004**, *37*, 48–61.
73. Fancy, D.A.; Kodadek, T. Chemistry for the analysis of protein-protein interactions: Rapid and efficient cross-linking triggered by long wavelength light. *Proc. Natl. Acad. Sci. USA* **1999**, *96*, 6020–6024, doi:10.1073/pnas.96.11.6020.
74. Bitan, G.; Teplow, D.B. Rapid Photochemical Cross-Linking: A New Tool for Studies of Metastable, Amyloidogenic Protein Assemblies. *Accounts Chem. Res.* **2004**, *37*, 357–364, doi:10.1021/ar000214l.
75. Schägger, H.; von Jagow, G. Tricine–sodium dodecyl sulfate polyacrylamide gel electrophoresis for the separation of proteins in the range from 1–100 kDa. *Anal. Biochem.* **1987**, *166*, 368–379.
- Saavedra, L.; Mohamed, A.; Ma, V.; Kar, S.; de Chaves, E.P. Internalization of β -Amyloid Peptide by Primary Neurons in the Absence of Apolipoprotein E. *J. Biol. Chem.* **2007**, *282*, 35722–35732, doi:10.1074/jbc.m701823



Article

Early Reactive A1 Astrocytes Induction by the Neurotoxin 3-Nitropropionic Acid in Rat Brain

Carmen Lopez-Sanchez ^{1,2,*}, Virginio Garcia-Martinez ^{1,2}, Joana Poejo ¹,
Virginio Garcia-Lopez ^{1,2,3}, Jairo Salazar ^{1,4} and Carlos Gutierrez-Merino ^{1,5}

¹ Instituto de Biomarcadores de Patologías Moleculares, Universidad de Extremadura, 06006 Badajoz, Spain; virginio@unex.es (V.G.-M.); joanapoejo86@gmail.com (J.P.); garcialopez@unex.es (V.G.-L.); jairochemsalazar@gmail.com (J.S.); carlosgm@unex.es (C.G.-M.)

² Departamento de Anatomía y Embriología Humana, Facultad de Medicina, Universidad de Extremadura, 06006 Badajoz, Spain

³ Departamento de Enfermería, Facultad de Medicina, Universidad de Extremadura, 06006 Badajoz, Spain

⁴ Departamento de Química, Universidad Nacional Autónoma de Nicaragua-León, Leon 21000, Nicaragua

⁵ Departamento de Bioquímica y Biología Molecular y Genética, Facultad de Ciencias, Universidad de Extremadura, 06006 Badajoz, Spain

* Correspondence: clopez@unex.es

Received: 7 April 2020; Accepted: 18 May 2020; Published: 20 May 2020



Abstract: 3-Nitropropionic acid (NPA) administration to rodents produces degeneration of the *striatum*, accompanied by neurological disturbances that mimic Huntington's disease (HD) motor neurological dysfunctions. It has been shown that inflammation mediates NPA-induced brain degeneration, and activated microglia secreting cytokines interleukin-1 α (IL-1 α) and tumor necrosis factor α (TNF α) can induce a specific type of reactive neurotoxic astrocytes, named A1, which have been detected in post-mortem brain samples of Huntington's, Alzheimer's, and Parkinson's diseases. In this work we used an experimental model based on the intraperitoneal (i.p.) administration of NPA to adult Wistar rats at doses that can elicit extensive brain degeneration, and brain samples were taken before and after extensive brain damage monitored using 2,3,5-triphenyltetrazolium chloride (TTC) staining. Western blots and immunohistochemistry of brain slices show that i.p. NPA injections elicit significant increase in the expression levels of C3 α subunit, a marker of generation of neurotoxic A1 astrocytes, and of cytokines IL-1 α , TNF α , and C1q within the *striatum*, *hippocampus*, and *cerebellum* before the appearance of the HD-related neurological dysfunctions and neuronal death induced by NPA. Noteworthy, NPA administration primarily induces the generation of A1 astrocytes in the more recent phylogenetic area of the rat *cerebellum*. We conclude that the activation of complement C3 protein in the brain from Wistar rats is an early event in NPA-induced brain neurodegeneration.

Keywords: 3-nitropropionic acid; rat brain; A1 astrocytes; complement component 3; cytokines IL-1 α ; TNF- α and C1

1. Introduction

3-Nitropropionic acid (NPA) is a natural toxin produced by some fungi and plants [1–4]. Systemic NPA administration to rodents and non-human primates produces degeneration of the *striatum*, accompanied by neurological disturbances that mimic Huntington's disease (HD) motor neurological dysfunctions. More precisely, systemic NPA administration produces a selective bilateral degeneration in the dorso-lateral region of the *striatum* [5–10], resembling severe damage observed in the caudate and dorso-lateral *putamen* of human brains affected by HD [11]. Moreover, preferential degeneration of the medium-sized GABAergic spiny striatal neurons has been reported after NPA systemic administration, alterations also observed in HD *striatum* [5,7]. However, the pre-motor symptomatic stages of HD are

commonly characterized by cognitive issues, including executive dysfunction, visuospatial deficits, perceptual deficits, memory loss, and difficulty in learning new skills [12,13]. It has been proved that systemic NPA administration to rodents also produces memory impairment [14,15], and significant metabolic alterations, not only in the *striatum* and vicinal cortical areas, but also in the *hippocampus* [15]. Furthermore, it has been shown that NPA administration to rats also elicits significant changes both to metabolism and neurotransmitters in the *cerebellum* [16,17]. Noteworthy, cerebellar *cortex* damage with extensive Purkinje cells loss has been reported recently in post-mortem samples of HD cases [18].

Mitochondrial functional alterations as well as associated generation of reactive oxygen species (ROS), that activate cell death pathways, have been demonstrated to play a major role in NPA neurotoxicity [19–21]. Additionally, both processes have been implicated in HD [22]. NPA is a suicide inhibitor of succinate dehydrogenase and causes rapid loss of ATP in neurons in vitro [19,23]. Depletion of neuronal ATP leads to a sustained rise in cytosolic calcium due to the large consumption of ATP to restore plasma membrane potential after repetitive synaptic activity in brain neurons. This potentiates excitatory neurotransmitter secretion and, eventually, neuronal death through calpains activation. Moreover, by means of cellular and animal experimental models, NPA has been shown to promote excitotoxic neuronal death, mediated by the excitatory neurotransmitters L-glutamate and dopamine [17,24,25], and by calpains activation [19,26,27]. Furthermore, it has been shown that NPA produces indirect excitotoxic damage to the *striatum* [28], making it unlikely that NPA-induced selective damage of neurons in specific regions of the brain can be solely related with the metabolic rate and density of receptors for L-glutamate and dopamine.

Activated microglia in the brain is a major source of ROS and nitric oxide in the brain and this can also impair the mitochondrial respiratory chain function [29], and in a previous publication [10] we have shown a large decrease of reduced glutathione in parallel with a large increase of protein nitrotyrosines in NPA-induced degeneration of the striatum of adult Wistar rats brain. This is consistent with activation of neuroinflammatory microglia by NPA administration reported by others [30–32] and strongly suggests that inflammation mediates NPA-induced brain degeneration. Noticeably, non-invasive imaging of the human brain has revealed significant microglial activation both in the *striatum* and cortical areas in HD patients [33]. Indeed, it has been proposed that pro-inflammatory cytokines stimulate the development of neurodegenerative diseases—including Huntington’s, Alzheimer’s, and Parkinson’s—where there is a slow and progressive damage of cerebral cortical areas: *substantia nigra*, *striatum*, and *hippocampus* [34]. Pro-inflammatory cytokines may potentiate oxidative stress-induced cell death through enhanced production of ROS and nitric oxide and stimulation of L-glutamate release to the extracellular space [35]. In addition, the release of endogenous cell molecules during brain degeneration (Damage Associated Molecular Patterns or DAMPs) can elicit further microglial activation, establishing a positive feedback loop in those brain areas undergoing a more extensive degeneration, such as the *striatum* and vicinal somatomotor *cortex* [36].

However, the molecular mechanisms through which brain inflammation can selectively produce cell death in specific neuronal structures remain unclear. Astrogliosis and loss of astrocytes have been noticed in the brain *striatum* in rats treated with NPA [28,31,32,37]. Recently, it has been shown that neuroinflammatory microglia activation can induce the formation of a specific type of reactive neurotoxic astrocytes, named A1, through the secretion of specific cytokines interleukin-1 α (IL-1 α), tumor necrosis factor α (TNF α) and complement component 1q (C1q), and that reactive A1 astrocytes are abundant in post-mortem tissue of HD patients [38]. Moreover, it has been noted that complement component 3 (C3) is a highly upregulated gene in A1 astrocytes, while it is not expressed by ischemic reactive astrocytes, named A2 [38]. Thus, C3 expression can be used to highlight the induction of reactive neurotoxic A1 astrocytes in neurodegenerative disorders.

In this work we used an experimental model based on the intraperitoneal administration of NPA to rats at doses that can elicit extensive brain degeneration, and brain samples were taken before and after extensive brain damage can be noticed. We show that reactive A1 astrocytes, expressing the activated C3 α fragment, are induced by NPA treatment in the *striatum*, as well as in highly relevant

neuronal structures inside both the *hippocampus* and the *cerebellum*. Consistent with this finding, an increase of the levels of pro-inflammatory cytokines IL-1 α , TNF α , and C1q was also detected in these areas of the brain of rats treated with NPA.

2. Results

In this work we designed an experimental NPA-treatment to induce progressive brain degeneration to investigate early biomarkers before the appearance of neurological defects and neuronal death.

2.1. The Increase of Activated Complement C3 Protein, a Reactive A1 Astrocyte Marker, Precedes Significant NPA-Induced Brain degeneration

Adult Wistar rats treated i.p. with a daily dose of 25 mg NPA/kg body weight up to 24 days (G24) already showed neurological defects based on increased dystonic movements of hind limbs and an abnormal gait, characterized by a wobbly gait and padding. These neurological symptoms are characteristics of this HD experimental model, as we previously described [10]. Furthermore, 2,3,5-triphenyltetrazolium chloride (TTC) staining of rat brain slices present evident damage of the *striatum* (Figure 1). Additionally, neuronal loss detected by means of neurogranin immunostaining and apoptotic cells observed with TUNEL staining reveal the neuronal damage related with the pathological events above described (Figure 1).

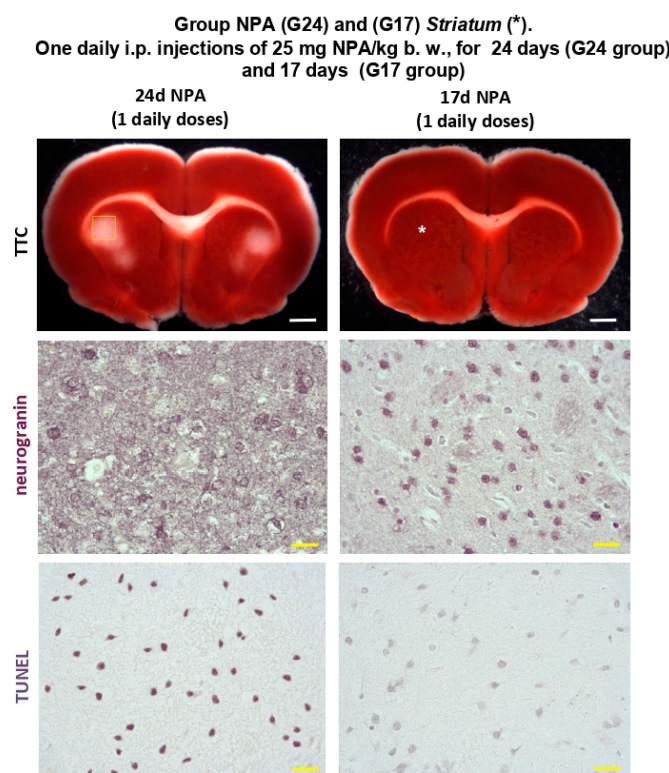


Figure 1. Rats of the G24 group show degeneration of the brain *striatum* (*) with respect to rats of the G17 group. Representative coronal sections stained with 2,3,5-triphenyltetrazolium chloride (TTC), neurogranin, and TUNEL, as indicated in Section 4. Treatment with one daily i.p. injection of 25 mg 3-nitropropionic acid (NPA)/kg b. w. for 24 days (G24 group) shows an initial unstained area of the *striatum* after TTC staining with respect to rats of the G17 group. Yellow square mark indicates the selected TTC unstained area neurogranin and TUNEL staining. Comparative neurogranin immunolabeling reveals a loss of neuronal somas in the *striatum* of rats of the G24 group with respect to rats of the G17 group. Comparative TUNEL staining shows neuronal cell death in the *striatum* (*) of rats of the G24 group. White scale bars: 2 mm. Yellow scale bars: 25 μ m.

Interestingly, rats treated i.p. with a daily dose of 25 mg NPA/kg body weight up to 17 days (G17) did not show significant sensorial or motor neurological dysfunctions yet, although after 17 doses some rats became hypoactive, but keeping a normal posture and gait. Indeed, G17 staining of coronal rat brain sections showed no differences with TTC staining of untreated control rats (Figure 2). The lack of noticeable unstained white areas in the *striatum*, *hippocampus*, and *cerebellum* of rats treated i.p. with one daily dose of 25 mg NPA/kg, for 17 days, pointed out that this treatment still did not produce observable degeneration of these brain areas. This result is supported by the neuronal soma labeling with neurogranin and no evident apoptotic cells with TUNEL in the *striatum* (Figure 1).

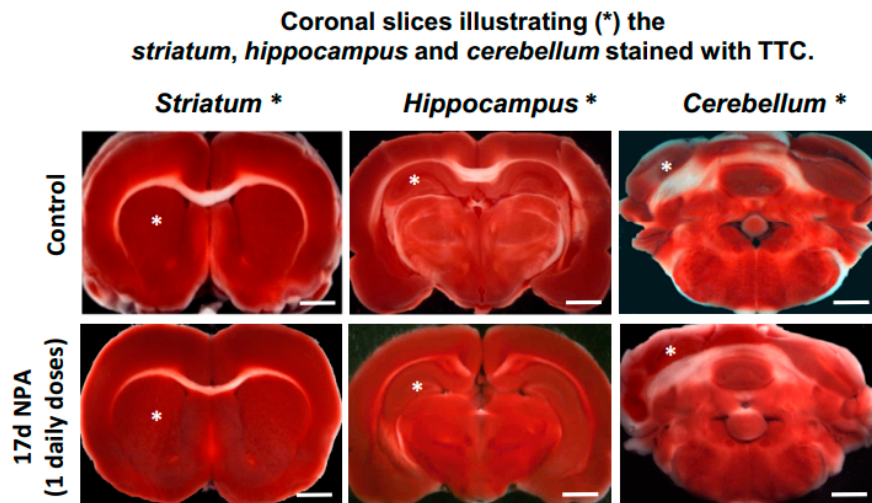


Figure 2. Representative fresh brain 1.5 mm thick coronal slices illustrating the *striatum*, *hippocampus*, and *cerebellum* (respectively marked with white asterisk) stained with TTC. Treatment with one daily i.p. injection of 25 mg NPA/kg b. w., for 17 days (G17 group) show no differences with TTC staining of control rats. Scale bars: 2 mm.

On these grounds, we selected rats subjected to 17 days treatment (G17) for an experimental assessment of brain biomarkers at early stages of the NPA-induced neurotoxic process (Figure 3). Western blots reveal that proteolytic fragment C3 α levels in the *striatum*, *hippocampus*, and *cerebellum* increased more than two-fold with respect to control untreated rats, namely 2.33 ± 0.17 , 3.7 ± 0.25 , and 2.2 ± 0.15 -fold, respectively (Figure 3A,C). Notably, it has been shown that reactive A1 astrocytes are also produced upon neuronal axotomy [38], which can account for the low levels of C3 α detected in these brain regions in control untreated rats. This result pointed out that reactive A1 astrocytes induced by this NPA treatment can be seen before significant NPA-induced brain damage is detected through TTC, neurogranin, and TUNEL staining, and precedes NPA-induced neurological dysfunctions.

Interestingly, brains of rats treated i.p. with a daily dose of 25 mg NPA/kg body weight for 6 days (G6) showed that a statistically significant increase of C3 α levels with respect to control rats can only be observed in the *hippocampus* and *cerebellum*, i.e., an increase of 2.5 ± 0.2 and 2.4 ± 0.2 -fold, respectively (Figure 3B). This fact indicates an early generation of reactive A1 astrocytes in these two brain regions.

2.2. The Increase of Proinflammatory Cytokines IL-1 α and TNF α Also Precedes Significant NPA-Induced Brain Degeneration

Recent studies have shown that cytokines IL1- α and TNF α are specifically expressed in activated microglia induced by different brain injuries inducing reactive A1 astrocytes [38–40]. Therefore, by means of Western blotting, we measured by the expression level of these cytokines in the *striatum*, *hippocampus*, and *cerebellum* of rats treated i.p. with one daily dose of 25 mg NPA/kg body weight for 17 days (G17). Figure 4 shows that both IL1 α and TNF α are increased in these brain areas with respect to control rats. The quantitative analysis yielded a similar increase of approximately 50% of the IL1 α

level in all brain areas under analysis (*striatum*, *hippocampus*, and *cerebellum*), while the increase of TNF α was higher in the *striatum* (160%) than in the *hippocampus* (80%) and *cerebellum* (70%).

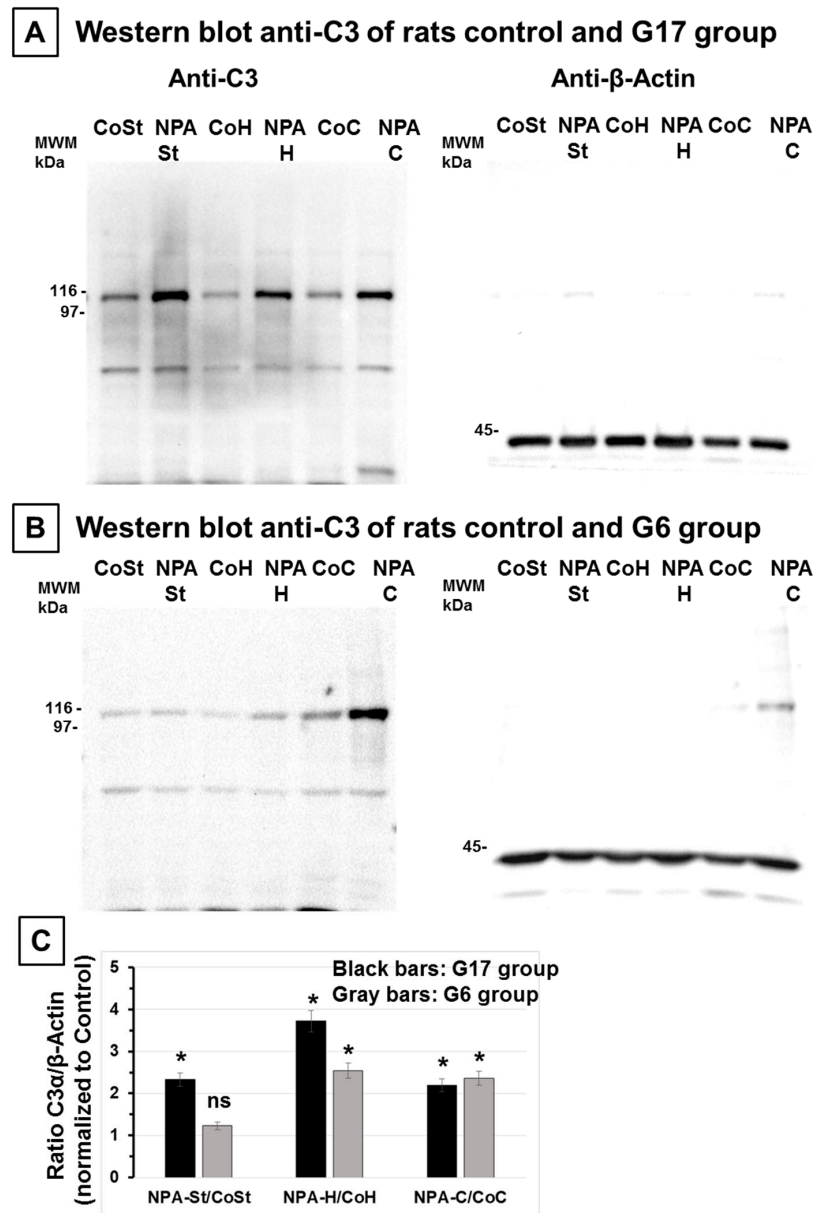


Figure 3. Rats of the G17 group show a large increase of the C3 α proteolytic fragment in the *striatum*, *hippocampus*, and *cerebellum* with respect to rats of the control group, while the C3 α proteolytic fragment only significantly increases in the *hippocampus* and *cerebellum* in the rats of the G6 group. Representative Western blots of C3 and β -actin of *striatum* (St), *hippocampus* (H), and *cerebellum* (C) homogenates of rats of control (Co) and G17 group (NPA rats) (A) and of control (Co) and G6 group (NPA rats) (B). After acquisition of images of the Western blot with anti-C3, the polyvinylidene difluoride (PVDF) membrane was stripped and processed for the Western blot of anti- β -actin, as indicated in Section 4. The molecular weights of the protein markers (MWM) closer to the target proteins (C3 α proteolytic fragment and β -actin) are indicated on the left-hand side. (C) Plot of the ratio of (C3 α / β -actin) in *striatum*, *hippocampus*, and *cerebellum* homogenates of rats of G17 (black bars) and G6 (gray bars) groups relative to control rats. The results shown are the average \pm s.e. of triplicate experiments. (*) $p < 0.05$ with respect to control rats; ns, statistically non-significant difference with respect to control rats.

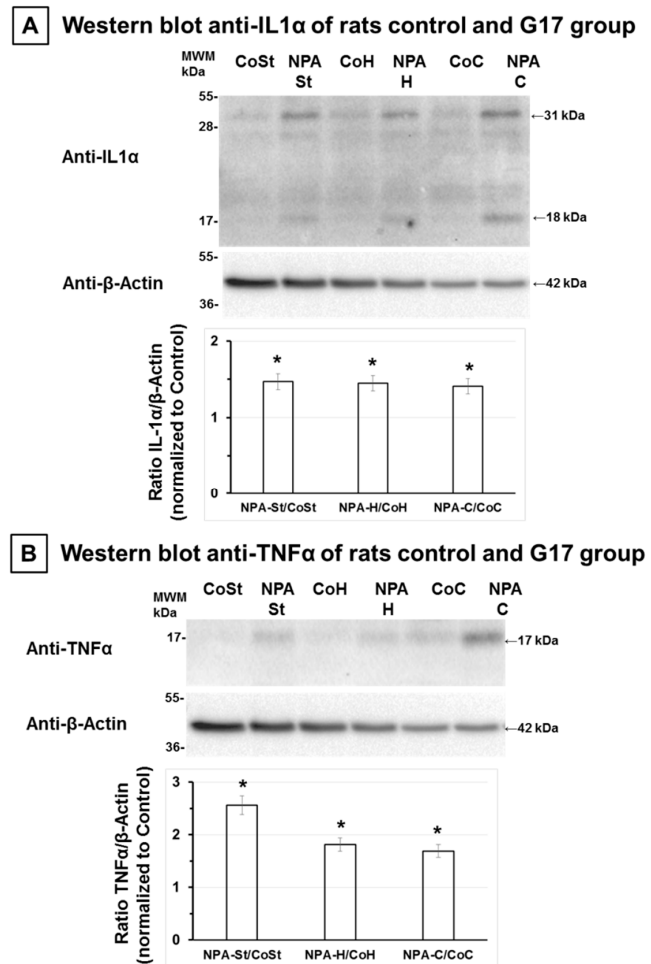


Figure 4. Rats of the G17 group show a significant increase of interleukin-1 α (IL-1 α) and tumor necrosis factor α (TNF α) in the *striatum*, *hippocampus*, and *cerebellum* with respect to rats of the control group. Representative Western blots of IL-1 α and β -actin (A) and of TNF α and β -actin (B) of *striatum* (St), *hippocampus* (H), and *cerebellum* (C) homogenates of rats of control (Co) and G17 group (NPA rats). After acquisition of images of the Western blot with anti-IL-1 α and TNF α , PVDF membranes were stripped and processed for the Western blot of anti- β -actin, as indicated in Section 4. The estimated molecular weights of the target proteins IL-1 α , TNF α , and β -actin are indicated on the right hand side, and on the left hand side the molecular weights of the protein markers (MWM) closer to the target protein are included. Plots of the ratios of (IL-1 α / β -actin) and (TNF α / β -actin) in *striatum*, *hippocampus*, and *cerebellum* homogenates of rats of G17 group relative to control rats are also inserted, respectively. The results shown are the average \pm s.e. of triplicate experiments. (*) $p < 0.05$ with respect to control rats.

2.3. Immunohistochemical Analysis of the Regionalization and Location of Complement C3 Protein Activation in the Striatum, Hippocampus, and Cerebellum

Our findings reveal a progressive increase in the activation of the complement component C3 protein from G6 through G17 groups. Since activation of C3 has earlier been identified as a reactive A1 astrocyte marker [38], we also used the astrocytic marker glial fibrillary acidic protein (GFAP).

As illustrated in Figure 5, an increase in reactive A1 astrocytes—expressing C3 α and GFAP—was observed in the dorsolateral region of the *striatum* (*caudate-putamen*) in NPA treated rats in experimental G17 group (Figure 5A). With respect to the *hippocampus*, we also observed an increase both in C3 α and GFAP, particularly significant within the pyramidal layer and *stratum radiatum* of CA1 area in Ammon's horn (Figure 5B). In addition, Figure 5 also highlights characteristic changes of the shape of astrocytes, and that C3 α and GFAP co-localize in the ameboid-shaped reactive A1 astrocytes, detected by using double immunohistochemistry.

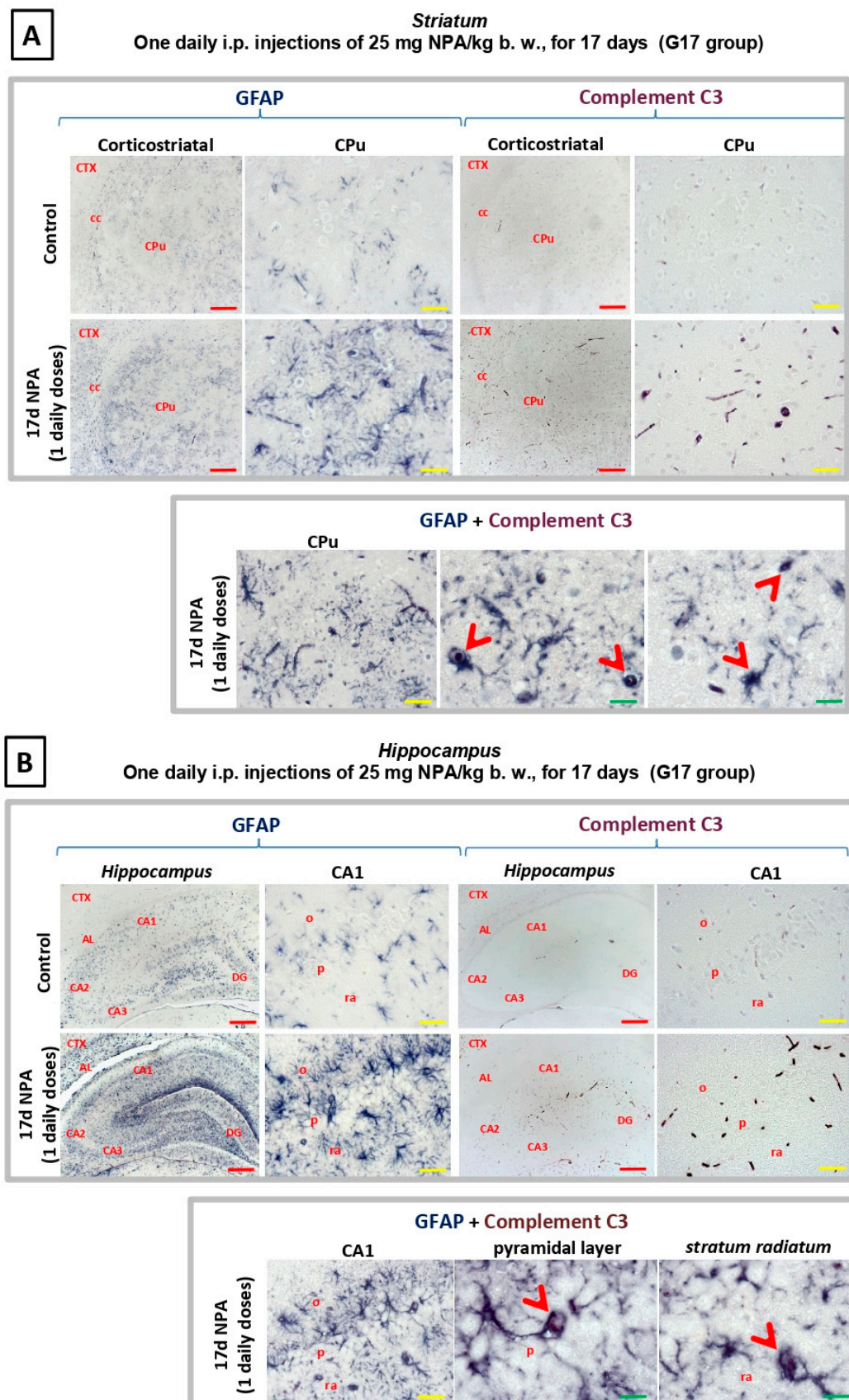


Figure 5. Rats of the G17 group (one daily i.p. injection of 25 mg NPA/kg b. w., for 17 days) show a significant increase of glial fibrillary acidic protein (GFAP) and Complement C3 in the *striatum*

and *hippocampus* with respect to rats of the control group. Light micrographs of coronal sections after immunohistochemistry with anti-GFAP and anti-Complement C3 antibodies. (A) Comparative immunolabeling showing an increase in astrocytes expressing C3 α and GFAP (upper panel), observed in the dorsolateral region of the *striatum (caudate putamen)* in experimental rats. Note that C3 α and GFAP co-localize in the ameboid-shaped astrocytes (arrowhead), detected by using double immunohistochemistry (lower panel). (B) At the level of the *hippocampus* an increase both in C3 α and GFAP is particularly significant within the pyramidal layer and *stratum radiatum* of CA1 area in Ammon's horn (upper panel). Note that C3 α and GFAP co-localize in astrocytes (indicated by red arrowheads), detected by using double immunohistochemistry (lower panel). In red letters: CPu: *striatum (caudate-putamen)*; CTX: Cerebral Cortex; cc: *corpus callosum*; CA1: field CA1 of *hippocampus*; CA2: field CA2 of *hippocampus*; CA3: field CA3 of *hippocampus*; DG: dentate gyrus; AL: *alveus*; o: *stratum oriens*; ra: *stratum radiatum*; p: pyramidal layer. Red scale bars: 200 μ m. Yellow scale bars: 25 μ m. Green scale bars: 10 μ m.

As shown in Figure 6, an increase in reactive A1 astrocytes expressing C3 α and GFAP was also present in the *cerebellum* of rats in G17, revealing the co-location of C3 α and GFAP in the ameboid-shaped reactive A1 astrocytes. The analysis of regionalization and distribution of reactive A1 astrocytes showed an increased expression in two specific locations, the cerebellar *nuclei*, and the cerebellar *cortex*. In the first location, C3 α is notably detectable at the level of dentate *nucleus*, while it is not observable either in the interposed or the fastigial cerebellar *nuclei* (Figure 6A). In the cerebellar *cortex* (Figure 6B), the increase of C3 α and GFAP is especially relevant within the Purkinje and granular layers. This distribution is evident in the most lateral zone of the cerebellar hemispheres and disappears progressively through the midline, being absent in the cerebellar *vermis*. Therefore, there is a significant regionalization of C3 activation that is clearly present in the cerebellar *neocortex*, and not detectable either in the paleo-or the archi-cerebellar *cortex*. Consequently, our data reveal that the corticonuclear lateral band, the most phylogenetically recent cerebellar area, is a highly sensitive cerebellar region to NPA-induced neurotoxicity.

2.4. Immunohistochemical Analysis of Regionalization and Location of IL1- α and TNF α Cytokines in the Striatum, Hippocampus, and Cerebellum

Generation of reactive A1 astrocytes in the brain has been shown to be induced by microglial activation and secretion of IL1 α and TNF α cytokines [38]. We experimentally assessed IL1- α and TNF α expressions in the three regions under analysis, that is *striatum*, *hippocampus*, and *cerebellum*. As observed in Figure 7, the treatment with 17 i.p. daily doses of 25 mg NPA/kg (G17) elicits an increase in these cytokines (Figure 7A) within the dorsolateral region of the *striatum (caudate putamen)*. This increase is also detected within the pyramidal layer and the *stratum radiatum* of CA1 area inside the Ammon's horn (Figure 7B).

As observed in Figure 8, cytokines IL1- α and TNF α are also expressed by NPA-activated cerebellar microglia. Our results show their regional distribution in the dentate *nucleus* (Figure 8A), as well as in the Purkinje and granular layers inside the most lateral zone of the cerebellar *cortex* (Figure 8B), highlighting microglial activation in the corticonuclear cerebellar lateral band.

Previous authors have reported an increase of cytokine C1q biosynthesis by activated microglia in HD, correlated to an increase of the activation of C3 complement protein [38,41,42]. Our results show a similar distribution of this cytokine in the three regions under analysis (Figure 9) in agreement with the above-mentioned cytokines. Overall, the pattern of increased expression of cytokines (IL1- α , TNF α , and C1q) in *striatum*, *hippocampus*, and *cerebellum* correlated with the regionalization of C3 positive reactive A1 astrocytes.

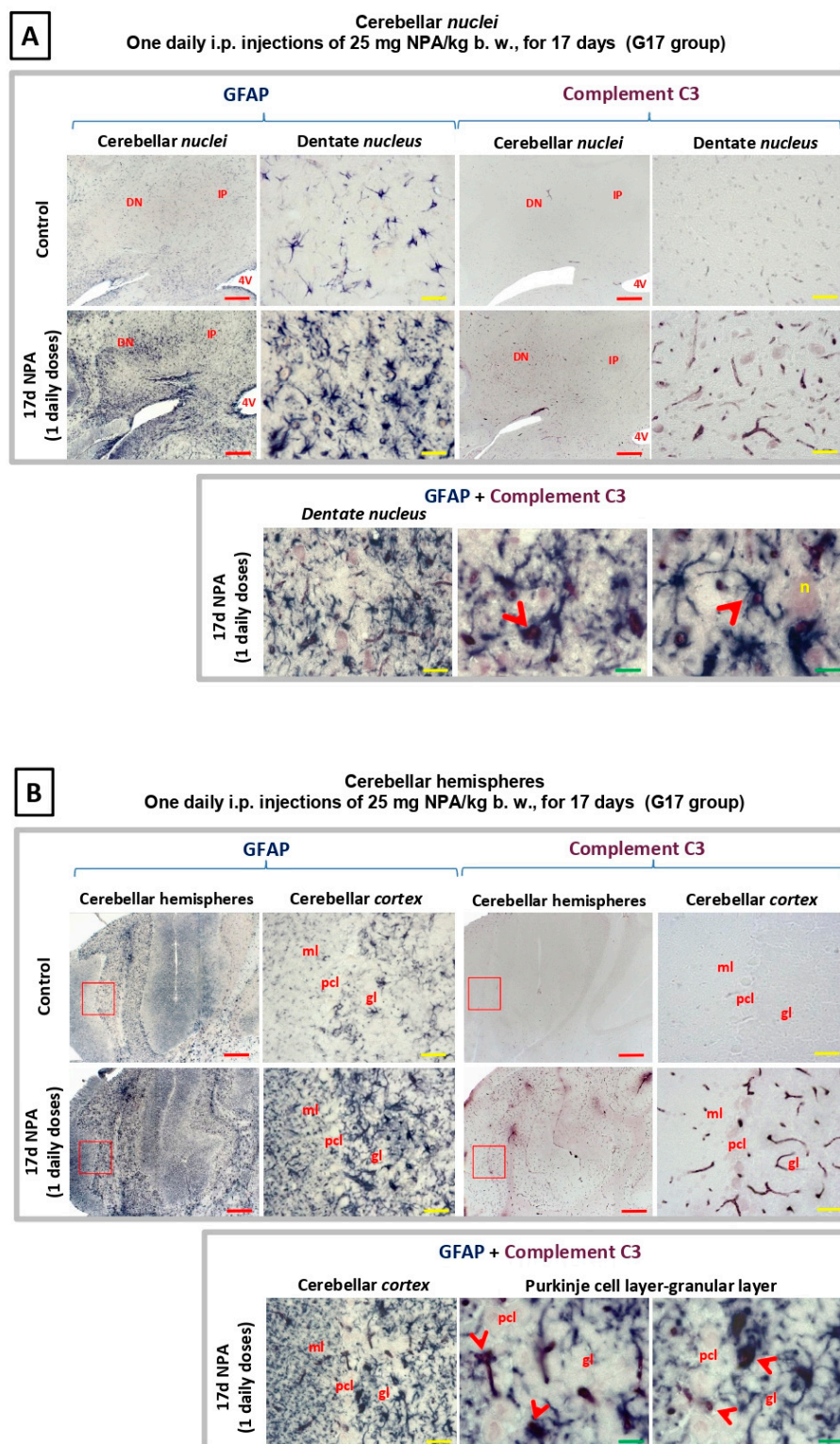


Figure 6. Rats of the G17 group (one daily i.p. injections of 25 mg NPA/kg b. w., for 17 days) show a significant increase of GFAP and Complement C3 in the cerebellum with respect to rats of the control group. Light micrographs of coronal sections after immunohistochemistry with anti-GFAP and anti-Complement C3 antibodies. (A) Comparative immunolabeling showing an increase in astrocytes expressing C3 α and GFAP (upper panel), observed in the cerebellar nuclei in experimental rats. C3 α is notably detectable at the level of dentate nucleus, while it is not observable either in the interposed or the fastigial cerebellar nuclei. Note that C3 α and GFAP co-localize in the ameboid-shaped astrocytes

(arrowhead), detected by using double immunohistochemistry (lower panel). (B) Comparative immunolabeling showing an increase in astrocytes expressing C3 α and GFAP (upper panel), observed in the cerebellar cortex in experimental rats, including the Purkinje and granular layers. Note that C3 α and GFAP co-localize in the astrocytes (indicated by red arrowheads), detected by using double immunohistochemistry (lower panel). The red squares indicate the enlarged area shown on respective image of the right side. In red letters: DN: dentate nucleus; IP: interposed nucleus; 4 V: forth ventricle; n: large or projecting neuron; ml: molecular layer; pcl: Purkinje cell layer; gl: granular layer. Red scale bars: 200 μ m. Yellow scale bars: 25 μ m. Green scale bars: 10 μ m.

Striatum. Hippocampus
One daily i.p. injections of 25 mg NPA/kg b. w., for 17 days (G17 group)

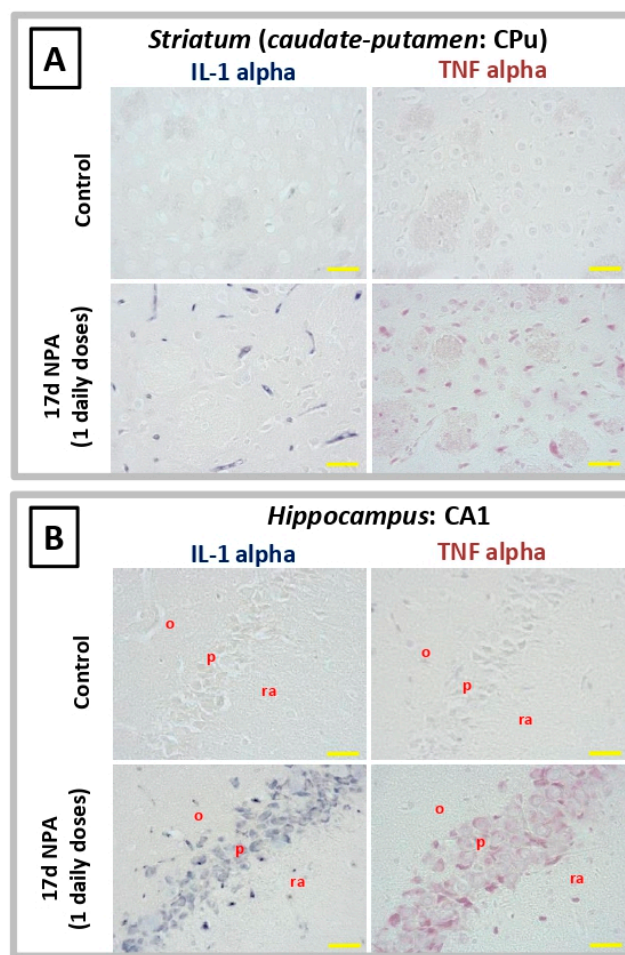


Figure 7. Rats of the G17 group (one daily i.p. injection of 25 mg NPA/kg b. w., for 17 days) show a significant increase of IL1 α and TNF α cytokines in the *striatum* and *hippocampus* with respect to rats of the control group. Light micrographs of coronal sections after immunohistochemistry with anti-IL1 α and anti-TNF α antibodies. Comparative immunolabeling showing an increase of IL1- α and TNF α expressions in the *striatum* (A) and *hippocampus*, within the pyramidal layer and the *stratum radiatum* of CA1 area inside the Ammon's horn (B). In red letters: o: *stratum oriens*; ra: *stratum radiatum*; p: pyramidal layer. Yellow scale bars: 25 μ m.

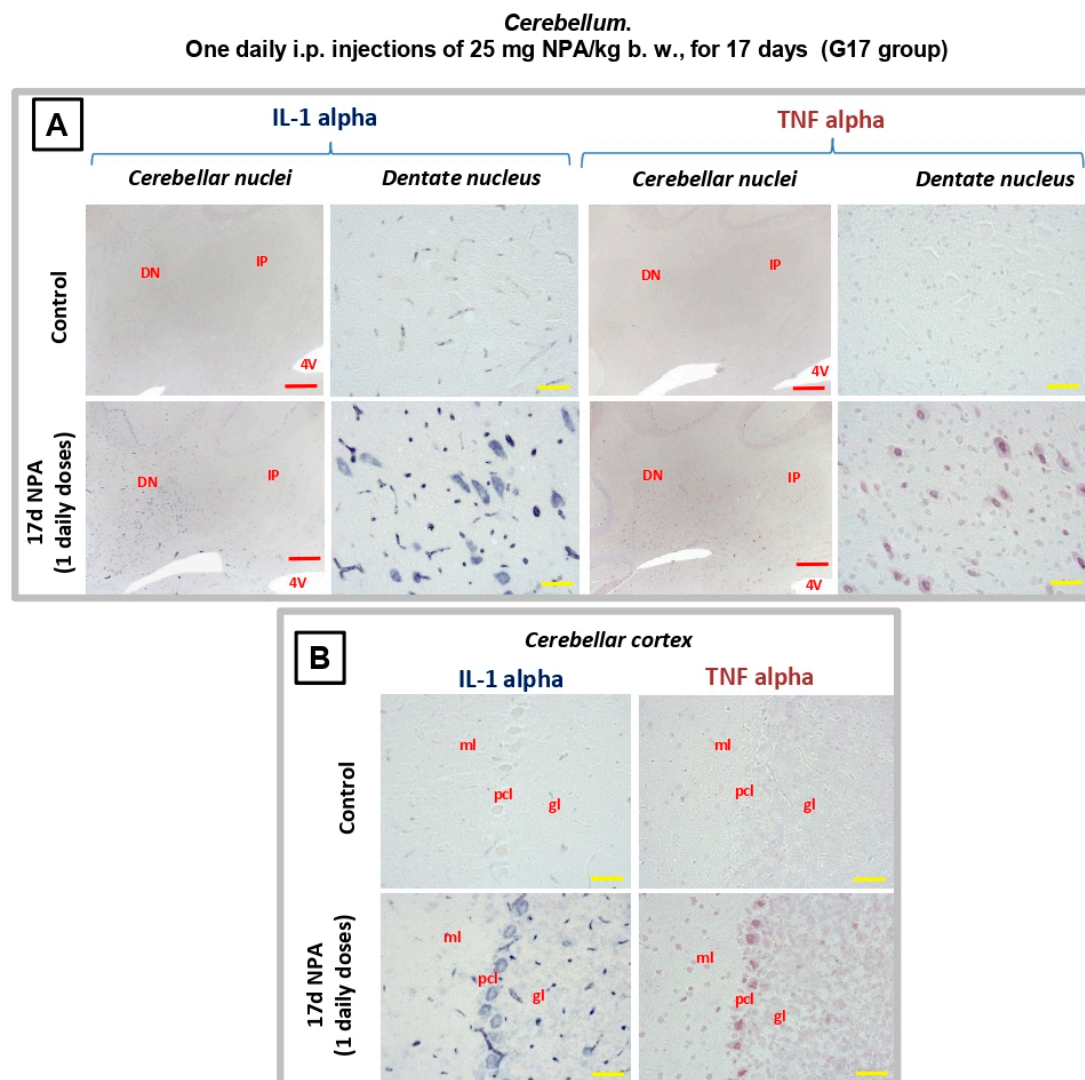


Figure 8. Rats of the G17 group (one daily i.p. injection of 25 mg NPA/kg b. w., for 17 days) show a significant increase of IL1 α and TNF α cytokines in the *cerebellum* and with respect to rats of the control group. Light micrographs of coronal sections after immunohistochemistry with anti-IL1 α and anti-TNF α antibodies. Comparative immunolabeling showing an increase of IL1- α and TNF α expressions in the *dentate nucleus* (A), as well as in the Purkinje and granular layers inside the most lateral zone of the cerebellar cortex (B). In red letters: DN: dentate nucleus; IP: interposed nucleus; 4 V: forth ventricle; ml: molecular layer; pcl: Purkinje cell layer; gl: granular layer. Red scale bars: 200 μ m. Yellow scale bars: 25 μ m.

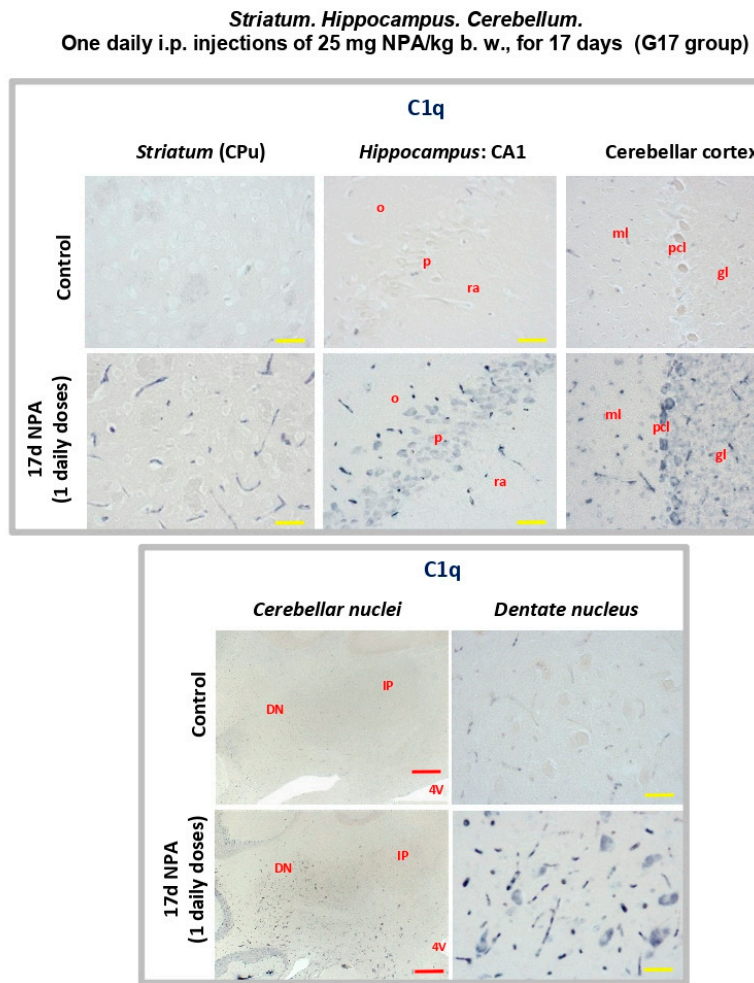


Figure 9. Rats of the G17 group (one daily i.p. injection of 25 mg NPA/kg b. w., for 17 days) show a significant increase of cytokine C1q in the three areas analyzed with respect to rats of the control group. Light micrographs of coronal sections after immunohistochemistry with anti-C1q antibody. Comparative immunolabeling showing an increase of cytokine C1q expression in the *striatum*, *hippocampus* (CA1 area), and cerebellar *cortex* (upper panel), as well as in the dentate nucleus (lower panel). In red letters: o: *stratum oriens*; ra: *stratum radiatum*; p: pyramidal layer; ml: molecular layer; pcl: Purkinje cell layer; gl: granular layer; DN: *dentate nucleus*; IP: *interposed nucleus*; 4 V: forth ventricle. Red scale bars: 200 μ m. Yellow scale bars: 25 μ m.

3. Discussion

The results of this work show a significant increase in the expression levels of C3 α subunit and cytokines IL-1 α , TNF α , and C1q within the *striatum*, *hippocampus*, and *cerebellum*, well before the appearance of the HD-related neurological dysfunctions induced by i.p. NPA injections to adult Wistar rats. Noteworthy, the release of specific cytokines IL-1 α , TNF α , and C1q upon microglial activation is required to induce reactive neurotoxic A1 astrocytes expressing C3 α subunit [38]. Thus, as a novel finding in NPA-induced neurotoxicity, our results demonstrate an earlier activation of complement C3 protein in the brain from Wistar rats that are treated with this neurotoxin. Other authors have also observed complement C3 expression in astrocytes in the *striatum* obtained from HD post-mortem brain samples [38,41]. However, unlike our observations in initial stages of NPA neurotoxicity, these authors have also described C3 expression in white matter and neurons in the *striatum* from the same patients [41], which is possibly well justified due to an advanced lesion stage (from Vonsattel grade 4), when neuronal loss is already evident.

NPA is a mitochondrial toxin that has been shown to produce microglial activation and neuronal death [30], and toxic effects of NPA on astrocytes at early stages of NPA-induced neurodegeneration has been reported [43]. Therefore, our results further validate the use of NPA i.p. administration to shed light on molecular mechanisms in the initial stages of neurotoxicity in HD. Consistently, the astrocytes—which are GFAP positive—present an increased expression of complement C3, suggesting an astrocytosis process characterized by the presence of A1 reactive astrocytes. In the present study, our results show an increase of A1 astrocytes in the three regions under analysis: *striatum*, *hippocampus*, and *cerebellum*. Histochemistry of brain slices in these regions point out that rats treated i.p. with NPA show a marked increase of anti-C3 staining with respect to control untreated rats in the vicinity of or in myelinated axons, striatal spiny neurons, pyramidal neurons of *hippocampus* Ammon's horn, Purkinje cerebellar neurons, and also in pyramidal neurons of the cerebellar *nuclei*. Since reactive A1 astrocytes are strongly neurotoxic [38], our results strongly support that these neuronal structures are highly vulnerable brain primary targets in NPA-induced neurotoxicity. Interestingly, these neuronal brain structures play a relevant role in motor neurological functions coordinated by the brain, and their degeneration can account for the motor dysfunctions induced by NPA treatment at a later stage. Indeed, kainic acid administration in rats, an animal model of epilepsy neuropathology, also induces a C3 expression increase in the glia of the *hippocampus* as well as in the pyramidal neurons corresponding to CA1 and CA3 areas, neurons particularly sensitive to kainic acid-induced neuronal death [44,45].

It has been proposed that HD is a neurodegenerative disease associated with a neuroinflammatory process mediated by microglial activation in the brain [34,36]. Pro-inflammatory cytokines can promote neuronal death through induction of ROS and also reactive nitrogen species production [29,46,47], excitotoxicity caused by the release of L-glutamate [35] and of damage-associated molecular products [47,48], as well as activation and proliferation of astrocytes [47]. It has been reported that the secretion of cytokines IL-1 α , TNF α , and C1q upon reactive microglial activation can induce the generation of reactive A1 astrocytes [38]. In a previous work [10] we have shown that there is a large increase of protein nitrotyrosines and depletion of reduced glutathione in NPA-induced degeneration of adult Wistar rat brains, pointing out a large induction of ROS and also reactive nitrogen species in this animal model of HD. In this work we showed that cytokines IL-1 α , TNF α , and C1q are also overexpressed in the *striatum*, *hippocampus*, and *cerebellum* of adult Wistar rats treated with daily i.p. injections of 25 mg NPA/kg b.w. In our experimental model, i.p. administration of NPA induced a gradual increase of these three cytokines starting long before the observation of any significant neurological motor impairment in treated rats, indicating an early induction of reactive microglia in the three regions under study (*striatum*, *hippocampus*, and *cerebellum*), and supporting the hypothesis of an early role of the three cytokines in the neuroinflammatory process. Furthermore, the increase of IL-1 α , TNF α , and C1q co-localizes with the appearance of C3 positive astrocytes in the three regions. Considering all these data, we conclude that, in our HD experimental animal model, extensive reactive microglial activation takes place in the brain, along with a reactive astrocytosis with generation of neurotoxic A1 astrocytes near or at neuronal structures which play a major role in brain motor coordination. These processes are likely to induce the brain neurodegenerative events that elicit motor disorders observed at an advanced stage of this neurological disease.

Finally, our results provide novel insights into *cerebellum* alterations after NPA administration, which may justify, at least in part, the motor symptoms in these kinds of patients. Previously, it has been reported [16] that NPA administration modifies the levels of metabolite concentrations, specifically of the neuronal activity markers N-acetylaspartate and the osmolyte taurine, in several areas of the rat brain, including the *cerebellum*. Recently, extensive Purkinje cells loss and overall cerebellar damage has been observed in the cerebellar *cortex* from the autopsy of HD cases [18]. As a novel contribution, our results reveal an early expression of inflammatory cytokines and complement C3 at the level of the *dentate nucleus* and the neocerebellar *cortex*. This highlights that NPA administration primarily affects the more recent phylogenetic area of the rat *cerebellum*. Therefore, our experimental NPA model

provides an alternate novel tool to study structure–function alterations of the *cerebellum* as a key target in the early stages of HD.

4. Materials and Methods

4.1. Animals and Treatments

Male Wistar rats, 9–10 weeks old, weighing 290–340 g were housed in a 12 h light/dark cycle and allowed free access to food and water during the experiment. The experimental procedures followed the animal care guidelines of the European Union Council Directive 86/609/EEC. The protocols were approved by the Ethics Committee for Animal Research of the local government.

3-Nitropropionic acid, (>97% by HPLC, Sigma, St. Louis, MO, USA) was administered by intraperitoneal (i.p.) injection of a 20-mg/mL solution in normal saline (0.9% *w/v* NaCl). Fresh solutions were prepared by dissolving solid NPA, the pH was adjusted to 7.4 with NaOH 5 M, and filtered through a 0.2 μm filter.

Rats were treated with 25 mg NPA/kg b.w. every 24 h for 6, 17, and 24 days, and are referred in the text as rats from G6 ($n = 7$), G17 ($n = 7$), and G24 ($n = 7$) groups. Of note, the total number of rats used for the G24 group was 10, because three rats died after developing severe pathological symptoms, an interindividual variability that we noticed when adult Wistar rats were treated with doses of 25 mg NPA/kg b.w. every 12 h [10]. Rats from control groups ($n = 6$) received 0.4 mL saline solution (NPA vehicle), with the same treatment schedule given in the experimental groups.

The animals were evaluated for motor impairment throughout the experiment. They were observed daily, just before the injection, and rated with a quantitative scale according to their motor deficiencies [10,49]. This rating scale measures gait abnormalities, hind limbs dystonia, grasping ability, balance, and recumbency.

4.2. Preparation of Rat Brain Slices and TTC Staining

The animals were anesthetized with ketamine (50 $\mu\text{g/g}$), diazepam (2.5 $\mu\text{g/g}$), and atropine (0.05 $\mu\text{g/g}$). The brains were immediately removed from the skull and washed in cold phosphate-buffered saline (PBS) pH 7.4, and then cut with a tissue slicer (Stoelting, Woodale, IL, USA).

Some sections (1.5 mm thick coronal slice) corresponding to the three regions analyzed (*striatum*, *hippocampus*, and *cerebellum*) were immersed in a 2% solution of 2,3,5-triphenyltetrazolium chloride (TTC) in PBS for 15 min at 37 °C, and observed under a Leica MZ APO stereomicroscope.

4.3. Brain Samples Homogenization and Western Blotting

A group of dissected brain sections of *striatum*, *hippocampus*, and *cerebellum* was weighed and immediately frozen in liquid nitrogen. Thereafter, samples were kept at –80 °C until use.

Brain sections were homogenized within an ice-cold recipient with a glass homogenizer followed by sonication, 30–40 pulses of 1 s, in buffer 25 mM tris-(hydroxymethyl) aminomethane hydrochloride (Tris-HCl) at pH 7.4, 150 mM NaCl, 5 mM ethylenediaminetetraacetic acid, 50 mM NaF, 5 mM NaVO₃, and 4-(1,1,3,3-Tetramethylbutyl)phenyl-polyethylene glycol (Triton X-100) 0.25%, supplemented with the protease inhibitor cocktail SIGMAFAST S8820 (Sigma-Aldrich). Brain homogenates were centrifuged at 500×*g* for 10 min at 4 °C to pellet tissue debris, the supernatant was carefully removed and supplemented with 40% glycerol, their protein concentration was determined using Bradford's method, and these samples were conserved at –80 °C until use for Western blotting.

Samples of the homogenates at 1–2 mg of protein/mL were denatured by heating at 98 °C for 5 min in 95 mM Tris-HCl buffer (pH 6.8), 3% sodium dodecyl sulfate (SDS), 1.5% *v/v* β -mercaptoethanol, 13% glycerol, and 0.005% bromophenol blue. Then, 20 μg of protein samples were loaded per lane in a polyacrylamide gel of 7.5% or 12% acrylamide, and after running the SDS-polyacrylamide gel electrophoresis the gel was transferred to a polyvinylidene difluoride (PVDF) membrane of 0.2 μm average pore size in standard transfer medium (Trans-BloT TransferMedium, BioRad). PVDF

membrane blocking was carried out by 1 h incubation and mild shaking with 3% bovine serum albumin (BSA) in Tris-buffered saline (TBS) supplemented with 0.05% polyoxyethylenesorbitan monolaurate (TBST). Before the incubation with the primary antibody, membranes were washed three times with TBST. The immunodetection of the selected protein (C3, IL-1 α , and TNF α) was performed with the following primary antibodies: rabbit monoclonal anti-C3 from Abcam (ab200999, dilution 1:2000), mouse monoclonal anti-IL-1 α from Santa Cruz Biotechnology (sc-9983, dilution 1:500) and rabbit polyclonal anti-TNF α from Abcam (ab6671, dilution 1:1000). After incubation with the first antibody overnight or 1 h at room temperature, membranes were washed six times with TBST and incubated for 1 h at room temperature with the appropriate secondary IgG antibody conjugated with horseradish peroxidase. Secondary anti-rabbit IgG-Horseradish peroxidase (Sigma-Aldrich-A0545) or anti-mouse IgG-Horseradish peroxidase (Sigma-Aldrich A0944) were used at a dilution of 1:5000 in TBST. Again, we washed the membrane six times with TBST followed by incubation for 2–3 min with Clarity TM Western ECL Substrate, BIO-RAD. Western blots were revealed with Bio-Rad ChemiDoc™ XRS+. The specificity of the detection of primary antibodies was then determined, and membranes were washed with deionized water and treated under continuous stirring at room temperature with the following stripping buffers: (1) 10 min with 0.2 M glycine/0.5 M NaCl brought to pH 2.8 with acetic acid and (2) 10 min with 0.5 M acetic acid/0.5 M NaCl at pH 2.5. After washing with distilled water for 10 min, membranes were blocked with 3% BSA in TBST and treated as indicated above to quantify β -actin to monitor protein load, using mouse monoclonal anti- β -actin (Sigma-Aldrich-A1978, dilution 1:5000) or rabbit polyclonal anti- β -actin (Sigma-Aldrich-A5060, dilution 1:750) as primary antibody, depending on the species of the selected target protein, and the appropriate secondary antibody conjugated with horseradish peroxidase (see above). Figure 10 shows a representative lane of the Western blots obtained with each one of the primary antibodies used for the selected proteins and against β -actin, highlighting the target protein band. Statistical analysis: results of Western blots are expressed as mean \pm standard error (s.e.). Statistical analysis was carried out by Mann–Whitney non-parametric test. Significant difference was accepted at the $p < 0.05$ level. All the results were confirmed with triplicate experiments.

Western blots of rat brain homogenates with the primary antibodies used in this work.

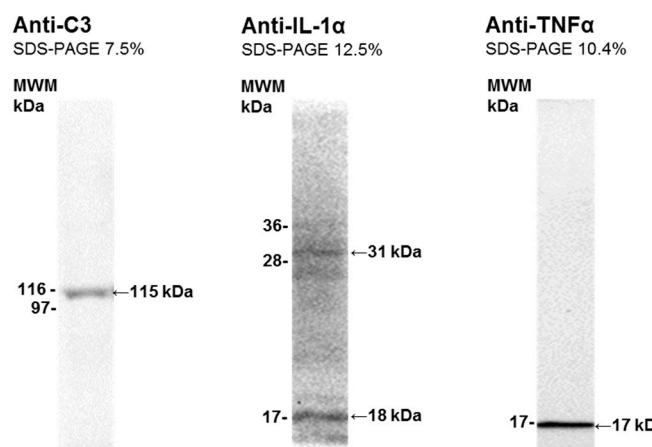


Figure 10. Western blotting of rat brain homogenates with the primary antibodies used in this work. The detection and specificity of primary antibodies for their corresponding target proteins was confirmed by Western blotting: rabbit monoclonal anti-C3 from Abcam (ab200999, dilution 1:2000), mouse monoclonal anti-IL-1 α from Santa Cruz Biotechnology (sc-9983, dilution 1:500), and rabbit polyclonal anti-TNF α from Abcam (ab6671, dilution 1:1000). MWM, molecular weight of protein markers closer to the target protein. See Section 4 for further experimental details.

4.4. Immunohistochemistry

A group of dissected brain sections of *striatum*, *hippocampus*, and *cerebellum* was immersed in 4% paraformaldehyde in PBS, dehydrated in a graded series of ethyl alcohol, cleared in xylene, and embedded in paraffin wax, using standard techniques. Afterwards, tissue blocks were cut in coronal sections (7 μ m thick) with a microtome Leica RM2125RT. Slices were hydrated and subjected to immunohistochemistry.

To identify and localize different cells populations we carried out the following procedures.

4.4.1. Glial Fibrillary Acidic Protein (GFAP), Interleukin 1 (IL-1 α), and Complement Component 1, Subcomponent q (C1q-C).

Tissue sections were blocked with 1% BSA in PBS for 30 min, followed by incubation with 5% normal goat serum in 1% BSA and 0.1% Triton X-100 for 2h. Next, slides were incubated overnight at 4 °C in humidified box, with primary antibodies: dilution 1:400 for mouse anti-GFAP (Sigma: G3893), and dilution 1:50 for both mouse anti-IL-1 α (Santa Cruz Biotechnology: sc-9983) and mouse anti-C1q-C (Santa Cruz Biotechnology: SC-365301). After extensive washing in PBS, sections were again blocked and the secondary antibody (dilution 1:200) was added, a goat anti-mouse immunoglobulin G conjugated with alkaline phosphatase (IgG-AP), Santa Cruz Biotechnology: sc 3698 for 3 h at room temperature. Finally, the sections were repeated rinsed in PBS, treated with 2 mm levamisole in reaction buffer (100 mm NaCl, 100 mm Tris-HCl pH 9.5, 0.25% polyoxyethylenesorbitan monolaurate, revealed with nitroblue tetrazolium/5-bromo-4-chloro-3-indolyl phosphate (NBT/BCIP) supplied by Roche (catalog n° 1681451) in reaction buffer, washed in PBS, dehydrated and mounted in Eukit.

4.4.2. Complement Component 3, (C3), Tumor Necrosis Factor Alpha (TNF α), and Neurogranin.

Tissue sections were blocked with 1% BSA in PBS for 30 min, followed by incubation with 5% normal goat serum in 1% BSA and 0.1% Triton X-100 for 2 h. Next, slides were blocked with endogenous avidin/biotin blocking kit (Abcam ab 64212) and incubated overnight at 4 °C in humidified box, with primary antibodies: dilution 1:2000 for rabbit anti-C3 (Abcam ab225539), dilution 1:100 for rabbit anti-TNF α (Abcam ab6671), and dilution 1:500 for rabbit anti-neurogranin (Chemicon AB5620). After extensive washing in PBS, endogenous peroxidase activity was quenched with 0.5% H₂O₂, again blocked, and incubated with the secondary antibody, a biotinylated goat anti-rabbit immunoglobulin G supplied by Vectastain ABC Kit, Vector Laboratories (PK-6101), for 3 h at room temperature. After rinsing in PBS, the sections were incubated with avidin-biotinylated horseradish peroxidase complex (Vectastain ABC Kit) for 30 min at room temperature. Chromogen development was performed with peroxidase substrate solution (Vector VIP substrate, SK-4600). Slides were washed in distilled water, dehydrated, and mounted in Eukit.

For double immunohistochemistry (GFAP and C3), primary antibodies mouse anti-GFAP and rabbit anti-C3 were applied together and incubated overnight at 4 °C in humidified box. Secondary antibodies, goat anti-mouse conjugated with alkaline phosphatase and biotinylated goat anti-rabbit Vectastain ABC Kit, were applied together, and incubated for 3 h at room temperature. The chromogen development AP anti-GFAP (blue) was developed before POD anti-C3 (red) due to the different pHs used (i.e., develop the more basic pH reaction first to avoid cross-reaction).

4.4.3. Terminal Deoxynucleotidyl Transferase-Mediated Deoxyuridine Triphosphate Nick-End Labelling (TUNEL).

Tissue sections were treated as we have described in a previous publication [50] with an in-situ cell death detection kit, POD (Roche). Apoptotic cells were observed under microscopy using a Vector VIP substrate kit (peroxidase detection; Vector Laboratories).

Author Contributions: The experimental study was designed and supervised by C.G.-M., C.L.-S., and V.G.-M., who also wrote the manuscript. All authors have contributed to the experimental work and analyzed and

discussed the results. Specific experimental tasks: C.L.-S. extracted brain samples, designed, and performed TTC staining and immunohistochemistry experiments with the direct collaboration of V.G.-M. and V.G.-L. J.P. and J.S. collaborated in animal treatments with NPA, prepared brain samples for Western Blotting, and ran Western blots. All authors have read and agreed to the published version of the manuscript.

Funding: This work has been supported by Grants: BFU2014-53641-P and BFU2017-85723-P of the Spanish Plan Nacional de I+D+i, and GR18185, AA-17-0099-1 and IDA1-18-0041-3 of the Junta de Extremadura. All these Grants have been co-financed by the European Funds for Structural Development (FEDER). Jairo Salazar has been supported by a predoctoral Fellowship of the Fundación Carolina (Spain).

Acknowledgments: We thank Laura Ortega Bermejo for her invaluable technical support with animal handling and sample preparation for immunohistochemistry.

Conflicts of Interest: The authors declare no conflict of interest.

References

1. Alston, T.A.; Mela, L.; Bright, H.J. 3-Nitropropionate, the toxic substance of *Indigofera*, is a suicide inactivator of succinate dehydrogenase. *Proc. Natl. Acad. Sci. USA* **1977**, *74*, 3767–3771. [[CrossRef](#)]
2. Liu, X.; Luo, X.; Hu, W. Studies on the epidemiology and etiology of moldy sugarcane poisoning in China. *Biomed. Environ. Sci.* **1992**, *5*, 161–177.
3. Ming, L. Moldy Sugarcane Poisoning—A Case Report with a Brief Review. *J. Toxicol. Clin. Toxicol.* **1995**, *33*, 363–367. [[CrossRef](#)]
4. Blumenthal, C.Z. Production of toxic metabolites in *Aspergillus niger*, *Aspergillus oryzae*, and *Trichoderma reesei*: Justification of mycotoxin testing in food grade enzyme preparations derived from the three fungi. *Regul. Toxicol. Pharmacol.* **2004**, *39*, 214–228. [[CrossRef](#)]
5. Beal, M.; Brouillet, E.; Jenkins, B.; Ferrante, R.; Kowall, N.; Miller, J.; Storey, E.; Srivastava, R.; Rosen, B.; Hyman, B. Neurochemical and histologic characterization of striatal excitotoxic lesions produced by the mitochondrial toxin 3-nitropropionic acid. *J. Neurosci.* **1993**, *13*, 4181–4192. [[CrossRef](#)]
6. Beal, M.F. Neurochemistry and toxin models in Huntington’s disease. *Curr. Opin. Neurol.* **1994**, *7*, 542–547. [[CrossRef](#)]
7. Brouillet, E.; Jenkins, B.G.; Hyman, B.T.; Ferrante, R.J.; Kowall, N.W.; Srivastava, R.; Roy, D.S.; Rosen, B.R.; Beal, M.F. Age-Dependent Vulnerability of the Striatum to the Mitochondrial Toxin 3-Nitropropionic Acid. *J. Neurochem.* **1993**, *60*, 356–359. [[CrossRef](#)]
8. Brouillet, E.; Condé, F.; Beal, M.F.; Hantraye, P. Replicating Huntington’s disease phenotype in experimental animals. *Prog. Neurobiol.* **1999**, *59*, 427–468. [[CrossRef](#)]
9. Blum, D.; Gall, D.; Cuvelier, L.; Schiffmann, S.N. Topological analysis of striatal lesions induced by 3-nitropropionic acid in the Lewis rat. *NeuroReport* **2001**, *12*, 1769–1772. [[CrossRef](#)]
10. Lagoa, R.; Lopez-Sanchez, C.; Samhan-Arias, A.K.; Gañan, C.M.; Garcia-Martinez, V.; Gutierrez-Merino, C. Kaempferol protects against rat striatal degeneration induced by 3-nitropropionic acid. *J. Neurochem.* **2009**, *111*, 473–487. [[CrossRef](#)]
11. Vonsattel, J.P.; Myers, R.H.; Stevens, T.J.; Ferrante, R.J.; Bird, E.D.; Richardson, E.P., Jr. Neuropathological classification of Huntington’s disease. *J. Neuropathol. Exp. Neurol.* **1985**, *44*, 559–577. [[CrossRef](#)]
12. Ho, A.; Sahakian, B.J.; Brown, R.G.; Barker, R.A.; Hodges, J.; Ane, M.-N.; Snowden, J.; Thompson, J.; Esmonde, T.; Gentry, R.; et al. Profile of cognitive progression in early Huntington’s disease. *Neurology* **2003**, *61*, 1702–1706. [[CrossRef](#)] [[PubMed](#)]
13. Phillips, W.; Shannon, K.M.; Barker, R.A. The current clinical management of Huntington’s disease. *Mov. Disord.* **2008**, *23*, 1491–1504. [[CrossRef](#)] [[PubMed](#)]
14. Browne, S.E.; Ferrante, R.J.; Beal, M.F. Oxidative stress in Huntington’s disease. *Brain Pathol.* **1999**, *9*, 147–163. [[CrossRef](#)]
15. Menze, E.; Esmat, A.; Tadros, M.G.; Abdel-Naim, A.B.; Khalifa, A.E. Genistein Improves 3-NPA-Induced Memory Impairment in Ovariectomized Rats: Impact of Its Antioxidant, Anti-Inflammatory and Acetylcholinesterase Modulatory Properties. *PLoS ONE* **2015**, *10*, e0117223. [[CrossRef](#)]
16. Tsang, T.M.; Haselden, J.N.; Holmes, E. Metabonomic Characterization of the 3-Nitropropionic Acid Rat Model of Huntington’s Disease. *Neurochem. Res.* **2009**, *34*, 1261–1271. [[CrossRef](#)]

17. Peraza, A.V.; Guzmán, D.C.; Brizuela, N.O.; Herrera, M.O.; Olguin, H.J.; Silva, M.L.; Tapia, B.J.; Mejía, G.B. Riboflavin and pyridoxine restore dopamine levels and reduce oxidative stress in brain of rats. *BMC Neurosci.* **2018**, *19*, 71. [[CrossRef](#)]
18. Singh-Bains, M.K.; Mehrabi, N.F.; Sehji, T.; Austria, M.D.; Tan, A.Y.S.; Tippett, L.J.; Dragunow, M.; Waldvogel, H.J.; Faull, R. Cerebellar degeneration correlates with motor symptoms in Huntington disease. *Ann. Neurol.* **2019**, *85*, 396–405. [[CrossRef](#)]
19. Nasr, P.; Gursahani, H.I.; Pang, Z.; Bondada, V.; Lee, J.; Hadley, R.W.; Geddes, J. Influence of cytosolic and mitochondrial Ca²⁺, ATP, mitochondrial membrane potential, and calpain activity on the mechanism of neuron death induced by 3-nitropropionic acid. *Neurochem. Int.* **2003**, *43*, 89–99. [[CrossRef](#)]
20. Rosenstock, T.R.; Carvalho, A.C.P.; Jurkiewicz, A.; Frussa-Filho, R.; Smaili, S. Mitochondrial calcium, oxidative stress and apoptosis in a neurodegenerative disease model induced by 3-nitropropionic acid. *J. Neurochem.* **2004**, *88*, 1220–1228. [[CrossRef](#)]
21. Brouillet, E.; Jacquard, C.; Bizat, N.; Blum, D. 3-Nitropropionic acid: A mitochondrial toxin to uncover physiopathological mechanisms underlying striatal degeneration in Huntington’s disease. *J. Neurochem.* **2005**, *95*, 1521–1540. [[CrossRef](#)]
22. Gil, J.M.; Rego, A.C. Mechanisms of neurodegeneration in Huntington’s disease. *Eur. J. Neurosci.* **2008**, *27*, 2803–2820. [[CrossRef](#)]
23. Zeevark, G.D.; Derr-Yellin, E.; Nicklas, W.J. NMDA receptor involvement in toxicity to dopamine neurons in vitro caused by the succinate dehydrogenase inhibitor 3-nitropropionic acid. *J. Neurochem.* **1995**, *64*, 455–458. [[CrossRef](#)]
24. Greene, J.G.; Sheu, S.-S.; Gross, R.A.; Greenamyre, J.T. 3-Nitropropionic acid exacerbates N-methyl-d-aspartate toxicity in striatal culture by multiple mechanisms. *Neuroscience* **1998**, *84*, 503–510. [[CrossRef](#)]
25. Calabresi, P.; Gubellini, P.; Picconi, B.; Centonze, D.; Pisani, A.; Bonsi, P.; Greengard, P.; Hipskind, R.A.; Borrelli, E.; Bernardi, G. Inhibition of Mitochondrial Complex II Induces a Long-Term Potentiation of NMDA-Mediated Synaptic Excitation in the Striatum Requiring Endogenous Dopamine. *J. Neurosci.* **2001**, *21*, 5110–5120. [[CrossRef](#)] [[PubMed](#)]
26. Bizat, N.; Hermel, J.-M.; Boyer, F.; Jacquard, C.; Creminon, C.; Ouary, S.; Escartin, C.; Hantraye, P.; Krajewski, S.; Brouillet, E. Calpain Is a Major Cell Death Effector in Selective Striatal Degeneration Induced In Vivo by 3-Nitropropionate: Implications for Huntington’s Disease. *J. Neurosci.* **2003**, *23*, 5020–5030. [[CrossRef](#)]
27. Crespo-Biel, N.; Camins, A.; Pelegrí, C.; Vilaplana, J.; Pallàs, M.; Canudas, A. 3-Nitropropionic acid activates calpain/cdk5 pathway in rat striatum. *Neurosci. Lett.* **2007**, *421*, 77–81. [[CrossRef](#)]
28. Fu, Y. 3-Nitropropionic acid produces indirect excitotoxic damage to rat striatum. *Neurotoxicol. Teratol.* **1995**, *17*, 333–339. [[CrossRef](#)]
29. Stewart, V.C.; Sharpe, M.A.; Clark, J.B.; Heales, S.J.R. Astrocyte-Derived Nitric Oxide Causes Both Reversible and Irreversible Damage to the Neuronal Mitochondrial Respiratory Chain. *J. Neurochem.* **2002**, *75*, 694–700. [[CrossRef](#)]
30. Ryu, J.K.; Nagai, A.; Kim, J.; Lee, M.C.; McLarnon, J.G.; Kim, S.U. Microglial activation and cell death induced by the mitochondrial toxin 3-nitropropionic acid: In vitro and in vivo studies. *Neurobiol. Dis.* **2003**, *12*, 121–132. [[CrossRef](#)]
31. Chakraborty, J.; Singh, R.; Dutta, D.; Naskar, A.; Rajamma, U.; Mohanakumar, K.P. Quercetin Improves Behavioral Deficiencies, Restores Astrocytes and Microglia, and Reduces Serotonin Metabolism in 3-Nitropropionic Acid-Induced Rat Model of Huntington’s Disease. *CNS Neurosci. Ther.* **2013**, *20*, 10–19. [[CrossRef](#)]
32. Jin, X.; Riew, T.-R.; Kim, H.L.; Choi, J.-H.; Lee, M.-Y. Morphological characterization of NG2 glia and their association with neuroglial cells in the 3-nitropropionic acid-lesioned striatum of rat. *Sci. Rep.* **2018**, *8*, 5942. [[CrossRef](#)] [[PubMed](#)]
33. Niccolini, F.; Politis, M. Neuroimaging in Huntington’s disease. *World J. Radiol.* **2014**, *6*, 301–312. [[CrossRef](#)]
34. Hong, H.; Kim, B.; Im, H.-I. Pathophysiological Role of Neuroinflammation in Neurodegenerative Diseases and Psychiatric Disorders. *Int. Neurourol. J.* **2016**, *20* (Suppl. 1), S2–S7. [[CrossRef](#)] [[PubMed](#)]
35. Takeuchi, H.; Jin, S.; Wang, J.; Zhang, G.; Kawanokuchi, J.; Kuno, R.; Sonobe, Y.; Mizuno, T.; Suzumura, A. Tumor Necrosis Factor- α Induces Neurotoxicity via Glutamate Release from Hemichannels of Activated Microglia in an Autocrine Manner. *J. Biol. Chem.* **2006**, *281*, 21362–21368. [[CrossRef](#)]

36. Crotti, A.; Glass, C.K. The choreography of neuroinflammation in Huntington’s disease. *Trends Immunol.* **2015**, *36*, 364–373. [[CrossRef](#)]
37. Nishino, H.; Kumazaki, M.; Fukuda, A.; Fujimoto, I.; Shimano, Y.; Hida, H.; Sakurai, T.; Deshpande, S.B.; Shimizu, H.; Morikawa, S.; et al. Acute 3-nitropropionic acid intoxication induces striatal astrocytic cell death and dysfunction of the blood-brain barrier: Involvement of dopamine toxicity. *Neurosci. Res.* **1997**, *27*, 343–355. [[CrossRef](#)]
38. Liddelow, S.A.; Guttenplan, K.A.; Clarke, L.E.; Bennett, F.C.; Bohlen, C.J.; Schirmer, L.; Bennett, M.L.; Münch, A.E.; Chung, W.-S.; Peterson, T.C.; et al. Neurotoxic reactive astrocytes are induced by activated microglia. *Nature* **2017**, *541*, 481–487. [[CrossRef](#)] [[PubMed](#)]
39. Zhang, Y.; Chen, K.; Sloan, S.; Bennett, M.L.; Scholze, A.R.; O’Keeffe, S.; Phatnani, H.P.; Guarneri, P.; Caneda, C.; Ruderisch, N.; et al. An RNA-sequencing transcriptome and splicing database of glia, neurons, and vascular cells of the cerebral cortex. *J. Neurosci.* **2014**, *34*, 11929–11947. [[CrossRef](#)] [[PubMed](#)]
40. Bennett, M.L.; Bennett, F.C.; Liddelow, S.A.; Ajami, B.; Zamanian, J.; Fernhoff, N.B.; Mulinyawe, S.B.; Bohlen, C.J.; Adil, A.; Tucker, A.; et al. New tools for studying microglia in the mouse and human CNS. *Proc. Natl. Acad. Sci. USA* **2016**, *113*, E1738–E1746. [[CrossRef](#)]
41. Singhrao, S.; Neal, J.; Morgan, B.P.; Gasque, P. Increased Complement Biosynthesis By Microglia and Complement Activation on Neurons in Huntington’s Disease. *Exp. Neurol.* **1999**, *159*, 362–376. [[CrossRef](#)] [[PubMed](#)]
42. Färber, K.; Cheung, G.; Mitchell, D.; Wallis, R.; Weihe, E.; Schwaeble, W.; Kettenmann, H. C1q, the recognition subcomponent of the classical pathway of complement, drives microglial activation. *J. Neurosci. Res.* **2009**, *87*, 644–652. [[CrossRef](#)] [[PubMed](#)]
43. Thomas, L.; Gates, D.J.; Richfield, E.K.; O’Brien, T.F.; Schweitzer, J.B.; Steindler, D.A. DNA End Labeling (TUNEL) in Huntington’s Disease and Other Neuropathological Conditions. *Exp. Neurol.* **1995**, *133*, 265–272. [[CrossRef](#)] [[PubMed](#)]
44. Morita, H.; Suzuki, K.; Mori, N.; Yasuhara, O. Occurrence of complement protein C3 in dying pyramidal neurons in rat hippocampus after systemic administration of kainic acid. *Neurosci. Lett.* **2006**, *409*, 35–40. [[CrossRef](#)] [[PubMed](#)]
45. Hernandez-Encinas, E.; Aguilar-Morante, D.; Morales-Garcia, J.A.; Gine, E.; Sanz-SanCristobal, M.; Santos, A.; Perez-Castillo, A. Complement component 3 (C3) expression in the hippocampus after excitotoxic injury: Role of C/EBP β . *J. Neuroinflamm.* **2016**, *13*, 276. [[CrossRef](#)]
46. Boje, K.M.; Arora, P.K. Microglial-produced nitric oxide and reactive nitrogen oxides mediate neuronal cell death. *Brain Res.* **1992**, *587*, 250–256. [[CrossRef](#)]
47. Murray, K.N.; Parry-Jones, A.R.; Allan, S.M. Interleukin-1 and acute brain injury. *Front. Cell. Neurosci.* **2015**, *9*, 1662–5102. [[CrossRef](#)]
48. Marinelli, C.; Di Liddo, R.; Facci, L.; Bertalot, T.; Conconi, M.; Zusso, M.; Skaper, S.; Giusti, P. Ligand engagement of Toll-like receptors regulates their expression in cortical microglia and astrocytes. *J. Neuroinflamm.* **2015**, *12*, 244. [[CrossRef](#)]
49. Ouary, S.; Bizat, N.; Altairac, S.; Ménétrat, H.; Mittoux, V.; Condé, F.; Hantraye, P.; Brouillet, E. Major strain differences in response to chronic systemic administration of the mitochondrial toxin 3-nitropropionic acid in rats: Implications for neuroprotection studies. *Neuroscience* **2000**, *97*, 521–530. [[CrossRef](#)]
50. Sun, F.; López-Sánchez, C.; Martin-Romero, F.J.; Luis, L.; Gutierrez-Merino, C.; Garcia-Martinez, V. Transfemoral selective “intraluminal wiring” technique for transient middle cerebral artery occlusion in rats. *J. Neurosci. Methods* **2005**, *149*, 82–89. [[CrossRef](#)]



© 2020 by the authors. Licensee MDPI, Basel, Switzerland. This article is an open access article distributed under the terms and conditions of the Creative Commons Attribution (CC BY) license (<http://creativecommons.org/licenses/by/4.0/>).

Food and Chemical Toxicology

Kaempferol Prevents the Activation of Complement C3 Protein and the Generation of Reactive A1 Astrocytes that Mediate Rat Brain Degeneration Induced by 3-Nitropropionic Acid.

--Manuscript Draft--

Manuscript Number:	
Article Type:	Full Length Article
Keywords:	kaempferol; 3-nitropropionic acid; Wistar rats; C3 protein; reactive A1 astrocytes; amyloid β peptides
Corresponding Author:	Carlos Gutierrez-Merino, PhD Universidad de Extremadura Badajoz, BADAJOZ SPAIN
First Author:	Carlos Gutierrez-Merino, PhD
Order of Authors:	Carlos Gutierrez-Merino, PhD Carmen Lopez-Sanchez Joana Poejo Virginio Garcia-Lopez Jairo Salazar Virginio Garcia-Martinez
Abstract:	Kaempferol is a natural antioxidant present in vegetables and fruits used in human nutrition. In a previous work, we showed that intraperitoneal (i.p.) kaempferol administration protects against striatum neurodegeneration induced by i.p. injections of 3-nitropropionic acid (NPA), an animal model of Huntington's disease. Recently, we have shown that reactive A1 astrocytes generation is an early event in the neurodegeneration induced by NPA i.p. injections. In the present work, we have experimentally evaluated the hypothesis that kaempferol protects both against the activation of complement C3 protein and generation of reactive A1 astrocytes in rat brain striatum and hippocampus . To this end, we have administered NPA and kaempferol i.p. injections to adult Wistar rats following the protocol described in a previous work. Kaempferol administration prevents against proteolytic activation of complement C3 protein and generation of reactive A1 astrocytes NPA-induced in the striatum and hippocampus . Also, it blocked the NPA-induced increase of NF- κ B expression and enhanced secretion of cytokines IL-1 α , TNF α and C1q, which have been linked to the generation of reactive A1 astrocytes. In addition, kaempferol administration prevented enhanced production of amyloid β peptides in striatum and hippocampus , a novel finding in NPA-induced brain degeneration found in this work.
Suggested Reviewers:	Guang Ji Shanghai University of Traditional Chinese Medicine Yueyang Hospital of Integrated Traditional Chinese Medicine and Western Medicine jiliver@vip.sina.com Expert in medicinal uses of kaempferol Ya-Ping Jin China Medical University School of Public Health ypjin@cmu.edu.cn Expert in reactive A1 astrocytes role in neurodegeneration Tao Wu Center of Chinese Medical Therapy and Systems Biology, Institute of Interdisciplinary Integrative Medicine Research, Shanghai University of Traditional Chinese Medicine wutao001827@163.com Expert in therapeutic uses of kaempferol Hanna Rosenmann The Agnes Ginges Center for Human Neurogenetics, Hadassah Hebrew University

	<p>Medical Center rosenman@hadassah.org.il Expert in NPA-induced neurodegeneration</p>
	<p>Domenico Nuzzo Consiglio Nazionale delle Ricerche -Istituto para la Riceca e Investigazione Biomedica, Palermo, Italy domenico.nuzzo@cnr.it Expert in beneficial effects of natural products in neurodegenerative diseases</p>
Opposed Reviewers:	

UNIVERSIDAD DE EXTREMADURA

DEPARTAMENTO DE BIOQUÍMICA Y BIOLOGÍA MOLECULAR Y GENÉTICA FACULTAD DE CIENCIAS

Avenida de Elvas, s/n
06006 – Badajoz, Spain.

Phone +34 924 289419
E-mail: carlosgm@unex.es

Dear Dr. José L. Domingo
Editor-in-Chief of the Journal Food and Chemical Toxicology

Enclosed, please, find the manuscript entitled: "*Kaempferol Prevents the Activation of Complement C3 Protein and the Generation of Reactive A1 Astrocytes that Mediate Rat Brain Degeneration Induced by 3-Nitropropionic Acid*", authored by Carmen Lopez-Sanchez, Joana Poejo, Virginio Garcia-Lopez, Jairo Salazar, Virginio Garcia-Martinez and myself to be considered for publication in the Journal of Food and Chemical Toxicology.

The main findings reported in this manuscript point out that administration of daily doses of 21 mg of kaempferol/kg b.w. prevents efficiently against the proteolytic activation of complement C3 protein and generation of reactive A1 astrocytes induced by acute treatment of adult Wistar rats with NPA in the brain regions studied in this work, i.e. *striatum* and *hippocampus*. This action of kaempferol correlates with its ability to afford protection against NPA-induced neurodegeneration of these brain areas. Kaempferol also blocks the activation of the NF- κ B signaling pathway, suggesting that this is the major molecular mechanism inducing the enhanced secretion of cytokines IL-1 α , TNF α and C1q that elicits the generation of reactive A1 astrocytes in the rat model used in this work. In addition, an enhanced production of amyloid β peptides has been found in NPA-induced brain degeneration, which is also prevented by kaempferol administration. Thus, this work highlights novel biological roles of this antioxidant flavonoid. In our opinion, the inhibition by kaempferol of C3 proteolytic activation in the brain suggest a potential novel therapeutic use of this flavonoid, because induction of neurotoxic reactive A1 astrocytes has been found in *post-mortem* samples of many human neurodegenerative diseases.

On behalf of all the authors, I declare that this manuscript is new and original and not under consideration for publication elsewhere, and that there is not potential conflict of interest.

Sincerely yours,



Signed. Carlos Gutierrez-Merino
Professor of Biochemistry and Molecular Biology

Highligths manuscript entitled “**Kaempferol Prevents the Activation of Complement C3 Protein and the Generation of Reactive A1 Astrocytes that Mediate Rat Brain Degeneration Induced by 3-Nitropionic Acid.**”

1. Kaempferol prevents the NPA-induced complement C3 protein activation in rat brain
2. Kaempferol protects against reactive A1 astrocytes induction by NPA in rat brain
3. Kaempferol blocks the NPA-induced increase of IL-1 α , TNF α and C1q in rat brain
4. Kaempferol prevents the NPA-induced NF- κ B expression in *striatum* and *hippocampus*
5. Kaempferol blocks NPA-induced amyloid β peptides production in *striatum* and *hippocampus*

1 **Kaempferol Prevents the Activation of Complement C3 Protein and the Generation of**
2 **Reactive A1 Astrocytes that Mediate Rat Brain Degeneration Induced by 3-Nitropropionic**
3 **Acid.**

7 Carmen Lopez-Sanchez ^{1,2†*}, Joana Poejo ^{1†}, Virginio Garcia-Lopez ^{1,2}, Jairo Salazar ^{1,3}, Virginio
8 Garcia-Martinez ^{1,2} and Carlos Gutierrez-Merino ^{1,4*}

10 1. Instituto de Biomarcadores de Patologías Moleculares, Universidad de Extremadura, 06006
11 Badajoz. Spain

14 2. Departamento de Anatomía y Embriología Humana, Facultad de Medicina, Universidad de
15 Extremadura, 06006 Badajoz. Spain

17 3. Departamento de Química, Universidad Nacional Autónoma de Nicaragua-León, León
18 21000, Nicaragua

20 4. Departamento de Bioquímica y Biología Molecular y Genética, Facultad de Ciencias,
21 Universidad de Extremadura, 06006 Badajoz. Spain

26 (†) Both should be considered first authors.

27 (*) Corresponding authors: clopez@unex.es (C.L.-S.); carlosgm@unex.es (C.G.-M.)

32 **Abbreviations:** A β , Amyloid β peptide; APP, Amyloid β Precursor Protein; ATP,
33 Adenosine triphosphate; BBB, Blood-Brain Barrier; BSA, Bovine Serum Albumin; C1q,
34 Complement protein component 1q; C3, Complement protein component 3; COX-2,
35 Cyclooxygenase-2; GFAP, Glial Fibrillary Acidic Protein; HD, Huntington's Disease; i.p.,
36 Intraperitoneal; IL-1 α , Interleukin 1 alpha; iNOS, inducible Nitric Oxide Synthase; NBT/BCIP,
37 Nitroblue Tetrazolium/5-Bromo-4-Chloro-3-Indolyl Phosphate; NF- κ B, Nuclear Factor kappa B;
38 NOS, Nitric Oxide Synthase; NPA, 3-Nitropropionic Acid; PBS, Phosphate-Buffered Saline; PVDF,
39 Polyvinylidene Difluoride; ROS, Reactive Oxygen Species; SDS, Sodium Dodecyl Sulfate; SDS-
40 PAGE, Sodium Dodecyl Sulfate-Polyacrylamide Gel Electrophoresis; TNF α , Tumor Necrosis
41 Factor alpha; TBS, Tris-Buffered Saline; TBST, TBS supplemented with 0.05% Triton X-100; TTC,
42 2,3,5-Triphenyltetrazolium Chloride.

1
2
3
4
5
6
7
8
9
10
11
12
13
14
15
16
17
18
19
20
21
22
23
24
25
26
27
28
29
30
31
32
33
34
35
36
37
38
39
40
41
42
43
44
45
46
47
48
49
50
51
52
53
54
55
56
57
58
59
60
61
62
63
64
65

Abstract

Kaempferol is a natural antioxidant present in vegetables and fruits used in human nutrition. In a previous work, we showed that intraperitoneal (i.p.) kaempferol administration strongly protects against *striatum* neurodegeneration induced by i.p. injections of 3-nitropropionic acid (NPA), an animal model of Huntington's disease. Recently, we have shown that reactive A1 astrocytes generation is an early event in the neurodegeneration induced by NPA i.p. injections. In the present work, we have experimentally evaluated the hypothesis that kaempferol protects both against the activation of complement C3 protein and the generation of reactive A1 astrocytes in rat brain *striatum* and *hippocampus*. To this end, we have administered NPA and kaempferol i.p. injections to adult Wistar rats following the protocol described in a previous work. Kaempferol administration prevents against proteolytic activation of complement C3 protein and generation of reactive A1 astrocytes NPA-induced in the *striatum* and *hippocampus*. Also, it blocked the NPA-induced increase of NF- κ B expression and enhanced secretion of cytokines IL-1 α , TNF α and C1q, which have been linked to the generation of reactive A1 astrocytes. In addition, kaempferol administration prevented the enhanced production of amyloid β peptides in *striatum* and *hippocampus*, a novel finding in NPA-induced brain degeneration found in this work.

Keywords: kaempferol; 3-nitropropionic acid; Wistar rats; C3 protein; reactive A1 astrocytes; amyloid β peptides

1. Introduction

Kaempferol is a natural antioxidant of the flavonoids group of flavonols that is present in many vegetables and fruits widely used in human nutrition. In a previous work, we reported that intraperitoneal (i.p.) kaempferol administration strongly protects against brain neurodegeneration of the striatum induced by i.p. injections of 3-nitropropionic acid (NPA) [Lagoa *et al.*, 2009]. Also, we have shown that intravenous administration of kaempferol afford

a large attenuation of brain damage induced by ischemia-reperfusion in a rat model of
1 transient focal ischemia caused by occlusion of the middle cerebral artery [Lopez-Sanchez *et*
2 *al.*, 2007]. Owing to the low toxicity of kaempferol in humans, we suggested that this
3 compound bears a significant potential therapeutic use as a protective agent against brain
4 damage induced by some insults and/or some neurodegenerative diseases. Indeed,
5 therapeutic applications of kaempferol have been reviewed recently, with particular emphasis
6 in its anti-inflammatory effects [Ren *et al.*, 2019].
7
8

NPA is a neurotoxin, produced by some fungi and plants, whose systemic
19 administration to rodents and non-human primates produces neurological dysfunctions that
20 closely mimic some neurological alterations found in human Huntington's disease (HD)
21 [Brouillet *et al.*, 1999, 2005]. Thus, systemic administration of NPA to rodents has been used as
22 an animal model to study the molecular and cellular mechanisms underlying the brain
23 neurodegeneration observed in this disease. *Striatum* degeneration is a major common
24 feature found in NPA-treated rats and in HD [Brouillet *et al.*, 2005]. Subsequently, it has been
25 shown that systemic administration of NPA also elicits metabolic alterations in cortical areas
26 vicinal to the *striatum*, as well as in the *hippocampus* and the *cerebellum* [Tsang *et al.*, 2009;
27 Menze *et al.*, 2015]. This correlates with cognitive dysfunction, visuospatial deficits, memory
28 loss and difficulty in learning new skills, reported in pre-motor stages of HD [Ho *et al.*, 2003;
29 Phillips *et al.*, 2008].
30
31

Neuroinflammation has been shown to be a common cause of tissue stress in brain
47 neurodegeneration that contributes to spread an initially focalized neuronal insult widely, and
48 it has been shown that NPA administration induces the activation of neuroinflammatory
49 microglia [Ryu *et al.*, 2003; Chakraborty *et al.*, 2014; Jin *et al.*, 2018], activation which has also
50 been reported in the striatum and vicinal cortical areas in HD patients [Niccolini and Politis,
51 2014]. Activated microglia secretes pro-inflammatory cytokines and enhances ROS and nitric
52
53
54
55
56
57
58
59
60
61
62
63
64
65

oxide production in the brain [Liu *et al.*, 2002], and oxidative stress caused by ROS overproduction has been shown to mediate NPA-induced brain neurodegeneration [Lagoa *et al.*, 2009; Brouillet *et al.*, 2005; Nasr *et al.*, 2003; Rosenstock *et al.*, 2004]. Furthermore, intracellular oxidative stress elicited by mitochondrial dysfunction is known to activate NF- κ B signaling pathway [Gutierrez-Merino *et al.*, 2011], and NF- κ B activation leads to enhanced secretion of the pro-inflammatory cytokines that mediate NPA-induced brain degeneration [Ryu *et al.*, 2003; Chakraborty *et al.*, 2014; Jin *et al.*, 2018]. Indeed, i.p. administration of NPA-induced degeneration of the striatum in adult Wistar rats produces a large decrease of reduced glutathione, as well as a large increase of protein nitrotyrosines [Lagoa *et al.*, 2009]. Also, an excess of ROS and nitric oxide causes both reversible and irreversible damage to the mitochondrial respiratory chain function [Stewart *et al.*, 2002], and this further potentiates NPA neurotoxicity, since NPA impairs the mitochondrial respiratory chain directly, acting as an irreversible inhibitor of succinate dehydrogenase [Brouillet *et al.*, 2005]. In addition, the inhibition of creatine kinase activity accelerates the neuronal energetic crisis in this nitroxidative scenario leading to a sustained ATP depletion that induces rapid cell death [Lagoa *et al.*, 2009]. Since many flavonoids are well-known inhibitors of proinflammatory cytokines, iNOS, as well as COX-2 gene expression in the brain through inhibition of NF- κ B activation, as reviewed in Gutierrez-Merino *et al.* (2011), it could be expected that flavonoids provide protection against brain neurodegeneration induced by systemic NPA-administration. Interestingly, when we administered i.p. kaempferol, it effectively protects against striatum degeneration and motor neurological dysfunctions induced by NPA administration, by preventing the decrease of reduced glutathione, the increase of protein nitrotyrosines and the inhibition of creatine kinase activity [Lagoa *et al.*, 2009]. Noteworthy, we also reported that intravenous administration of kaempferol elicits a large inhibition of protein nitrotyrosines production in brain lesion areas during the insult of transient focal cerebral ischemia [Lopez-Sanchez *et al.*, 2007]. In agreement, *Ginkgo biloba* extract EGb761, which major component is

kaempferol, present neuroprotective properties in brain ischemia models [Saleem et al., 2008].

Additionally, the administration of another flavonol, quercetin, has demonstrated to have beneficial effects to improve behavioral deficiencies and restore astrocytes and microglia in the NPA-induced rat model of HD [Chakraborty et al., 2014].

Some neuroinflammatory cytokines secreted by activated microglia in the brain can induce the generation of reactive A1 astrocytes that are highly neurotoxic [Zhang et al., 2014; Bennett et al., 2016; Liddelow et al., 2017], and also astrocytes dysfunctions or gliosis have been reported in the striatum of rats treated with systemic administration of NPA [Lagoa et al., 2009; Jin et al., 2018; Fu, 1995; Nishino et al., 1997; Lopez-Sanchez et al., 2020]. Recently, we have shown that the induction of reactive A1 astrocytes in the striatum, hippocampus and cerebellum of rat brains by NPA i.p. administration is an early event in the NPA-induced neurodegeneration [Lopez-Sanchez et al., 2020]. Astrocytes have been increasingly viewed as critical contributors to neurological disorders [Escartin et al. 2021], and can secrete pro-inflammatory mediators that induce neuroinflammation and result in disruption in tight junctions, finally leading to BBB integrity breakdown and brain edema formation [Farina et al. 2007; Lee and MacLean 2015]. Of note, neuroinflammation could be induced due to astrocytes and microglia activation during brain edemas in 1,2-dichloroethane intoxicated mice [Jin et al., 2019; Wang et al., 2021]. Furthermore, it has been recently shown that rat astrocytes are more sensitive than microglia to 2-choloroethanol, an intermediate metabolite in subacute poisoning with 1,2-dichloroethane, and that reactive astrocytes induced by 2-chloroethanol poisoning can stimulate microglia polarization [Wang et al., 2021]. Thus, reactive astrocytes induced by some chemical insults can also lead to microglia activation. In addition, reactive astrocytes can produce neurotoxic amyloid β peptides [Nadler et al., 2008; Zhao et al., 2011; Frost and Li, 2017], and this possibility deserved to be studied in NPA-induced brain neurodegeneration because it has been recently shown that this neurodegenerative process is also a tauopathy [Lahiani-Cohen et al, 2020].

1 Complement C3 protein gene expression is highly upregulated in reactive A1
2 astrocytes [Liddelow *et al.*, 2017]. Thus, C3 protein expression has been used as a specific
3 marker of reactive A1 astrocytes generation, as reported in post-mortem tissue of HD patients,
4 in which abundant reactive A1 astrocytes have been identified [Liddelow *et al.*, 2017].
5
6 Nevertheless, it has to be recalled that complement C3 protein is initially produced in an
7 inactive form that, in order to be activated, requires partial proteolysis [Huber-Lang *et al.*,
8 2018]. Apart from the classical/lectin and alternative pathway C3 proteases that produce the
9 larger C3 α fragments (C4bC2a and C3bBb, respectively), additional proteases have been shown
10 to act as auxiliary proteases producing further cleavage of C3 [Huber-Lang *et al.*, 2018].
11
12 Several of these proteases are activated and/or released into the extracellular medium during
13 brain neurodegenerative processes, such as extracellular metalloproteases [Rosenberg, 2009]
14 and cathepsins [Nakanishi, 2020]. To the best of our knowledge, the possibility that flavonoids
15 can be potent inhibitors of the pathways (classical or alternative) of C3 activation has been
16 overlooked to date, although some medicinal plants have shown to contain active ingredients
17 such as flavonoids, among others, which are inhibitors of the complement system activation
18 [Kulkarni *et al.*, 2005].
19
20

21 On these grounds, we hypothesize that kaempferol may protect against both the
22 activation of complement C3 protein and generation of reactive A1 astrocytes in the brain
23 regions, striatum, hippocampus, that become dysfunctional and degenerate upon systemic
24 administration of NPA. To experimentally evaluate this hypothesis, we have used adult Wistar
25 rats treated with i.p. injections to administrate NPA and kaempferol as animal model,
26 following the protocol of acute NPA injections and co-administration of a protective
27 kaempferol dose that we have established in a previous work [Lagoa *et al.*, 2009].
28
29
30
31
32
33
34
35
36
37
38
39
40
41
42
43
44
45
46
47
48
49
50
51
52
53
54
55
56
57

58 **2. Materials and Methods**

59
60
61
62
63
64
65

1
2 **2.1. Chemicals**
3
4
5
6
7
8
9
10
11
12
13
14
15

Kaempferol and NPA were supplied by Sigma-Aldrich Spain (Sigma-Aldrich, St. Louis, MO, USA). Glycerol and paraformaldehyde were purchased from Panreac (Barcelona, Spain). Ketamine was from Pfizer, Madrid, Spain. Diazepam and atropine were obtained from B. Braun, Rubí-Barcelona, Spain. All other products were obtained from Sigma-Aldrich or Merck (Darmstadt, Germany), unless specified otherwise.

16 **2.2. Animals and treatments**
17
18
19
20
21
22
23
24
25
26
27
28
29
30
31
32
33
34
35
36
37
38
39
40
41
42
43
44
45
46
47
48
49
50
51
52
53
54
55
56
57
58
59
60
61
62
63
64
65

We have followed protocols previously established in our laboratory for the systemic administration of NPA and kaempferol, [Lagoa *et al.*, 2009; Lopez-Sanchez *et al.*, 2020]. Due to this, these protocols are briefly summarized next.

Male Wistar rats, 9–10 weeks old, weighing 290–340 g, were housed in a 12 h light/dark cycle and allowed free access to food and water during the experiment. The experimental procedures followed the animal care guidelines of the European Union Council Directive 86/609/EEC. The protocols were approved by the Ethics Committee for Animal Research of the local government.

Rats were divided into three experimental groups: KNPA, NPA and Control. The KNPA-group ($n = 6$) received a first injection of kaempferol solution, at a dose of 21 mg/kg, 48 h before initiation of NPA-treatment. From day 0 to 5 of treatment, a dose of 25 mg of NPA/kg body weight (b.w.) was administered every 12 h. Daily, 30 min before the morning NPA injection, another 21 mg/kg dose of kaempferol was injected to the rats. Rats from NPA-group ($n = 6$) were treated with 25 mg NPA/kg b.w. every 12 h during 5 days and, instead of kaempferol, received 1-mL injections with 2.4%v/v DMSO in saline 48 h before NPA-treatment and every day 30 min prior to the morning NPA injection. Control-group ($n = 6$) received 1 mL 2.4%v/v DMSO in saline (kaempferol vehicle) and 0.4 mL saline solution (NPA vehicle), with the same time schedule of treatment groups. Systemic administration of NPA at a dose of 25 mg/kg b.w. every 12h caused marked behavioral alterations in the rats, as reported in a

1 previous work [Lagoa *et al.*, 2009]. After the first and second NPA injections, the animals
2 showed reduced reactive activity during handlings with respect to control animals, although
3 maintained a normal posture and gait. Through days 2 and 3, the animals showed dystonic
4 movements of hind limbs and wobbling gait and paddling. On the 4th day, the animals lost
5 grasping ability and balance capacity. By day 4-5, the rats became recumbent, with a
6 progressive limbs paralysis and moribund appearance. The co-administration of kaempferol
7 drastically reduces the neurological disorders induced by NPA.
8
9

10 To avoid a further loss of animals in the fifth day of treatment, the rats in this group
11 with severe pathological symptoms (motor deficit ≥ 6 or weight loss $\geq 15\%$) were sacrificed at
12 the end of day 4. The rats from the KNPA-group, as well as Control-group, were all treated
13 until day 5 and sacrificed at this time.
14
15

16 At the end of treatments, the animals were anesthetized with ketamine (50 $\mu\text{g/g}$),
17 diazepam (2.5 $\mu\text{g/g}$) and atropine (0.05 $\mu\text{g/g}$). The brains were immediately removed from the
18 skull and washed in cold phosphate-buffered saline (PBS) pH 7.4, and then cut with a tissue
19 slicer. All the immunohistochemistry and Western blots shown in this work have been
20 performed with brain slices vicinal to those used for TTC staining and without signs of
21 microvessel's hemorrhage.
22
23

2. 3. 2,3,5-Triphenyltetrazolium chloride (TTC) staining

24 TTC staining has been performed as described in previous works of our laboratory [Sun
25 *et al.*, 2005; Lopez-Sanchez *et al.*, 2007; Lagoa *et al.*, 2009; Lopez-Sanchez *et al.*, 2020].
26 Routinely one *striatum* slice of the rats of each group was excised for TTC staining to evaluate
27 the extent of *striatum* damage, which is an index of the severity of the neurological lesion
28 correlated with the motor deficit of the rats [Ouary *et al.*, 2000].
29
30

31 From each of the three experimental groups (KNPA, NPA and Control) sections (1,5
32 mm thick coronal slice) corresponding to the regions analyzed, *striatum* and *hippocampus*,
33
34

were immersed in a 2% solution of 2,3,5-triphenyltetrazolium chloride (TTC) in PBS for 15 min
1
2 at 37°C, and observed under a Leica MZ APO stereomicroscope.
3
4

2.4. Brain samples homogenization and Western blotting

Dissected brain sections of *striatum* and *hippocampus* were immediately frozen in
7 liquid nitrogen. Thereafter, samples were kept at -80°C until use. Samples homogenization and
8
9 Western blotting has been performed as described in detail in a recent publication [Lopez-
10 Sanchez *et al.*, 2020]. Briefly, weighed brain sections were homogenized in the following ice-
11 cold buffer: 25 mM tris-(hydroxymethyl)aminomethane hydrochloride (Tris-HCl) at pH 7.4, 150
12 mM NaCl, 5 mM ethylenediaminetetraacetic acid, 50 mM NaF, 5 mM NaVO3 and 4-(1,1,3,3-
13 Tetramethylbutyl)phenyl-polyethylene glycol (Triton X-100) 0.25 %, supplemented with the
14 protease inhibitor cocktail SIGMAFAST S8820 (Sigma-Aldrich). After homogenization with a
15 glass homogenizer, samples were transferred to a plastic Eppendorf tube and sonicated with
16 30-40 pulses of 100 w of 1 s each using a titanium-tip sonicator in an ice-cold recipient. The
17 protein concentration of homogenates was determined using Bradford's method using bovine
18 serum albumin (BSA) as protein standard, and later supplemented with 40% glycerol and
19 conserved at -80°C until use for Western blotting.
20
21

SDS-PAGE have been performed in a BIO-RAD mini-Protean Tetra cell following a
37 standard protocol with 7.5% acrylamide. Samples were loaded at 20 µg protein per lane after
38
39 heat-denaturation of homogenate samples in 95 mM Tris-HCl buffer (pH 6.8), 3% sodium
40 dodecyl sulfate (SDS), 1.5% v/v β-mercaptoethanol, 13% glycerol and 0.005% bromophenol
41 blue. After SDS-PAGE, the gel was transferred to a polyvinylidene difluoride (PVDF) membrane
42 of 0.2 µm average pore size in standard transfer medium (Trans-BloT TransferMedium,
43 BioRad). PVDF membranes were blocked with 3% BSA, washed 6 times with Tris-buffered
44 saline (TBS) supplemented with 0.05% Triton X-100 (TBST), incubated with the primary
45 antibody against the protein target for 1h at room temperature with shaking. Afterwards, the
46 PVDF membrane was washed 6 times with TBST, then incubated with the appropriate
47 antibody for 1h at room temperature with shaking. Finally, the membrane was washed 6 times with
48 TBST and processed for Western blot analysis.
49
50

secondary antibody conjugated with horseradish peroxidase for 1h at room temperature with
1 shaking, washed 6 times with TBST and treated with Clarity TM Western ECL Substrate, BIO-
2 RAD. Western blots were revealed with Bio-Rad ChemiDocTM XRS+. Primary antibodies used in
3 this work: anti-C3 antibody (Abcam ab200999 –rabbit monoclonal, dilution 1:2,000), anti-NF-
4 kB-p65 polyclonal antibody (Proteintech 10745-1-AP produced in rabbit, dilution 1:1,000) and
5 anti-β-amyloid antibody (Sigma-Aldrich A8354 -mouse monoclonal, at 2 µg/mL). Later,
6 membranes were washed with deionized water, stripped, blocked with 3% BSA and treated to
7 quantify β-actin to monitor protein load as indicated above, using mouse monoclonal anti-β-
8 actin antibody (Sigma-Aldrich A1978, dilution 1:5,000) or polyclonal anti-β-actin antibody
9 produced in rabbit (Sigma-Aldrich A5060, dilution 1:500) as primary antibody, and anti-mouse
10 or anti-rabbit IgG-Horseradish peroxidase (Sigma-Aldrich A0944 and A0545, respectively,
11 dilution of 1:5,000 -1:10,000). See Lopez-Sanchez *et al.* (2020) for additional experimental
12 details.
13

14 All the results were confirmed with Western blots of n =6 different samples of each
15 experimental condition. Statistical analysis: results of Western blots are expressed as mean ±
16 standard error (s.e.). Statistical analysis was carried out by Mann–Whitney non-parametric
17 test. Significant difference was accepted at the $p < 0.05$ level.
18

19 **2.5. Immunohistochemistry**

20 Dissected brain coronal sections of *striatum* and *hippocampus* were embedded in
21 paraffin wax and cut 7 µm thick.
22

23 In order to identify and localize different cells populations we carried out the following
24 immunohistochemistry procedures, described in more detail in Lopez-Sanchez *et al.* (2020).
25

26 **2.5.1. Glial fibrillary acidic protein (GFAP), Interleukin 1α (IL-1α), and Complement 27 component 1, subcomponent q (C1q).**

28 After blocking with 1% BSA for 30 min and incubation with 5% normal goat serum in
29 1% BSA and 0.1% Triton X-100 for 2h, tissue sections were incubated with primary antibodies:
30

1 dilution 1:400 for mouse anti-GFAP antibody (Sigma: G3893), and dilution 1:50 for both mouse
2 anti-IL-1 α antibody (Santa Cruz Biotechnology: sc-9983) and mouse anti-C1q-C antibody (Santa
3 Cruz Biotechnology: SC-365301). Then, secondary antibody (dilution 1:200) was added, a goat
4 anti-mouse immunoglobulin G conjugated with alkaline phosphatase (IgG-AP), Santa Cruz
5 Biotechnology: sc 3698. Finally, it was revealed with nitroblue tetrazolium/5-bromo-4-chloro-
6 3-indolyl phosphate (NBT/BCIP) supplied by Roche (catalog nº 1681451).

7
8
9
10
11
12
13
14 **2.5.2. Complement component 3 (C3), Tumor necrosis factor alpha (TNF α) and Nuclear factor
15 k B (NF- κ B p65).**

16
17
18 Tissue sections were blocked with endogenous avidin/biotin blocking kit (Abcam ab
19 64212) and incubated with primary antibodies: dilution 1:2000 for rabbit anti-C3 antibody
20 (Abcam ab225539), dilution 1:100 for rabbit anti- TNF α antibody (Abcam ab6671)), and
21
22 dilution 1:50 for rabbit anti- NF- κ B-p65 (Proteintech 10745-1-AP). Sections were incubated
23
24 with avidin-biotinylated horseradish peroxidase complex (Vectastain ABC Kit). Chromogen
25
26 development was performed with peroxidase substrate solution (Vector VIP substrate, SK-
27
28 4600).

29
30
31
32
33 **2.5.3. Double immunohistochemistry (GFAP+C3; GFAP+ NF- κ B).**

34
35 For double immunohistochemistry, primary antibody mouse anti-GFAP was applied
36
37 together with rabbit anti-C3,or rabbit anti-NF- κ B-p65. Secondary antibodies, goat anti-mouse
38
39 conjugated with alkaline phosphatase and biotinylated goat anti-rabbit Vectastain ABC Kit,
40
41 were applied together. The chromogen development was performed sequentially as follows:
42
43 first, anti-GFAP and secondary antibody conjugated with alkaline phosphatase (blue) and,
44
45 thereafter, the red colour was developed with anti-C3 or anti-NF- κ B-p65 and a biotinylated
46
47 secondary antibody conjugated with peroxidase.

48
49
50
51
52 **2.6. Image analysis**

53
54 Quantitative analysis of microscopy images has been performed using the Image J®
55
56 software.

1
2 **3. Results**
3
4
5
6
7
8

9 **3.1. Kaempferol prevents the increase of complement C3 protein expression and activation, a**
10 **reactive A1 astrocyte marker in NPA-induced brain damage.**

11 Brain samples have been taken from brain slices vicinal to those that display brain
12 damage in TTC-stained slices (**Supplementary Figure S1**), and homogenized as indicated in the
13 Materials and Methods.

14 Western blots reveal that C3 α levels in the *striatum* and *hippocampus* strongly
15 increased in rats of the NPA-group with respect to Control-group, namely $4,44 \pm 0,4$ and $5,9 \pm$
16 0.5 -fold, respectively (**Figure 1** and **Supplementary Figure S2**). In addition, these results also
17 revealed an enhanced proteolytic processing of C3 α in rats of the NPA-group leading to lower
18 molecular weight fragments, i.e. C3 protein activation. Of note, in the *striatum* and
19 *hippocampus* this increase is much higher if the increase is calculated from the sum of the C3 α
20 and all C3 α fragments detected by the anti-C3 antibody used in this work (Abcam, ab200999).
21
22 Thus, these results suggested an enhanced generation of reactive A1 astrocytes in the *striatum*
23 and *hippocampus*, the brain areas that have been shown in many studies to be more prone to
24 NPA-induced degeneration. Indeed, no significant increase of C3 α and all C3 α fragments can
25
26 be seen in the brain stem of rats of the NPA-group with respect to rats of the Control-group
27
28 (**data not shown**).
29
30
31
32
33
34
35
36
37
38
39
40
41
42
43
44
45
46
47
48
49
50
51
52
53
54
55
56
57
58
59
60
61
62
63
64
65

1
2
3
4
5
6
7
8
9
10
11
12
13
14
15
16
17
18
19
20
21
22
23
24
25
26
27
28
29
30
31
32
33
34
35
36
37
38
39
40
41
42
43
44
45
46
47
48
49
50
51
52
53
54
55
56
57
58
59
60
61
62
63
64
65

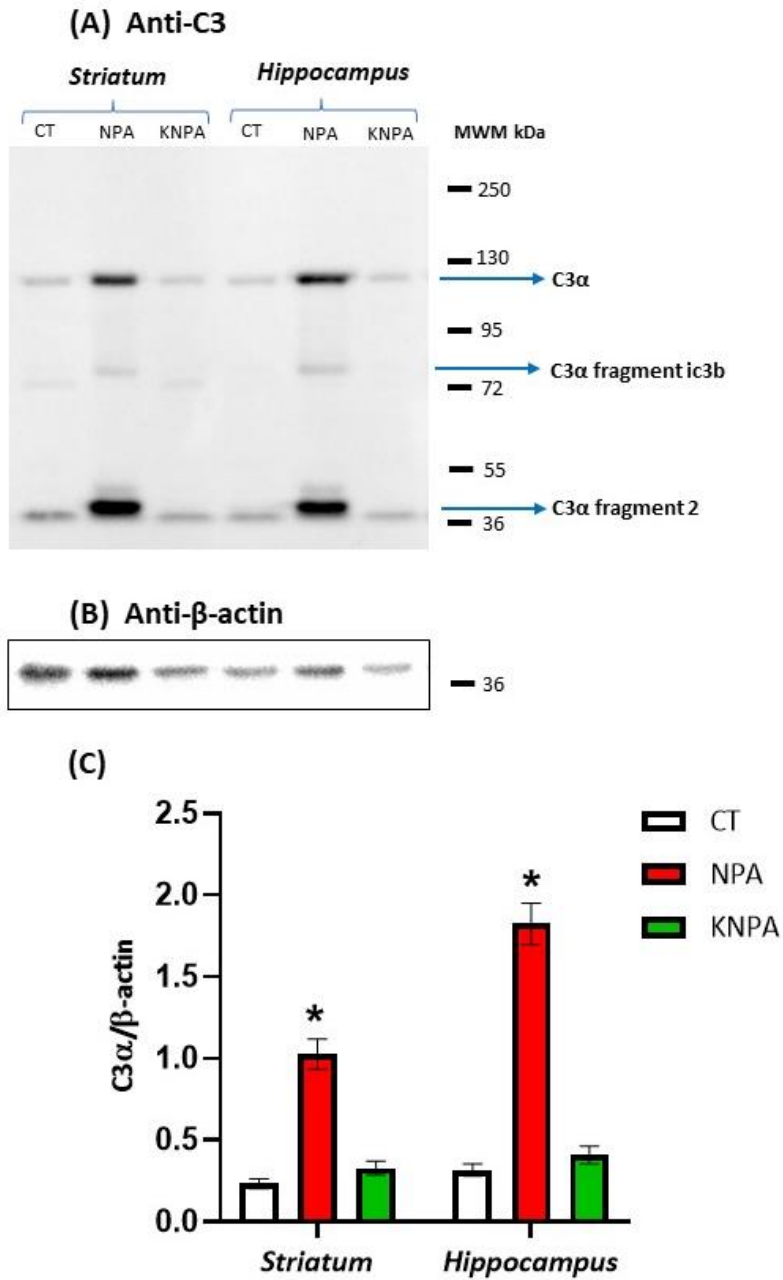


Figure 1. Kaempferol i.p. administration protects against the increase of C3 α and C3 α proteolytic fragments induced by i.p. administration of NPA in the striatum and hippocampus with respect to rats of the Control-group. (A) Representative Western blot of C3 protein and β -actin of striatum and hippocampus homogenates of rats of Control-group (CT), NPA-group (NPA) and KNPA-group (KNPA). (B) After acquisition of images of the Western blot with anti-C3 antibody, the PVDF membrane was stripped and processed for the Western blot of anti- β -actin, as indicated in the Materials and Methods. The β -actin band has been cropped from **Supplementary Figure S2** included at the end of this manuscript. The molecular weights of the protein markers (MWM) are indicated on the left-hand side. (C) Plot of the ratio of (C3 α / β -actin) in striatum and hippocampus homogenates of rats of CT-, NPA- and KNPA-groups. The results shown are the average \pm s.e. of Western blots of n = 6 homogenate samples of each group of rats. (*) p<0.05 with respect to Control rats.

In addition, the results shown in the **Figure 1** demonstrated that the increase of the C3 α was statistically non-significant ($p > 0.05$) in the *striatum* and *hippocampus* of rats treated with kaempferol and NPA (KNPA group). The same result was obtained if the calculations are performed from the sum of C3 α plus all the C3 α fragments, instead of only the C3 α expression level.

3.2. Immunohistochemical analysis of the regionalization and location of complement C3 protein and major proteolytic fragments show that kaempferol also protects against reactive A1 astrocytes induction in Wistar rats brain by acute i.p. NPA treatment.

By means of immunohistochemical analysis, we observed the location and regionalization of complement C3 protein in brain coronal sections. Since the manufacturer indicates that the anti-C3 α antibody used in this work can also bind to blood plasma components, this point was experimentally assessed using excised rat brain slices of the NPA-group [**Supplementary Figure S3**]. Despite that in all this work we have taken special care to use in immunohistochemistry brain slices not showing signs of a significant micro-hemorrhage in the observation area, small thin lines observed in some of the images are likely fingerprints of capillaries.

Since activation of C3 protein has earlier been identified as a reactive A1 astrocyte marker [Liddelow *et al.*, 2017; Lopez-Sanchez *et al.*, 2020], we identified both C3 protein and GFAP by means of double immunochemistry in NPA-group (**Figures 2A and 2B**). C3 α and GFAP immunostaining is revealed by red and blue color, respectively. The localization and distribution of pixels stained in blue and red in the low magnification images of **Figures 2A and 2B** can be better seen in the **Supplementary Figure S4**, which shows the overlay of blue and red channel images obtained using Image J software as indicated in the Materials and Methods section. Our results show high C3 immunostaining in the lesion core, overlapping with the necrotic area, labeling cellular somas. However, ameboid-shape reactive A1 astrocytes are hardly seen in this largely degraded lesion core, a results that is consistent with the large drop

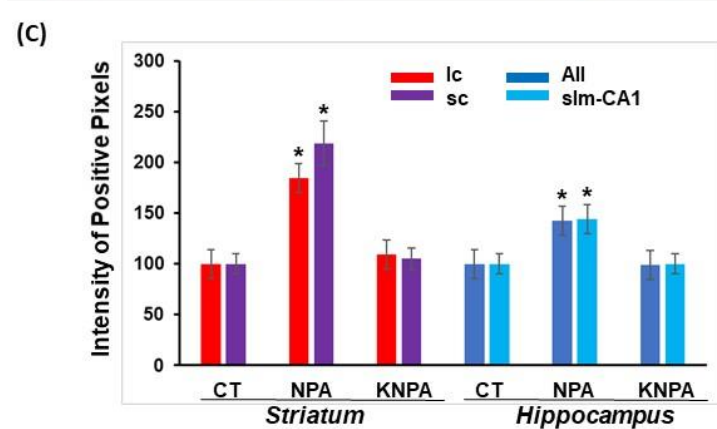
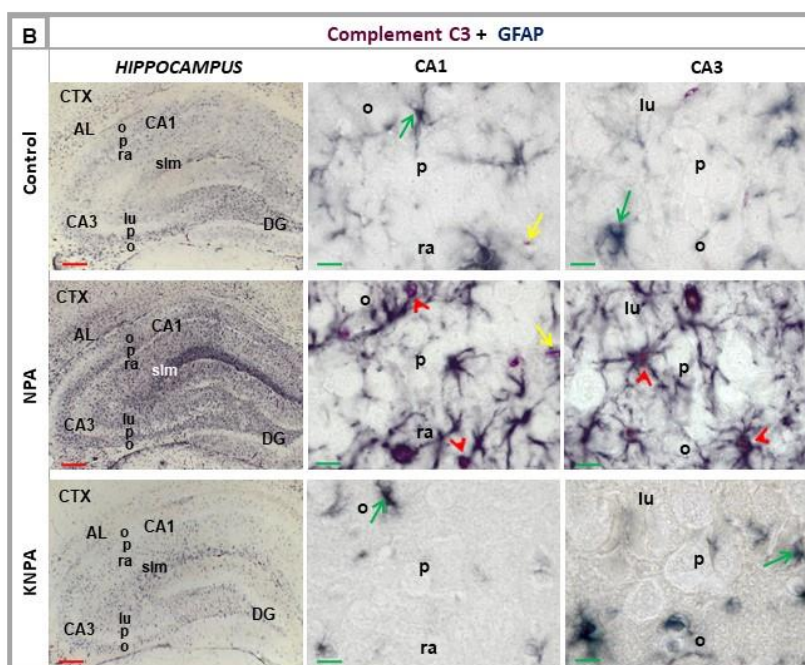
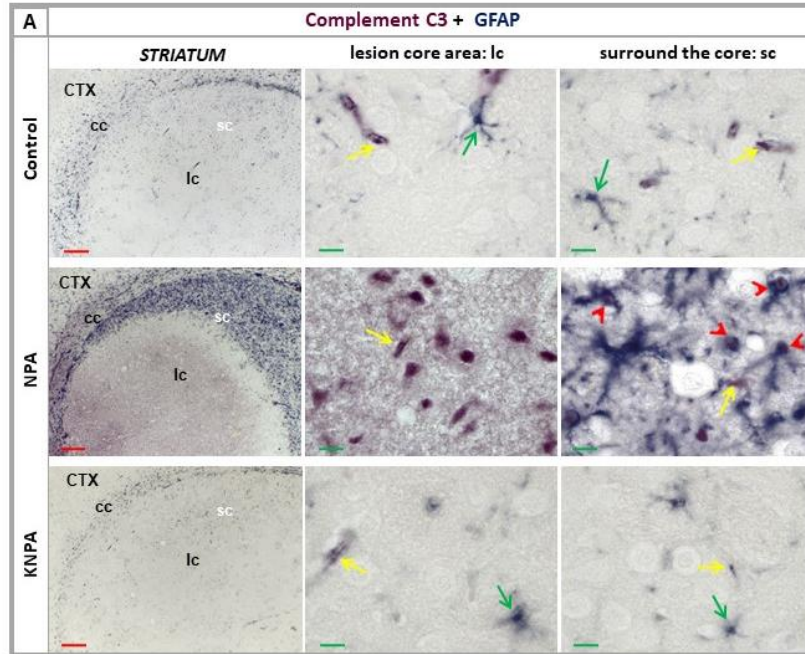


Figure 2. Double immunohistochemistry with anti-C3 (in red) and anti-GFAP (in blue) antibodies in the striatum (A) and hippocampus (B) in the brain coronal sections obtained from Control-, NPA- and KNPA- groups. In NPA-group, note C3 immunostaining in the cellular somas of the lesion core (lc) in the *striatum (A)*. In contrast, in the area surrounding the core (sc) in the *striatum (A)*, ameboid-shape reactive A1 astrocytes (red arrowheads) show a co-location of C3 and GFAP, also observed (red arrowheads) in CA1 as well as CA3 (Ammon's horn) fields in the *hippocampus (B)*. Co-location of complement C3 and GFAP is not observed in Control- and KNPA-groups. As a significant characteristic of anti-C3 antibody, small blood vessels are marked in the three groups (yellow arrows). Abbreviations used in this Figure: AL, *alveus*; cc, *corpus callosum*; CTX, Cerebral cortex; DG, *dentate gyrus*; lu, *stratum lucidum*; o, *stratum oriens*; p, *pyramidal layer*; ra, *stratum radiatum*; slm, *stratum lacunosum-moleculare*. Green arrows: astrocytes. Red scale bars: 200 µm. Green scale bars: 10 µm. **(C)** Histograms of the intensity of positive pixels of the images of C3 staining, obtained from n =3 different rats of each group obtained with Image J® software. Positive pixels means pixels with an intensity higher than 80% of the saturation value and the average intensity shown is the normalized value (100% for controls). Rat brain sections treated with kaempferol (KNPA-group) show a low immunoreactivity, similar to the Control-group. (*) p < 0.05 with respect to Control-group.

of astrogliosis in this area indicated by the results of GFAP immunostaining. On the other hand, we observed high C3 immunolabeling in the area surrounding the core but, in this area, double immunohistochemistry revealed co-location of C3 and GFAP in the ameboid-shape reactive A1 astrocytes (**Figure 2A**). Similarly, our results show co-location of C3 and GFAP in the ameboid-shape reactive A1 astrocytes located in the *hippocampus* (**Figure 2B**), intensively observed in CA1 and CA3 areas and the vicinal *dentate gyrus*.

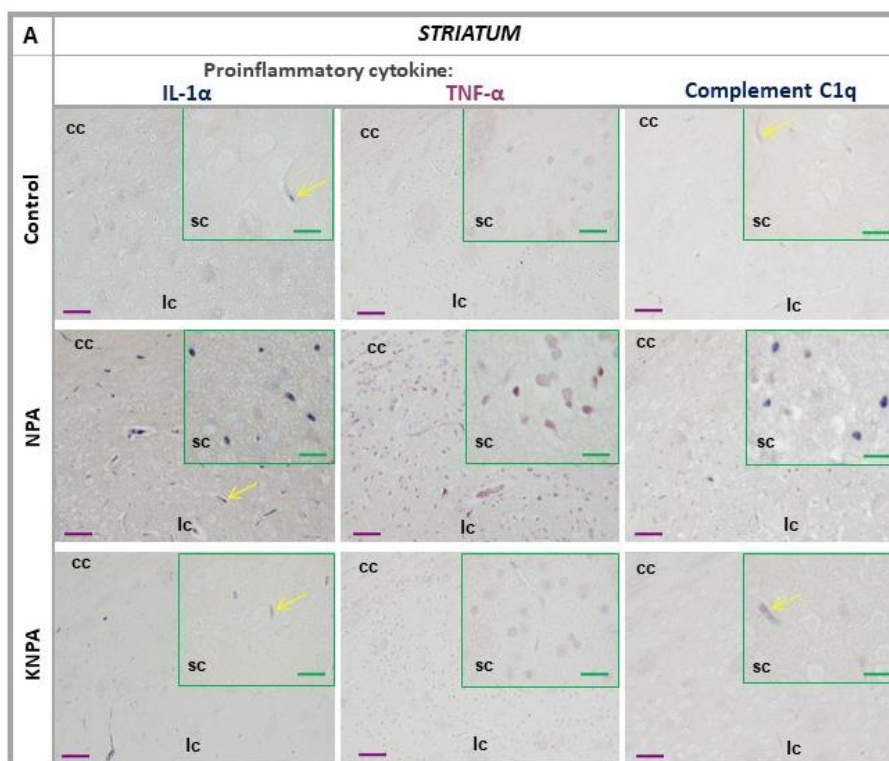
Histograms of the average counts of pixels with high intensity of the images of C3α staining obtained from different rats of each group are shown in the **Figure 2C**. The quantification of high intensity pixels points out that the average increase is 1.85- and 2.2-fold in the lesion core and the surrounding area of the *striatum*, respectively, and 1.45-fold in the *hippocampus*.

This increase of distribution and regionalization of complement C3 protein expression, as well as the presence of reactive A1 astrocytes, detected in NPA-group is fully prevented in rats treated with kaempferol and NPA (KNPA-group) in the regions analyzed, which shows an immunostaining pattern very similar to the Control-group of rats (**Figures 2A and 2B**).

1
2 **3.3. Kaempferol prevents the increase of proinflammatory cytokines IL-1 α , TNF α and**
3 **complement C1q in the striatum and hippocampus of NPA-treated rats.**

4
5 As shown in a recent publication of our laboratory [Lopez-Sanchez *et al.*, 2020], the
6 treatment with NPA also induces increased levels of the proinflammatory cytokines IL-1 α ,
7 TNF α and C1q in the brain regions of Wistar rats that generate reactive A1 astrocytes. It has
8 been shown by other investigators that these cytokines are secreted by activated microglia
9 inducing neurotoxic A1 astrocytes [Zhang *et al.*, 2014; Bennett *et al.*, 2016; Liddelow *et al.*,
10 2017]. A careful selection of brain slices with low capillarity is also of relevance here, since
11
12 **Supplementary Figure S3** show the unspecific staining of the blood plasma with anti-
13 complement C3, anti-IL-1 α and anti-C1q antibodies (yellow arrows), in good agreement with
14 the indications of the manufacturers.
15
16

17 Immunostaining with specific antibodies reveals the increase of IL-1 α , TNF α and C1q in
18 *striatum* brain slices of rats of the NPA-group with respect to Control-group (**Figure 3A**). More
19 than two-fold increase can be calculated for the cytokines and complement C1q from cell
20 counting of selected higher magnification images.
21
22



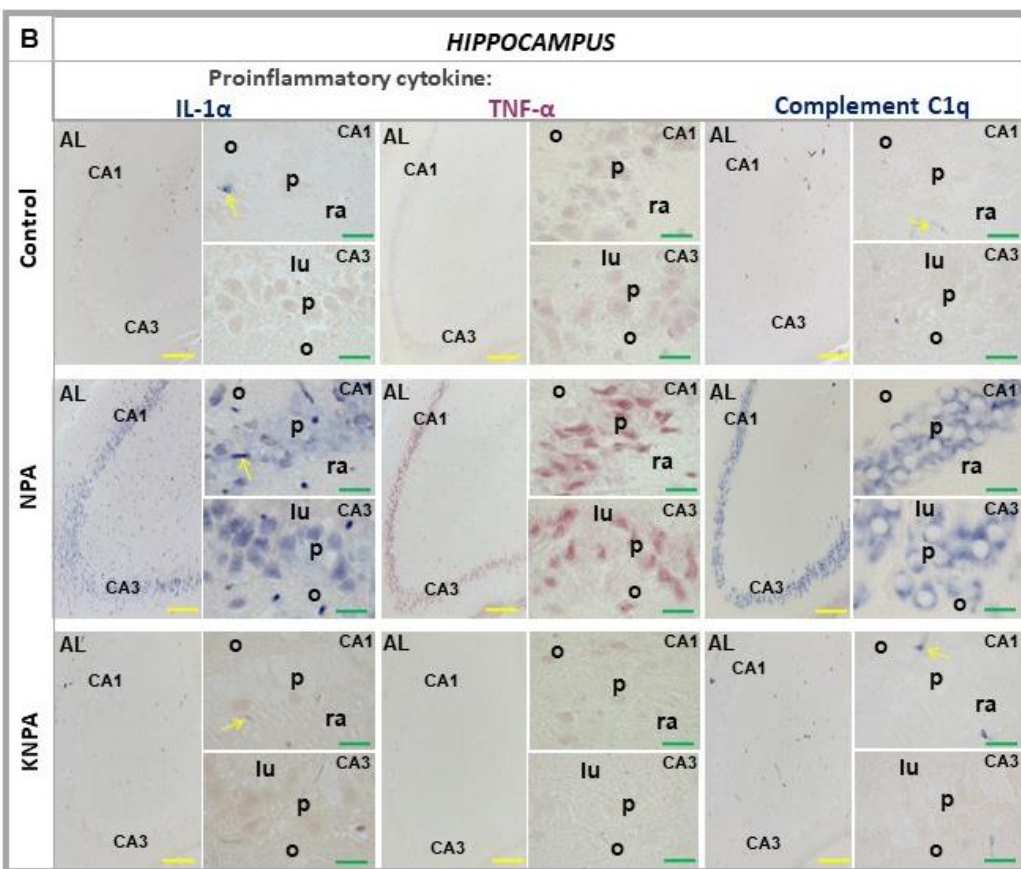


Figure 3. Kaempferol prevents an increase in proinflammatory cytokines IL-1 α , TNF α and complement C1q in the striatum (A) and in the hippocampus (B) of NPA-treated rats. (A) Representative coronal sections of striatum (A) and hippocampus (B) after immunohistochemistry with anti-IL-1 α , anti-TNF α and anti-C1q antibodies corresponding to Control-, NPA- and KNPA-groups. In NPA-group note the cellular somas stained in the area surrounding the core (sc) in the striatum (A), and in CA1 and in CA3 (Ammon's horn) fields in the hippocampus (B). Brain sections of rats treated with kaempferol (KNPA-group) show a low immunoreactivity, similar to the Control- group. No staining in the cellular soma is observed in Control- and KNPA-groups. As a significant characteristic of anti-IL-1 α and anti-C1q antibodies, small blood vessels are marked in the three groups (yellow arrows). Abbreviations used in this Figure: AL, alveus; cc, corpus callosum; lc, lesion core area; lu, stratum lucidum; o, stratum oriens; p, pyramidal layer; ra, stratum radiatum. Yellow scale bars: 100 μ m. Purple scale bars: 50 μ m. Green scale bars: 10 μ m.

The frames with higher magnification in the **Figure 3A** point out the strong staining of cell bodies by these cytokines and the small apparent particle size of the cells heavily stained with TNF α is consistent with the known nuclear translocation of this cytokine. In addition, the striatum brain slices prepared from the KNPA-group display a pattern of immunostaining with

the cytokines and complement C1q that is not significantly different to Control-group for C1q
1 and TNF α , and at most 20% higher for IL-1 α (**Figure 3A**).
2

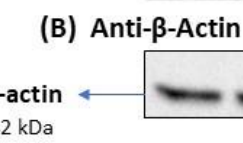
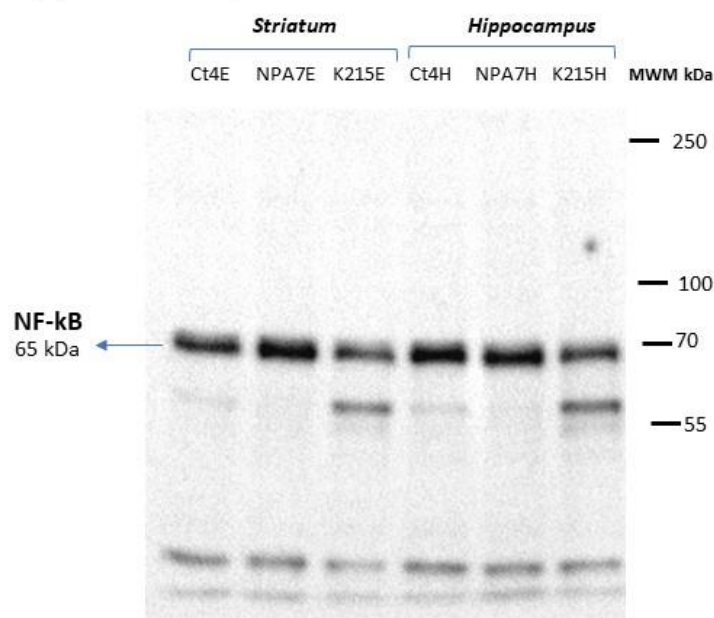
3 The results obtained with *hippocampus* slices also show that NPA treatment increases
4 the expression of these cytokines and complement C1q in this brain area and that this is fully
5 prevented by co-administration of kaempferol at the doses that prevent C3 α activation (**Figure**
6 **3B**). Anti-IL-1 α , anti-TNF α and anti-C1q immunostaining of *hippocampus* slices point out that
7 NPA treatment induced a large increase of these cytokines in the Ammon's horn CA1 and CA3
8 regions, heavily staining the soma of pyramidal neurons. Note that this is not seen in the
9 *hippocampus* slices prepared from the KNPA-group, whose immunostaining pattern is not
10 significantly different from those of rats of the control group.
11

12 **3.4. Kaempferol prevents the NPA-induced increase of NF- κ B expression in the striatum and**
13 ***hippocampus*.**

14 Next, we have experimentally assessed whether kaempferol co-administration can
15 prevent the NPA-induced rise of NF- κ B expression, because activation of NF- κ B has been
16 shown to take place in NPA-induced brain neurodegeneration [Ryu *et al.*, 2003; Chakraborty *et*
17 *al.*, 2014; Jin *et al.*, 2018] and this is a molecular mechanism underlying the enhanced
18 expression of many cytokines [Gutierrez-Merino *et al.*, 2011]. Western blots reveal that NF- κ B-
19 p65 levels in the *striatum* and *hippocampus* increased in rats of the NPA-group with respect to
20 Control-group, and also that this increase was fully prevented by co-administration of
21 kaempferol at the doses that prevented C3 α activation (**Figure 4**).
22

1
2
3
4
5
6
7
8
9
10
11
12
13
14
15
16
17
18
19
20
21
22
23
24
25
26
27
28
29
30
31
32
33
34
35
36
37
38
39
40
41
42
43
44
45
46
47
48
49
50
51
52
53
54
55
56
57
58
59
60
61
62
63
64
65

(A) Anti-NF- κ B p65



(C)

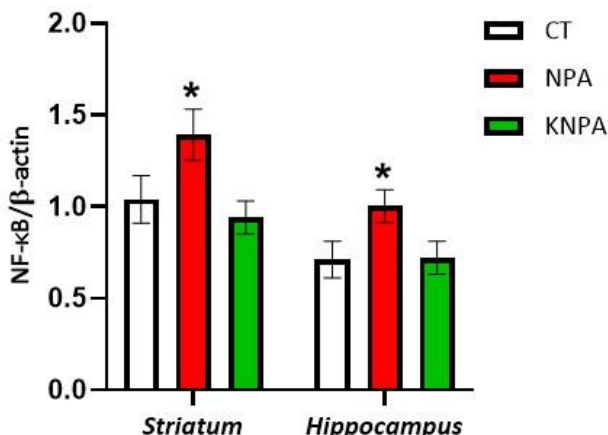


Figure 4. Kaempferol co-administration prevents the increase in NF- κ B induced by NPA-treatment. (A) Representative Western blot of NF- κ B and and β -actin of striatum and hippocampus homogenates of rats of Control-group (CT), NPA-group (NPA) and KNPA-group (KNPA). (B) After acquisition of images of the Western blot with anti- NF- κ B-p65 antibody, the PVDF membrane was stripped and processed for the Western blot of anti- β -actin, as indicated in the Materials and Methods. The molecular weights of the protein markers (MWM) are indicated on the left-hand side. (C) Plot of the ratio of (NF- κ B / β -actin) in striatum and hippocampus homogenates of rats of CT-, NPA- and KNPA-groups. The results shown are the average \pm s.e. of Western blots of $n = 6$ homogenate samples of each group of rats. (*) $p < 0.05$ with respect to Control rats.

These results were confirmed using double immunohistochemistry of coronal slices of
1
the *striatum* and *hippocampus* (**Figure 5**). The immunohistochemistry results of the *striatum*
2
presented in the **Figure 5A** show that the lesion core is only weakly stained both with anti-NF-
3
κB-p65 and with the glial marker anti-GFAP, which is consistent with the advanced tissue
4
damage revealed by TTC staining, as pointed out in a previous work [Lagoa *et al.*, 2009] and
5
also in the **Supplementary Figure S1**. In contrast, the slices of NPA-treated rats displays a large
6
increase of anti-NF-κB-p65 and anti-GFAP staining in the area surrounding the *striatum* lesion
7
core with respect to control rats, in good agreement with the immunohistochemistry results
8
obtained with anti-C3α staining commented above. The *hippocampus* of NPA-treated rats is
9
not extensively damaged, as shown by TTC staining in the **Supplementary Figure S1**. The
10
immunohistochemistry results shown in the **Figure 5B** demonstrate that NPA-treatment elicits
11
a large increase of anti-GFAP staining in CA1 and CA3 fields of the *hippocampus*. Co-location of
12
NF-κB and GFAP in ameboid-shape reactive astrocytes (labelled with red-arrowheads) can be
13
seen in the area surrounding the lesion core of the *striatum* (**Figure 5A**) and in CA1 and CA3
14
fields of the *hippocampus* (**Figure 5B**). **Figure 5** also demonstrates that kaempferol at the
15
doses that prevented C3α activation also prevents the appearance of co-location between NF-
16
κB and GFAP immunostaining, being NF-κB immunostaining restricted to neuronal soma of
17
hippocampal CA1 and CA3 pyramidal neurons like in the Control group (**Figure 5B**). It is to be
18
recalled that high basal constitutive NF-κB activity was found in glutamatergic neurons of the
19
CNS, such as the *hippocampus* granule cells and CA1 and CA3 pyramidal neurons [Kaltschmidt
20
et al., 1994; Kaltschmidt *et al.*, 1995].

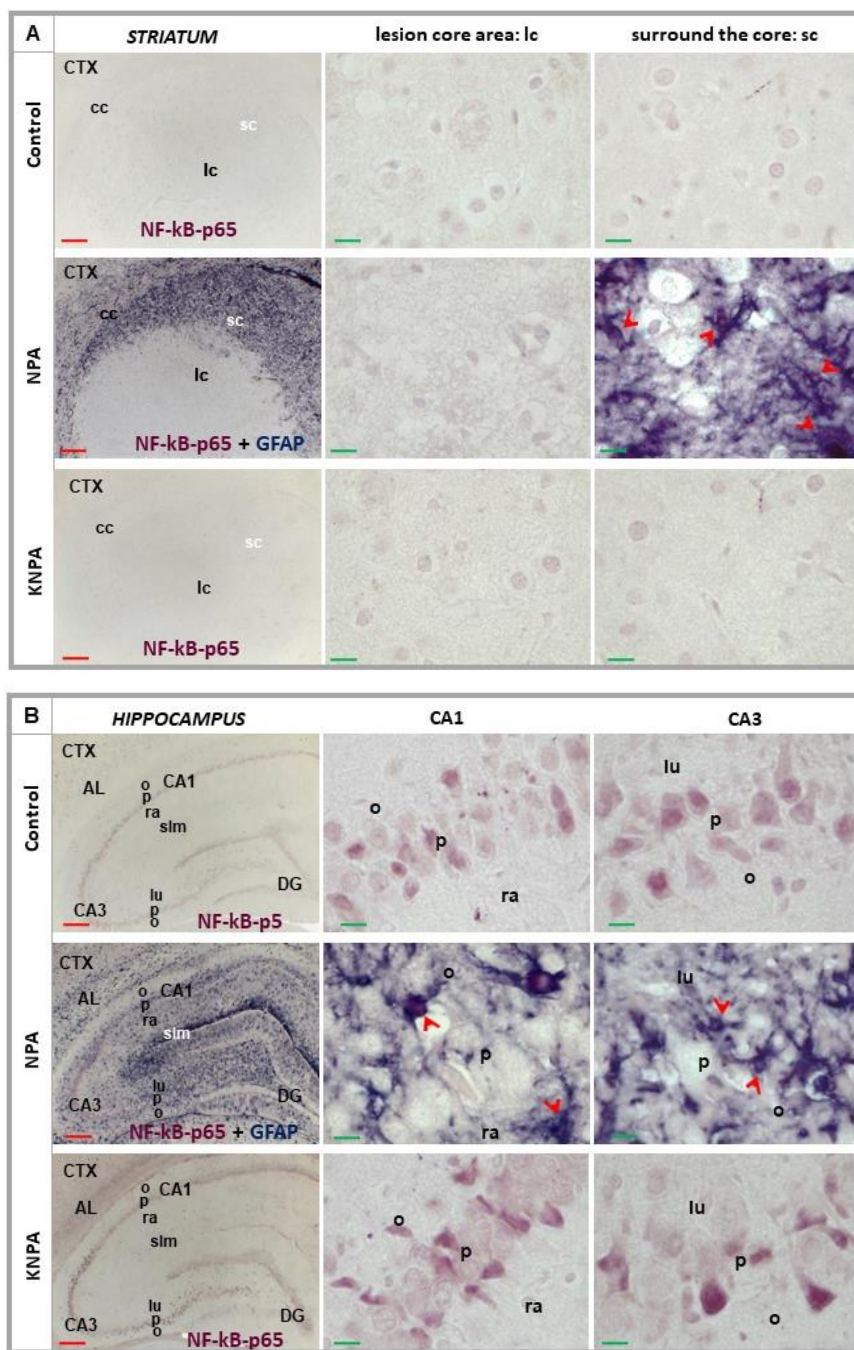


Figure 5. Representative coronal sections corresponding to the striatum (A) and hippocampus (B) after immunohistochemistry with anti-NF-κB-p65 (in red) of Control- and KNPA-groups. And double immunohistochemistry with anti-NF-κB-p65 (in red) and anti-GFAP (in blue) antibodies in NPA-group. In NPA-group, note co-location of NF-κB-p65 and GFAP in ameboid-shape reactive A1 astrocytes (red arrowheads) in the area surrounding the core (sc) in the striatum (A) and in CA1 and in CA3 (Ammon's horn) fields in the hippocampus (B). In the lesion core area (lc) of the striatum (A) no staining in cellular somas is observed with NF-κB-p65 in Control-, NPA- and KNPA- groups. In contrast, in the hippocampus (B) pyramidal neurons (p) of CA1 and CA3 show staining with NF-κB-p65 in Control-and KNPA- groups. Abbreviations used in this Figure: AL: alveus; cc: corpus

1 *callosum*; CTX: Cerebral cortex; DG: dentate gyrus; lu: stratum lucidum; o: stratum oriens;
2 ra: stratum radiatum. Red scale bars: 200 µm. Green scale bars: 10 µm.

3
4
5 **3.5. Kaempferol protects against the increase of amyloid β peptides production in the**
6 **hippocampus and striatum of NPA-treated rats.**

7
8
9
10 A recent study has pointed out that NPA-induced brain neurodegeneration can be also
11
12 classified as a tauopathy [Lahiani-Cohen et al., 2020]. As neurofibrillary tangles of tau and
13
14 amyloid β peptides are major hallmarks in Alzheimer's disease neurodegeneration, a
15
16 neurodegenerative disease in which the generation of reactive A1 astrocytes has also been
17
18 reported [Liddelow et al., 2017], we decided to experimentally assess whether astroglia
19
20 activation leads to an increased production of amyloid β peptides in the *striatum* and
21
22 *hippocampus* during NPA-induced brain neurodegeneration. The results of Western blots of
23
24 homogenates of *striatum* and *hippocampus* slices stained with anti-amyloid β peptides of rats
25
26 of control, NPA-treated and KNPA-treated groups are shown in the **Figure 6**. In the **Figure 6C** it
27
28 is presented the analysis of the ratio C99-cleavage fragment of APP/ β -actin, but a similar trend
29
30 can be seen in the protein bands corresponding to smaller size amyloid β peptides, bands
31
32 between 35 and 50 kDa and peptides of less than 15 kDa migrating near the front of the gel.
33
34
35 These results demonstrated that treatment with NPA induces amyloid β peptides production in
36
37 both brain areas and, also, that co-administration of kaempferol at the doses that prevent C3 α
38
39 activation completely protect against the increase of amyloid β peptides production induced
40
41 by i.p. treatment of rats with NPA.

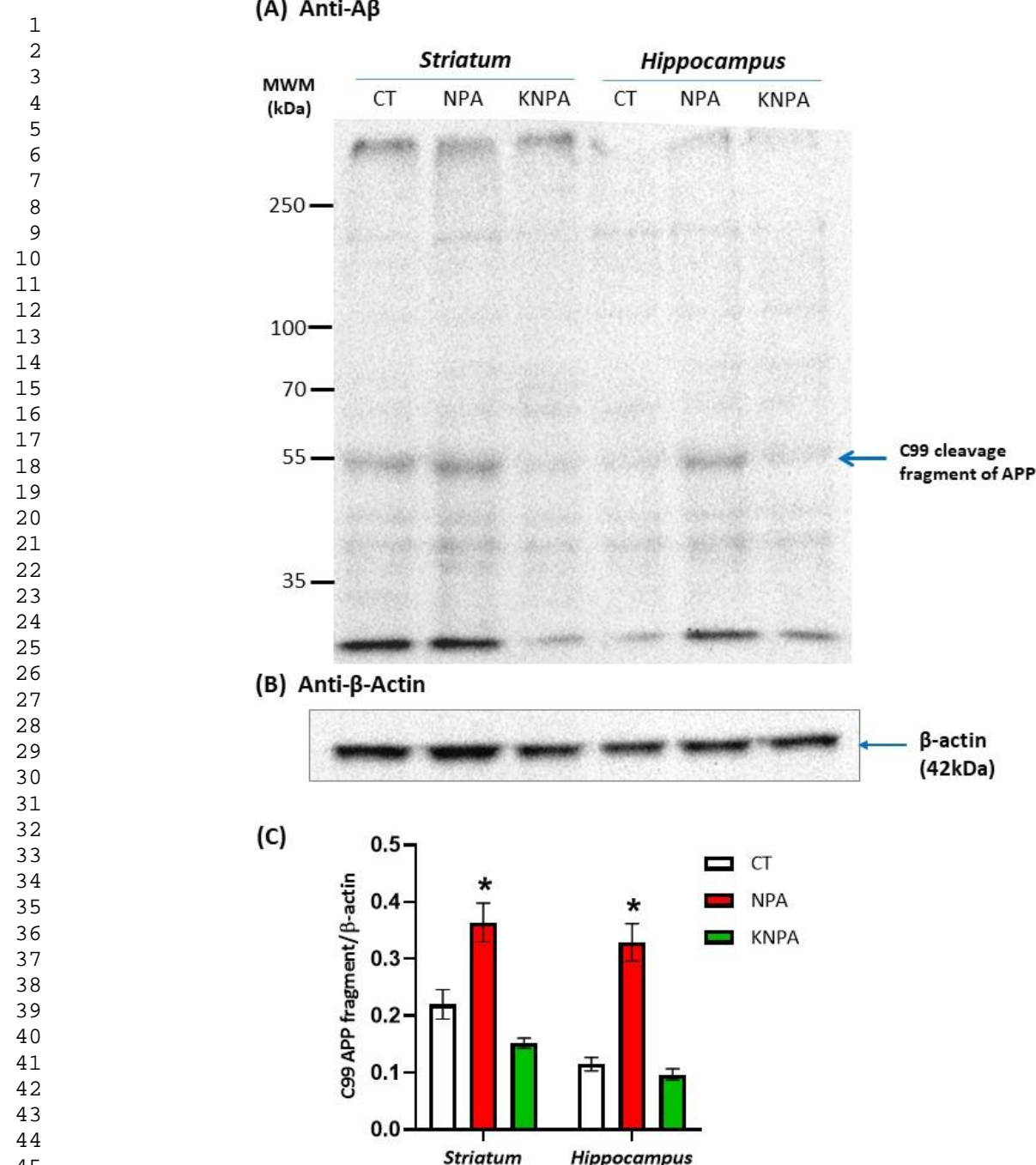


Figure 6. Kaempferol co-administration prevents the increase in amyloid β peptides induced by NPA-treatment. (A) Representative Western blot of amyloid β -peptides and β -actin of *striatum* and *hippocampus* homogenates of rats of Control-group (CT), NPA-group (NPA) and KNPA-group (KNPA). (B) After acquisition of images of the Western blot with anti- β -amyloid antibody, the PVDF membrane was stripped and processed for the Western blot of anti- β -actin, as indicated in the Materials and Methods. The molecular weights of the protein markers (MWM) are indicated on the left-hand side. (C) Plot of the ratio of (C99 cleavage fragment of APP of 50–55 kDa / β -actin) in *striatum* and *hippocampus* homogenates of rats of CT-, NPA- and KNPA-groups. The results shown are the average \pm s.e. of Western blots of $n = 6$ homogenate samples of each group of rats. (*) $p < 0.05$ with respect to Control rats.

4. Discussion

The major result of this work is the protection against proteolytic activation of complement C3 protein by i.p. administration of kaempferol at a dose that also protects efficiently against the rise of markers of neurodegeneration and against the neurological dysfunctions induced by acute i.p. injections of the neurotoxin NPA in male adult Wistar rats, as shown by the good neurological scores of the rats of the KNPA-group, which are in good agreement with those reported in an earlier work [Lagoa *et al.*, 2009]. To the best of our knowledge this a novel finding not previously reported elsewhere. The kaempferol dose used to perform this work, 21 mg/kg b.w., was chosen on the basis of a previous study of our laboratory with this experimental model of i.p. injections of NPA [Lagoa *et al.*, 2009]. Lower doses of kaempferol afforded only a partial protection against *striatum* degeneration [Lagoa *et al.*, 2009]. Also, it is to be noted that herbal extracts of *Persicaria lapathifolia* that contains kaempferol glycoside has been shown to be inhibitors of the classical pathway of complement C3 protein activation [Park *et al.*, 1999]. The results of this work show that i.p. administration of kaempferol results in an almost complete blockade of the NPA-induced increase of C3 α and other proteolytic fragments of C3 (iC3b, C3 α fragment 2 and lower molecular weight fragments) in the brain regions studied, i.e. *striatum* and *hippocampus*. Of note, in a recent study we have shown that a rise of C3 α levels is an early event in NPA neurotoxicity that precedes the appearance of severe neurological dysfunctions [Lopez-Sanchez *et al.*, 2020]. Taking into account that the TTC staining of brain slices of rats of the NPA-group shows large differences between the extent of damage in the *striatum* and the *hippocampus*, this result by itself points out that kaempferol bears a large therapeutic potential to protect against NPA-induced brain degeneration in major brain regions affected by this neurotoxin. Indeed, histochemical results lend further support to this conclusion, since the levels of tissue markers of NPA-induced brain neuroinflammation (C3 activation, NF- κ B immunostaining, astrogliosis and pro-inflammatory cytokines IL-1 α , TNF α and C1q) and neurodegeneration (TTC staining

1 and TUNEL labelling), in *striatum* and *hippocampus* slices from rats of the KNPA-group are
2 similar to those found in the slices of these brain areas from the Control-group, this work and
3 our previous work [Lagoa *et al.*, 2009].
4
5

6 The histochemical studies shown in this work also reveal that C3 α immunostaining in
7 the brain show a remarkable regional and cellular pattern after i.p. injections with acute NPA
8 doses leading to neurological dysfunctions that mimic those found in Huntington's disease. Li
9 et al. (2019) have reported that neurons showing signs of degeneration are marked by
10 upregulated proteins C3 and C1q and are surrounded by activated microglia. In the *striatum*,
11 the brain region undergoing the more extensive damage according to our TTC staining results,
12 the immunostaining with anti-C3 antibody is largely enhanced not only in the necrotic area
13 visualized with TTC staining, but also in the vicinal cortical and *striatum* areas surrounding the
14 lesion core. Indeed, the anti-C3 antibody immunostaining is more intense in these latter vicinal
15 areas, as expected due to the extensive cell loss and tissue degradation observed in the lesion
16 core in this work, accompanied by a significant loss of protein mass as shown in a previous
17 work [Lagoa *et al.*, 2009]. As we have shown in a recent work [Lopez-Sanchez *et al.*, 2020], in
18 early stages of NPA-induced neurotoxicity the immunostaining pattern observed with anti-C3
19 antibody in the *striatum* slices of rats of the NPA-group closely mimics the immunostaining
20 pattern observed with the glial marker anti-GFAP antibody, which revealed astrogliosis. In this
21 work, at an advanced stage of NPA-induced *striatum* degeneration, double immunostaining
22 with anti-C3 and anti-GFAP antibodies showed their co-localization in ameboid-shape
23 astrocytes mostly in areas surrounding the lesion core of the *striatum* in this work, likely
24 because most of reactive A1 astrocytes have been already degraded in the lesion core
25 However, secreted activated C3, a specific marker of these neurotoxic astrocytes [Liddelow *et*
26 *al.*, 2017], seems to remain high in the lesion core of the *striatum* for some time after A1
27 astrocytes are degraded, becoming a fingerprint of earlier generation of these type of
28 astrocytes. Furthermore, this conclusion is also supported by the similarity between
29
30
31
32
33
34
35
36
37
38
39
40
41
42
43
44
45
46
47
48
49
50
51
52
53
54
55
56
57
58
59
60
61
62
63
64
65

1 immunostaining patterns obtained with anti-TNF α , anti-IL-1 α and anti-C1q antibodies, because
2 these cytokines secreted by activated microglia are known to foster reactive A1 astrocytes
3 generation [Liddelow *et al.*, 2017]. Noteworthy, the immunostaining patterns of C3, GFAP, IL-
4
5 1 α , C1q and TNF α antibodies obtained with *striatum* slices of the rats of the KNPA-group are
6 not significantly or only weakly different to those obtained with *striatum* slices of the rats of
7 the Control-group. Therefore, we can conclude that i.p. administration of kaempferol at the
8 dose used in this work prevents efficiently against the activation of complement C3 protein
9 and generation of reactive A1 astrocytes induced by acute treatment with NPA in the *striatum*.
10
11

12 In a previous work, we have shown that induction of reactive A1 astrocytes by i.p. NPA
13 administration is an early event in NPA neurotoxicity that takes place not only in the *striatum*,
14 but also in the *hippocampus* [Lopez-Sanchez *et al.*, 2020]. It is to be recalled here that systemic
15 NPA administration to rodents has been shown to produce memory impairment [Menze *et al.*,
16 2015; Browne *et al.*, 1999]. Noteworthy, the immunohistochemical results obtained in this
17 work with slices of the *hippocampus* of rats of the NPA-group show the presence of A1
18 astrocytes in CA1 and CA3 hippocampal regions, and the vicinal *dentate gyrus* area. We wish to
19 note that anti-C3 antibody will give positive immunostaining of all type of cells expressing C3 α
20 or C3 α -derived fragments or their corresponding complement receptors bound to these C3
21 fragments, which are transmembrane proteins anchored at the cell surface [Li *et al.*, 2011]. In
22 addition, other proteases like extracellular metalloproteinases and cathepsins, which are
23 activated in brain neurodegeneration [Rosenberg, 2009; Nakanishi, 2020], can act as auxiliary
24 proteases in the proteolytic processing C3 [27]. Indeed, C3 expression has been reported in
25 experimental models of neuronal apoptotic cells [Thomas *et al.*, 2000; Morita *et al.*, 2006;
26 Hernandez-Encinas *et al.*, 2016]. In contrast, the weak immunostaining with anti-C3, anti-IL-1 α ,
27 anti-C1q and anti-TNF α antibodies found in the *hippocampus* slices from rats of the KNPA-
28 group is not significantly different to that found in slices from rats of the Control-group.
29
30 Therefore, we can conclude that i.p. administration of kaempferol also prevents efficiently
31

1 against the activation of complement C3 protein and generation of reactive A1 astrocytes
2 induced by acute treatment with NPA in the *striatum* and the *hippocampus*.

3
4 In a previous work we showed that i.p. co-administration of 21 mg of kaempferol/kg
5 b.w. largely prevents the rise of cellular oxidative stress markers in NPA-induced brain
6 degeneration [Lagoa *et al.*, 2009]. In this work, we show that i.p. co-administration of this dose
7 of kaempferol fully prevents against the rise of the expression of NF- κ B in the *striatum* and in
8 the *hippocampus* of NPA-treated rats. In addition, it has been shown that the secretion of pro-
9 inflammatory cytokines that mediate NPA-induced brain degeneration is elicited by NF- κ B
10 activation [Ryu *et al.*, 2003; Chakraborty *et al.*, 2014; Jin *et al.*, 2018]. Therefore, our results
11 lend support to the hypothesis that the activation of NF- κ B signaling pathway by cellular
12 oxidative stress is the major molecular mechanism underlying the enhanced production of pro-
13 inflammatory cytokines IL-1 α , TNF α and C1q in NPA-induced degeneration of the *striatum* and
14 of the *hippocampus*. However, the putative implication of other cellular stress signaling
15 pathways in the production of these cytokines cannot be excluded. Thus, the molecular
16 mechanisms of the blockade by kaempferol of reactive A1 astrocyte generation in the rat brain
17 induced by i.p. administration of NPA deserve to be further investigated. Nevertheless, the
18 results reported in this work reveal a potential novel therapeutic use of this flavonoid, because
19 induction of neurotoxic reactive A1 astrocytes has been found in *post-mortem* samples of
20 many human neurodegenerative diseases, like Alzheimer's, Parkinson's and Huntington's
21 diseases and in amyotrophic lateral sclerosis and multiple sclerosis [Liddelow *et al.*, 2017].
22 Indeed, Stanek *et al.* (2019) using the YAC128 mouse model have suggested that astrocyte
23 dysfunction may play a critical role on Huntington's disease pathogenesis, although this is still
24 a controversial point because it has been questioned by other authors using another mouse
25 models [Diaz-Castro *et al.*, 2019]. The effective doses of kaempferol that afford protection
26 against activation of complement C3 protein in the brain are likely to be strongly dependent
27 upon the administration route of this flavonoid. Indeed, in a previous work we showed that
28

intravenous injections of only 100-200 μ M of kaempferol in the blood produce an extensive
protection against the striatal neurodegeneration caused by transient focal cerebral ischemia
induced by middle cerebral artery occlusion in adult rats [Lopez-Sanchez *et al.*, 2007]. For
comparison, the amount of kaempferol used for intravenous injections in Lopez-Sanchez *et al.*
(2007) were 0.16-0.25 mg of kaempferol/kg b.w., while i.p. injections used in this work have
been 21 mg of kaempferol/kg b.w.

Finally, in this work we found an increase of amyloid β peptides in the *striatum* and a
higher increase in the *hippocampus* of NPA-treated rats. To the best of our knowledge this is a
novel finding in NPA-induced brain neurodegeneration and it has a special relevance, because
exposure to NPA has been recently shown to induce tau pathology in tangle-mouse model and
also in wildtype-mice [Lahiani-Cohen *et al.*, 2020]. Therefore, this neurodegenerative process
shares these molecular biomarkers with Alzheimer's disease, in which reactive A1 astrocytes
have been reported to be generated as well [Liddelow *et al.*, 2017]. Also, our results show that
co-administration of kaempferol prevents the increase of amyloid β peptides induced by NPA.
This is likely due to the protection afforded by kaempferol against the generation of reactive
astrocytes, as it has been shown that they can produce neurotoxic amyloid β peptides [Nadler
et al., 2008; Zhao *et al.*, 2011; Frost and Li, 2017]. Yet, the putative beneficial effects of
kaempferol in Alzheimer's disease is a pending issue, although clinical trials have reported
improvements in cognitive function and memory impairment from treatment with the
flavonoid-rich *Ginkgo biloba* extract [Praticó and Delanty, 2000; Ward *et al.* 2002], a extract
that contains kaempferol.

In summary, i.p. administration of daily doses of 21 mg of kaempferol/kg b.w. prevents
efficiently against the proteolytic activation of complement C3 protein and generation of
reactive A1 astrocytes induced by acute treatment of adult Wistar rats with NPA in the brain
regions studied in this work, i.e. *striatum* and *hippocampus*. This action of kaempferol
correlates with its ability to afford protection against NPA-induced neurodegeneration of these

1 brain areas. Kaempferol also blocks the activation of the NF- κ B signaling pathway, suggesting
2 that this is the major molecular mechanism inducing the enhanced secretion of cytokines IL-
3
4 1 α , TNF α and C1q that elicits the generation of reactive A1 astrocytes in the rat model used in
5 this work. In addition, an enhanced production of amyloid β peptides has been found in NPA-
6 induced brain degeneration, which is also prevented by kaempferol administration. Thus, this
7 work highlights novel biological roles of this antioxidant flavonoid. The inhibition by
8 kaempferol of C3 proteolytic activation in the brain suggest a potential novel therapeutic use
9 of this flavonoid, because induction of neurotoxic reactive A1 astrocytes has been found in
10 *post-mortem* samples of many human neurodegenerative diseases.
11
12
13
14
15
16
17
18
19
20
21
22
23
24
25
26
27
28
29
30
31
32
33
34
35
36
37
38
39
40
41
42
43
44
45
46
47
48
49
50
51
52
53
54
55
56
57
58
59
60
61
62
63
64
65

1
2
3
4
5
6
7
8
9
10
11
12
13
14
15
16
17
18
19
20
21
22
23
24
25
26
27
28
29
30
31
32
33
34
35
36
37
38
39
40
41
42
43
44
45
46
47
48
49
50
51
52
53
54
55
56
57
58
59
60
61
62
63
64
65

Acknowledgements

This work has been supported by Grants: BFU2014-53641-P and BFU2017-85723-P of the Spanish Plan Nacional de I+D+i, and GR21174 and IDA1-19-0055-3 of the Junta de Extremadura. All these Grants have been co-financed by the European Funds for Structural Development (FEDER). Joana Poejo has been funded, in part, by Cafés Delta Foundation (Campomaior, Portugal). Jairo Salazar has been supported by a predoctoral Fellowship of the Fundación Carolina (Spain). We thank our laboratory technician Ms. Laura Ortega Bermejo for her invaluable technical support with animal handlings and samples preparation for immunohistochemistry

References

- 1
2 Bennett, M.L., Bennett, F.C., Liddelow, S.A., Ajami, B., Zamanian, J.L., Fernhoff, N.B.,
3
4 Mulinyawe, S.B., Bohlen, C.J., Adil, A., Tucker, A., Weissman, I.L., Chang, E.F., Li, G., Grant, G.A.,
5
6 Hayden-Gephart, M.G., Barres, B.A., 2016. New tools for studying microglia in the mouse and
7
8 human CNS. Proc. Natl. Acad. Sci. USA 113, E1738–E1746.
9
10 https://doi.org/10.1073/pnas.1525528113
11
12 Brouillet, E., Condé, F., Beal, M.F., Hantraye, P., 1999. Replicating Huntington's disease
13
14 phenotype in experimental animals. Prog. Neurobiol. 59, 427–468.
15
16 https://doi.org/10.1016/s0301-0082(99)00005-2
17
18 Brouillet, E., Jacquard, C., Bizat, N., Blum, D., 2005. 3-Nitropropionic acid: A mitochondrial
19
20 toxin to uncover physiopathological mechanisms underlying striatal degeneration in
21
22 Huntington's disease. J. Neurochem. 95, 1521–1540. https://doi.org/10.1111/j.1471-
23
24 4159.2005.03515.x
25
26 Browne, S.E., Ferrante, R.J., Beal, M.F., 1999. Oxidative stress in Huntington's disease. Brain
27
28 Pathol. 9, 147–163. https://doi.org/10.1111/j.1750-3639.1999.tb00216.x
29
30 Chakraborty, J., Singh, R., Dutta, D., Naskar, A., Rajamma, U., Mohanakumar, K.P., 2014.
31
32 Quercetin improves behavioral deficiencies, restores astrocytes and microglia, and reduces
33
34 serotonin metabolism in 3-nitropropionic acid-induced rat model of Huntington's disease. CNS
35
36 Neurosci. Ther. 20, 10–19. https://doi.org/10.1111/cns.12189
37
38 Diaz-Castro, B., Gangwani, M.R., Yu, X., Coppola, G., Khakh, B.S., 2019. Astrocyte molecular
39
40 signatures in Huntington's disease. Sci. Transl. Med. 11, eaaw8546.
41
42 https://doi.org/10.1126/scitranslmed.aaw8546
43
44
45
46
47
48
49
50
51
52
53
54
55
56
57
58
59
60
61
62
63
64
65

1 Escartin, C., Galea, E., Lakatos, A., O'Callaghan, J.P., Petzold, G.C., Serrano-Pozo, A., *et al.*,
2 2021. Reactive astrocyte nomenclature, definitions, and future directions. *Nat Neurosci* 24(3),
3 312-325. <https://doi.org/10.1038/s41593-020-00783-4>
4
5
6
7 Farina, C., Aloisi, F., Meinl, E., 2007. Astrocytes are active players in cerebral innate immunity.
8 *Trends Immunol* 28, 138-45. <https://doi.org/10.1016/j.it.2007.01.005>
9
10 Frost, G.R., Li, Y.M., 2017. The role of astrocytes in amyloid production and Alzheimer's
11 disease. *Open Biol.* 7, 170228. <https://doi.org/10.1098/rsob.170228>
12
13 Fu, Y., 1995. 3-Nitropropionic acid produces indirect excitotoxic damage to rat striatum.
14 *Neurotoxicol. Teratol.* 17, 333–339. [https://doi.org/10.1016/0892-0362\(94\)00076-P](https://doi.org/10.1016/0892-0362(94)00076-P)
15
16 Gutierrez-Merino, C., Lopez-Sanchez, C., Lagoa, R., Samhan-Arias, A.K., Bueno, C., Garcia-
17 Martinez, V., 2011. Neuroprotective actions of flavonoids. *Curr. Med. Chem.* 18, 1195-1212.
18
19 <https://doi.org/10.2174/092986711795029735>
20
21
22 Hernandez-Encinas, E., Aguilar-Morante, D., Morales-Garcia, J.A., Gine, E., Sanz-SanCristobal,
23
24 M., Santos, A., Perez-Castillo, A., 2016. Complement component 3 (C3) expression in the
25 hippocampus after excitotoxic injury: Role of C/EBP β . *J. Neuroinflamm.* 13, 276.
26
27
28 <https://doi.org/10.1186/s12974-016-0742-0>
29
30
31 Ho, A.K., Sahakian, B.J., Brown, R.G., Barker, R.A., Hodges, J.R., Ané, M.-N., Snowden, J.,
32
33 Thompson, J., Esmonde, T., Gentry, R., Moore, J.W., Bodner, T., 2003. Profile of cognitive
34 progression in early Huntington's disease. *Neurology* 61, 1702–1706.
35
36
37 <https://doi.org/10.1212/01.WNL.0000098878.47789.BD>
38
39
40 Huber-Lang, M., Ekdahl, K.N., Wiegner, R., Fromell, K., Nilsson, B., 2018. Auxiliary activation of
41 the complement system and its importance for the pathophysiology of clinical conditions.
42
43 Semin Immunopathol. 40, 87–102. <https://doi.org/10.1007/s00281-017-0646-9>

1 Jin, X., Riew, T.-R., Kim, H.L., Choi, J.-H., Lee, M.-Y., 2018. Morphological characterization of
2 NG2 glia and their association with neuroglial cells in the 3-nitropropionic acid–lesioned
3 striatum of rat. *Sci. Rep.* 8, 5942. <https://doi.org/10.1038/s41598-018-24385-0>
4
5
6
7 Jin, X., Wang, T., Liao, Y., Guo, J., Wang, G., Zhao, F., Jin, Y., 2019. Neuroinflammatory
8 Reactions in the Brain of 1,2-DCE-Intoxicated Mice during Brain Edema. *Cells* 8(9), 987.
9
10 <https://doi.org/10.3390/cells8090987>
11
12
13
14
15 Kaltschmidt, C., Kaltschmidt, B., Neumann, H., Wekerle, H., Baeuerle, P.A., 1994. Constitutive
16 NF-kappa B activity in neurons. *Mol Cell Biol.* 14, 3981-3992.
17
18 <https://doi.org/10.1128/mcb.14.6.3981-3992.1994>.
19
20
21
22
23 Kaltschmidt, C., Kaltschmidt, B., Henkel, T., Stockinger, H., Baeuerle, P.A., 1995. Selective
24 recognition of the activated form of transcription factor NF-kappa B by a monoclonal antibody.
25
26 *Biol Chem Hoppe Seyler* 376, 9-16. <https://doi.org/10.1515/bchm3.1995.376.1.9>.
27
28
29
30 Kulkarni, A.P., Kellaway, L.A., Kotwal, G.J., 2005. Herbal complement inhibitors in the
31 treatment of neuroinflammation. Future strategy for neuroprotection. *Ann. N.Y. Acad. Sci.*
32
33 1056, 413–429. <https://doi.org/10.1196/annals.1352.020>
34
35
36
37
38 Lagoa, R., Lopez-Sanchez, C., Samhan-Arias, A.K., Gañan, C.M., Garcia-Martinez, V., Gutierrez-
39 Merino, C., 2009. Kaempferol protects against rat striatal degeneration induced by 3-
40 nitropropionic acid. *J. Neurochem.* 111, 473–487. <https://doi.org/10.1111/j.1471-4159.2009.06331.x>
41
42
43
44
45
46
47
48 Lahiani-Cohen, I., Touloumi, O., Lagoudaki, R., Grigoriadis, N., Rosenmann, H., 2020. Exposure
49 to 3-Nitropropionic Acid Mitochondrial Toxin Induces Tau Pathology in Tangle-Mouse Model
50 and in Wild Type-Mice. *Front. Cell Dev. Biol.* 7, 321. <https://doi.org/10.3389/fcell.2019.00321>
51
52
53
54 Lee, K.M., MacLean, A.G., 2015. New advances on glial activation in health and disease. *World*
55
56
57
58
59 *J Virol* 4(2), 42-55. <https://doi.org/10.5501/wjv.v4.i2.42>
60
61
62
63
64
65

Li, K., Fazekasova, H., Wang, N., Sagoo, P., Peng, Q., Khamr, W., Gomes, C., Sacks, S.H.,
1
2 Lombardi, G., Zhou, W., 2011. Expression of complement proteins, receptors and regulators by
3
4 human dendritic cells. Mol. Immunol. 48, 1121-1127.
5
6
7 <https://doi.org/10.1016/j.molimm.2011.02.003>
8
9
10 Li, Y., Severance, E.G., Viscidi, R.P., Yolken, R.H., Xiao, J., 2019. Persistent Toxoplasma infection
11
12 of the brain induced neurodegeneration associated with activation of complement and
13
14 microglia. Infec. Immun. 87, e00139-19. <https://doi.org/10.1128/IAI.00139-19>
15
16
17 Liddelow, S.A.; Guttenplan, K.A.; Clarke, L.E.; Bennett, F.C.; Bohlen, C.J.; Schirmer, L.; Bennett,
18
19 M.L.; Münch, A.E.; Chung, W.-S.; Peterson, T.C.; Wilton, D.K., Frouin, A., Napier, B.A., Panicker,
20
21 N., Kumar, M., Buckwalter, M.S., Rowitch, D.H., Dawson, V.L., Dawson, T.M., Stevens, B.,
22
23 Barres, B.A., 2017. Neurotoxic reactive astrocytes are induced by activated microglia. Nature
24
25 541, 481–487. <https://doi.org/10.1038/nature21029>
26
27
28 Liu, B., Gao, H.-M., Wang, J.-Y., Jeohn, G.-H., Cooper, C.I., Hong, J.-S., 2002. Role of nitric oxide
29
30 in inflammation-mediated neurodegeneration. Ann. N.Y. Acad. Sci. 962, 318-331.
31
32
33 <https://doi.org/10.1111/j.1749-6632.2002.tb04077.x>
34
35
36 Lopez-Sanchez, C., Martin-Romero, F.J., Sun, F., Luis, L., Samhan-Arias, A.K., Garcia-Martinez,
37
38 V., Gutierrez-Merino, C., 2007. Blood micromolar concentrations of kaempferol afford
39
40 protection against ischemia/reperfusion induced damage in rat brain. Brain Res. 1182, 123-
41
42
43 137. <https://doi.org/10.1016/j.brainres.2007.08.087>
44
45
46 Lopez-Sanchez, C., Garcia-Martinez, V., Poejo, J., Garcia-Lopez, V., Salazar, J., Gutierrez-Merino,
47
48 C., 2020. Early reactive A1 astrocytes induction by the neurotoxin 3-nitropropionic acid in rat
49
50 brain. Int. J. Mol. Sci. 21, 3609. <https://doi.org/10.3390/ijms21103609>
51
52
53 Menze, E., Esmat, A., Tadros, M.G., Abdel-Naim, A.B., Khalifa, A.E., 2015. Genistein improves 3-
54
55 NPA-induced memory impairment in ovariectomized rats: Impact of its antioxidant, anti-
56
57
58
59
60
61
62
63
64
65

inflammatory and acetylcholinesterase modulatory properties. PLoS ONE 10, e0117223.
1
2 https://doi.org/10.1371/journal.pone.0117223
3
4
5 Morita, H., Suzuki, K., Mori, N., Yasuhara, O., 2006. Occurrence of complement protein C3 in
6
7 dying pyramidal neurons in rat hippocampus after systemic administration of kainic acid.
8
9
10 Neurosci. Lett. 409, 35–40. https://doi.org/10.1016/j.neulet.2006.09.037
11
12 Nadler, Y., Alexandrovich, A., Grigoriadis, N., Hartmann, T., Rao, K.S.J., Shohami, E., Stein, R.,
13
14 2008. Increased expression of the gamma-secretase components presenilin-1 and nicastrin in
15
16 activated astrocytes and microglia following traumatic brain injury. Glia 56, 552-567.
17
18
19 https://doi.org/10.1002/glia.20638
20
21
22 Nakanishi, H., 2020. Microglial cathepsin B as a key driver of inflammatory brain diseases and
23
24 brain aging. Neural Regen. Res. 15, 25-29. https://doi.org/10.4103/1673-5374.264444
25
26
27 Nasr, P., Gursahani, H.I., Pang, Z., Bondada, V., Lee, J., Hadley, R.W., Geddes, J.W., 2003.
28
29 Influence of cytosolic and mitochondrial Ca²⁺, ATP, mitochondrial membrane potential, and
30
31 calpain activity on the mechanism of neuron death induced by 3-nitropropionic acid.
32
33
34 Neurochem. Int. 43, 89–99. https://doi.org/10.1016/S0197-0186(02)00229-2
35
36
37 Niccolini, F., Politis, M., 2014. Neuroimaging in Huntington's disease. World J. Radiol. 6, 301–
38
39 312. https://doi.org/10.4329/wjr.v6.i6.301
40
41
42 Nishino, H., Kumazaki, M., Fukuda, A., Fujimoto, I., Shimano, Y., Hida, H., Sakurai, T.,
43
44 Deshpande, S.B., Shimizu, H., Morikawa, S., Inubushi, T., 1997. Acute 3-nitropropionic acid
45
46 intoxication induces striatal astrocytic cell death and dysfunction of the blood-brain barrier:
47
48 Involvement of dopamine toxicity. Neurosci. Res. 27, 343–355.
49
50
51
52
53
54 https://doi.org/10.1016/S0168-0102(97)01170-X
55
56
57 Ouary, S., Bizat, N., Altairac, S., Ménétrat, H., Mittoux, V., Condé, F., Hantraye, P., Brouillet, E.,
58
59 2000. Major strain differences in response to chronic systemic administration of the
60
61
62

mitochondrial toxin 3-nitropropionic acid in rats: Implications for neuroprotection studies.
1
2 Neuroscience 97, 521–530. [https://doi.org/10.1016/s0306-4522\(00\)00020-8](https://doi.org/10.1016/s0306-4522(00)00020-8)
3
4
5 Park, S.H., Oh, S.R., Jung, K.Y., Lee, I.S., Ahn, K.S., Kim, J.H., Kim, Y.S., Lee, J.J., Lee, H.K., 1999.
6
7 Acylated flavonol glycosides with anti-complement activity from *Persicaria lapathifolia*. Chem.
8 Pharm. Bull. 47, 1484–1486. <https://doi.org/10.1248/cpb.47.1484>
9
10 Phillips, W., Shannon, K.M., Barker, R.A., 2008. The current clinical management of
11 Huntington's disease. Mov. Disord. 23, 1491–1504. <https://doi.org/10.1002/mds.21971>
12
13 Praticò, D., Delanty, N., 2000. Oxidative injury in diseases of the central nervous system: Focus
14 on Alzheimer's disease. Am. J. Med. 109, 577-585. [https://doi.org/10.1016/S0002-9343\(00\)00547-7](https://doi.org/10.1016/S0002-9343(00)00547-7)
15
16 Ren, J., Lu, Y., Qian, Y., Chen, B., Wu, T., Ji, G., 2019. Recent progress regarding kaempferol for
17 the treatment of various diseases. Exp. Ther. Med. 18, 2759-2776.
18
19 <https://doi.org/10.3892/etm.2019.7886>
20
21 Rosenberg, G.A., 2009. Matrix metalloproteinases and their multiple roles in
22 neurodegenerative diseases. The Lancet Neurology 8, 205–216.
23
24 [https://doi.org/10.1016/S1474-4422\(09\)70016-X](https://doi.org/10.1016/S1474-4422(09)70016-X)
25
26 Rosenstock, T.R., Carvalho, A.C.P., Jurkiewicz, A., Frussa-Filho, R., Smaili, S.S., 2004.
27
28 Mitochondrial calcium, oxidative stress and apoptosis in a neurodegenerative disease model
29 induced by 3-nitropropionic acid. J. Neurochem. 88, 1220–1228.
30
31 <https://doi.org/10.1046/j.1471-4159.2003.02250.x>
32
33 Ryu, J.K., Nagai, A., Kim, J., Lee, M.C., McLarnon, J.G., Kim, S.U., 2003. Microglial activation and
34 cell death induced by the mitochondrial toxin 3-nitropropionic acid: *In vitro* and *in vivo* studies.
35
36 Neurobiol. Dis. 12, 121–132. [https://doi.org/10.1016/S0969-9961\(03\)00002-0](https://doi.org/10.1016/S0969-9961(03)00002-0)

- 1 Saleem, S., Zhuang, H., Biswal, S., Christen, Y., Doré, S., 2008. *Ginkgo biloba* extract
2 neuroprotective action is dependent on heme oxygenase 1 in ischemic reperfusion brain
3 injury. *Stroke* 39, 3389-3396. <https://doi.org/10.1161/STROKEAHA.108.523480>
- 4 Stanek, L.M., Bu, J., Shihabuddin, L.S., 2019. Astrocyte transduction is required for rescue of
5 behavioral phenotypes in the YAC128 mouse model with AAV-RNAi mediated HTT lowering
6 therapeutics. *Neurobiol. Dis.* 129, 29-37. <https://doi.org/10.1016/j.nbd.2019.04.015>
- 7 Stewart, V.C., Sharpe, M.A., Clark, J.B., Heales, S.J.R., 2002. Astrocyte-derived nitric oxide
8 causes both reversible and irreversible damage to the neuronal mitochondrial respiratory
9 chain. *J. Neurochem.* 75, 694–700. <https://doi.org/10.1046/j.1471-4159.2000.0750694.x>
- 10 Sun, F., López-Sánchez, C., Martin-Romero, F.J., Luis, L., Gutierrez-Merino, C., Garcia-Martinez,
11 V., 2005. Transfemoral selective “intraluminal wiring” technique for transient middle cerebral
12 artery occlusion in rats. *J. Neurosci. Methods* 149, 82–89.
13 <https://doi.org/10.1016/j.jneumeth.2005.05.008>
- 14 Thomas, A., Gasque, P., Vaudry, D., Gonzalez, B., Fontaine, M., 2000. Expression of a complete
15 and functional complement system by human neuronal cells in vitro. *Int. Immunol.* 12, 1015–
16 1023. <https://doi.org/10.1093/intimm/12.7.1015>
- 17 Tsang, T.M., Haselden, J.N., Holmes, E., 2009. Metabolomic Characterization of the 3-
18 Nitropropionic Acid Rat Model of Huntington’s Disease. *Neurochem. Res.* 34, 1261–1271.
19 <https://doi.org/10.1007/s11064-008-9904-5>
- 20 Wang, T., Sun, Q., Yang, J., Wang, G., Zhao, F., Chen, Y., Jin, Y., 2021. Reactive astrocytes
21 induced by 2-chloroethanol modulate microglia polarization through IL-1 β , TNF- α , and iNOS
22 upregulation. *Food and Chemical Toxicology* 157, 112550.
23 <https://doi.org/10.1016/j.fct.2021.112550>

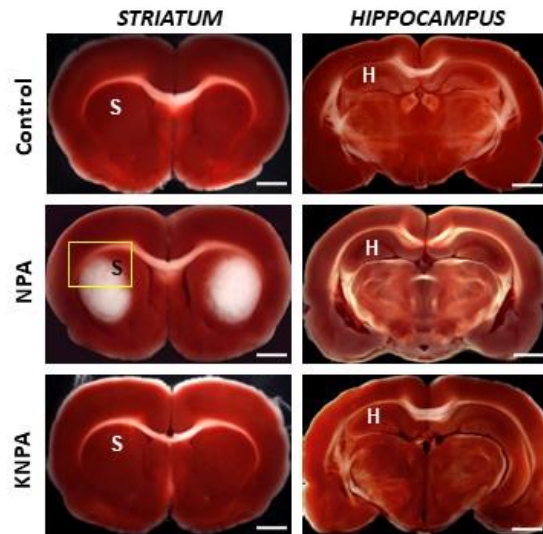
Ward, C.P., Redd, K., Williams, B.M., Caler, J.R., Luo, Y., McCoy, J.G., 2002. *Ginkgo biloba*
extract: cognitive enhancer or antistress buffer. *Pharmacol. Biochem. Behav.* 72, 913-922.
[https://doi.org/10.1016/S0091-3057\(02\)00768-2](https://doi.org/10.1016/S0091-3057(02)00768-2)

Zhang, Y., Chen, K., Sloan, S.A., Bennett, M.L., Scholze, A.R., O'Keeffe, S., Phatnani, H.P.,
Guarnieri, P., Caneda, C., Ruderisch, N., Deng, S., Liddelow, S.A., Zhang, C., Daneman, R.,
Maniatis, T., Barres, B.A., Wu, J.Q., 2014. An RNA-sequencing transcriptome and splicing
database of glia, neurons, and vascular cells of the cerebral cortex. *J. Neurosci.* 34, 11929–
11947. <https://doi.org/10.1523/JNEUROSCI.1860-14.2014>

Zhao, J., O'Connor, T., Vassar, R., 2011. The contribution of activated astrocytes to A β
production: Implications for Alzheimer's disease pathogenesis. *J Neuroinflammation* 8, 150.
<https://doi.org/10.1186/1742-2094-8-150>

1
2
3
4
5
6
7
8
9
10
11
12
13
14
15
16
17
18
19
20
21
22
23
24
25
26
27
28
29
30
31
32
33
34
35
36
37
38
39
40
41
42
43
44
45
46
47
48
49
50
51
52
53
54
55
56
57
58
59
60
61
62
63
64
65

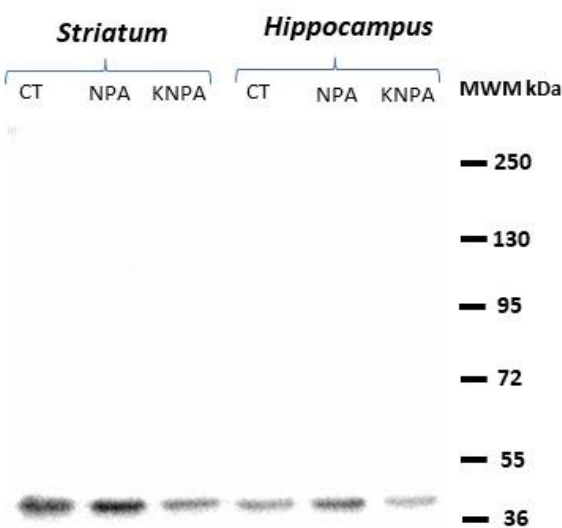
SUPPLEMENTARY FIGURES



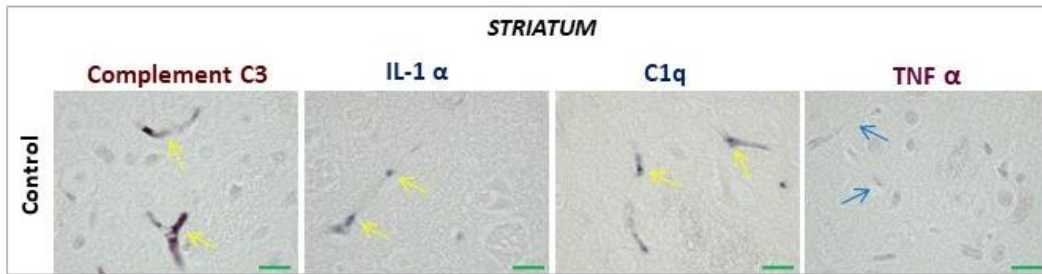
Kaempferol reduces NPA-induced brain degeneration. The images show representative fresh brain 1.5 mm thick coronal sections of the *striatum* (S) and *hippocampus* (H), stained with 2,3,5-triphenyltetrazolium chloride (TTC) in the three groups. The white areas observed in the *striatum* reveal large lesions in NPA-group. No damaged tissue is observed in KNPA-group, which shows similar TTC staining to Control-group. The yellow square mark indicates those *striatum* areas illustrated in the immunohistochemistry images. In the *hippocampus* is observed a weaker TTC staining in NPA-group with respect to Control- and KNPA-groups. Scale bars: 2mm.

Supplementary Figure S1 –C. Lopez-Sanchez, J. Poejo *et al.* (2021)

Western blot of anti- β -actin from which it has been cropped the image shown in the Figure 1B.



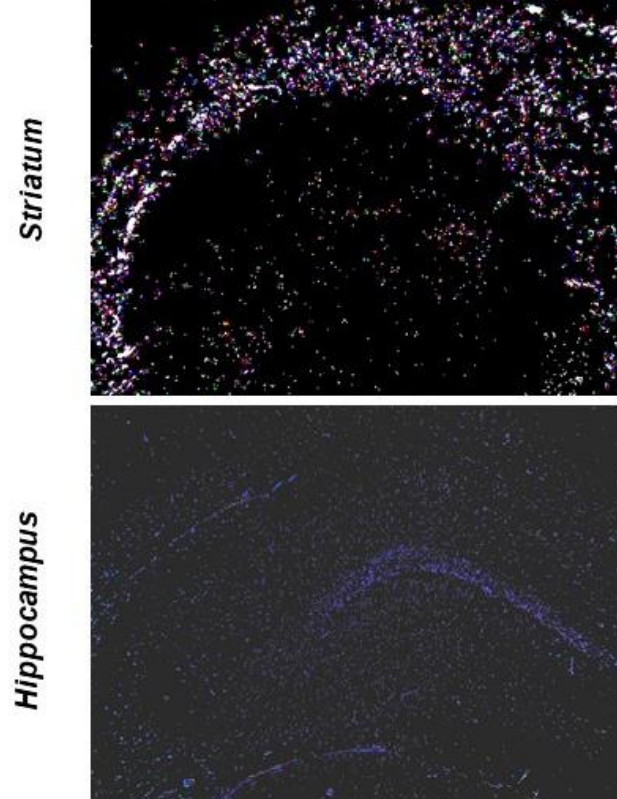
Supplementary Figure S2 –C. Lopez-Sanchez, J. Poejo et al. (2021)



Representative *striatum* coronal sections of a rat of the Control-group after immunohistochemistry showing the unspecific staining of the blood plasma with anti- complement C3, IL1 α and C1q (yellow arrows mark the position of some blood vessels), in agreement with the specifications indicated by manufacturers. Note that anti-TNF α do not afford a significant staining of the blood plasma (blue arrows mark the position of some blood vessels). Green scale bars: 10 μ m.

Supplementary Figure S3 –C. Lopez-Sanchez, J. Poejo *et al.* (2021)

1
2
3 **Overlay of blue and red channels of the low magnification**
4 **images of the Figures 2A and 2B.**
5
6
7
8
9
10
11
12
13
14
15
16
17
18
19
20
21
22
23
24
25
26
27
28
29
30
31
32
33
34
35
36
37
38
39
40
41
42
43
44
45
46
47
48
49
50
51
52
53
54
55
56
57
58
59
60
61
62
63
64
65



Supplementary Figure S4 –C. Lopez-Sanchez, J. Poejo *et al.* (2021)

Declaration of interests

The authors declare that they have no known competing financial interests or personal relationships that could have appeared to influence the work reported in this paper.

The authors declare the following financial interests/personal relationships which may be considered as potential competing interests:



Signed on behalf of all the authors.

GUTIERREZ Firmado
MERINO digitalmente por
CARLOS - GUTIERREZ
08756360F MERINO CARLOS -
08756360F Fecha: 2021.12.14
13:33:26 +01'00'